Control Strategies for Supercritical Carbon Dioxide Power Conversion Systems

by:

Nathan A. Carstens

Master of Science, Nuclear Engineering
Massachusetts Institute of Technology, February 2004

Honors Bachelor of Science, Nuclear Engineering
Oregon State University, June, 2001

Submitted to the Department of Nuclear Engineering in partial fulfillment of the requirements for the degree of

Doctor of Science in Nuclear Engineering

at the

Massachusetts Institute of Technology

June 2007

Author....

Department of Nuclear Engineering
April 20, 2007

Certified by.....

Dr. Michael Driscoll
Professor Emeritus of Nuclear Engineering
Thesis Supervisor

Certified by.....

Dr. Pavel Hejzlar
Principal Research Scientist
Thesis Supervisor

Accepted by.....

Dr. Jeffrey Coderre
Chairman, Department Committee on Graduate Students

Control Strategies for Supercritical Carbon Dioxide Power Conversion Systems

by

Nathan A. Carstens

Submitted to the Department of Nuclear Engineering
On April 20, 2007, in partial fulfillment of the
requirements for the degree of Doctor of Science

Abstract

The supercritical carbon dioxide (S-CO_2) recompression cycle is a promising advanced power conversion cycle which couples well to numerous advanced nuclear reactor designs. This thesis investigates the dynamic simulation of, control strategies for, and selected transient results for an indirect S-CO_2 recompression cycle.

The cycle analyzed is a 600 MWth, highly recuperated, single shaft recompression power conversion cycle with a turbine inlet temperature of 650°C. The cycle features relatively high net efficiency (~47%) at relatively low heat addition temperatures, primarily due to efficient compression. The bottom of this cycle approaches (but in the steady state does not cross) carbon dioxide's critical point, where high fluid densities (~600 kg/m^3) allow efficient compression.

Dynamic simulation of this cycle is complicated by its key features: single-shaft constant-speed turbomachinery, main and recompression compressor in parallel, operation of the main compressor inlet very close to the critical point, and rapid fluid property changes surrounding the critical point. A dynamic simulation and control code for gas-cooled Brayton Cycle reactor power conversion systems (PCS) has been significantly modified and enhanced to use supercritical carbon dioxide as the working fluid. These modifications include the incorporation of accurate yet fast fluid properties, more detailed modeling of turbomachinery performance, and rapid yet accurate calculation of heat exchange in printed circuit heat exchangers, even with rapid fluid property changes. Of particular significance are the methods devised to overcome convergence problems caused by compression near the critical point of CO_2, and the attendant large variations in properties in the main compressor, precooler and low temperature recuperator. Coding innovations have made faster than real time simulation possible (on today's off the shelf hardware), which makes plant simulator and control applications feasible.

This code was used to devise and investigate some of the major control strategies required to operate the cycle: high and low temperature control, three variations of turbine bypass, and inventory control. Using these strategies various transients were investigated including part-load operation, loss-of-load, loss of heat sink, over-power, and startup/shutdown.

The results of these simulations show that the S-CO_2 recompression cycle can be controlled for the transients analyzed, including steady state operation, a variety of part-load operation methods, and the loss-of-load transient. The plant also shows the ability to move between zero and 100% power and can operate at part-load efficiently by combining several control methods. Of particular note, are the advantages of a method devised for simultaneously using properly coupled low temperature and inventory control during part-load operation to avoid rapid fluid property changes near the critical point.

Thesis Supervisor:	Dr. Michael Driscoll
Title:	Professor Emeritus of Nuclear Engineering
Thesis Supervisor:	Dr. Pavel Hejzlar
Title:	Principal Research Scientist
Thesis Reader:	Dr. Richard Vilim
Title:	Nuclear Engineer, Argonne National Laboratory

Acknowledgements

I would like to express my deep gratitude to my advisors Dr. Michael Driscoll and Dr. Pavel Hejzlar for their help and sage advice over many years. Dr. Driscoll has frequently aided directly in my research, provided the guidance that enabled me to successfully navigate new and difficult problems, and supported me throughout my time at MIT. He never ceases to amaze me by scoping out on a piece of paper problems that frequently take me a large simulation code and a week to improve upon.

Dr. Hejzlar has been instrumental in my thesis. Besides being a full time advisor and an expert in this very new and very unique power cycle he has been the integral part of countless working discussions that helped me make progress on everything from day to day programming problems to deciphering complicated and uncertain thermal-hydraulic phenomena never seen before. His experience and expert advice are a key reason for my success modeling this cycle.

I would like to thank Dr. Richard Vilim of Argonne National Laboratory, the original developer of GAS-PASS. His close, continuous, and extensive involvement has greatly aided this project -- this thesis would not have been possible without his help. His expertise in the simulation code and control system modeling saved me countless hours of unnecessary and unrewarding research. Despite my hundreds of phone calls he was always available, willing, and able to help.

I would like to thank my research group members especially Dr. Yifang Gong, of the MIT Gas Turbine Laboratory of the Department of Aeronautics and Astronautics, and Dr. Shih-Ping Kao, a research scientist in the MIT CANES group, for their close and constant involvement which have greatly aided this project. I would also like to thank Jon Gibbs for his expert help with the cycle layout. The working discussions with this group have consistently flushed out unforeseen issues with this cycle and greatly aided my understanding.

Many people have contributed to parts of my research.

- Expertise on modeling the turbomachinery belongs to Jeff Wang and Dr. Gong. Mr. Wang originally modeled the S-CO_2 turbomachinery which made development of correlations for turbine and compressor performance possible. Dr. Gong greatly expanded Mr. Wang's work, provided frequent data updates. His advice regarding turbomachinery has provided me a firm base for understanding these complicated machine and ability to make progress.
- Dr. Mike Pope helped me benchmark the most complicated component in my system – the S-CO_2 precooler. His RELAP expertise was invaluable in simulating this difficult component.
- Dr. Vaclav Dostal created the S-CO_2 recompression cycle design and left an excellent thesis that gave me a firm base to work from.
- Two interns in the Summer 2006 MIT MSRP, Isaac Matthews and Dustin Langewisch, made very useful contributions in the component modeling area.

- Dr. Eric Lemmon, the developer of the NIST RefProp code helped resolve fluid property equation of state issues several times.

I'd like to thank Sandia National Laboratory for funding this research under the contract with MIT for "Qualification of the Supercritical CO_2 Power Conversion Cycle for Advanced Reactor Applications" and its successor "Supercritical CO_2 Cycle Control System Simulation and Plant Design Studies."

Finally, I'd like to dedicate this thesis to my family. The constant encouragement of my grandparents, uncle and aunt, and, especially, my parents are the reason I finished this undertaking. My parents deserve high praise for giving me the tools and encouragement to successfully start my college education in a community college on one side of the country and work my way through a Doctorate in Nuclear Engineering at MIT on the other. I can't thank them enough.

Biography

I began a nearly lifelong involvement with nuclear energy at the Reed Reactor Facility beginning at the age of 14. My career began with becoming the youngest NRC licensed reactor operator at Reed before I moved on to become the only person ever licensed to operate two reactors simultaneously at the Oregon State University Reactor.

Besides operating reactors I have enjoyed several wonderful internships including studying technology public policy in Washington DC with NEI, learning my way around the real thing at the Diablo Canyon Nuclear Power Plant, and completing research at the Pacific Northwest and Los Alamos National Laboratories.

My Nuclear Engineering education began with an Honors Bachelor of Science, Nuclear Engineering Cum Laude from Oregon State University in 2001, progressed with a Masters of Science, Nuclear Engineering from the Massachusetts Institute of Technology in 2004, and now culminates in my Doctorate of Science in Nuclear Engineering at MIT. When I'm asked to explain my focus on nuclear energy, I say that after my first look at Cerenkov radiation and I was hooked.

Table of Contents

List of Figures

List of Tables

1 Introduction

This chapter will briefly introduce the reader to the work carried out in this thesis. It will look at the need for the research, preview the primary research accomplishments, and outline the organization of the thesis.

1.1 Motivation

The development of advanced nuclear power plants promises lower cost electricity while improving upon other key factors such as safety and proliferation resistance. The economic growth of our modern society is tied to the availability of electricity and both appear set to grow significantly over the coming decades[1]. Electricity from nuclear power offers numerous benefits including a relatively stable fuel source and almost no carbon emissions, but its growth will depend significantly upon its ability to compete with the cost of other electricity sources.

The Generation IV[2] effort is an organized assessment of some of the most promising future reactors. While quite different, they all share the common feature of moving to higher operating temperatures than the Generation III reactors operating today.

Increasing the temperature range a cycle operates over is a key factor affecting plant efficiency and ultimately the cost of electricity. In an ideal power cycle, a Carnot Cycle, the cycle efficiency depends only upon the ratio of the low to high temperature. To increase efficiency one must decrease the low temperature, at which heat is rejected, and/or increase the high temperature, at which heat is added. Since the cycle low temperature is typically constrained by local ambient water/air conditions, the designer must increase the high temperature to improve the possible cycle efficiency.

How the nuclear reactor accommodates these higher temperatures is a key design element, but the higher reactor temperatures are of little value if they cannot be efficiently converted into electricity. The power conversion system (PCS) used almost universally for today's reactors, the Rankine Cycle, cannot be easily adapted to exploit these higher temperatures, which imply very high pressures – now approaching 30 MPa. Therefore, a key consideration of the Generation IV effort is the creation of a power cycle which works efficiently at the higher temperatures envisioned. Closed Brayton Cycles are prominent candidates for this service.

One such, the supercritical carbon dioxide (S-CO_2) recompression system, couples well to advanced nuclear reactor designs. The cycle features relatively high efficiency at temperatures significantly lower (for the same efficiency – see Figure 2-1) than those found in helium gas cycles. Furthermore, this cycle is relatively compact for a given power rating (see Figure 2-4), which provides significant advantages in component costs and applications where space is at a premium. Therefore, the S-CO_2 recompression cycle

appears well suited to couple to the Generation IV effort. However, interest in this cycle has only recently been revived[3], and significant research needs to be carried out before its suitability can be confirmed. A key area requiring resolution is the dynamic behavior of the cycle.

Dynamic simulation of this cycle is complicated by its key features: single shaft constant speed turbomachinery, main and recompression compressor in parallel, operation of the main compressor inlet very close to the critical point, and, especially, the rapid fluid property changes surrounding the critical point. The significant property changes near the critical point are the primary reason that this cycle is more efficient than a helium power cycle at the same temperatures (and thus attractive) but they are also inherently complicating.

Many analyses have been carried out for Ideal Gas power cycles, especially helium (see Section 2.2), which share numerous characteristics – fluid properties change smoothly with pressure and temperature. Near carbon dioxide's critical point fluid properties respond in a highly non-linear manner (see Section 2.1.2) that greatly complicate the behavior and modeling of most of the components in this cycle. These complications make many of the methods used to model the Ideal Gas cycle difficult, and frequently impossible, to use. The dynamic modeling of this new, non-linear cycle requires careful and significant development of methods to handle these issues.

Once this cycle can be realistically simulated, the questions of how it will respond to the many transients encountered in a real power plant arise. These questions will require designing and simulating a control system that allows safe and efficient operation of this unique cycle. Note that achieving high efficiency during part-load operation is a key control system consideration. This thesis is dedicated to the development of the necessary modeling methods and answering these questions as to its controllability.

1.2 Thesis Objectives & Contributions

Very little research has gone into the modeling, analyzing, or controlling the dynamics of the S-CO_2 recompression cycle. Virtually all past work, dated back to 1948[3], has focused on steady state full power performance. A parallel effort at Argonne National Laboratory (ANL) has resulted in some recent publications (see Section 2.2.2).

This thesis will look at methods which can rapidly yet accurately model this highly non-linear cycle, the dynamic response of the cycle to a variety of transients, and a control system which allows the cycle to respond safely and efficiently to all the transients simulated. The basic framework for simulation code development has been to start with an existing Ideal Gas (helium) Brayton cycle code, GAS-PASS/H[4], developed by ANL, and to substantially rewrite all subroutines affected by non-ideal gas behavior.

The major contributions of this thesis can be fall into three categories: simulation methods, dynamic simulation results, and control development.

1. Simulation methods:
    a. Rapidly and accurately allowing fluid property interpolation from carbon dioxide's critical point through the highest temperature encountered in the cycle. The method developed can be readily applied to virtually any fluid and can be readily adapted to other non-linear fluids.
    b. The development of a method to accurately and rapidly model S-CO_2 turbomachinery in both design and off-design conditions. While the off-design relations are currently crude, the method is extremely rapid and will become more accurate as experimental data become available.
    c. Developing a rapid method to simulate printed circuit heat exchanger heat exchange, mass and energy storage, and pressure drop. Simulating this process, especially in the precooler where fluid properties change rapidly, is difficult and can be quite computationally expensive. After optimization, runtime improvements approaching 5 orders of magnitude were found without a loss in accuracy – without these improvements the simulation code would not function in a truly useful manner.
    d. Numerically formulating the S-CO_2 recompression cycle in a fashion to allow numerical convergence (increasing Jacobian linearity) and improving the ability of a digital computer to solve the system. To the best of the author's knowledge, no other similar code can simulate the whole cycle simultaneously without significant assumptions. Furthermore, this simulation code uses a fully implicit formulation of equations with a Newtonian system of equations numerical solver, which would normally require a relatively linear system to converge.
    e. Developing several techniques to recover from convergence difficulties, that allow the simulation code to make progress even when highly non-linear regions are encountered.
    f. Optimizing the whole simulation code to the point that it can now run faster than real time on today's off-the shelf hardware.
2. Dynamic simulations:
    a. Identifying a region of difficulty around the main compressor pseudo-critical point which may cause unstable oscillations during inventory control.
    b. Highlighting and numerically benchmarking the importance of transient fluid storage in the precooler heat exchanger.
    c. Investigating low temperature control and its significant ability to affect main compressor performance.
    d. Characterizing the relative efficiency of, and key differences, among six different part-load control methods. In particular, the significant differences encountered with different bypass locations is worthy of note.
3. Control design:
    a. Proposing and simulating a solution to avoid the main compressor's region of difficulty encountered during inventory control.
    b. Simulating the ability to move to low cycle powers using combined inventory and low temperature control.

1.3 Thesis Organization

This report is organized in seven chapters and four appendices:

Chapter 1 presented a brief introduction to this thesis.

Chapter 2 presents the steady state plant model and review the relevant literature.

Chapter 3 analyzes the code used to simulate this cycle in detail. The chapter is broken into several key parts:

- The previously used Ideal Gas cycle simulation code, GAS-PASS, which has been adapted and enhanced to simulate the S-CO_2 recompression cycle
- Section 3.2 examines the modeling approach take in this work. This section provides an overview of how the conservation equations are applied in the overall solution process.
- The fluid property methods and data sources used to allow rapid and accurate calculation of real fluid properties are examined in Section 3.3. The difficulties associated with fluid properties in this cycle and how these problems have been over-come are described.
- Turbomachinery performance is analyzed in Section 3.4. This section will look at the methods and models used to simulate S-CO_2 turbomachinery and also address one of the key uncertainties in the current research – simulating off-design turbomachinery fluid property effects.
- Section 3.5 looks at the methods and models used to calculate heat transfer and pressure drop in the printed circuit heat exchangers used in this cycle. The emphasis of the chapter is on the development of a computational model appropriate for use in a transient performance code.
- Finally, Section 3.6 presents the overall (greatly modified and enhanced) GAS-PASS code. It will provide a description of the code, the integration of the various methods and models addressed in this chapter, and a description of the techniques used to allow a Newtonian solver to be used with a highly non-linear system.
- A brief numerical comparison of inventory control results between GAS-PASS/CO_2 and an independent simulation code are offered in Section 3.7.
- The chapter summary is offered in Section 3.8.

Chapter 4 will briefly look at the various control systems used in GAS-PASS with the S-CO_2 recompression cycle and some of the problems that have arisen. It is not meant as a complete cycle control description but should provide a good background to the major control strategies and they interact with this unique cycle. It is also a primer for future research & development needs to resolve key uncertainties.

Chapter 5 gives the results of the major simulations run with GAS-PASS. The focus of the chapter will be on part-load operation. The unique fluid

properties of this cycle make efficient part-load operation complex in ways not seen in other cycles.

Chapter 6 presents a summary of this thesis and makes recommendations for future work.

Several appendices are included for reference to document details in support of the main text:

- Appendix A: GAS-PASS/CO2 Equations, compiles the differential/difference equations which constitute the mathematical underpinnings of the GAS-PASS code.
- Appendix B: Suggested Future Improvement presents the logical next steps in the code evolution and major possible future improvements.
- Appendix C: GAS-PASS/CO_2 User Manual presents the future user and developer with basic instructions on how to work with the code.
- Appendix D: Simple Turbomachinery Performance Equations presents the compressor performance maps and off-design fluid property relations as approximate polynomials.
- Appendix E: References presents the complete references for this thesis.

1.4 Chapter Summary

This chapter presented the reader with the need and rational for this research, the major thesis accomplishments, and a brief overview of the thesis content. It was intended solely to give the reader a broad overview of the thesis before its detailed components are presented.

2 S-CO_2 Recompression Cycle

The S-CO_2 recompression cycle is unique. The first part of this chapter will describe the major features and components of the MIT 600 MWth indirect PCS. The rest of the chapter will review literature relevant to dynamic simulation and control of this cycle.

2.1 S-CO_2 Recompression Cycle Plant Model

The steady state design of the S-CO_2 recompression cycle has been explored in detail elsewhere[3], but the key features of this cycle merit review. These features not only drive transient performance but they are frequently quite different than those found in other power cycles and therefore deserve examination before transient cycle aspects are introduced.

This cycle uses supercritical carbon dioxide to convert heat to electricity in a closed Brayton cycle. The cycle operates very close (in both temperature and pressure) to carbon dioxide's critical point at the cycle bottom temperature, 32°C, primarily to increase the fluid's density, thereby enabling efficient compression, but never enters the two-phase region. While a condensing cycle (e.g. Rankine) offers many attractive options it requires cooling water too cold to be geographically available throughout the world thus in the present work the critical point will be approached but not crossed to allow widespread deployment.

The cycle maximum temperature, the turbine inlet temperature, is 650°C, in the reference design, making this cycle widely applicable to next generation reactors. The pressures within the cycle operate between 7.69 MPa to 20 MPa, making this a relatively high pressure cycle but by no means the highest pressure cycle being designed for advanced nuclear applications. For example, the supercritical water GEN-IV concept operates at 25 MPa (water's supercritical pressure is 22.1 MPa)[5]. The cycle mass flow rates are also relatively high, approaching 3,000 kg/s. The efficiency of this power cycle is quite attractive at, roughly, 47%.

Dostal compared[3] the efficiency of several advanced nuclear power cycles as a function of turbine inlet temperature as shown in Figure 2-1. The reader should note that at 650°C the S-CO_2 recompression cycle offers higher efficiencies than those available to the water cycles and is about 200°C cooler than a helium cycle with the same efficiency. The ability to achieve this high efficiency without dealing with the materials issues present at substantially higher temperatures is a key reason for interest in this cycle.

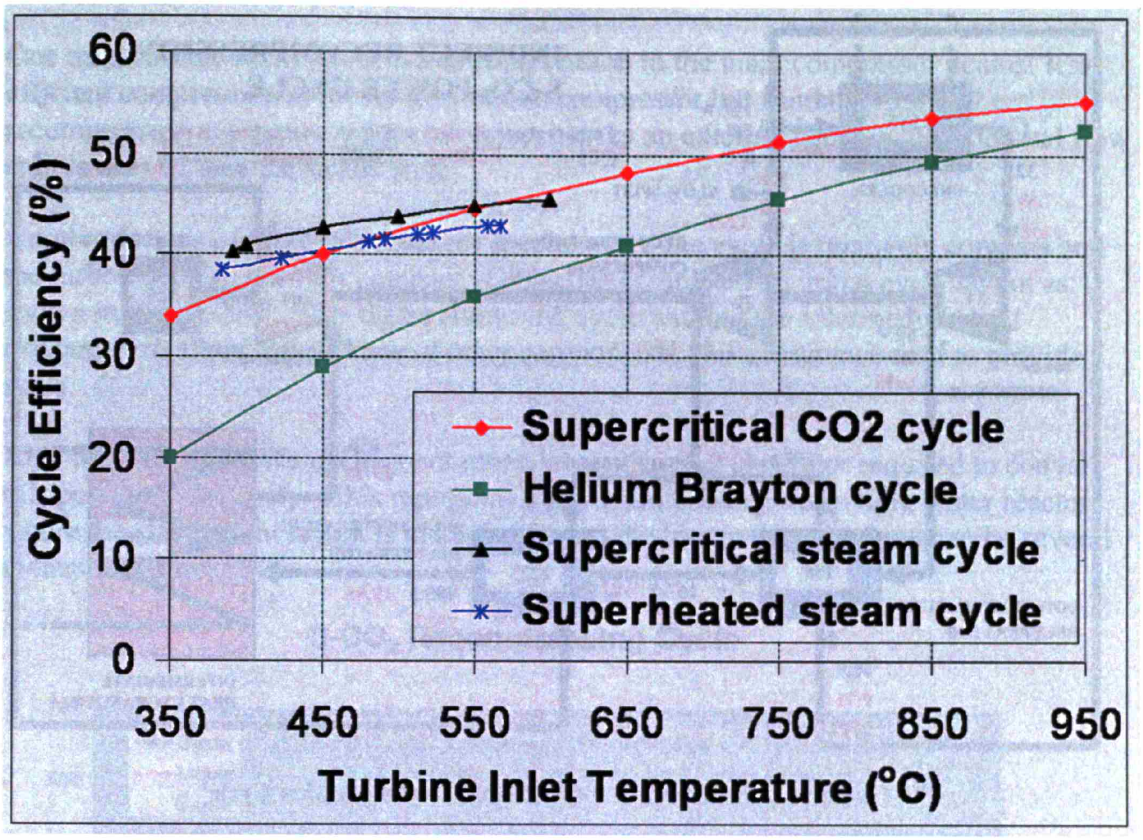

Figure 2-1: Advanced Nuclear Power Cycle Efficiency Comparison[3]

The cycle layout is shown Figure 2-2. The reader should note several features which will be explored in greater detail shortly:

- all the turbomachines operate on a single shaft
- there are two compressors – the main compressor receives externally cooled fluid
- a flow split sends 42% of the flow to the recompression compressor
- there are two recuperators and the low temperature recuperator only receives the main compressor fluid on the cold side to avoid a pinch point
- the power cycle is indirect
- fluid properties vary greatly within the single phase cycle
- there are three turbomachines: an axial turbine and two radial compressors
- heat exchange occurs inside four printed circuit heat exchangers

This cycle uses a single shaft for several reasons. While a multiple shaft arrangement allows more turbomachine control options and the turbomachinery could be optimized for non-grid rotation speeds, a multiple shaft arrangement would require more turbomachines*.

*The multiple shaft layout would probably put each compressor on a separate shaft with a separate turbine, and a generator on a third shaft being driven by a second turbine. The turbines could be in series or in parallel.

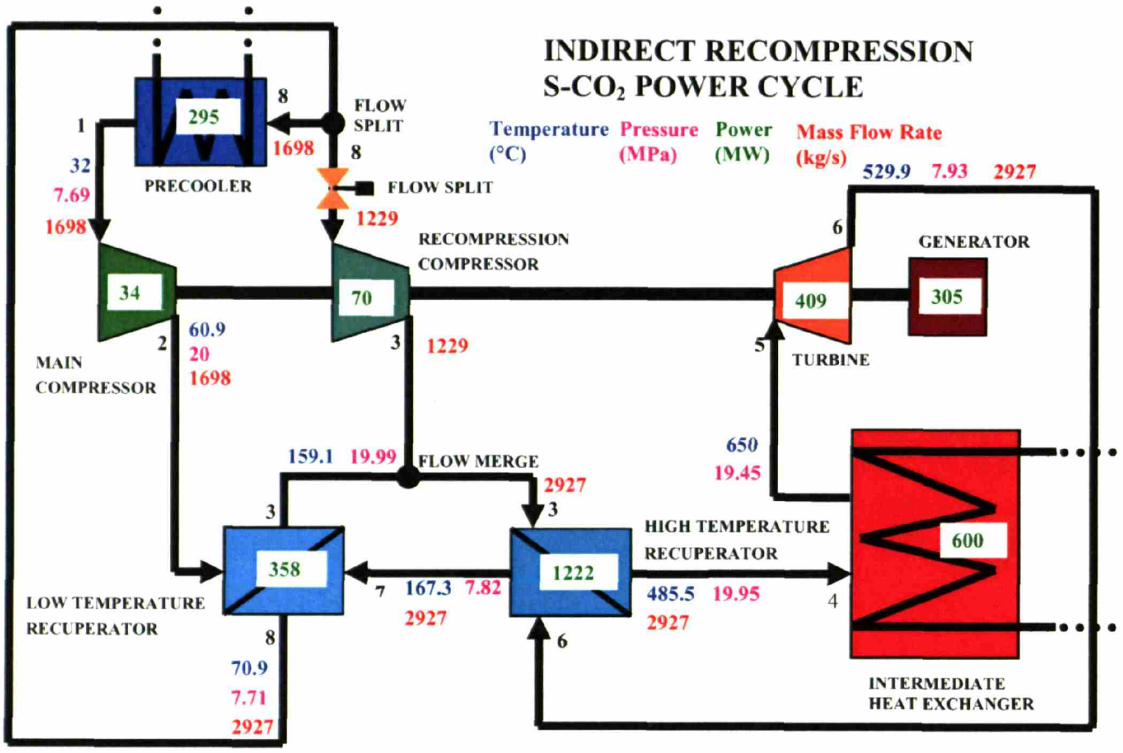

Figure 2-2: Reference Version, S-CO_2 Recompression Cycle

Furthermore, a shaft containing only a turbine and the generator is more difficult to control during loss-of-load events due to smaller inertia and the absence of compressor work to slow the shaft. To minimize cycle cost and size and to provide better overspeed control a single shaft will be adopted unless significant unmet control needs arise.

This cycle uses the flow split and two recuperators to avoid a pinch point during recuperation. Recuperation is performed to further separate the temperatures of heat addition and heat removal, thereby moving closer to the ideal Carnot cycle performance (which has a single temperature for heat addition and a single temperature for heat removal) and increasing efficiency.

Significant isobaric specific heat variation (see Section 2.1.2) near carbon dioxide's critical point can create a pinch point within a recuperator[3]. A pinch point is important because this cycle has substantial gains in efficiency with recuperation that will be lost, as further heat transfer is impossible following the pinch point. The temperature and entropy diagram of this cycle is shown as Figure 2-3, where each number corresponds to a component/number shown in Figure 2-2 – these numbers will be referenced throughout this chapter. Figure 2-3 shows three important features: the bottom of the cycle operates very close to the critical point, about 2/3 of the heat added to the cycle comes from recuperation, and the intermediate heat exchanger adds heat over a relatively narrow temperature range (roughly 150°C). A pinch point will prevent about 10%[3] of the available heat from being recuperated. A parallel recompression stream is a simple and economical way to avoid this pinch point.

One may balance relatively efficient compression in the main compressor against less efficient compression in the recompression compressor but fluid moving to the recompression compressor, does not reject heat to an external coolant. The optimal flow split is near 42% in the steady state.

Another feature of this cycle deserves special note: the cycle is relatively compact and the turbomachines are very compact. Gibbs has completed an initial cycle layout as shown in Figure 2-4[6]. This figure shows the cycle without the intermediate heat exchanger to allow a clear view of other components, and a reference man to provide scale.

Note that the 300 MWe cycle is not much larger than the generator required to convert this power to electricity. This represents a significant change from light water reactors where the steam plant layout is much larger and the low pressure turbine can be several meters in diameter.

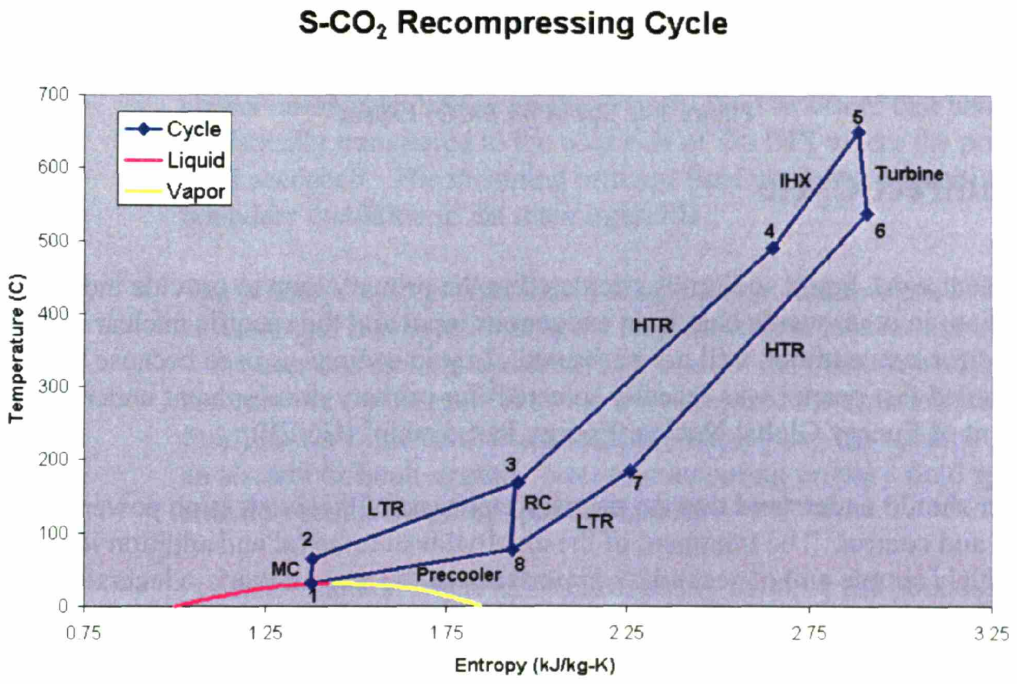

Figure 2-3: S-CO_2 Cycle Temperature vs. Entropy Diagram

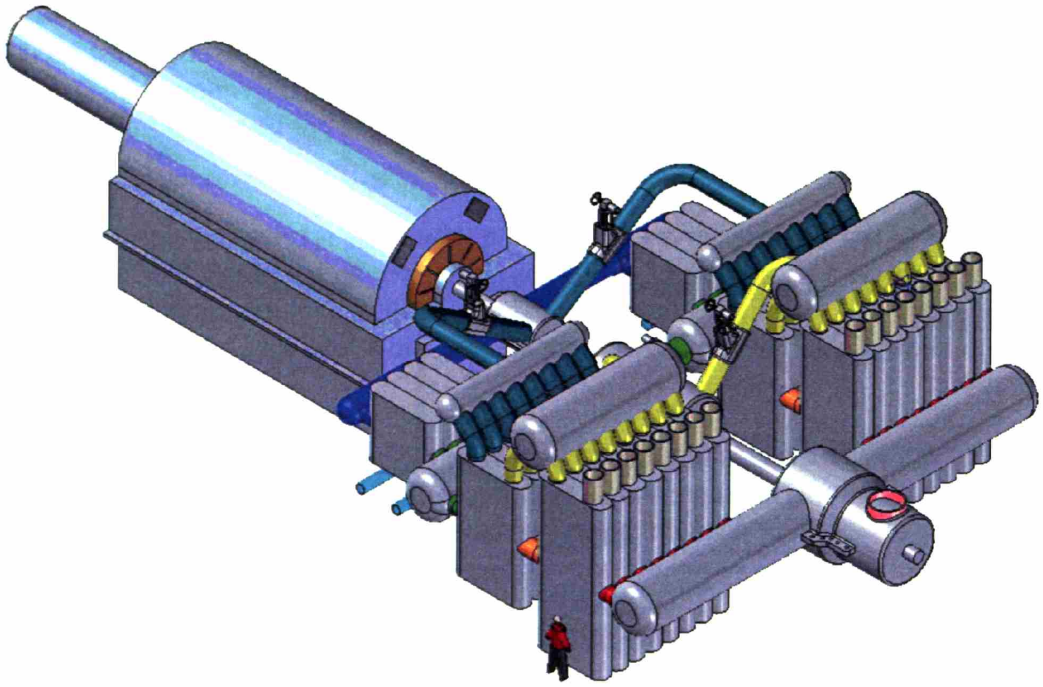

Figure 2-4: 300 MWe S-CO_2 Layout[6]

2.1.1 Indirect Cycle

In the present work liquid sodium is circulated in the primary loop to provide indirect heat addition; in other words heat is an exogenous input and the specific nuclear reactor envisioned for heat addition will not be treated. Liquid sodium* is used because the sodium cooled fast reactor was recently selected[7] for primary development under the U.S. Department of Energy Global Nuclear Energy Partnership[8] (GNEP).

The reader should understand that the primary emphasis of this work is on power cycle dynamics and control. The treatment of the external heat removal and addition loops is comparatively simple and of secondary importance to the present work. Generally, the boundaries of the power cycle have been treated in the simplest manner possible which still preserves the accuracy of power cycle behavior. The treatment of the primary loop is somewhat detailed and thus deserves further analysis.

The primary loop is treated in a simple manner that, while assuring accurate power cycle calculations, does not significantly complicate simulation. Future developers can easily improve the treatment of the primary loop by properly closing the primary loop

* Current liquid sodium reactor designs typically feature a maximum temperature of 550°C, yet this work uses a liquid sodium temperature maximum of, roughly, 670°C. It is not the intention of the present work to investigate the primary coolant system but to investigate the power cycle. Therefore, a maximum CO_2 temperature of 650°C was set to match the power cycle needs, and the sodium coolant temperature was arbitrarily raised to make that possible.

conservation equations and adding a realistic reactor model (see Section 6.4.2 for recommendations) but there are several reasons for the current simple treatment:

1. The rapid CO_2 fluid property changes near the critical point are not directly affected by reactor behavior. Moreover in the intermediate heat exchanger (IHX) the CO_2 is a near ideal gas.
2. A direct cycle would couple the power conversion cycle's behavior closely with the specific behavior of a particular reactor (i.e. temperature coefficient feedback) thus limiting the applicability of the present analysis. A direct cycle S-CO_2 gas cooled fast reactor (GFR) is under evaluation at MIT[9].

Thus, considering the early state of research into the dynamics and control of this cycle, investigating the indirect cycle driven by a general primary loop will be of significant value at this time.

The heat addition primary loop is modeled in a simple but reasonable manner in the simulation code used for this work (see Section 3.6.2 for more detail). The primary loop consists of three components:

- The hot (sodium) side of the IHX. This component performs accurate energy conservation, quasi-static momentum conservation, and mass conservation calculations on the primary fluid to assure that heat is realistically transferred to the cold side of the IHX where the power cycle fluid accepts it. The incoming primary fluid pressure is specified as a boundary condition in the main input file.

- The primary "system" includes a simple pump. Pump work is an input file variable that is proportional to the loop mass flow rate for this component -- the user can directly and arbitrarily control the mass flow rate. These laws are not met because they are not necessary for accurate (secondary fluid) power cycle calculations and can complicate the solution process of an already difficult system. Note that incoming primary fluid specific enthalpy equals outgoing specific enthalpy.

- A reactor module where heat (specified by an input file boundary condition) is added to the incoming primary fluid enthalpy. In this module the incoming primary coolant mass flow rate always equals the outgoing flow rate and there is no pressure drop i.e. the pressure equals the outlet of the IHX.

This simple model provides excellent convergence (avoiding pressure drop and mass storage issues), allows hot primary coolant temperatures to adjust to the colder power cycle fluid, and allows the user control over the mass flow rate with a simple pump work variable. This method of treating the primary system should work for any liquid fluid where the fluid's properties do not vary significantly over the small pressure differences in the primary loop (e.g. liquid sodium, lead, or water) but is not suited for boiling water or gas applications.

Note that a direct cycle GFR has been examined by Pope[9], and indirect coupling of this cycle with a lead cooled reactor has been examined by Moisseytsev[10]. This cycle may also be applicable to plants with similar temperature ranges. Recent advances in coal plants[11] may make this cycle attractive, and initial work has been carried out on coupling this cycle to a fusion power plant[12].

2.1.2 Non-linear S-CO_2 Fluid Property Behavior

Carbon dioxide shows rapidly varying property behavior near its critical point (30.978°C, 7.3773 MPa). This is one of the key enabling features for the S-CO_2 recompression cycle, but it presents challenges for modeling, and exhibits unique behavior during transients.

The cycle design points (component outlet states numbered 1 through 8 in Figure 2-2) are plotted on a density versus temperature diagram in Figure 2-5. The reader should note both the wide variation in densities within the cycle (for a single phase fluid) and especially note the very steep increase in fluid density at lower pressures as the fluid nears its critical temperature. It should be apparent from the plot that a small change in fluid temperature or pressure at this point of the cycle results in a large change in fluid density.

This impression is further reinforced when one looks at other fluid properties such as isobaric specific heat. The cycle design points from Figure 2-2 are plotted on an isobaric specific heat versus temperature diagram in Figure 2-6. Compared to the density figure this property shows an even steeper rise as the fluid approaches its critical point. The rapidly changing nature of these fluid properties makes working with an equation of state non-trivial – this will be examined in detail in Section 3.3.

Unfortunately, (from a property calculation standpoint), CO_2 shows non-linear behavior in several parts of this cycle. While this behavior is expected close to the critical point, it can also be manifested at pressures well above the critical pressure and temperatures above the critical temperature. An example of this behavior shows up clearly when one plots the main compressor operating region on an enthalpy and entropy diagram, as shown in Figure 2-7.

Figure 2-7 shows a narrow region where the main compressor operates in enthalpy and entropy space. The main compressor operates over a wider range of enthalpies than entropies (the slope is steep), thus the compressor is relatively isentropic (and efficient). However, small changes in enthalpy or entropy create comparatively large and non-linear changes in temperature and pressure. Therefore, fluid property conversions must be very accurate to avoid introducing significant error, because they are inherently non-linear.

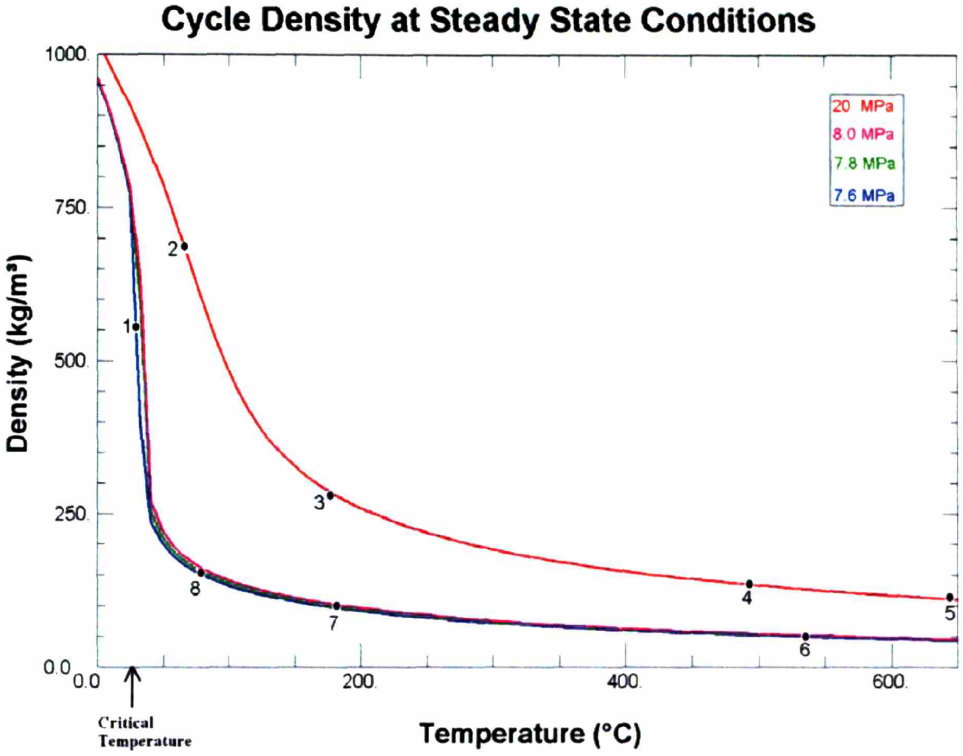

Figure 2-5: S-CO_2 Cycle Density

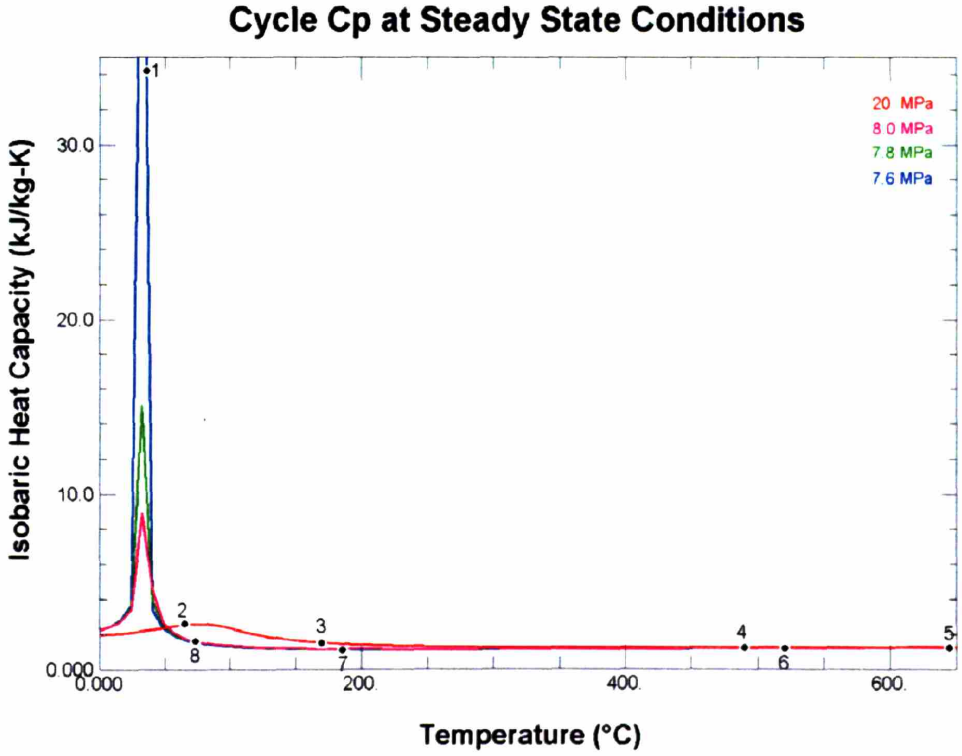

Figure 2-6: S-CO_2 Cycle Isobaric Specific Heat

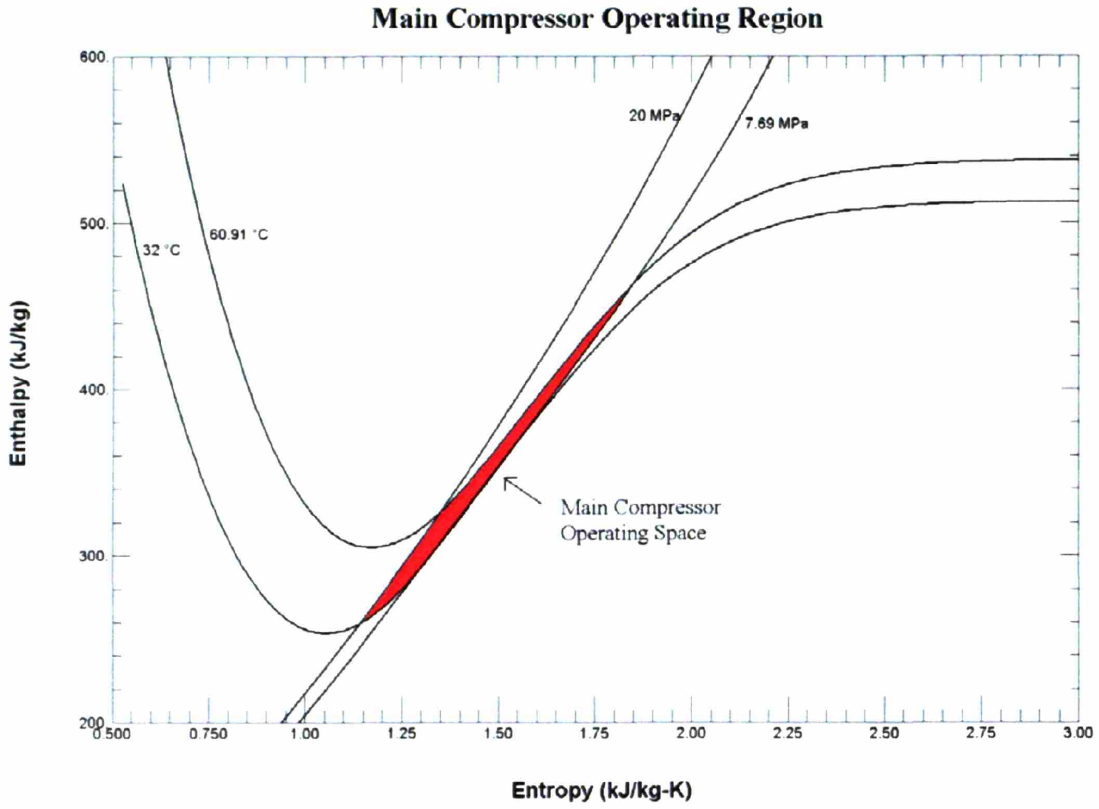

Figure 2-7: Main Compressor Enthalpy vs. Entropy Region

To summarize, CO_2 fluid properties show highly non-linear behavior in the S-CO_2 recompression cycle. This behavior is concentrated near the fluid's critical point but can also present itself in other regions such as the outlet of the main compressor. The sharpness of this behavior requires highly accurate property conversions thus making large demands upon the equation of state.

2.1.3 Turbomachinery

The turbomachinery in this cycle is quite different from that encountered in typical Brayton Cycles. Compared to Ideal Gas Brayton Cycles these turbomachines have a large mass flow rate, a significant bending stress, a small Mach number, and are very compact[13]. Due to the higher "density of CO_2, the specific enthalpy change is much smaller given a pressure ratio. That translates into reduced compression work and the potential for higher efficiency."[13]

The turbine operates far from the critical region and thus works in a quasi-ideal gas environment (near constant specific heat ratio and gas constant) and hence its design is somewhat similar to that of other power cycles. The turbine receives fluid at about 110 kg/m^3 and exhausts fluid near 50 kg/m^3.

The main compressor receives externally cooled precooler effluent fluid to take advantage of higher fluid densities near the critical point. At steady state this compressor receives fluid at a density of about 600 kg/m^3 and ejects fluid about 720 kg/m^3, which is approximately the liquid water densities found in pressurized water reactors. In many respects, this compressor operates like a pump (see Section 3.4.4.2 for comparison), but can move to much lower fluid densities during off-design operation (examined in detail in Section 5.1.1). There is considerable uncertainty over this compressor's performance when fluid properties change rapidly along its length.

The recompression compressor receives fluid at a density of about 160 kg/m^3 and ejects fluid at about 310 kg/m^3. This machine requires significantly more specific work due to the greater difficulty of compressing a more dilute compressible fluid.

The modeling of these performance maps and off-design behavior of these turbomachines will be analyzed in detail in Section 3.4.

2.1.4 Printed Circuit Heat Exchangers

The S-CO_2 recompression cycle's advantageous performance is greatly enhanced by using high efficiency, yet compact, heat exchangers to significantly recuperate the cycle as seen in Figure 2-3. This cycle's design[3] takes advantage of new heat exchanger technology in the form of printed circuit heat exchangers (PCHEs) developed by Heatric™. PCHEs have been described elsewhere[3] but the basic idea of a channel layout is shown in Figure 2-8 (note that in an actual PCHE there are tens of thousands of channels).

A PCHE is created by chemically etching out small (1-2 mm diameter) semi-circular channels on a thin metal plate. Alternating hot and cold fluid plates are arranged in a counter flow fashion and then diffusion bonded together to create a solid block of metal with many channels. Besides having a large heat transfer area per unit volume, PCHEs are robust, allowing large pressure and temperature differences that could require significant design changes in other types of heat exchangers[3].

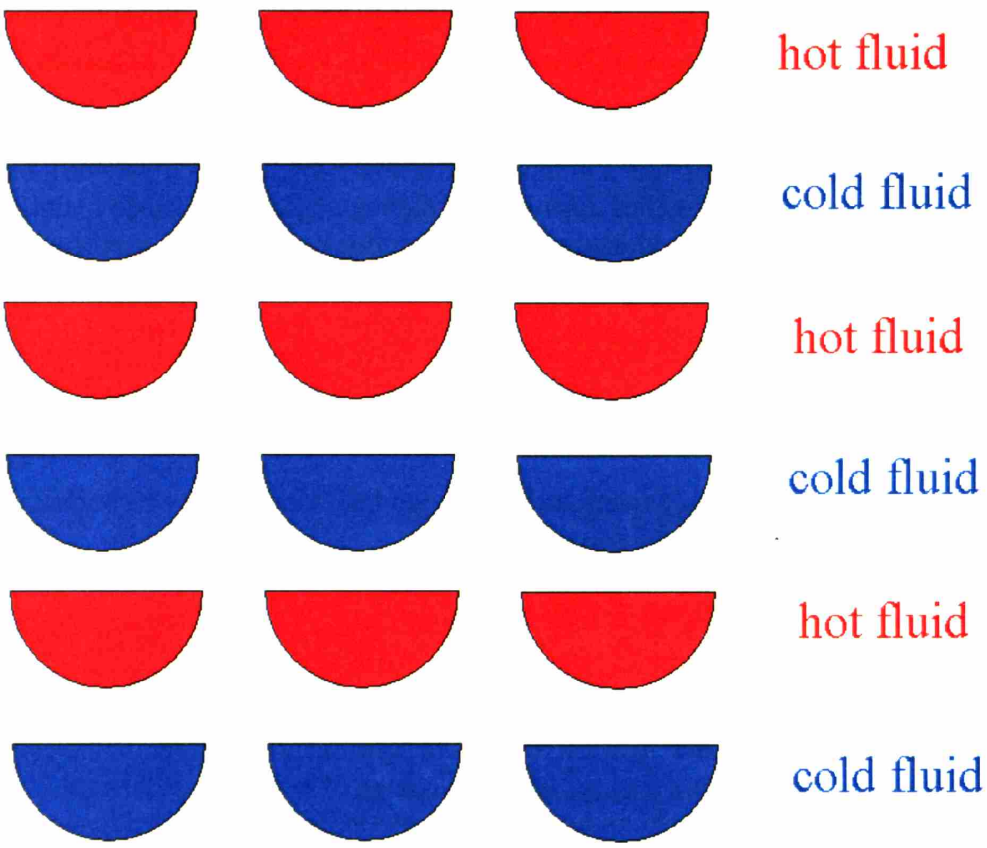

Figure 2-8: Face of a Printed Circuit Heat Exchanger

The cycle layout shown in Figure 2-4 shows four heat exchangers which must be modeled. Unfortunately, while the large CO_2 property variations previously outlined in Section 2.1.2 allow high efficiency, they also complicate standard analysis assumptions. This is especially true in the heat exchangers where standard procedures like log-mean temperature heat transfer are not valid. Section 3.5 will examine problems encountered, and methods used, to model PCHEs.

2.2 Cycle Simulation & Control Background & History

This section will focus upon literature most relevant to simulating and controlling the S-CO_2 recompression cycle. It is intended to provide the reader with an overview of the literature that enabled the completion of this work. The section is subdivided into several parts; the cycle steady state design, dynamic simulation and control of the S-CO_2 recompression cycle, dynamic simulation and control of cycles with analogous features, and several component-specific sections.

Note that sections within this work examining detailed features will provide literature references within that section. These sections include the examination of the original

GAS-PASS code used only for Ideal Gases, Section 3.1) and the fluid property correlations used in the heat exchangers, Section 3.5.1.1.

2.2.1 Steady State Design

The steady state design of the S-CO_2 recompression cycle was analyzed in depth by Dostal. He looks at the history of carbon dioxide cycles, investigates various cycle layouts with an emphasis on efficiency and cost, and selects a reference design (the supercritical recompression cycle) and investigates their behavior in his topical report[3] and thesis[14]. His work included developing a steady state modeling code for this cycle, which will introduce the reader to many of the issues found in dynamic modeling. Several of the steady state techniques will be expanded upon in this work. Two papers provide a brief introduction to, and summary of, this work; one by Dostal[15] and one by Hejzlar[16].

2.2.2 Dynamic Simulation and Control of the S-CO_2 Recompression Cycle

At the beginning of this work, no published work (to the author's knowledge), which focused upon simulating or controlling this cycle, was available. During the completion of the work several interesting publications have been released.

The direct S-CO_2 recompression cycle coupled to a gas fast reactor (GFR) was examined by Pope[9]. His thesis focused upon developing a 2400 MWth steady state core design and coupling that cycle to 4 S-CO_2 recompression cycle loops. Using a RELAP5 model he examines how the plant responds to several transients including natural circulation, loss-of-load (LOL), and a loss of coolant accident (LOCA). While much of the thesis discusses issues related to reactor design and protection (and thus not directly relevant to this work), the thesis also introduces the reader to many of the issues present in this cycle. Note that the precooler PCHE model used in GAS-PASS/CO_2 was benchmarked to Pope's RELAP5 precooler model with good agreement.

Moisseytsev has investigated the indirect coupling of this cycle to a lead fast reactor designed for autonomous load following. His paper on control modeling[17] briefly introduces and presents results for using several control mechanisms quite relevant to this work including turbine inlet throttle, turbine bypass, and inventory control. His paper on transient anylysis[10] presents greater detail on his simulation code and the results of this cycle with several transients including loss of heat sink (LOHS), LOL, and LOCA. His code shares several similarities with the simulation code developed for this work including solving one-dimensional transient equations with a simplified momentum equation. Comparisons to Moisseytsev's results will be made in Section

2.2.3 Cycle Analogues

Frutschi[18] provides a comprehensive overview of closed Brayton cycles, focusing mainly on numerous air working fluid systems operating in Europe in the 1960's, including other past studies (including a condensing cycle, two shaft S-CO_2 cycle) and a review of ideal gas control. His work serves as an excellent general reference.

The helium Brayton cycle has been researched by numerous authors; only two of the most relevant will be presented here. Yan completed a thesis[19] similar to this work looking at the dynamic analysis and control system of the Modular High-Temperature Gas-Cooled Reactor Gas Turbine power plant (MGR-GT). It provides a close look at the necessary control systems for this helium reactor and the transient simulation program created to analyze the cycle. He concluded that inventory control provided the highest part-load efficiency but examines numerous faster control options.

C. Wang[20] looked at the dynamic analysis and control of the modular pebble bed reactor (PBMR). His thesis developed a reference design using only existing technology, for which he then performed transient simulation and control development. He concludes that bypass and inventory control are the primary control methods for this cycle, with the former used for fast action and the more efficient inventory control used for slower action.

The supercritical water reactor (SCWR) shares several features with the S-CO_2 recompression cycle. A brief overview of this cycle was presented by Buongiorno[5], a stability analysis has been completed by Zhao[21], and basic control features of this cycle have been analyzed by Burns and Roe[22]. The control of this system is accomplished primarily by control rods for reactor power, a turbine control valve for pressure, and feedwater flow is controlled by the coolant pumps which control reactor outlet temperature.

2.2.4 Fluid Property Equation of State

Providing an accurate and computationally fast carbon dioxide equation of state is rather difficult. Aungier provided[23] a modified Redlich-Kwong equation of state which employs an accentric and compressibility factor to correct for real fluid properties including CO_2. This equation is very fast and quite accurate when appropriate factors are used but it is designed for use in turbomachinery design and does not cover the range of the temperatures and pressures experience in the S-CO_2 recompression cycle. Aungier later offers[24] a pseudo-perfect gas model with methods to implement it in computer codes. This model is also optimized for turbomachinery design and requires updating factors between each stage.

A slow but accurate equation of state for carbon dioxide (and many other fluids) can be found in the NIST RefProp[25] computer code. This code was used to generate fluid property tables for the simulation code used in this work, as discussed in Section 3.3.

The equation of state selected within RefProp is based upon the Span and Wagner Helmholtz equation of state[26].

2.2.5 Fluid Choice

Dostal briefly surveyed the available power cycle fluids in his introduction[3]. Looking at basic principles he surveys a variety of the different gases that could be used and provides efficiency comparisons against helium and advanced water cycles. He selected carbon dioxide for a variety of reasons, including high efficiency at the desired temperature range.

Oh[27] also evaluated several indirect working cycles when coupled to a very high temperature gas cooled reactor using the HYSIS computer code and a Visual Basic model. Using the same primary system, helium, CO_2, and a nitrogen-helium mixture were parametrically compared. Oh concludes that CO_2 provides the most efficient indirect cycle, with smaller heat exchangers. Note that Oh earlier investigated[28] means to improve Brayton cycle efficiency focusing upon various cycle layouts such as multiple shafts and helium, and provided a brief comparison to CO_2.

El-Genk[29] has compared various noble gas mixtures for use in a Brayton cycle, focusing upon maximizing heat transfer and minimizing pumping power requirements.

2.2.6 Similar Transient Modeling Codes

This section will briefly document codes similar to that used in this work. A general (albeit brief) review of dynamic simulation codes is provided by Tauveron[30].

Vilim[4] created the GAS-PASS transient ideal gas simulation code which was adapted and expanded for this work. This code will be analyzed in greater detail in Section 3.1.

C. Wang[31] created the MPBRSim transient simulation code for the MPBR. His code is a one dimensional lumped parameter model using an implicit integration operator and a fourth order Runge-Kutta technique to solve the differential equations. Note that he converged only on the most sensitive variable, pressure.

Yan[19] created the GTSim transient simulation code for the helium based MGR-GT. His code implicitly and simultaneously solved a one dimensional lumped system of non-linear stiff equations. While quite similar to the process performed in this work, it was created for an ideal gas cycle and thus would require significant modification for use with carbon dioxide.

A similar code, Flownex, has been applied to the PBMR by Kemp[32]. This code simulated the system with an implicit one-dimensional CFD approach to the PCS and a 2D model of the reactor. The model used SIMULINK for control system design. The code has undergone significant validation studies for use with the PBMR.

Also note that while RELAP5-3D is quite different in complexity and computational method from the codes overviewed in this section, it has been used by Pope[9], as previously described, to simulate the S-CO_2 recompression cycle.

2.2.7 Turbomachinery Performance

Turbomachinery performance in the S-CO_2 recompression cycle is an area of active research. The unique real property behavior of carbon dioxide, especially near the critical point, creates difficulties when designing and simulating turbomachinery performance.

Initial axial turbomachinery design was completed by Wang[13]. The turbomachinery was designed for the previously outlined cycle conditions (see Figure 2-2) except that the turbine used a lower inlet temperature of 550°C, which matched an earlier cycle design. Wang used the Concepts/NREC AXIAL™ and/or a set of NASA codes to simulate the turbomachinery at design and off-design conditions.

The axial analysis of the main compressor was improved and expanded upon by Gong[33]. Due to the rapidly changing fluid properties near the critical point existing design codes have convergence difficulties. Gong's analysis improved upon previous work by using enthalpy and entropy, which move relatively smoothly through the critical region, as state parameters instead of temperature and pressure, which do not, to create an operating map.

Gong also analyzed[34] (per recommendation of Barber-Nichols Inc.[35]) the possibility of using radial (instead of axial) compressors for this cycle. Different options and performance attributes were reviewed and design recommendations were made for a one stage main compressor and a three stage recompression compressor. Initial design and off-design performance maps are offered as well as basic relations for scaling off-design performance – these will be used in this work.

A procedure to scale performance maps for compressors is offered by Kurzke[36]. Based upon a statistical survey of literature and data the authors define three parameters they relate to pressure ratio. Using these relations the authors create a method to scale similar, known compressor maps to specific needs during the preliminary design phase.

A significantly different design for S-CO_2 axial turbomachinery was presented by Muto[37]. While this design was optimized for a different supercritical carbon dioxide cycle, the design was similar enough that differences in turbomachinery were surprising. The primary difference in design was the large number of stages use by Muto, including 2 in the low and 10 in the high pressure compressor (combined as a single compressor, called main, in this work) and 21 in the recompression compressor. Muto calculated that high bending stresses require a large number of stages – this is not confirmed by Gong or Wang's work.

The design and operation of a large, constant speed, centrifugal, carbon dioxide compressor is discussed by Olson[38]. This compressor takes CO_2 from atmospheric

pressure and a variety of atmospheric temperatures to 18.7 MPa and 43-49°C for use in pipelines. The paper presents the control mechanisms used within the compressor to avoid "dramatic" compressibility variations including; strict temperature outlets for inter-stage cooling and pressure control on every other stage. The primary flow control device used was variable inlet guide vanes (VIGVs).

The design and operation of a large, centrifugal, carbon dioxide compressor designed for power plant CO_2 sequestration has been discussed by Wada[39] and Sato[40]. The compressor takes carbon dioxide from atmospheric pressure and discharges the fluid at 20.3 MPa and 173°C (quite similar to the outlet properties of the present study's recompression compressor outlet – see Figure 2-2). The authors discuss the challenges associated with this large molecular weight gas such as smaller operating range, vibration instability due to high fluid specific gravity, and impeller resonance.

The design of a wide flow range radial compressor is examined by Uchida[41]. The authors investigate the ability of casing treatment and VIGVs to extend the operating range between stall and choke in a radial compressor with a pressure ratio of 2.5. The authors conclude that a 59% increase can be had with a "synergistic" effect between casing treatments and VIGVs.

Efficiently operating centrifugal compressors in parallel have been studied by Staroselsky[42]. The authors examine the parallel operation of ideal gas compressors from an efficiency, control, and stability perspective. They conclude that for parallel ideal gas compressors and simultaneous load changes, reducing recycling and simultaneously reaching surge provide an excellent control method.

2.2.8 Heat Exchangers

Dostal investigated two types of heat exchangers for S-CO_2 recompression cycle, with the primary design goal of compactness. Due to the poor ability of a gas to exchange heat with another gas these heat exchangers can become prohibitively large – especially in a highly recuperated cycle. As the size of heat exchanger increases, the associated pressure drop typically increases, which can create a significant efficiency penalty in a Brayton Cycle. The types of heat exchanger examined were plate-fin and PCHEs. Due to the large pressure differentials experienced in this cycle the plate-fin heat exchangers were rejected due to their large size when such a large pressure differential was accommodated.

PCHEs are described and modeled by Dostal[3] for this cycle. While there was considerable uncertainty over the heat transfer correlation to use, conservative assumptions were made and conduction lengths were modeled with the Fluent code. Preliminary designs for the recuperators and precooler were created and were expanded upon for this work.

The intermediate heat exchanger was analyzed in detail in Gezelius[43]. His report examines PCHEs, looks at the options for modeling the friction factor, benchmarks the

conduction model with a two-dimensional conduction code Fluent, and compares various intermediate heat exchanger designs including shell & tube and plate-fin. The overall conclusion is that PCHEs are the appropriate choice for intermediate heat exchange, offering the same or superior performance in a small volume.

There have been several PCHE developments worth note. Instead of straight channel PCHEs Heatric™ has introduced zigzag channels which trip the boundary layer of the fluid to increase turbulence and heat transfer at the expense of a pressure drop increase. Ishizuka[44] has published a paper comparing the heat transfer and pressure drop effects of the zigzag to straight channel designs. Finally, Muto[45] presented ongoing work at the Tokyo Institute of Technology using an interrupted sine-wave shaped PCHE channel to enhance heat transfer with a lower pressure drop.

2.3 Chapter Summary

This chapter provided a brief overview of the S-CO_2 recompression cycle. The first part of the chapter provided a synopsis of the key cycle features including the reasons for a choice of single shaft, recompression, and a review of fluid property effects, especially near the critical point, and the rational for investigating an indirect cycle. The rest of the chapter looked at the literature relevant to simulation and controlling this cycle with an overview of the steady state, the small amount of literature available on the actual dynamics of the cycle, and some analogues found in ideal gas and water cycles.

3 Simulation Code & Methods

In this chapter the simulation code, Gas Plant Analyzer and System Simulator (GAS-PASS), is examined in detail. The chapter will provide the reader with the ideas and methods used to simulate the highly non-linear S-CO_2 recompression power cycle. Unfortunately, many of the techniques and methods applicable to other cycles (see Section 2.2.3) do not apply. The chapter is subdivided into seven sections:

1. The first section will provide a brief overview of the original, ideal gas, simulation code called GAS-PASS/He in this work (GAS-PASS/H in prior ANL work). It will introduce the reader to the basic solution method and how it was applied to several ideal gas plants.
2. The second section provides an overview of the system model. The GAS-PASS/CO_2 solution process will be briefly analyzed, the assumptions going into modeling of the components, and a general set of equations will be specified. These equations will be applied for the turbine to provide an example. Note that the full set of GAS-PASS/CO_2 solution equations is lengthy and primarily of interest to future developers. The full set of equations is therefore relegated to, "Appendix A: GAS-PASS/CO_2 Equations."
3. The third section will look at the problems and solutions to modeling S-CO_2 fluid properties which change very rapidly near the critical point. The reader will learn about the accurate but computationally intensive source of the properties data and how this data was put into a format which allowed rapid and accurate use.
4. The fourth section will discuss a method to model turbomachinery performance based upon the data available today. This work will not attempt to calculate the complex behavior of a turbomachine directly ab initio.
5. The fifth section will analyze in detail the heat exchangers modeled in this work. These heat exchangers are responsible for the vast majority of the computational work in solving this cycle, and due to the sometimes rapidly changing S-CO_2 properties can be difficult to model accurately.
6. The sixth section of this chapter will review the significantly updated and enhanced general fluid property code called GAS-PASS/CO_2 (note that this new code can, in principle, simulate dozens of different fluids, not just CO_2). The section will focus upon the way the solution equations are expressed and the newly developed solution methods used to overcome difficulties encountered in this cycle.
7. The final section will provide a brief summary of this chapter.

By the end of this chapter the reader should attain an appreciation for the methods used to solve this real fluid cycle.

3.1 Ideal Gas Simulation Code: GAS-PASS/He

Dr. Richard Vilim at Argonne National Laboratory developed the ideal gas GAS-PASS/H[4] code. This code will be called GAS-PASS/He in this study*. The GAS-PASS/He code was adopted, modified, and expanded for this work (see Section 3.6). Readers interested in learning more about this code can read a brief paper[46] or a more in depth summary[4]. Several papers published[47,48] using this code are available as well. This sub-section will review the original simulation code.

GAS-PASS/He is a transient simulation control design and cycle scoping code designed for gas cycles directly coupled to a nuclear reactor. The code is intended for rapid assessment and appropriate placement of major system components based upon their dynamic response in an integrated plant. To accomplish this mission GAS-PASS/He was constructed in a rapidly executable, modular, and flexible manner.

GAS-PASS/He used a one-dimensional lumped parameter with perfect mixing solution process that appropriately conserved mass and energy but used quasi-static momentum conservation. Note that the simplification of the momentum equation avoids creating a stiff system in the numerical sense. Numerous plant phenomena occur over the seconds to minutes time frame (e.g. structure thermal conduction) but transient momentum effects (such as density wave oscillations) typically occur much more quickly. Using only quasi-static momentum effects avoids combining phenomena which exist on very different timescales – a stiff system.

Using the above simplifications most plant component equations are directly derived from conservation equations, except for the reactor core neutronics and decay heat models which use the liquid-metal version of MINISAS, the heat exchangers which use log-mean temperature, and the turbomachinery which is explored in Section 3.4.1. Frictional pressure losses are typically specified via a user input friction coefficient. These equations are generally computationally trivial, which allowed GAS-PASS/He to run much faster than real-time.

GAS-PASS/He is modular and flexible, allowing any number or order of (predefined) system components because a defined component can be generally introduced throughout the plant. The set of defined components form a system of non-linear equations which, along with the appropriate boundary conditions, is fed to a non-linear system of equations numerical solver. The solver uses a general Newtonian root solving technique that allows the user to change the order, number, and content of the conservation equations and variables at will.

---

* In this work the simulation code naming convention is as follows. GAS-PASS/He refers to the original ideal gas, direct cycle code written by Dr. Vilim. GAS-PASS/CO_2 refers to the updated and expanded code used with the indirect S-CO_2 recompression cycle examined and used in this work. GAS-PASS refers to general features common to both GAS-PASS/He and GAS-PASS/CO_2.

A second part of GAS-PASS/He flexibility is the ability to interchange boundary conditions and variables. While the number of equations must match the number of unknowns, the user can readily exchange most variables for most boundary conditions. For example, if the external cooling loop is set up to provide a constant heat transfer one can solve the system by fixing either the cooling loop mass flow rate or the cooling fluid incoming temperature; then the numerical solver determines the variable's value. Later the user can switch fixed heat rate and temperature. This allows the GAS-PASS/He user to rapidly solve the system for almost any behavior desired and proves quite valuable for scoping calculations.

GAS-PASS/He required significant updating before it could be applied to the S-CO_2 recompression cycle. This chapter is largely devoted to describing the required updates that went into creating GAS-PASS/CO_2. To simulate this cycle GAS-PASS/He required:

1. The ability to very accurately and very rapidly simulate a wide variety of real fluid properties. GAS-PASS/He used a very simple equation of state, which is not possible for carbon dioxide in this application. The process of updating GAS-PASS/CO_2 to meet these requirements is described in Section 3.3.
2. The ability to accurately model complex turbomachinery performance. Ideal gas turbomachinery perform in a relatively simple and smooth manner that may allow a single simple polynomial to describe their behavior. This was the approach taken by GAS-PASS/He, but the behavior of S-CO_2 recompression cycle turbomachinery, while still uncertain in many respects, is significantly more complex. The process of updating turbomachinery models is described in Section 3.4.
3. The ability to accurately and rapidly model printed circuit heat exchangers was lacking. Due to the rapidly varying fluid properties encountered with S-CO_2, traditional simplifications such as log-mean temperature, the approach used in GAS-PASS/He, are not appropriate. Therefore the developer must nodalize and iteratively solve this component, which rapidly becomes computationally prohibitive. The methods to rapidly and accurately model these components for GAS-PASS/CO_2 are described in Section 3.5.
4. Numerous modifications to allow the solution process to converge the numerical system. Due to the inherently more non-linear nature of the S-CO_2 recompression cycle, using a Newtonian numerical solver presents numerous problems not seen in ideal gas applications. GAS-PASS/He required several basic modifications to make this cycle more readily solvable, and numerous computational methods to make the solution process more robust before the S-CO_2 recompression cycle could be simulated. These are described in Section 3.6.

Overall, GAS-PASS/He performed its function well and contains several features that made its adoption for the S-CO_2 recompression cycle attractive. The process of updating and expanding the code was non-trivial and will be detailed throughout the rest of this chapter.

3.2 Modeling Approach

The GAS-PASS/CO_2 model, as it applies to the S-CO_2 recompression cycle, will be overviewed in this sub-section. The code solution process, fundamental assumptions, and basic equations will be briefly overviewed. The sub-section will conclude with an application of the conservation equations to the turbine.

3.2.1 GAS-PASS Solution Process

GAS-PASS uses a general Newtonian root-finding algorithm (a modified Powell-Hybrid method[49]), designed for non-linear systems of equations, to compute all variable values implicitly. The user specifies which inputs are variables, boundary conditions, and constants within the input deck. Once basic checks are preformed, the solution process begins with a call to the numerical solver. Note that a discussion of the various non-linear solution techniques is included in Section 3.6.3, but the general technique is unchanged from GAS-PASS/He.

The numerical solver then calls a custom made function, *Fcn(x)*, which contains all of the equations necessary to solve the system at a time step. *Fcn* is organized by code modules which correspond to components within the system. Each component will contain one or more equations in the form:

$$F(i) = Fcn_i(x)$$

This must equal 0 to satisfy the system. Typically these equations are conservation laws or the output variables of other subprograms which apply conservation laws. In any case, these equations take the variable, x, inputs supplied by the numerical solver, and evaluate the given equation. The solver then compares the error of the solution to the change in the x inputs and modifies the variables accordingly, until tolerance is reached.

The numerical solution process is fully implicit, with iterative refinement of the user-specified variables at each time step until the system of equations is within tolerance of the system root, as outlined below:

1. At time $t_i > t_{i-1}$
2. Take X_i inputs from X_{i-1} (temperature, work …), an initial guess
3. Calculate Jacobian (see Figure 3-1)
4. Use Jacobian to guess new X_i
5. Evaluate $F(X_i)$
6. Repeat (3), (4), and (5) as necessary to find system solution

$$J = \begin{bmatrix} \frac{\partial F_1}{\partial x_1} & \frac{\partial F_1}{\partial x_2} & \cdots & \frac{\partial F_1}{\partial x_n} \\ \frac{\partial F_2}{\partial x_1} & \frac{\partial F_2}{\partial x_2} & \cdots & \frac{\partial F_2}{\partial x_n} \\ \vdots & \vdots & \vdots & \vdots \\ \frac{\partial F_m}{\partial x_1} & \frac{\partial F_m}{\partial x_2} & \cdots & \frac{\partial F_m}{\partial x_n} \end{bmatrix}$$

Figure 3-1: Jacobian

A flowchart of the overall code solution process is shown in Figure 3-2. This flow chart shows that the code preprocesses numerous data sets, converges the steady state system, and then converges the transient system. Data is output at the conclusion of the steady state solution and the conclusion of each transient iteration.

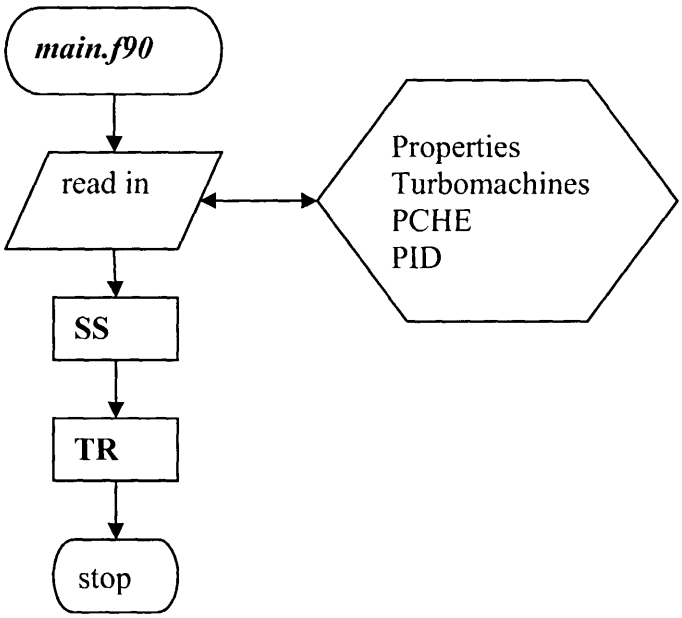

Figure 3-2: GAS-PASS/CO_2 Overall Flow Chart

A more detailed look at the steady state solution process is shown in Figure 3-3 (the source code is discussed in Section 3.6.1.2). This figure shows the solution process and the major module calls. The user should note that all of the plant components are accessed through a single module called *fcn*. Components within *fcn* may be relatively simple to the point where they are only a set of conservation equations (e.g. *primary*) or may be relatively complex as in *Qpche*. This component iteratively solves a nodalized PCHE before reporting the aggregate results back to *fcn*. The user should also note that the completion of the numerical solver code is only one of the steps taken in arriving at a converged system. Section 3.6.3 discusses the techniques used to handle the non-linear

S-CO_2 recompression cycle within a Newtonian solution process. Finally, note that a stall/choke check is performed on each turbomachine after the converged solution is reached. If stall or choke are predicted then the code exits. The reason for checking for this problem only after solution convergence is reached is outlined in Section 3.6.3.3.3.

The transient solution process is shown in Figure 3-4. This figure is quite similar to the steady state solution process with a few significant exceptions:

- The transient PCHE solution process is not shown. This process is unique, detailed, and will be shown in Figure 3-67 and discussed in the surrounding text.
- The transient solution process involves an iterative convergence of the system at each of the consecutive time steps. Therefore, the transient solution is akin to solving the steady state at each time step, except with transient conservation equations.
- Before each transient solution process begins the boundary condition variables are updated. This behavior is specified by the user in the main input file.
- After each transient solution process ends, the controlled plant values are updated by PID controllers.

3.2.2 Approximations

GAS-PASS is designed to be a dynamic analysis and control system design scoping tool. GAS-PASS/CO_2 has been adapted to model the S-CO_2 recompression cycle to allow the simulation of major control systems to determine appropriate placement and approximate cycle performance. The code is not intended to give the best possible simulation estimate of cycle performance and is wholly unsuited to several types of transients as outlined below.

The major GAS-PASS/CO_2 assumptions are briefly discussed below. Most entries will provide a reference to a more detailed discussion at a later point in this work. Many of the relevant assumptions* were also previously used in GAS-PASS/He[4].

1. Flow is simulated in only one dimension, and control volume regions are lumped. These are common modeling assumptions and are used in other Brayton cycle simulation codes such as FlowNex[32], and MPBRSim[20].
2. The heat exchangers are nodalized while all other components are lumped into a single control volume with their following piping. In general, components in the S-CO_2 recompression cycle perform an action on the fluid over a small distance (e.g. a splitting-T or a radial compressor) and in the vast majority of (the relatively large) control volume no work occurs. This is similar to the method used in MPBRSIM.
3. Control volumes experience perfect mixing (except in the heat exchangers). This assumption states that fluid values in the interior are equal to the values for the fluid at the exit of the component. This assumption generally provides better numerical stability than using average fluid values[50].

* GAS-PASS/He uses assumptions 1-9. Further assumptions do not apply because new code was added to simulate the S-CO_2 recompression cycle.

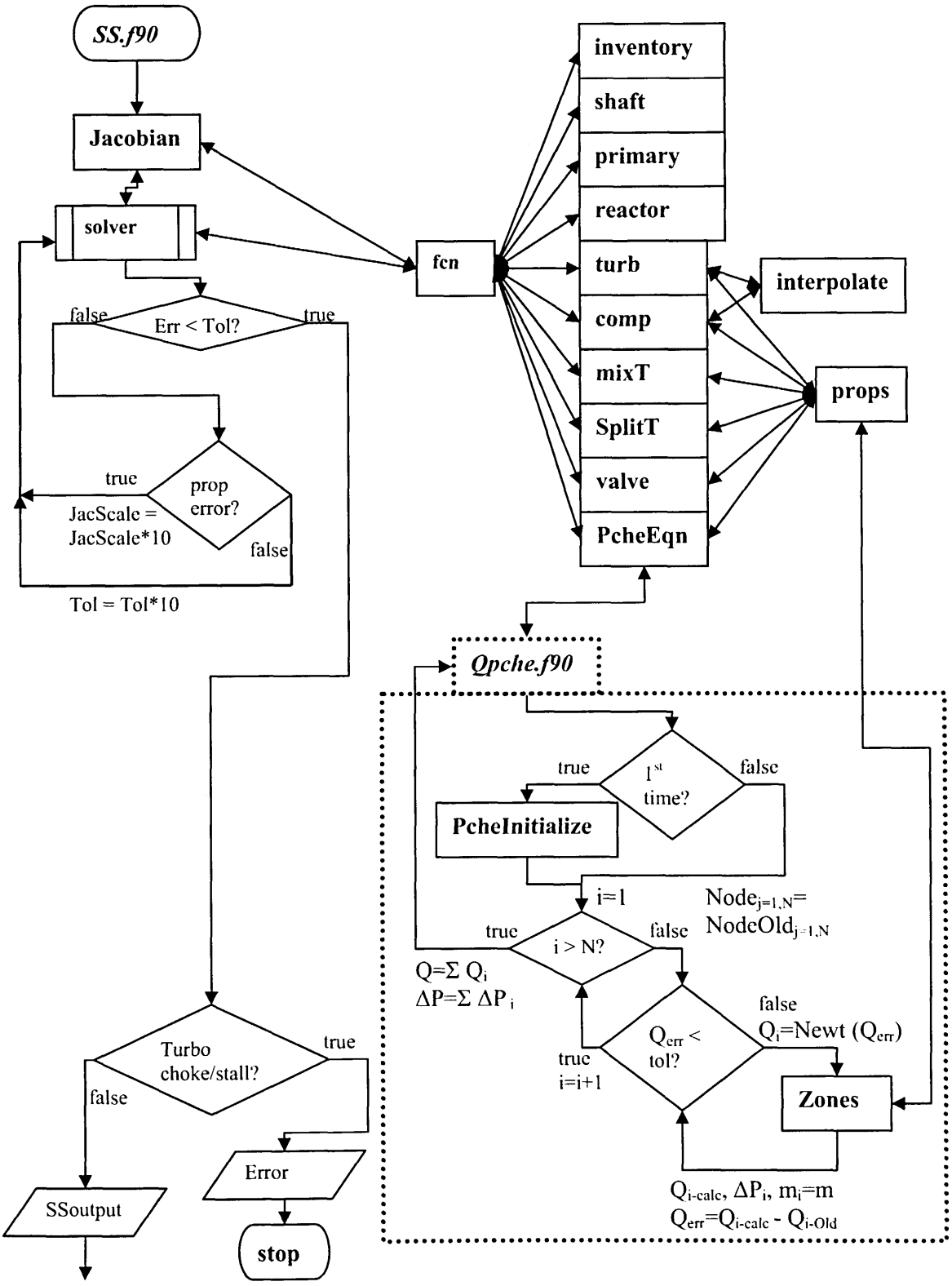

Figure 3-3: GAS-PASS/CO_2 Steady State Flowchart

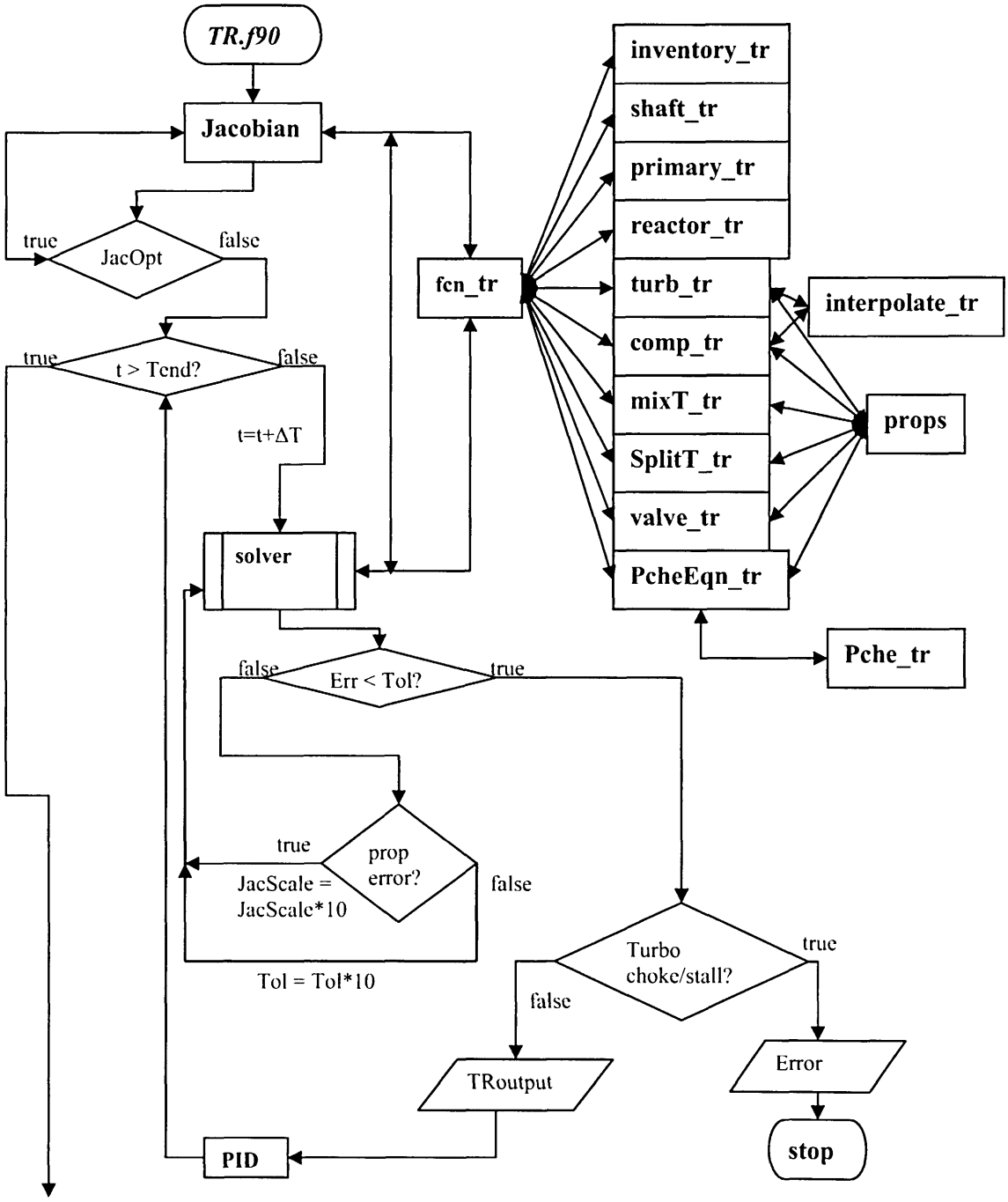

Figure 3-4: GAS-PASS/CO_2 Transient Flowchart

4. Momentum conservation can be simplified to a quasi-static equation. Thus inertial effects are not modeled. Most momentum inertial effects occur over relatively small time scales that will not be investigated by GAS-PASS/CO_2. By using a quasi-static equation for momentum GAS-PASS/CO_2 can simulate cycles with time steps that are, very likely, orders of magnitude larger than those which would be required with a full momentum equation. Note that this assumption

restricts GAS-PASS/CO_2 from simulating transients that have rapid inertial momentum changes, such as the effect of slamming a valve closed.

5. Fluid kinetic energy and gravity effects may be neglected, as they are typically quite small relative to the fluid internal and work energies.
6. The structure mass is currently assumed to be in thermal equilibrium with the fluid. A method has been outlined in, "Appendix B.3 Approximating Structure Conduction," to alleviate this constraint, but it was not implemented in GAS-PASS/CO_2 due to time constraints. This assumption will change the time constants of the system during fast transients.
7. The system is adiabatic to the environment. The heat lost to the environment from a properly insulated power cycle is relatively small compared to the heat transferred within the cycle.
8. Pressure drops are not calculated in the piping. The amount of pressure lost to friction can be important, especially in a Brayton cycle, but GAS-PASS/CO_2 assumes that piping has been sized appropriately to render these losses a secondary effect. Also constant pressure drop pipe loses can, and are, lumped with the PCHE plena via input files.
9. The area inside turbomachinery blades is too small to have appreciable storage, energy or mass, which will affect the work equation. Thus, the turbomachinery performance maps operate directly on the fluid coming into the component and fluid mass and energy storage affects are later added to the this result. Note that the volume inside the turbomachinery is tiny compared to our system and the amount of energy which changes inside this volume with temperature changes is negligible compared to the work going through it. For example, in the S-CO_2 recompression cycle the total turbine volume is less than 5 m^3, of which only a fraction is inside the blades. The piping following the turbine before the next active component is slightly less than 33 m^3.
10. Turbomachinery performance will be estimated from performance maps calculated from other codes, as outlined in Section 3.4. This method is commonly used in transient simulation codes, but note that GAS-PASS/CO_2 uses basic fluid behavior relations to simulate off-design property effects, as discussed in Section 3.4.4. These relations are somewhat crude, but important to system behavior. They are used due to a lack of available computational and or experimental performance data.
11. The heat exchanger subroutines calculate heat transfer coefficients using the Gnielinski correlation, which is probably conservative, especially in the precooler, as referenced in 3.5.1.1.
12. The heat exchangers use straight channels, unlike some recent printed circuit heat exchanger designs which use other channel geometries such as zig-zag channels.
13. The heat exchanger walls are in thermal equilibrium. Note that these walls are about 1.5 mm thick, thus they rapidly approach thermal equilibrium, as discussed for the precooler in Section 3.5.4.2.

3.2.2.1 Component Equations

GAS-PASS equations are grouped by component and follow from simple conservation laws, or are set to match more complex modeling calculations (e.g. the PCHE model).

All the equations shown refer to the plant network layout shown in Figure 3-5. This figure shows the components modeled in the S-CO_2 recompression cycle.

The GAS-PASS conservation equations are formulated based upon treating a component as a black box. GAS-PASS provides a component with guesses of its inputs and outputs, which the component module uses to do its calculations, and the results are plugged into conservation equations. The numerical solver then takes care of changing the input and output guesses so as to converge to a balanced set of conservation equations. Generally one component's outputs become the next component's inputs.

Although there are a number of ways to derive the conservation equations, it is only necessary that the derivation process be consistent. An easy way to determine the number of equations is to treat a component as a black box with a set of inputs that produce a set of outputs. If one assumes that the incoming fluid state is determined, then setting the number of equations can be boiled down to two simple ideas:

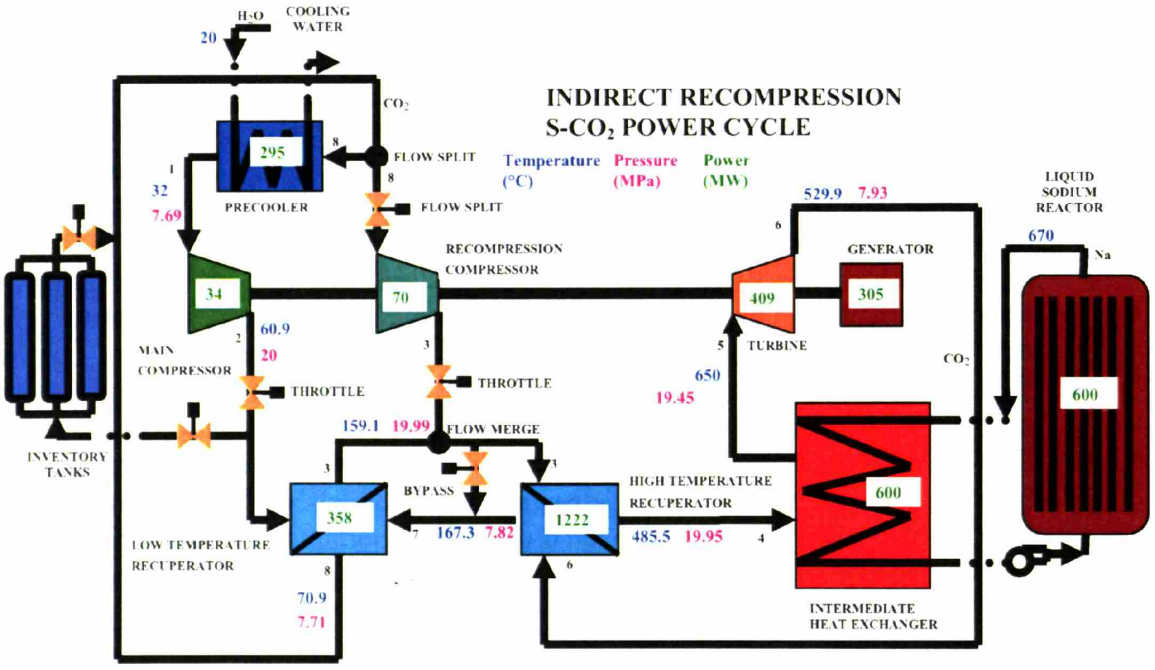

Figure 3-5: S-CO_2 Recompression Cycle Component Layout

1. A fluid flow stream has three properties which completely define it: mass flow rate, specific enthalpy, and pressure.
2. What happens within a component is irrelevant except when energy is transferred:
    - If the energy transfer is *external* to the system it is a boundary condition.

- If the energy is transferred to or from another component *within* the system then there must be a conservation of energy equation for this process.

In practice the first rule dictates that for each fluid coming out of a component there are three equations. The second rule is a little more involved, thus several examples will be given:

- A reactor has only three equations because the heat that is added is not from another component – it is a boundary condition.
- A heat exchanger has only six equations (three for each outgoing stream) because the heat transfer occurs within the component.
- A turbomachine has four equations because work is added or removed from the shaft, which affects other components in the system.
- A generator has one equation because there is no fluid flow but there is work added and removed from other system components via the shaft.

The fundamental conservation equations are quite simple, as shown in Equation 3-1 through Equation 3-3. Note that Equation 3-3 is included solely to indicate that the momentum equation contains a significant assumption.

Equation 3-1: Mass Conservation Equation **(3-1)**

$$\frac{\partial M}{\partial t} = \dot{m}_{in} - \dot{m}_{out}$$

Equation 3-2: Energy Conservation **(3-2)**

$$\frac{dE}{dT} = \dot{E}_{in} - \dot{E}_{out}$$

Equation 3-3: Simplified Momentum Equation -- Pressure Drop **(3-3)**

$$dP^{time} = \Delta P^{time}_{calculated}$$

The momentum equation is reduced to quasi-steady state pressure drop calculations. This allows a significant simplification of the solution with a relatively small loss of accuracy in flow dynamics. Note that this dictates that GAS-PASS/CO_2 cannot be used to accurately analyze rapid (roughly less than a second) fluid pressure effects. The application of these equations in the steady state and in transient processes is elaborated upon in, "*Appendix* A: GAS-PASS/CO2 Equations," but the next section will provide an example by applying these equations to the turbine.

3.2.2.2 Turbine Conservation Equations

The turbine will use mass, momentum, and energy conservation laws and the equation of state of carbon dioxide and the turbomachinery performance maps to provide constitutive relationships.

The turbine and its following piping will be simulated as shown in Figure 3-6. This figure shows that the turbine receives the incoming fluid, extracts work, and the fluid then proceeds through the piping and exits the control volume. All the equations derived refer to this system.

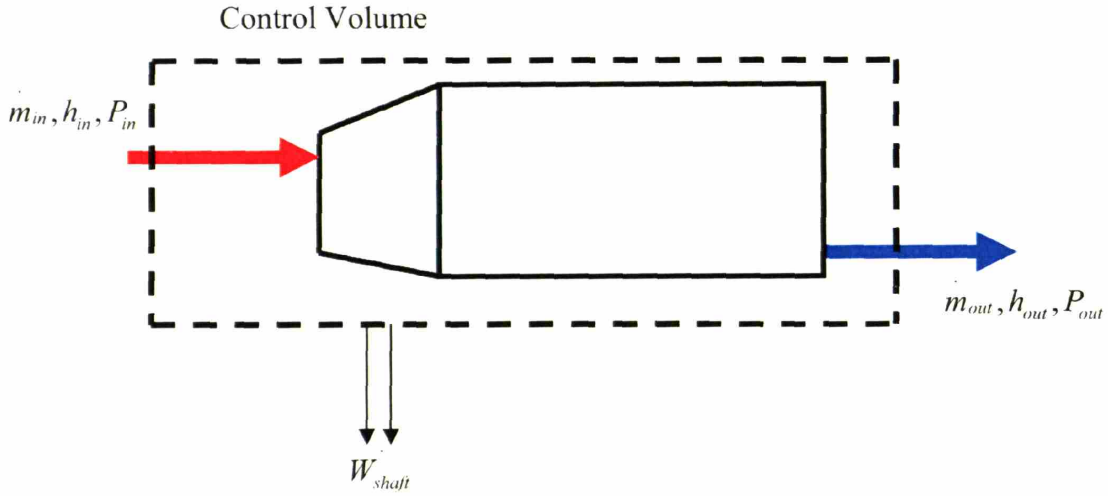

Figure 3-6: Control Volume for a Turbine

3.2.2.2.1 Turbine Mass Conservation

The mass flow rates and mass storage in the system come directly from the mass conservation equation, Equation 3-1:

$$\frac{\partial M}{\partial t} = \dot{m}_{in} - \dot{m}_{out}$$

Discretizing yields:

$$\frac{M_{c.v.}^{i+1} - M_{c.v.}^{i}}{\Delta t} = \dot{m}_{in} - \dot{m}_{out}$$

GAS-PASS/CO_2 solves the numerical system implicitly, thus:

$$\frac{M_{c.v.}^{i+1} - M_{c.v.}^{i}}{\Delta t} = \dot{m}_{in}^{i+1} - \dot{m}_{out}^{i+1}$$

Finally, one may apply assumptions 2 and 3, stating that the control volume interior conditions are equal to the fluid outlet conditions, to yield the full mass conservation equation for the turbine as shown in Equation 3-4.

Equation 3-4: Turbine Mass Conservation Equation **(3-4)**

$$\frac{M_{c.v.-fluid-out}^{i+1} - M_{c.v.-fluid-out}^{i}}{\Delta t} = \dot{m}_{in}^{i+1} - \dot{m}_{out}^{i+1}$$

The amount of mass in the control volume is calculated as:

$f_{equation\_of\_state}(h_{out}, P_{out}) => \rho_{out}$ and $M_{c.v.-fluid-out} = \rho_{out} V$.

3.2.2.2.2 Turbine Momentum Conservation

The momentum equation is applied in a highly simplified form due to several assumptions. The piping may be neglected altogether regarding pressure loss due to assumption 4, which restricts pressure loss to friction in a pipe, and 8, which neglects frictional losses in piping. For the turbine the pressure change will be determined from a constitutive relationship via the performance maps and off-design fluid property relations as stated in assumption 10.

To use the turbine's performance maps requires first applying the off-design fluid relations to the interpolated variables. Note that the fluid properties used are the inlet values to the control volume which relies on assumption 9. Then the "normalized" inputs variables, ($\dot{m}_{normalized}, U_{normalized}$), are applied to the performance maps calculated at design conditions to determine the pressure ratio. The variable U denotes the turbine/shaft rotational speed.

I. $f_{properties}(h_{in}, P_{in}, \dot{m}_{in}, U) => \dot{m}_{normalized}, U_{normalized}$

II. $f_{curves}\left(\dot{m}_{normalized}, U_{normalized}\right) => P_{ratio}$

III. $P_{out} = P_{in} P_{ratio}$

Thus, the turbine's momentum conservation becomes the combination of two constitutive relationships as shown in Equation 3-5 in a discrete and implicit form.

Equation 3-5: Turbine Momentum Conservation **(3-5)**

$$\frac{P_{out}^{i+1}}{P_{in}^{i+1}} = P_{ratio} = f_{curves}\left(f_{properties}(h_{in}^{i+1}, P_{in}^{i+1}, \dot{m}_{in}^{i+1}, U_{shaft}^{i+1})\right)$$

3.2.2.2.3 Turbine Energy Conservation

The turbine energy conservation can be broken into two equations: the turbine work equation, which is provided from the constitutive relationships already mentioned, and the overall conservation of energy equation of the control volume.

The turbine's work is found by calculating isentropic efficiency from the performance maps and off-design fluid property relations. The off-design fluid property relations are identical to those used in the pressure ratio case shown above and will not be repeated here thus:

I. $f_{equation\_of\_state}(h_{in}, P_{in}) => S_{in}$

II. $f_{equation\_of\_state}(S_{in}, P_{out}) => h_{ideal}$

III. $f_{curves}\left(\dot{m}_{normalized}, U_{normalized}\right) => \eta$

Recall that the definition of isentropic efficiency for a turbine is:

IV. $$\eta = \frac{\dot{W}_{actual}}{\dot{W}_{ideal}} = \frac{\dot{m}(h_{out-turbine} - h_{in})}{\dot{m}(h_{ideal} - h_{in})} = \frac{h_{out-turbine} - h_{in}}{h_{ideal} - h_{in}}$$

Thus the turbine's work, which is delivered to the shaft, is:

V. $$-\dot{W}_{shaft-calc} = \eta \dot{m}_{in}(h_{ideal} - h_{in})$$

Note that this is equivalent to:

VI. $$-\dot{W}_{shaft-calc} = \dot{m}(h_{out-turbine} - h_{in})$$

The complete (discrete and implicit) equation for calculating the turbine's work is shown in Equation 3-6.

Equation 3-6: Turbine Work Equation **(3-6)**

$$-W_{shaft}^{i+1} = \eta \dot{m}_{in}(h_{ideal} - h_{in}) = f_{properties}(h_{in}^{i+1}, P_{in}^{i+1}, \dot{m}_{in}^{i+1}, U_{shaft}^{i+1}) * \dot{m}_{in}^{i+1}, *$$
$$\left(f_{curves}\left(f_{equation\_of\_state}\left(h_{in}^{i+1}, P_{in}^{i+1}, P_{out}^{i+1}\right)\right) - h_{in}^{i+1}\right)$$

Once the turbine work is known the familiar first law of thermodynamics may be solved. Todreas and Kazimi[51] express this equation (for one dimensional flow in a stationary control volume, Equation 4-39) as:

$$\dot{E}_{cv} = \sum_{i=1}^{I} \dot{m}_i\left(h_i^{\circ} + gz_i\right) + \dot{Q} + \dot{Q}_{gen} - \dot{W}_{shaft} - \dot{W}_{normal} - \dot{W}_{shear}$$

If shear work and the differences between kinetic and potential energy are neglected while $\dot{Q}_{gen}$ is conflated with $\dot{E}$ then the previous equation becomes (Equation 6-2 in Todreas and Kazimi[51]):

$$\dot{E}_{cv} = \sum_{i=1}^{I} \dot{m}_i h_i + \dot{Q} - \dot{W}_{shaft} - \dot{W}_{normal}$$

For a turbine the control volume is assumed to be adiabatic and kinetic energy effects are neglected, as stated in assumptions 5 and 7, thus:

$$\frac{dE_{cv}}{dt} = -\dot{W}_{c.v.} + \dot{m}_{in} h_{in} - \dot{m}_{out} h_{out}$$

Once again the lumped component will assume perfect mixing, assumptions 2 and 3, to produce:

$$\frac{dE_{c.v.-out}}{dt} = -\dot{W}_{c.v.} + \dot{m}_{in} h_{in} - \dot{m}_{out} h_{out}$$

The control volume will be solved implicitly and discretely which yields the complete turbine energy conservation equation shown in Equation 3-7.

Equation 3-7: Turbine Energy Conservation (3-7)

$$\frac{M_{c.v.-out}^{i+1} e_{c.v.-out}^{i+1} - M_{c.v.-out}^{i} e_{c.v.-out}^{i}}{\Delta t} = -\dot{W}_{c.v.}^{i+1} + \dot{m}_{in}^{i+1} h_{in}^{i+1} - \dot{m}_{out}^{i+1} h_{out}^{i+1}$$

The internal energy of the control volume is the sum of the fluid's internal energy, $E_{c.v.-fluid} = M_{c.v.-fluid-out} e_{fluid-out}$ where $f_{equation\_of\_state}(h_{out}, P_{out}) => e_{fluid-out}$, and the structure's stored energy. Using assumption 6 the structure's stored energy is $E_{struct} = M_{struct} e_{struct} = M_{struct} C_{struct} * T_{out}$.

Note that a subtle part of Equation 3-7 is that the control volume outlet enthalpy includes the work taken from the fluid by the turbine and the change in internal energy in the control volume which was stated in assumption 9. If one substitutes with a previous work relationship this yields the full turbine energy conservation equation:

$$\frac{M_{c.v.-out}^{i+1} e_{c.v.-out}^{i+1} - M_{c.v.-out}^{i+1} e_{c.v.-out}^{i+1}}{\Delta t} = \dot{m}_{in}^{i+1}\left(h_{turbine-out}^{i+1} - h_{in}^{i+1}\right) + \dot{m}_{in}^{i+1} h_{in}^{i+1} - \dot{m}_{out}^{i+1} h_{out-guess}^{i+1}$$

Canceling redundant terms yields Equation 3-8.

Equation 3-8: Turbine Energy Conservation with Substitution (3-8)

$$\frac{M_{c.v.-out}^{i+1} e_{c.v.-out}^{i+1} - M_{c.v.-out}^{i+1} e_{c.v.-out}^{i+1}}{\Delta t} = \dot{m}_{in}^{i+1} h_{turbine-out}^{i+1} - \dot{m}_{out-guess}^{i+1} h_{out-guess}^{i+1}$$

In other words, after the turbine is done with the fluid the change in the control volume's internal energy goes into changing the (outlet) enthalpy of the fluid, which is as expected.

3.3 Fluid Properties

This section provides methods to rapidly and accurately introduce real fluid properties into the GAS-PASS/CO_2 simulation code. Previously the GAS-PASS/He code simulated only ideal fluids like helium, thus allowing the use of the Ideal Gas Law for most fluid properties. The property requirements for the S-CO_2 cycle are considerably more complex.

The key challenges of properties in this cycle are:

- S-CO_2 shows highly non-linear behavior near its critical point which, by design, is a key area of operation in this cycle. These non-linear changes are fast enough that solving the equation of state may become challenging both in machine precision and in root finding as described in Section 3.3.1.
- The difficulty of using a Newtonian solver with a non-linear system requires solving the system of equations using enthalpy instead of temperature, as addressed in Sections 3.5.2.2 and 3.6. Fluid properties must be based upon enthalpy and pressure (instead of temperature and pressure) but there is also a need to convert back and forth with temperature in the heat exchangers.
- The complexity of heat exchange with S-CO_2 requires detailed heat transfer and pressure drop calculations, preventing the use of simple but common relations like log-mean temperature (addressed in detail in Section 3.5). These detailed

calculations require thermodynamic transport properties such as thermal conductivity and viscosity. Even if a simple relation like the Ideal Gas Law could be developed for S-CO_2 one would have to find a way to provide transport properties.

- Simulating the turbomachinery performance curves requires converting to and from entropy. The turbomachinery efficiencies are expressed in isentropic efficiency (as is typical), so the property code must be able to calculate entropy using enthalpy and pressure then to calculate back to enthalpy using entropy and pressure.
- Besides S-CO_2 it is necessary to accurately simulate liquid water for heat rejection, and liquid sodium* for heat addition. Since these fluids are used for heat exchange with S-CO_2 one must also be able to calculate their transport properties.
- Finally, CO_2 fluid properties must be available above and below the critical pressure to allow for part-load operation with inventory control.

In summary, the fluid properties calculations must be robust, very accurate, able to convert to and from a wide variety of properties, and able to use a variety of fluids. While this is a challenging list already, the most difficult requirement for fluid property simulation is that these requirements have to be met very quickly to minimize computational time.

When running a typical transient simulation GAS-PASS/CO_2 may easily make over 10^9 calls to the fluid property routine. The vast majority of code runtime will be spent in the fluid property routines; therefore it is crucial that this code run rapidly if the ultimate design code continues to serve its purpose of rapid scoping calculations.

This section will explain the developments that were incorporated into GAS-PASS to meet the above requirements. The section is subdivided into three sub-sections:

Section 3.3.1 addresses the use and the improvements made to the ultimate source of CO_2 fluid properties, NIST RefProp.

Section 3.3.2 details how the fluid properties are put into linear and log-indexed fluid property tables.

Section 3.3.4 summarizes this section.

---

* Note that the indirect S-CO_2 recompression cycle can be readily coupled to a variety of primary system fluids. Liquid sodium was used because the sodium cooled fast reactor was recently selected[7] for primary development under the U.S. Department of Energy Global Nuclear Energy Partnership[8] (GNEP).

3.3.1 Using NIST RefProp with CO_2

The ultimate source of real fluid property for GAS-PASS is the NIST RefProp code[25]. The NIST RefProp code can accurately calculate a variety of fluid properties for numerous fluids. The documentation included with the code states:

> REFPROP is based on the most accurate pure fluid and mixture models currently available. It implements three models for the thermodynamic properties of pure fluids: equations of state explicit in Helmholtz energy, the modified Benedict-Webb-Rubin equation of state, and an extended corresponding states (ECS) model. Mixture calculations employ a model which applies mixing rules to the Helmholtz energy of the mixture components; it uses a departure function to account for the departure from ideal mixing. Viscosity and thermal conductivity are modeled with either fluid-specific correlations or an ECS method.[52]

The RefProp code was selected for a variety of reasons but primarily because of its accuracy and wide ranging applicability to carbon dioxide. Other authors have modeled CO_2 properties from a "pseudo-perfect" gas model that fixes the ideal gas law with compressibility factors. Aungier makes a compelling case for using these very rapid calculations in compressor design as previously discussed in Section 2.2.4.

Unfortunately, these pseudo-perfect models require constants that are not readily available, compressibility factors must be recalculated within turbomachinery stages[24] (a level of detail not desired in GAS-PASS), and, in general, will not be as accurate as the NIST RefProp models. Furthermore, the varied requirements of simulating fluid properties for simulation of the recompression cycle prohibit the use of a simplified equation.

Therefore, NIST RefProp was selected as GAS-PASS's ultimate property source whenever possible. This section will provide a brief background of key RefProp features, recommend an equation of state, and warn the user of several problems encountered and solutions found when calculating S-CO_2 properties with RefProp.

3.3.1.1 Key NIST RefProp Features

RefProp provides the ability to calculate numerous different fluid properties ranging from common properties like enthalpy, to more exotic properties like fugacity. More importantly, it allows the user to input various properties to get the desired value e.g. one may use enthalpy and entropy to calculate temperature. RefProp accomplishes this with an equation of state in temperature and pressure by performing numerical convergence iterations when properties other than temperature and pressure values are entered. For simulating the S-CO_2 recompression cycle RefProp provides far more property flexibility than is required.

RefProp 7.0 also features the choice of simulating 52 different fluids as shown in Table 3-1. While not offering liquid sodium, RefProp offers all other fluids necessary, including water.

Of importance to future work is the ability of RefProp to calculate fluid mixtures. Fluid mixtures (e.g. helium and nitrogen) Brayton cycles are an area of active research, and mixtures also allow the simulation of plant performance during accidents such as air ingress. RefProp 7.0 supports mixing up to 20 fluids and includes a mixtures file, *Hmx.bnc*, which provides the mixture rules. The mixtures supported are somewhat limited at the time of this writing but common combinations with fluids like helium, nitrogen, and carbon dioxide are available.

3.3.1.2 RefProp CO_2 Equation of State

RefProp allows the user to specify the equation of state. This subsection will compare the Benedict-Webb-Rubin, (BWR), model to the default Span and Wagner[26] Helmholtz model, (FEQ), using CO_2 density, since this is a key property of interest. The RefProp CO_2 fluids file, *co2.fld*, states that the FEQ model is more accurate in the critical region of CO_2 while the BWR model is recommended for general use.

Data points ranging from 300 K to 440 K (the maximum temperature in the BWR model is 440.1 K) at every 0.5 K and at each integer MPa value between 1 MPa and 20 MPa were tested.

The results may be seen in *Figure 3-7* (only a few pressure lines are shown for clarity) showing the percent difference between the BWR and FEQ models. The reader should note that there are systematic differences but they are relatively small (note the percent scale). The differences are centered near the critical temperature and slightly above the critical pressure but persist in all the data.

Due to the relatively small differences between these model values, the limited temperature range of the BWR model: to only 440.1 K (the FEQ model goes to 1100 K, a realistic temperature for possible applications), the emphasis on the critical region, and the difficulty in coding a variable model program, only the NIST default model, FEQ, will be used.

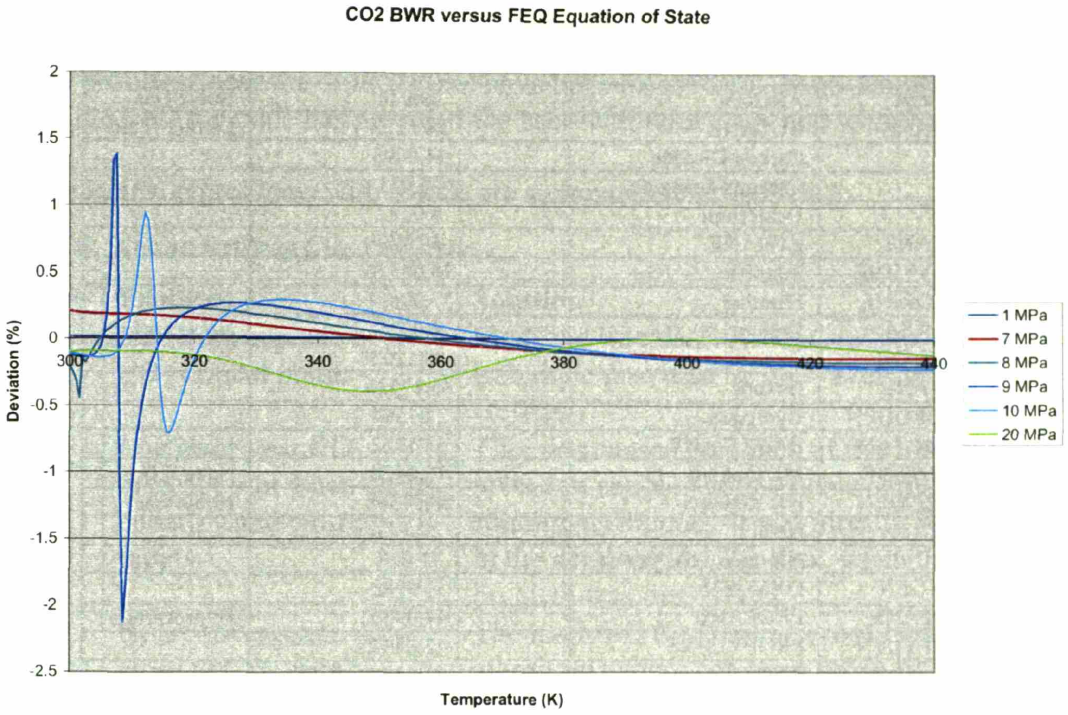

Figure 3-7: CO_2 BWR versus FEQ Equations of State

Table 3-1: NIST RefProp 7.0 Available Fluids

Number	Symbol	Fluid	Molecular Weight [g/cm^3]	Description
1	AMMONIA	AMMONIA	17.03026	
2	ARGON	ARGON	39.948	Noble Gas
3	BUTANE	BUTANE	58.1222	Lighter Fluid
4	CO2	Carbon Dioxide	44.0098	
5	CO	Carbon Monoxide	28.011	
6	D2	Deuterium	4.0282	
7	ETHANE	ETHANE	30.070	
8	ETHYLENE	Ethylene	28.05376	
9	FLUORINE	Fluorine	37.99681	
10	HELIUM	Helium	4.0026	Noble Gas
11	HEPTANE	Heptane	100.202	
12	HEXANE	Hexane	86.17536	
13	HYDROGEN	Hydrogen	2.01594	
14	ISOBUTAN	ISOBUTANE	58.1222	
15	METHANE	METHANE	16.0428	Natural Gas
16	NITROGEN	NITROGEN	28.01348	Noble Gas
17	NEON	Neon	20.179	
18	NF3	Nitrogen Tri-Fluoride	71.019	
19	OXYGEN	OXYGEN	31.9988	
20	PROPANE	PROPANE	44.0956	Hydrocarbon
21	PROPYLEN	PROPYLENE	42.0804	
22	PARAHYD	Parahydrogen	2.01594	
23	PENTANE	Pentane	72.14878	
24	R11	R11	137.368	Refrigerant
25	R113	R113	187.375	Refrigerant
26	R114	R114	170.921	Refrigerant
27	R115	R115	154.4667	Refrigerant
28	R116	R116	138.01	Refrigerant
29	R12	R12	120.913	Refrigerant
30	R123	R123	152.931	Refrigerant
31	R124	R124	136.4762	Refrigerant
32	R125	R125	120.022	Refrigerant
33	R13	R13	104.459	Refrigerant
34	R134A	R134A	102.032	Refrigerant
35	R14	R14	88.0046	Refrigerant
36	R141B	R141B	116.95	Refrigerant
37	R142B	R142B	100.495	Refrigerant
38	R143A	R143A	84.041	Refrigerant
39	R152A	R152A	66.051	Refrigerant
40	R218	R218	188.019	Refrigerant
41	R22	R22	86.468	Refrigerant
42	R227EA	R227EA	170.0289	Refrigerant
43	R23	R23	70.01385	Refrigerant
44	R236EA	R236EA	152.03928	Refrigerant
45	R236FA	R236FA	152.0393	Refrigerant
46	R245CA	R245CA	134.04882	Refrigerant
47	R245FA	R245FA	134.04882	Refrigerant
48	R32	R32	52.024	Refrigerant
49	R41	R41	34.033	Refrigerant
50	RC318	RC318	200.0312	Refrigerant
51	WATER	WATER	18.015268	
52	Xenon	Xenon	131.3	

3.3.1.3 RefProp CO_2 Caveats

While RefProp accurately calculates CO_2 properties in the vast majority of circumstance several problems near the critical point have been discovered. In all known cases of failure the RefProp code has provided the user with error flags and warning messages.

Known RefProp problems with S-CO_2 are summarized in Table 3-2.

Table 3-2: Known RefProp CO_2 Problems

Version	Problem	Solution
5.0	Non-convergence near CO_2 critical point.	Modified Regula-Falsi root finding technique provided by Dr. Pavel Hejzlar.
7.0	Log error near CO_2 critical point when using enthalpy and entropy inputs.	This was caused by a lack of machine precision coupled with a non-optimal solution technique. It was already fixed in the next version, 7.1 beta, when the problem was discovered.
7.1	Non-convergence very close to CO_2 critical point using non-temperature and pressure inputs.	The modified Regula-Falsi root finding algorithm cannot converge some CO_2 data points. An updated algorithm and patch were provided by Nate Carstens.

The first problem listed in the table was fixed several years ago and the main code now features the solution. The second problem in the table has a fix available for those willing to use the current beta code version. The final problem deservers further attention.

RefProp iteratively converges non-temperature and pressure roots with numerical root finding algorithms, currently a modified Regula-Falsi method. While this works well in the vast majority of cases, S-CO_2 is non-linear enough that this technique will not work very close to the critical point.

A solution was developed that changed the root finding algorithm to Brent's method[53]. Brent's method uses inverse quadratic interpolation and the secant method (when possible) for speed, and falls back on the bisection method when progress isn't made. When provided with bracketing roots, convergence is guaranteed for continuous functions.

This method has been applied to RefProp 7.1 and a patch was sent to RefProp's developer. To date this new code has converged in every case tried, including very close to the CO_2 critical point and with a variety of fluids and properties. The new code also runs slightly faster than the previous version.

To summarize, when patched the NIST RefProp code provides the required accuracy for all of the fluids (except liquid sodium) and properties required to simulate the S-CO_2

recompression cycle. It is the source of all water and CO_2 fluid properties used in GAS-PASS/CO_2.

3.3.2 Tabular Fluid Properties

The benefits of the NIST RefProp code come at the cost of considerable complexity and therefore slow runtime. When GAS-PASS/He was originally updated to allow real fluid properties it used RefProp directly. Unfortunately, this slowed code runtime by quite a few orders of magnitude. While runtime isn't a primary concern, GAS-PASS is designed as a rapid scoping tool and this large an increase in runtime would negate much of its rationale.

The solution adopted for GAS-PASS/CO_2 is to pre-compute fluid property data and store it in tabular form. The user can still have the flexibility to create tabular data for any fluid or fluid mixture and can create tables with any input or output properties. Tables also offer the advantage of easily combining disparate property sources such as simple liquid sodium polynomials with the very complex RefProp carbon dioxide Helmholtz equation of state. Finally, tables offer the advantage of unrestricted distribution, whereas NIST RefProp is a commercial code.

GAS-PASS uses indexed property tables to save space and avoid searching. An indexed table contains only the desired property data but by carefully setting up the table one may know the location of the desired data a priori. For example, a table might be indexed by temperature and pressure and contain 1,001 temperature indexes between 0 and 1000 K and 1,001 pressure indexes between 100 kPa and 10,100 kPa with a density calculated at each point. When the interpolation routine is called with a desired temperature and pressure it calculates the position in the table where those values would lie. Once the points surrounding the desired value are found the approximate value is calculated via double linear interpolation as shown in Equation 3-9.

Equation 3-9: Double Linear Interpolation **(3-9)**

$$x_t = {(t - T_{low})}\Big/{(T_{high} - T_{low})}$$

$$x_p = {(p - P_{low})}\Big/{(P_{high} - P_{low})}$$

$$r_{p\ low} = V(P_{low}, T_{low}) + x_t * (V(P_{low}, T_{high}) - V(P_{low}, T_{low}))$$

$$r_{p\ high} = V(P_{high}, T_{low}) + x_t * (V(P_{high}, T_{high}) - V(P_{high}, T_{low}))$$

$$V(t, p) = r_{p-low} + x_p * (r_{p-high} - r_{p-low})$$

This code is very fast and can be implemented with little overhead, especially compared to a sorting algorithm.

The user should be aware that GAS-PASS/CO_2 will not extrapolate and returns an error flag if properties are requested outside tabular bounds. This will become important during Jacobian calculation, addressed in detail in Section 3.6. If necessary, the user may simply recreate the appropriate data table with larger bounds to avoid this problem.

3.3.2.1 Linearly Indexed Property Tables

The obvious way to index tabular data is linearly. This creates a constant spacing between values and makes it trivial to calculate the appropriate data position within the table by knowing the minimum and maximum index values and grid spacing. When this method was implemented in GAS-PASS/CO_2 the runtime improved significantly compared to the NIST RefProp version, as shown in Table 3-3. The reader should note that this is an optimal RefProp runtime using assumptions that probably couldn't be maintained during transient simulation.

Table 3-3: GAS-PASS/CO_2 Run Times by Data Source

Run	Time (sec.)	% Change vs. Ideal Gas Law
Ideal Gas Law	236	0
NIST RefProp	15730*	6665
Linearly Indexed Tables	444	88.1

*Estimated from 10% of run time

3.3.2.2 Log Indexed Property Tables

Unsurprisingly, the highly non-linear behavior of S-CO_2 properties leads to difficulty when used with linearly indexed tables. The first CO_2 tables were linearly indexed and numerical problems were encountered during simulation that prevented solver convergence. Upon investigation it was discovered that during the calculation of the main compressor outlet pressure the property tables were creating significant errors -- over 1 MPa in pressure at the outlet of the main compressor (see Section 2.1.2).

The reason for this error can be visually seen in Figure 2-7. Despite using millions of data points in the property table, the non-linear behavior of the fluid properties in the main compressor required a much tighter table spacing to avoid large property conversion errors when converting from values of enthalpy and entropy to pressure. Unfortunately, tables with this tight of a grid spacing would be far too large to be practical.

Using a variable mesh could effectively solve this problem at the cost of requiring a searching routine to find the appropriate position in table. The large increase in computation time (compared to indexed tables) would remove much of the advantage of using tabular data in the first place. Log-indexed property tables offer many of the benefits of both methods with few drawbacks.

3.3.2.2.1 Background

One significant advantage of non-linear CO_2 behavior is that its challenging areas are well defined and furthermore lie in only one region. In many complex problems that

would benefit from a variable mesh, it is very difficult to predict the region, or more probably regions, of difficulty. One may take advantage of this specific knowledge by using a non-linearly indexed property data table.

Carbon dioxide's properties become highly non-linear near its critical point, thus any property table would benefit from a larger number of data points in this area. For the S-CO_2 recompression cycle the temperatures and pressures of interest range from the critical point upwards during normal operation.

During off-design operation (e.g. part-load operation with inventory control) the S-CO_2 recompression cycle will move well below the critical pressure. To handle this transient a second set of log-indexed fluid property tables that range from low pressures up to super-critical pressure have been created. These tables have been combined into one file and switching between them is automatic within GAS-PASS/CO_2.

3.3.2.2.2 Log Function

If one were to plot the desired number of data points versus property value it would create a function that, beginning at the critical point, bends sharply upward then tapers off towards a limit. The most common simple function that resembles this shape is a natural log. For supercritical properties Equation 3-10 & Equation 3-11 apply. For subcritical fluid properties (only pressure in this work) Equation 3-12 & Equation 3-13 are appropriate. Note that the α, β, γ variables are constants unique to each property table and that each table has a fixed number of data points which cover the area between minimum and maximum property values in that table.

Equation 3-10: Number of Data Points as a Function of Supercritical Property Value **(3-10)**

$$Np = \alpha * \ln(P^*) + \beta$$

$$P^* = P - \gamma$$

Equation 3-11: Supercritical Property Value as a Function of the Number of Data Points **(3-11)**

$$P^* = e^{\frac{Np-\beta}{\alpha}}$$

$$P = P^* + \gamma$$

Equation 3-12: Number of Data Points as a Function of Subcritical Property Value **(3-12)**

$$Np = \alpha * \ln(P^*) + \beta$$

$$P^* = -P - \gamma$$

Equation 3-13: Subcritical Property Value as a Function of the Number of Data Points **(3-13)**

$$P^* = e^{\frac{Np-\beta}{\alpha}}$$

$$P = -P^* + \gamma$$

Equation 3-10 (for supercritical values) & Equation 3-12 (for subcritical values) calculate the desired table data point a given property value will be at. Note that a given property

value will probably lie between table data points due to the finite number of data points in the table, but with expected mesh densities the bounding values should be close. Correspondingly, when creating the data tables, Equation 3-11 (for supercritical values) & Equation 3-13 (for subcritical values) may be used to calculate the property value for a given table data point.

The requirements of rapidly solving turbomachinery and converging a non-linear system with a Newtonian solver dictate (discussed in detail in Section 3.6.3) that pressure, enthalpy, and entropy are the properties that must be log-indexed.

3.3.2.2.3 Property Indexes

The outlined process will be used for CO_2 pressure in the S-CO_2 recompression cycle by using Equation 3-10 through Equation 3-13 to find appropriate coefficients. Experimentation has shown that a multiplicative coefficient, alpha, near 100 provides a reasonable degree of high initial density and reasonable end of table density. The value of beta and gamma may be iteratively solved for. First, by deciding upon the number of data points in the table, i.e. 500, and then solving for beta by setting the last point to be equal to the largest desired property value. Then one may solve for gamma by setting point 1 equal to the minimum desired pressure. By iterating several times to keep both points close to their targets one may arrive at the desired values, which for the S-CO_2 cycle are shown in Table 3-4.

One finds that by starting with data point 1 at 7,385 kPa (for the supercritical table -- note that the coefficients are sized in terms of Pascal), where there is one data point every 0.46 kPa, that at the 750th data point the pressure is 30,185 kPa, where there is one data point every 228 kPa. This encompasses our range of interest, provides more detail in the critical region, and provides a reasonable guess of an appropriate mesh density. The number of data points as a function of pressure for the supercritical table is graphically shown in Figure 3-8. The number of data points as a function of pressure for the subcritical table is shown graphically in Figure 3-9.

Table 3-4: Log-Indexed Pressure Table Coefficients

Coefficient	Supercritical Pressure	Subcritical Pressure
α	100	100
β	-944.2829591	-1075.386425
γ	7372255.825	-7547281.021
# of points	750	500

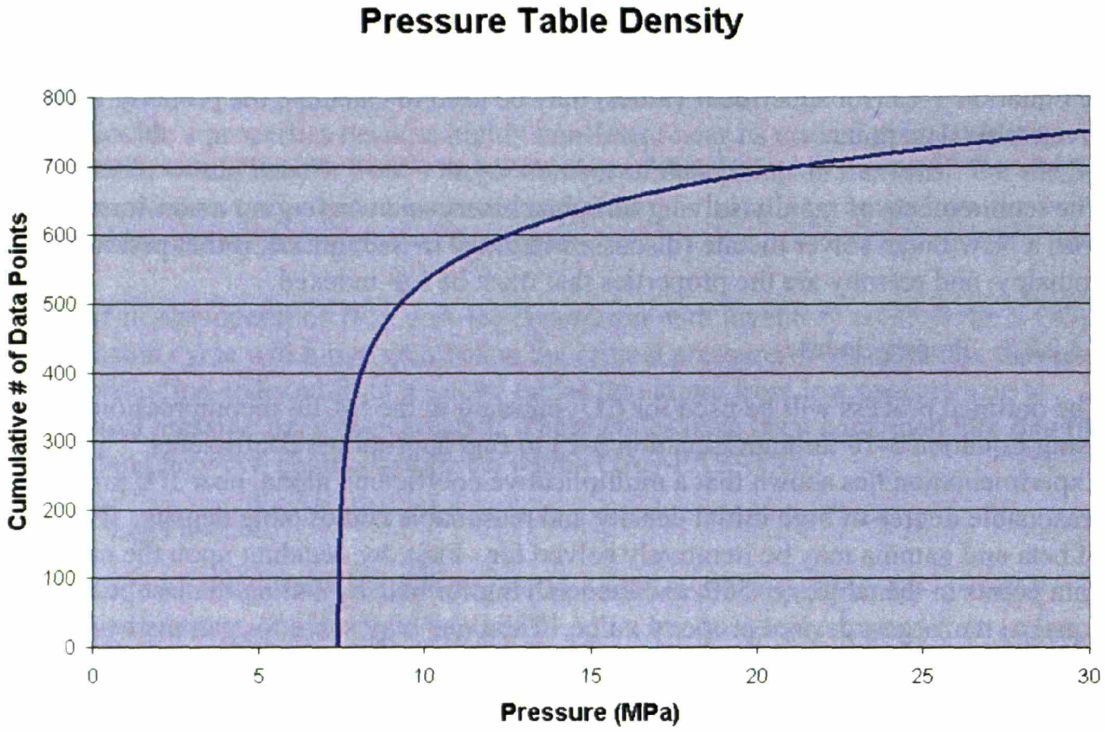

Figure 3-8: Supercritical Pressure Table Data Density

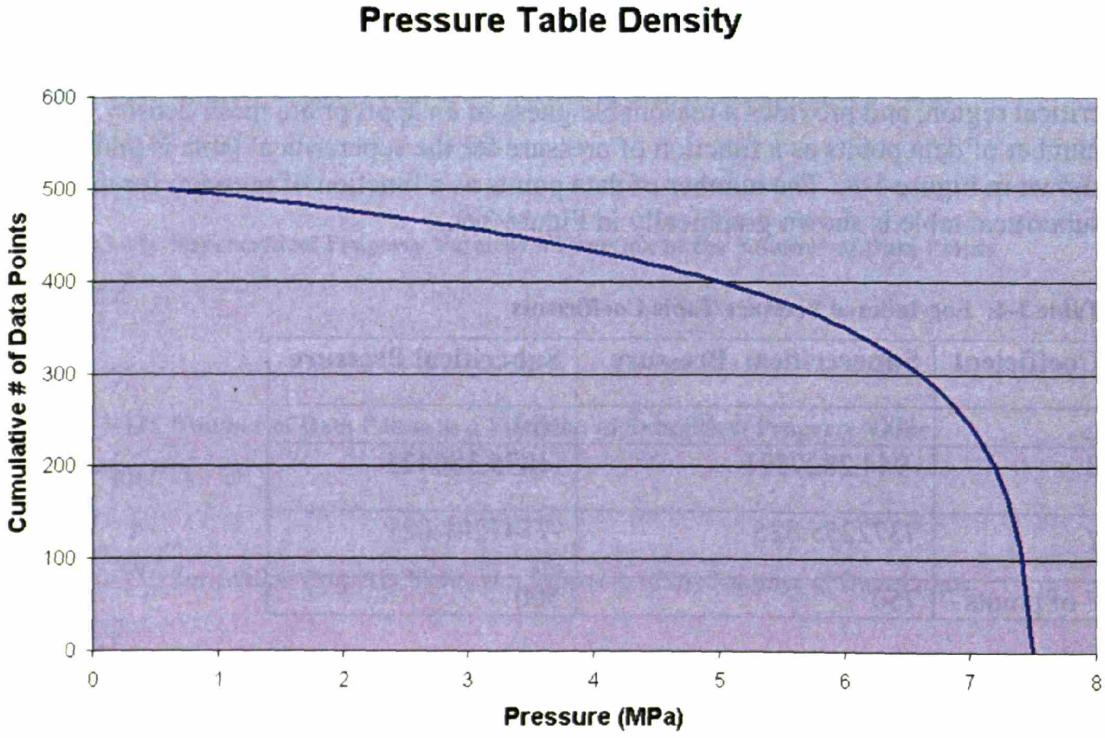

Figure 3-9: Subcritical Pressure Table Data Density

A similar process may be used with enthalpy. Using the equations previously shown for enthalpy (in J/kg units) one can create Table 3-5.

Table 3-5: Log-Indexed Enthalpy Table Coefficients

Coefficient	Supercritical Pressure	Subcritical Pressure
α	100	100
β	-889.555	-887.1129357
γ	267627	295015.407
# of points	500	500

It should be noted that enthalpy is a function temperature and pressure. Thus this table type must cover both expected temperatures and pressures, which may require several iterations during initial table creation.

While temperature determines enthalpy more strongly than pressure, the wide range of pressures of interest above the critical pressure (7.385-30 MPa) leads to a significant enthalpy range. For example, at the critical point the enthalpy is 326.08 kJ/kg. However, at 31°C (just above T_c=30.978°C) and 30 MPa the enthalpy is 242.68 kJ/kg. To be conservative, this table starts at 31°C and 10 MPa which has an enthalpy of 275 kJ/kg*. This trades table density of pressures near the critical point for table completeness. Future use should establish the appropriateness of this tradeoff. The upper bound is simply set to 800°C and 30 MPa, which are well above expected operating parameters.

A similar process may be used with entropy. Using the previously shown equations (in J/kg-K units) results in Table 3-6. This table encompasses the same range as the minimum to maximum pressures and enthalpies as previously noted.

Table 3-6: Log-Indexed Entropy Table Coefficients

Coefficient	Supercritical Pressure	Subcritical Pressure
α	100	100
β	-22.14641102	-279.421067
γ	1243.539556	1317.686672
# of points	750	500

Temperature may also be put into this format. Only supercritical values will be used (since below critical temperatures are not needed and temperature is independent of pressure, unlike enthalpy and entropy). Using the previously outlined process, with temperatures ranging between 31°C and 800°C, results in Table 3-7.

* At 31°C and 7 MPa carbon dioxide has an enthalpy of 399.57 kJ/kg

Table 3-7: Log-Indexed Temperature Table Coefficients

Coefficient	Value
α	100
β	-22.14641102
γ	1243.539556
# of points	500

These tables encompass our range of interest, provide greater detail in the critical region, allow below-critical pressure operation and provide a reasonable mesh density for projected applications.

3.3.2.2.4 Speed and Accuracy

The speed and accuracy of the log-indexed tables were compared to linearly-indexed tables. The linearly-indexed tables had approximately 4x as many data points as the log-indexed tables and covered the same range (the S-CO_2 recompression cycle with extra margin). Virtually the full range of both tables was tested and compared to the NIST RefProp code to assess their accuracy.

Figure 3-10 shows the error of the log-indexed properties versus the error of the linearly indexed properties. It is apparent that log-indexed properties are much more accurate (150x more accurate on average) especially near the critical region (towards the beginning of the table) despite the much larger amount of data in the linear table. Unfortunately, the log tables ran approximately 3.6x slower than the linear tables (a log is more difficult to calculate than a linear function). However, the log tables were still about 2,300x faster than the NIST RefProp code with default inputs.

The error present in the log-indexed tables is more clearly seen in Figure 3-11. The critical region is extremely accurate but the log function, as currently configured, does not place enough emphasis on the transition between the critical region and higher values. One might desire approximately the same error throughout the table, but this table appears appropriate for our purpose, where the critical region is the key area of interest.

In any case, a maximum error of less than 0.003% is more accuracy than necessary for dynamic analysis. Also note that the original NIST RefProp FEQ CO_2 equation of state has uncertainty ranging from 0.03-0.15% in the vapor region and up to 1.5% in the liquid region[25] hence striving for smaller error offers little reward.

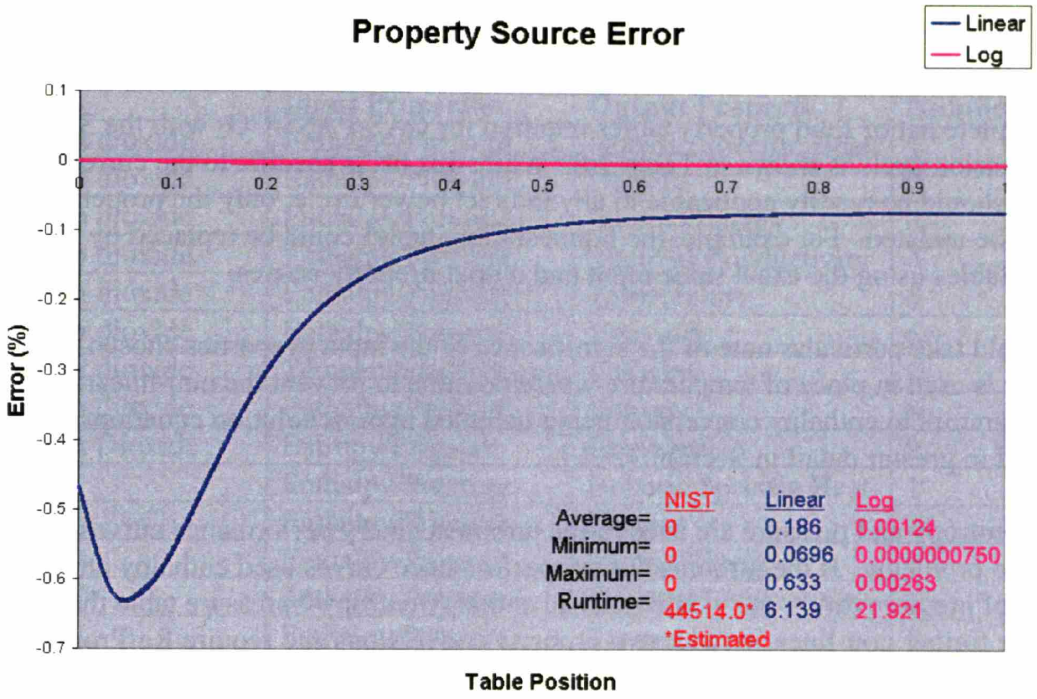

Figure 3-10: Relative Tabular Error

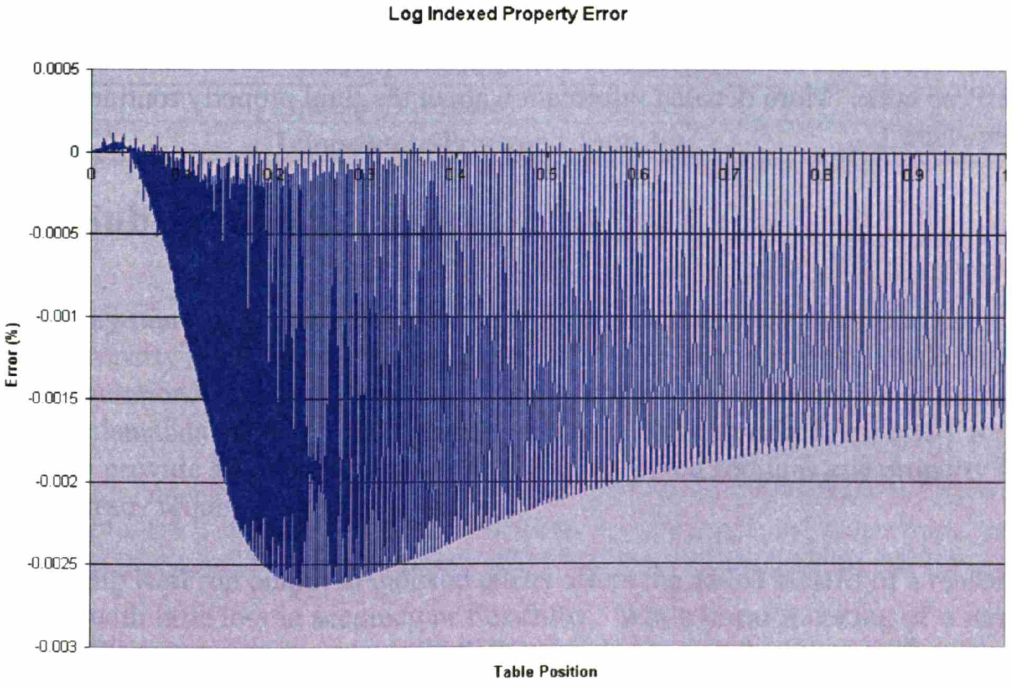

Figure 3-11: Log-Indexed Tabular Error

3.3.3 GAS-PASS/CO_2 Property Tables

The complete list of fluid property tables required for GAS-PASS/CO_2 with the S-CO_2 recompression cycle is shown in Table 3-8. While this list is specific to the current plant model it should be readily applicable to any indirect power cycle; only the property table needs to be updated. For example, the liquid sodium tables could be replaced by lead bismuth tables using the exact same input and output property entries.

One should take particular note of the significance of the input properties chosen. Enthalpy is used in place of temperature where possible to prevent the non-linearity of the temperature to enthalpy conversion being included in most solution equations, as described in greater detail in Section 3.5.2.2.

Second, entropy and pressure are used in the turbomachinery performance curves to avoid two problems. If the turbomachinery performance curves used enthalpy change (instead of pressure ratio) one would need an enthalpy/entropy->pressure table that would introduce further non-linearity with two property conversions and require RefProp to perform a much more difficult double root find. Using pressure ratio performance curves avoids these problems and is the more common practice; therefore it was adopted for GAS-PASS/CO_2.

Finally, a brief description of how to use the standalone property table creation code is provided in, "Appendix C: GAS-PASS/CO_2 User Manual." This appendix should provide the reader with the ability to create simple fluid property tables based upon the NIST RefProp code. More detailed information about the fluid property routines can be found elsewhere[54].

Table 3-8: GAS-PASS Property Tables

Fluid	Input Properties	Output Property	Number
Carbon dioxide	Enthalpy/Pressure	Isobaric Specific Heat	1
Carbon dioxide	Enthalpy/Pressure	Density	2
Carbon dioxide	Enthalpy/Pressure	Internal Energy	3
Carbon dioxide	Enthalpy/Pressure	Thermal Conductivity	4
Carbon dioxide	Enthalpy/Pressure	Temperature	5
Carbon dioxide	Enthalpy/Pressure	Viscosity	6
Carbon dioxide	Temperature/Pressure	Enthalpy	7
Carbon dioxide	Enthalpy/Pressure	Entropy	8
Carbon Dioxide	Entropy/Pressure	Enthalpy	9
Water	Enthalpy/Pressure	Isobaric Specific Heat	1
Water	Enthalpy/Pressure	Density	2
Water	Enthalpy/Pressure	Internal Energy	3
Water	Enthalpy/Pressure	Thermal Conductivity	4
Water	Enthalpy/Pressure	Temperature	5
Water	Enthalpy/Pressure	Viscosity	6
Water	Temperature/Pressure	Enthalpy	7
Sodium	Enthalpy/Pressure	Isobaric Specific Heat	1
Sodium	Enthalpy/Pressure	Density	2
Sodium	Enthalpy/Pressure	Internal Energy	3
Sodium	Enthalpy/Pressure	Thermal Conductivity	4
Sodium	Enthalpy/Pressure	Temperature	5
Sodium	Enthalpy/Pressure	Viscosity	6
Sodium	Temperature/Pressure	Enthalpy	7

3.3.4 Sub-Section Summary

The highly non-linear property behavior of carbon dioxide near its critical point, the varied property requirements for simulating the S-CO_2 recompression cycle, and the need for computational efficiency when used within dynamic simulation places a set of difficult demands upon any fluid property method. When patched, the NIST RefProp code can provide all of the necessary fluid (except liquid sodium) and property flexibility and accuracy required for simulation.

Combining RefProp output in indexed tables offers the added benefit of a reasonable runtime with little loss in accuracy or flexibility. While linear indexing of water and liquid sodium properties works well, S-CO_2 required log indexing to achieve the necessary accuracy in a reasonably efficient manner. By using a super and a subcritical log indexed table this code can seamlessly simulate inventory control operations, where pressures become subcritical, without a loss in accuracy.

Overall, these property methods and sources allow GAS-PASS/CO_2 to flexibly, accurately, and rapidly calculate fluid properties. This will enable this simulation code to continue to meet its design goal of being a rapid scoping tool.

3.4 Turbomachinery Performance Modeling

Due to the complexity of modeling turbomachinery, GAS-PASS/CO_2 will use pre-computed performance curves to estimate turbomachinery performance. This has the advantage of removing a significant computational burden from the transient code as well as allowing rapid changes to turbomachinery, such as switching from radial to axial turbomachines, by simply switching input files. Furthermore, it will allow more realistic experimental data to be easily introduced into simulations as this data becomes available.

GAS-PASS/He also used basic performance curves but, as discussed in Section 3.4.1, the simple assumptions that are made for an ideal gas cannot be accurately applied to S-CO_2, hence a more complex modeling process will be employed which will be discussed in this section.

Note that all turbomachinery performance modeling will take place at the whole-machine level. Individual blades will not be examined within GAS-PASS/CO_2 for several reasons, including avoiding an unnecessarily detailed treatment in a scoping tool, and significant uncertainties over main compressor behavior near the critical point, especially at the blade level.

Also note that the turbine efficiency used in the present work assumes the use of a diffuser with a, roughly, 90% recovery of the kinetic energy of the exiting fluid. The use of total-to-static* versus total-to-total† efficiency has been treated in greater detail elsewhere[13,55].

This section is subdivided into five subsections:

1. The first subsection will briefly look at the assumptions used with the ideal gas code, GAS-PASS/He.
2. The second subsection will present the turbomachinery performance maps used in this work. It will graphically display the maps and briefly document their sources and major features.
3. The third subsection will detail how GAS-PASS/CO_2 uses turbomachinery performance maps. Note that while some of the methods used are relatively simple, they represent the results of numerous iterations between the dynamic simulation code and modeling methods – only the best result is shown.
4. The fourth subsection will analyze the fluid property relations used to predict off-normal turbomachinery performance. These relations will prove key to transient behavior and can produce undesirable effects. This is a key area of uncertainty which future work should investigate.

---

* Total-to-static efficiency assumes that the kinetic energy of the exiting fluid is lost.

† Total-to-total efficiency assumes that the moving fluid is adiabatically and reversibly brought to rest.

5. The final subsection will provide a brief overview of the whole turbomachinery performance modeling section.

By the end of this section the reader should understand where the turbomachinery performance maps come from and how they are applied in GAS-PASS/CO_2. Turbomachinery performance will prove central to cycle performance during transients, especially for part-load operation with inventory control (see Section 4.5.4).

3.4.1 GAS-PASS/He Turbomachinery Performance Modeling

GAS-PASS/He simulated (only ideal gas) helium Brayton cycles. The turbomachinery in an ideal gas cycle exhibit relatively simple behavior that allow several greatly simplifying assumptions. These assumptions are:

- Changing fluid properties do not affect turbomachinery performance. For an ideal gas several properties such as isobaric specific heat are constant across a turbomachine. Relatively small changes in incoming temperature and pressure (for the same mass flow rate) will not significantly affect performance.
- The efficiency of a turbomachine does not depend on shaft speed. An example GAS-PASS/He map axial turbine efficiency is shown in Figure 3-12. This figure shows a rapid parabolic rise in efficiency, peaking near 1 then a gradual almost linear decrease following the peak. This turbomachine was modeled to perform in this manner regardless of shaft speed*.
- The enthalpy change of a turbomachine can be characterized by a simple polynomial with two variables. This method can is shown in Figure 3-13. In this figure two performance curves at (quite) different shaft speeds are modeled with one equation. Due to the simple and similar nature of these curves little error is introduced.

Unfortunately, none of these assumptions can be applied in the S-CO_2 recompression cycle without introducing potentially large errors. As previously shown, Figure 2-5, the S-CO_2 recompression cycle has rapidly changing fluid properties, especially in the main compressor. The performance maps (both efficiency and pressure ratio) for S-CO_2 show complex shapes (e.g. Figure 3-18) that prevent simple treatment. While curves at nearby shaft speeds frequently resemble their neighbors, no simple relation has been discovered which describes behavior over a full performance map. One might be tempted to neglect small variations but shaft speed curves change significantly, as will be shown shortly. Therefore, GAS-PASS/CO_2 will avoid collapsing shaft speed curves in favor of interpolating on and between individual shaft speed curves.

* Note that this assumption was used due to a lack of data rather than a physical reason.

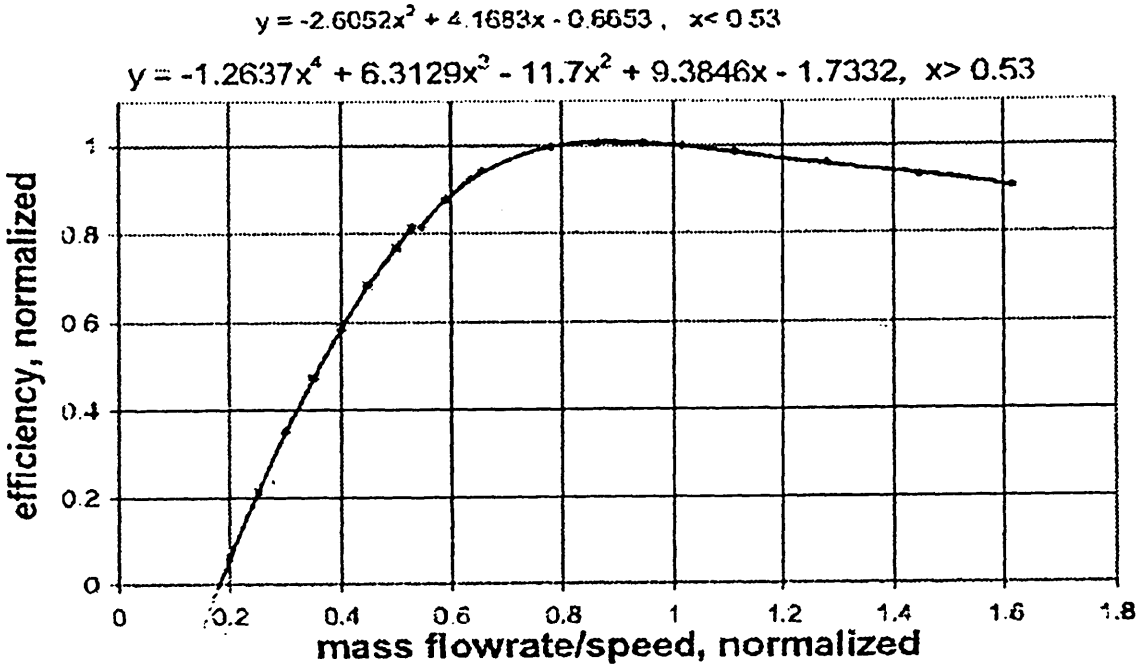

Figure 3-12: Original GAS-PASS/He Helium Axial Turbine Efficiency Performance Map[56]

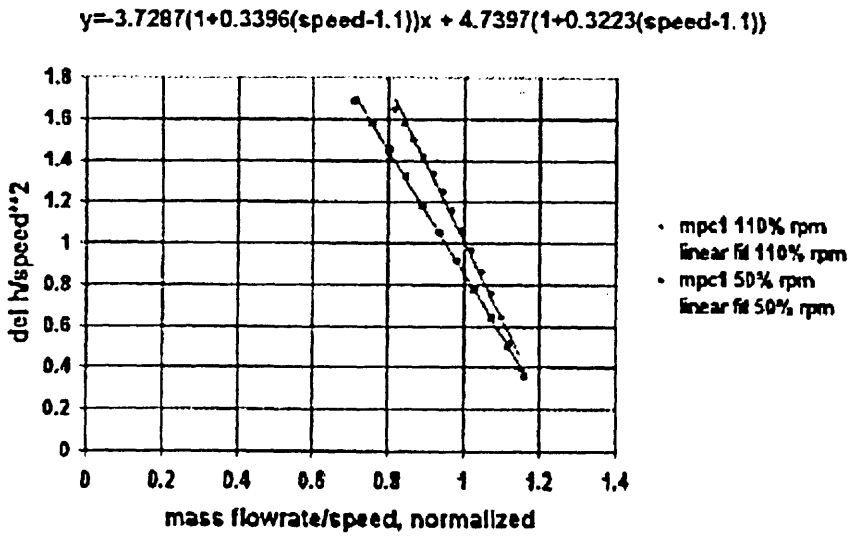

Figure 3-13: Original Gas-Pass Helium Axial Compressor Enthalpy Change Performance Map[56]

3.4.2 Turbomachinery Performance Maps

The turbomachinery performance maps used in GAS-PASS/CO_2 are displayed in this section. The shapes of these maps are quite important during transient simulations since they will largely determine how pressure ratios and mass flow rates change during transient simulation.

Note that the format of the maps and the scaling used to generate them are based on comparing normalized mass flow rates to normalized pressure ratios and normalized efficiencies. There are a variety of, typically dimensionless, factors that can be applied to scale performance maps. Matthews[57] has reviewed several of the prominent methods, and determined that the present work is consistent with that recommended by Japikse[58].

In general, the stall and choke limits were not explicitly reached in the performance map data. While many of the curves show behavior which suggests the approach of phenomena like choke (such as a sharp drop in pressure ratio), the actual value of these limits was not reached due, primarily, to the difficulty of converging the S-CO_2 turbomachinery near performance failure in the detailed design codes. Therefore, GAS-PASS/CO_2 will use the smallest shown mass flow rates as a proxy for stall and the highest mass flow rate as a proxy for choke.

The radial compressor maps are based upon Dr. Yifang Gong's radial compressor report[59]. The radial main and recompression compressor efficiency maps are shown in Figure 3-14 and Figure 3-15 respectively. They show a definite efficiency peak with a relatively steep drop off on either side. The curves show a wider mass flow rate operating range at higher shafts speeds, but are similar. This stems from scaling and extrapolation from a single normalized shaft speed curve, as detailed in the referenced report.

The radial main and recompression compressor pressure ratio maps are shown in Figure 3-16 and Figure 3-17. These curves have a flat pressure ratio at low mass flow rates that eventually smoothly slopes to a minimum at high mass flow rates. The shaft speed curves become more widely spaced and have ever wider mass flow ranges as the speed increases. Once again, these curves are scaled and extrapolated from a single normalized shaft speed curve data source.

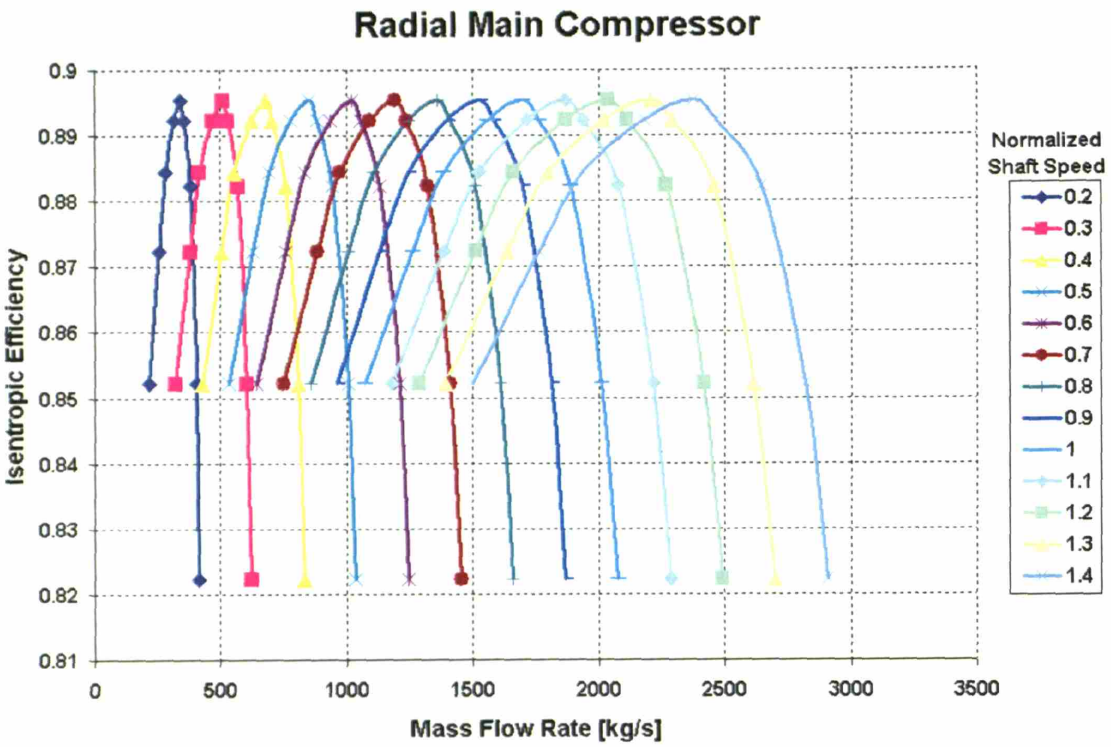

Figure 3-14: Radial Main Compressor Efficiency Map

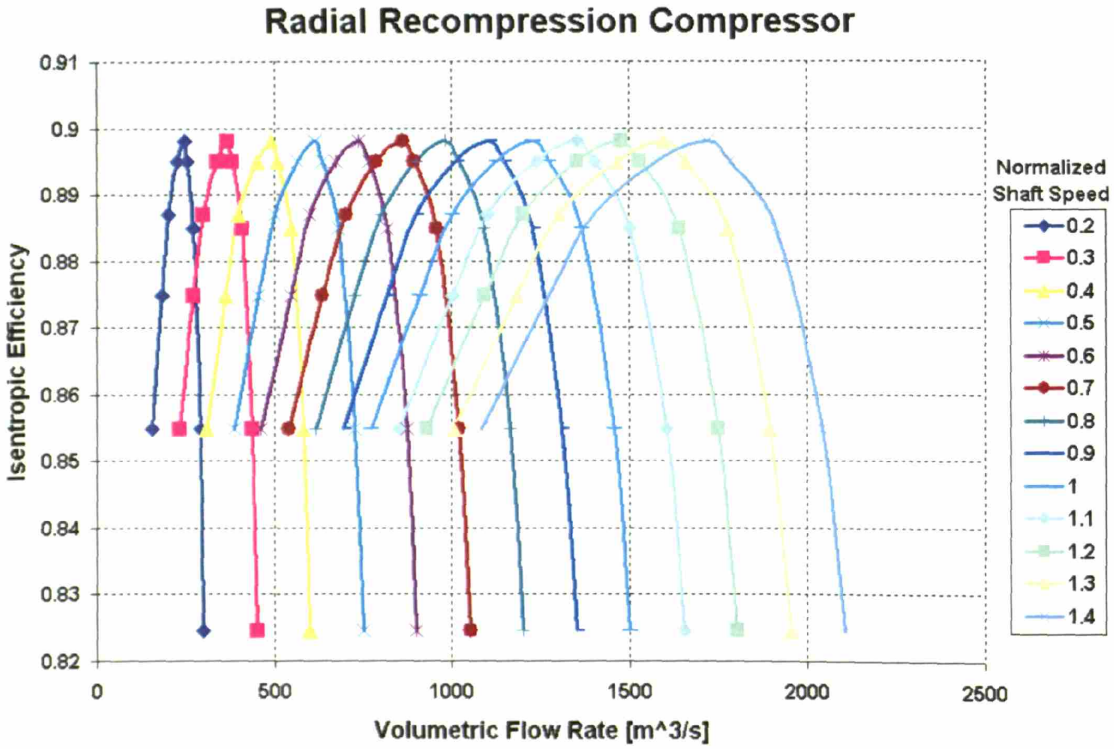

Figure 3-15: Radial Recompression Compressor Efficiency Map

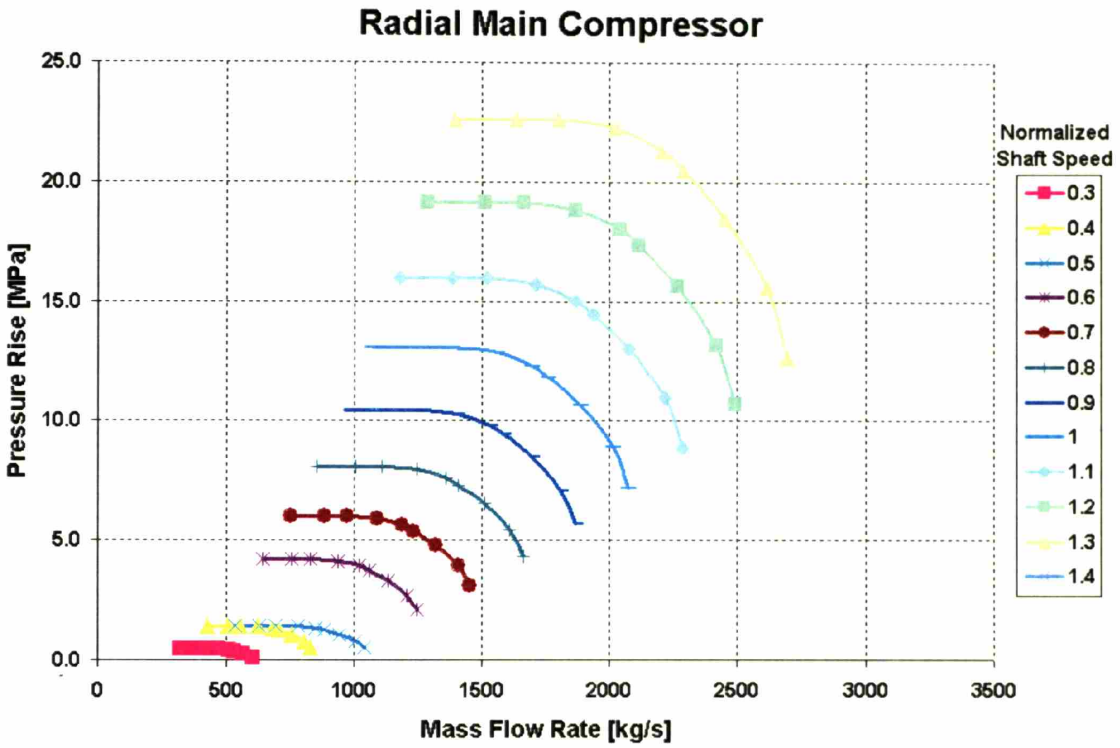

Figure 3-16: Radial Main Compressor Pressure Ratio Map

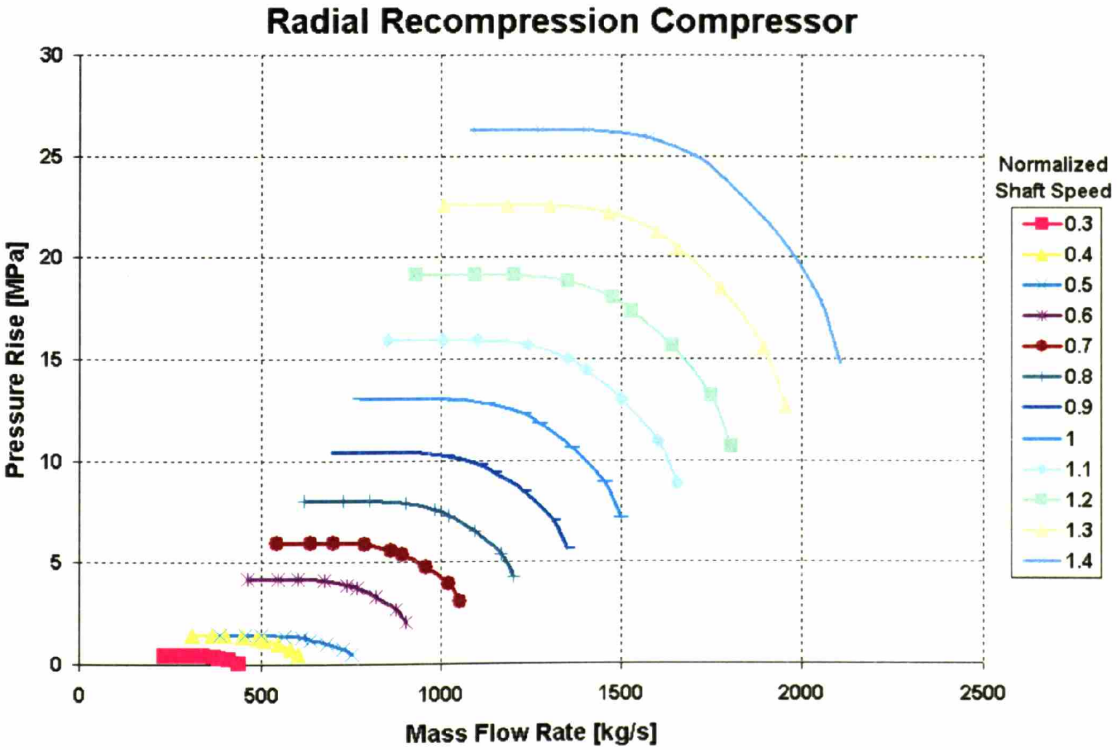

Figure 3-17: Radial Recompression Compressor Pressure Ratio Map

The axial data, shown in Figure 3-18 through Figure 3-23, are based originally upon Wang's report[13], as subsequently modified by Gong[33]. Due to the difficulty caused by highly non-linear fluid properties near the critical point the axial main compressor shown here was designed at 42°C. The axial compressor maps will not be used in the results shown in this work, for reasons addressed later in this section, but they are included for reference.

It should be noted that the original curves showed numerical "noise" that was smoothed before the curves were incorporated into GAS-PASS/CO_2. The noise was concentrated in the axial compressor data points at high shafts speeds, and the absolute values of the noise were quite small (see reference[60]). Removing the noise by smoothing was judged to be more faithful to compressor physics and necessary for proper use in a transient simulation code. It is thought that the noise in the curves stems primarily from insufficiently tight convergence tolerance in the detailed design codes when they are used with non-linear fluid properties[61].

The axial turbine efficiency curves are shown in Figure 3-18. At high shaft speeds (note that the 120% curve visually covers the 100% curve) these curves show a slight increase in efficiency as mass flow rates increase, until the peak efficiency is met, then a rapid decrease. At low shaft speeds these curves show a linearly decreasing efficiency with increasing mass flow rates and a sudden final drop in efficiency. The shaft speed curves operate over a wider mass flow rate range at lower shaft speeds. It is worth noting that if the turbine is operated at the peak efficiency, then small increases in mass flow rate will rapidly drop efficiency and move beyond the known data.

The axial turbine pressure change curves are shown in Figure 3-19 (note that the 120% curve visually covers the 100% curve). These curves show a gently sloping increase in pressure ratio that becomes increasingly steep as mass flow rate increases. At the end of the curve the increase in pressure ratio is nearly straight up suggesting choke. The mass flow rate operating range increases as the shaft speed decreases.

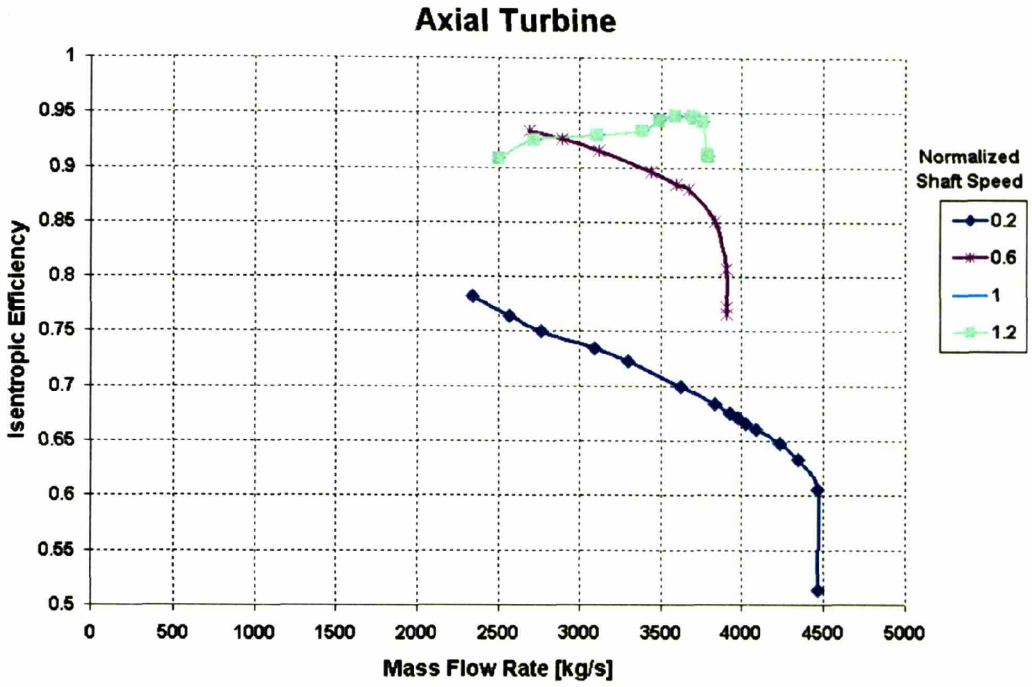

Figure 3-18: Axial Turbine Efficiency Map*

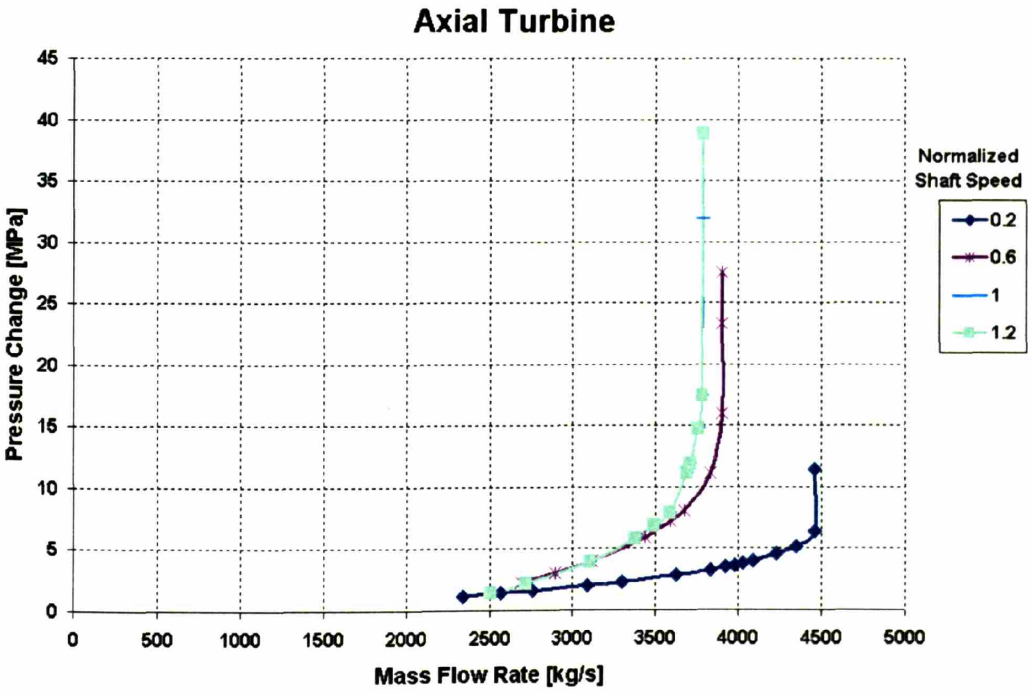

Figure 3-19: Axial Turbine Pressure Ratio Map*

* Note that the axial turbine curves were trimmed to prevent simulation difficulties. The original numerical data created overlapping curves due to the very small pressure ratio differences encountered at higher shaft speeds. The intent was to remain true to the data without introducing confusing oscillations into the dynamic simulation code. The original designer, Dr. Gong, has viewed and agreed with the final result.

3.4.2.1 Reference Axial Compressor Maps

The (unused) axial compressor maps are included for comparison. The axial compressor curves were used in original S-CO_2 recompression cycle simulations. The relatively restricted mass flow rates in the axial versus radial compressor curves caused numerous simulations to reach the predicted choke or stall limits. To alleviate this restriction GAS-PASS/CO_2 adopted radial compressors.

Compared to the radial compressor performance maps, the following generalizations apply:

- The pressure rise of an axial compressor is quasi-linear and steep compared to the gently sloping curve seen in radial machines. Therefore, the pressure ratio of an axial compressor will be quite different from that of a radial compressor at a low flow rate. The radial compressor is typically designed to operate close to its maximum pressure ratio at the design point while the axial compressor can move to significantly higher pressures than available at the design point by decreasing the incoming mass flow rate. This may change part-load control mechanisms – for example throttling will be more restricted with radial compression than axial compression[62].
- Efficiency is of secondary importance during dynamic simulation. While an axial compressor typically features higher steady state efficiency than a radial machine, it is difficult to draw significant generalizations from the maps seen in this chapter if for no other reason than the differences between the axial main and recompression compressor efficiency curve is large.

The axial main compressor efficiency map is shown in Figure 3-20. At low shaft speeds these curves begin near their peak efficiency and rapidly decrease in efficiency as mass flow rates are increased. At high shaft speeds the curves become nearly flat with an efficiency peak towards the middle of the curve. The widest range of mass flow rates is found towards the middle shaft speeds.

The axial recompression compressor efficiency map is shown in Figure 3-21. This map shows similar behavior to the main compressor at low shaft speeds. At high shaft speeds the curves show considerably more curvature than in the main compressor. The efficiency begins near the peak shaft speed, gently slopes to the peak as mass flow rate increases, and gently but increasingly drops off after the peak.

The axial main compressor pressure ratio curves are shown in Figure 3-22. At low mass flow rates these curves are nearly flat but slope downwards with increasing mass flow rates. At high shaft speeds the curves become somewhat steeper but still decrease monotonically as mass flow rate increases. The widest range of mass flow rates is found towards the middle shaft speeds.

The axial recompression compressor pressure ratio curves are shown in Figure 3-23. These curves show similar behavior to the axial main compressor curves at low shaft speeds but have a much steeper slope at high shaft speeds. It is worth noting that the

recompression compressor has a relatively small mass flow rate operating range at high shaft speeds.

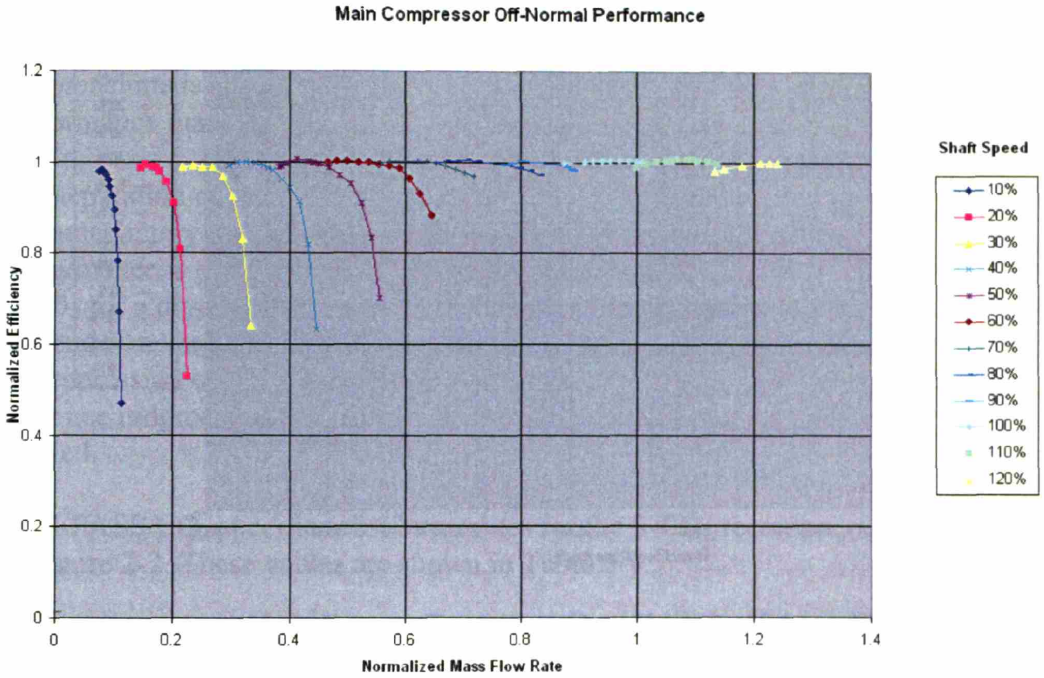

Figure 3-20: Axial Main Compressor Efficiency Map

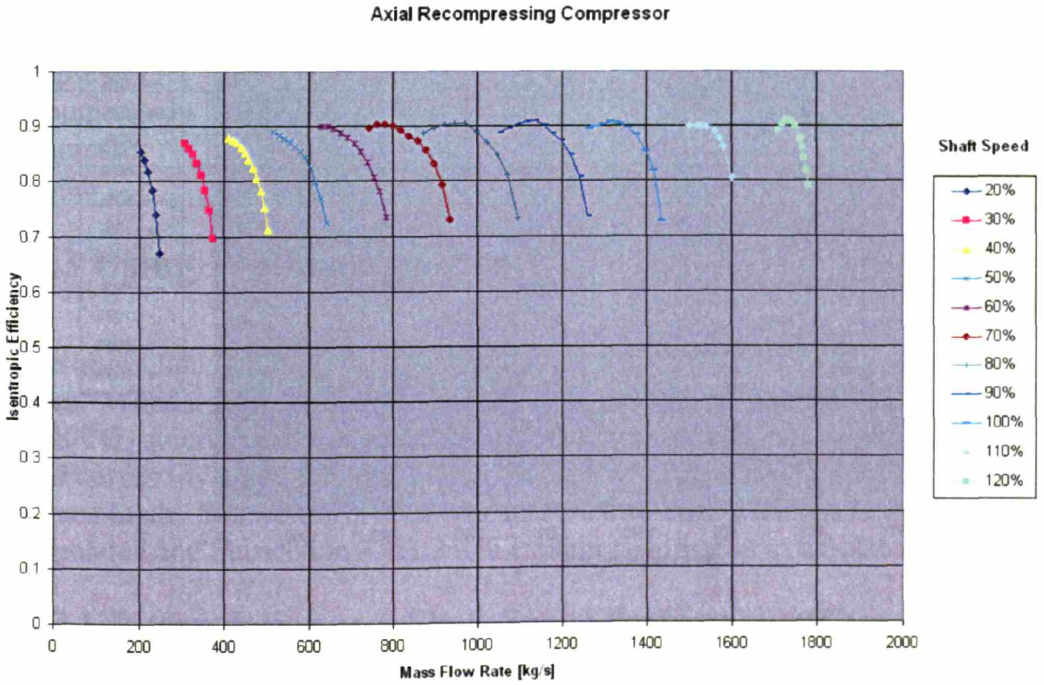

Figure 3-21: Axial Recompression Compressor Efficiency Map

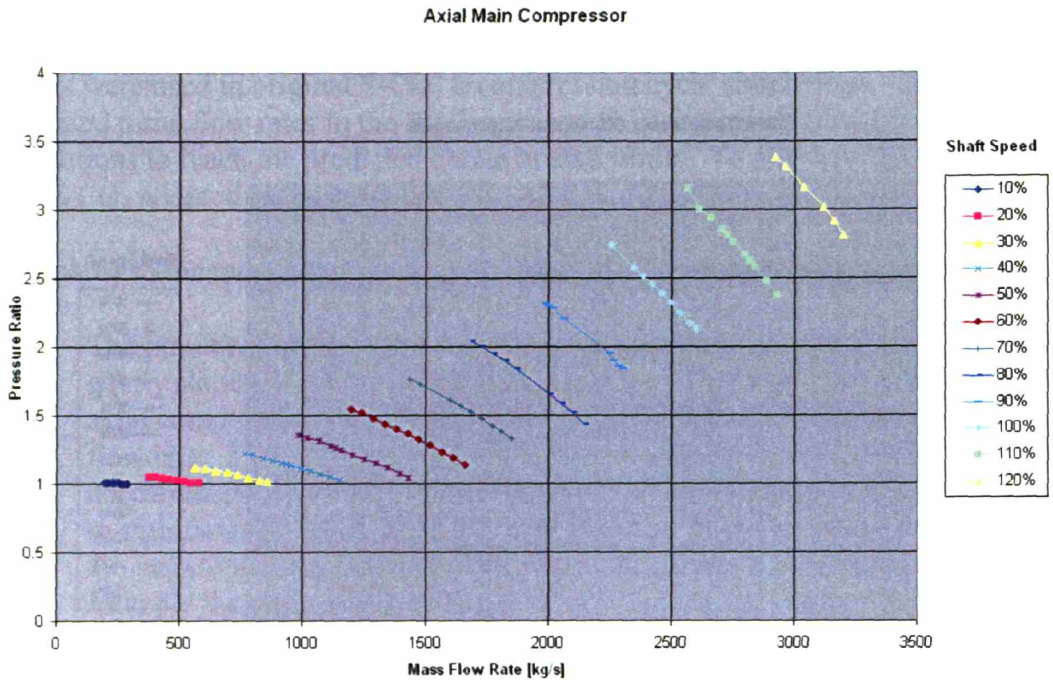

Figure 3-22: Axial Main Compressor Pressure Ratio Map

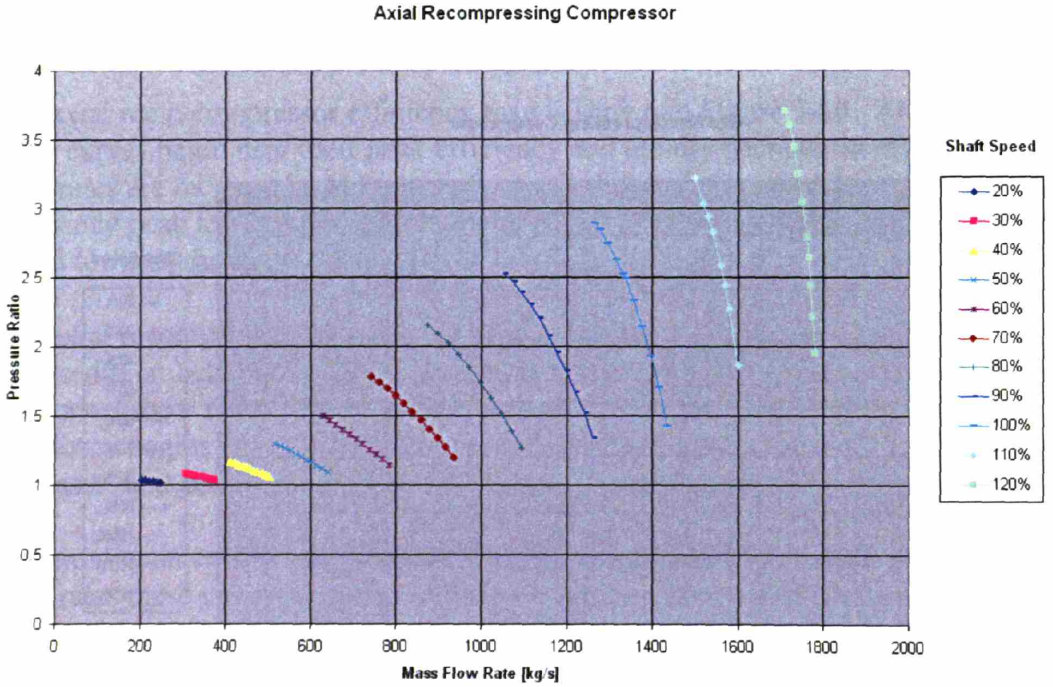

Figure 3-23: Axial Recompression Compressor Pressure Ratio Map

3.4.2.2 Map Normalization

GAS-PASS/CO_2 uses performance maps to specify relative turbomachinery performance – not its absolute value. Each shaft speed curve is normalized to the full power, full flow, and normal rotational speed values used when creating its data (e.g. in the detailed turbomachinery design codes). The absolute value, in the form of a multiplier, for a turbomachine is specified by the user in an input file and then applied to the normalized performance map.

The separation of relative performance from absolute value allows the designer to use turbomachinery that behaves similar to a desired component even if the absolute performance is quite different. For example, a small S-CO_2 radial compressor pumping S-CO_2 for a dry cleaning service pumps only a few kilograms per minute but may respond in a very similar manner to the large main compressor envisioned for the S-CO_2 recompression cycle, which pumps thousands of kilograms per second. The developer must use judgment to determine what turbomachinery performance maps should be applied.

GAS-PASS/CO_2 specifies absolute values for the S-CO_2 recompression cycle as shown in Figure 2-2. These values are shown in Table 3-9.

Table 3-9: GAS-PASS/CO_2 Turbomachinery Design Values

Component	Mass Flow Rate	Shaft Speed	Pressure Ratio	Efficiency
-	[kg/s]	[RPM]	-	-
Main Compressor	1698	3600	2.60	0.895
Recompression Compressor	1229	3600	2.59	0.898
Turbine	2927	3600	2.46	0.945

3.4.3 Using Performance Maps

This sub-section will describe how GAS-PASS/CO_2 uses the normalized shaft speed curves. When a set of turbomachinery data is sent for interpolation from the main GAS-PASS/CO_2 solution process, the turbomachinery code first determines the bounding shaft speed curves (by shaft speed), then interpolates on each curve, and finally interpolates between them. Subsection 3.4.3.1 will analyze how each shaft speed curve is interpolated and Subsection 3.4.3.2 will explain how data is interpolated between curves.

3.4.3.1 Interpolating on a Shaft Speed Performance Curve

Interpolating on shaft speed curves is non-trivial due to the variety of curve shapes encountered in practice. A technique that works well on a radial compressor curve is unlikely to work well on an axial turbine curve without significant modification.

The interpolation method used in this work must also account for significant uncertainty in the current performance maps themselves. For a variety of reasons, which will be addressed within the text, the supplied shaft speed curves exhibit non-physical behavior such as jitter. Due to the importance of these curves in determining cycle performance, these non-physical behaviors are, largely, removed before interpolation. This concern will be largely eliminated as experimental data become available.

GAS-PASS/CO_2 uses a simple but general approach to these problems that arose from numerous attempts at modeling shaft speed curves.

3.4.3.1.1 Monotonic Trimming

The first step in modeling shaft speed curves is removing non-monotonic data from the curves. At the highest pressure ratios, for a given shaft speed, the mass flow rate (the independent variable) may decrease by a fraction of a percent despite the increase in the pressure ratio (the dependent variable) and the power. Having a non-monotonic function would add significant complexity, and removing these points loses little real data.

In all observed cases this phenomenon occurs when the efficiency is decreasing very rapidly, and only at the end of the data set (e.g. a turbine is nearing choke). A representative example is shown in Figure 3-24, where the last data point also decreases on the **X** axis (probably not visually observable) by a fraction of a percent. Aside from the problems of non-monotonic functions this point creates a very steep slope that causes problems in many interpolation methods. Therefore any point at the end of a shaft speed data set that would create a non-monotonic curve is removed.

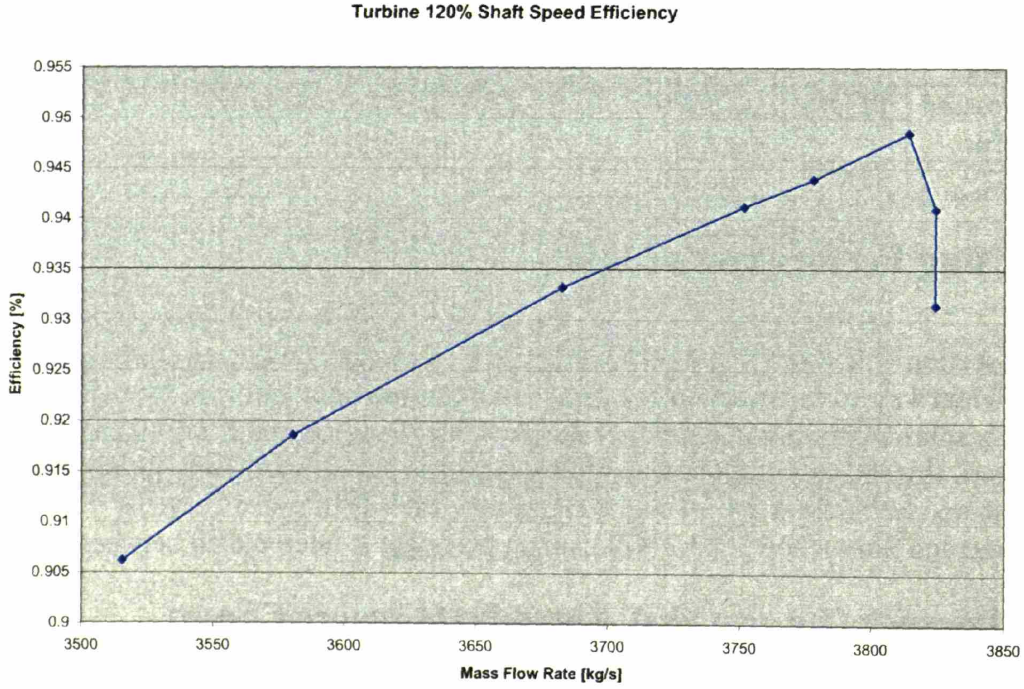

Figure 3-24: S-CO_2 Turbine 120% Shaft Speed Efficiency versus Mass Flow Rate

3.4.3.1.2 Linear Interpolation

Linear interpolation between known points offers the simplest shaft speed curve modeling method and typically performs surprisingly well. Unfortunately, pure linear interpolation also has instant changes in slope due to discontinuous first derivatives at data points, which has the potential to create convergence problems later, aside from being a non-physical phenomenon. When linear interpolation is used this problem is avoided by smoothing the transition between lines.

When linear interpolation is used the first 10% of a line is combined with the previous line to smooth the transition. For example, at 5% of a linear line's length (of the dependent variable) 95% of the independent variable's value comes from the current line and 5% of the independent value comes from the previous spline. The combination process progressively merges the slopes of both curves for the first 10% of a line's length, which creates a visually smooth transition and prevents abrupt slope changes.

Linear interpolation may offer reasonable performance from an absolute error point of view but it will always underestimate points near significant slope changes such as around a peak (a key area of interest). Therefore, it will only be used as a backup method when more advanced methods fail.

3.4.3.1.3 Cubic Spline Interpolation

More advanced interpolation methods may yield better results than linear interpolation. Two properties of the shaft speed curves stand out when picking an interpolation method:

> -every data point is equally accurate (best estimate)
> -all the normalized performance curves (generally) gently curve between each point

These two properties suggest cubic spline interpolation (fitting a polynomial via regression will be addressed later) which exactly models each point and adds curvature between points. Cubic is selected because higher order splines could add unwanted oscillation between points.

Cubic spline interpolation gives a formula which is "smooth in the first derivative, and continuous in the second derivative, both within an interval and at its boundaries."[63] The method creates a cubic function between each consecutive data point that passes exactly through the data point, matches the first derivatives, and has a continuous second derivative. In short, it makes a smooth curved line between each known data point.

Since all the data points are known, only two additional pieces of information are required to solve this system. After some experimentation it was decided that the best general method for setting the end point derivatives is to use a natural spline. Natural splines set the second derivative equal to 0 at the end points which allows the curve to move freely at other points. A code, SPLINE, for this purpose is available[63], very fast (linear, tridiagonal system, *O(N)* operations), and need be run only once. These

equations can then be used to calculate the actual curve values by finding the appropriate position via bisection and solving the cubic equation. This code, SPLINT, is also available[63], very fast, and is called each time a value on a shaft speed curve is desired. Using cubic spline interpolation one may calculate any position along a smooth performance curve with significant accuracy.

An example of cubic spline interpolation is shown in Figure 3-25. This figure shows both linear and cubic spline interpolation for the axial main compressor at shaft speed curve at 90% of the normal shaft speed. The reader may observe that all data points match exactly, there are no wild oscillations in the curve, and that the cubic splines closely match linear interpolation except where the slope changes.

While both methods match most of the curve well, the linear method shows deviation from the cubic spline method when the curve's slope changes direction at the peak. The cubic spline curve more faithfully models expected physics. Real turbomachines show smoothly varying peaks and do not change first derivatives instantly.

Note that the absolute deviation between the curves is small (check the **Y** scale) but from the perspective of using these curves with a Jacobian it is apparent that the linear curve will introduce instantly changing slopes into the solution process. This could prevent solution convergence in the affected regions.

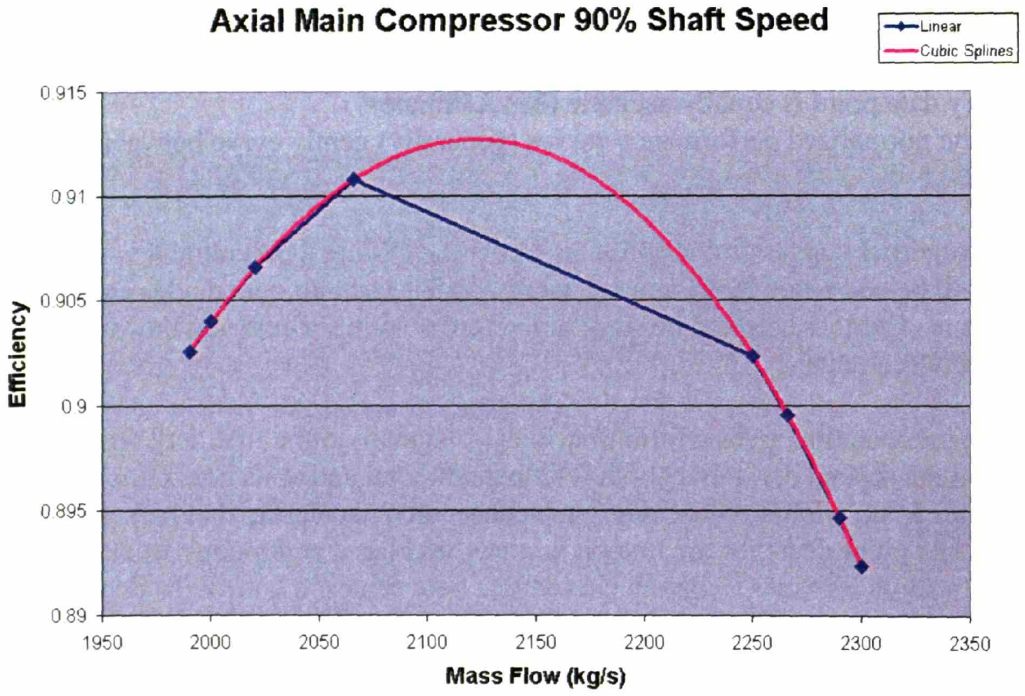

Figure 3-25: Linear and Cubic Spline Interpolation Example

Looking at Figure 3-25 closely one sees that the linear line uses a single slope between mass flow rates 2065.5 and 2250 (kg/s). When the numerical solver enters this region it

will test to see what happens to the system as it varies mass flow rates, pressures, and enthalpies. With linear interpolation it would find that there is only one possible solution (at a given efficiency/pressure ratio) between these mass flow rates. With cubic spline interpolation it would find two possible solutions at different mass flow rates. Thus the smoothly varying slopes of the cubic spline method allow GAS-PASS/CO_2 to use more of, and use more faithfully, the performance curves. This will produce more accurate solutions and allow solutions in places where linear interpolation would not predict one is possible. However, cubic splines present a special challenge: how to handle rapid slope changes.

3.4.3.1.4 Cubic Spline Problems with Rapid Slope Changes

In some shaft speed curves cubic splines oscillate due to extremely large slope changes. For example, in axial turbine efficiency curves the last few data **X** points change little while the last few **Y** points change greatly (due to proximity to choke), producing slopes that cubic splines cannot handle appropriately. The problem is best described with Figure 3-26.

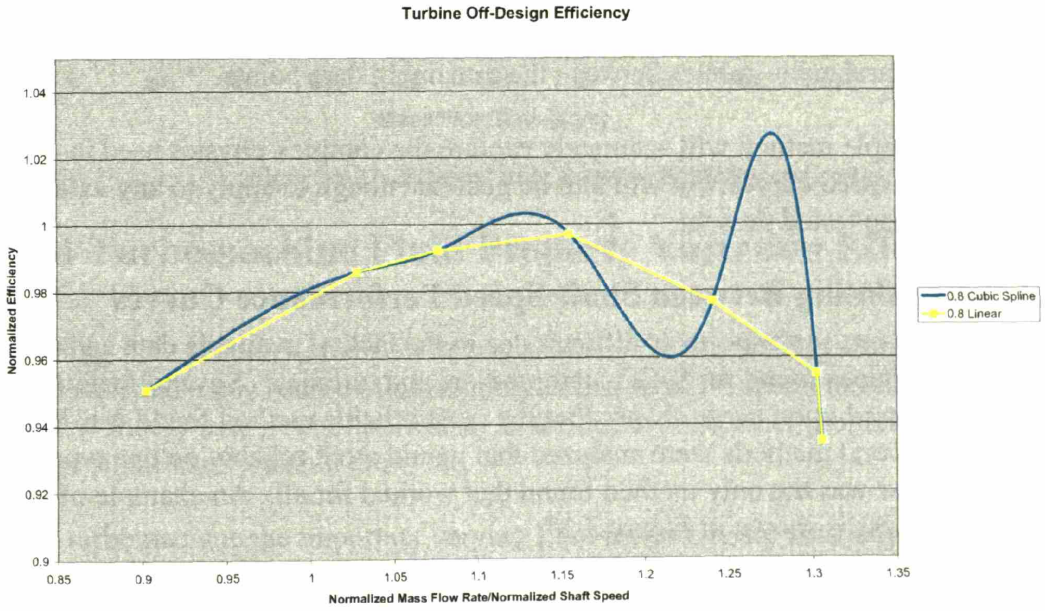

Figure 3-26: Cubic Spline Slope Oscillation

The reader will notice that the last two data points produce a relatively large slope. The last two data points are:

X	Y
1.302256	0.955096
1.305341	0.93484

These points create a linear slope of -6.56 compared to the median slope of the whole curve of -0.088. The large difference between these slopes between consecutive points

creates problems when matching first derivatives and imposing continuous second derivatives with the cubic spline method.

Since this high slope region represents a small part of the **X** range (6% in Figure 3-26) linear interpolation will be used here and cubic spline interpolation will be used over the other 94%.

One could argue that this small region may be neglected without significantly affecting the turbine curve, however this may not be true when it comes to studying extreme transients. It is expected that turbomachinery efficiency will rapidly decrease at certain mass flow rates and shaft speeds, thus this could be a real physical phenomenon that may be needed in dynamic studies.

3.4.3.1.5 Shaft Speed Curve Modeling Summary

In GAS-PASS/CO_2 a shaft speed curve is modeled in a three step process:

1. Remove any (always end) data points that make the curve non-monotonic.
2. If any set of points creates a linear slope that is greater than 4x the median linear slope use linear interpolation here.
3. Create natural cubic splines between the remaining data points.

This relatively simple method will accurately capture the complex physics used in creating the shaft speed curves, but will still be general enough to apply to any axial or radial turbomachine tested thus far.

3.4.3.2 Interpolating Between Shaft Speed Performance Curves

Interpolating between shaft speeds is difficult due to the lack of available data and the variety of curve shapes found for S-CO_2 compressors and turbines. Several methods were attempted based upon curve shapes, but the most reliable method found was linear interpolation. Several methods were analyzed that would work reliably on one type of machine, but linear was the only method found that worked for all. An example of this interpolation process is shown in Figure 3-27.

Figure 3-27 shows a dashed line connecting the 120% shaft speed curve to the 100% shaft speed curve near 1200 kg/s: the 110% curve is included solely for reference and is not used during this example interpolation. If GAS-PASS/CO_2 needed a pressure ratio at 110% shaft speed, but this curve did not exist, then it can interpolate for the desired shaft speed by calculating the pressure rise for both the 100% and 120% curves. In this case the desired point is halfway between the two curves, in terms of shaft speed, thus GAS-PASS/CO_2 calculates the pressure rise halfway between the curves. This is shown as the dotted line in the figure. In the case of the radial recompression compressor, the interpolated point lands directly on the (unused) 110% shaft speed curve.

Note that there are relatively few curves at a given **X** value, thus it is frequently not possible to interpolate on three or more shaft speed curves and fit a function to the resulting data. Linear interpolation will be adopted between shaft speed curves until more turbomachinery performance data are available.

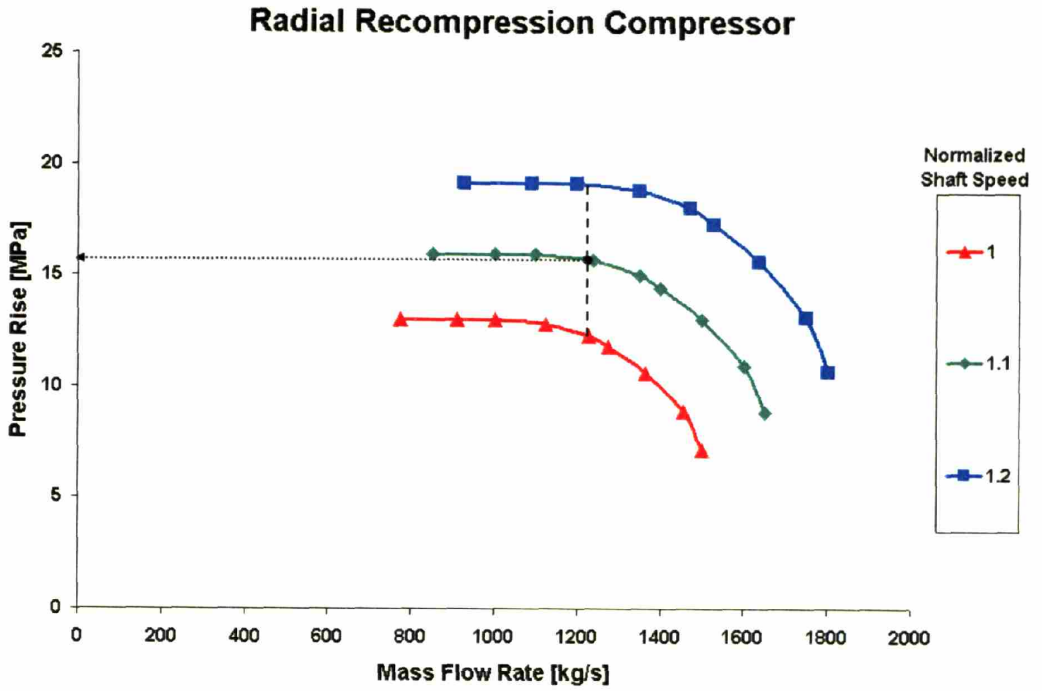

Figure 3-27: Interpolating Between Shaft Speed Curves

3.4.4 Turbomachine Fluid Property Variation Effect

Handling fluid property effects in turbomachinery for the S-CO_2 recompression cycle is non-trivial and a key source of uncertainty in this work. Typical turbomachinery fluid property theory may not be applicable, as the density and other properties of S-CO_2 change significantly within the cycle.

For a turbomachine the important varying fluid properties are viscosity and density. As viscosity changes, the flow profile will change and frictional losses will change, both of which affect turbomachine performance. As density changes the turbomachine's velocity triangle will change, as will the ease of compressing or expanding the fluid, therefore the pressure rise will change. To compute these effects is non-trivial and in general must be done with detailed finite element codes in a computationally expensive manner.

Note that the gas flow velocity triangle between the blade and fluid vector is a critical factor in turbomachinery performance. Changes in these vectors force the gas flow to move in ways not intended and, in extreme cases, can lead to problems such as gas flow separation*. When the shaft speed is fixed (as occurs in power plants for the vast majority of the time, since they must synchronize with the electrical grid frequency) the

* Air flow separation occurs when the incoming fluid vector no longer matches the blade vector to a degree that the blade no longer propels the fluid, aka stall. Depending upon the cause, stall can frequently lead to surge, which is an abrupt gas flow reversal that may damage the machine.

tangential velocity is fixed. Thus changes to the velocity triangle come solely from changes to the incoming fluid velocity. Since a turbomachine typically has a fixed geometry the fluid velocity is proportional to the volumetric flow rate. Thus, for the purposes of this work, changes in volumetric flow rate encompass how fluid property changes affect a turbomachine's velocity triangle. In general, the fluid property relations used in this work are scaled as a function of changes in volumetric flow rate.

In GAS-PASS/CO_2 the accurate and rapid calculation of fluid property effects could eventually be done by allowing interpolation between multiple sets of performance curves. Each set of performance curves will allow interpolation in mass flow rate and shaft speed (i.e. two independent variables). Between performance curve sets one could interpolate in the changing fluid properties such as temperature and pressure (i.e. an additional two independent variables).

Unfortunately, these sets of performance curves are not currently available. As turbomachinery modeling codes evolve to incorporate S-CO_2 and as experimental data are generated these performance curve sets will be incorporated into GAS-PASS/CO_2. Until then fluid property effects will be approximated using the two basic relations outlined in this section, which approximate the fluid property effects in the compressors and turbine.

Near the main compressor the fluid is quite dense (roughly 720 kg/m^3 at the outlet), but the fluid can still be quite sensitive to pressure changes due to its proximity to the critical point (at the compressor inlet), as shown in Figure 3-28. This figure shows the main compressor operating range, with constant density lines on a pressure versus temperature diagram. At the main compressor's outlet the constant density lines have a relatively large spacing compared to the inlet, where the lines converge at the two-phase dome (note that two-phase values are not shown). Similar diagrams are shown for the recompression compressor in Figure 3-29 and for the turbine in Figure 3-30.

Compared to the main compressor the recompression compressor operates at significantly lower densities and farther from the converging constant density lines near the critical point. The turbine operates well above the critical point in a quasi-ideal region (at steady state the turbine fluid's isobaric specific heat changes by less than 5% and γ, the ratio of specific heats, varies by less than 1%). Thus the turbine will be approximated employing ideal gas relations while the compressors will be approximated using incompressible fluid relations.

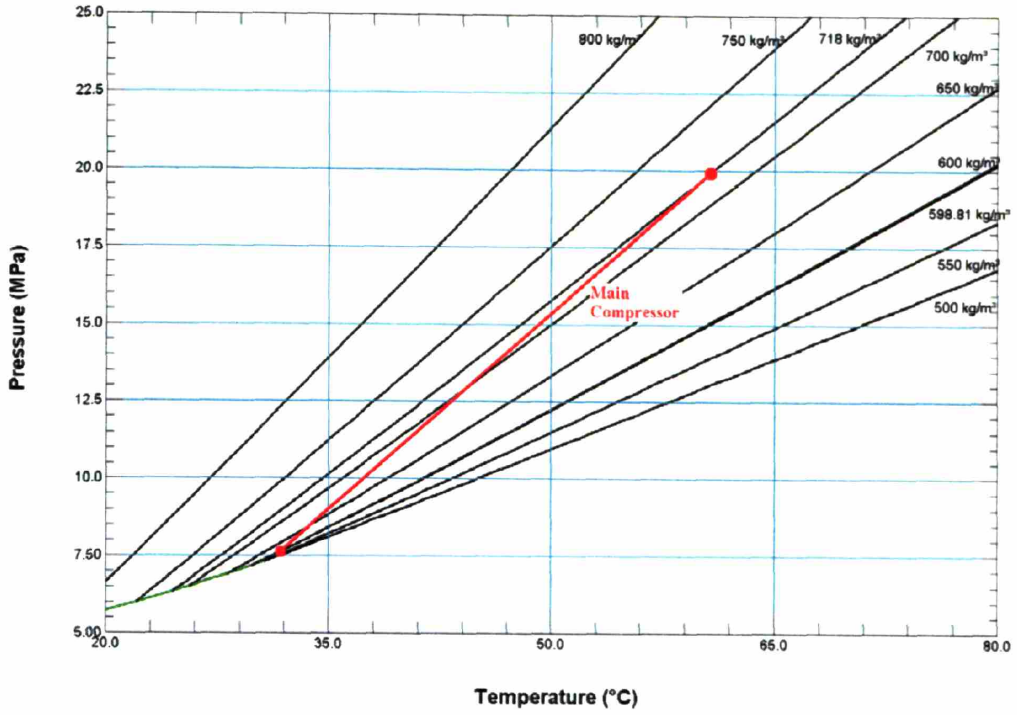

Figure 3-28: Main Compressor Operating Path Showing Pressure vs. Temperature

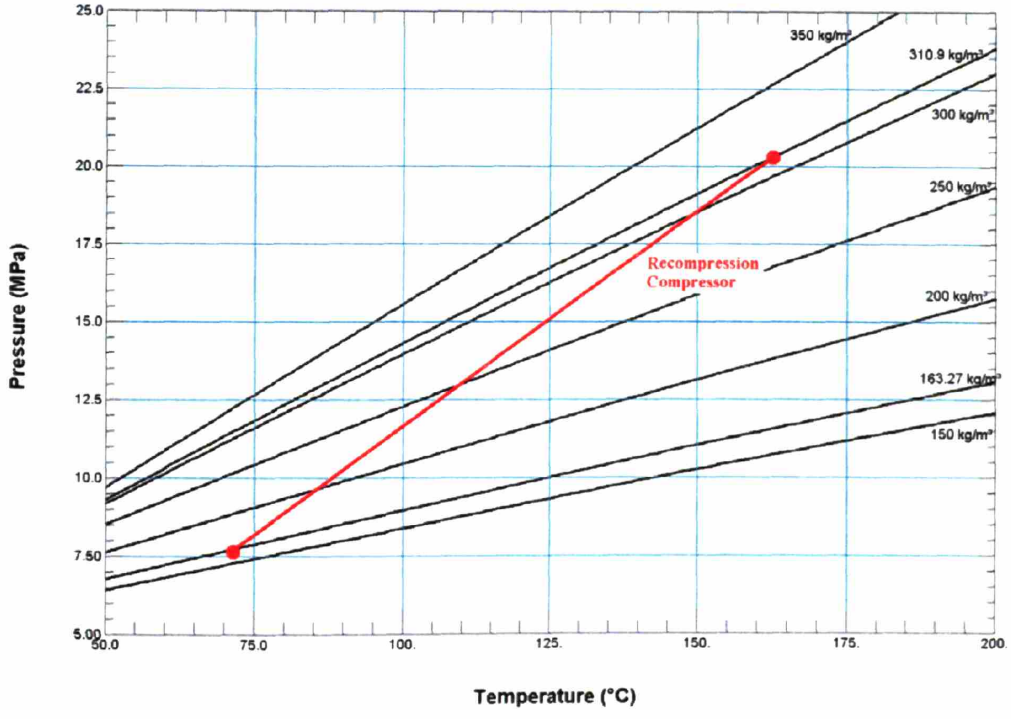

Figure 3-29: Recompression Compressor Operating Path Showing Pressure vs. Temperature

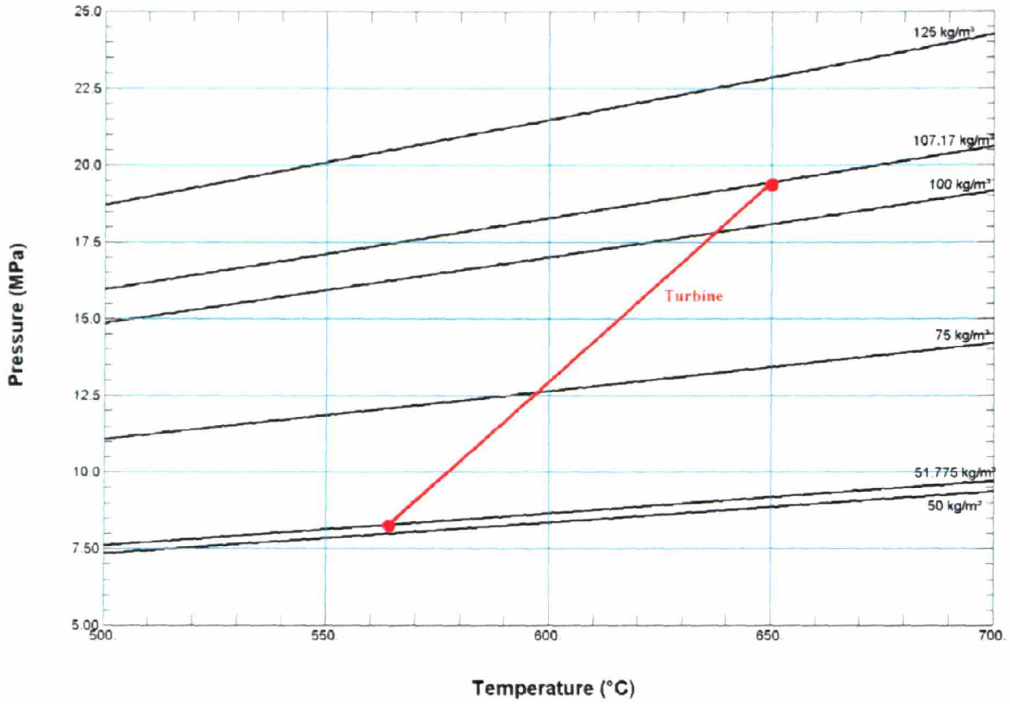

Figure 3-30: Turbine Operating Path Showing Pressure vs. Temperature

3.4.4.1 Ideal Gas Relations

For the turbine in the S-CO_2 recompression cycle the fluid conditions are assumed to be ideal as the turbine inlet conditions are near 650°C and 19.5 MPa, which are far from the rapidly changing property region near the critical point. The compressibility factor* for the steady state turbine is 1.00406 at the inlet and 1.0095 at the outlet. From standard ideal gas theory (see reference[59] section 4.2) one may correct the mass flow rate and shaft speed for changing inlet conditions and then use these "normalizing" values to interpolate on performance maps at the design point fluid conditions.

For ideal gas relations one may "normalize" the properties used for performance map interpolation, in this case mass flow rate and shaft speed, to correct for changing fluid properties[3,34]. The ideal gas correction for mass flow rate is shown in Equation 3-14, which states that as the square root of temperature increases, then mass flow rate increases, and as pressure increases, then mass flow rate decreases†. The normalizing

---

* The compressibility factor, $Z = \frac{P\tilde{V}}{RT}$, is used to determine a fluid's deviation from ideal properties and has a value of one in an ideal gas[60].

† The reader is encouraged to think in terms of volumetric flow rates. Since $\dot{Q} = \frac{\dot{m}}{\rho}$ we can determine first order behavior by density changes or mass flow rate changes.

relation for shaft speed is shown in Equation 3-15 which states that as the square root of temperature increases then the shaft speed increases.

Equation 3-14: Turbine Mass Flow Rate Property Normalization **(3-14)**

$$\dot{m}_{norm} = \dot{m}\frac{\sqrt{T}}{\sqrt{T_{ref}}}\frac{P_{ref}}{P}$$

Equation 3-15: Turbine Shaft Speed Property Normalization **(3-15)**

$$\omega_{norm} = \omega\frac{\sqrt{T}}{\sqrt{T_{ref}}}$$

Note that for ideal gas fluid property effects, the turbine's overall ability to extract work is not affected (as occurs in incompressible fluids). Normalizing inlet properties for performance map use is all that is necessary to correct ideal gas effects.

3.4.4.2 Incompressible Fluid Relations

In the compressors the fluid is very dense and the machines operate like a pump in many respects. The main compressor's steady state compressibility factors are 0.223 at the inlet, and at the outlet 0.455. Note that in the main compressor's behavior may change significantly if there are small changes in fluid properties near the inlet due to the fluid's proximity to the critical point. This is highlighted in Figure 3-31 which shows that, near the main compressor's inlet, the compressibility factor increases significantly and steeply (especially as the temperature approaches the critical temperature) if the pressure dips slightly.

As pressure and temperature increase in the main compressor, the fluid will rapidly move away from the critical point and thus become relatively insensitive to pressure change. Proximity to the critical point is less of an issue for the recompression compressor.

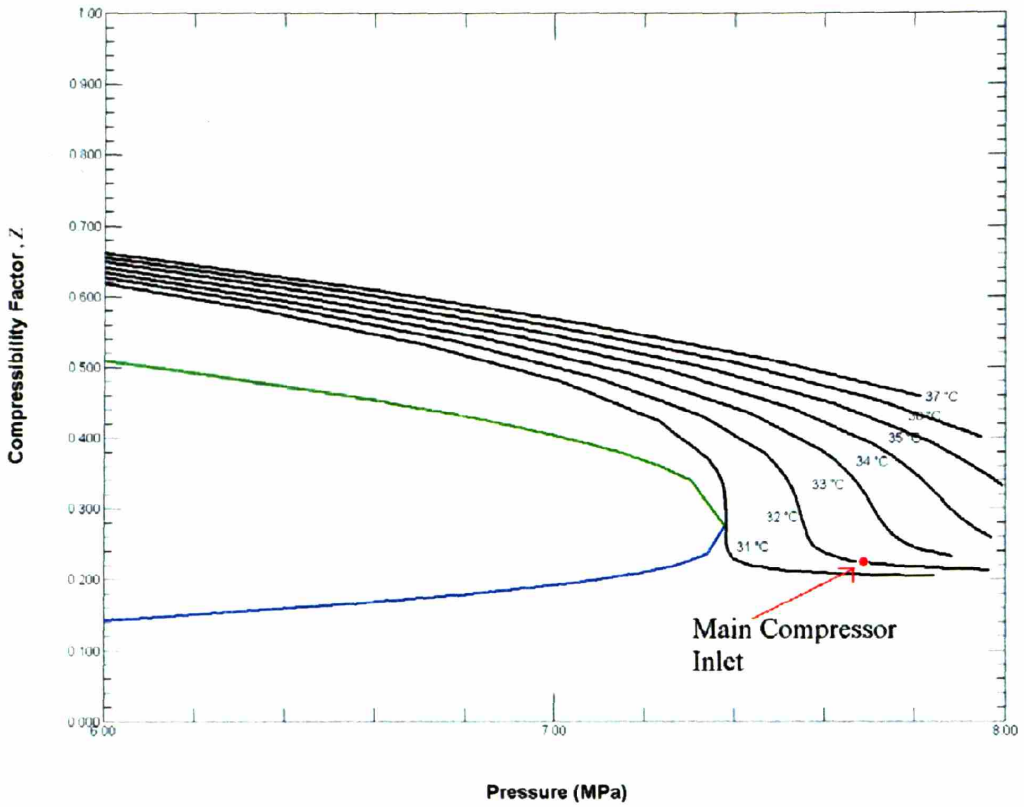

Figure 3-31: Compressibility Factors Near Main Compressor Inlet

The incompressible fluid relations (see reference[59] section 4.3) are described in two sections: the first deals with how to scale the incoming mass flow rate for interpolation on the curves (i.e. where the compressor operates on the curve). The second section details how the compressor's ability to increase pressure changes with changing fluid properties. Compression is highly sensitive to the fluid density, thus a compressor will not only operate on a different part of the curve with a density change but it will experience a change in its ability to increase fluid pressure.

3.4.4.2.1 Mass Flow Rate Normalization

For incompressible flow one may "normalize" the properties used for performance map interpolation, in this case mass flow rate, to correct for changing fluid properties. This normalization process moves along the design point performance curves. The incompressible mass flow rate correction is based upon volumetric flow rates and can be derived from basic relations. Fluid velocity is: $V = \frac{\dot{m}}{\rho A}$ and the volumetric flow rate is: $\dot{Q} = \frac{\dot{m}}{\rho}$, which for a constant flow area is proportional to fluid velocity. Thus to match velocity triangles one need only match volumetric flow rates. For matching volumetric

flow rates $\dot{Q}_1 = \dot{Q}_2$, then $\frac{\dot{m}_2}{\rho_2} = \frac{\dot{m}_1}{\rho_1}$. Therefore, design point performance curves can be used by normalizing the mass flow rate by multiplying by the fluid density ratio as shown in Equation 3-16.

Equation 3-16: Mass Flow Rate Normalization for Compressors **(3-16)**

$$\dot{m}_{norm} = \dot{m}\frac{\rho_{ref}}{\rho}$$

Equation 3-16 states that as density increases the scaled mass flow rate decreases (i.e. the volumetric flow rate goes down as density goes up) which is what one would expect.

3.4.4.2.2 Pressure Ratio Normalization

This section will derive an equation which allows a simple approximation to a compressor's ability to increase pressure, it is based on a reference[64]. Note that only final equations will be labeled.

The first law of thermodynamics for a control volume where shaft and flow work are separated is:

$$dU_{cv} = dH_{in} - dH_{out} + \delta Q - \delta W_{shaft}$$

For a steady state system which is adiabatic with respect to the environment and where work is input:

$$H_{out} - H_{in} = W_{shaft}$$

Separating the enthalpy into internal energy and neglect kinetic energy changes the flow work becomes:

$$U_{out} + P_{out}V_{out} - U_{in} - P_{in}V_{in} = W_{shaft}$$

Assuming that the fluid density is constant with pressure changes*, then:

$$P_{out} - P_{in} = \frac{W_{shaft} - (U_{out} - U_{in})}{V}$$

This equation states that a compressor's pressure rise is proportional to the shaft work minus the energy lost to increasing fluid temperature (viscous forces) which is conceptually what is expected. Dividing both sides by the fluid density times gravity:

$$\frac{P_{out} - P_{in}}{\rho g} = \frac{W_{shaft} - (U_{out} - U_{in})}{V\rho g}$$

* This assumption is not strictly true in the compressors but is not without basis. The compressors operate far from the ideal gas region and the main compressor inlet, in particular, has an extremely low compressibility factor.

The right hand side is also known as actual pump head (h now refers to head not enthalpy – they will not appear in the same equation):

$$\frac{P_{out} - P_{in}}{\rho g} = h_{actual}$$

This can be restated:

$$\Delta P = h_{actual} \rho g$$

This equation expresses the pressure rise as proportional to density. If one further assumes that the actual head term does not change with changing properties then:

$$\Delta P_{ref} = \alpha \rho_{ref}$$

$$\Delta P_2 = \alpha \rho_2$$

Therefore, pressure rise at a new fluid density can be computed with Equation 3-17.

Equation 3-17: Compressor Fluid Property Variation Effect* **(3-17)**

$$\Delta P_2 = \Delta P_{ref} \frac{\rho_2}{\rho_{ref}}$$

Equation 3-17 requires that:

- A steady state exists
- Adiabatic isolation applies
- Gravitational and kinetic energy may be neglected
- Flow is inviscid
- Fluid is incompressible as a result of pressure changes
- Actual head is constant with changing fluid properties

For fluid flow, viscous forces become important when they become significant compared to inertial forces (i.e. when the fluid has a high Reynolds number). Therefore, one may generally approximate a fluid with a high Reynolds number, i.e. turbulent flow, as inviscid (over short flow distances). The S-CO_2 recompression cycle turbomachinery experience highly turbulent flow, therefore this analysis will assume inviscid flow. Furthermore, this only neglects the difference in viscous effects between the design and new fluid properties. Viscous effects are properly accounted for at design fluid conditions.

The assumption of incompressible flow is an approximation*. However, when the S-CO_2 leaves the compressors it has largely stopped increasing in density and is relatively incompressible, especially when compared to an ideal gas system. Furthermore, even within the compressors the fluid is relatively incompressible. Table 3-10 compares the

* In certain cases the main compressor in this work may achieve speeds close to a Mach number and the incompressible assumption is no longer valid. Due to the lack of a simple alternative it will be used, but with reservation, in this work.

density ratios of an incompressible fluid and an ideal gas to S-CO_2 for the main compressor inlet and outlet design conditions. The relative compressibility of the fluids suggests that the S-CO_2 behaves roughly as an incompressible fluid.

Table 3-10: Density Ratios at Main Compressor Operating Conditions

Fluid:	$\rho_{outlet}/\rho_{inlet}$
Incompressible	1
Ideal Gas	2.38
S-CO_2	1.24

Finally, the steady state assumption will be applied solely to the fluid property corrections in the turbomachine performance curves. Typical energy and mass storage effects in the turbomachines will be much smaller and faster than those occurring within the overall cycle, due to these machines' relatively small volumes and masses. The overall plant analysis will continue to account for transient energy and mass storage.

Note that all compressor efficiency changes will be taken care of by using the scaled mass flow rate, shown in Equation 3-16, to move along the shaft speed curve. The efficiency shaft speed curve does not change with fluid property changes in a compressor.

3.4.4.3 Approximating Choke & Stall

Choke and stall are approximated in GAS-PASS/CO_2 as if they occur at the limits of the interpolated performance curves, as seen in Figure 3-14 through Figure 3-19. Generally, these curves show clear behavior (rapidly changing pressure ratios and rapidly lowering efficiencies) that suggests the turbomachine is approaching its limits. In any case, it is undesirable to introduce the possibility of extrapolation beyond the end points considering the numerous uncertainties at this stage of the design process.

During off-design operation fluid properties change, which affects the turbomachine's performance. To approximate this effect on the choke and stall limits each of the performance maps are compared on the basis of volumetric flow rates instead of mass flow rates. This captures the effects of the changing velocity triangle while simplifying the process of checking for choke and stall, and is equivalent to Equation 3-16.

Off-Design Fluid Property Conclusion

The performance of a turbomachine depends not only on the fluid mass flow rate and rotational speed but also upon fluid properties. As fluid temperatures and pressures vary so will turbomachine performance. This section 3.4.4 briefly outlined this problem and how GAS-PASS/CO_2 models fluid properties changes.

Basic fluid property relations assuming ideal gas behavior in the turbine and incompressible fluid behavior in the compressors are used in GAS-PASS/CO_2. While these simple relations cannot account for the all fluid property effects, they should

provide first order behavior, which proves crucial to cycle dynamic and control simulation.

When calculated or experimental data curves are available for a range of fluid conditions, then these simple relations can be replaced by interpolation between known curves. For example, when performance maps for a S-CO_2 main compressor have been generated, if the simulation code desires to estimate the main compressor performance at 31.75°C, then the performance may be interpolated from both the 32°C and 31.5°C maps and the desired value calculated by averaging the results.

3.4.5 Turbomachinery Modeling Section Summary

S-CO_2 turbomachinery performance is complex and, currently, contains considerable uncertainties especially as regards off-design fluid property effects. The Ideal gas approximation allowed GAS-PASS/He to be based on assumptions about turbomachinery performance modeling that cannot be made in GAS-PASS/CO_2, as applied to the S-CO_2 recompression cycle. In particular, the current code must accurately interpolate along individual shaft speed lines, provide a means to interpolate between shaft speed lines, and handle fluid property variation effects.

To summarize, modeling turbomachinery performance maps in GAS-PASS/CO_2 is done in a three step process:

1. Apply fluid property relations to the incoming data to correct for off-normal property effects.
2. Use performance maps:
    a. Normalize incoming data.
    b. Interpolate on both (bounding) shaft speed curves.
        i. Monotonically trim the shaft speed curve.
        ii. Use cubic splines to interpolate between data points where possible. Fall back on linear interpolation where necessary.
    c. Linearly interpolate (by shaft speed) between the values from the bounding shaft speed curves.
    d. Convert normalized data to absolute values.
3. Apply, if necessary, fluid property relations to the resulting value to correct for off-normal property effects.

As experimental data become available, it should be simple to allow GAS-PASS/CO_2 to accurately interpolate between shaft speed lines (as more curves become available) and between temperature and pressure (or density) sets – interpolating on a shaft speed line does not need to change. Until then the methods outlined in this chapter should capture the major physics effects.

3.5 Printed Circuit Heat Exchangers

Modeling printed circuit heat exchanger performance (PCHE) is a key area of research in the S-CO_2 recompression cycle. This cycle is highly recuperated, as shown in Figure 2-3 where, roughly, twice the amount of heat added to the cycle is recuperated. Due to the large variation in carbon dioxide properties (especially near the critical point in the precooler) it is not trivial to accurately calculate PCHE performance.

This section will examine efficient methods to model PCHEs in the S-CO_2 recompression cycle (the reader is referred Section 2.1.4 for brief overview of PCHEs, and Section 2.2.8 for detailed application of these heat exchangers to this cycle). Complete fluid dynamic simulations are computationally expensive, with runtimes of hours to days, and would not be feasible for this work.

Dynamic simulation (for applications such as control studies) may require millions of PCHE simulations, and a much faster solution process is required. Using methods proposed in this section one may solve for heat transfer and other properties of a PCHE very rapidly, thus allowing the accurate assessment of internal PCHE performance while meeting the overall simulation goals.

This section is subdivided into six sub-sections:

1. Section one provides an overview of heat transfer and pressure drop correlations.
2. Section two describes how a PCHE is nodalized and computed efficiently.
3. Section three provides a graphical overview of the steady state performance of the various PCHEs.
4. Section four analyzes the precooler PCHE thermal inertia.
5. Section five derives the transient equations implicitly applied to the PCHEs in GAS-PASS/CO_2.
6. Section six summarizes this chapter.

3.5.1 1-D Straight Channel Correlations

The appropriate correlation to use with S-CO_2 heat exchange is an area of active research at this time. Due to the variety of designs and the lack of published data only semi-circular (current available PCHE designs use semi-circular channels) straight channels will be considered in this chapter.

Converting to wavy channels should be relatively simple as better correlations become available. Ishizuka et. al.[65] have performed initial wavy channel experiments and published results and updated correlation factors. They recommend a simple multiplicative factor for converting straight channel to wavy channel correlations. For now, GAS-PASS/CO_2 will use only straight channel correlations.

3.5.1.1 Applicable Literature

There is a long history of property correlations, but according to Wang and Hihara[66] many turbulent correlations stem from Petukhov et. al.[67]. The Petukhov correlation was improved upon by Gnielinski[68] into what has become a widely applied correlation shown in Equation 3-18 (note that this does not include his recommend entrance length or property corrections). According to Wang and Hihara[66] Gnielinski's constant property correlation has been cited by numerous authorities as the most accurate for constant property turbulent flow in a tube, but was found inaccurate for variable property flows by Olsen[69] and to under-predict heat transfer for conditions near CO_2's critical point by Pitla[70].

Equation 3-18: Gnielinski Constant Property Turbulent Heat Transfer Correlation **(3-18)**

$$Nu = \frac{\xi/8\,(\mathrm{Re}-1000)\mathrm{Pr}}{1+12.7\sqrt{\xi/8}\left(\mathrm{Pr}^{2/3}-1\right)}$$

Note ξ is the drag coefficient.

Wang and Hihara computationally compared several correlations for S-CO_2 PCHE heat transfer and found that that the Gnielinski constant property correlation significantly underestimates the heat transfer compared to other correlations. Wang and Hihara conclude that the more recently developed methods use variable property models and predict higher heat transfer coefficients. They did not compare data with a Gnielinski correlation including property correction.

Oslen[69] also compared several correlations that attempt to correct for supercritical property variations based on experiments. Unfortunately, he concluded that no correlations "were found to adequately predict the measurements over the entire range of experimental parameters." The Gnielinski constant property correlation was found to consistently under-predict heat transfer, and fixes to account for property variation were not entirely successful. It should be noted that Olsen used the correlations to predict integral heat transfer (i.e. only based upon inlet and outlet conditions) and did not attempt to apply these correlations in a nodalized fashion. However, it is likely that even if the Gnielinski constant property correlation was applied in a nodalized fashion it would under-predict the true heat transfer.

Pitla[70] experimentally analyzed and numerically simulated conditions quite similar to those found in the present cycle's precooler. This is a key area of uncertainty, because when CO_2 approaches its critical point (as happens in the precooler in this cycle) fluid properties change rapidly and significantly. Pitla also proposed a new correlation that is significantly more accurate than Gnielinski or the other compared correlations, but comes with the cost of knowing the wall conditions. Pitla states:

> By studying the flow in the near-wall region it was observed that the superficial profiles of the velocity and the temperature look very similar to

constant property turbulent flows. However, upon close examination it was seen that the velocity and temperature law of the wall that can be derived for constant property flows is not valid here.[70]

Thus, it appears that heat transfer correlations may require a wall temperature effect to become accurate for carbon dioxide near the critical region.

For laminar flow Hesselgreaves (2001)[71] recommends Equation 3-19 for our conditions.

Equation 3-19: Laminar Heat Transfer Correlation **(3-19)**

$$Nu = 4.089$$

Hesselgreaves further recommends a set of tabular data from Shah and Bhatti (1987)[72] for the laminar thermal entrance length effect, which will be linearly interpolated in practice. This data is plotted in Figure 3-32.

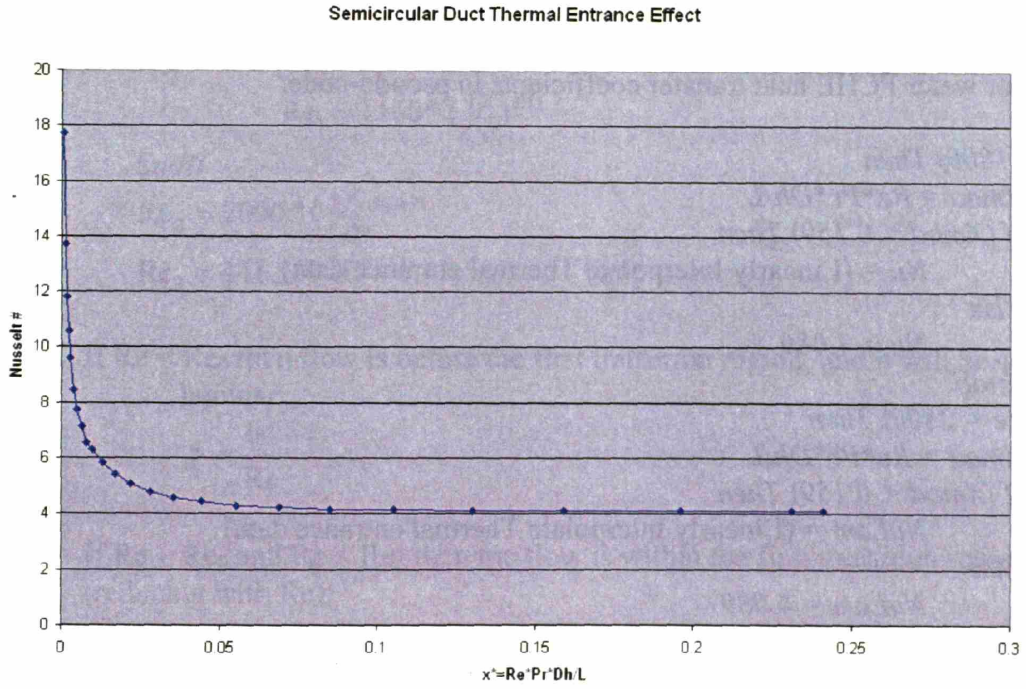

Figure 3-32: Semi-circular Tube Laminar Thermal Entrance Length

3.5.1.2 Straight Channel Heat Transfer Correlation

The method presented here is slightly modified from a code developed by Dostal[14]. It is presented here in an abbreviated form, with basic computer logic and loop constructs for brevity and clarity.

There are few accurate correlations or data for smooth, semi-circular S-CO_2 heat transfer. While the Pitla[70] correlation holds the promise of significant accuracy, its use of wall

temperature within the correlation seriously complicates transient equation expression and numerical solver convergence. It will not be adopted in this work for those reasons.

Therefore, the simple and typically conservative Gnielinski correlation will be adopted. The Gnielinski correlation shown in Equation 3-18, with entrance length correction, will be used for turbulent flow in water and CO_2, since it is simple, experimentally based, widely used, and a recommended correlation that includes entrance length effects.

For laminar fluid flow in CO_2 and water the Hesselgreaves' recommendations will be followed, including interpolating tabular data for the entrance length effects.

Finally, a transition region will be used to create a smooth change from laminar to turbulent correlations. Since the turbulent correlation begins at 2300, a transition region was chosen to range from 500 above and below the transition point i.e. $1800 < Re < 2800$. This region will simply use linear interpolation to create a smooth transition between the laminar and turbulent Nusselt numbers to calculate the heat transfer coefficient.

These correlations are modular and simple to change if desired. To summarize findings, for CO_2 or water PCHE heat transfer coefficients in pseudo-code:

If (Re < 1800) Then
    *Xmod = Re*Pr*Dh/L*
    If (Xmod < 0.159) Then
        Nu = (Linearly Interpolate Thermal entrance data)
    Else
        Nu = 4.089
    Endif
ElseIf (Re < 2800) Then
    *Xmod = Re*Pr*Dh/L*
    If (Xmod < 0.159) Then
        NuLam = (Linearly Interpolate Thermal entrance data)
    Else
        NuLam = 4.089
    Endif

    $f=(1.8*LOG10(2800)-1.5)^{-2} / 4$
    $NuTurb = f/2*((2800-1000) * Pr / (1 + 12.7 * (f/2)^{0.5} * (Pr^{2/3}-1)$
    $NuTurb=NuTurb*(1+(d/L)^{2/3}$

    *Nu = (Re – 1800)/(2800-1800) * (NuTurb – NuLam) + NuLam*
Else
    $f=(1.8*LOG10(2800)-1.5)^{-2} / 4$
    $NuTurb = f/2*((2800-1000) * Pr / (1 + 12.7 * (f/2)^{0.5} * (Pr^{2/3}-1)$
    $NuTurb=NuTurb*(1+(d/L)^{2/3}$
Endif

3.5.1.3 Straight Channel Pressure Drop

The method presented here is taken directly from code originally created by Hejzlar and used by Dostal[14], and is presented here solely for completeness. The approach is based upon Idelchik[73]. It is shown in an abbreviated form with basic computer logic and loop constructs for brevity and clarity.

The heat transfer coefficient will also be calculated as a function of Reynolds Number and tube smoothness. The Reynolds Number flow transition points depend upon tube smoothness. The relative smoothness is the ratio of deviation peak size to tube diameter:

$$\delta_{rel} = \frac{\delta}{D}$$

- The Reynolds Number transition points are:

If $\delta_{rel} < 0.007$ *Then*

$$\mathrm{Re}_0 = 2000$$

$$\mathrm{Re}_1 = 2000$$

ElseIf $\delta_{rel} \geq 0.007$ *Then*

$$\mathrm{Re}_0 = 754 e^{0.0065/\delta}$$

$$\mathrm{Re}_1 = 1160 * (1/\delta)^{0.11}$$

EndIf

$$\mathrm{Re}_2 = 2090 * (1/\delta)^{0.0635}$$

$$\mathrm{Re}_3 = 441.19 * \delta^{-1.1772}$$

- If $\mathrm{Re} < \mathrm{Re}_0$ then flow is before the first transition region, and it will be considered laminar:

$$f = \frac{64}{\mathrm{Re}}$$

- If $\mathrm{Re} > \mathrm{Re}_0$ and $\mathrm{Re} < \mathrm{Re}_1$ then the flow is within the first transition region (reducing with Re):

If $\delta_{rel} < 0.007$ *Then*

$$f = 0.032 + 3.895 * 10^{-7} * (\mathrm{Re} - 2000)$$

Else

$$f = 4.4 * \mathrm{Re}^{-0.595} * e^{-0.00275/\delta}$$

EndIf

- If $\mathrm{Re} > \mathrm{Re}_1$ and $\mathrm{Re} < \mathrm{Re}_2$ then the flow is within the second transition region (increasing with Re):

$$f = 0.11 * \left(\delta_{rel} + 68/\mathrm{Re}_2 \right)^{0.25}$$

Do

$$f_n = \left(\frac{1}{2 * \log_{10}\left(\frac{2.51}{\mathrm{Re}_2 \sqrt{f}} + \frac{\delta_{rel}}{3.7} \right)} \right)^2$$

If $ABS\left(\frac{f_n - f}{f_n} \right) < 0.01$ *Then*

$f = f_n$

Exit Loop

EndIf

$f = f_n$

EndDo Loop

If $(\delta_{rel} < 0.007)$ *Then*

$f_1 = 0.032$

$f_2 = f$

Else

$f_1 = 0.0758 - \frac{0.0109}{\delta}$

$f_2 = f$

EndIf

$f = (f_2 - f_1) * e^{-(0.0017*(\mathrm{Re}_2 - \mathrm{Re}))^2} + f_1$

- If $\mathrm{Re} > \mathrm{Re}_2$ and $\mathrm{Re} < \mathrm{Re}_3$ then the flow is within the third region (decreasing with Re):

$$f = 0.11 * \left(\delta + \frac{68}{\mathrm{Re}} \right)^{0.25}$$

Loop2: Do

$$f_n = \left(\frac{1}{2 * \log_{10}\left(\frac{2.51}{\mathrm{Re}\sqrt{f}} + \frac{\delta_{rel}}{3.7} \right)} \right)^2$$

If $ABS\left(\frac{f_n - f}{f_n} \right) < 0.01$ *Then*

$f = f_n$

Exit Loop2

EndIf

$f = f_n$

EndDo Loop2

- If Re > Re_3 then the flow is highly developed (independent of Reynolds Number):

$$f = 0.11 * \left(\delta_{rel} + 68/\mathrm{Re}_3 \right)^{0.25}$$

Loop3: Do

$$f_n = \left(\frac{1}{2 * \log_{10}\left(\frac{2.51}{\mathrm{Re}_3 \sqrt{f}} + \frac{\delta_{rel}}{3.7} \right)} \right)^2$$

$$If\ ABS\left(\frac{f_n - f}{f_n} \right) < 0.01\ Then$$

$f = f_n$

Exit Loop3

EndIf

$f = f_n$

EndDo Loop3

Once the friction factor has been calculated it is applied as follows:

$$\Delta P_{node} = f_{node} \frac{\Delta X_{node}}{D_{eq-node}} \frac{G_{node}^{\ 2}}{2 * \rho_{node}}$$

Note that G_{node} is the mass flux.

3.5.1.4 Correlation Section Summary

This section has presented a quick one-dimensional method to calculate heat transfer and pressure drop within a straight channel printed circuit heat exchanger using supercritical carbon dioxide or water. This method should be useful for applications that require repeated and rapid analysis, such as dynamic simulation, until more accurate correlations become available.

3.5.2 Computational Application

Computationally modeling a S-CO_2 PCHE provides many opportunities for efficiency that should be realized. While runtime may not be a primary consideration in a steady state analysis, any transient simulation will typically require thousands to millions of the individual evaluations (e.g. fluid properties, heat transfer coefficient, and friction factor)

occurring in a steady state code, therefore making computational efficiency very important.

This section will provide an overview of the highlights of efficient PCHE modeling, including simplifying a PCHE to a single axial channel, solving in enthalpy space, averaging in nodes, using nodal memory, and avoiding 2 nested iteration loops.

3.5.2.1 Using a Single Nodalized Axial Channel

One may take advantage of the regularity in a PCHE's channels by assuming it to be adiabatic to the environment and knowing that there is (typically) a one to one correspondence between hot and cold channels, as shown in Figure 2-8. This allows the whole PCHE to be reduced to single hot and cold channels, as shown in Figure 3-33. This approach was followed by Dostal[14].

The user may solve these single channels with a one-dimensional (1D) code by assuming that the conditions within a channel are uniform at any given distance into the PCHE. Although this is a significant assumption, the S-CO_2 flow is typically turbulent, a typical channel diameter is 2 mm and therefore small, and the heat transfer has been found to be insensitive to this assumption[74].

In the one-dimensional quick up the PCHE is axially divided into small sections. By using small enough sections one may assume that properties are constant (within a section) and it becomes relatively simple to arrive at a solution. An example of splitting up a PCHE axially and averaging fluid properties is shown in Figure 3-34.

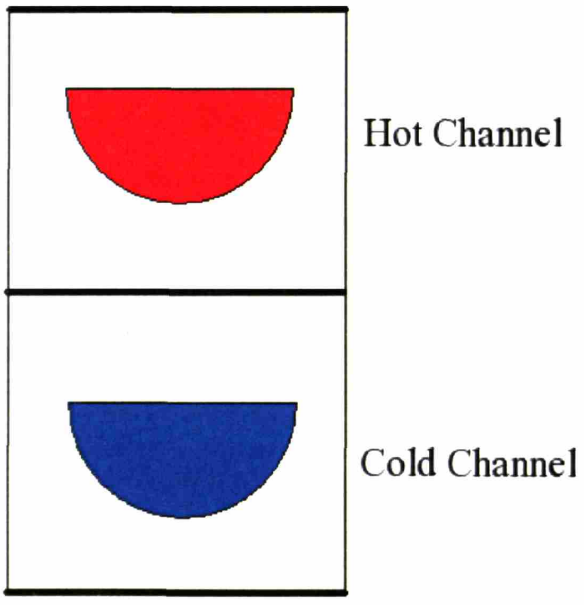

Figure 3-33: PCHE Single Channel Unit Cell Model

Note that only the outlet values of pressure, enthalpy, and mass flow rate, and mass and energy storage are used in the overall solution code. This fits with the overall GAS-PASS solution process of separating detailed component treatment from the actual system root finding.

Similar methods for one-dimensional straight channel printed circuit heat exchanger (PCHE) design codes were previously developed by Dostal[14], which inspired this expanded approach.

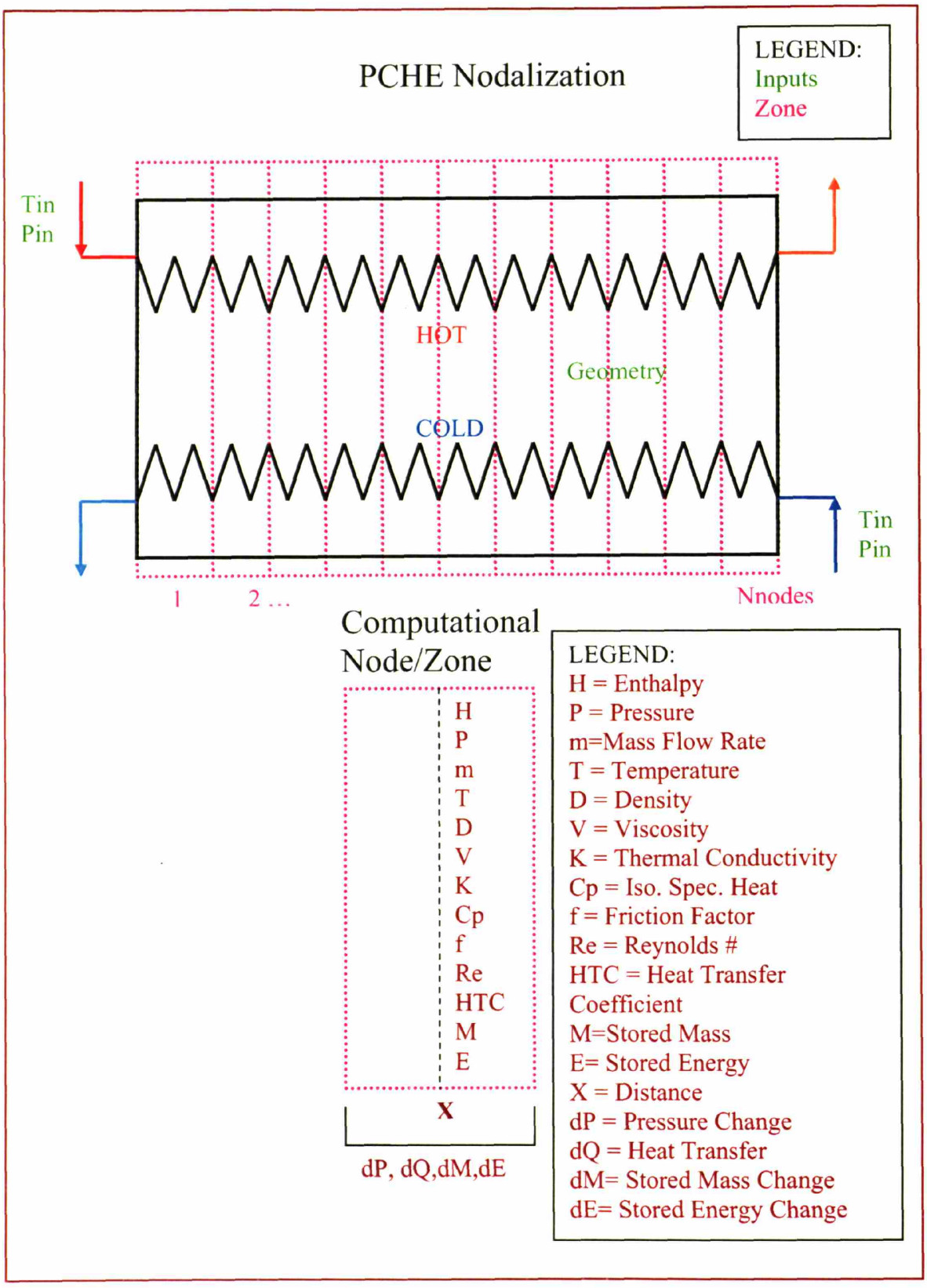

Figure 3-34: PCHE Computation Method

3.5.2.2 Solving in Enthalpy Space

The typical designer thinks in terms of temperature and pressure, but it is far more advantageous to calculate in enthalpy and pressure, especially in the S-CO_2 cycle. Where temperature is highly non-linear and relatively rarely used in typical solution code thermodynamic equations, enthalpy is frequently linear and shows up in most solution equations (see *Appendix* A: GAS-PASS/CO2 Equations).

The precooler clearly shows the advantage of calculating in enthalpy versus temperature space. Figure 3-35 shows the steady state precooler temperature profile. While the water temperature profile is relatively linear, the CO_2 profile drops rapidly to a nearly asymptotic limit. Any numerical approach will encounter difficulty in predicting the appropriate CO_2 temperature, even when many nodes are used, thus requiring numerous evaluations to achieve an accurate solution.

Figure 3-36 shows the enthalpy profile of the precooler in the steady state. This profile shows nearly linear behavior for both the water and the CO_2. Simple linear estimation will provide a relatively accurate enthalpy guess even on the first try. Furthermore, this benefit will extend to subsequent iterations, since each guess will be more accurate for a linear profile than for a non-linear one.

Figure 3-37 is included to show the reader that pressure is relatively linear in a PCHE as well. It shows the pressure profile in the precooler during the steady state.

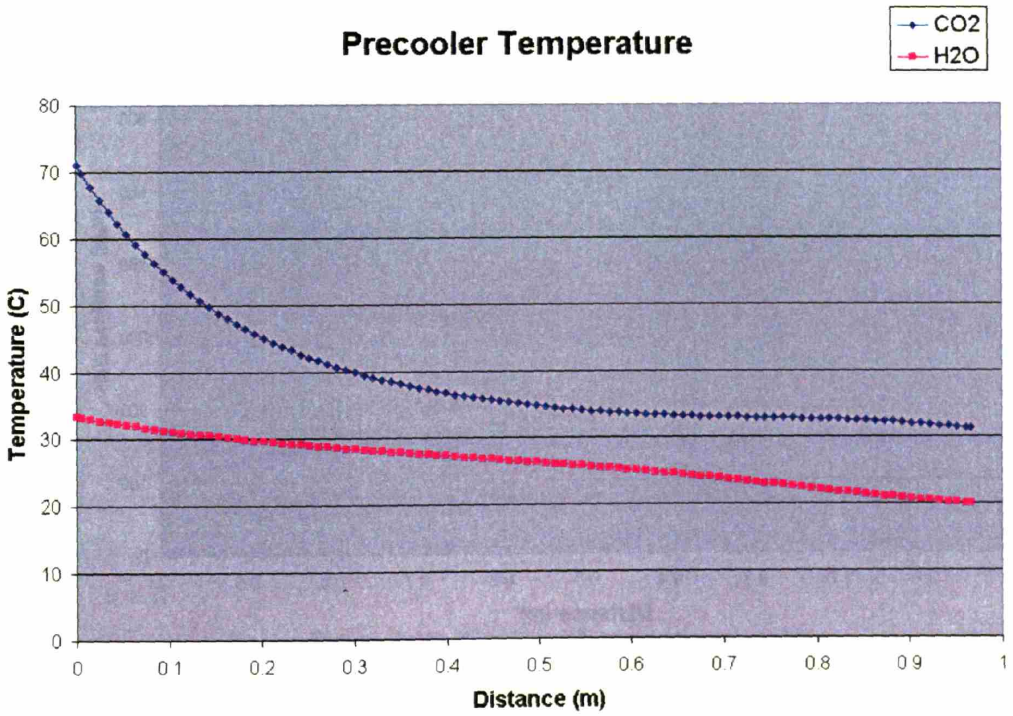

Figure 3-35: Precooler Temperature Profile

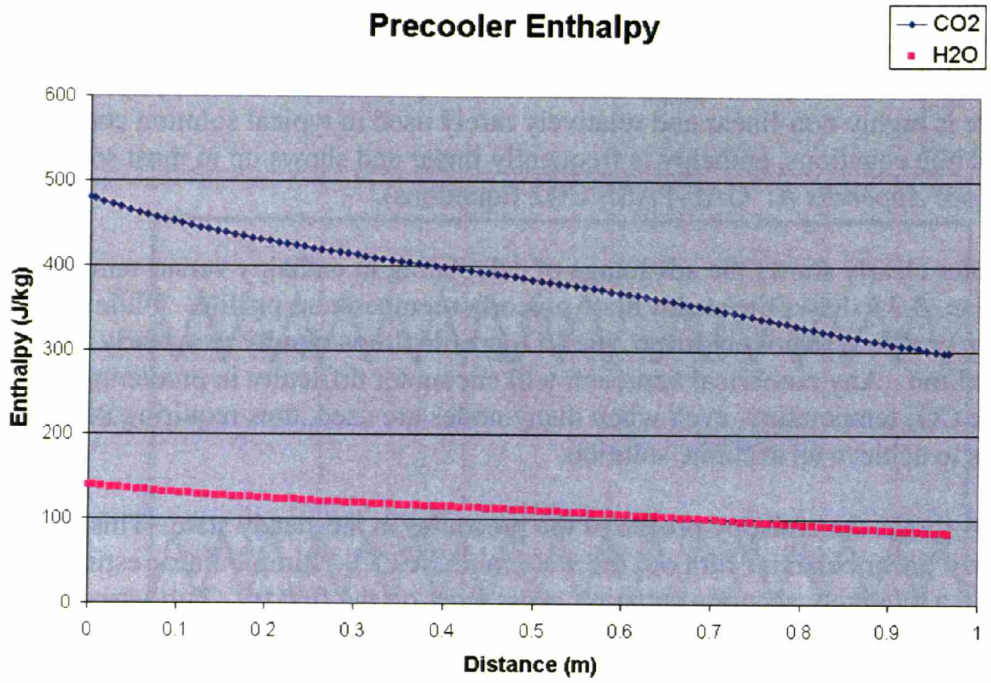

Figure 3-36: Precooler Enthalpy Profile

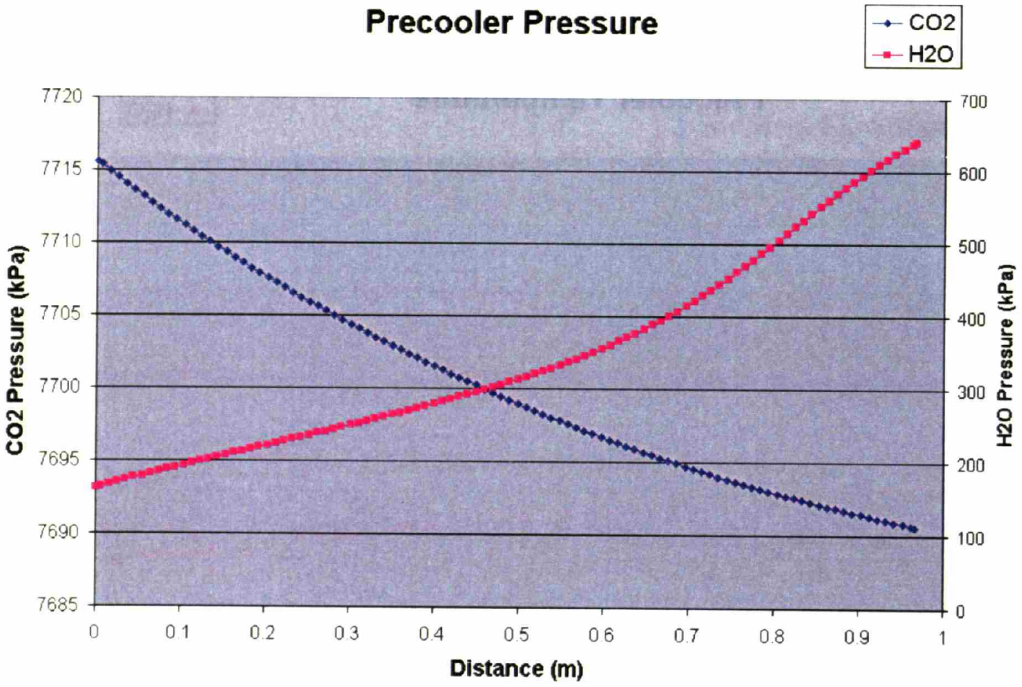

Figure 3-37: Precooler Pressure Profile

It is also important to note that one may greatly decrease the non-linearity of a solution process by solving in enthalpy instead of temperature. If most of the solution equations are in enthalpy (as are typical representations of the first law) and one is solving in temperature, then this does a great disservice to the solver. While ideal gas enthalpy converts proportionally to temperature, S-CO_2 converts highly non-linearly.

Recall Figure 2-7 which shows the steady state operating region of the main compressor (shaded) on an enthalpy and pressure graph. Incoming and outgoing pressure and temperature lines are shown as well. The reader need only glance at the graph to see that small changes in enthalpy can produce relatively large changes in pressure and temperature. Therefore, any solution process that attempts to convert between temperature and enthalpy will need to be highly accurate *solely* because of the property conversion process.

This sensitivity can be clearly seen by comparing the GAS-PASS/CO_2 Jacobians of the S-CO_2 recompression cycle solved in temperature and enthalpy space. Figure 3-38 shows the original Jacobian when the system was solved in temperature. Large peaks suggest that small changes in the solution variables produce large changes in the solution equations. Figure 3-39 shows a later GAS-PASS/CO_2 Jacobian whose primary change is solving the system in enthalpy and pressure instead of temperature and pressure. The reader will note that there are many fewer peaks, that are much smaller in magnitude.

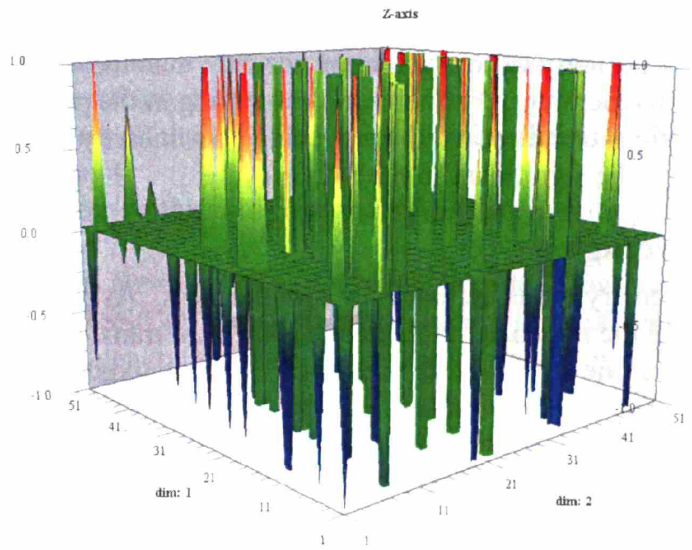

Figure 3-38: Gas-Pass Temperature Jacobian

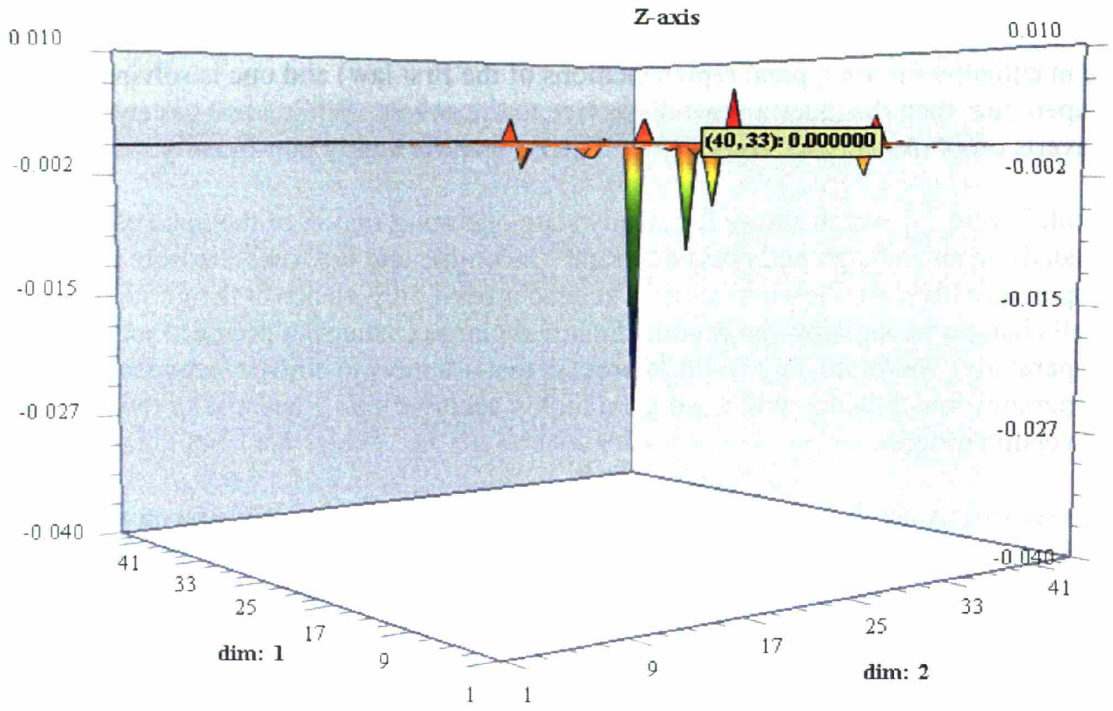

Figure 3-39: Gas-Pass Enthalpy Jacobian (note the expanded vertical scale)

In conclusion, one may take advantage of the linear behavior of enthalpy and pressure even in S-CO_2 PCHEs to accurately predict fluid properties. This linearity will allow each guess of a fluid property to be much more accurate than those offered by a non-linear property like temperature. Furthermore, by solving in the primary variables used in the solution equations one may avoid introducing non-linearity solely from property conversion, which can be significant in the S-CO_2 cycle.

3.5.2.3 Nodal Averaging

This section is elementary but is included for completeness. As previously mentioned, the primary output of the nodalized PCHE code is the heat transfer and pressure drop in each node. Assuming one starts a node with a guess of the node's heat transfer, pressure drop, and mass flow rate it is important to choose an appropriate position within the node to evaluate the guesses. The position in the node determines the enthalpy and pressure at which the correlations will be evaluated.

The appropriate position in the node is where "average" values are found. Choosing any other position will introduce an inherent bias in the correlation inputs which will make it more difficult for the node to converge, thereby requiring more iterations or more nodes. By choosing enthalpy and pressure (which vary linearly) as the state variables the average values in a node are likely to be at the midpoint. This assumption is applied in the present work.

3.5.2.4 Node Memory

One may significantly speed-up the calculation of PCHE performance by remembering past nodal values such as enthalpy, pressure, and heat transfer (a more complete list is shown in Figure 3-34). Initial guesses of PCHE properties and performance are likely to be quite crude and require many iterations to converge accurately. Correspondingly, past solutions are likely to be quite similar (and not infrequently identical) to current solutions, therefore likely providing a good initial guess. In practice this was observed to speed runtime by nearly an order of magnitude despite using a relatively sophisticated initial performance guess.

However, the reader is warned that memory updating* should not be done during system Jacobian evaluation. Having PCHE nodes start with different values during each step of the Jacobian calculation will almost surely introduce a significant error in the Jacobian that may prevent root finding: a problem that was observed. GAS-PASS/CO_2 updates the PCHE node memory the first time a new time step is evaluated (but before the numerical solver is called or Jacobian calculated) and then holds the memory values for the initial guess constant until the next time step.

3.5.2.5 Avoiding Nested Iteration Loops

Typically, a PCHE will be calculated from the fluid inlets to outlets. For a counter-flow heat exchanger a standalone code will require a four step iterative process:

1. Starting with total heat transfer and pressure drop guesses, move to one end of the heat exchanger (in this example the hot fluid inlet/cold fluid outlet) and iteratively solve for each node's pressure drop, heat transfer, and mass flow rate.
2. Evaluate the error on the overall pressure drop guess to obtain cold side inlet pressure and iteratively refine it.
3. Evaluate the error on the cold flow inlet enthalpy (heat transfer guess) and iteratively refine it.
4. Evaluate the error on the cold flow mass flow rate and iteratively refine it.

Thus four iterative loops are required in a standalone code. However, in an integrated plant code like GAS-PASS/CO_2 it may not be necessary to use the final three loops. GAS-PASS/CO_2 uses a general non-linear numerical solver which does not distinguish variables by such things as component inputs and outputs – every variable is simply a knob to twist until the equations are satisfied. Therefore, one does not need to supply a PCHE within GAS-PASS/CO_2 with fluid inlet or outlet conditions.

One could, and GAS-PASS/CO_2 does, supply a PCHE with fluid properties at a single end of the (counter-flow) heat exchanger. Since GAS-PASS/CO_2 is only providing a guess of the inputs to check the outputs (to see if the system equations are satisfied) there is no reason to solve for outlets instead of one outlet and one inlet – they are both system variables.

---

* In this work node memory refers to using the last converged solution as the initial estimate for the solution currently sought.

By solving from one end of the PCHE, GAS-PASS/CO_2 does not need the three outer loops required of a standalone code and therefore should calculate PCHE performance at least one order of magnitude faster than it would by evaluating from the fluid inlets. A flowchart showing the steady state calculation process (using constant mass flow rates) is shown in Figure 3-40.

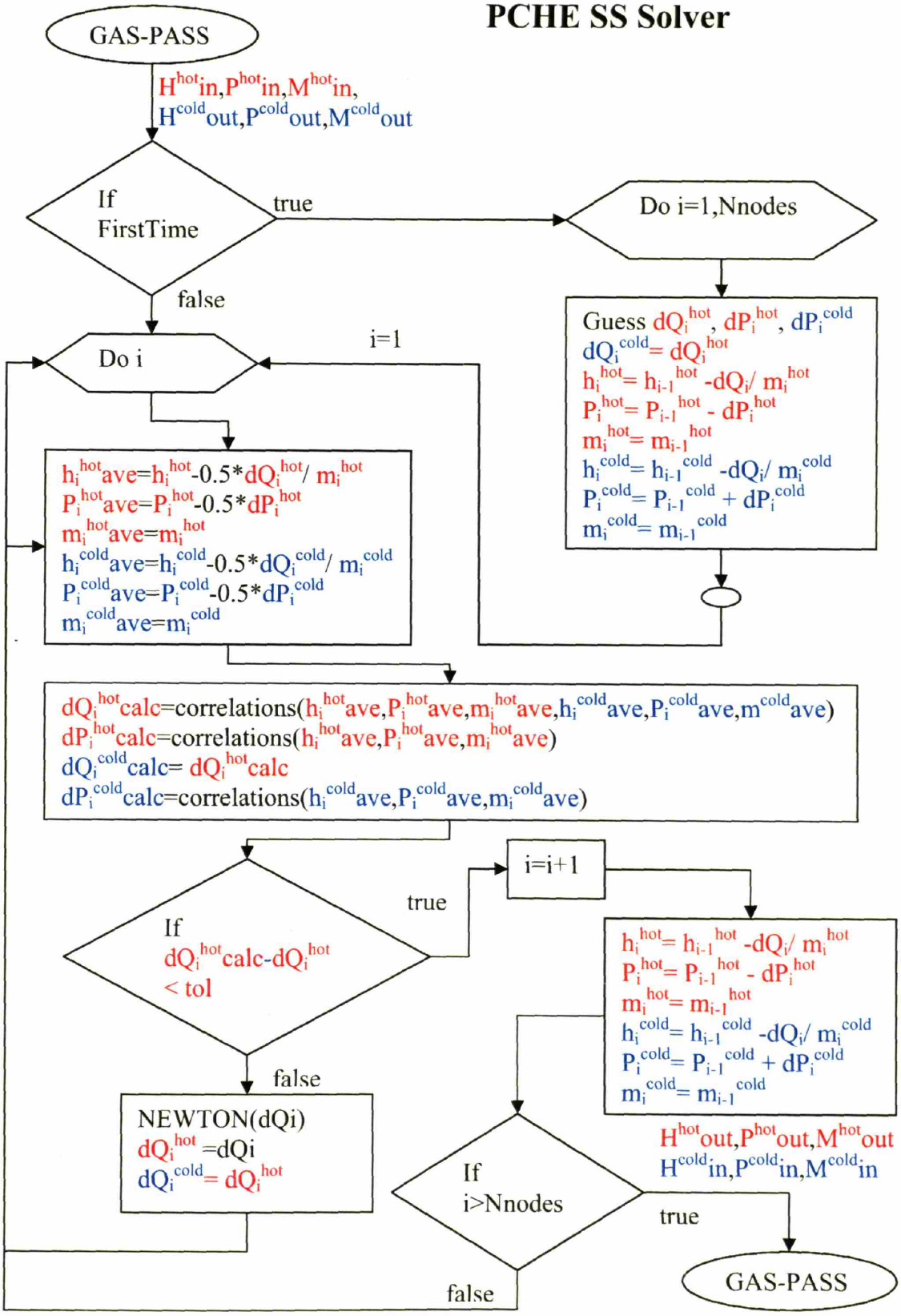

Figure 3-40: PHCE SS Code Flow Chart

3.5.2.6 Computation Section Conclusion

One may use a careful understanding of the problem to greatly speed the calculation of PCHE performance. Examples of the estimated speed-ups due to the various factors are noted subsequently.

Note that the user should determine the appropriate number of nodes to use in the PCHEs via experimentation. A representative experiment is shown in Figure 3-41. This figure shows the percentage error on calculated power in various components when the GAS-PASS/CO_2 code is run with different numbers of nodes in the steady state. For this graph, the correct solution is assumed to be the 10 node case.

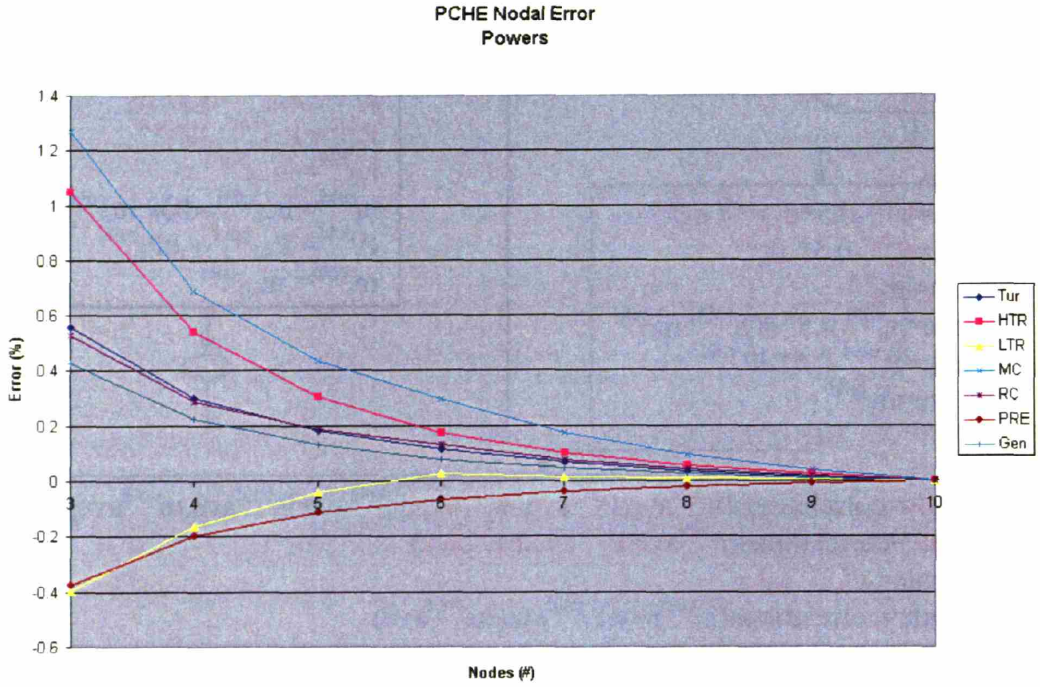

Figure 3-41: PCHE Node Induced Error in GAS-PASS

Starting with the axial 1D nodalized code outline in Section 3.5.2.1:

1. Using enthalpy instead of temperature and calculating at the node midpoint instead of at the beginning of the node allows one to reduce the number of computational nodes from approximately 40 to approximately 2 for the same accuracy, therefore a 20 fold speed-up.
2. Using node memory to speed-up PCHE calculations decreases runtime about 10x.
3. Avoiding the outer two iteration loops speeds up the PCHE calculation by about 50x.
4. Avoiding unnecessary PCHE solutions (see Section 3.6.3.4), especially during Jacobian calculation, speeds the solution process by about another order of magnitude.

Thus we have sped up the PCHE calculation by roughly a factor of 10^5 without any loss in accuracy. Since the PCHE is, by far, the most computationally demanding component

in GAS-PASS/CO_2, the overall code runtime is proportional to the PCHE sub module runtime.

Furthermore, if one counts the greater linearity of solving a S-CO_2 system where variables are in the same property as is commonly used in solution equations (enthalpy instead of temperature) then we can probably add at least another order of magnitude in speed-up compared to the original GAS-PASS/He, which solved in temperature and pressure. This suggests that GAS-PASS/CO_2 may run 6 orders of magnitude faster than might otherwise take place, by simply adopting already-simplified standalone codes.

3.5.3 Steady State PCHE Results

This section shows the performance of S-CO_2 recompression cycle PCHEs in both steady state and several anticipated transient conditions. The conditions are meant to provide an overview of possible performance during plant operation. All cases are for the 650°C turbine inlet temperature design.

3.5.3.1 Precooler Heat Exchanger Performance

The precooler has hot S-CO_2 coming into the precooler and being cooled by liquid water that is external to the thermodynamic cycle. It is the only heat sink for the recompression cycle.

Several cases were computed:

- Normal/steady state (CO_2 inlet pressure = 7.69 MPa)
- CO_2 inlet pressure = 8 MPa
- CO_2 inlet pressure = 7.5 MPa

In all cases the inlet CO_2 temperature was varied between 40°C and 100°C (nominal is 70.953°C). The water stream conditions were not changed. Highlights of these runs are shown in Figure 3-42 through Figure 3-45. Note that the Reynolds numbers in the precooler are turbulent and generally range between 45,000 at the inlet and 15,000 at the (colder) outlet.

The plots suggest several generalizations. CO_2 in the precooler features an isobaric specific heat peak (which is sometimes referred to as the pseudo-critical peak) that moves within the PCHE with temperature and pressure. Lower temperatures and higher pressures move the peak towards the CO_2 inlet and vice versa.

The operating pressure largely determines the height of the isobaric specific heat peak. As the pressure approaches the critical pressure (the critical point occurs at 30.978 °C, 7.3773 MPa[25]) the peak magnitude increases rapidly, and vice versa. The CO_2 heat transfer coefficient shows peaks similar to that of the isobaric specific heat. Its behavior is significantly affected by the isobaric specific heat profile and will show related behavior.

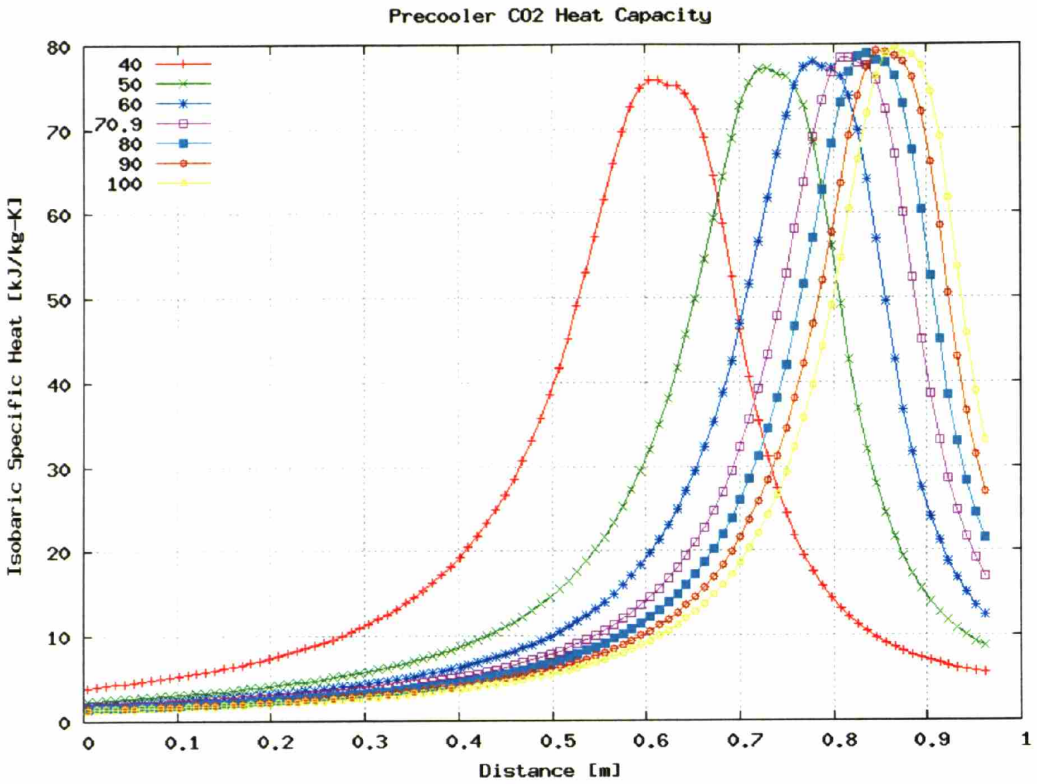

Figure 3-42: Precooler CO_2 Isobaric Specific Heat Capacity

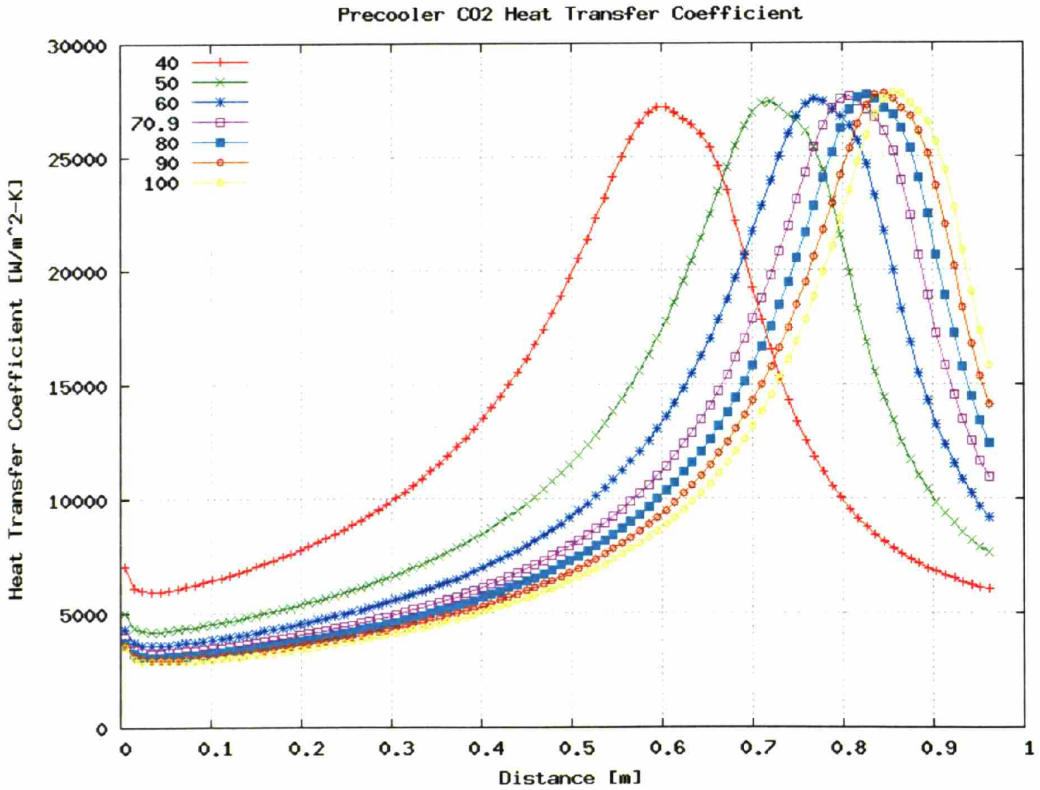

Figure 3-43: Precooler CO_2 Heat Transfer Coefficients

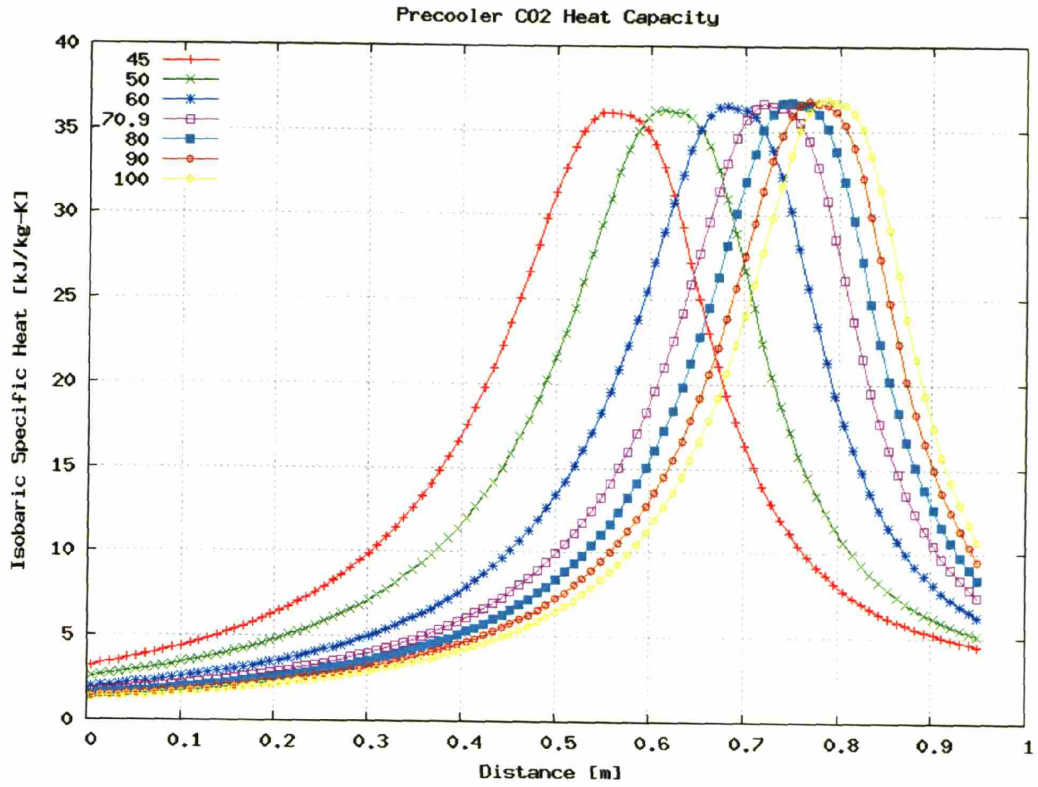

Figure 3-44: Precooler CO_2 Isobaric Specific Heat Capacity with Pin=8MPa

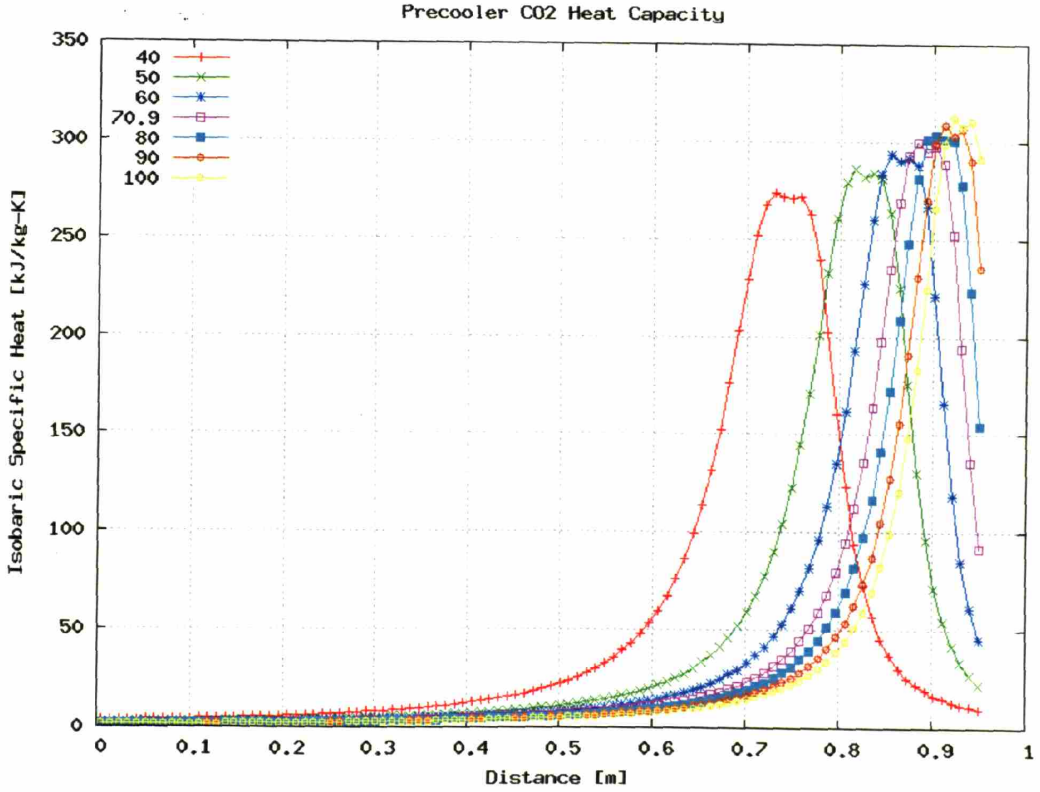

Figure 3-45: Precooler CO_2 Isobaric Specific Heat Capacity with Pin=7.5MPa

3.5.3.2 Low Temperature Recuperator Performance

The low temperature recuperator has hot S-CO_2 at the full mass flow rate being cooled by cold S-CO_2 at approximately 60% of the full CO_2 flow rate. The cold side flow split avoids a recuperator pinch point that would significantly decrease cycle efficiency.

Cases were run at steady state values, except that the cold inlet CO_2 temperature was varied between 45°C and 90°C (nominal is 60.9°C). Highlights of these runs are shown in Figure 3-46 and Figure 3-47. The figure legends list temperatures next to both the hot and cold fluids to identify the case that was run. In all cases the cold fluid temperature was varied while the hot fluid stream was unchanged (except for the effects of the cold stream). All pressures and mass flow rates were kept at design values.

The Reynolds number on the hot side of the low temperature recuperator are turbulent and range between 30,000 at the inlet and slightly increase to 40,000 at the outlet. The cold side of the low temperature recuperator begins with Reynolds numbers which approach the transition region as temperature fall. At 45°C the inlet Reynolds number is about 5,500 but rises to over 10,000 by 90°C. In all cases observed the outlet Reynolds number approaches 15,000 on the cold side.

Figure 3-46 shows that the hot side heat transfer coefficients begin in the same position and then drop rapidly initially (due to entrance effects) and later gradually spread out as different amounts of heat are transferred in the different cases. As more heat is transferred the heat transfer coefficient increases.

The cold side heat transfer coefficients have nearly the same value at the cold fluid outlet (distance 0) and the cold inlet (distance 0, where entrance effects dominate) but vary in between. Around distance 1.2 meters the colder fluid inlet temperatures show a peak due to changes in isobaric specific heat. It is clear from Figure 3-47 that the isobaric specific heats of the CO_2 differ between the two sides of the LTR. This confirms the need for the different flow rates present in the LTR.

Figure 3-47 shows peaks in the cold fluid isobaric specific heat capacity near distance 1.2 meters, especially at lower temperatures. These curves gradually converge to nearly the same value at the outlet regardless of inlet temperature. The hot fluid shows identical fluid inlet isobaric specific heat (they are all at the same state) that gradually diverges as different amounts of heat are transferred to the fluid. As more heat is transferred the hot fluid experiences an increase in isobaric specific heat. Relative to the precooler this is a small change in heat capacity.

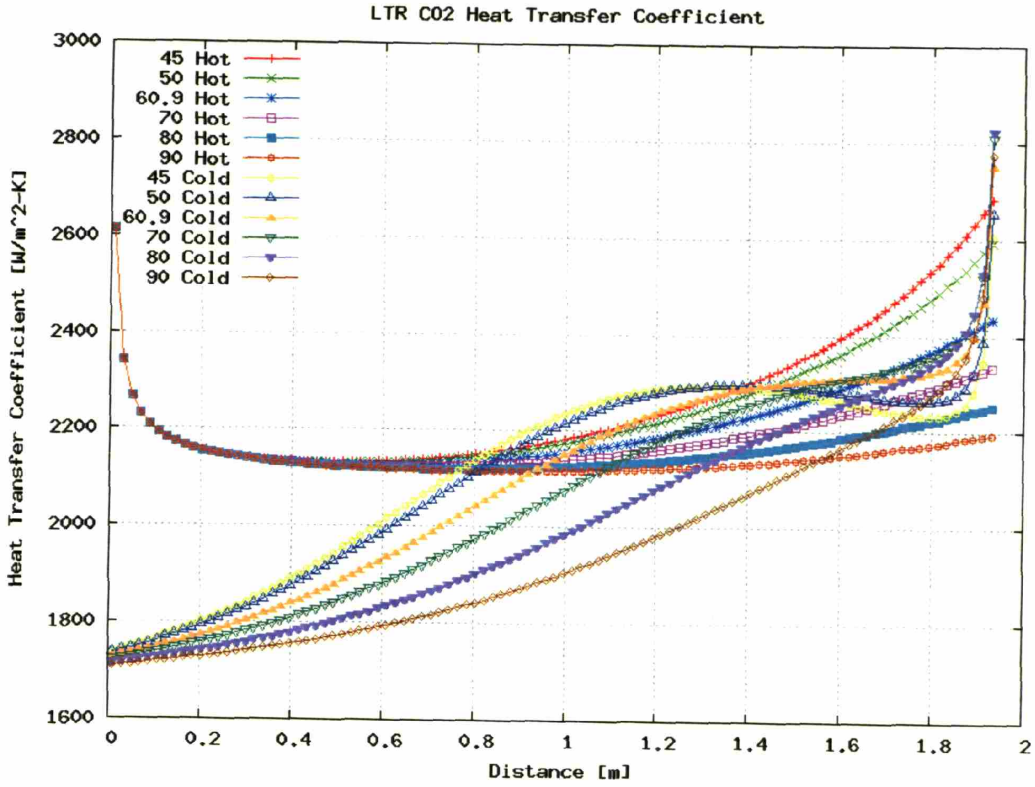

Figure 3-46: LTR CO_2 Heat Transfer Coefficients

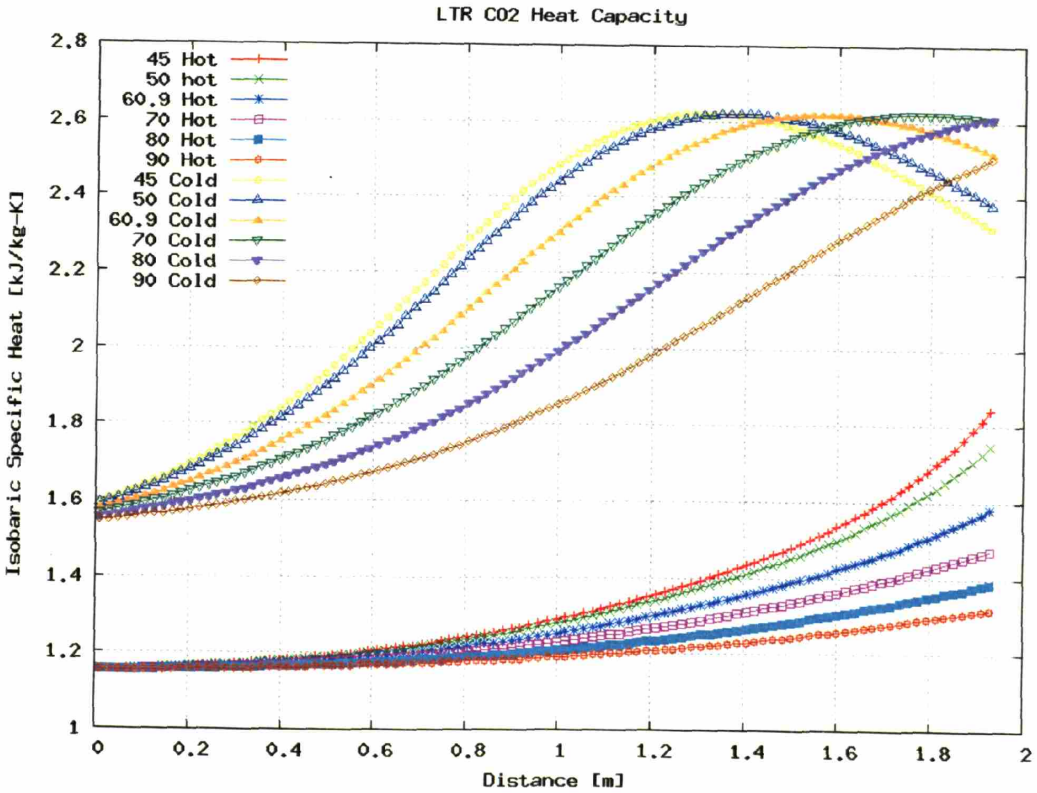

Figure 3-47: LTR CO_2 Isobaric Specific Heat Capacity

3.5.3.3 High Temperature Recuperator Performance

The high temperature recuperator has S-CO_2 cooled by S-CO_2, both at 100% of the full flow rate. The inlet "cold" CO_2 temperature was varied between 130°C and 190°C (nominal is 159.1°C) while all other inlet properties (pressure, mass flow rates, and hot fluid temperature) were held constant. Highlights of these runs are shown in Figure 3-48 through Figure 3-49. Once again, the legend of the figures labels the hot fluid with the cold fluid temperature to identify the case run.

Figure 3-48 shows the now familiar entrance length effect on the hot and cold heat transfer coefficients. The cold fluid shows an increase in heat transfer coefficient, especially at lower CO_2 inlet temperatures, toward the cold fluid outlet. The hot fluid shows a decrease in heat transfer coefficient, with the values converging near the fluid outlet.

The isobaric specific heats do not show a peak, as seen in Figure 3-49. While the cold fluid shows an increase, especially for colder inlet temperatures, it does not show a peak and subsequent decrease within this PCHE. The hot fluid shows a dip and gradual spread as different amounts of heat are transferred in the different cases. Note that compared to the precooler there is only a small change in heat capacity.

The Reynolds numbers in the high temperature recuperator deserve discussion, and are shown in Figure 3-50. The hot side of the high temperature recuperator shows increasing Reynolds numbers from about 15,000 at the inlet to 20-25,000 at the outlet. The cold side of the high temperature recuperator shows unique behavior since the cold fluid generally decreases in Reynolds number from around 18,000 at the inlet to about 15,000 at the outlet. Furthermore, the cold fluid lines, especially the 130°C line, show an initially increasing Reynolds number before decreasing.

The reason for this behavior becomes clear from Figure 3-51 which plots carbon dioxide's viscosity versus temperature for the pressures experienced in the high temperature recuperator. The low pressure/hot side of the recuperator shows a linearly changing viscosity but the high pressure/cold side of the recuperator has a linear decrease at high temperatures, then a parabolic rise in viscosity at lower temperatures. This large rise in viscosity at low temperature is responsible for the unique Reynolds number behavior on the high pressure/cold side of the high temperature recuperator. Note that the change in the viscosity's behavior may signal the start of the pseudo-critical peak at 20 MPa, which occurs near 75°C.

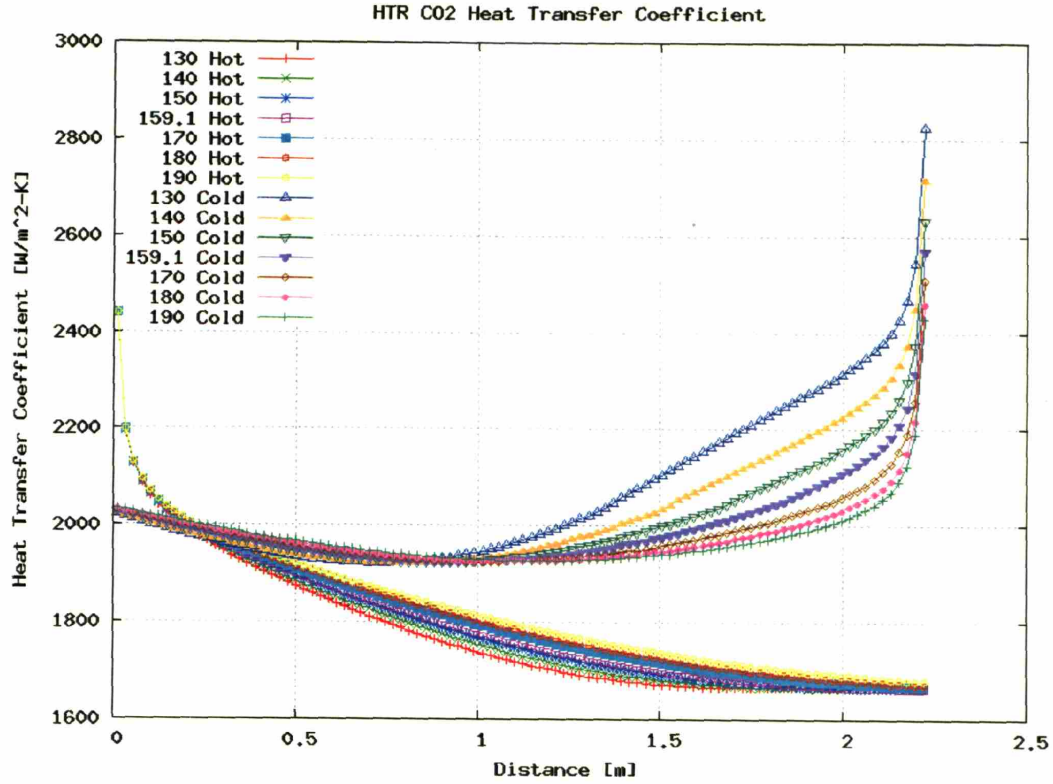

Figure 3-48: HTR CO_2 Heat Transfer Coefficients

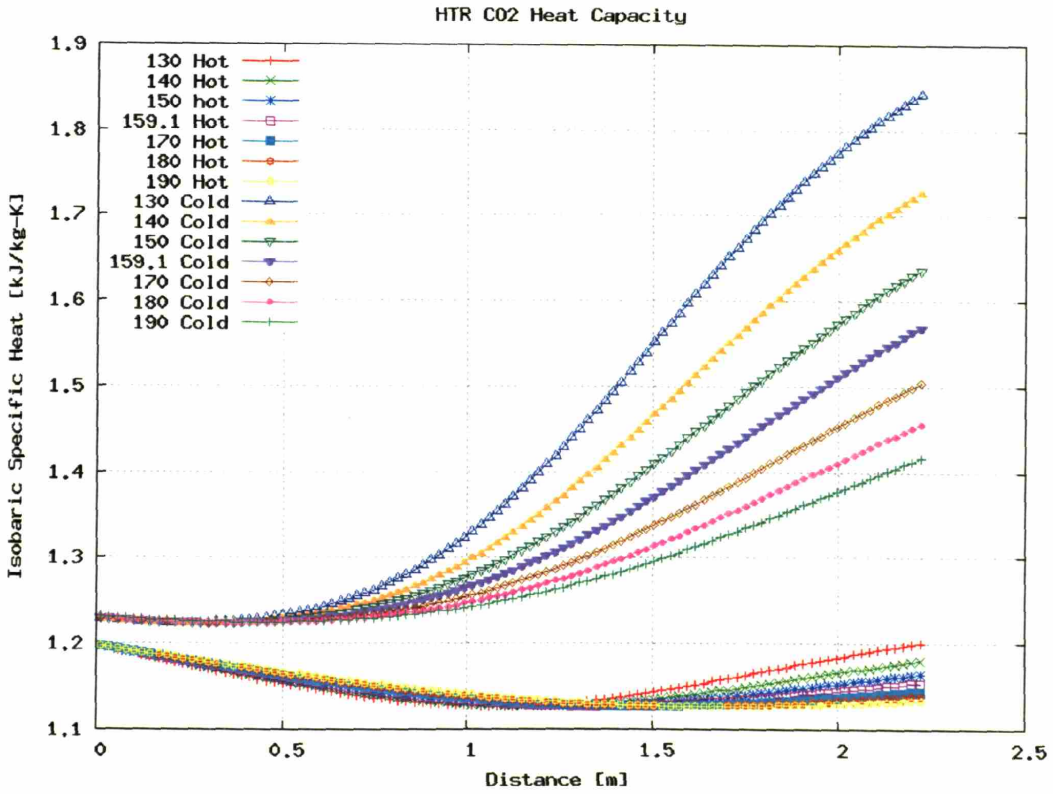

Figure 3-49: HTR CO_2 Isobaric Specific Heat Capacity

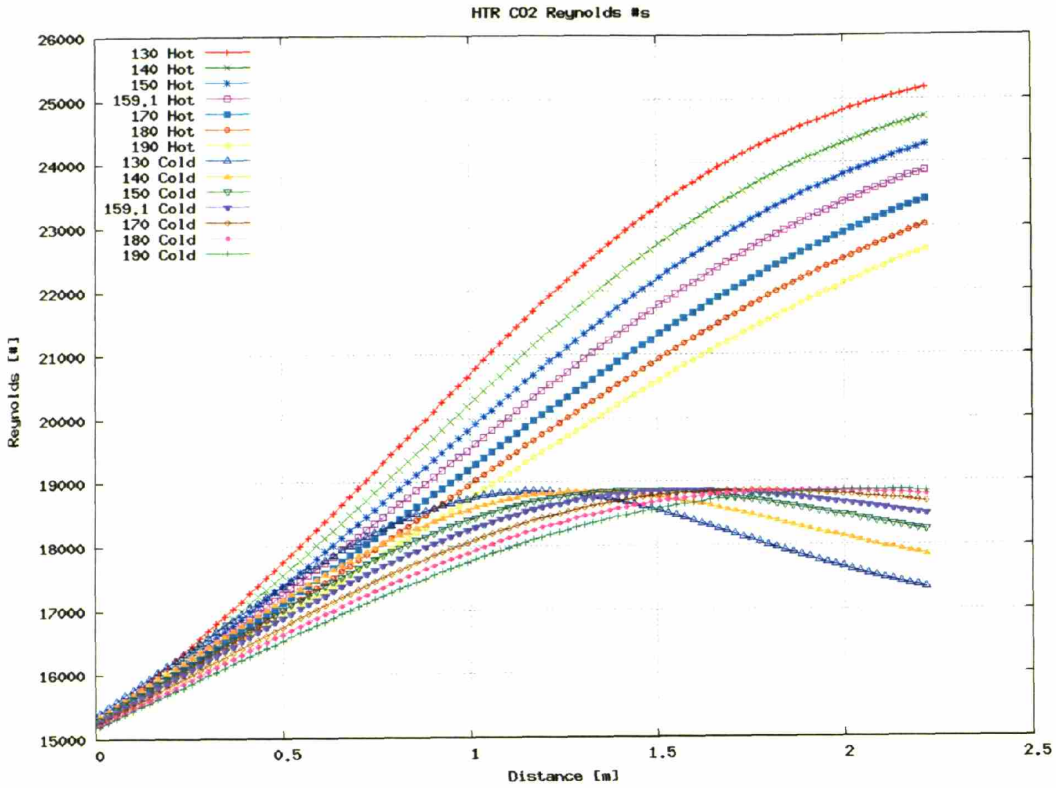

Figure 3-50: HTR CO_2 Reynolds Numbers

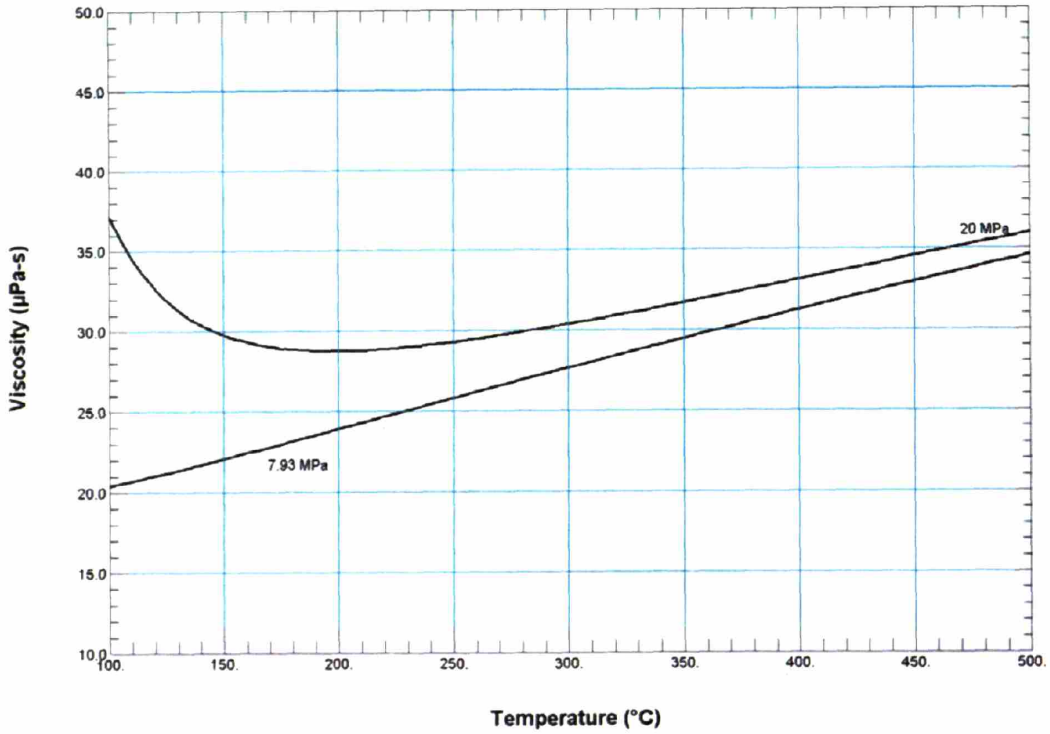

Figure 3-51: HTR CO2 Viscosity

3.5.3.4 Intermediate Heat Exchanger Performance

The intermediate heat exchanger has hot liquid sodium cooled by (relatively) cold S-CO_2. The inlet cold CO_2 temperature was varied between 450°C and 525°C (nominal is 485.5°C). Highlights of these runs are shown in Figure 3-52 and Figure 3-53.

Figure 3-52 shows a rapid decrease (moving from right to left) in CO_2 heat transfer coefficient following the entrance length effect, then a gradual increase as the CO_2 receives energy.

Figure 3-53 shows a continuous but small increase in CO_2 isobaric specific capacity (note the scale) as the fluid is heated. The hotter inlet cases have a higher specific capacity than the colder inlet cases.

The carbon dioxide Reynolds numbers in the intermediate heat exchanger are turbulent. If the incoming CO_2 cools to 450°C then the fluid enters with a Reynolds number near 36,500. At 525°C the inlet possesses a slightly lower Reynolds number of about 34,500. The outlet Reynolds number is above 31,500 in the observed cases.

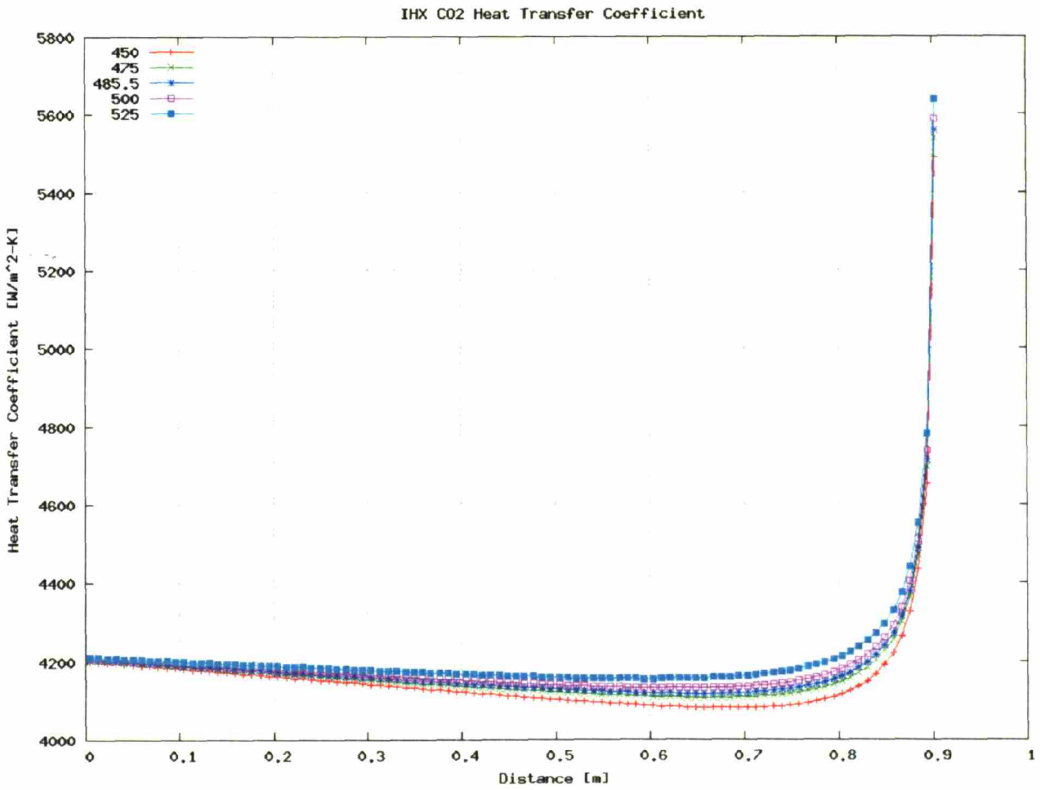

Figure 3-52: IHX CO_2 Heat Transfer Coefficients

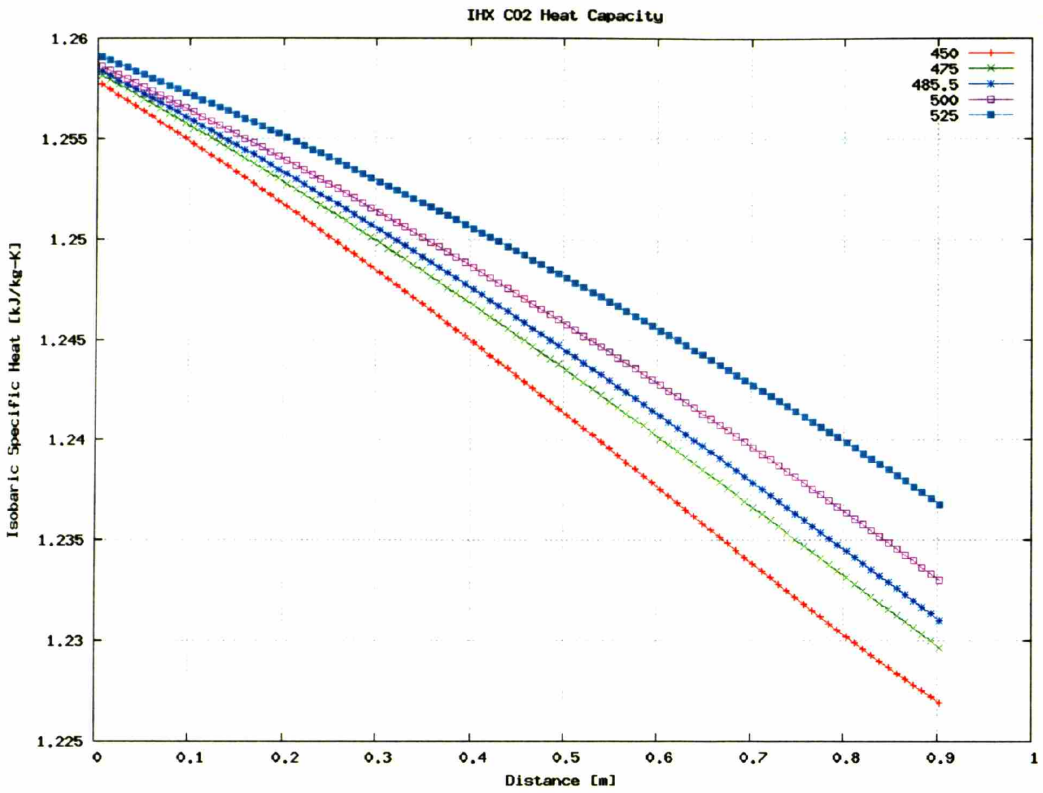

Figure 3-53: IHX CO_2 Isobaric Specific Heat Capacity

3.5.3.5 PCHE Steady State Section Conclusion

Initial studies dealing with the PCHEs suggest that isobaric specific heat varies with length in each PCHE, but is quite important in the precooler, and to a lesser extent the LTR. The integral log-mean temperature model does not hold due to the varying specific heats and heat transfer coefficients experienced with CO_2.

3.5.4 Precooler Thermal Inertia

This section will analyze and will attempt to characterize the thermal inertia present in the S-CO_2 recompression cycle precooler. The precooler design is preliminary but it represents the current best design. Recently, a standalone transient code was developed and computational transients in the precooler were analyzed[75].

3.5.4.1 Precooler Background

The precooler (shown in Figure 2-2) is a single module, straight channel, printed circuit heat exchanger (PCHE) with the geometry shown in Table 3-11. The volumes within the precooler are shown in Table 3-12.

Component	Distance (m)
Hot channel diameter	0.002
Cold channel diameter	0.002
Hot pitch	0.0024
Cold pitch	0.0024
PCHE height	18.52
PCHE width	0.6
PCHE Length	0.9664

Table 3-11: Precooler Geometry

Component	Volume (m^3)
CO_2	2.395
H_2O	2.395
Titanium	5.949

Table 3-12: Precooler Volumes Excluding Plena

The precooler is constructed out of titanium with a thermal conductivity of 25 [W/m-K] and a surface roughness of $1E^{-5}$ [m]. In the recompression cycle with a 650°C reactor outlet temperature and 300 MWe design the precooler transfers 295 MW. The PCHE is counter-flow, with the inlet and outlet properties shown in Table 3-13.

Fluid	In	Out
CO_2 Temperature (°C)	70.95	31.99
CO_2 Pressure (MPa)	7.7516	7.6899
H_2O Temperature (°C)	20.00	32.72
H_2O Pressure (MPa)	0.50132	0.39505

Table 3-13: Precooler Inlet and Outlet Properties

The steady state precooler internal profiles are shown in Figure 3-54 through Figure 3-60. These figures are included for reference purposes only, but the reader should note the CO_2 isobaric specific heat peak and how it ends up affecting the heat transfer, and the very large change in carbon dioxide density.

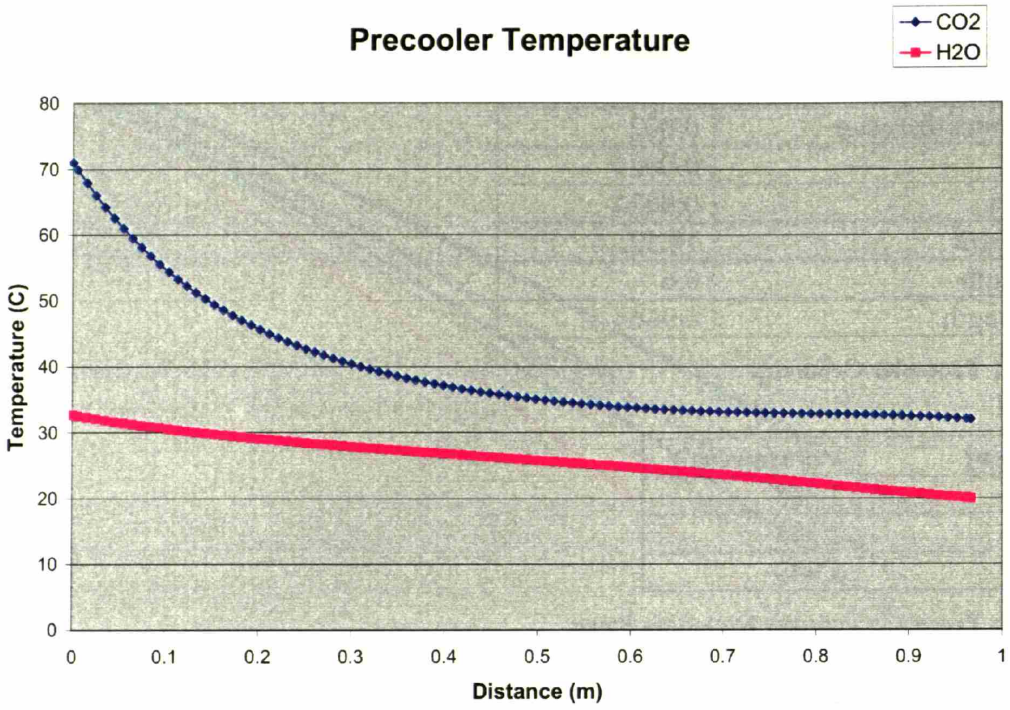

Figure 3-54: Precooler Temperatures

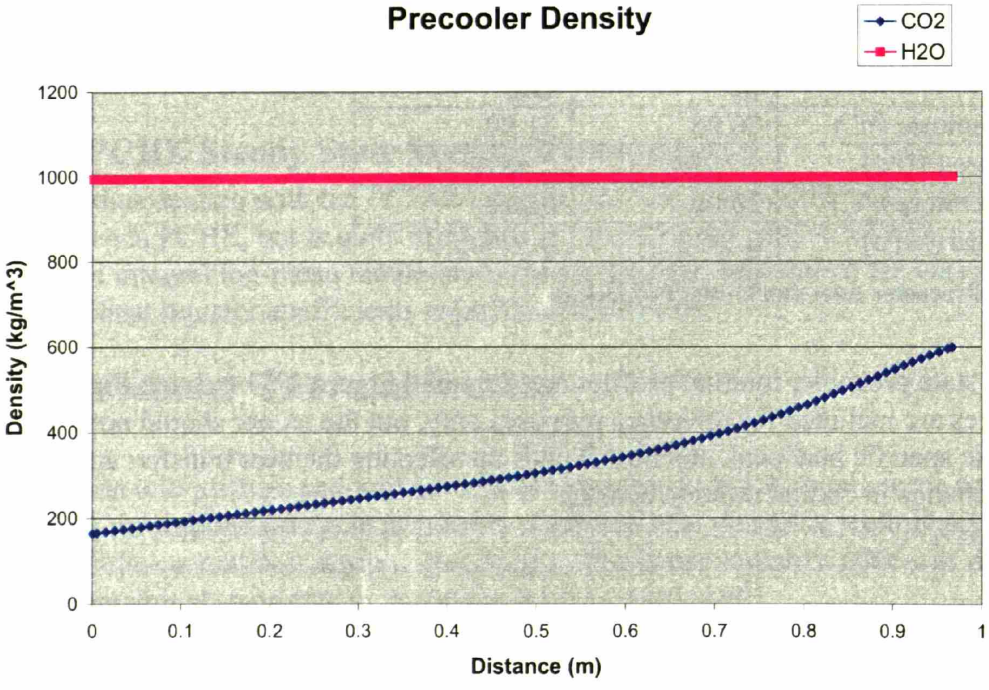

Figure 3-55: Precooler Density

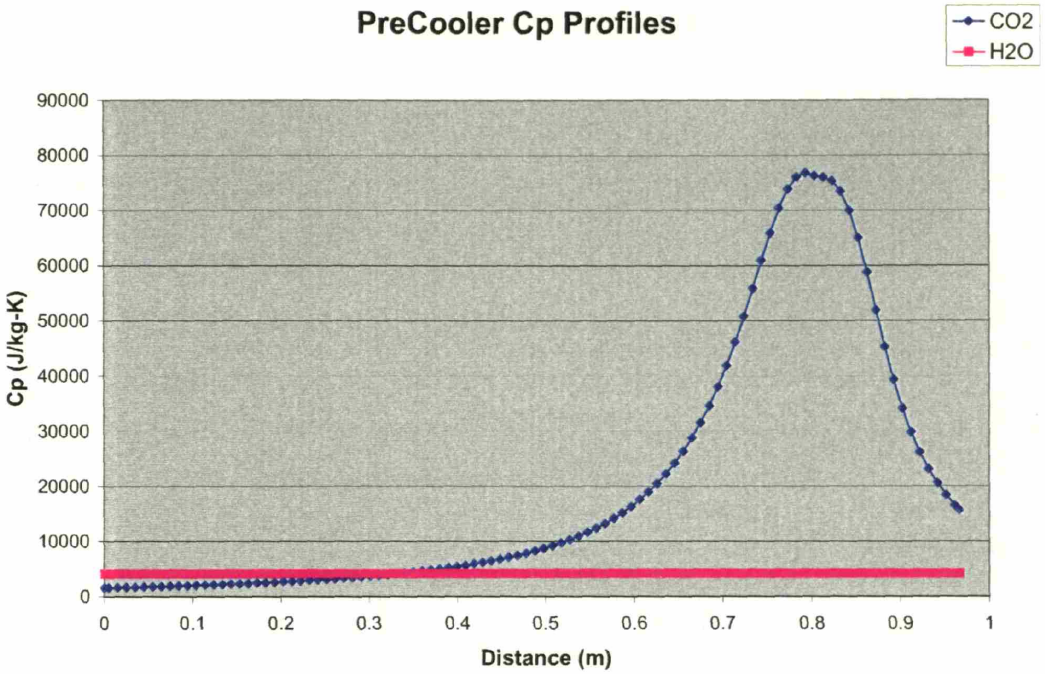

Figure 3-56: Precooler Isobaric Specific Heat

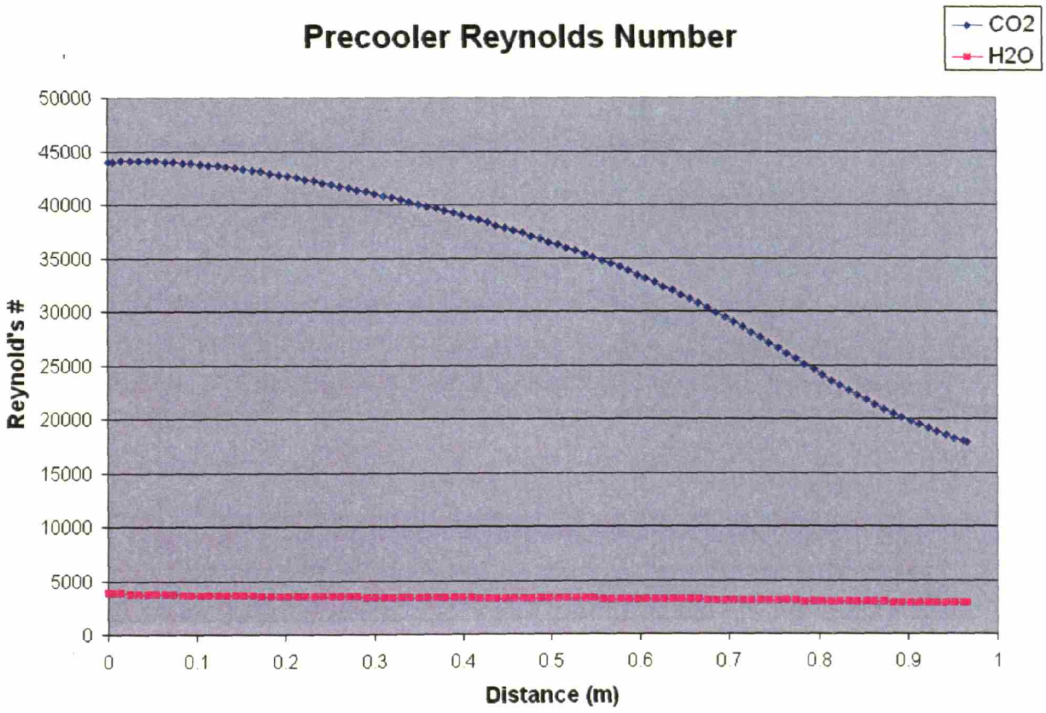

Figure 3-57: Precooler Reynolds Numbers

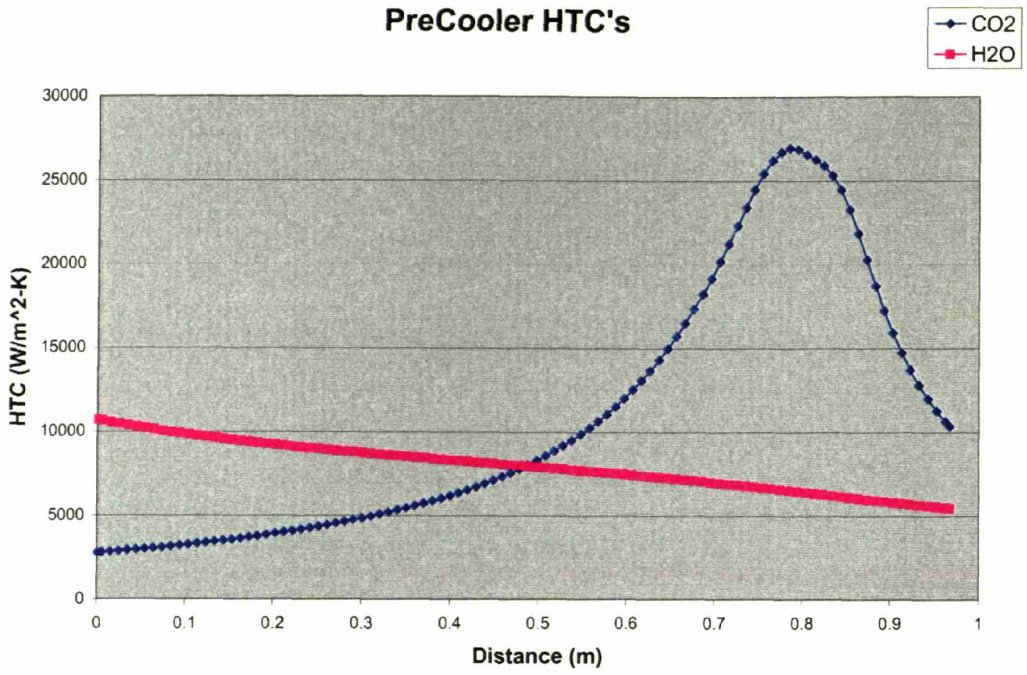

Figure 3-58: Precooler Heat Transfer Coefficient

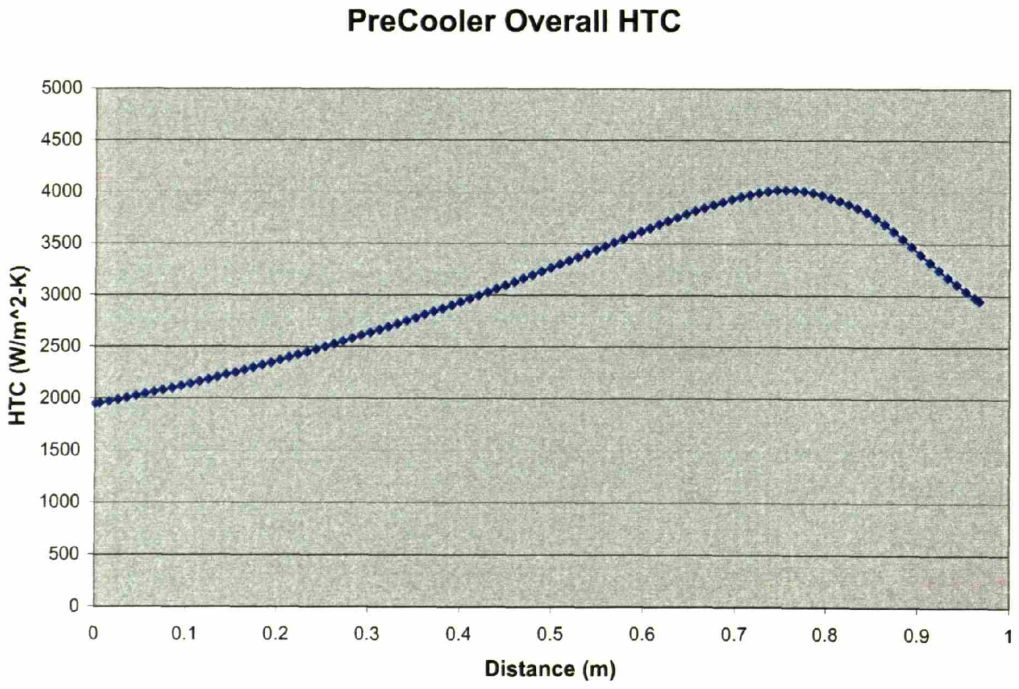

Figure 3-59: Precooler Overall Heat Transfer Coefficient

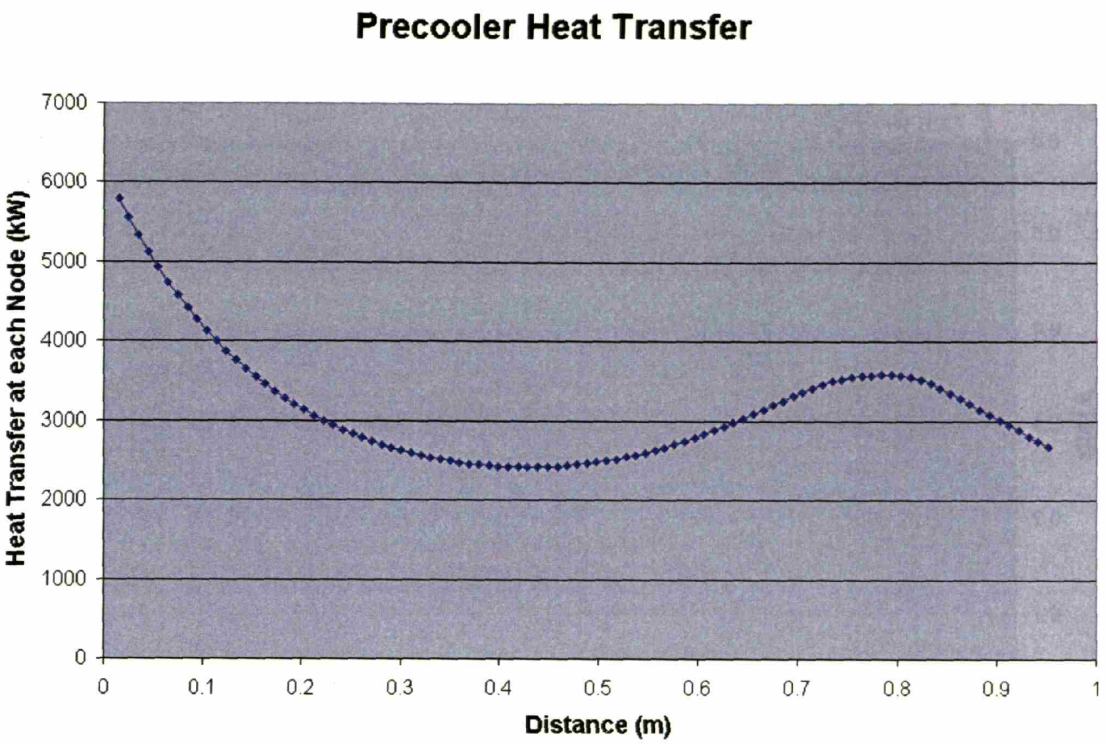

Figure 3-60: Precooler Heat Transfer

3.5.4.2 Precooler Thermal Inertia Analysis

The thermal inertia of the precooler is not simple to characterize due to the complexity of fluid behavior in the component. However, several general observations may be readily made.

The Biot Number is a measure of a structure's internal versus external/surface resistance to heat transfer[76]. The Biot Number is defined in Equation 3-20, where h is the heat transfer coefficient.

Equation 3-20: Biot Number **(3-20)**

$$Bi = \frac{hL_c}{k_{struct}}$$

$$L_c = \frac{V_{struct}}{A_{surface}}$$

A value much less than one implies that the structure's conduction resistance is sufficiently small relative to the surface resistance that structure temperature gradients may be neglected. Looking at this number from the perspective of the titanium block we can calculate this number for both fluids, which results in Figure 3-61.

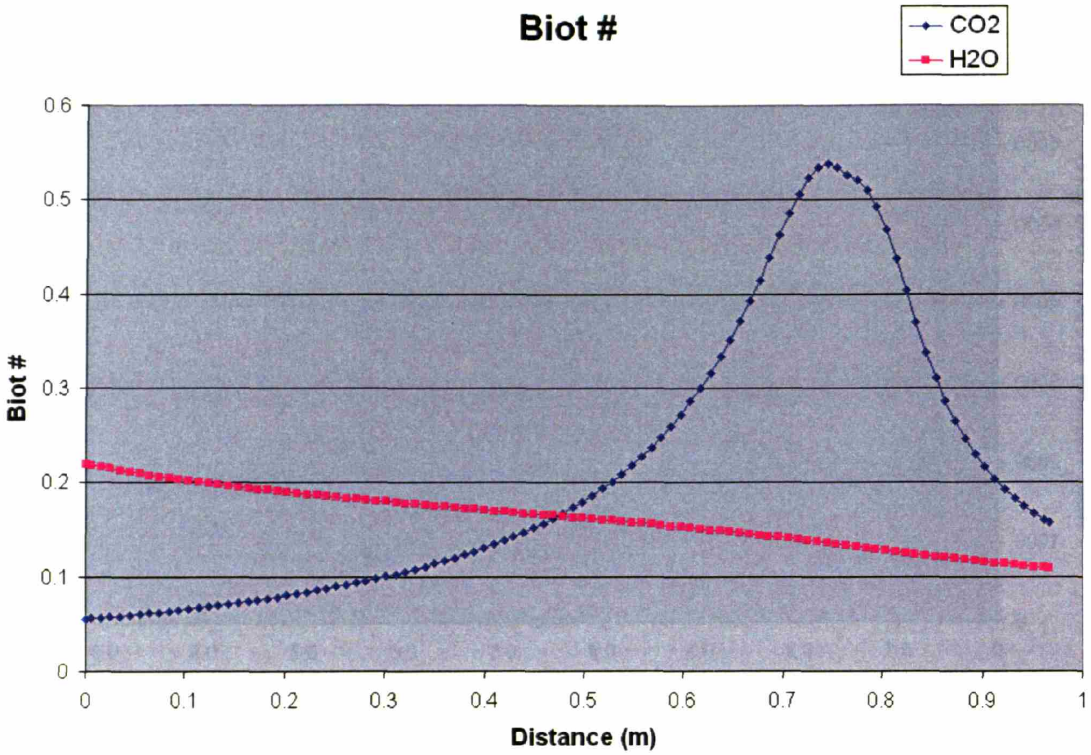

Figure 3-61: Precooler Biot Number

These figures suggest that external (i.e. the fluid's) resistance is the dominant barrier to heat transfer but that the metal's resistance is somewhat comparable, especially as the temperature gradient of the CO_2 decreases with increasing isobaric specific heat. The Biot number for CO_2 ranges from a system almost wholly dominated by the fluid resistance at the entrance to a system partially determined by the metal resistance near 0.8 meters. The Biot number for water is more constant and mainly dominated by fluid resistance.

One might also look at the steady state temperature distribution within the titanium. Figure 3-62 features the previously seen fluid temperatures and the titanium wall temperature on the hot and cold sides and the midpoint temperature. Clearly, there is a much larger temperature difference between the fluids than within the titanium. However, the titanium temperature difference is neither negligible nor constant as seen in Figure 3-63. Note that the peak within this figure coincides with the carbon dioxide isobaric specific heat peak and represents a small temperature difference between the fluids – the titanium heat transfer resistance may become significant in this region.

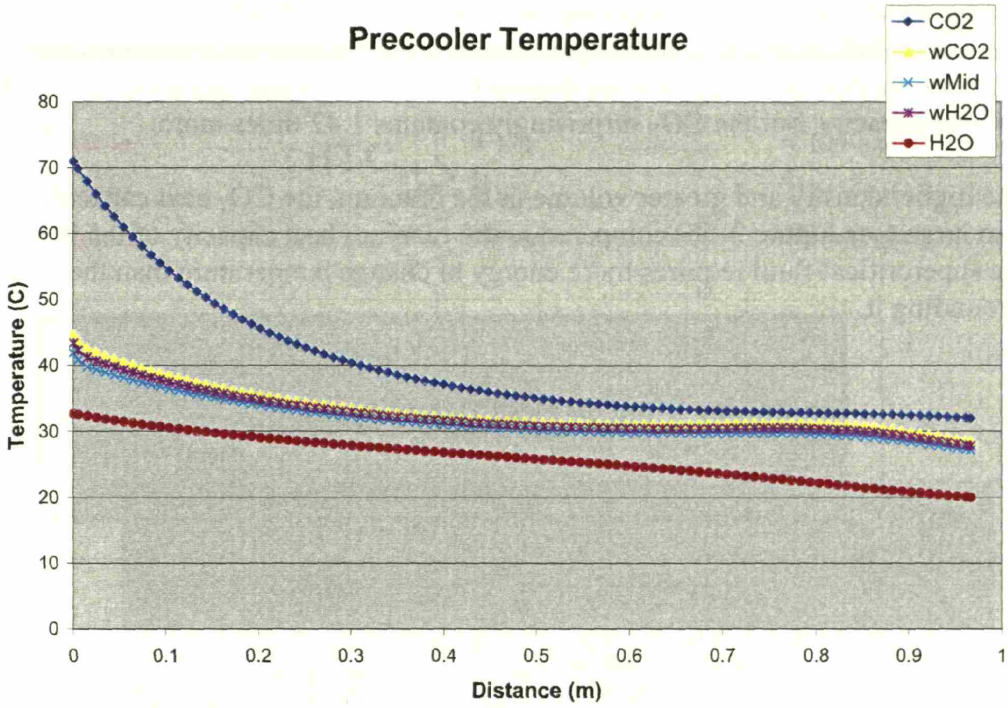

Figure 3-62: Titanium Temperature Distribution

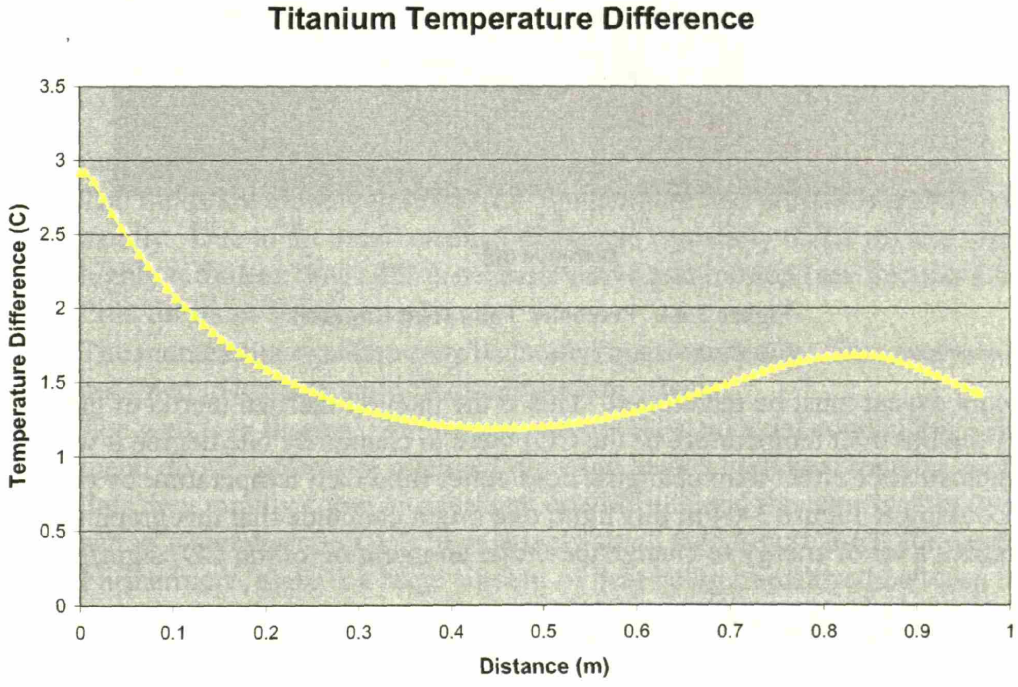

Figure 3-63: Titanium Temperature Difference

An interesting result comes from comparing the total heat capacity of the CO_2, water, and titanium as shown in Figure 3-64. This figure shows the amount of energy required to raise the temperature of the substance one degree Kelvin. The water has about 2/3 of the titanium's heat capacity, but the CO_2 surprisingly contains 1.42 times more.

Despite the higher density and greater volume in the titanium, the CO_2 heat capacity becomes so large (see Figure 3-56) compared to the titanium heat capacity of 0.5 [kJ/kg-K] that the supercritical fluid requires more energy to change temperature than the metal block surrounding it.

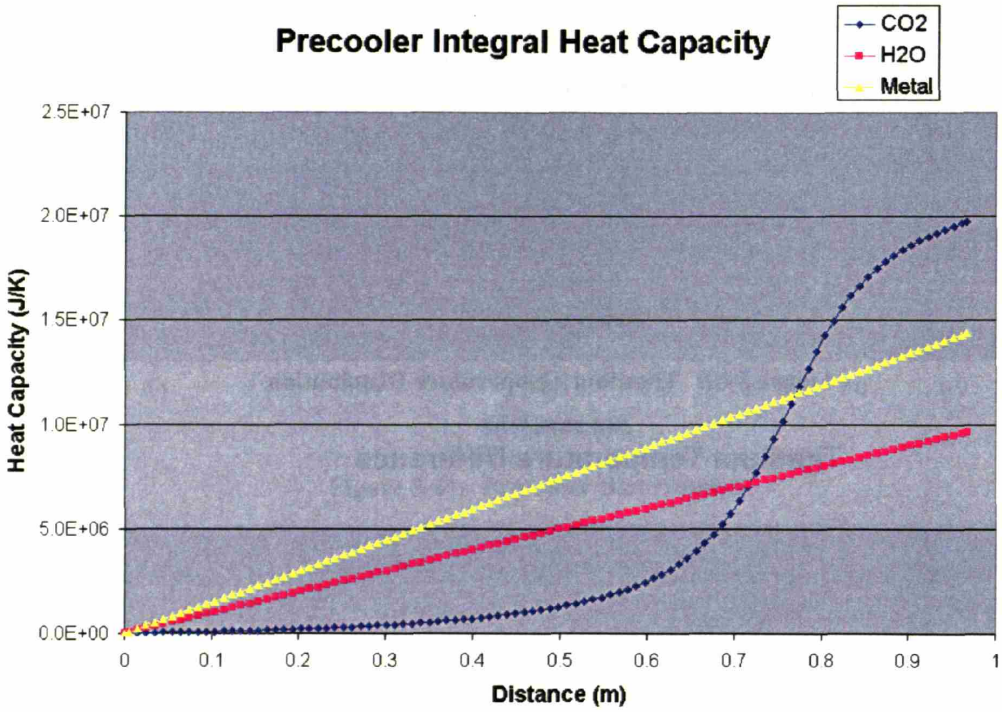

Figure 3-64: Precooler Total Heat Capacity

A significant caveat must be mentioned. This is the integral thermal inertia of the (entire) PCHE. If the hot inlet temperature of the CO_2 were to change by one degree it would have a much smaller effect than changing cold outlet fluid CO_2 temperature by one degree. Looking at Figure 3-64 in this light, one might conclude that this graph states that it requires a lot of energy to change the outlet temperature of the CO_2 significantly.

3.5.5 PCHE Implicit Solution Method

This section will derive the system of equations used to solve a nodalized PCHE implicitly during a transient. The reader is assumed to have already read the preceding sections for background on computationally nodalizing a PCHE and the various performance models used. Incropera and Dewitt offer a good overview[77] of the implicit transient energy transfer process which will be used as a guideline here.

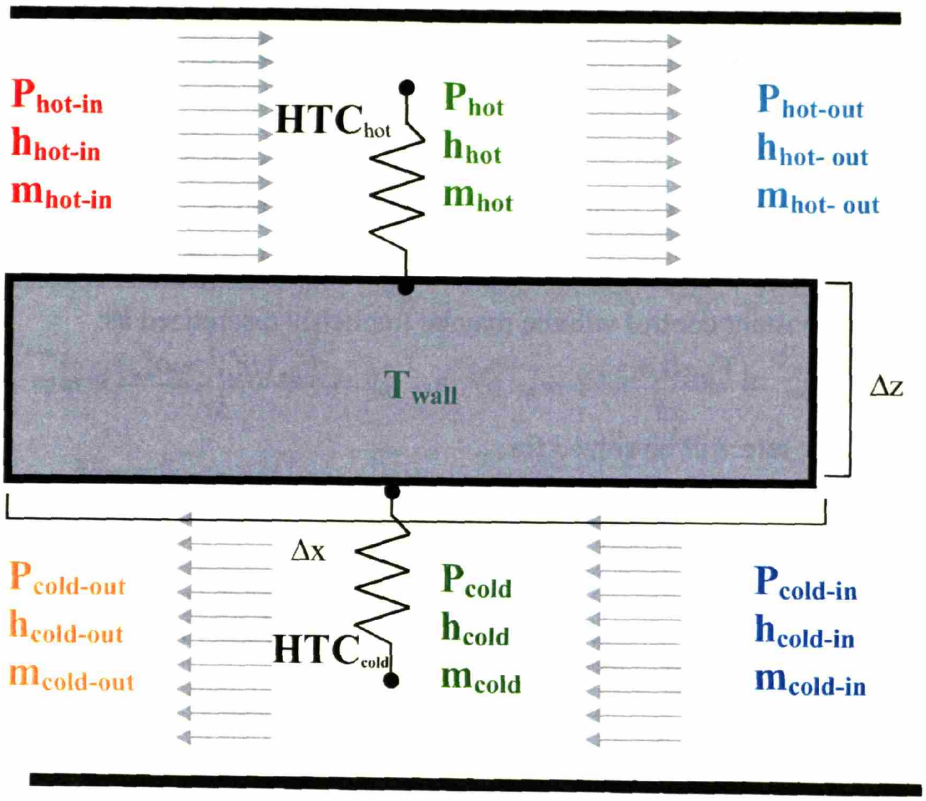

Figure 3-65: PCHE Zone Model

The assumptions of this model are the following:

- The fluids are radially uniform (i.e. temperature and pressure) and only change axially. Due to the small channel diameters (typically 0.002 m) and typically highly turbulent flows this is a conservative assumption (see Section 3.5.1.1under Pitla for more information).
- The momentum equation may be treated quasi-statically. This analysis is not designed to capture rapid fluid momentum effects.
- The wall is in thermal equilibrium and provides no axial conduction. The PCHE metal divider plates are relatively thin and have a high heat transfer coefficient thus they rapidly come into thermal equilibrium and the temperature difference across a metal section will be relatively small (see Figure 3-63, for example). Furthermore, there is a large amount of heat being transferred between the fluid streams, hence axial conduction will add a negligible amount of heat transfer.
- Within a zone one may perform all calculations at the average fluid properties based upon assumed linear enthalpy and pressure changes. In practice, one may simply increase the number of computational nodes until this assumption is adequately satisfied.

Using these assumptions this chapter will derive a set of non-linear mass and energy conservation equations and will match fluid pressure drops to model a PCHE section.

Note that local, time dependent mass flow rates amongst the nodes along each side of the heat exchanger are not assumed constant due to the relatively large fluid volumes inside some of the PCHEs and the large density difference that can arise near carbon dioxide's critical point (see Figure 3-55).

3.5.5.1 Derivation

Conservation of mass for a control volume (represented by a node) is:

$$\frac{dM}{dt} = \dot{m}_{in} - \dot{m}_{out}$$

The hot fluid with a constant control volume may be implicitly discretized as:

$$\frac{dM_{hot}}{dt} = \dot{m}_{hot-in} - \dot{m}_{hot-out} \rightarrow \frac{V_{hot} d(\rho_{hot})}{dt} = \dot{m}_{hot-in} - \dot{m}_{hot-out} \rightarrow \frac{V_{hot}(\rho_{hot}^{p+1} - \rho_{hot}^{p})}{\Delta t} = \dot{m}_{hot-in}^{p+1} - \dot{m}_{hot-out}^{p+1}$$

The average mass flow rate will be solved for:

$$\dot{m}_{hot}^{p+1} = \frac{\dot{m}_{hot-in}^{p+1} + \dot{m}_{hot-out}^{p+1}}{2} \rightarrow \dot{m}_{hot-out}^{p+1} = 2\dot{m}_{hot}^{p+1} - \dot{m}_{hot-in}^{p+1}$$

Substituting:

$$\frac{V_{hot}(\rho_{hot}^{p+1} - \rho_{hot}^{p})}{\Delta t} = \dot{m}_{hot-in}^{p+1} - \left(2\dot{m}_{hot}^{p+1} - \dot{m}_{hot-in}^{p+1} \right)$$

$$\left(2\dot{m}_{hot}^{p+1} - \dot{m}_{hot-in}^{p+1} \right) = \dot{m}_{hot-in}^{p+1} - \frac{V_{hot}(\rho_{hot}^{p+1} - \rho_{hot}^{p})}{\Delta t}$$

$$2\dot{m}_{hot}^{p+1} = 2\dot{m}_{hot-in}^{p+1} - \frac{V_{hot}(\rho_{hot}^{p+1} - \rho_{hot}^{p})}{\Delta t}$$

which yields:

Equation 3-21: PCHE Hot Fluid Mass Conservation **(3-21)**

$$\dot{m}_{hot}^{p+1} = \dot{m}_{hot\ in}^{p+1} - \frac{V_{hot}(\rho_{hot}^{p+1} - \rho_{hot}^{p})}{2\Delta t}$$

Energy conservation for a control volume can be simply expressed as:

$$\frac{dE}{dt} = \dot{E}_{in} - \dot{E}_{out} \rightarrow \frac{d(Mu)}{dt} = \dot{E}_{in} - \dot{E}_{out}$$

When this is applied implicitly and discretely to the hot fluid:

$$\frac{M_{hot}^{p+1} U_{hot}^{p+1} - M_{hot}^{p} U_{hot}^{p}}{\Delta t} = \dot{m}_{hot-in}^{p+1} h_{hot-in}^{p+1} - \dot{m}_{hot-out}^{p+1} h_{hot-out}^{p+1} - \dot{Q}_{hot}^{p+1}$$

Note that the enthalpy terms capture the fluid flow work and that there is no shaft work in a PCHE. The hot fluid only loses heat from internal surface convection:

$$\dot{Q}_{hot}^{p+1} = HTC_{hot}^{p+1} A\left(T_{hot}^{p+1} - T_{wall}^{p+1} \right)$$

The fluid heat transfer coefficient and temperature are calculated from the average node enthalpy and pressure.

Assuming our control volume is constant:

$$\frac{V_{hot}\left(\rho_{hot}^{p+1}u_{hot}^{p+1}-\rho_{hot}^{p}u_{hot}^{p}\right)}{\Delta t}=\dot{m}_{hot-in}^{p+1}h_{hot-in}^{p+1}-\dot{m}_{hot-out}^{p+1}h_{hot-out}^{p+1}-HTC_{hot}^{p+1}A\left(T_{hot}^{p+1}-T_{wall}^{p+1}\right)$$

We will solve this equation for the average hot fluid enthalpy for later computational convenience:

$$h_{hot}^{p+1}=\frac{h_{hot-in}^{p+1}+h_{hot-out}^{p+1}}{2}\rightarrow h_{hot-out}^{p+1}=2h_{hot}^{p+1}-h_{hot-in}^{p+1}$$

Substituting:

$$\frac{V_{hot}\left(\rho_{hot}^{p+1}u_{hot}^{p+1}-\rho_{hot}^{p}u_{hot}^{p}\right)}{\Delta t}=\dot{m}_{hot-in}^{p+1}h_{hot-in}^{p+1}-\dot{m}_{hot-out}^{p+1}\left(2h_{hot}^{p+1}-h_{hot-in}^{p+1}\right)-HTC_{hot}^{p+1}A\left(T_{hot}^{p+1}-T_{wall}^{p+1}\right)$$

$$\dot{m}_{hot-out}^{p+1}\left(2h_{hot}^{p+1}-h_{hot-in}^{p+1}\right)=\dot{m}_{hot-in}^{p+1}h_{hot-in}^{p+1}-HTC_{hot}^{p+1}A\left(T_{hot}^{p+1}-T_{wall}^{p+1}\right)-\frac{V_{hot}\left(\rho_{hot}^{p+1}u_{hot}^{p+1}-\rho_{hot}^{p}u_{hot}^{p}\right)}{\Delta t}$$

$$2h_{hot}^{p+1}=\frac{\dot{m}_{hot-in}^{p+1}h_{hot-in}^{p+1}-HTC_{hot}^{p+1}A\left(T_{hot}^{p+1}-T_{wall}^{p+1}\right)-\frac{V_{hot}\left(\rho_{hot}^{p+1}u_{hot}^{p+1}-\rho_{hot}^{p}u_{hot}^{p}\right)}{\Delta t}}{\dot{m}_{hot-out}^{p+1}}+h_{hot-in}^{p+1}$$

which leads to:

Equation 3-22: PCHE Hot Fluid Energy Conservation **(3-22)**

$$h_{hot}^{p+1}=\frac{\dot{m}_{hot-in}^{p+1}h_{hot-in}^{p+1}-HTC_{hot}^{p+1}A\left(T_{hot}^{p+1}-T_{wall}^{p+1}\right)-\frac{V_{hot}\left(\rho_{hot}^{p+1}u_{hot}^{p+1}-\rho_{hot}^{p}u_{hot}^{p}\right)}{\Delta t}}{2\dot{m}_{hot-out}^{p+1}}+\frac{h_{hot-in}^{p+1}}{2}$$

The hot fluid pressure is the correlation-predicted pressure drop for the quasi-static momentum case. For this simulation code this can be simplified to:

$$\Delta P=F_{friction}$$

The frictional force will be calculated by a variety of methods specific to the component model. Applying this implicitly:

$$P_{hot-out}^{p+1}=P_{hot-in}^{p+1}-\Delta P_{hot}^{p+1}$$

Once again we will solve for average pressure:

$$P_{hot}^{p+1}=\frac{P_{hot-in}^{p+1}+P_{hot-out}^{p+1}}{2}$$

Substituting:

Equation 3-23: PCHE Hot Fluid Pressure **(3-23)**

$$P_{hot}^{p+1}=\frac{P_{hot-in}^{p+1}+\left(P_{hot-in}^{p+1}-\Delta P_{hot}^{p+1}\right)}{2}$$

Similarly, we will derive the same equations for the cold fluid. Care should be taken regarding sign conventions here. Recall that for computational efficiency all of the PCHEs are solved from one side to the other and it was arbitrarily chosen to be the hot fluid inlet to outlet/the cold fluid outlet to inlet. Thus the cold fluid is computationally solved in reverse of the flow direction as suggested by Figure 3-66.

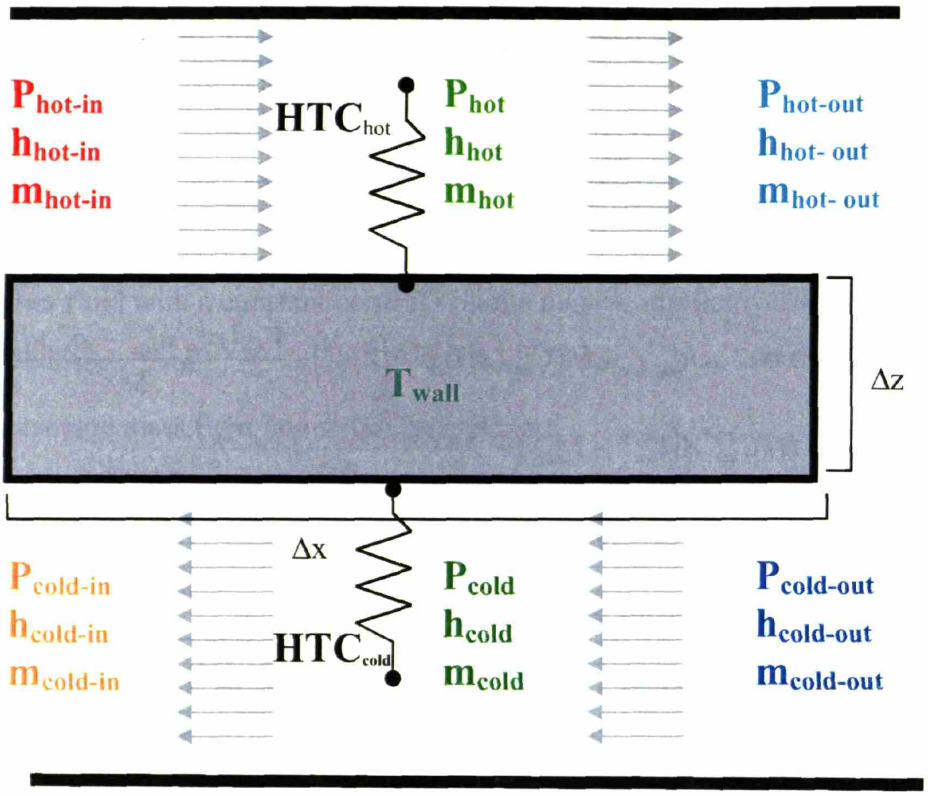

Figure 3-66: PCHE Zone Computational Model

For mass conservation of the cold fluid in a control volume with reversed flow:

$$\frac{dM_{cold}}{dt} = \dot{m}_{cold-out} - \dot{m}_{cold-in} \rightarrow \frac{V_{cold} d(\rho_{cold})}{dt} = \dot{m}_{cold-out} - \dot{m}_{cold-in} \rightarrow$$

$$\frac{V_{cold}(\rho_{cold}^{p+1} - \rho_{cold}^{p})}{\Delta t} = \dot{m}_{cold-out}^{p+1} - \dot{m}_{cold-in}^{p+1}$$

Again solving for the average value:

$$\dot{m}_{cold}^{p+1} = \frac{\dot{m}_{cold-in}^{p+1} + \dot{m}_{cold-out}^{p+1}}{2} \rightarrow \dot{m}_{cold-out}^{p+1} = 2\dot{m}_{cold}^{p+1} - \dot{m}_{cold-in}^{p+1}$$

Substituting:

$$\frac{V_{cold}(\rho_{cold}^{p+1} - \rho_{cold}^{p})}{\Delta t} = 2\dot{m}_{cold}^{p+1} - \dot{m}_{cold-in}^{p+1} - \dot{m}_{cold-in}^{p+1}$$

$$\frac{V_{cold}(\rho_{cold}^{p+1} - \rho_{cold}^{p})}{2\Delta t} = \dot{m}_{cold}^{p+1} - \dot{m}_{cold-in}^{p+1}$$

which yields:

Equation 3-24: PCHE Computational Cold Fluid Mass Conservation **(3-24)**

$$\dot{m}_{cold}^{p+1} = \dot{m}_{cold-in}^{p+1} + \frac{V_{cold}(\rho_{cold}^{p+1} - \rho_{cold}^{p})}{2\Delta t}$$

The cold fluid energy conservation equation is:

$$\frac{M_{cold}^{p+1}u_{cold}^{p+1} - M_{cold}^{p}u_{cold}^{p}}{\Delta t} = \dot{m}_{cold-out}^{p+1} h_{cold-out}^{p+1} + \dot{Q}_{cold}^{p+1} - \dot{m}_{cold-in}^{p+1} h_{cold-in}^{p+1}$$

This equation states that:

- as more fluid and hotter are found in the "*in*" location (which is the exiting flow – see Figure 3-66), then more energy is required from the control volume
- as more heat flows from the structure to the cold fluid, then the "*in*" location must increase in energy

This preserves the correct directionality for energy conservation and is a convenient form for computation (when the cold fluid is solved against the direction of flow).

Note that the enthalpy terms capture the fluid flow work and that there is no shaft work in the cold fluid of a PCHE. The cold fluid only loses heat from internal surface convection:

$$\dot{Q}_{cold}^{p+1} = HTC_{cold}^{p+1} A\left(T_{wall}^{p+1} - T_{cold}^{p+1}\right)$$

The fluid heat transfer coefficient and temperature are calculated from the average node enthalpy and pressure.

Once again we will solve for the average cold fluid enthalpy in the zone for computational convenience:

$$h_{cold}^{p+1} = \frac{h_{cold-in}^{p+1} + h_{cold-out}^{p+1}}{2} \rightarrow h_{cold-out}^{p+1} = 2h_{cold}^{p+1} - h_{cold-in}^{p+1}$$

Substituting:

$$\frac{V_{cold}\left(\rho_{cold}^{p+1}u_{cold}^{p+1} - \rho_{cold}^{p}u_{cold}^{p}\right)}{\Delta t} = \dot{m}_{cold-out}^{p+1}\left(2h_{cold}^{p+1} - h_{cold-in}^{p+1}\right) + HTC_{cold}^{p+1}A\left(T_{wall}^{p+1} - T_{cold}^{p+1}\right) - \dot{m}_{cold-in}^{p+1} h_{cold-in}^{p+1}$$

$$\dot{m}_{cold-out}^{p+1}\left(2h_{cold}^{p+1} - h_{cold-in}^{p+1}\right) = \dot{m}_{cold-in}^{p+1} h_{cold-in}^{p+1} - HTC_{cold}^{p+1}A\left(T_{wall}^{p+1} - T_{cold}^{p+1}\right) + \frac{V_{cold}\left(\rho_{cold}^{p+1}u_{cold}^{p+1} - \rho_{cold}^{p}u_{cold}^{p}\right)}{\Delta t}$$

$$2h_{cold}^{p+1} = \frac{\dot{m}_{cold-in}^{p+1} h_{cold-in}^{p+1} - HTC_{cold}^{p+1}A\left(T_{wall}^{p+1} - T_{cold}^{p+1}\right) + \frac{V_{cold}\left(\rho_{cold}^{p+1}u_{cold}^{p+1} - \rho_{cold}^{p}u_{cold}^{p}\right)}{\Delta t}}{\dot{m}_{cold-out}^{p+1}} + h_{cold-in}^{p+1}$$

which results in:

Equation 3-25: PCHE Computational Cold Fluid Energy Conservation **(3-25)**

$$h_{cold}^{p+1} = \frac{\dot{m}_{cold-in}^{p+1} h_{cold-in}^{p+1} - HTC_{cold}^{p+1}A\left(T_{wall}^{p+1} - T_{cold}^{p+1}\right) + \frac{V_{cold}\left(\rho_{cold}^{p+1}u_{cold}^{p+1} - \rho_{cold}^{p}u_{cold}^{p}\right)}{\Delta t}}{2\dot{m}_{cold-out}^{p+1}} + 2h_{cold-in}^{p+1}$$

The cold fluid pressure is simply the correlation-predicted pressure drop for the quasi-static momentum case, as in the hot fluid case:

$$\Delta P = F_{friction}$$

Applying this implicitly (to a reverse-flow control volume):

$$P_{cold\_out}^{p+1} = P_{cold-in}^{p+1} + \Delta P_{cold}^{p+1}$$

Once again solve for average pressure:

$$P_{cold}^{p+1} = \frac{P_{cold-in}^{p+1} + P_{cold-out}^{p+1}}{2}$$

Substituting:

Equation 3-26: PCHE Cold Fluid Pressure **(3-26)**

$$P_{cold}^{p+1} = \frac{P_{cold-in}^{p+1} + \left(P_{cold-in}^{p+1} + \Delta P_{cold}^{p+1}\right)}{2}$$

Finally, we need only solve for the metal wall energy conservation. Once again we implicitly discretize the energy conservation equation:

$$\frac{dE}{dt} = \dot{E}_{in} - \dot{E}_{out} \rightarrow \frac{d(Mu)}{dt} = \dot{E}_{in} - \dot{E}_{out} \rightarrow \frac{M_{wall}(u_{wall}^{p+1} - u_{wall}^{p})}{\Delta t} = \dot{E}_{in} - \dot{E}_{out}$$

The only energy transfer is from the fluid surface convection:

$$\frac{M_{wall}(u_{wall}^{p+1} - u_{wall}^{p})}{\Delta t} = \dot{Q}_{hot} - \dot{Q}_{cold}$$

$$\frac{M_{wall}(u_{wall}^{p+1} - u_{wall}^{p})}{\Delta t} = \dot{Q}_{hot} - \dot{Q}_{cold}$$

For a metal the specific heat may be assumed constant over the small temperature differences encountered in this type of heat exchanger:

$$\frac{M_{wall}C_{wall}(T_{wall}^{p+1} - T_{wall}^{p})}{\Delta t} = HTC_{hot}^{p+1}A\left(T_{hot}^{p+1} - T_{wall}^{p+1}\right) - HTC_{cold}^{p+1}A\left(T_{wall}^{p+1} - T_{cold}^{p+1}\right)$$

Separating:

$$\frac{M_{wall}C_{wall}(T_{wall}^{p+1} - T_{wall}^{p})}{\Delta t} = HTC_{hot}^{p+1}A\left(T_{hot}^{p+1} - T_{wall}^{p+1}\right) - HTC_{cold}^{p+1}A\left(T_{wall}^{p+1} - T_{cold}^{p+1}\right)$$

$$\frac{M_{wall}C_{wall}}{\Delta t}T_{wall}^{p+1} - \frac{M_{wall}C_{wall}}{\Delta t}T_{wall}^{p} = HTC_{hot}^{p+1}AT_{hot}^{p+1} - HTC_{hot}^{p+1}AT_{wall}^{p+1} - HTC_{cold}^{p+1}AT_{wall}^{p+1} + HTC_{cold}^{p+1}AT_{cold}^{p+1}$$

$$\frac{M_{wall}C_{wall}}{\Delta t}T_{wall}^{p+1} + HTC_{hot}^{p+1}AT_{wall}^{p+1} + HTC_{cold}^{p+1}AT_{wall}^{p+1} = HTC_{hot}^{p+1}AT_{hot}^{p+1} + HTC_{cold}^{p+1}AT_{cold}^{p+1} + \frac{M_{wall}C_{wall}}{\Delta t}T_{wall}^{p}$$

$$T_{wall}^{p+1}\left(\frac{M_{wall}C_{wall}}{\Delta t} + HTC_{hot}^{p+1}A + HTC_{cold}^{p+1}A\right) = HTC_{hot}^{p+1}AT_{hot}^{p+1} + HTC_{cold}^{p+1}AT_{cold}^{p+1} + \frac{M_{wall}C_{wall}}{\Delta t}T_{wall}^{p}$$

to obtain:

Equation 3-27: PCHE Wall Energy Conservation (3-27)

$$T_{wall}^{p+1} = \frac{HTC_{hot}^{p+1} AT_{hot}^{p+1} + HTC_{cold}^{p+1} AT_{cold}^{p+1} + \frac{M_{wall} C_{wall}}{\Delta t} T_{wall}^{p}}{HTC_{hot}^{p+1} A + HTC_{cold}^{p+1} A + \frac{M_{wall} C_{wall}}{\Delta t}}$$

There are now seven equations and seven unknowns which must be simultaneously solved for to arrive at a new time step solution. Unfortunately, the common practice of putting these equations into a tridiagonal matrix and solving for the various values is difficult due to the nature of this calculation. Both fluid's properties (i.e. density and internal energy) and performance models (i.e. heat transfer coefficient and friction factor) are calculated based upon the node's average enthalpy and pressure. The equation of state for carbon dioxide is quite complex, but even if one were able to express the various fluid properties succinctly enough to put them into a matrix, one would still have the problem of updating the performance models. Therefore, these equations will be solved by a general non-linear numerical solver.

At a new time step the solver will be supplied with the initial guesses for the seven variables to be solved for: $X_{guess} = (\dot{m}_{hot}^{p+1}, h_{hot}^{p+1}, P_{hot}^{p+1}, \dot{m}_{cold}^{p+1}, h_{cold}^{p+1}, P_{cold}^{p+1}, T_{wall}^{p+1})$ at the node's average values. The solver will then update the various fluid properties based upon each fluid's average enthalpy and pressure and then update the pressure drop and heat transfer models using these new values.

The newly calculated fluid properties and performance model results are then plugged into Equation 3-22 through Equation 3-27 along with the known incoming fluid property values: $X_{in} = (\dot{m}_{hot-in}^{p+1}, h_{hot-in}^{p+1}, P_{hot-in}^{p+1}, \dot{m}_{cold-in}^{p+1}, h_{cold-in}^{p+1}, P_{cold-in}^{p+1})$, which are the outputs of previous calculations, and the previous time step's known values to predict the current time step's average fluid values: $X_{calculated} = (\dot{m}_{hot}^{p+1}, h_{hot}^{p+1}, P_{hot}^{p+1}, \dot{m}_{cold}^{p+1}, h_{cold}^{p+1}, P_{cold}^{p+1}, T_{wall}^{p+1})$. By iteratively refining the guessed values until they match the calculated values to tolerance (typically 10^{-7}%), the PCHE node may be solved at the current time step. Using the converged variables the code then calculates the fluid outlet values:

$X_{out} = (\dot{m}_{hot-out}^{p+1}, h_{hot-out}^{p+1}, P_{hot-out}^{p+1}, \dot{m}_{cold-out}^{p+1}, h_{cold-out}^{p+1}, P_{cold-out}^{p+1})$, which become the next calculation's inputs. A flowchart of the overall process is shown in Figure 3-67. The general non-linear system of equation solver is labeled *DNEQF*. Since each calculation only depends upon the previous calculation's results we maintain our implicit assumption.

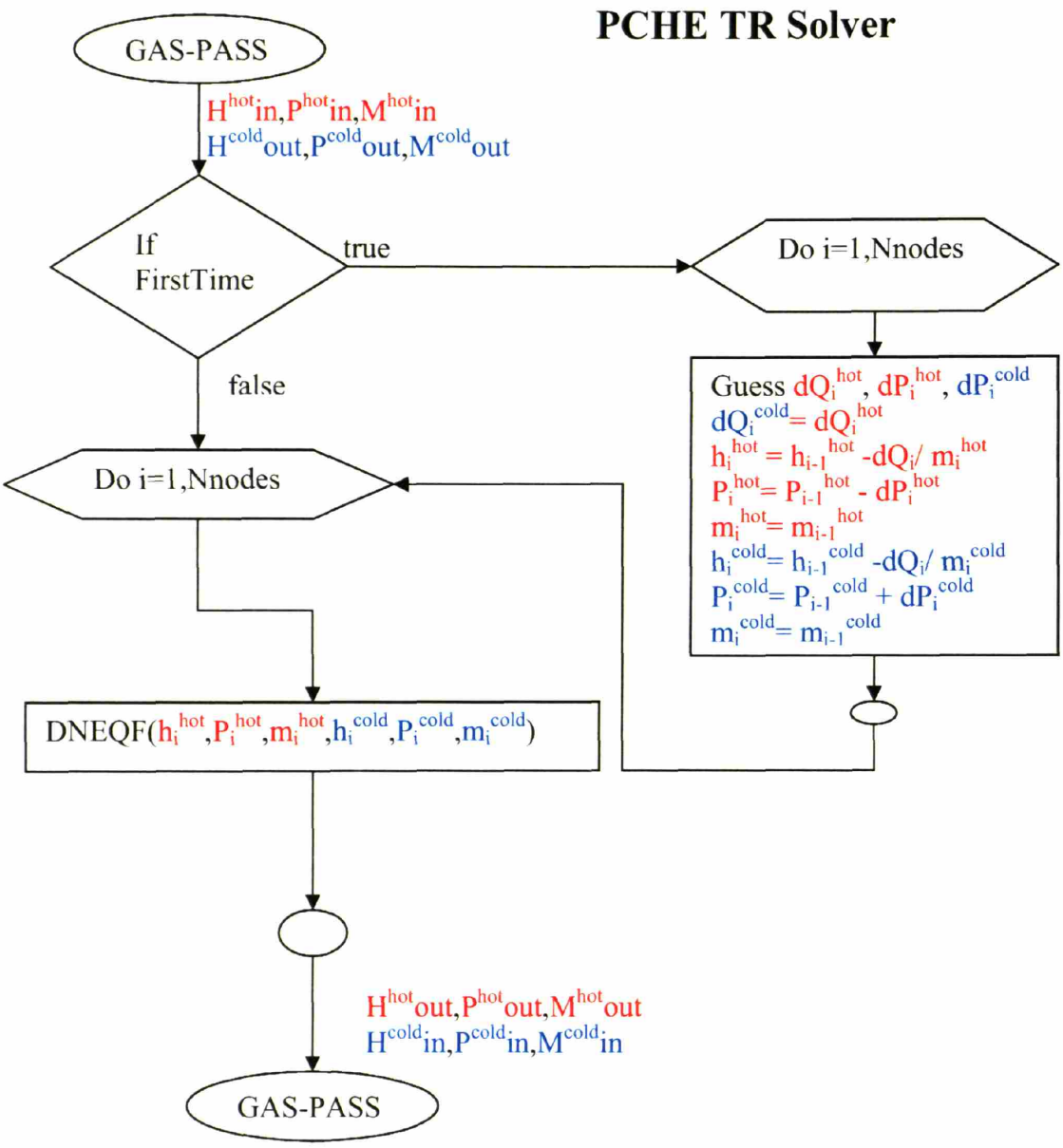

Figure 3-67: PCHE Transient Code Flow Chart

3.5.5.2 Results

The PCHE implicit solution method used in GAS-PASS/CO_2 was tested in a standalone code, called HXSIM (see solution process flowchart in Figure 3-67), both to characterize component performance and to benchmark the solution method against other codes and techniques. This subsection will briefly document the code with several transient PCHE simulations of interest and compare the results against other solution methods.

The transient behavior of the precooler used in the S-CO_2 recompression cycle has largely been documented by Langewisch[75]. However, several aspects deserve further treatment.

During transient PCHE behavior, fluid density changes can make significant changes in mass flow rates for short periods of time, even if the incoming mass flow rate does not change. If the fluid density decreases (i.e. temperature rises) then the PCHE will reject fluid for a short amount of time, as shown in the large peak in Figure 3-68. Furthermore, the heat transfer between the wall structure and the carbon dioxide are large enough that the carbon dioxide density decreases as the metal structure warms and allows the carbon dioxide temperature to rise. This is seen as the tail of the sharp peak in Figure 3-68.

This figure comes shows that a significant rise in the CO_2 inlet temperature can lead to a greater than 15% spike in outlet mass flow rate. Most expected transients will be more gradual than the case shown, but the designer should be aware that the various PCHE components can produce sharp changes in mass flow rate solely due to changing fluid density.

To quantify this newly observed effect, Dr. Pavel Hejzlar ran a similar case with RELAP5 which HXSIM was then compared to. The results of this run are shown in Figure 3-69. This figure shows that both HXSIM and RELAP5 predict a significant spike in outlet mass flow rate due to thermal heating of the CO_2. However, HXSIM predicts a higher spike than RELAP5 does.

This "overestimation" should be expected, since RELAP5 has proper treatment of the momentum equation while HXSIM uses a highly simplified momentum conservation relation. Thus, RELAP5 shows the effect of fluid inertia, while HXSIM does not; therefore the RELAP5 spike will be smaller and slower, both of which are clearly seen.

HXSIM's performance is considered acceptable because expected transients will be much slower than the case shown here. Therefore the error will be much less, and HXSIM over predicts this phenomenon, and therefore will produce a conservative result.

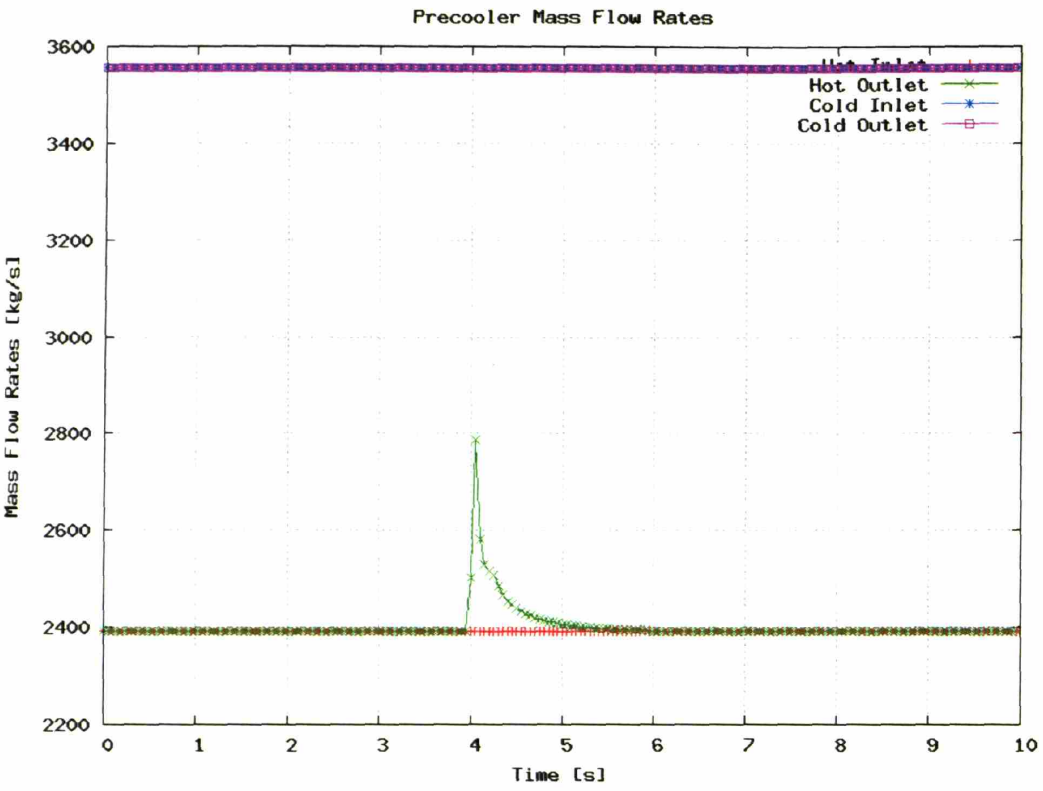

Figure 3-68: Precooler Mass Flow Rate - Density Decrease

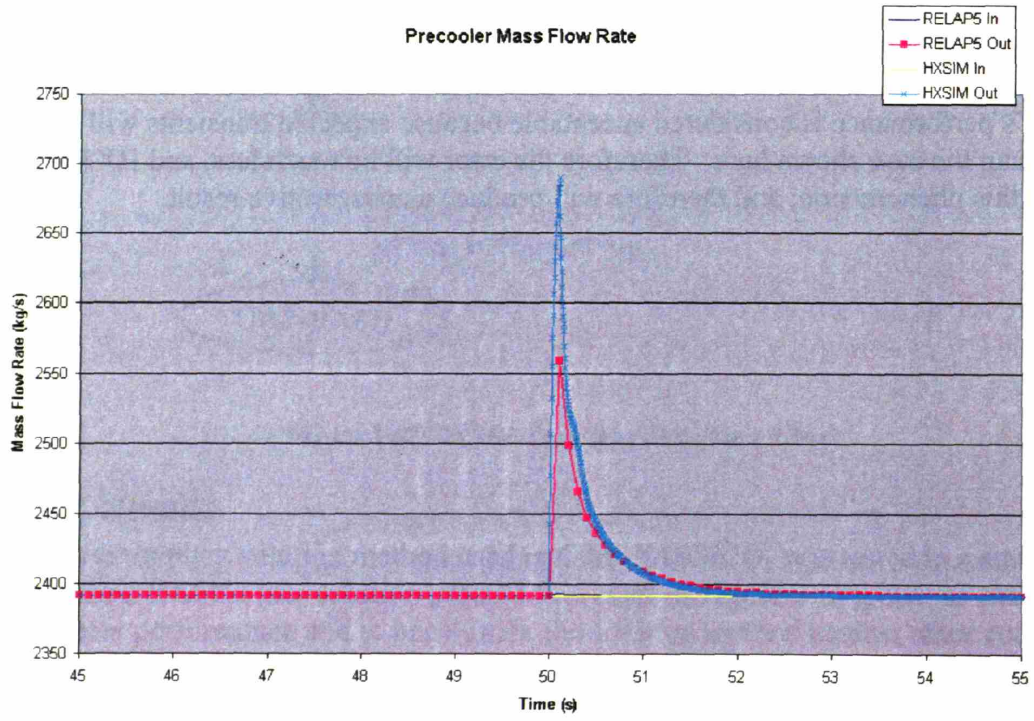

Figure 3-69: HXSIM vs. RELAP5 Mass Flow Rates

3.5.5.2.1 Precooler Numerical Comparison

To compare HXSIM, the 42°C precooler design was compared to (nearly) identical transient cases run by HXMOD and RELAP5. HXMOD is a program written by Langewisch[75] which is highly similar to HXSIM except for a few key differences noted below. RELAP5 is an industry standard heat transfer simulation code using sophisticated models. The RELAP5 simulation performed here was completed by Pope[78].

Compared to HXMOD, HXSIM has several major differences:

- Fluid properties are provided by tables.
- The code is fully implicit.
- PCHE zones are solved iteratively instead of simultaneously.
- The code uses a general numerical solver (instead of matrix inversion).

HXSIM also relaxes several assumptions that HXMOD makes:

- Pressure drop effects on fluid properties are accounted for.
- Mass storage is accounted for (i.e. as fluid densities change).
- Laminar entrance length effects on heat transfer are accounted for.

Note that HXMOD does use the Gnielinski correlation recommended wall temperature correction correlations while HXSIM does not. HXSIM was used to test these correlations during steady state simulations and found that they produced negligible differences on heat transfer for PCHE simulated for the S-CO_2 recompression cycle. This probably stems from the relatively small temperature difference between the fluid stream and the structure wall in these small channels. They were removed for transient simulation due to their complicating effects with the fully implicit transient solution.

Both HXSIM and HXMOD used 10 axial nodes for the simulation shown. Recall that the models used for these codes assume that the metal wall instantly comes into thermal equilibrium with the surrounding fluids i.e. the wall is not nodalized. RELAP5 used a more complex nodalization scheme as shown in Figure 3-70.

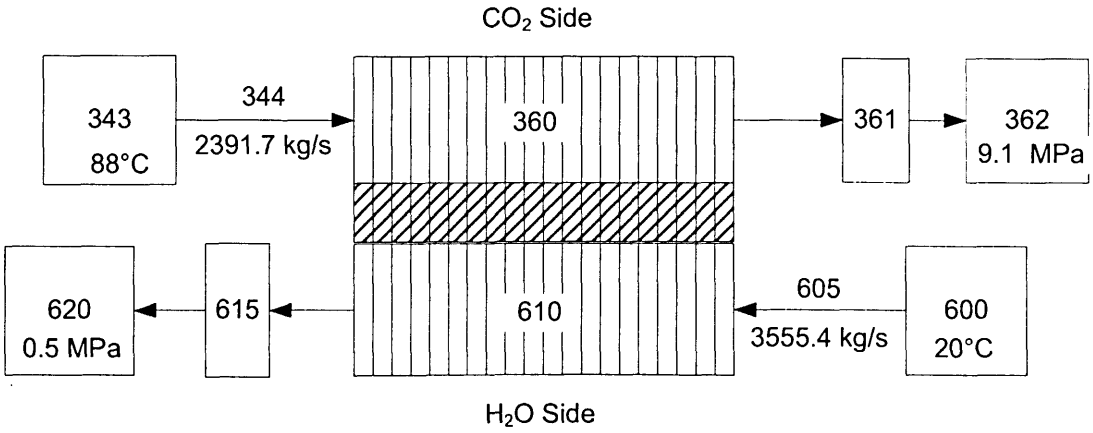

Figure 3-70: RELAP Nodalization Diagram of Comparison Precooler Model[78]

The transient simulation began with steady state conditions, then the hot fluid inlet was temperature linearly increased until 0.05 seconds, when the hot fluid (CO_2) inlet temperature was 40°C hotter -- a close approximation of a step change. This higher temperature was held for the rest of the simulation and the other fluid inlet values were not changed.

The results of the simulation are shown for transient outlet temperatures for RELAP5 and HXMOD in Figure 3-71 and for HXSIM in Figure 3-72 and Figure 3-73. These figures show highly similar time dependent behavior, but in all cases RELAP5 predicted the largest heat transfer and HXMOD the least. Note that there is a small bump in Figure 3-73 where the convergence criteria were relaxed to converge a difficult time step.

The steady state outlet values and heat transfer are compared in Table 3-14 and Table 3-15 to RELAP5 and HXMOD respectively. In both cases the relative errors are well within the expected heat transfer correlation uncertainties and HXSIM calculates values between the other two codes. Note that a key area of uncertainty in heat transfer stems from the laminar to turbulent transition on the water side of the precooler.

The highly similar time dependent behavior and the relatively small error between heat transfer predictions shown between HXSIM, HXMOD, and RELAP5 suggest that HXSIM is sufficiently accurate for use in GAS-PASS/CO_2. As more accurate heat transfer correlations become available and are incorporated, this assertion should be revisited.

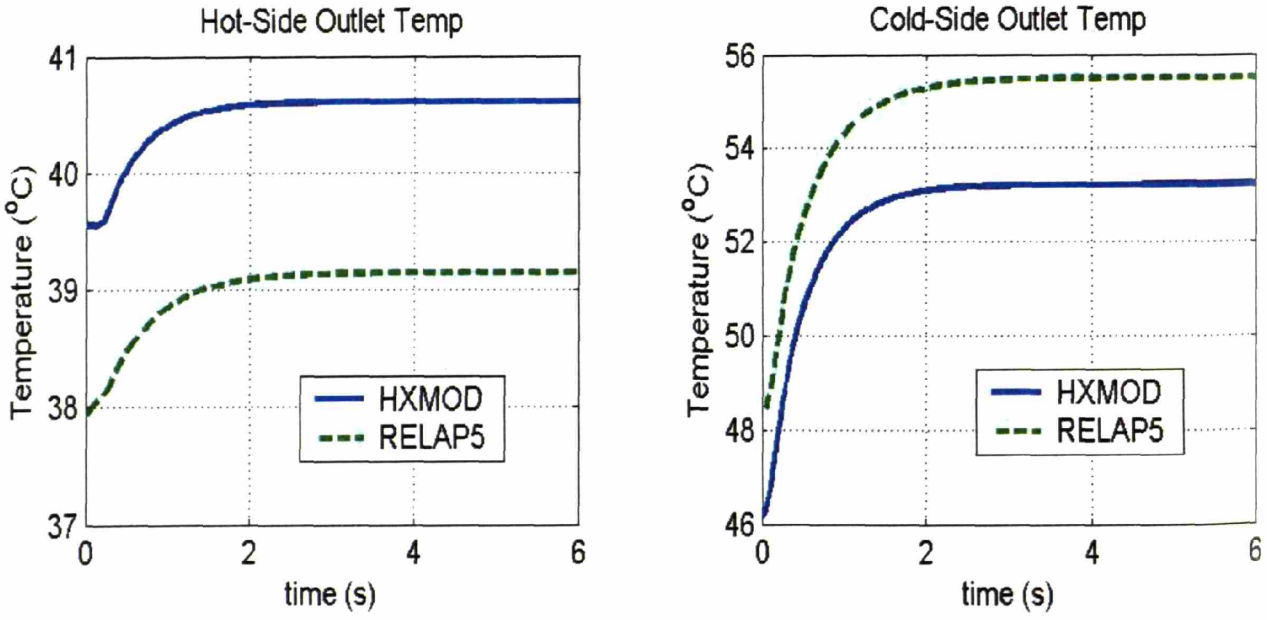

Figure 3-71: CO_2 and H_2O Outlet Temperatures for RELAP5 vs. HXMOD Comparison (transition Re 1800-2800)[75]

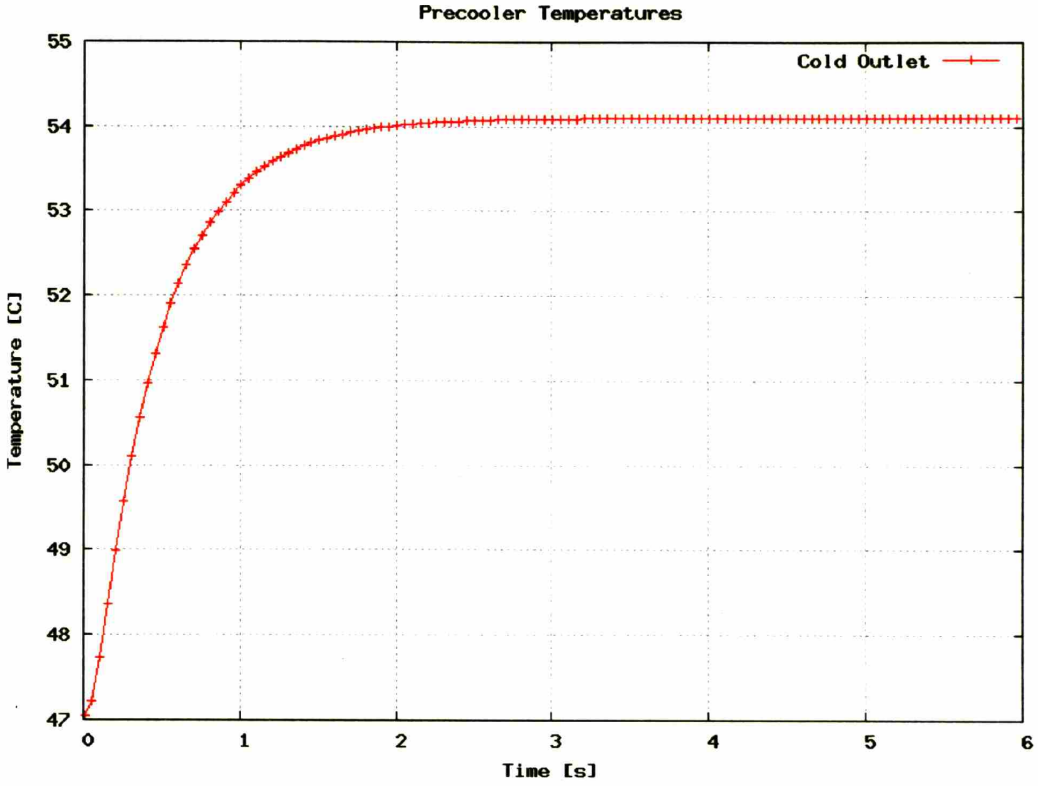

Figure 3-72: HXSIM (GAS-PASS/CO_2) Precooler Comparison Water Cold Outlet Temperature

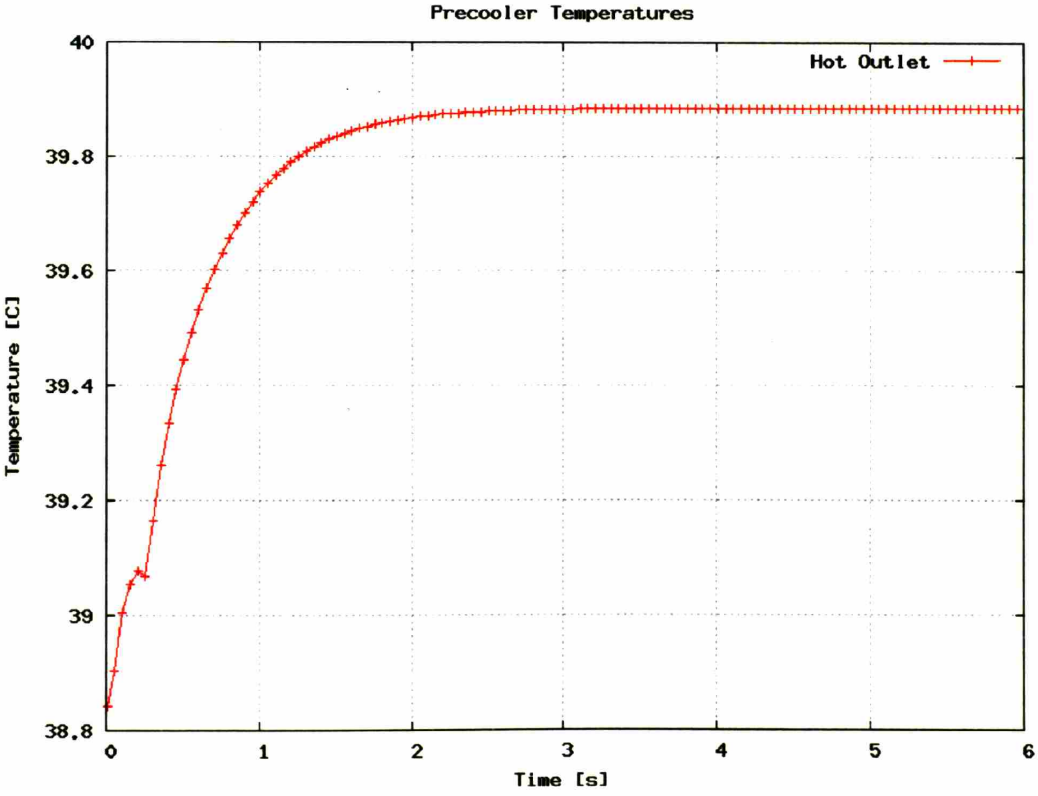

Figure 3-73: HXSIM (GAS-PASS/CO_2) Precooler Comparison CO_2 Hot Outlet Temperature

Table 3-14: Steady State Precooler Comparison vs. RELAP5

	RELAP5	HXSIM	Discrepancy
Hot-Side Outlet Temp (°C)	37.90	38.85	+0.95°C
Cold-Side Outlet Temp (°C)	48.40	47.05	-1.35°C
Heat Transfer Rate (MW)	425.9	402.2	-5.6%

Table 3-15: Steady State Precooler Comparison vs. HXMOD (Transition Re 1800-2800)

	HXMOD	HXSIM	Discrepancy
Hot-Side Outlet Temp (°C)	39.66	38.85	-0.81°C
Cold-Side Outlet Temp (°C)	46.03	47.05	+1.02°C
Heat Transfer Rate (MW)	386.9	402.2	+4.0%

3.5.6 Section Summary

Printed circuit heat exchangers are a key component for the highly recuperated S-CO_2 recompression cycle. Although there is some uncertainty about the selection of appropriate heat transfer and pressure drop correlations, it is judged that current GAS-PASS/CO_2 correlations are sufficiently accurate and conservative, and that the transient and steady state modeling coding has been validated.

Due to the non-linear property changes of S-CO_2, simple analytical correlations are not available to model heat exchanger performance. However, PCHEs can be efficiently computed by axially nodalizing a single channel, computing with enthalpy at the midpoint of a node, using past solutions as initial guesses, and avoiding excess computational loops when PCHEs are computed within a general non-linear solver. Efficient computation allows realistic transient simulation where a small non-linear set of equations must be solved within each node of every PCHE. All things considered, GAS-PASS/CO_2 offers a fast and accurate method to compute heat exchange and pressure drop in this cycle.

3.6 The GAS-PASS Simulation Code

Over the past two years GAS-PASS/CO_2 has been significantly modified and improved, as documented in this chapter. The code is now fully functional and can successfully simulate the S-CO_2 recompression cycle. It is still a work in progress, but future changes will stem primarily from simulation results and the introduction of new control capabilities instead of fundamental code development. Appendix B: Suggested Future Improvements contains a discussion on attractive future code improvements.

This chapter contains five sections:

1. A brief description of the current code.
2. A review of the unchanged GAS-PASS solution process.
3. An explanation and analysis of the new component conservation equations.

4. A description of the techniques used to make the code robust.
5. A summary of this section.

3.6.1 GAS-PASS/CO_2

GAS-PASS/CO_2 represents a comprehensive update to GAS-PASS/He. It retains the original code structure and solution process but has been rewritten on a line by line basis where original code was retained and the majority of the current code was written from scratch. The current code is about 24,000 lines of Fortran 90* in 27 source files.

GAS-PASS/CO_2 now includes all real fluid properties, detailed turbomachinery performance interpolation with correction for fluid property effects, and detailed PCHE heat transfer and pressure drop calculations.

While tailored to the S-CO_2 cycle the code is modular and general, allowing the end user to change almost any part of the plant simply by modifying simple text input files. New capabilities will, of course, require modifying the source code but the end user could easily change the current code to something quite different without coding. For example, the current model could be converted to a helium plant, heated by lead bismuth, with a radial turbine, and axial-radial hybrid compressors without editing the source. The major task to creating new plant designs is creating and combining new component input files.

Due to the general nature of the fluid properties code, any fluid that can be pre-computed and put in tabular format can be used. Due to the general nature of the turbomachinery methods, any design that offers sets of shafts speed curves can be modeled. Due to the general nature of the heat transfer code any type of PCHE can be modeled for any set of fluids (assuming the current heat transfer and pressure drop correlations may be used). These capabilities should place GAS-PASS/CO_2 in an excellent position for future use.

3.6.1.1 Input/Output

GAS-PASS/CO_2 takes 33 input files, and produces 11 output files when set up to model the S-CO_2 recompression cycle. The large number of files separates different aspects of the code and is solely for user convenience. The only command line argument GAS-PASS/CO_2 takes is the name of the input file, which lists all of these other files. Table 3-16 provides a brief description of the input and output files.

The filename input file is separated into five sections:

1. The first section contains the main GAS-PASS/CO_2 input file, the transient normalization factors input file, and the PID settings file.
2. The second section contains the heat exchanger geometry and characteristics with every PCHE in a separate file.
3. The third section contains the performance curves for the turbomachinery. Each turbomachine has one file.

---

* GAS-PASS/CO_2 is programmed and developed with Compaq Visual Fortran 6.6.C. Older Compaq Visual Fortran compilers will not work with some of the new features.

4. The fourth section contains the property table files for all three fluids: the external heat addition fluid, the cycle working fluid, and the external cooling fluid.
5. The fifth file contains the various output files.

Generally, the main GAS-PASS/CO_2 input and PID settings file will be the only files that the user will want to edit -- all other files need to be set up only once. The reader should note that the fluid property tables are a repetitive set of tables for the various fluids except that the working fluid has two extra fluid tables which are used to perform turbomachinery performance calculations.

Table 3-16: GAS-PASS/CO_2 Input and Output Files

Input Order	Purpose	Name	Description
1	Input	inputs\gp.i	The main GAS-PASS/CO_2 input file.
2	Input	inputs\ cond_num.i	Previously created transient equation normalization factors.
3	PID Input	inputs\control.i	PID controller settings.
4	PCHE Input	inputs\pre.i	The precooler specifications.
5	PCHE Input	inputs\ltr.i	The low temperature recuperator specifications.
6	PCHE Input	inputs\htr.i	The high temperature recuperator specifications.
7	PCHE Input	inputs\ihx.i	The intermediate heat exchanger specifications.
8	TURBO Input	inputs\main.i	The main compressor performance curves.
9	TURBO Input	inputs\recomp.i	The recompression compressor performance curves.
10	TURBO Input	inputs\turbine.i	The turbine performance curves.
11	PROP Input	inputs\tables\ NA-HP-Cp.dat	The heating fluid enthalpy and pressure to isobaric specific heat table.
12	PROP Input	inputs\tables\ NA-HP-D.dat	The heating fluid enthalpy and pressure to density table.
13	PROP Input	inputs\tables\ NA-HP-E.dat	The heating fluid enthalpy and pressure to internal energy table.
14	PROP Input	inputs\tables\ NA-HP-K.dat	The heating fluid enthalpy and pressure to thermal conductivity table.
15	PROP Input	inputs\tables\ NA-HP-T.dat	The heating fluid enthalpy and pressure to temperature table.
16	PROP Input	inputs\tables\ NA-HP-V.dat	The heating fluid enthalpy and pressure to viscosity table.
17	PROP	inputs\tables\	The heating fluid temperature and pressure to

	Input	NA-TP-H.dat	enthalpy table.
18	PROP Input	inputs\tables\ CO2-HP-Cp.dat	The working fluid enthalpy and pressure to isobaric specific heat table.
19	PROP Input	inputs\tables\ CO2-HP-D.dat	The working fluid enthalpy and pressure to density table.
20	PROP Input	inputs\tables\ CO2-HP-E.dat	The working fluid enthalpy and pressure to internal energy table.
21	PROP Input	inputs\tables\ CO2-HP-K.dat	The working fluid enthalpy and pressure to thermal conductivity table.
22	PROP Input	inputs\tables\ CO2-HP-T.dat	The working fluid enthalpy and pressure to temperature table.
23	PROP Input	inputs\tables\ CO2-HP-V.dat	The working fluid enthalpy and pressure to viscosity table.
24	PROP Input	inputs\tables\ CO2-TP-H.dat	The working fluid temperature and pressure to enthalpy table.
25	PROP Input	inputs\tables\ CO2-HP-S.dat	The working fluid enthalpy and pressure to entropy table.
26	PROP Input	inputs\tables\ CO2-SP-H.dat	The working fluid entropy and pressure to enthalpy table.
27	PROP Input	inputs\tables\ H2O-HP-Cp.dat	The cooling fluid enthalpy and pressure to isobaric specific heat table.
28	PROP Input	inputs\tables\ H2O-HP-D.dat	The cooling fluid enthalpy and pressure to density table.
29	PROP Input	inputs\tables\ H2O-HP-E.dat	The cooling fluid enthalpy and pressure to internal energy table.
30	PROP Input	inputs\tables\ H2O-HP-K.dat	The cooling fluid enthalpy and pressure to thermal conductivity table.
31	PROP Input	inputs\tables\ H2O-HP-T.dat	The cooling fluid enthalpy and pressure to temperature table.
32	PROP Input	inputs\tables\ H2O-HP-V.dat	The cooling fluid enthalpy and pressure to viscosity table.
33	PROP Input	inputs\tables\ H2O-TP-H.dat	The cooling fluid temperature and pressure to enthalpy table.
34	Output	outputs\gp.o	The main GAS-PASS/CO_2 outputs file containing the simulation results.
35	Output	outputs\ variables.o	An output file listing boundary conditions and solved for variables.
36	Output	outputs\gp.i	An output file that creates a new main GAS-PASS/CO_2 input file with converged steady state solutions from the current simulation.
37	Output	outputs\log.o	A run log containing all screen output and warning messages.
38	Output	outputs\ss_jac.o	The steady state Jacobian.
39	Output	outputs\tr_jac.o	The (initial) transient Jacobian.
40	Output	outputs\	The transient equation normalization factors used.

		cond_num.i	
41	PID Output	outputs\ control.o	The PID controller inputs, error, and rate of change.
42	TURBO Output	outputs\ turbine.o	The turbine volumetric flow rate, limits, and off-design data.
43	TURBO Output	outputs\ recomp.o	The recompression compressor volumetric flow rate, limits, and off-design data.
44	TURBO Output	outputs\ main_comp.o	The main compressor volumetric flow rate, limits, and off-design data.

3.6.1.2 Source Code

The source code has changed significantly from the ideal gas code GAS-PASS/He. The 27 files are grouped by function and include the new sections of properties, turbomachinery, and PCHE simulation. Commonly used code has been grouped into libraries and the general input/output routines have been grouped as well. These source files are briefly explained in Table 3-17. The reader may also consult the previously presented steady state flow chart in Figure 3-3 and the transient flow chart in Figure 3-4.

Table 3-17: GAS-PASS/CO_2 Source Files

#	Name	Folder	Function
1	Main.f90	.	To control the flow of the program
2	Imsl.f90	.	To provide the exact interface expected by IMSL solver routines. Note that these subroutines are the only code in the whole program which are not in modules.
3	Common.f90	Library	To provide commonly used general routines
4	Engineering.f90	Library	To provide commonly used engineering routines.
5	Gp.f90	Library	GAS-PASS specific commonly used routines.
6	Math.f90	Library	To provide commonly used mathematical routines.
7	System.f90	Library	To provide commonly used routines that interface with the operating system.
8	Input.f90	IO	To read in and process: the filename input file and the main GAS-PASS input file.
9	Control.f90	IO	To read in and process PID settings.
10	ssOutPout.f90	IO	To output a detailed variable list and to create a new GAS-PASS input file based upon converged results.
11	Props.f90	Properties	To handle all property related routines including table read in & interpolation (linear & log).
12	Turbodata.f90	Turbomap	To read in and process turbomachinery characteristics & performance curves.

13	Turbointerpolate.f90	Turbomap	To interpolate along & between shaft speed curves.
14	Turbolibrary.f90	Turbomap	To provide commonly used turbomachinery routines.
15	Qpche.f90	PCHE	To calculate steady state PCHE performance using Newton's method.
16	Pche_tr.f90	PCHE	To calculate transient PCHE performance using non-linear equation solver.
17	Pcheinitialize.f90	PCHE	To initialize a PCHE's zone data with good guesses.
18	Pcheinput.f90	PCHE	To read in & process a PCHEs characteristics.
19	Pchestruct.f90	PCHE	Provide custom memory structures for zone data and PCHE characteristics.
20	Pchethermo.f90	PCHE	To hold PCHE heat transfer and pressure drop correlations.
21	Zones.f90	PCHE	Calculate a zone's heat transfer, pressure drop, mass inventory, and energy inventory. Used in both steady state and transient calculations.
22	Components.f90	SS	Provide the solution equations and model calls for steady state components.
23	Fcn.f90	SS	Supervise the execution of one plant evaluation given variable inputs.
24	SS.f90	SS	Supervise calculations of steady state solution.
25	Components_tr.f90	TR	Provide the equations and model calls for transient components.
26	Fcn_tr.f90	TR	Supervise the execution of one transient plant evaluation given variable inputs.
27	TR.f90	TR	Supervise the calculations of the transient solution and outputting data.

3.6.2 Component Conservation Equations

This section will discuss two unique aspects of the component conservation equations: the primary loop equations and avoiding linear dependence in mass loop equations. A general discussion of the conservation equations was already presented in Section 3.2.2.1 and the full set of solution equations are presented in, "*Appendix* A: GAS-PASS/CO2 Equations".

3.6.2.1 Primary Loop Equations

GAS-PASS/CO_2 has been designed to simulate the indirect S-CO_2 recompression cycle, but the primary system deserves further analysis. The primary system consists of a loop of liquid sodium with an intermediate heat exchanger (IHX), reactor, and other components lumped into a single component called "primary."

While such a simple physical loop is easy to envision, it is complicated to incorporate in GAS-PASS/CO_2 due to two interlinked factors:

- Sodium properties do not depend on pressure.
- The primary loop cannot use a typical set of closed loop mass equations.

3.6.2.1.1 Primary Pressure

The fluid properties used for liquid sodium come from simple polynomials which account for temperature effects but do not deal with pressure. Physically this should be expected since liquid sodium will not change fluid properties significantly (the fluid is largely incompressible) and the sodium loop will not operate under high pressures nor pressure variations. Therefore, accounting for pressure is not useful except to deal with pressure loss.

Pressure loss in a liquid sodium loop is a secondary effect where GAS-PASS/CO_2 is concerned. Pumping liquid sodium will require only a small amount of work compared to pumping S-CO_2 and thus will not impact plant efficiency appreciably. Hence there is little reason to deal with pressure in the primary loop at this stage of analysis.

This is the approach taken in GAS-PASS/CO_2 where pressure is fixed in the reactor and primary loop and they do not have pressure equations. The IHX still properly accounts for pressure drop (and has a pressure drop equation) because it uses shared code with other PCHE heat exchangers, but the output of this module, the outgoing pressure, is neglected at the next component. The (input file) pressure specifications used in the GAS-PASS/CO_2 loop should therefore be:

```
0.20 :Primary
1        1
0.20 :Reactor
1        1
0.151193395252949 :IHX-Hot
0        0
```

The first number of each component specifies the pressure in mega-Pascal and the rest of the line is simply a description provided to the user. The second line specifies how the values is treated in the steady sate and the transient computation. A value of 1 signifies that the variable is a boundary condition while a value of 0 signifies it is a variable. Thus this command states that the primary and reactor pressure are fixed, while the output of the IHX (hot side) is allowed to match the calculated pressure drop. The interested reader can read more about the input files and format in, "Appendix C: GAS-PASS/CO_2 User Manual."

3.6.2.1.2 Primary Mass Conservation

It will been shown in Section 3.6.2.3 that setting incoming mass flow rate equal to outgoing mass flow rate (even if mass storage is enabled) in a closed loop produces an linearly dependent set of equations and simulation failure. The typical solution to this

problem is to use a total loop inventory equation for one component's (arbitrarily selected) mass conservation equation. This approach was not taken for the liquid sodium primary loop for several reasons:

1. Modeling the primary system's volumes and fluid inventories is not necessary for simulation of the indirect S-CO_2 recompression cycle.
2. Mass flow rate is a function of pumping power and pressure drop. Since pressure drop is not modeled, there is no feedback to determine the mass flow rate.
3. Liquid sodium (as modeled here) is completely incompressible, therefore no stored fluid can move between components. This may create a stiff solution loop where very small changes in mass flow rate/fluid storage are calculated to solve the loop.
4. Easier alternatives exist.

GAS-PASS/CO_2 models primary loop mass conservation by opening the mass conservation loop in the primary component. Regardless of the incoming fluid mass flow rate, the outgoing fluid mass flow rate is determined solely by pump work. This solution prevents an over-determined matrix and allows the user to control fluid mass flow rates. The primary mass conservation equation is:

$$0 \sim F(i) = W_{pump} - C * \dot{m}_{out}$$

This equation states that pump work is proportional to mass flow rate: as mass flow rates increase work must increase and vice-versa. While crude, this equation is only used to provide a "knob" to control loop mass flow rate.

The other components use a standard balance: incoming equals outgoing mass flow rate:

$$0 \sim F(i) = \dot{m}_{in} - \dot{m}_{out}$$

Therefore the component feeding the primary component has its outgoing mass flow rate neglected. Since the mass flow is determined from the outlet of the primary component, and all other components have constant mass flow rates, then the whole loop has an identical mass flow rate.

This solution prevents matrix problems, is simple, and allows the user complete control over mass flow rates even allowing the user of GAS-PASS/CO_2 to determine the mass flow rate via energy conservation.

3.6.2.1.3 Primary Energy Conservation

GAS-PASS/CO_2 conserves specific enthalpy* throughout the primary loop. The loop energy conservation equations are shown in Equation 3-28 through Equation 3-30.

These equations preserve fluid specific enthalpy (with constant pressure enthalpy becomes solely a function of temperature) and effectively conserve energy. In every primary component, the incoming mass flow rate is equal to outgoing mass flow rate, therefore these equations conserve energy. By preserving fluid temperature the liquid

* Specific enthalpy is the amount of enthalpy per unit mass and defined as $h = u + pv$.

sodium properties will be accurately calculated and used in heat transfer calculations with the S-CO_2, and appropriate sodium temperatures will be used to transfer heat to the S-CO_2 as well.

Equation 3-28: Primary Equation **(3-28)**

$$0 \sim F(i) = h_{in} - h_{out}$$

Equation 3-29: Reactor Equation **(3-29)**

$$0 \sim F(i) = \left(h_{in} + \frac{Q_{reactor}}{\dot{m}_{out}} \right) - h_{out}$$

Equation 3-30: IHX Equation **(3-30)**

$$0 \sim F(i) = \left(h_{in} - \frac{Q_{ihx}}{\dot{m}_{out}} \right) - h_{out}$$

The reactor and IHX equations also contain a heat transfer and a mass flow rate term. Thus, if the user decides to fix a loop temperature, then the mass flow rate or the reactor heat addition can be solved for. In general the user will want to fix the reactor heat addition and let all three temperatures be solved for.

3.6.2.1.4 Primary Section Conclusion

GAS-PASS/CO_2 uses a very simple primary loop model but still allows the user full control over relevant variables. This simple treatment avoids complicated calculations and numerous equations, which would slow the overall simulation when this loop is of small importance as in the present study. This model is appropriate for the system being studied, but would be wholly inappropriate for a helium primary loop.

3.6.2.2 Preventing Mass Equation Linear Dependence

Setting up a closed system of components (such that there is no mass (typically) leaving the system) requires care that the solution matrix does not become linearly dependent in the mass equations. When setting up component conservation equations the mass conservation equation is typically the most straightforward. However, if the system loop is closed then this system of equations will become linearly dependent, as shown in the following examples.

3.6.2.2.1 Linear Mass Dependence Example – Steady State

Figure 3-74 shows a very simple closed system where component **A** feeds directly into component **B** which feeds directly back into component **A**. There is no mass storage in the pipes (the connectors between components), no mass can escape the system, and the volumes of the components do not change.

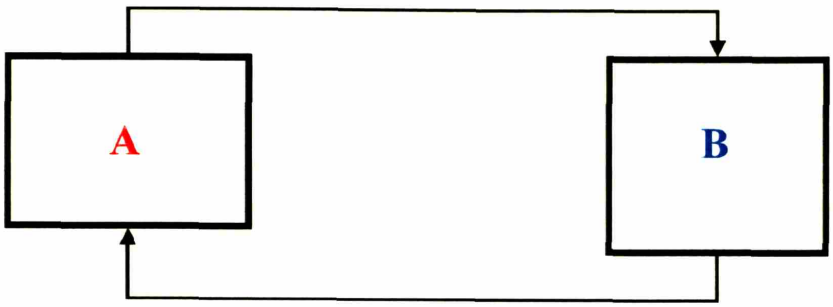

Figure 3-74: Component Mass Equations

The mass conservation equation for a control volume is:

$$\frac{dM}{dt} = \dot{m}_{in} - \dot{m}_{out} \rightarrow \dot{m}_{in} - \dot{m}_{out} = \dot{M}$$

Thus setting up a system of mass conservation equations gives:

$$1 * \dot{m}^{A}_{in} - 1 * \dot{m}^{A}_{out} = \dot{M}^{A}$$

$$1 * \dot{m}^{B}_{in} - 1 * \dot{m}^{B}_{out} = \dot{M}^{B}$$

If we set up this system for the steady state (no mass storage) it follows that:

$$1 * \dot{m}^{A}_{in} - 1 * \dot{m}^{A}_{out} = 0$$

$$1 * \dot{m}^{B}_{in} - 1 * \dot{m}^{B}_{out} = 0$$

By definition what comes out of a pipe must go into the next pipe, therefore:

$$\dot{m}^{A}_{out} = \dot{m}^{B}_{in}$$

$$\dot{m}^{B}_{out} = \dot{m}^{A}_{in}$$

Thus, substituting the **A** variables for **B** variables, our system becomes:

$$1 * \dot{m}^{A}_{in} - 1 * \dot{m}^{A}_{out} = 0$$

$$1 * \dot{m}^{A}_{out} - 1 * \dot{m}^{A}_{in} = 0$$

This in matrix form is:

$\dot{m}^{A}_{in}$	$\dot{m}^{A}_{out}$	$\dot{M}$
1	-1	0
-1	1	0

Alternatively both equations can be rearranged to yield:

$$\dot{m}^{A}_{in} = \dot{m}^{A}_{out}$$

$$\dot{m}^{A}_{in} = \dot{m}^{A}_{out}$$

From either perspective it is apparent that we have two equations but only one unknown, which is an over-determined or linearly-dependent system of equations. Therefore, any answer will satisfy these equations and the simulation will appear to work quite robustly regardless of the behavior of the closed loop mass equations i.e. we are not simulating a real/physical system.

3.6.2.2.2 Linear Mass Dependence Example – Transient

It is worth showing that this problem applies to the transient case as well. Once again we will use Figure 3-74 which shows a very simple closed system where component **A** feeds directly into component **B** which feeds directly back into component **A**.

The transient mass equations are:

$$1*\dot{m}^{A}_{in} - 1*\dot{m}^{A}_{out} = \dot{M}^{A}$$

$$1*\dot{m}^{B}_{in} - 1*\dot{m}^{B}_{out} = \dot{M}^{B}$$

Even though there can be storage in a component, by definition, what comes out of a pipe must go into the next pipe, therefore:

$$\dot{m}^{A}_{out} = \dot{m}^{B}_{in}$$

$$\dot{m}^{B}_{out} = \dot{m}^{A}_{in}$$

Thus, substituting the **A** variables for **B** variables the system becomes:

$$1*\dot{m}^{A}_{in} - 1*\dot{m}^{A}_{out} = \dot{M}^{A}$$

$$1*\dot{m}^{A}_{out} - 1*\dot{m}^{A}_{in} = \dot{M}^{B}$$

This in matrix form is:

$\dot{m}^{A}_{in}$	$\dot{m}^{A}_{out}$	$\dot{M}$
1	-1	$1\ \dot{M}^{A}$
-1	1	$1\ \dot{M}^{B}$

Alternatively both equations can be substituted for each other:

$1*\dot{m}^{A}_{in} = \dot{M}^{A} + 1*\dot{m}^{A}_{out}$ -> substituting for $\dot{m}^{A}_{in}$ in the **B** equation:

$$1*\dot{m}^{A}_{out}-\left(\dot{M}^{A}+1*\dot{m}^{A}_{out}\right)=\dot{M}^{B} \;\text{->}\; -\dot{M}^{A}=\dot{M}^{B}$$

From either perspective this result makes common sense -- if component **A** stores more mass then it has to come from component **B** and vice-versa. However, this still involves two identical equations. If one substitutes only the **A** values into the **B** equations the result is:

$$1*\dot{m}^{A}_{in}-1*\dot{m}^{A}_{out}=\dot{M}^{A}$$

$$1*\dot{m}^{A}_{out}-1*\dot{m}^{A}_{in}=-\dot{M}^{A}$$

Or:

$\dot{m}^{A}_{in}$	$\dot{m}^{A}_{out}$	$\dot{M}$
1	-1	$\dot{M}^{A}$
-1	1	$-\dot{M}^{A}$

Therefore the system is still over-determined with two identical equations, where any $\dot{m}^{A}_{in}$ will work. The situation is the same as in the steady state example.

3.6.2.3 Avoiding Linear Mass Dependence

It is now evident that, that for a two component closed loop, setting up mass conservation in both components creates a linearly dependent system. What is true for two components is true for any number. This counterintuitive result should be clearly stated:

> ***in a closed loop system setting up mass conservation equations for each component leads to simulation failure.***

Fundamentally, what has been lacking thus far is the amount of fluid in the system. The equations so far have described rates of change without mentioning the amount; therefore they are conceptually as well as mathematically incomplete.

To create linear independence and fully describe the system one can simply remove one component's mass conservation equation and replace it with a system fluid storage/inventory equation. This will be made clear with an example.

Again referencing the system in Figure 3-74, the mass equations can be setup as shown in Equation 3-31 and Equation 3-32.

Equation 3-31: Component A Mass Conservation Equation (3-31)

$$1^{*}\dot{m}_{in}^{A} - 1^{*}\dot{m}_{out}^{A} = \dot{M}^{A}$$

Equation 3-32: Loop Mass Inventory Equation (3-32)

$$\sum_{i=1}^{n} M^{i} = M^{Total}$$

Equation 3-32 simply states that the total fluid in the system is equal to the sum of the fluid masses in individual components. This equation becomes slightly more sophisticated if it is recognized that the mass in each component can change with time, but the system inventory does not as shown in Equation 3-33.

Equation 3-33: Time Dependent Loop Mass Inventory Equation (3-33)

$$\sum_{i=1}^{n} M(t)^{i} = M^{Total}$$

The amount of fluid in a component may be calculated from (assuming a fixed control volume) fluid density:

$$M(t) = \rho(t) * Vol$$

Similarly, the rate of change in mass storage can be expressed in terms of fluid density:

$$\frac{dM}{dt} = \dot{M} = \frac{d\rho}{dt} * Vol$$

Substituting these ideas into Equation 3-31 and Equation 3-33 yields Equation 3-34 and Equation 3-35.

Equation 3-34: Component A Mass Conservation Equation by Fluid Density (3-34)

$$1^{*}\dot{m}_{in}^{A} - 1^{*}\dot{m}_{out}^{A} = \frac{d\rho^{A}}{dt} * Vol^{A}$$

Equation 3-35: Loop Mass Inventory Equation by Fluid Density (3-35)

$$\sum_{i=1}^{n} \rho(t)^{i} Vol^{i} = M^{Total}$$

Since there are only two components **A** and **B** the inventory control equation can be expressed as Equation 3-36.

Equation 3-36: Complete Loop Mass Inventory Equation by Fluid Density (3-36)

$$\rho(t)^A Vol^A + \rho(t)^B Vol^B = M^{Total}$$

By now it should be clear that Equation 3-34 and Equation 3-36 are not linearly dependent. However, it bears further clarification that this still allows us to properly simulate a real system. If one takes a time derivative Equation 3-36:

$$\frac{d\rho^A}{dt}Vol^A + \frac{d\rho^B}{dt}Vol^B = 0 \rightarrow -\frac{d\rho^A}{dt}Vol^A = \frac{d\rho^B}{dt}Vol^B \rightarrow -\dot{M}^A = \dot{M}^B,$$

the same result that follows as previously achieved with the mass conservation equations. Therefore, the conservation of system inventory equation added is simply the *integral of the mass flow rate equations with time*. Conceptually this means that the first equation contains time varying mass information and the second equation contains time integrated (not invariant) mass information. This suggests that these equations completely describe system mass while managing to avoid linear dependence.

Looking at the Equation 3-31 and Equation 3-32 from a physical perspective may make this clear. Figure 3-74 shows that if the mass flow rates coming in and out of component **A** are known, then every mass flow rate in the system (since the pipes do not have storage in this example) is known. Equation 3-31 contains these terms and it also describes how the amount of fluid stored in component **A** is changing, which is by definition equal to the how the amount of fluid stored in component **B** is changing. Thus this first equation describes everything about mass in the system except:

- the amount of mass stored in component **A**
- the amount of mass stored in component **B**

Equation 3-32 describes the amount of mass stored in the components, therefore complete system mass information is contained in these two equations.

3.6.2.4 Implementing the Solution

In practice one must calculate the amount of fluid mass stored in the system before the mass flow rate equations can be applied. In the steady state this is easily accomplished by simply setting the total mass equal to the calculated sum of the individual masses the first time the code is called, and holding it constant thereafter. In pseudo-code:

In all but one component:

F(1) = Min - Mout
*Mass(i) = Rho(i) * Vol(i)*

In one component:

*Mass(i) = Rho(i) * Vol(i)*
CalcMass=SUM(Mass(*))

If(FirstTime) Then

```
        TotalMass = CalcMass
Endif

F(1) = (TotMass - CalcMass)
```

In the transient the already-calculated total fluid mass can be used, thus the pseudo code would be:

In all but one component:

```
Mass(i) = Rho(i) * Vol(i)
F(1)=(Mass(i)- MassOld(i))/dT – (Min-Mout)
```

In one component:

```
Mass(i) = Rho(i) * Vol(i)
CalcMass=SUM(Mass(*))
F(1) = (TotMass - CalcMass)
```

When computing the total fluid mass, care should be taken not to include components that will have time invariant fluid mass. If a component doesn't store mass during the transient then:

$$\frac{dM^i}{dt} = 0 \rightarrow \dot{m}_{in}^{\,i} = \dot{m}_{out}^{\,i}$$

This does not mean that the component cannot have a fluid mass; it just means that the stored mass cannot change thus:

$$M^i(t) = M^i$$

However, if the component's fluid mass is: $M(t) = \rho(t) * Vol$ then this dictates that the fluid density in that component cannot change, thus its temperature and pressure cannot change with time if the fluid is compressible. Since any real simulation will have changing temperatures and pressures and compressible fluids, in practice this means that if a mass is computed for components that do not have transient mass storage then this mass cannot be added to the total fluid inventory without violating mass conservation. An excellent way to avoid this issue altogether is to set the volume of components to 0 for those components that have time invariant mass storage.

GAS-PASS/CO_2 provides volumes for transient mass storage in all the modeled components for the S-CO_2 recompression cycle containing carbon dioxide except the splitting-T* and valves. The valves have a very small volume, thus may be neglected and the splitting-T has proven numerically difficult to implement for the case with storage.

* The splitting-T is simply the name of the component containing the compressor flow split. While simple in operation, this component contains significant volume since it also serves as a collection point for the outlet of the parallel modules of the low temperature recuperator (shown in Figure 2-4).

The S-CO_2 recompression cycle is quite sensitive to the compressor flow split. Small changes in the flow split fraction produce large changes in cycle performance (an example is available in Section 5.1.1). Furthermore, how the splitting-T is simulated has a significant effect on the ability of a computer to solve this system. If the flow split is treated as a boundary condition then the system condition number* is similar to the ideal gas systems previously simulated by GAS-PASS/He and readily solved by GAS-PASS/CO_2. However, if the flow split is allowed to vary† then the condition number approaches machine precision and simulation reliability drops. If the splitting-T is not only allowed to vary but contains stored fluid (recall that fluid is assumed lumped and experiences perfect mixing) then the system condition number drops significantly and the numerical system will not converge as simulated in this work. Since the mass storage in the splitting-T is not crucial to cycle dynamics it has been omitted.

3.6.3 GAS-PASS/CO_2 Solution Techniques

Converging the S-CO_2 recompression cycle initially proved quite difficult. This was expected given the strong non-linearity in the S-CO_2 properties (see Section 2.1.2) near the critical point, where parts of the cycle operate. The reader has probably noted numerous "tricks" and techniques to promote system linearity throughout this report. This section is the outgrowth of what happens when those tricks and techniques fail.

GAS-PASS/CO_2 is quite robust compared to past versions of GAS-PASS/He. Previously, the failure of almost any process during simulation would lead to simulation failure. Numerous attempts have been made to allow GAS-PASS/CO_2 to continue with a simulation, for as long as is reasonable, even if computation becomes difficult.

The major techniques developed are: progressive solution tolerance, time step failure, Jacobian scaling, and numerical turbomachinery performance extrapolation. Note that two solution techniques; Jacobian sparsity, and user controlled dynamic time stepping, are not strictly used to produce a more robust solution, but are important in practice, and therefore included in the solution techniques section. This section will briefly analyze each of these techniques.

3.6.3.1 Progressive Solution Tolerance

The user sets the numerical solver steady state and transient solution tolerance (roughly 10^{-9} with the current solver) via the input file. If this tolerance is not met and no extrapolation errors have been detected, then GAS-PASS/CO_2 will inform the user it is having trouble and attempts to converge with a looser tolerance. This process is repeated

* A condition number represents the ability of a system to be solved digitally. If the condition number is large then the system can easily be solved by a computer. If the condition number approaches (or becomes smaller than) machine precision then problems like round off will prevent the system from being solved reliably, if at all.

† The parallel compressors in the S-CO_2 recompression cycle will automatically control the flow split to balance their outlet pressures if this is not controlled elsewhere (see Section 4.3).

until the solution converges, or until a very large tolerance is not met and the calculation fails.

In general, this can allow a simulation to run past one or two difficult steps. The S-CO_2 cycle can have unexpected difficult regions such as when the pseudo-critical peak is encountered in the main compressor due to a changing pressure or temperature. By allowing the code to run through one or two difficult time steps a simulation can get past things like the pseudo-critical peak without failure.

A more common occurrence is for this technique to only delay failure by a few time steps. If the code needs to converge to a looser tolerance because it can't converge the transient, then no amount of tolerance relaxation will prevent failure. If this is the case, then once the code stops converging tightly it will rapidly run away from a realistic solution and fail within a few steps. The only advantage of this technique in this case is that it gives the user a warning to carefully check the run, since GAS-PASS/CO_2 is being asked to simulate something very difficult.

3.6.3.2 Time Step Failure

If GAS-PASS/CO_2 cannot converge a time step then it will report the error and simply move on to the next time step. The next time step will be attempted with the last converged set of values. Therefore, if necessary, GAS-PASS/CO_2 will skip a time step it cannot converge.

It is not uncommon for GAS-PASS/CO_2 when running the S-CO_2 recompression cycle to fail at a single time step but recover and successfully run afterwards. This occurs in practice when a boundary condition changes sharply or the system hits a difficult point such as a pseudo-critical property peak. By allowing GAS-PASS/CO_2 to fail but recover, the user can gain a lot more information about the simulation and the problem encountered than by simply letting the code exit.

3.6.3.3 Jacobian Guessing

When using a Newtonian numerical solver with a non-linear system it is frequently necessary, for numerical purposes, to provide system values well outside of operating regions. A Newtonian solver works well in a linear region, which in benign systems (i.e. when simulating an ideal gas plant) can be quite large, but in more non-linear systems (a S-CO_2 plant) the linear region, always present near the root, can be quite small.

Therefore, in non-linear systems it is necessary either to assure that one stays within the linear region or that the code can handle some operations in the non-linear region. While the former goal is desirable, it is probably not possible for realistic operating conditions or transients and may be quite difficult numerically. However, the second goal can be accomplished in several ways.

When simulating a plant, several variables are likely to go well outside of expected bounds, including fluid properties and turbomachinery performance curves, when numerical perturbations of the system, during root finding, are performed. Obviously, it

is desirable to have a wide range on the property tables and the performance curves but these are limited by fundamental physics e.g. freezing and dissociation or stall or choke. Even if one makes the fluid property tables and turbomachinery performance curves as large as is physically possible, it is entirely plausible, if not likely, that a Newtonian numerical solver will request values well outside of these bounds. This is especially likely to occur during the solver's first solution after a Jacobian has been calculated.

3.6.3.3.1 Jacobian Slope Estimation

Figure 3-75 shows a two dimensional example of guessing the system root using the Jacobian. If the dotted line in the figure represents the function being modeled and the root is sought, then the difference in calculating the slope from the non-linear point *A* or the more linear point *B* is large.

Since a Newtonian solver is being used, the Jacobian is a one dimensional derivative, thus we are just taking a slope from the initial guess shown by the lines connected to *A* and *B*. Unfortunately, if the function is non-linear then this slope can easily predict an approximation to the root that is a long way from the true value, as happens with *A*. Correspondingly, point *B*, which is relatively close to point *A* on the *X* axis, predicts a value much closer to the true root.

In practice this means that the guess from point *A* will probably put the system outside of realistic performance bounds and generate some type of error, while point *B* will converge nicely. This can be quite frustrating to the user since point *B* may be only slightly different from point *A*.

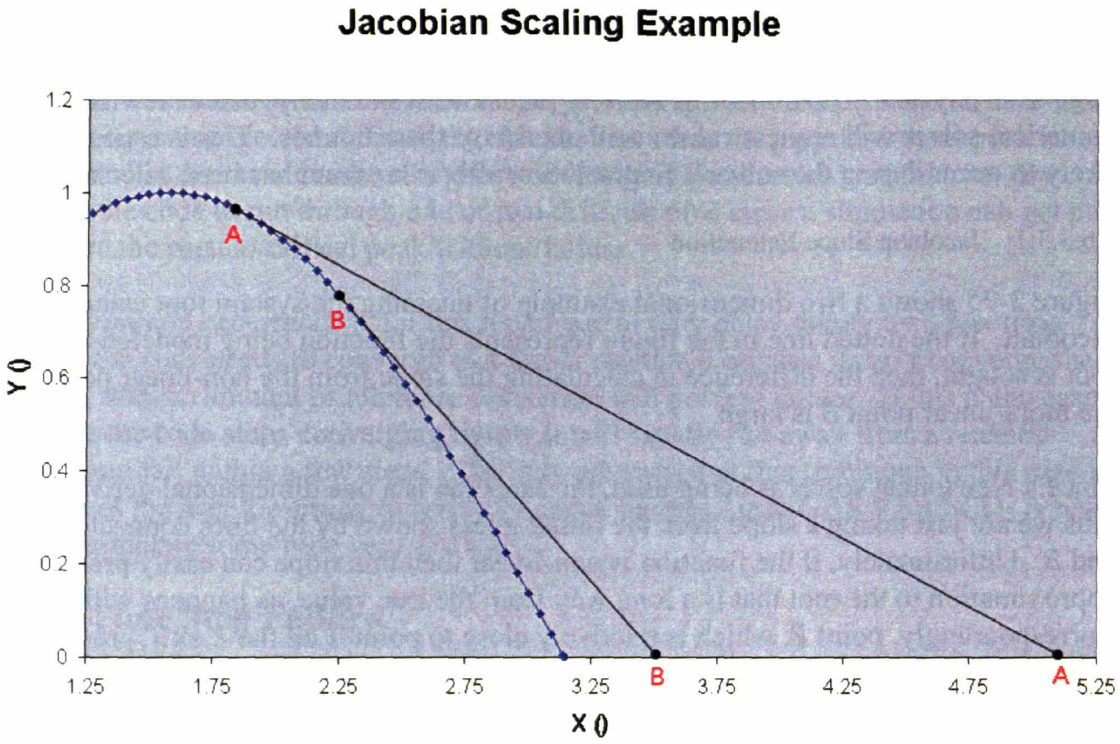

Figure 3-75: Jacobian Scaling Example

3.6.3.3.2 Jacobian Scaling

One method to minimize this problem is to scale the Jacobian. A scaling factor may be applied to the (whole) Jacobian to prevent the solver from taking unrealistically large steps and may simply be thought of as decreasing the predicted distance to the root. Note that when multiplying the Jacobian by this factor a larger scaling factor decreases the distance to the root. The scaling factor should not be less than 1.0, since good numerical solvers will automatically converge on the root without external assistance.

GAS-PASS/CO_2 handles this Jacobian scaling in two manners:

1. The user can specify a default Jacobian scaling factor for both the steady state and the transient in the input file. A large scaling factor is appropriate for a highly non-linear system and a value of 1.0 is appropriate for a more linear problem. A larger factor will slow the solution process (more steps are required to find the root) but may be necessary if the solver is taking many unrealistically large steps.

   GAS-PASS/CO_2 normally runs with a value of 10 for the steady state (since the user may be making some significant guesses about the root location, and the steady state is a small percentage of runtime), and a value of 1 during the transient since GAS-PASS/CO_2 can scale automatically.

2. GAS-PASS/CO_2 automatically increases the Jacobian scaling factor if property errors are detected. In practice, the first indication of an unrealistically large step

will be the solver asking for a fluid property that is out of table bounds. When this happens an error flag is generated, the solver stops computation and increases the Jacobian scaling factor, and then the solution process begins again (this is shown in the solution process flow charts: Figure 3-3 and Figure 3-4). This recovering and rescaling happens repeatedly until the system converges or the Jacobian scaling factor becomes unrealistically large and the time step fails.

If the system converges then a true root has been found, all is well, and the code moves on to the next time step. If the system does not converge then GAS-PASS/CO_2 will give up on this time step and try the next in hopes that changing boundary conditions will allow a future solution (observed to occur in practice). All of these actions are printed to the screen and written to the log file to warn the user and allow appropriate action.

Jacobian scaling is one of the most important solution-enabling techniques used in GAS-PASS/CO_2.

3.6.3.3.3 Numerical Extrapolation

Unfortunately, Jacobian scaling may not prevent all out of bound errors. An example of where this might occur is in the performance curve of the axial main compressor used in the S-CO_2 recompression cycle. The efficiency curve of this compressor at normal shaft speed is shown in Figure 3-76.

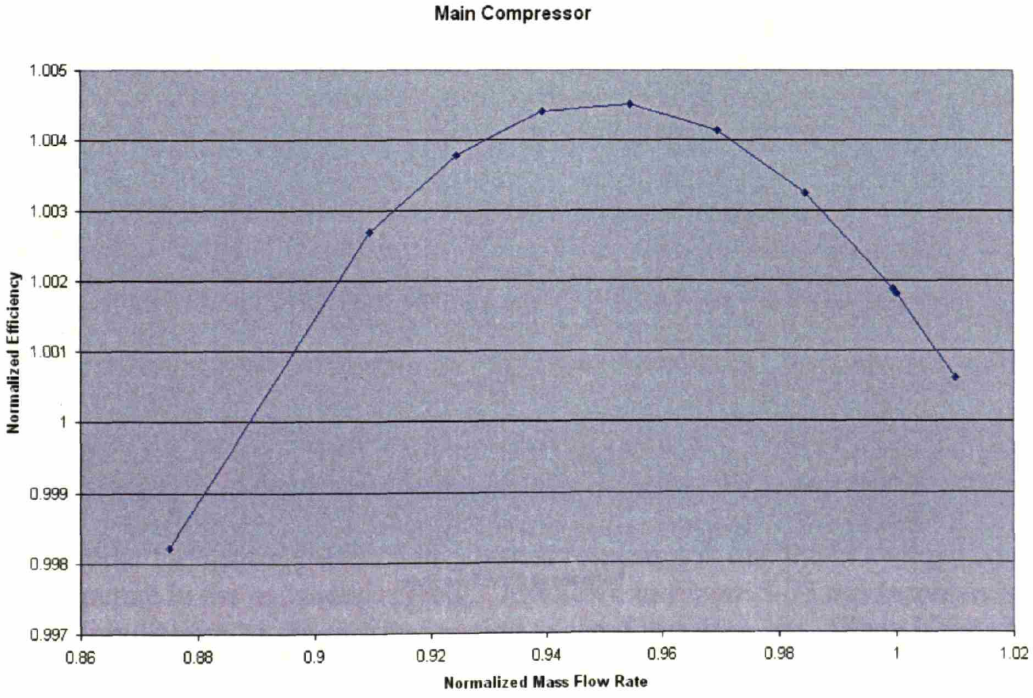

Figure 3-76: Axial Main Compressor Efficiency

This curve shows the expected physical performance of an axial compressor, but note that the operating range is quite small. The detailed compressor design code used to create this curve was only able to converge data points slightly less than 1% higher than the design mass flow rate.

An obvious solution to this problem is to extrapolate the performance curves past their expected region; however, one must be careful how this is implemented. Not only will an axial turbomachine stall and choke in a narrow range but simple linear extrapolation is insufficient. Figure 3-77 shows the same performance curve linearly extrapolated (from the last two data points) to 10% above design flow rate. This figure clearly shows that even relatively small mass flow rate changes can cause negative efficiency values resulting from such tight compressor curves.

One solution to this problem is to create non-physical but numerically significant extrapolation. This numerical extrapolation would only be used to tell the solver that it is overshooting the root, while simultaneously assuring that nonsensical answers (i.e. a negative efficiency) do not produce mathematical errors. An example of what this might look like is shown in Figure 3-78.

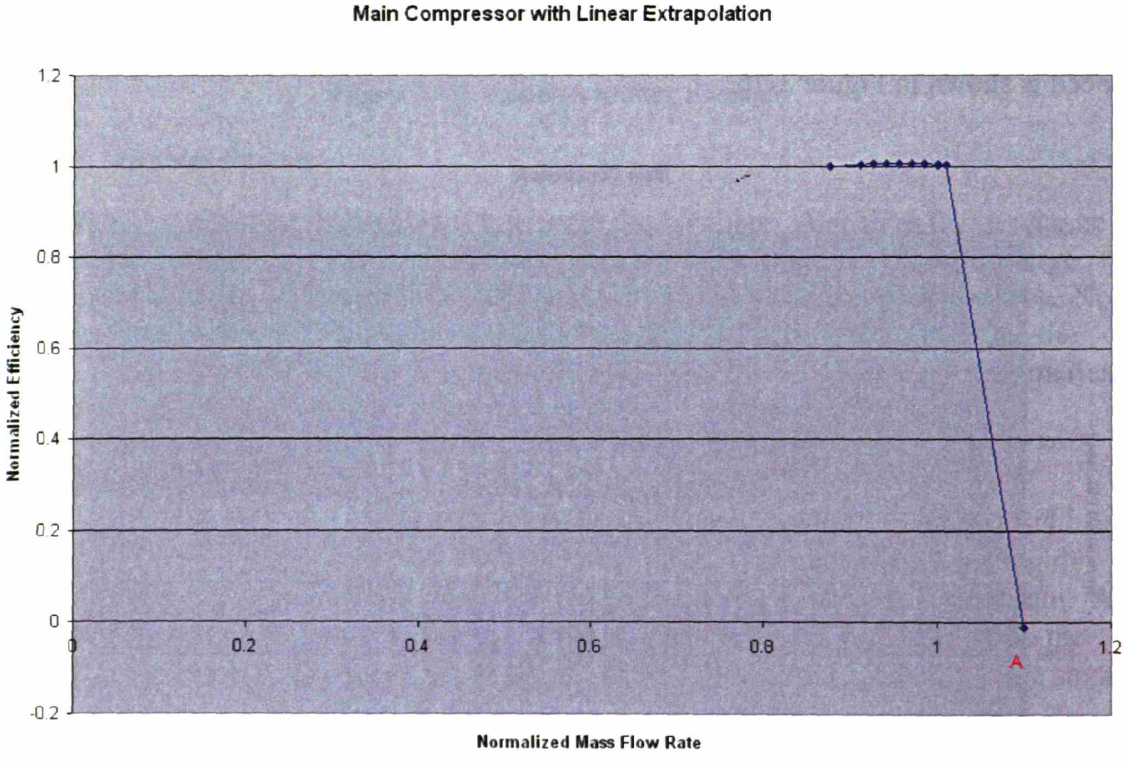

Figure 3-77: Axial Main Compressor Efficiency with Linear Extrapolation

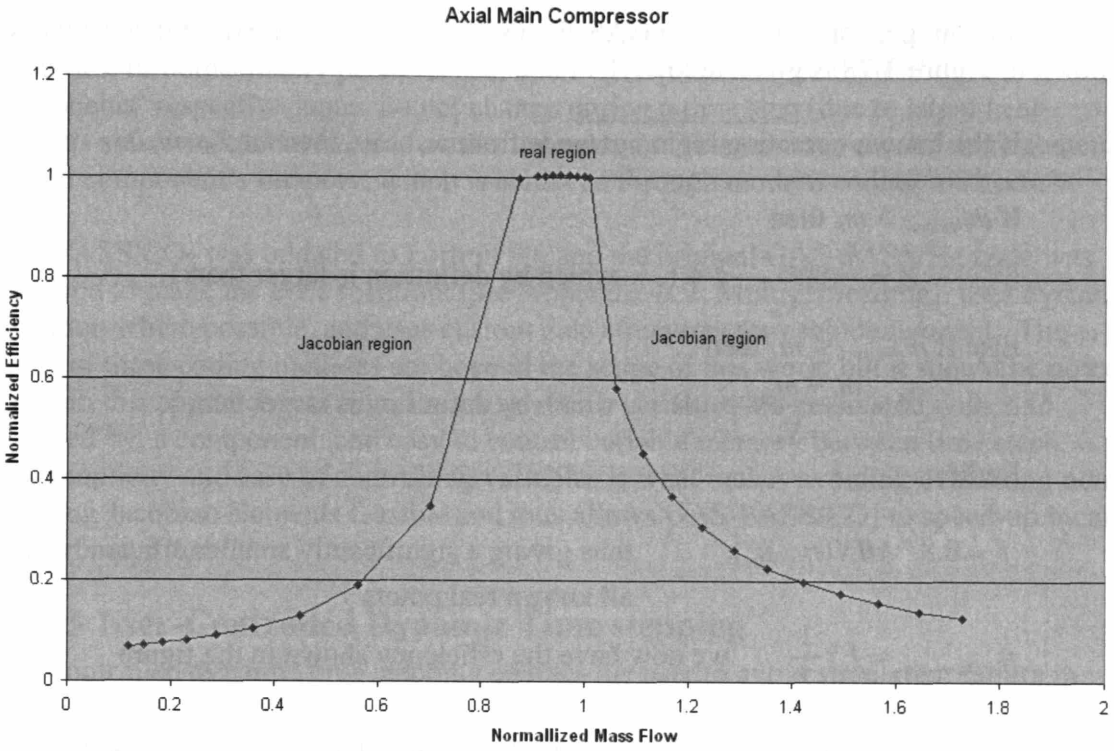

Figure 3-78: Axial Main Compressor Efficiency with Added Extensions

Figure 3-78 shows the narrow real operating region with much larger but non-physical efficiency curves attached to either side. These curves show a significant drop in initial efficiency that asymptotically decreases as the mass flow rates become ever further from the operating region. These curves were devised to show this behavior for several reasons:

- Everywhere outside of the real region they will predict a very low efficiency that will inform the Jacobian it is not near the root (i.e. solution equations will be non-zero to a significant degree).
- The extrapolated curves are smoothly sloping, with a derivative that informs the Jacobian that to achieve higher efficiencies it must move back towards the real region.
- The curves cover a very wide mass flow rate range without introducing unrealistic values (i.e. a negative or much greater then than 100% normalized efficiency).

The rational for allowing these non-physical responses is that the converged code will never operate in the expanded regions. As shown in Figure 3-75 the Jacobian is simply making predictions of the root and testing to see if it is accurate. When it tests these extrapolated data points it will discover that it has moved too far from the root and move back towards its original point. This stratagem will also keep the code from mathematically failing. GAS-PASS/CO_2 includes a check to make sure that no converged operating conditions (i.e. a time step's root) ever include non-physical extrapolation, as shown in the solution process flow charts of Figure 3-3 and Figure 3-4.

The simple but general way used in GAS-PASS/CO_2 to create the extrapolated curves shown in Figure 3-78 is given below:

If the known operating region extends from m_1 ...m_n then let X_m=m_n-m_1

If $m_{desired} > m_n$ then

$$Z = \frac{m_{desired} - m_n}{X_m} + 1$$ which by definition is larger than 1.

Else If $m_{desired} < m_1$ then

$$Z = \frac{m_1 - m_{desired}}{X_m} + 1$$ which by definition is larger than 1.

Endif

$f = 0.8 * MIN(\eta_1 ... \eta_n)$ thus giving a significantly smaller efficiency than all known real points

$\eta_{extrapolated} = f * \frac{1}{Z}$ we now have the efficiency shown in the figure

Note that this process may prevent GAS-PASS/CO_2 from failing due to extrapolation during root finding – it will not prevent the solution from moving past the turbomachinery performance map bounds*. For example, note that in Figure 3-76 there is very little mass flow rate margin above the design operating point of 1. Any simulation that increases the mass flow rate will probably exceed this map's boundaries. The reader should also note that this was a primary reason for moving to radial compression in the S-CO_2 recompression cycle.

3.6.3.4 Sparse Jacobian Evaluation

When a Jacobian is evaluated, every unknown variable is perturbed one at a time and the impact of each perturbation on every conservation equation within the system is calculated. The majority of the equations are not directly affected by perturbations in a variable, thus creating a sparse Jacobian. Examples of GAS-PASS/CO_2 Jacobians are shown in Figure 3-38 and Figure 3-39. If the reader looks carefully it will be noted that these Jacobians are approximately 93% sparse.

A sparse Jacobian means that numerous conservation equations were tested for variables that do not affect them, and thus constitute wasted computations. Several methods were tested to avoid this waste, but the easiest method found was computing a component only if its inputs have not changed from the last computation. This simple idea provides an order of magnitude improvement in runtime when dealing with the S-CO_2 recompression cycle.

* Any turbomachinery extrapolation produces warning messages which are logged.

While simple in theory, this can become quite complex in practice, due to memory management complexity. GAS-PASS/CO_2 as a compromise avoids recalculating fluid properties, turbomachinery performance, and PCHE performance if all of these components' respective inputs do not change during a time step (due to latent heat, previous solutions cannot be used across time steps). This requires careful management of each component's memory, which is achieved through modern coding methods.

GAS-PASS/CO_2 was updated to Fortran 90, and the original GAS-PASS/He code was improved to make the code reentrant (see Appendix B.2 Multi-Threading), uses dynamic allocation where possible, and uses custom data structures for each component. The merits of these coding methods are beyond the scope of this work, but it should be noted that with this approach it is trivial to know which variables are associated with, and modified by, a component, and easy to control variable memory between time steps. This simplicity and ease of controlling variables is what makes avoiding evaluating non-changing Jacobian elements feasible and thus allows GAS-PASS/CO_2 to speed-up by an order of magnitude.

3.6.3.5 User-Controlled Dynamic Time stepping

User-controlled dynamic time stepping enables the user to avoid simulation failure in practice. In an ideal world a simulation would occur employing the smallest time step necessary at any point in the simulation, and the code would run fast enough that this would not matter (as was the case with GAS-PASS/He simulating ideal gases). For GAS-PASS/CO_2 it is frequently necessary to have a small time step during rapid boundary condition changes, but this is unnecessarily detailed during the vast majority of the simulation, when boundary conditions vary slowly or not at all.

GAS-PASS/CO_2 allows the user to avoid this problem by controlling the time step size. This tactic has been used quite successfully to simulate sharp perturbations in boundary conditions. For example, a transient previously simulated had a very rapid change during ¼ of a 1000 second simulation. Before the perturbation the simulation is effectively in a steady state and large time steps could be used. During and shortly after the perturbation very small time steps were required to capture the mass storage and major energy storage effects. Gradually, the mass storage effects decrease and the energy storage became less important and progressively larger time steps were used until, at large timescales, the system again reached a steady state.

The time step instructions used for the simulation just described were:

```
1000.0          :total problem runtime  [s]
0.01            :default time step size [s]
4               :# of time step instructions
0.0 5.0  1.0 1.0  1.25 1.0  1001.0 1000.0
```

The last line is in standard GAS-PASS boundary condition format. It tells the code to take 0.05 second (five multiplied by the default value of 0.01 seconds) time steps at time 0, linearly decrease the step size until it is taking 0.01 second (1 multiplied by the default time step) time steps at the perturbation, hold that time step size until the perturbation is

over, then linearly increase the time step size until, at 1001 seconds, 10 second time steps are being taken.

The net results of these instructions are to run this simulation with 638 time steps instead of the 10^6 steps which would be used with the 0.01 second step size. This represents a, roughly, 157 fold speed-up. The user will observe that the code takes longer to run the first 13 seconds of the simulation than it does the last 987 seconds.

While this is not strictly a solution technique, the great speed-up it allows encourages the user to take appropriately small time steps during changing conditions and to run the simulation until it reaches a new steady state. This makes GAS-PASS/CO_2 more likely to run a successful simulation, and it is therefore included in this section on solution techniques.

3.6.3.6 Solution Techniques Conclusion

GAS-PASS/CO_2 has benefited from the difficult process of developing and initially converging the S-CO_2 recompression cycle by introducing a progressively more robust solution process. The code may still fail if asked to simulate a very difficult transient, but the code will now adapt to and survive many difficult transients without changing the fundamental solution process.

3.6.4 GAS-PASS/CO_2 Runtime

GAS-PASS/CO_2 runtime depends on many factors. However, there are a few factors that dominate:

1) How many time steps are used. This will depend upon the speed with which the system changes (the minimum required time step) in the simulation, how the user sets up the transient run (with dynamic time stepping), and, of course, how long the simulation should run.
2) How many components, and especially how many PCHE components, must be solved at every time step.
3) How many PCHE zones are used. The runtime will be almost proportional to the number of zones.
4) How difficult the simulation is. When the system changes rapidly and or becomes highly non-linear then the solver must work much harder to find the solution. A hard problem will be several times slower than an easy problem.

Due to the numerous speed-up methods already outlined, the S-CO_2 recompression cycle can now simulate faster than real time using off the shelf hardware. This result was for the reference cycle during inventory control (a difficult simulation), using a constant time step of 0.05 seconds, and two PCHE nodes.

Note that it is likely that GAS-PASS/CO_2 could be sped-up by at least two more orders of magnitude for only a small programming effort, as outlined in Appendix B: Suggested

Future Improvements. Due to the lack of current need and time constraints these steps were not implemented in the current work.

3.6.5 Section Summary

GAS-PASS/CO_2 is a complete code, able to successfully simulate the S-CO_2 recompression cycle. It has the capability to simulate real fluid properties, turbomachinery performance maps, and PCHE heat exchange, even in the S-CO_2 recompression cycle. The coding and input/output processes have been significantly improved, making it much easier for the user and the developer to work with the code, and the solution process has been made much more robust, allowing greater success with more difficult cycles. Finally, several PID controllers have been added to the cycle layout to enable proper and realistic control of the cycle for a variety of transients.

GAS-PASS/CO_2 will continue to be improved but only in response to future simulation needs and control system design requirements. Code testing has shown that relatively non-linear systems can be successfully simulated with Newtonian solvers given careful consideration of the system being modeled.

3.7 Inventory Control Numerical Comparison

Inventory control is complicated, difficult, and uncertain in the S-CO_2 recompression cycle and should serve as an excellent comparison between simulation codes. This section will provide a brief comparison against a similar, but independent, simulation code simulating this power cycle coupled to a lead cooled fast reactor[10,17]. The complication and uncertainty encountered with inventory control in this cycle is analyzed in Section 4.5, and the full simulation results of inventory control are shown in Section 5.1.1.

The cycle efficiency versus nominal generator power is shown in Figure 3-79. This figure shows the GAS-PASS/CO_2 result versus the ANL results of Dr. Anton Moisseytsev using axial compressors[17]. Both curves show similar behavior and values until 47% nominal generator power. Note that the GAS-PASS/CO_2 efficiency has been decreased everywhere by 2.5% to equal the steady state value of the Moisseytsev work, which primarily just matches non-modeled cycle inefficiencies (such as generator efficiency), thereby allowing easier comparison.

Near 47% generator power the main compressor inlet pressure drops rapidly with only a small drop in density as the inlet temperature decreases (see Figure 4-18). Below 30% generator power the wide operating range of the radial compressors combined with the PID controller trading flow between the parallel compressors, allows the GAS-PASS/CO_2 result to proceed to much lower powers. At approximately 6% generator power the turbine is predicted to stall by GAS-PASS/CO_2.

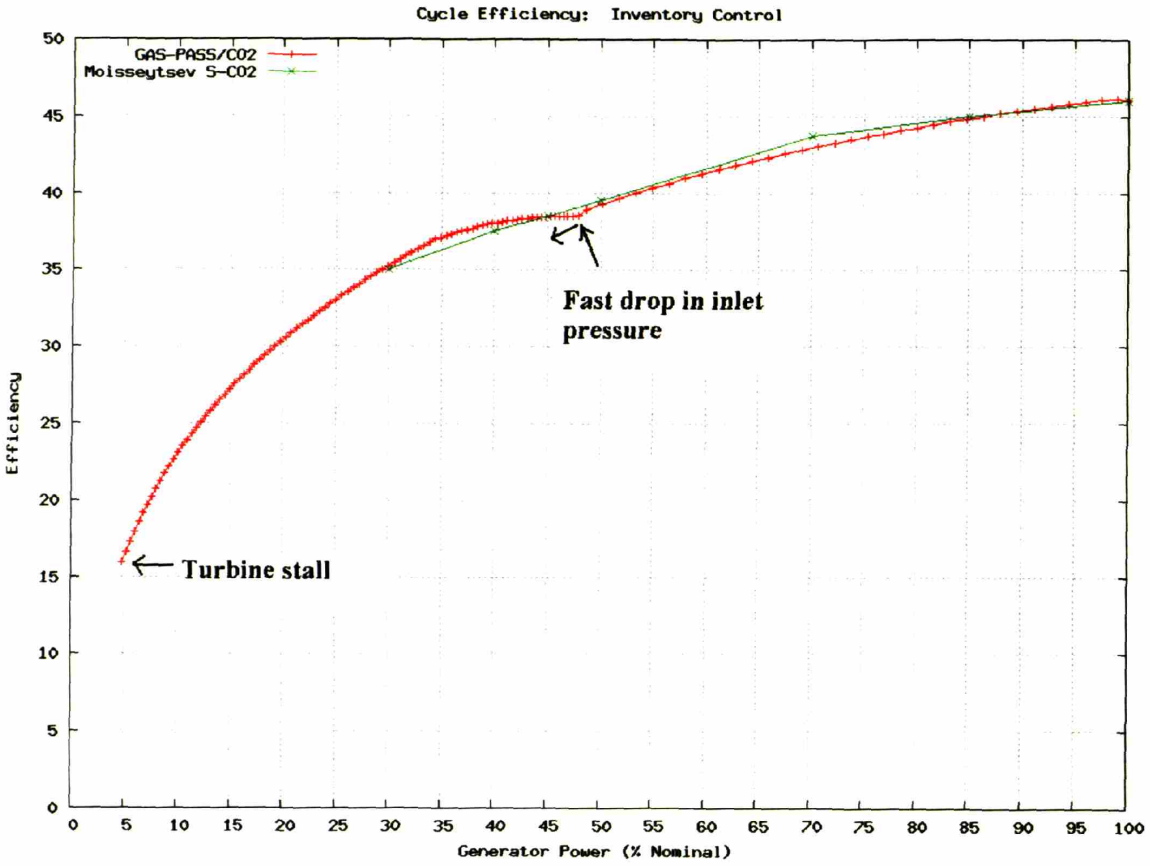

Figure 3-79: Inventory Control Efficiency Comparison

In general, the inventory control efficiency curves are quite similar. The general trends and slopes of both simulation codes show significant similarity until the flow split change near 47% power. While not a rigorous numerical comparison, the similarity of the results for one of the most difficult simulations in this cycle between two independent codes is encouraging. When more simulations, or preferably experimental results, become available for this cycle, a detailed benchmark should be pursued.

3.8 Chapter Summary

This chapter provided the reader with a detailed examination of the GAS-PASS/CO_2 solution process. The ideal gas GAS-PASS/He code was introduced as were the use of the NIST RefProp equation of state in log indexed property tables, and the use of pre-calculated turbomachinery performance maps with basic fluid property relations. A detailed analysis was provided for the newest and most difficult to simulate component, printed circuit heat exchangers, including available correlations and rapid modeling methods that accurately predict heat exchange. Finally, relevant discussion of the overall GAS-PASS/CO_2 code was included, which concentrated on the system of non-linear equations and the solution techniques that allow this non-linear cycle to be solved with a Newtonian solution method faster than real time.

The reader should have a detailed understanding of the GAS-PASS/CO_2 solution process and some of the key uncertainties in the work. The precooler has been closely compared to RELAP5, and an inventory control simulation of the whole cycle between independent codes shows good agreement. As experimental data become available for this cycle benchmarking should highlight areas for GAS-PASS/CO_2 improvement.

4 Control Strategies and Issues

This chapter will focus upon the control system used in the GAS-PASS/CO_2 code and issues that have arisen with its implementation. The control system is by no means complete, but features some of the fundamental methods which allow the cycle to operate appropriately.

This chapter is subdivided into six sections:

1. Section one will review proportional-integral-derivative (PID) controllers as they apply to GAS-PASS/CO_2. The section will briefly review PID theory, look at variable sampling, offer a PID tuning example, and address low pass filtering needs.
2. Section two will look at the controls used in the S-CO_2 recompression cycle. The controls developed for this work represent a basic set of methods to allow this complex cycle to operate appropriately during a variety of transients.
3. Section three will briefly examine the issues involved in parallel compression. The complex fluid property changes experienced by the main compressor may make this an important area of future research.
4. Section four will consider the merits of simplifying (to a single compressor or a single recuperator) the recompression cycle layout during off-design performance. The original reasons for the recompression cycle layout diminish during inventory control operation but no attractive options exist which simplify the cycle.
5. Section five will describe a region of concern encountered during inventory control. While the overall inventory control results will be presented in Section 5.1.1, this section will examine the importance of careful operation near the critical point, introduce a method to avoid the region of concern, and highlight a key modeling uncertainty in this work.
6. The sixth section will mention an inventory control system which does not require an extra compressor. This design would solely use cycle pressures to drive inventory control mass flow but is not examined in thesis. It is included to alert the reader to future work that is unique to this cycle.

By the end of the chapter the reader should understand what controls are used in the cycle, and several unique control challenges in this cycle. Future chapters will focus upon simulation results.

4.1 PID Controllers

One of the most common closed loop (feedback) controllers used is the proportional-integral-derivative (PID) controller. This controller is used to keep a measured value at the design point, called "reference*" in control theory.

* Also known as "set point."

A PID controller uses three inputs to determine how to change the controlled value to force the measured value to reference (note this discussion is based upon Wikipedia[79]).

- The first input is the proportional gain, *P*. This input multiplies the controller error, between the measured value and the reference value, by a constant, labeled *Kp*, to modify the controlled value. This input will drive the error to small values but will never completely eliminate error.
- The second input is the integral gain, *I*, which serves as a kind of past history for the controller. This input multiplies the integral of the controller error with time (starting from time zero) by a constant, *Ki*. The integral error can accumulate rapidly and drive the system to its reference more quickly than the proportional input alone. The integral gain will, inevitably, overshoot the reference and create opposite error. The overshoot will gradually diminish as the integral error approaches zero.
- The final input is the derivative gain, *D*, and represents the future response of the system. This value stems from the derivative of the controller error and can create a large response for fast system changes. The derivative term prevents rapid, significant overshoot. The derivative term also slows down the speed at which the measured value is driven to reference, since it minimizes the integral error by preventing overshoot.

A common formulation for implementing this controller is shown in Equation 4-1 and is known as the ideal parallel form.

Equation 4-1: PID Formula - Continuous[79] **(4-1)**

$$\text{Output(t)} = K_p \left(e(t) + K_{ip} \int_0^t e(\tau)\, d\tau + K_{dp} \frac{de}{dt} \right)$$

This formulation has the advantage of being easily implemented, is general, and still allows control over each (parallel) input individually[79]. Note that "e" is the difference between the actual process value and its reference value, the error. When put into discrete form the PID formula is shown in Equation 4-2 where $t^n - t^{n-1}$ is the time step size.

Equation 4-2: PID Formula – Discrete **(4-2)**

$$Int^n = Int^{n-1} + e^n * \left(t^n - t^{n-1}\right)$$

$$der^n = \frac{e^n - e^{n-1}}{t^n - t^{n-1}}$$

$$Output^n = K_p \left(e^n + K_{ip} * Int^n + K_{dp} * der^n\right)$$

In GAS-PASS/CO_2 the output of the PID controller is added to the controlled value at the next time step; $v^{n+1} = v^n + O^n_{PID}$. Thus, if there is no error (and the integral and derivative

terms remain zero) then the PID controller will produce no control action leaving the controlled value unchanged between time steps.

This formula is shown graphically in Figure 4-1. This figure shows the logic behind implementing Equation 4-2 in GAS-PASS/CO_2. The reader should note that the control reference values are set by the user via input files and can vary with time.

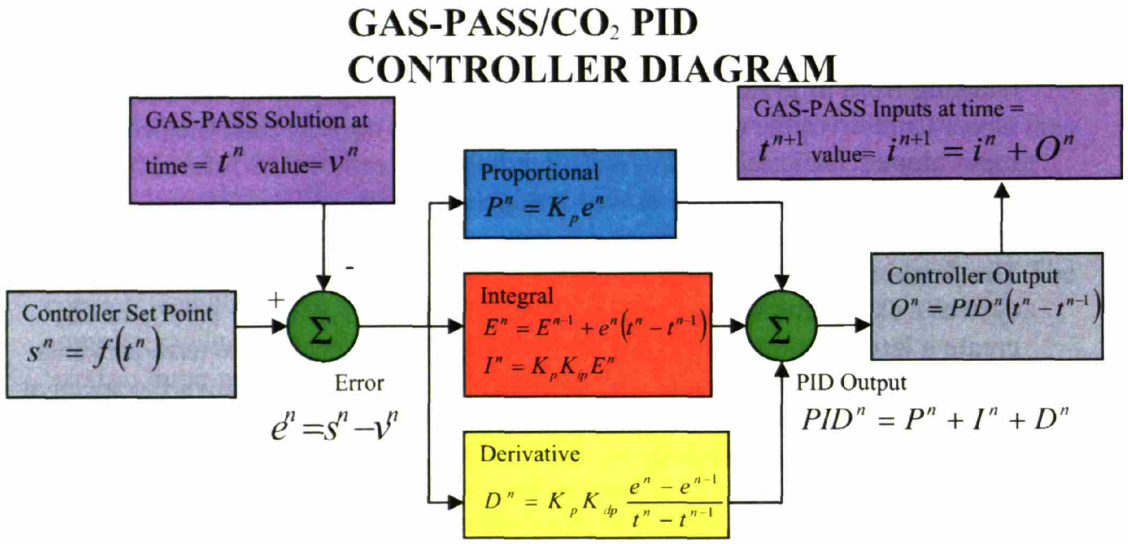

Figure 4-1: PID Controller Diagram

4.1.1 Variable Sampling

While typical PID control equations, as shown in Equation 4-1, can be readily tuned for constant time steps, they do not handle variable time steps well. In control theory this is known as variable sampling. Simply put, if time steps are short, then more control is used per unit time and vice versa. The effects of this are shown in the figures below.

The simulations will show a PI controller which measures the CO_2 outlet temperature of the precooler against the 32°C reference temperature. The controller changes the external cooling water mass flow rate. All the simulations will start from a steady state system at 25 seconds. At 35 seconds the incoming cooling water temperature will be linearly increased from 20°C to 21°C by 36 seconds and held there – a quasi-step change. The PI controller will then move the measure back to reference.

Figure 4-2 shows the original behavior of the controller with a 0.05 time second constant time step. This figure shows a large error peak at 36 seconds which the PI controller corrects by 52 seconds and then gradually integrates the accumulated error away, eventually approaching reference at 95 seconds.

Figure 4-3 shows the same transient except the time steps are cut in half to 0.025 seconds. While the trends are identical, the numerical values are not. In this case the PI controller forces the measured value to cross reference around 44 seconds and later approach reference around 85 seconds. Changing the time step changes the behavior of a PI controller.

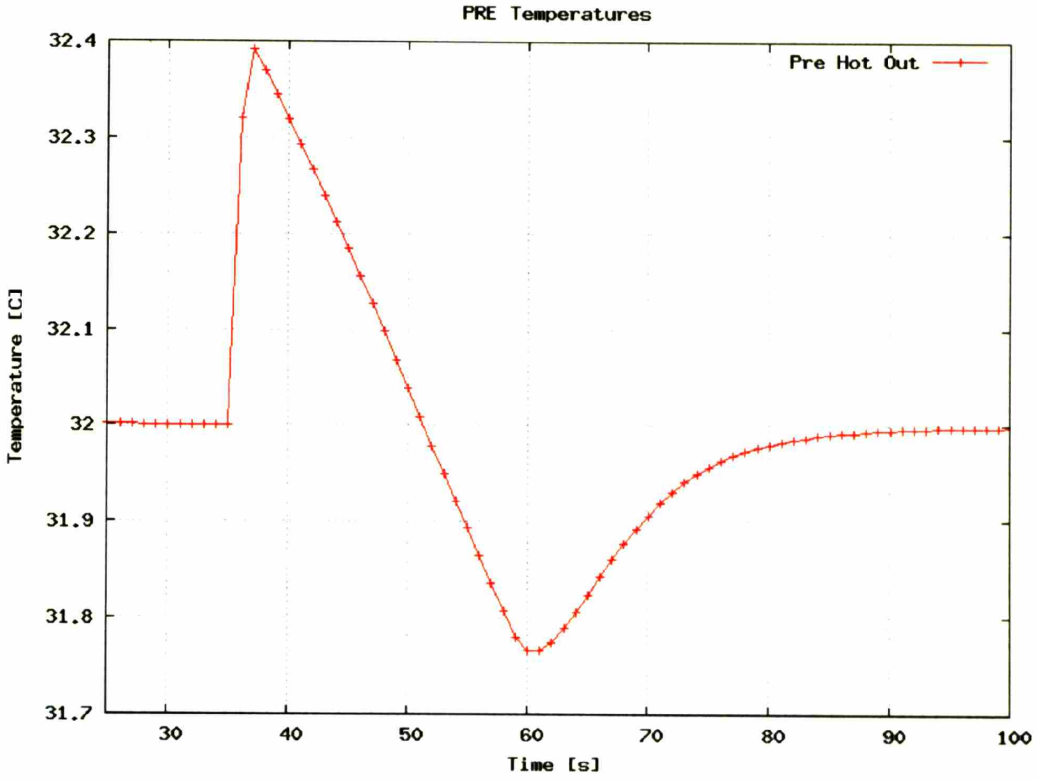

Figure 4-2: PI Control on Precooler Water Mass Flow Rate - dt = 0.005

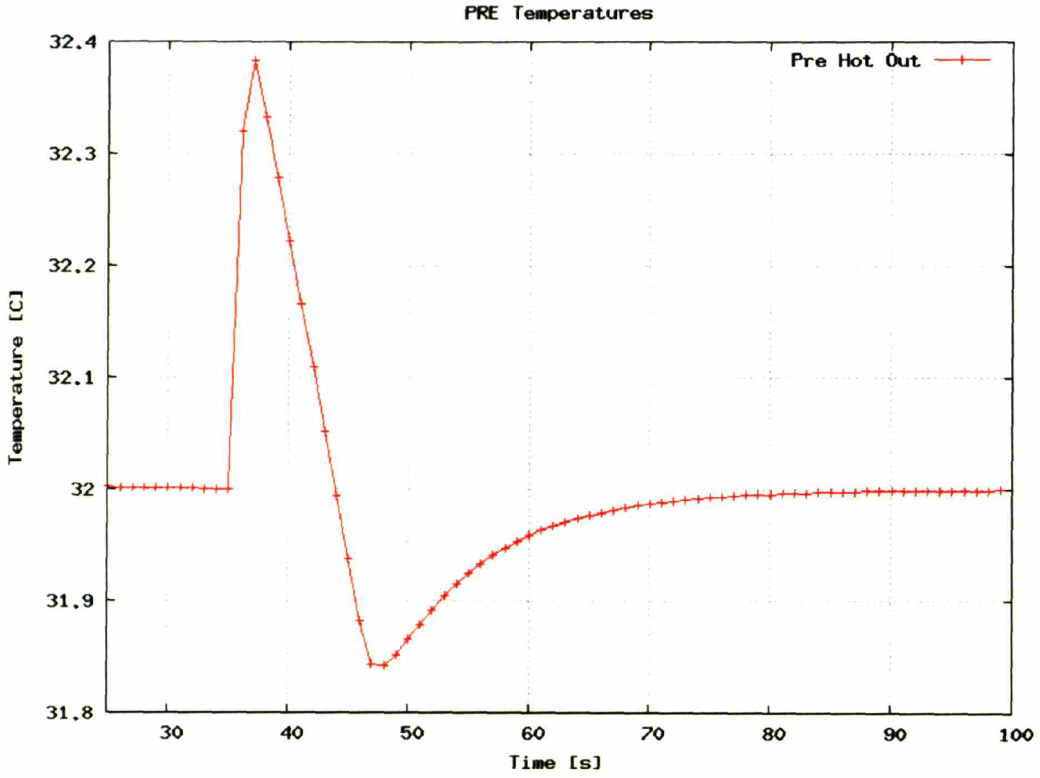

Figure 4-3: PI Control on Precooler Water Mass Flow Rate - dt = 0.0025

The example shown exhibited desirable behavior but it is inherently undesirable to have controllers sensitive to the time step:

- Using GAS-PASS/CO_2's variable time step capability, the user could encounter different PID responses within the same simulation. What works well during one part of a simulation may begin oscillating during short time steps or working slowly during long time steps.
- Even if the time step is held constant it is undesirable to tune a PID controller for only a single time step. Tuning a PID is a considerable amount of work (see Section 4.1.2) and there are a variety of reasons the designer may wish to change the time step. If the time step is changes the PID coefficients must change.

A solution to this problem is to add a time element to the overall PID equation as shown in Equation 4-3. Multiplying by the time step makes the controller output proportional to the length of the time step thus giving large time steps large control reactions and vice versa.

Equation 4-3: PID Equation with Time Step Control **(4-3)**

$$Int^n = Int^{n-1} + e^n * \left(t^n - t^{n-1}\right)$$

$$der^n = \frac{e^n - e^{n-1}}{t^n - t^{n-1}}$$

$$Output^n = K_p\left(e^n + K_{ip} * Int^n + K_{dp} * der^n\right) * \left(t^n - t^{n-1}\right)$$

When this new equation was implemented with the short time steps shown in Figure 4-2, it resulted in Figure 4-4. This figure shows identical behavior to Figure 4-3 thus eliminating* the PI controller's sensitivity to the time step. Unless future needs arise this (simple) modified PID equation will be used to account for time step length.

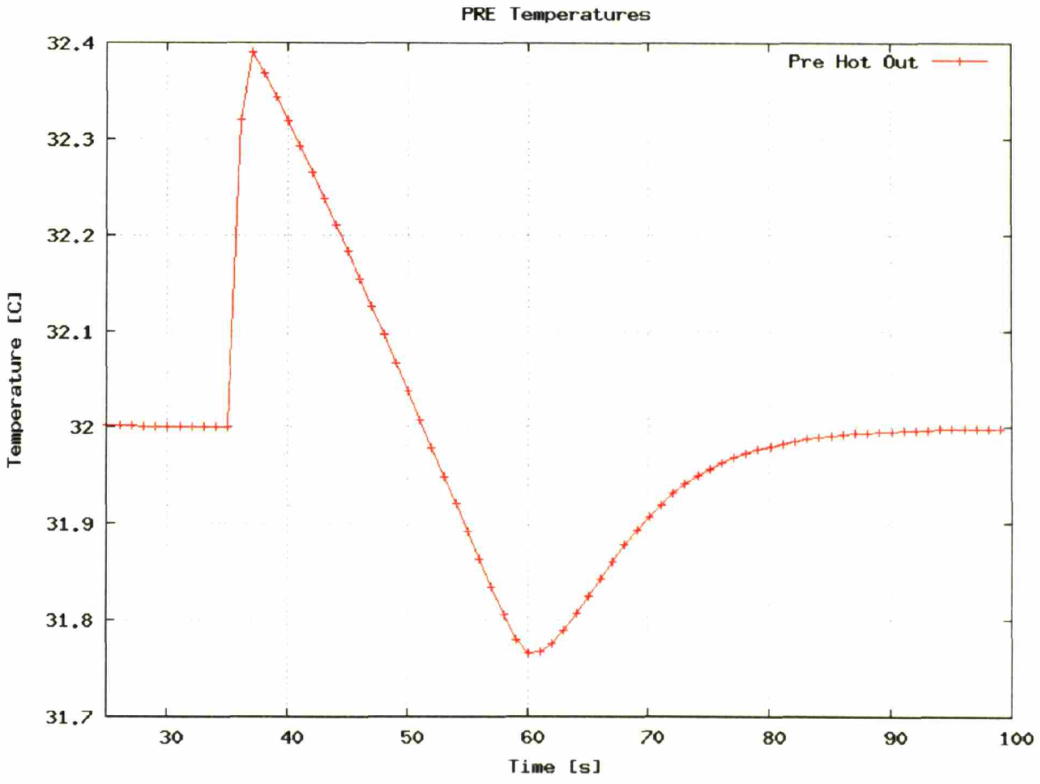

Figure 4-4 Variable Time Step PI Control on Precooler Water Mass Flow Rate - dT = 0.005

* Note that if time steps vary during a simulation the behavior of the modified PID formula, shown in Equation 4-3, with will not be identical. However, in all the cases tested the behavior of the modified formula was found to be acceptable and much improved from the original PID formula, shown in Equation 4-2.

4.1.2 PID Tuning Example

This section will present the tuning method used for PID controllers in the S-CO_2 recompression cycle, with an example. The section is meant to introduce the reader to the basic and pragmatic PID tuning methods used to control this cycle with GAS-PASS/CO_2. The example controller uses the external water mass flow rate through the precooler to drive the measured CO_2 outlet temperature to the reference value. All the simulations begin from the steady state. The incoming cooling water temperature is linearly increased by 1°C between 1 and 2 seconds and then held there.

4.1.2.1 Setting the Proportional Gain

The overall gain, K_p, is the most important PID variable. In general it should be the maximum allowable value before oscillation occurs. Figure 4-5 shows the effect of several gain values around the oscillation point.

The "natural" line shows a steadily increase away from the desired temperature. When K_p = 1000 the temperature is rapidly decreased, until at around six seconds the temperature goes below the reference value, and then slight oscillations occur. The K_p = 750 line shows slight oscillation at the cost of slower response, and the K_p = 200 line shows no oscillation, but the measured value takes a relatively long time to achieve the desired temperature. The line K_p = 200 is chosen as the best case since it shows no oscillation and quickly approaches reference.

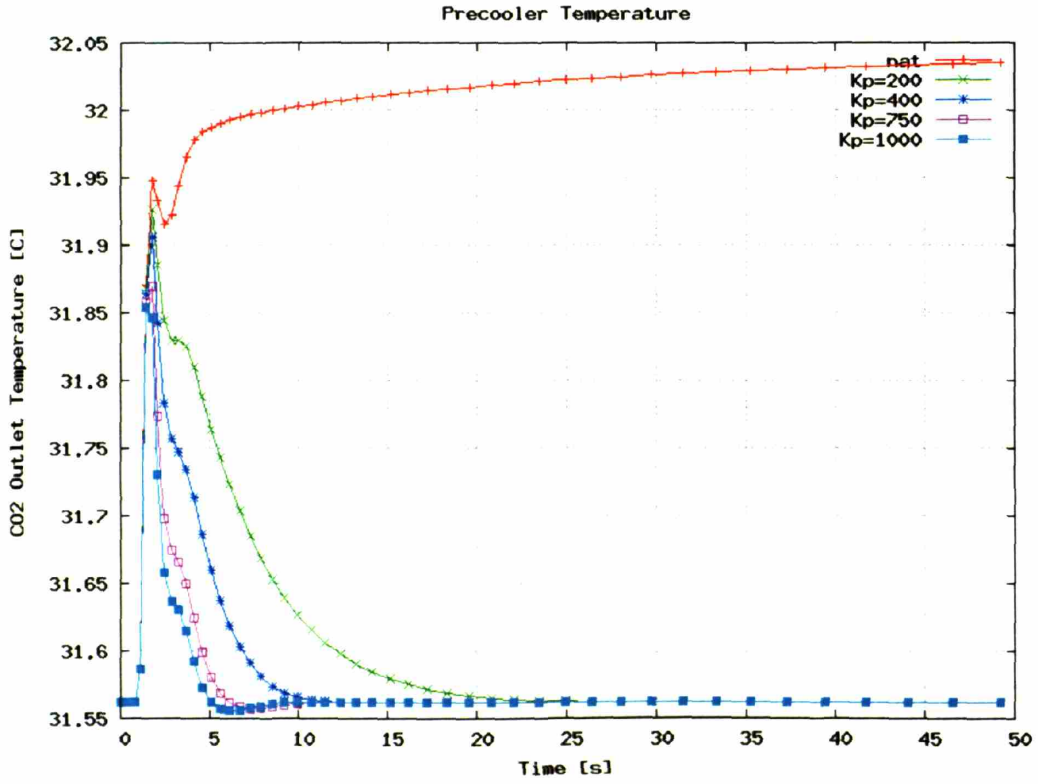

Figure 4-5: Proportional Gain Tuning

4.1.2.2 Setting the Integral Gain

The K_{ip} value was set using the optimal K_p value. Using the same transient as shown in Figure 4-5, several K_{ip} values were tried, as shown in Figure 4-6. These lines show similar behavior, where $K_{ip} = 1.0$ greatly overshoots the steady state and oscillates significantly. The $K_{ip} = 0.2$ line shows only a single oscillation above reference. The selected value of $K_{ip} = 0.1$ comes quite close without ever crossing the reference value. The addition of the K_{ip} factor drives the measured value to cross reference faster than the proportional gain did alone. Note that the integral gain also keeps the measured value much closer to reference than the proportional gain did, but this is not visually distinguishable on Figure 4-5.

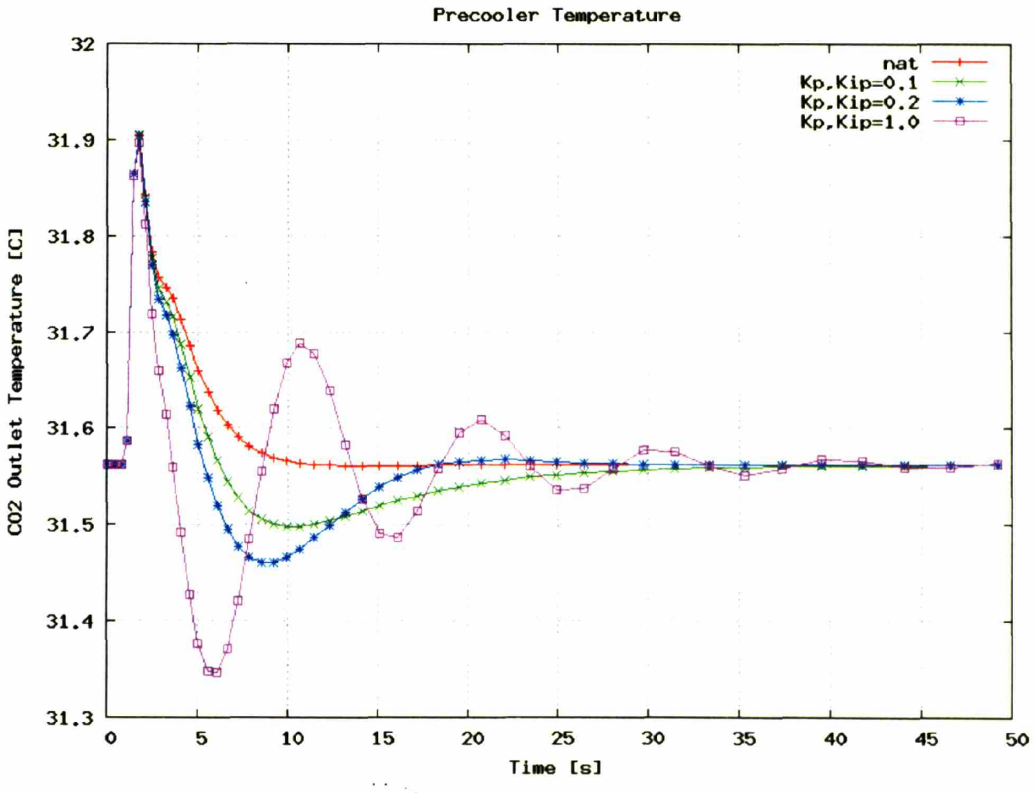

Figure 4-6: Integral Gain Tuning*

4.1.2.3 Setting the Derivative Gain

The K_{dp} value was set using the optimal K_p and K_{ip} values. Using the same transient as shown in Figure 4-5 and Figure 4-6, several K_{dp} values were tested, as shown in Figure

* Note that chosen integral value drives the error to reference more quickly than in the proportional-output-only, called "nat", case. However, the integral term does create overshoot which takes time to be integrated away – this is how an integral term is designed to function. See the PID description in Section 4.1 for more information.

4-7. These lines show different behavior than previously seen, since the derivative term prevents the large initial peak previously present. The derivative term prevents large overshoot but also prevents the rapid accumulation of the inventory term, which otherwise would quickly drive the pressure to its design point. Therefore, the derivative gain term is most desirable if the maximum error is of higher concern than reaching the design point quickly.

In Figure 4-7 the $K_{dp} = 4$ line shows a much smaller peak than for the PI controller, but does not cross reference until 12 seconds instead of 7 seconds for the PI controller. Furthermore, this large derivative term allows a small oscillation above reference around 42 seconds.

The $K_{dp} = 1$ line shows an intermediate initial overshoot peak and no oscillation. The selected line is $K_{dp} = 2$, whose behavior lies between the two previously discussed factors. This line shows the smallest overshoot peak without oscillation.

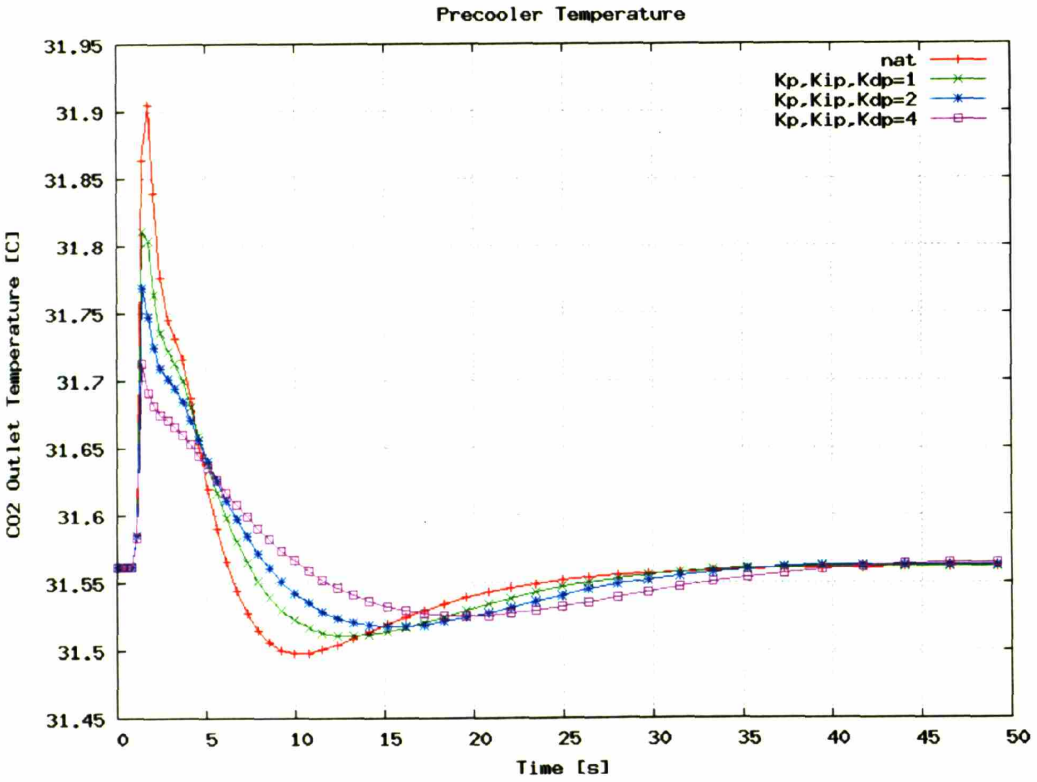

Figure 4-7: Derivative Gain Tuning

4.1.3 Simultaneously Using Multiple PID Controllers

The results of combining the two PID controllers is worth noting. The first controller discussed here changed the amount of inventory in the cycle to keep the main compressor outlet pressure constant. The second PID controller attempted to keep the precooler outgoing CO_2 temperature constant by modifying the cooling water mass flow rate.

These controllers were given a combination of two simultaneous changes in the boundary conditions:

- A quasi-step* change 10% increase in reactor power at 1 second.
- A quasi-step change 5% increase in cooling water enthalpy at 1 second.

Both PID controllers performed quite well during the simulation but failed around 500 seconds when both controlled variables approached close to their reference points. The failure stemmed from a runaway oscillation being produced, primarily by the derivative term in both controllers. Further investigation isolated the problem to the size of the time step, which had become quite large, 1 second, near the time of failure.

To prevent simulation failure and allow further analysis, a maximum allowable rate of change was added to both controllers. Figure 4-8 shows the results of this simulation using a maximum rate of change (100 kg/s on both controllers – 5.8% of CO_2 mass flow rate and 2.1% of water mass flow rate). It is clear that near 500 seconds, when the time step approaches 1 second, the system begins oscillating significantly.

When the maximum time step was decreased to 0.5 seconds, both PID controllers performed well as shown in Figure 4-9. In this case the controlled value gradually approaches the reference point as desired, unlike the larger time step case, where the system moves away from the design point during oscillation.

This problem appears to stem from higher frequency effects becoming shorter than simulation time steps. A simple solution for this case would keep time steps shorter than 1 second, but the frequency of these higher order effects may change during other simulations, such as at different power levels. One could add a low-pass filter but the level of required filtering may change depending on the simulation and this level of controller sophistication is not required for the present work.

The recommended solution is to remove the derivative term from PID controllers whenever possible. Removing the derivative term is a frequently used control solution which typically has little effect on the controllability of the system[80]. The derivative term is by far the most sensitive term to system fluctuations since it tries to predict the future behavior of the system.

When the derivative term is removed, but large time steps are retained, the simulation leads to Figure 4-10. This figure shows the system rapidly crosses the reference and features good long-term behavior but has the additional cost of larger short-term oscillations. However, these larger oscillations are still less than 10 kPa, and acceptable for this transient and system.

* The use of the term "quasi" signifies practical effect rather than dictionary definition. The step changes in these values are not instantaneous, which can be difficult for a Newtonian solver to simulate. However, the time scale of the non-step change is so short, compared to the system response time, that the effect of this fast change is the same as an instantaneous change, hence, a "quasi-step" change.

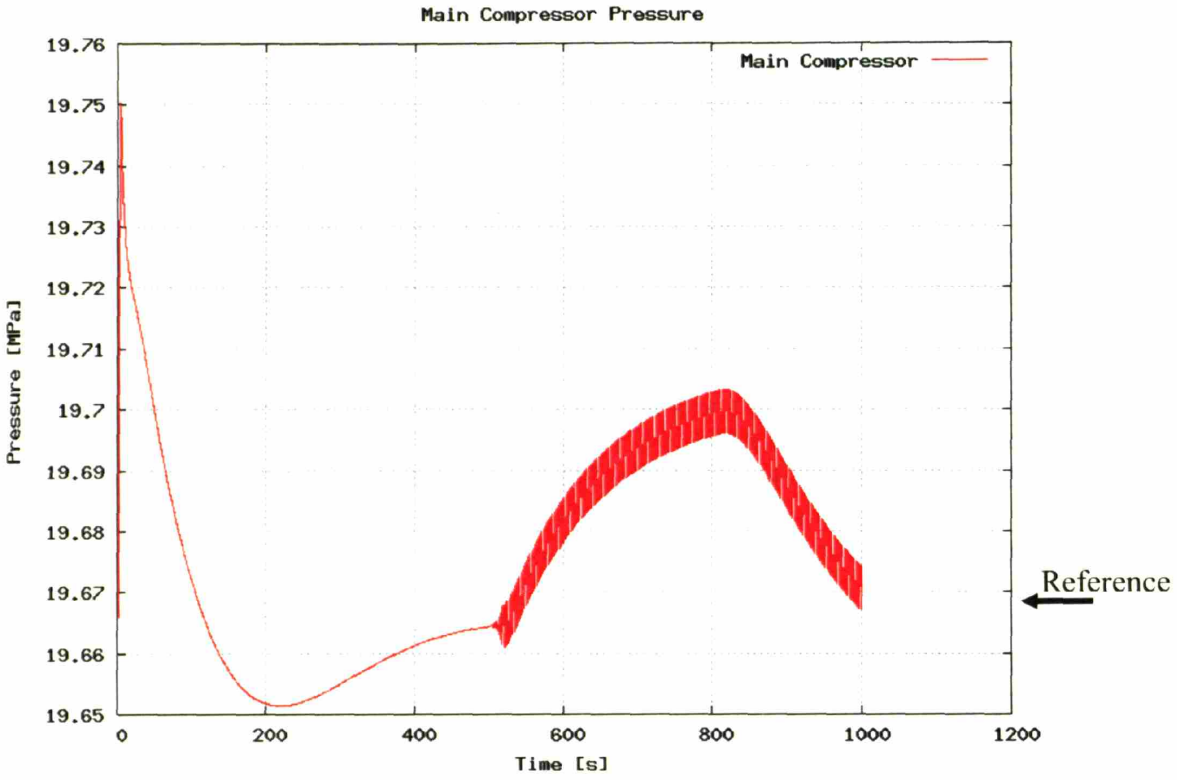

Figure 4-8: Competing PID Controllers - Maximum Time Step 1.0 Second

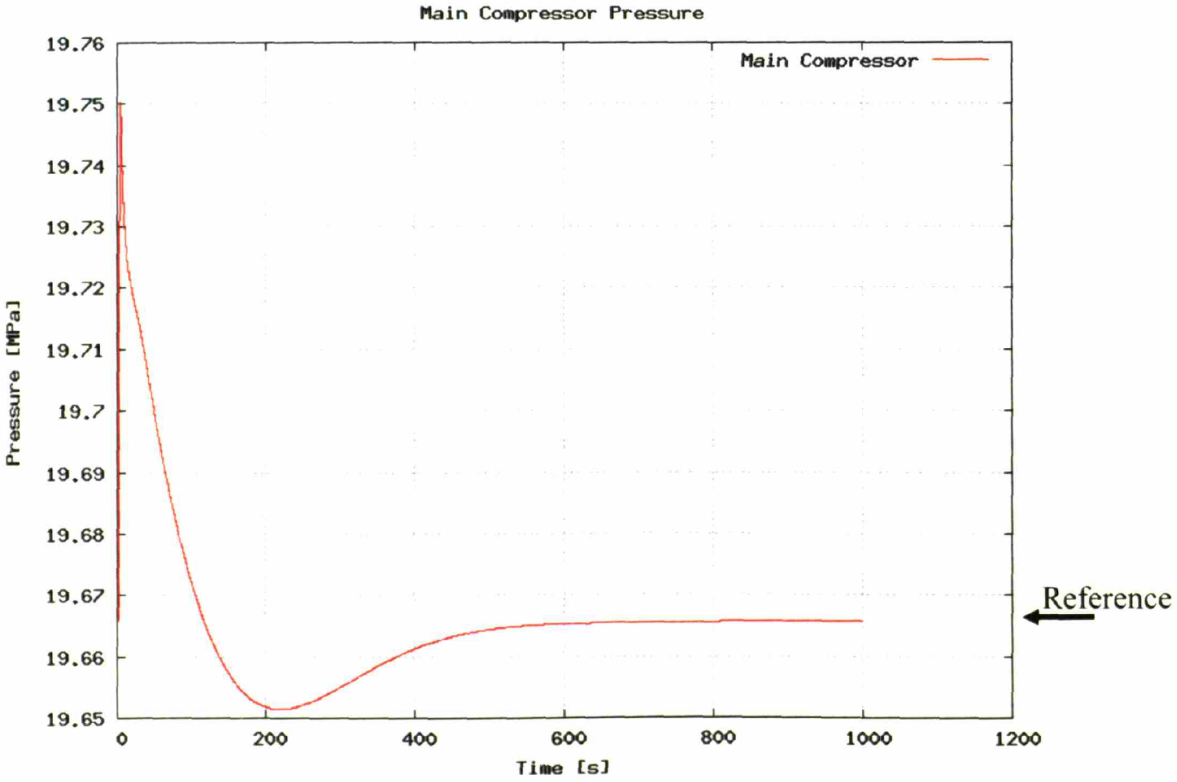

Figure 4-9: Competing PID Controllers - Maximum Time Step 0.5 Second

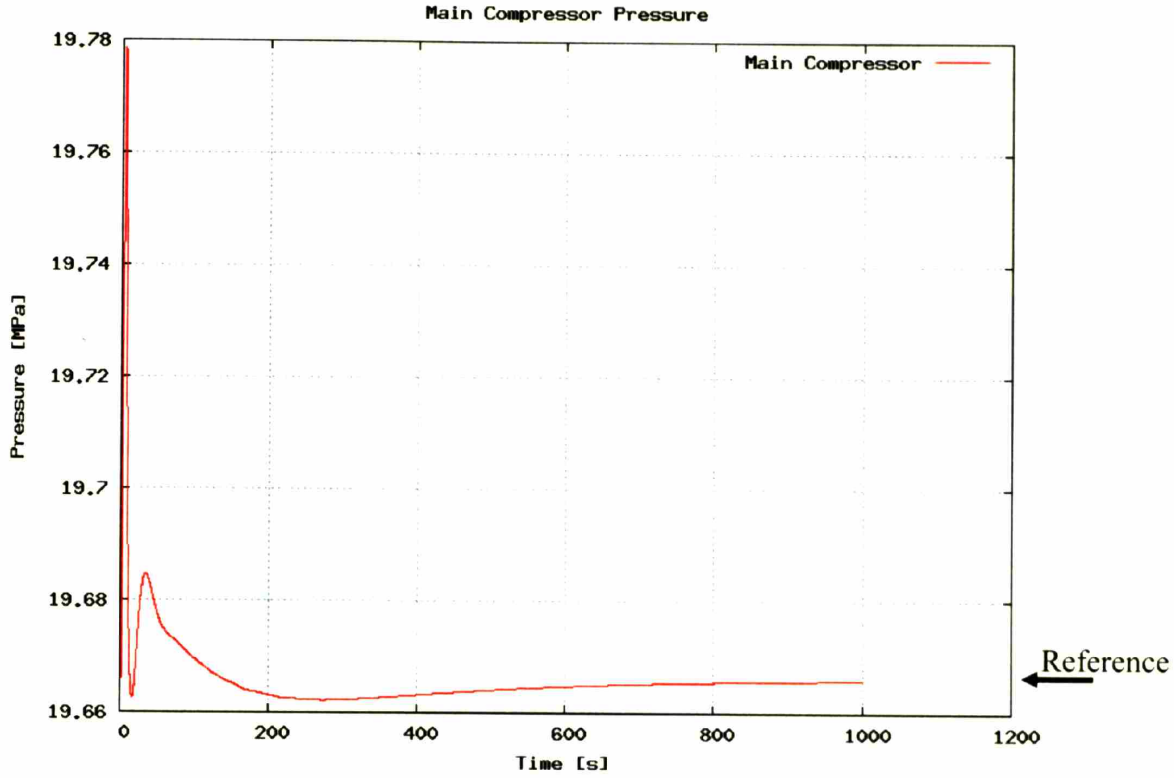

Figure 4-10: Competing PI Controllers - Maximum Time Step 1.0 Second

4.2 Basic Plant Controls

The S-CO_2 recompression cycle was successfully simulated for a variety of transients using GAS-PASS/CO_2 by employing a basic set of controls. These controls provide appropriate plant response during part-load operation and loss-of-load events in particular. The basic controls used are shown in Figure 4-11.

The controls shown in Figure 4-11 are:

- The flow split valves before the compressors. These variable valves are used to introduce a slight pressure drop to control the mass flow split going to the compressors. They can be operated in a completely open position allowing each of the compressors to balance mass flow rates by matching outlet pressure, or one valve can be used to introduce a pressure drop until the desired mass flow rate split is achieved. Since the operator may need to introduce a pressure drop for either compressor, depending upon desired operational parameters, one valve on each line is needed even though only one operates at any given time.

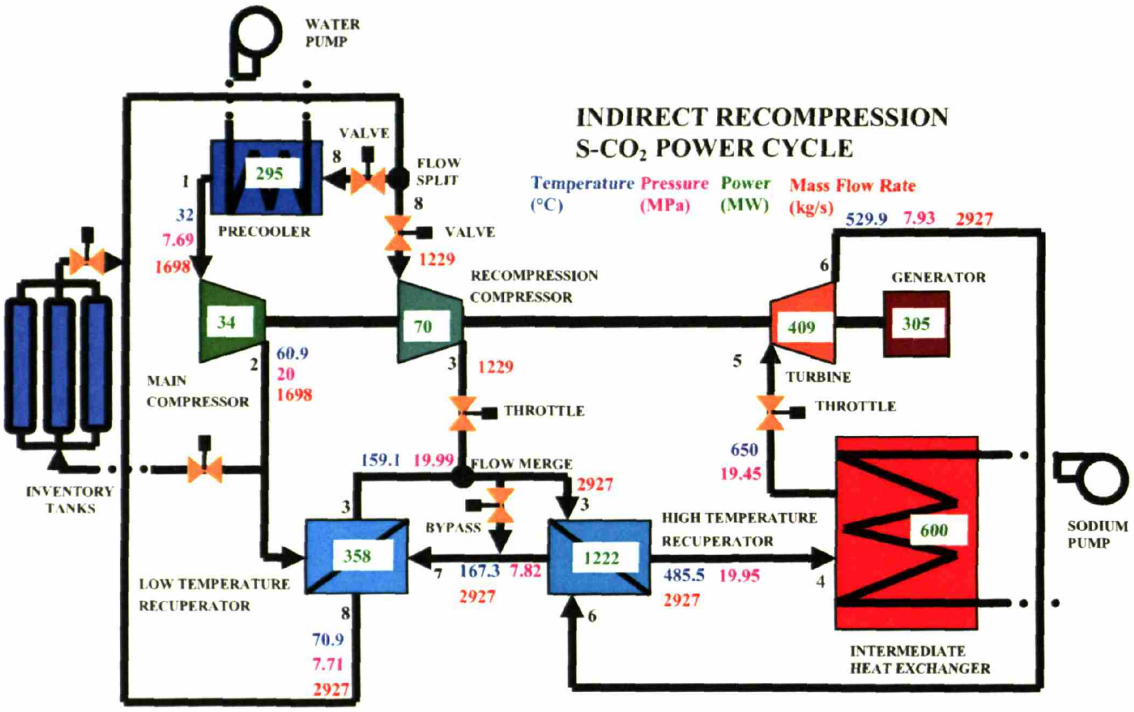

Figure 4-11: S-CO_2 Recompression Cycle with Basic Controls

- A variable throttle is needed after the recompression compressor. If a flow split is maintained across the compressors, which does not match outlet pressures, then a throttle is needed to drop the higher outlet pressure to match the lower outlet pressure to prevent flow stoppage in the lower pressure line. In all observed cases the recompression compressor has achieved higher pressure than the main compressor, thus the throttle is needed only downstream of the recompression compressor. If unforeseen needs arise, then a throttle may be required after the main compressor as well.
- Valves are needed at the inlet and outlet of the inventory control tanks. The optimization of inventory control with this cycle is an area of active research[62] but the current version of GAS-PASS/CO_2 the ability to add and remove up to (typical removal rates are less than 10 kg/s during inventory control)100 kg/s during part-load operation was assumed. The valve locations are also an area of research, but the outlet of the main compressor is a high pressure and low temperature location within the cycle, thus suggesting its use for an inventory control inlet. The precooler inlet is suggested for the inventory tank outlet since the precooler inlet is nearly the lowest cycle pressure, and the precooler will act as an attemperator for the main compressor, whose performance is quite sensitive to temperature.
- The bypass valve is used for rapid power changes, such as loss-of-load. This valve bypasses part of the flow around the turbine, thus reducing the amount of work added to the shaft, and bypasses the intermediate heat exchanger, which will decrease the amount of heat added to the cycle. The valve is placed between the high and low temperature recuperator lines because they have a small temperature

difference, (7°C at steady state) which avoids thermal shock, and the flow would naturally move from high to low pressure in this location.

- The turbine inlet throttle can be used to decrease the pressure ratio available to the turbine to perform work. This is another means to allow part-load operation.
- The water pump is used to control the amount of energy removed from the cycle in the precooler. The pump is used to vary the water mass flow rate, primarily to control the CO_2 outlet temperature. Note that the water temperature may need to increase during low power operation, which can be accomplished by a recirculation loop on the water side.
- The sodium pump is used to control the energy added to the cycle via the IHX. Typically, it is used to proportionally match sodium mass flow rate to reactor power. By keeping these values proportional, the sodium inlet and outlet temperatures are held close to the steady state value.

Note that this list does not include several other possible control systems or the detailed control systems required within components. For example, an S-CO_2 compressor may need a complex control system including temperature control and recirculation loops within the compressor[38,40] to provide stable operation. In the present work note that recirculation loops have not been provided for the compressors. This common control technique (employed to help prevent surge) was not needed for the transients analyzed in this work. They would likely prove useful during LOL transients, when the shaft rapidly gains excess work, for the design shaft speed to support. Recirculating compressor flow would create additional shaft work. Recirculation loops are necessary to prevent compressor surge in any case.

The location of the turbine bypass valve merits discussion. The plant reference layout, with a control system, is shown Figure 4-11. This figure shows that the inlet to the proposed bypass line is before the inlet to the cold/high pressure side of the HTR; however there are at least two other possible locations for turbine bypass.

4.2.1 Turbine Bypass Valve Location

Figure 4-12 shows three turbine bypass valves, labeled bypass 1-3, on a basic S-CO_2 recompression cycle layout diagram. Bypass valve 1 bypasses only the turbine (which is common in Rankine cycles) by taking flow from the outlet of the IHX and supplying it before the inlet to the hot/low pressure side of the HTR. This method of bypass may be undesirable for two reasons:

- The fluid being bypassed is much hotter, by a 120.1°C temperature difference at steady state, than the fluid it is returned to. This presents the possibility of thermal shock to the piping, especially since the bypassed fluid is at the highest temperature in the cycle. For this reason Dostal[3] rejected this bypass location.
- The IHX is not directly affected by turbine bypass. If a reactor is self-controlled to a significant degree by temperature feedback, then this method of bypass will prevent the necessary information being rapidly transmitted to the reactor. This may lead the reactor to produce unnecessarily high power during turbine bypass.

Instead of using turbine bypass at the location of bypass 1 one could operate at bypass 2. This location shifts fluid before the IHX to the HTR and minimizes the two concerns associated with bypass 1. The temperature difference is less at this point, 44.4°C at steady state, and the IHX directly experiences the effects of turbine bypass by receiving less fluid flow. This is the method of bypass used in several helium Brayton cycles[19,20]. However, this bypass method may lead to flow reversal during rapid bypass operation, such as loss-of-load transients[9].

The S-CO_2 recompression cycle offers a relatively unique opportunity for bypass at bypass location 3 in Figure 4-12. This location bypasses flow between the LTR and HTR recuperators. The advantage of using bypass at this location is that the temperature difference is minimal, 8.2°C at steady state.

Note that a concern with this location might be that part of the fluid flow will not enter the HTR, thus there is potential for less recuperation. This is not actually the case since the fluid that does not enter the HTR is directly injected into the low pressure side and the HTR will experience a decrease in flow on both the high and low pressure sides. Thus the HTR should become more effective, with lower mass flow rate (and the same geometry), while the bypassed flow is "directly" recuperated.

All three bypass methods will be investigated during part-load operation in Sections 5.1.5 through 5.1.7. However, only turbine and IHX bypass will be used during the loss-of-load transient analyzed in Section 5.2.

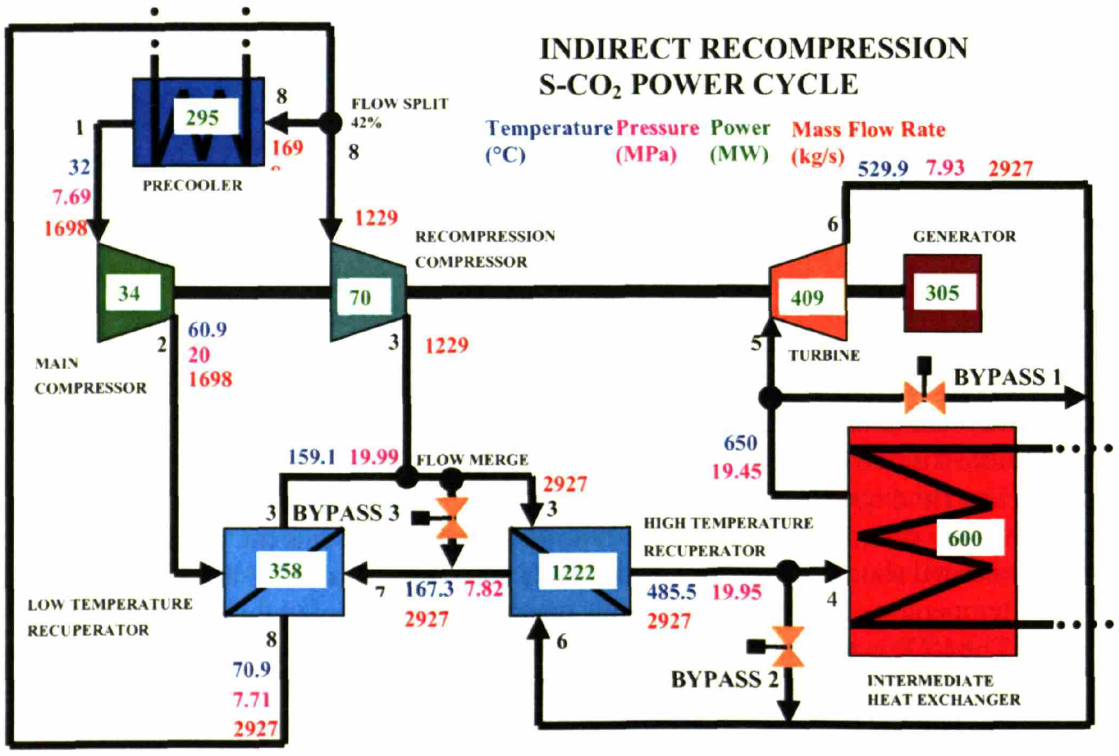

Figure 4-12: Possible Turbine Bypass Locations

4.3 Parallel Compression

Parallel compression is inherently more complex than single compressor operation. Compressor performance in the S-CO_2 recompression cycle is quite sensitive to incoming mass flow rate (thus the flow split) and changing fluid properties (especially the main compressor), yet the outgoing outlet pressures must match for stable operation. If the outlet pressures do not match, and no active control actions, such as throttling, are taken, then the lower pressure line will decrease its flow rate, changing the mass flow split, until both compressors balance.

For example, if the main compressor starts to output too high a pressure, then the recompression compressor will immediately respond to this pressure imbalance by decreasing its mass flow rate, thus increasing its pressure ratio (see the shape of the pressure ratio curves shown in Figure 4-13). As the recompression compressor decreases its mass flow rate the main compressor gains this flow and therefore decreases its pressure ratio. Thus, the compressors automatically balance their pressure ratios by exchanging mass flow.

Turbomachines have a limited range of volumetric flow rates over which they can operate. Figure 4-13 shows the pressure ratio curves for the S-CO_2 recompression cycle turbomachines at nominal shaft speed. While the curves stretch over a relatively wide flow rate range, the range can become limiting due to fluid property effects during off-design operation.

This effect is particularly important for the main compressor, where fluid density changes rapidly with small changes in temperature (and pressure). Figure 2-5 shows the cycle fluid densities, with a number marking the location of each major component. During inventory control the main compressor inlet density can drop by over a factor of two, see Figure 4-20, which pushes the main compressor well beyond stall given the same mass flow rate, to say nothing of the effects on the compressor's pressure ratio.

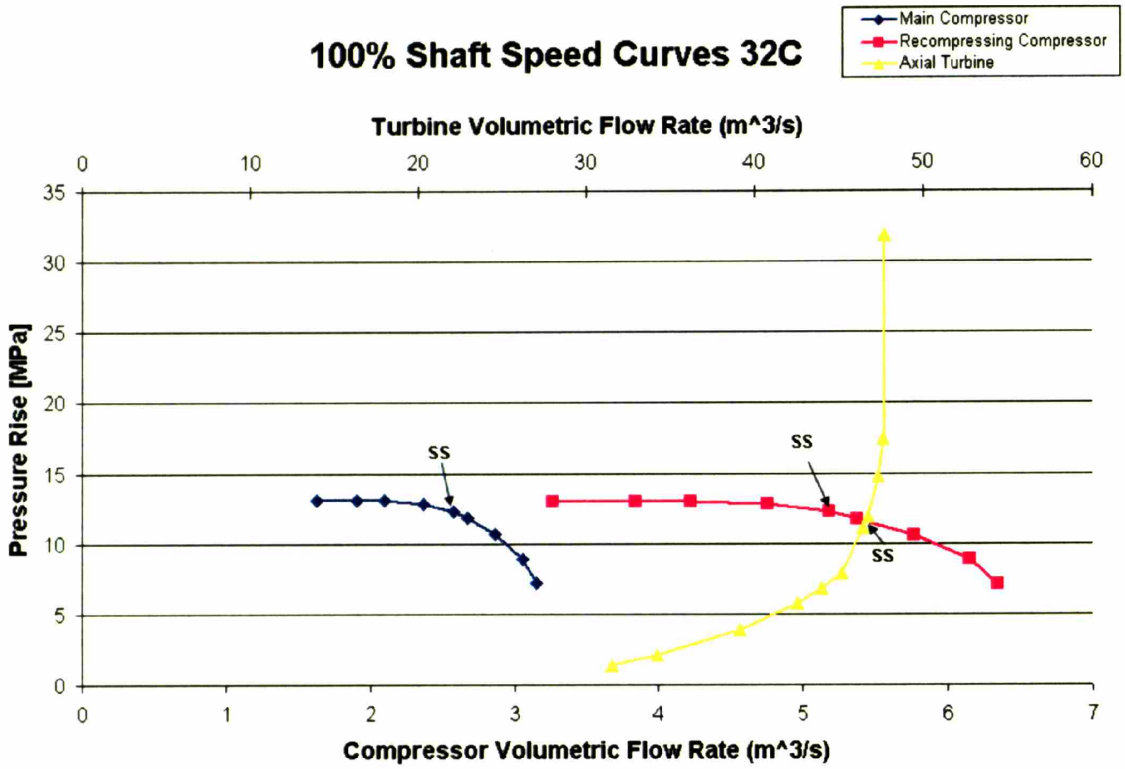

Figure 4-13: Turbomachinery 100% Shaft Speed Pressure Ratio Curves

The optimal manner to operate these unique parallel compressors is at an early stage of research. Previous experience with ideal gases by Staroselsky[42] provides several guidelines:

- Recycling flow is inherently inefficient and should be minimized.
- Compressors should reach stall/surge at the same time.
- Biasing flow or shaft speeds requires constant readjustment.
- Staroselsky concludes that for an ideal gas the optimal operation method is simultaneous loading/unloading of both compressors.

A modification of these conclusions was used during simulation with the S-CO_2 recompression cycle. Note that since both compressors are on the same shaft the designer can only control the flow rate to the compressors.

Both compressors adjust to changing conditions simultaneously, but the flow split is controlled by valves. Thus, while each compressor simultaneously sees load changes, the operator can move the compressors to a region where the outlet pressures do not balance, which is needed during inventory control. During inventory control the main compressor drops in volumetric flow rate quickly, due to fluid property changes, which forces the recompression compressor to choke. To avoid this problem the mass flow split must be controlled and the recompression compressor outlet throttled.

Within these constraints there is significant flexibility on how to shift flow between the compressors. While optimization studies have not been performed, repeated runs suggest that during inventory control the most efficient method is to keep more flow in the main compressor. This occurs naturally due to the increases in volumetric flow rate experienced by the main compressor, solely due to changes in fluid properties* even if the flow split is held constant. Therefore, at some point, near 47% generator power during quasi-static runs, flow must be shift from the main compressor to the recompression compressor.

For simplicity a PI controller was added to the flow split valves, which keeps the steady state mass flow split, 42%, until the main compressor reaches 95% of the way to choke, based upon volumetric flow rate. At this point the flow split is increased, shifting flow to the recompression compressor if the main compressor increases its volumetric flow rate.

Referring again to Staroselsky, the compressors are operated with simultaneous loading/unloading near full power. During inventory control the main compressor, typically the more efficient compressor, gradually assumes its maximum flow rate (due to property changes, not controller action). From this point on the main compressor operates near its maximum flow rate, but both compressors continue to see simultaneous load changes. Flow is shifted to the recompression compressor as necessary.

This method of control (or something quite similar) will be required during lower power operation with inventory control. It is quite likely that active control of the flow split and throttle will require continuous readjustment, which may be detrimental to equipment lifetime. Future studies should determine the optimal flow split during part-load operation and if the compressors can be allowed to self balance, i.e. the flow split valves are not active, near full power.

4.4 Cycle Layout with Off-Design Operation

During off-design operation it may become possible to simplify the S-CO_2 recompression cycle by adding a bypass line to redirect flow from the outlet of the recompression compressor to the outlet of the main compressor, as shown in Figure 4-14, but it is probably undesirable. This section will discuss the reason for the recompression layout, why the layout may not be necessary during off-design operation, and why the layout should remain the same.

---

* Due to the strong fluid property effects near the main compressor inlet the operator could control the main compressor to a significant degree by changing the external cooling water mass flow rate to affect the CO_2 temperature entering the main compressor. Unfortunately, this control, while effective, can generally only be used to increase the main compressor volumetric flow rate, the opposite of the desired effect, during inventory control. The main compressor inlet temperature is quite close to CO_2's critical point, ~1°C above, thus decreasing the temperature would put the main compressor inlet into the two-phase fluid region. The introduction of liquid to a compressor is undesirable and may damage the machine. This issue will be examined closely, for different reasons, in Section 4.5.

Dostal found that in a simple cycle arrangement (one recuperator and one compressor) a pinch point (where the hot and cold streams reach the same temperature and further heat transfer cannot occur) can arise due to the significant variation in isobaric specific heat between the two streams[3]. Near carbon dioxide's critical point isobaric specific heat and density increase greatly. The supercritical cycle is designed to operate near this point mainly to take advantage of the efficiency of compression with a dense fluid. A pinch point will prevent about 10%[3] of the available heat from being recuperated. Parallel recompression is a simple and economical way to avoid this pinch point.

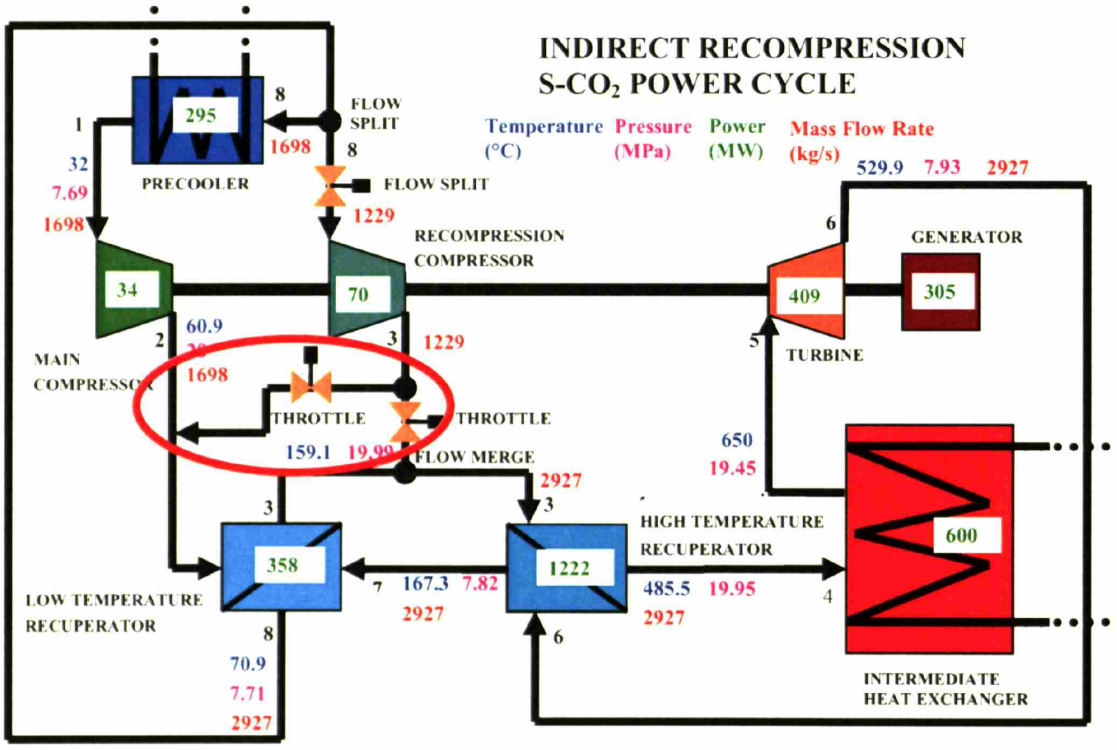

Figure 4-14: Simplified Cycle Layout During Off-Design Operation

During off-design operation with inventory control, the low pressure side of the system will drop below the critical pressure, and the behavior of the isobaric specific heat on the cold side will change significantly. This may make it possible to simplify the cycle layout by shifting flow to a single compressor and one recuperator. Unfortunately, it isn't possible to shift all the flow into a single compressor and undesirable to (effectively) combine the recuperators into a single unit.

The main compressor experiences a significant drop in inlet density as pressure drops with inventory control. This increases the compressor's volumetric flow rate even as mass flow rates decrease (at part-load operation). Since a turbomachine's behavior is largely determined by the velocity triangles, which are proportional to the volumetric flow rate, it is unlikely that a compressor can operate with a significantly larger volumetric flow rate. Current design calculations predict that the main compressor can drop its fluid inlet density by over a factor of two, while mass flow rate drops by less than

half, thus creating a limiting large volumetric flow rate in the main compressor even if the cycle layout does not change. Therefore, the main compressor cannot absorb extra flow and the recompression compressor cannot handle as much flow as the main compressor.

Even if the compressors cannot be combined, one could combine the two recuperators. By shifting the fluid from the outlet of the recompression compressor to the low temperature recuperator inlet one would, effectively, combine the high and low temperature recuperators into a single heat exchanger. This would be desirable from a control standpoint and simplify the cycle operation significantly, but it would decrease the cycle efficiency.

During both steady state and off-design operation, the outlet of the main compressor is, roughly, 100°C colder than the outlet of the recompression compressor (due to the main compressor inlet fluid being cooled by the precooler). By combining the fluid flows one would move to the average enthalpy at some intermediate temperature. This higher temperature fluid stream would then be used to cool the hot, low pressure fluid coming from the turbine. By definition, one would warm the cold fluid being used in recuperation, thus decreasing the effectiveness of the recuperation thus one would cool down the turbine's stream as well. Combining the warmer cold stream (from the recompression compressor) with the colder cold stream (from the main compressor and precooler) would mix a desirable with a less desirable fluid for recuperation and result in a loss of cooling ability.

While the original reason for using a recompression cycle is alleviated during inventory control, due to the limitations in volumetric flow rate in the compressors and the loss in efficiency created by mixing a cold and a warm stream it is undesirable to change the cycle layout. Note that part-load operation without inventory control, and above design load operation, do not change the reasons or need for the recompression layout, and they are thus not addressed in detail. Unless unforeseen future needs arise, the S-CO_2 recompression cycle layout should not be changed during off-design operation.

4.5 Inventory Control Region of Concern

Controlling the S-CO_2 recompression cycle presents unique problems and opportunities not seen in ideal gas cycles. In particular, part-load operation using inventory control may create undesirable turbomachinery behavior which can be alleviated if cycle low temperature control is used as well. A set of procedures are proposed for part-load operation with inventory control for this cycle.

Inventory control removes fluid from the cycle to keep high efficiency during part-load operation. As fluid is removed system pressure drops which leads to lower fluid density and smaller mass flow rates. The smaller mass flow rates allow the same temperature difference (Carnot efficiency) at lower powers. In this cycle, non-linear fluid property effects dictate that, as system pressure drops, each turbomachine responds differently.

4.5.1 Non-Linear Density Change at Main Compressor Inlet

This subsection provides the motivation for a control scheme of partial load operation described in Sections 4.5.2 and 4.5.3. Main compressor performance is especially sensitive to pressure decrease due to its proximity to the critical point. The critical point of CO_2 is 30.978°C and 7.3773 MPa* while the steady state main compressor inlet conditions are at 32°C and 7.69 MPa. As pressure drops, the inlet to this compressor moves through its pseudo-critical point and the incoming fluid density changes rapidly and significantly. Proximity to the critical temperature determines the magnitude of this change, as shown in Figure 4-15.

This figure shows several temperatures of interest and the liquid-vapor dome. The reader should note three key features in this graph:

1. There are large density changes for relatively small pressure changes at the main compressor inlet. Starting at the design conditions the main compressor inlet density is 599 kg/m^3. If the fluid pressure drops to 7.3 MPa, then the inlet density drops by over a factor of two, to 288 kg/m^3. Note that a large density change will occur regardless of the temperature: on the right side of the dome fluid density is high while on the lower pressure left side of the dome the densities are low.
2. The isothermal lines on either side of the dome are nearly vertical. A perfectly vertical line would mean the fluid is incompressible during a pressure change. However, when lines cross over the dome they become more horizontal, especially as temperatures approach the critical temperature. This means the fluid is becoming more compressible with pressure changes. Therefore, there is a large and fundamental change in how the fluid behaves as it crosses over the dome, especially as the temperature approaches the critical temperature.
3. The rate of density change versus pressure change becomes quite rapid when CO_2 approaches its critical temperature. The rate of (isothermal) density change per unit pressure is clearly shown in Figure 4-16.

Figure 4-16 shows a very large rate of density change versus pressure change close to the critical temperature. The magnitude of the $\frac{d\rho}{dP}$ peak decreases rapidly as the width of the peak spreads with increasing temperature. For example, at 31°C the main compressor inlet density would drop from 551.37 to 375.61 kg/m^3 (31.8% density change) between 7.39 and 7.37 MPa (0.2% pressure drop).

Large density changes will significantly affect main compressor performance -- especially pressure rise. The exact effects of these large non-linear density changes near the CO_2 critical point on a compressor are complex and uncertain at this time, since the performance maps are currently based on analytical models and numerical simulation

* According to NIST RefProp 7.0.

(see Section 3.4) and not yet supported by experimental data on actual compressors in the near critical region*.

If one assumes that the main compressor works with incompressible fluid (a good approximation for present purposes where, as we will see, operation near the critical point is avoided) then the fluid property (density) change effect is expressed by Equation 3-16 and Equation 3-17. The first equation states that the main compressor will increase its volumetric flow rate by nearly a third (based on conditions given in the second paragraph above), and thus significantly decrease its pressure rise (see Figure 4-17 where, for a constant mass flow rate, the volumetric flow rate is inversely proportional to density). The second equation states that the compressor's ability to raise pressure will drop by nearly a third, thus significantly decreasing the compressor's pressure rise. There is considerable uncertainty over the validity of these equations, as discussed in Section 3.4.4.2, but they will be used, with reservation, until better data becomes available.

Thus, a 20 kPa pressure decrease at the inlet to the main compressor can significantly decrease main compressor pressure rise† at 31°C. The size and speed of the drop in pressure rise presents at least two concerns:

1. The change in pressure may produce pressure spikes in the system.
2. The main compressor may stall and/or the recompression compressor may choke.

The first concern stems from the shock introduced to the system when an almost prompt drop in fluid density (for a decrease in pressure at the inlet to the main compressor) and pressure change move through the cycle. The compressor outlet pressures will not balance‡, and mass flow will significantly decrease in the main compressor as the flow through the recompression compressor rises to try to balance pressure§. Nearly simultaneously, the turbine will see a reduced pressure ratio and thus decrease its outgoing mass flow rate.

The combination of the main compressor, recompression compressor, and turbine nearly simultaneously making prompt changes in pressure ratio and mass flow rate may not be desirable. Furthermore, these effects may produce feedback which could make the system unstable.

---

* Note that S-CO_2 compressors have been successfully operated and controlled while passing from subcritical to supercritical conditions.[38,39] However, in all known cases the critical point was avoided by a significant margin.

† As this density decrease happens to the main compressor, the cycle will respond with changing flow rates and, perhaps, a flow split change. It is not trivial to estimate the exact effect of fluid property changes on the main compressor due to this cycle feedback.

‡ Recall that a decrease in density in the compressors increases the volumetric flow rate, which moves the compressor to lower pressure ratios along its shaft speed curve, and the thinner fluid decreases the ability of the compressor to raise pressure.

§ Note that if the system is operated with valves to control the flow split and a throttle to match the compressor pressure rise, then the change in conditions in the main compressor may not change the flow split, depending upon how the control system on these valves is implemented.

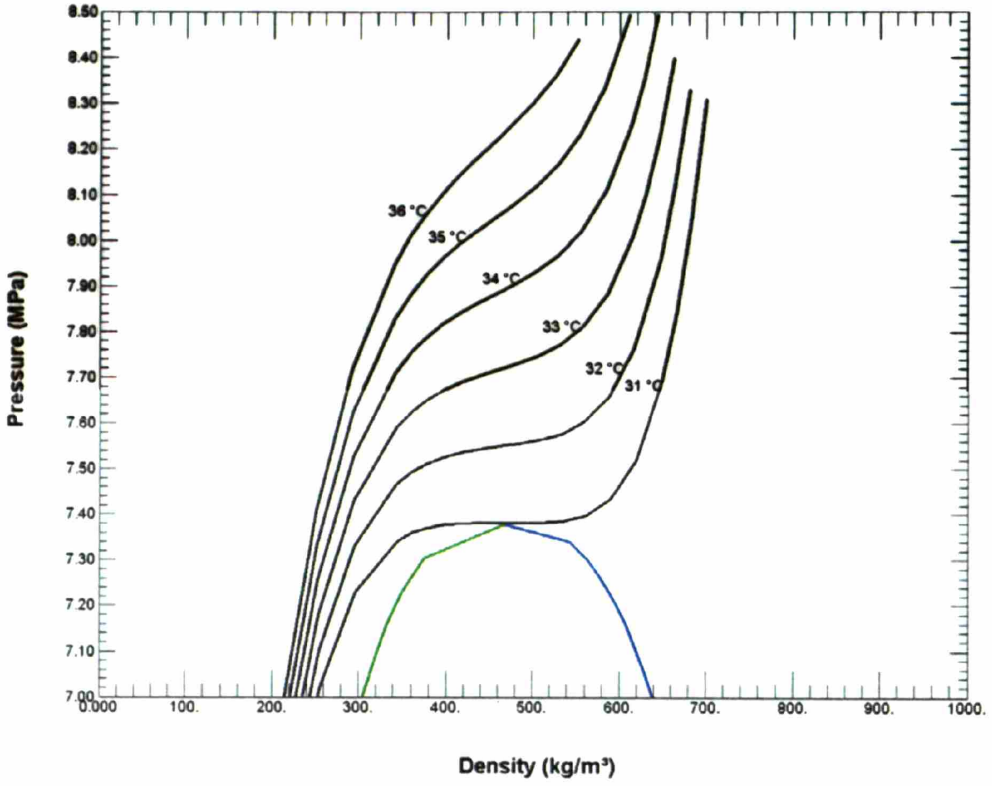

Figure 4-15: Pressure vs. Density along Main Compressor Inlet Isotherms

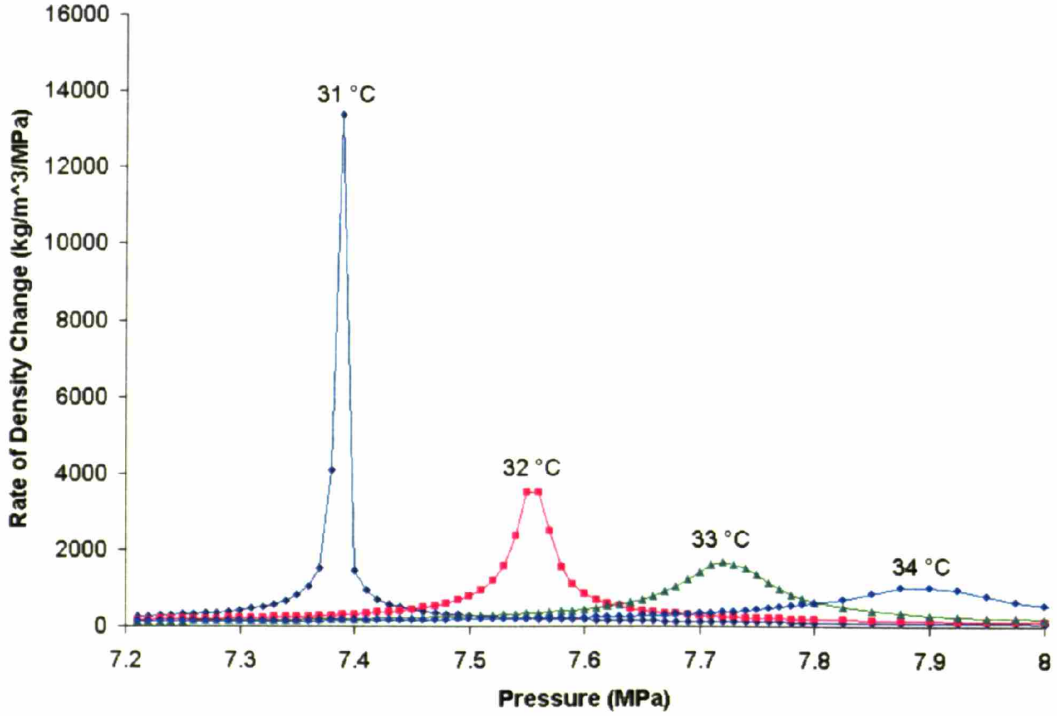

Figure 4-16: Rate of Density Change vs. Pressure along Main Compressor Inlet Isotherms

GAS-PASS/CO_2 simulations (see Section 4.5.4.3) using simple compressor off-density property relations (see Section 3.4.4.2) show that the large and fast density changes experienced on the 32°C isotherm near the pseudo-critical point that result during inventory control can produce significant oscillation. At this time there is considerable uncertainty over the behavior in this region, as will be described in Section 4.5.4.

The second concern is that the main compressor will move below its stalling mass flow rate in an attempt to increase its pressure ratio. The compressor pressure ratios (at 100% shaft speed) are shown in Figure 4-17. From its design point the main compressor can only increase its pressure rise by 6.2% before stall (assuming constant fluid properties). While the recompression compressor will reduce its pressure rise as it receives more mass flow rate it is limited to an 11.7% decrease in pressure rise before choke (starting from its design point and assuming constant fluid properties). Therefore, it is likely that such a large pressure change will require other actions (such as valves controlling the flow split and throttling) to prevent turbomachine failure starting from the given design points and using the radial turbomachine curves shown in Section 3.4.2.

The concerns seen at 31°C are significantly alleviated when operating at 32°C. A similar change in density requires a change from roughly 7.6 to 7.5 MPa. Thus, a 1°C rise in compressor inlet temperature provides a density (and pressure drop) that is 500% less sensitive to pressure drop. For 33°C a similar density change requires a pressure change about 0.3 MPa and is about 300% less sensitive than the 32°C case.

The limiting isothermal temperature which the main compressor can pass through will require detailed analysis of the effects of rapid density changes in this cycle, but its is clear that the designer can greatly alleviate the rate of change by operating at temperatures even a few degrees higher than the critical temperature. Moreover, a preferred approach to isothermal operation is to use inventory control in combination with temperature control at the low-temperature end of the cycle. This we describe next.

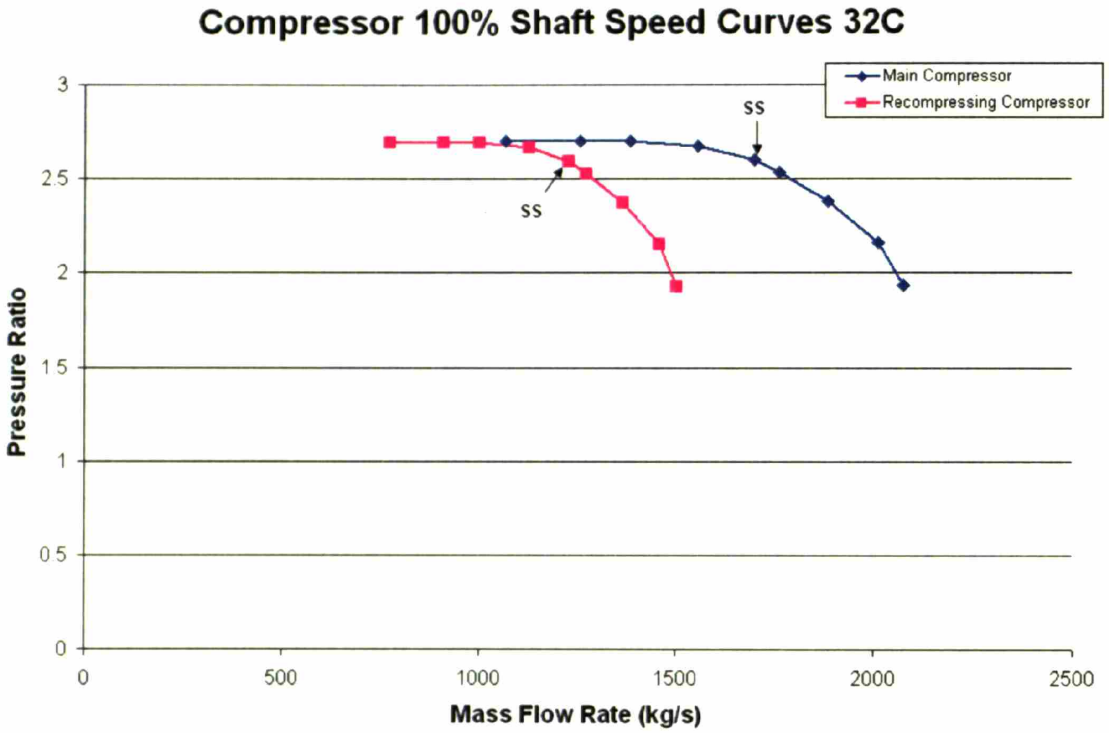

Figure 4-17: Radial Compressor Pressure Ratios

4.5.2 Low Temperature Control

Due to the strong non-linear fluid property effects near the main compressor inlet, shown in Figure 4-15 and Figure 4-16, the designer has a significant and unique method of control available. Increasing the cycle lower temperature (the main compressor inlet temperature) a few degrees has little direct affect on the cycle efficiency but a significant affect on the main compressor performance.

As the main compressor inlet pressure drops during inventory control, it experiences large changes in fluid properties, which decreases compressor pressure rise. If the designer keeps the main compressor inlet at a constant temperature during this process then the large fluid property changes are solely dependent upon the pressure.

Controlling the cycle low temperature (i.e. the inlet temperature to the main compressor) has three major advantages over pure inventory control:

1. By increasing the fluid temperature a few degrees, the rate of fluid property changes may be greatly reduced (see Figure 4-16).
2. The vast majority of the large main compressor fluid density changes (at part-load operation) can be affected through temperature control without decreasing pressure (i.e. moving isobarically between points A and B in Figure 4-18).

3. The desired main compressor inlet temperature control can be achieved by varying the external cooling water mass flow rate in the precooler immediately preceding the main compressor.

Numerical simulations using temperature control to gradually warm the main compressor inlet temperature were completed for a variety of scenarios.

- Isobarically increasing the cycle low temperature from 32°C to 38°C allows the reactor power to drop over 5% (while keeping the same turbine inlet temperature). However, due to increased cycle pressures from the displaced main compressor fluid* the cycle mass flow rates actually increase, making this method inefficient.
- The recommended method of operation analyzed in the next section.

4.5.3 Recommended Inventory & Low Temperature Control Method

A more efficient part-load control method was found by combining inventory and low temperature control. Essentially inventory control will be used to ameliorate the system pressure increase referred to in the first bullet above. Following various numerical simulations, a recommended operational path has been developed shown as the dotted line in Figure 4-18.

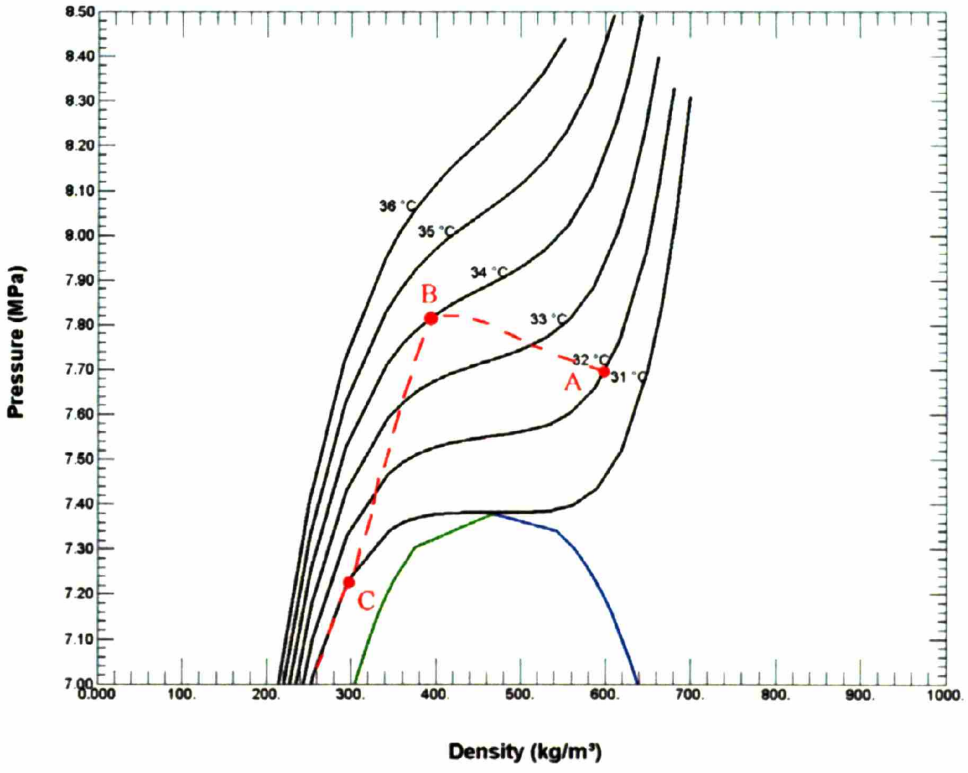

Figure 4-18: Proposed Main Compressor Inlet Operation Path with Inventory Control

*There is a relatively large inventory of fluid (in the piping) downstream of the main compressor due to the fluid's high density as shown in, "Appendix B.4 Separating vs. Lumping Piping Volumes in the S-CO_2 Recompression Cycle."

If the main compressor inlet pressure is allowed to gradually peak (the dotted line between point A and B in Figure 4-18) while the fluid temperature is increased, then the large fluid density change occurs significantly further from the critical point than in either the isothermal or isobaric case (for the same starting temperature and pressures). This significantly alleviates the rate of fluid property changes and the associated concerns.

Numerical simulations have shown that if inventory control is used to keep the turbine inlet temperature constant, then the pressure peak shown between A and B is approximately correct. Furthermore, these simulations show that point B is an appropriate temperature, 34°C, for the highest main compressor inlet temperature. Above this temperature the density is unnecessarily decreased and below this temperature there are still large density changes when decreasing fluid pressure.

From point B one could move towards point C without a significant reduction in density (pressure can now be reduced without approaching the critical point) by removing more fluid from the system and cooling the fluid back towards the critical temperature. Below point C in pressure the temperature should be kept at 31°C: the highest density value which does not risk entering the two phase region.

Note that at some point in this path it is highly likely that flow will need to be shifted from the main to the recompression compressor to prevent the main compressor from choking. Due to the large decrease in fluid density, without a proportional decrease in loop mass flow rate, the main compressor receives ever larger volumetric flow rates during the shown operation path.

The results of using the proposed path for inventory control will be shown in Section 5.1.1.

4.5.4 Uncertainty in the Application of Fluid Property Relations

An unexpected result of using the off-design fluid property corrections, previously outlined in Section 3.4.4, is the difference in cycle response encountered depending upon where fluid property relations are applied. The fluid property relations may be applied at any point within a turbomachine (e.g. to the inlet, average, or outlet properties of the turbomachine; the turbomachine models are integral models, not stage by stage models) but the point chosen will affect simulation results. During typical simulations the location of application makes no noticeable change to the S-CO_2 recompression cycle performance but, during inventory control the cycle performance can change significantly.

This subsection will briefly show the difference in behavior for each location and offer a possible explanation. Note that the examples used in this subsection come from a simulation with a control system which allowed the cycle flow split to adjust to the

changes in compressor pressure rise (i.e. the compressor flow split and throttling valves were completely open) to balance the main compressor against the recompression compressor.

Two figures will aid the discussion in this section. During inventory control the main compressor, especially at the inlet, experiences a large and potentially rapid change in fluid properties. This is clearly seen in Figure 4-20, which shows two operation lines. Line 1 shows the main compressor's inlet and outlet states during steady state operation and line 2 shows an approximate operation line after inventory control moves the main compressor's inlet pressure below carbon dioxide's critical pressure. It is clear from this diagram that the main compressor experiences a large decrease in fluid density at the inlet and a significant, but smaller, decrease in density at the outlet.

Figure 4-19 shows the recompression compressor's operation lines. Line 1 shows the recompression compressor's inlet and outlet states during steady state operation and line 2 shows an approximate operation line after inventory control moves the main compressor's inlet pressure below carbon dioxide's critical pressure. The reader should note that there is a larger density change at the outlet of the recompression compressor than at the inlet to the recompression compressor.

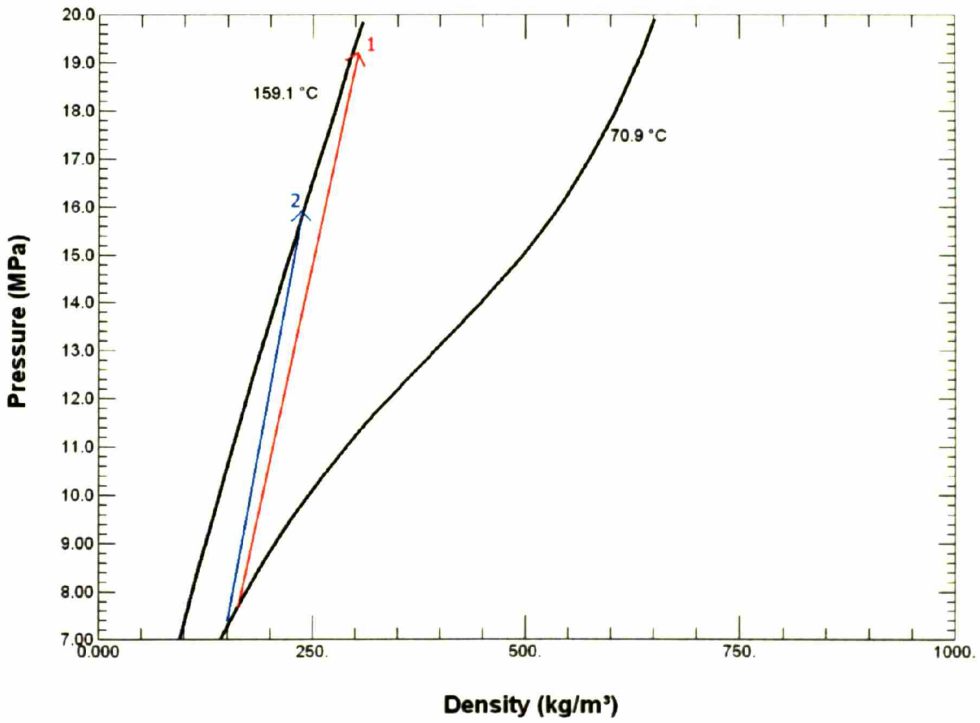

Figure 4-19: Recompression Compressor Operating Region during Inventory Control

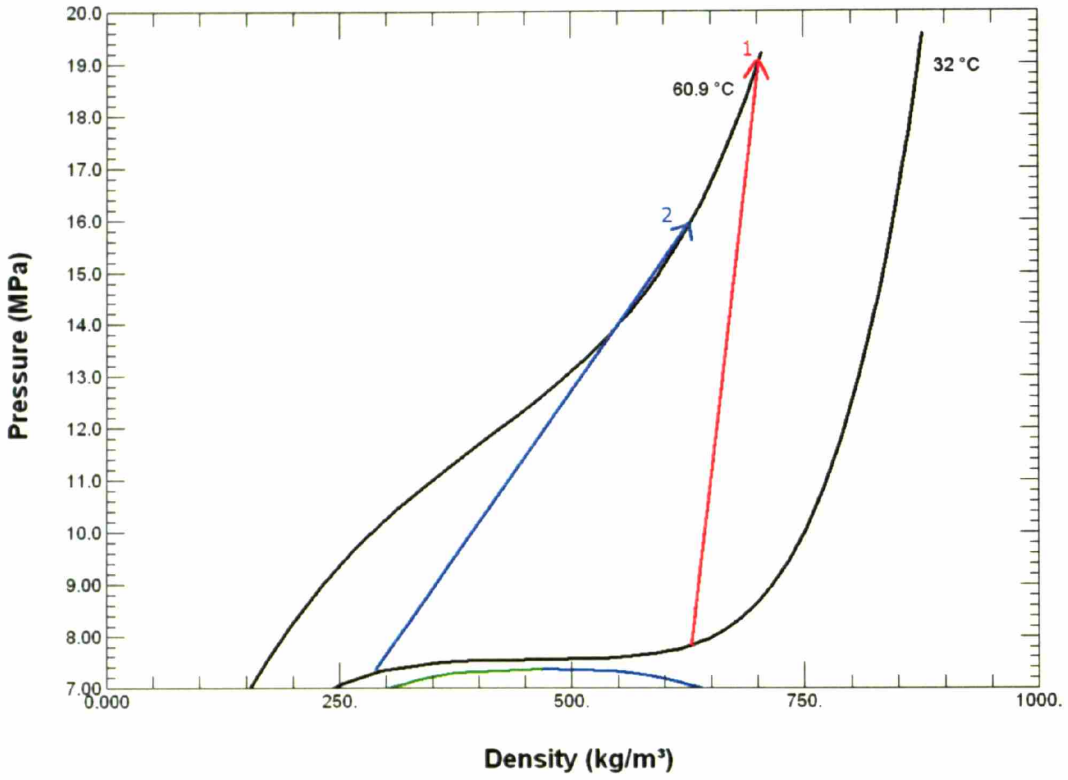

Figure 4-20: Main Compressor Operation during Inventory Control

4.5.4.1 Inlet Fluid Properties

When inlet fluid properties are used the main compressor experiences an especially large (proportional) density change. This large change has two effects:

1. Increasing volumetric flow rate, which moves the machine on the performance curves to lower pressure rises.
2. Dropping the machine's ability to increase pressure.

These effects combine to drop the main compressor pressure rise significantly. The recompression compressor must match these drops by increasing its volumetric flow rate significantly by shifting the flow split fluid to the recompression compressor, as seen in Figure 4-21. Since the recompression compressor operates with smaller mass flow rate this turbomachine runs to choke, as seen in Figure 4-22.

Therefore, if fluid inlet properties dominate off-design turbomachinery performance the designer will have to control the flow split and throttle the recompression compressor to create a matching pressure rise to the main compressor. Note that using inlet property relations, with GAS-PASS/CO_2, has not produced unstable oscillations as seen with average and outlet simulations which will be discussed shortly.

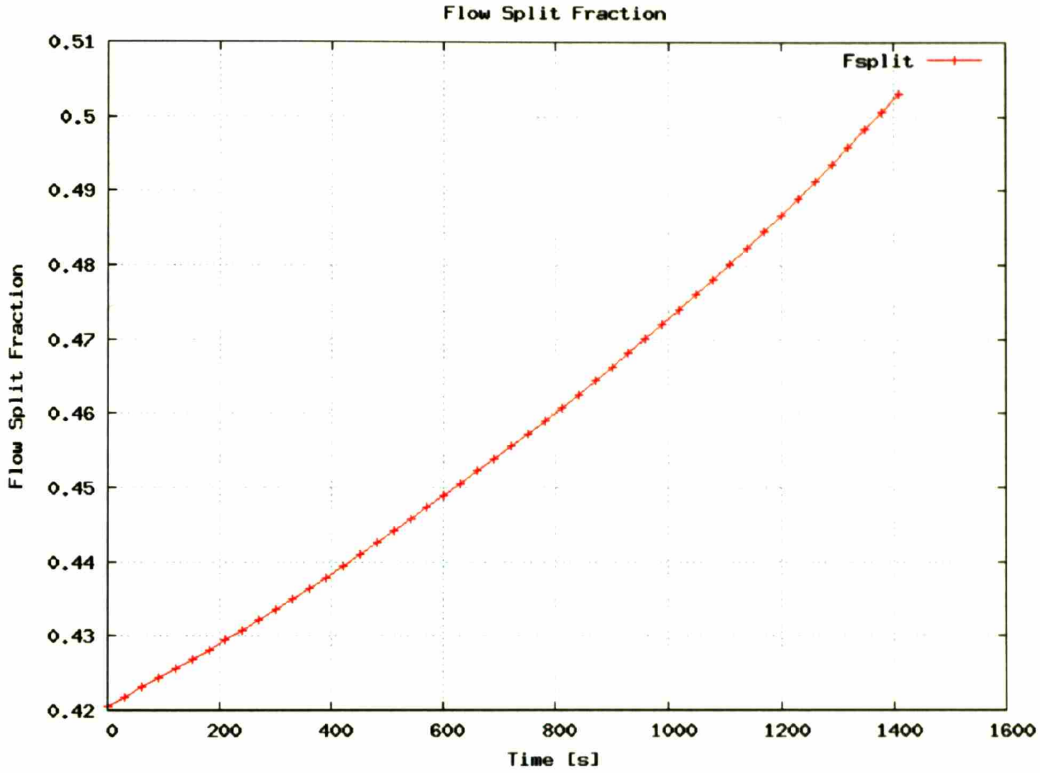

Figure 4-21: Flow Split Fraction Using Inlet Properties

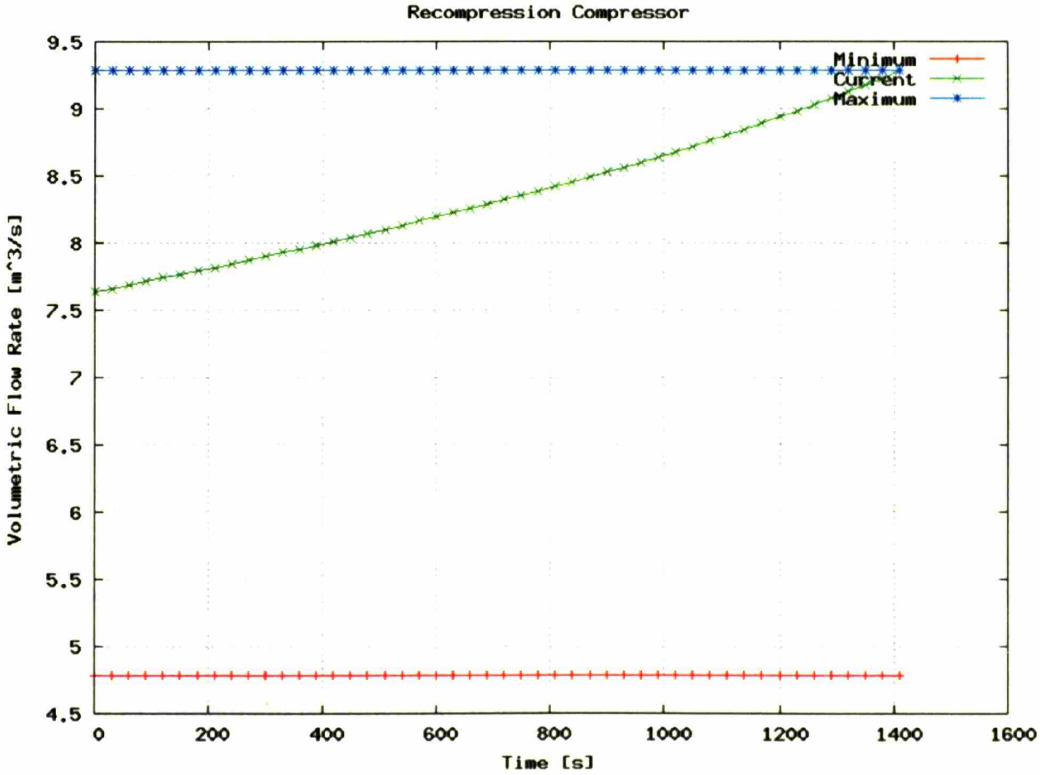

Figure 4-22: Recompression Compressor Volumetric Flow Rate Using Inlet Properties

4.5.4.2 Average Fluid Properties

Using average (within the turbomachine) fluid properties results in Figure 4-23 and Figure 4-24. These figures are quite similar to Figure 4-21 and Figure 4-22, except that the recompression compressor's volumetric flow rate increases faster than for the inlet fluid properties case.

This stems not from the main compressor's property changes (which change more slowly using average properties than inlet properties, as seen Figure 4-20) but stems from the recompression compressor property changes, as shown in Figure 4-19. From this diagram it is clear that the recompression compressor experiences a smaller density change at the inlet than at the outlet.

Using average fluid properties makes both compressors' performance sensitive to the pressure and mass flow rate in the cycle. This can lead to undesirable oscillation, since any change in pressure affects both compressors pressure rise, which affects system pressure. Depending upon the speed with which main compressor inlet pressure moves through the critical point the compressors can experience flow stoppage, as shown in the outlet properties section below, but was not the case in the simulation shown here.

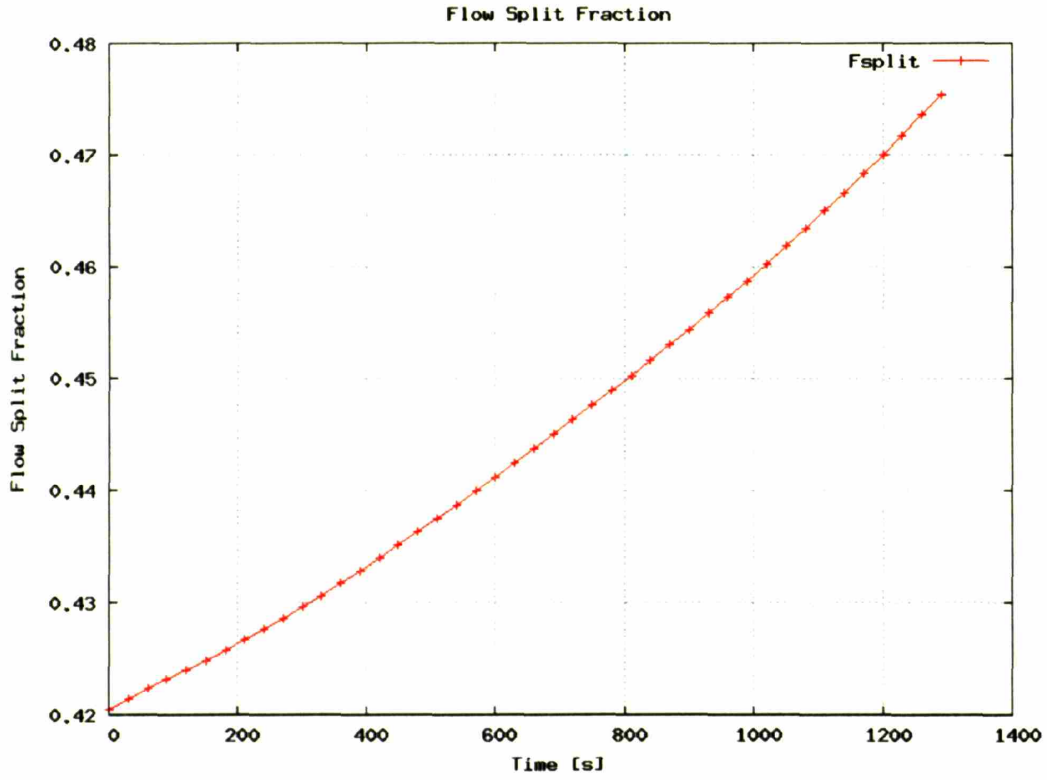

Figure 4-23: Flow Split Fraction Using Average Properties

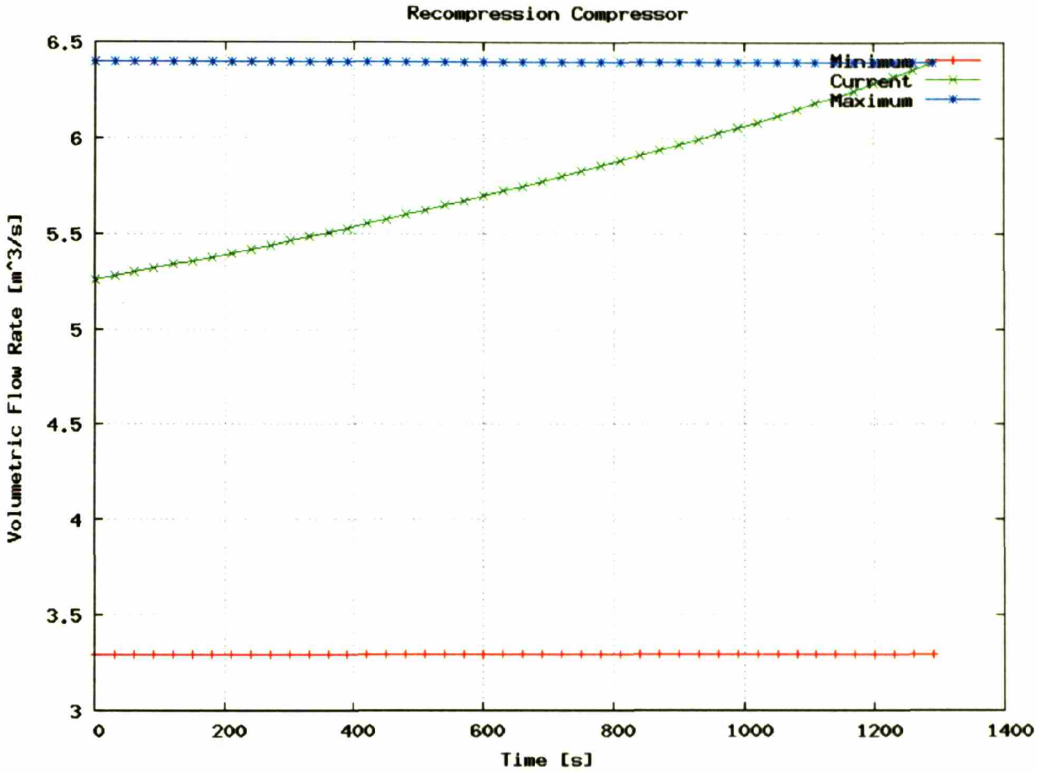

Figure 4-24: Recompression Compressor Volumetric Flow Rate Using Average Properties

4.5.4.3 Outlet Fluid Properties

Using outlet fluid properties to simulate off-design turbomachine performance results in Figure 4-25 and Figure 4-26. Figure 4-25 also shows the compressor flow split versus time. Using outlet fluid properties, the split shows now familiar behavior until about 140 seconds when rapid and large oscillations occur. These oscillations begin when the main compressor inlet pressure nears its pseudo-critical pressure.

At the point of maximum change, the main compressor inlet pseudo-critical pressure, the oscillation becomes too large and the simulation fails. Note that pressure oscillations will indirectly drive mass flow rates and work, so these spikes will show up in virtually every aspect of the plant. This is shown in Figure 4-26.

This figure shows how the inlet, average, and outlet density in the main compressor vary with time. These values show that when the power cycle pressures begin to oscillate the fluid density is affected significantly. The change in fluid further changes the system pressure and a growing oscillation is the result. In a real plant these spikes could very well lead to component or structural damage.

Note that while the density oscillation in Figure 4-26 is larger at the inlet than the outlet, the outlet oscillations are comparable.

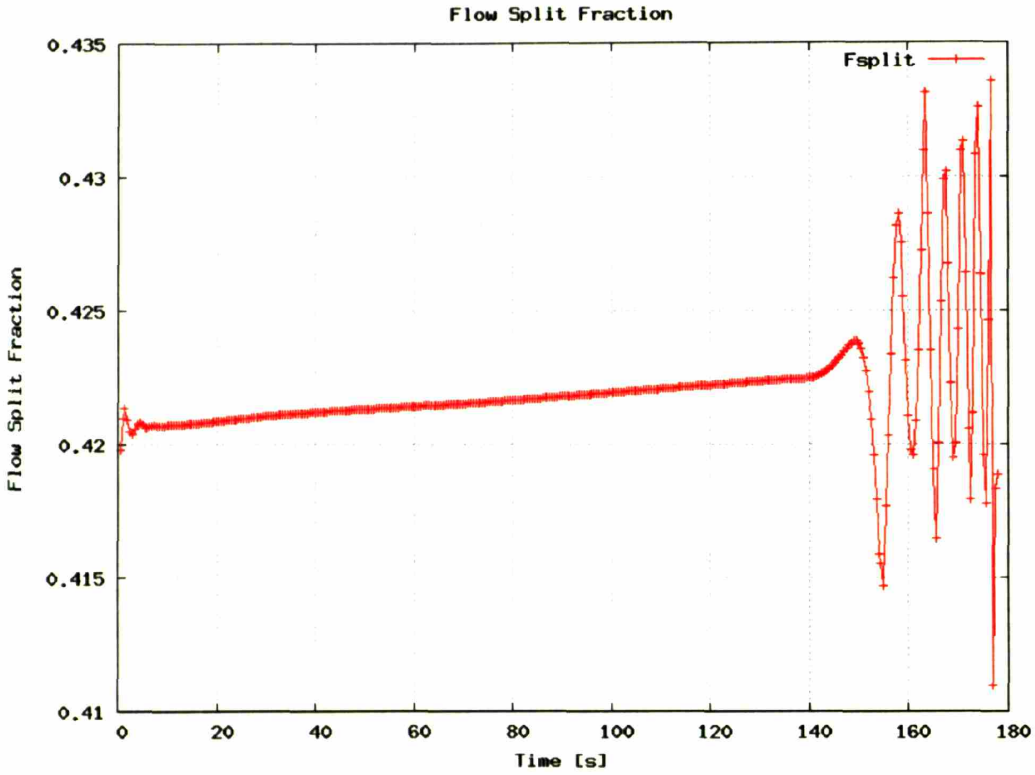

Figure 4-25: Flow Split Fraction Using Outlet Properties

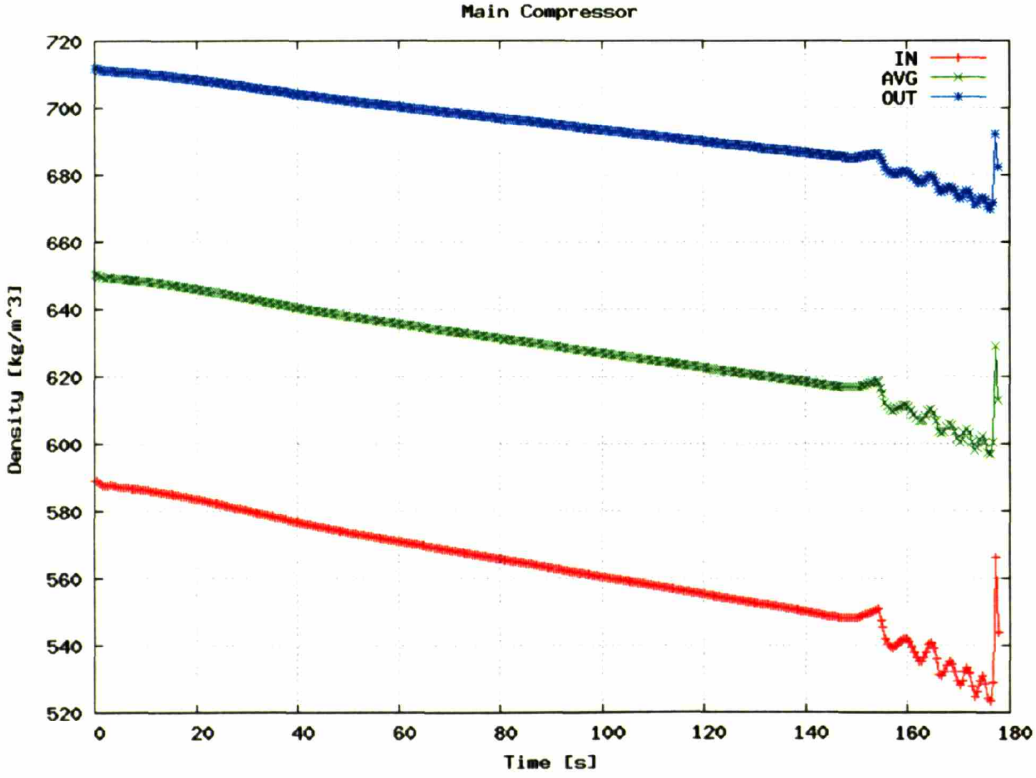

Figure 4-26: Main Compressor Fluid Density Using Outlet Properties

4.5.4.4 Possible Reason for Location Importance

The reason for this oscillation's dependence upon the location that the fluid properties are applied is somewhat subtle. While Figure 4-20 shows a smooth isothermal line at the main compressor outlet between points 1 & 2, this is not what occurs in practice. When the main compressor inlet nears the pseudo-critical point the fluid becomes very easily compressible (i.e. large density changes for small pressure changes). Therefore, even though the outlet fluid properties are being used to drive the incompressible property change equations, the effect of system pressure changes will be felt on the fluid which enters the compressor almost perfectly compressible.

This was, of course, the situation for the using either inlet or average fluid properties. The difference in using outlet properties is that the recompression compressor experiences larger fluid density changes (than it did in the other cases) which also drives the system pressure ratio. Both the main compressor and the recompression compressor experience density changes, thus they will both drive the flow split and pressure rise. This works well until the main compressor inlet becomes easily compressible, where large and fast density changes begin to occur. This is shown in Figure 4-26, which illustrates when the main compressor fluid density begins to oscillate.

The serious problems appear to stem from the main compressor and recompression compressor simultaneously driving pressure changes as the main compressor inlet becomes readily compressible. If the recompression compressor performance is also sensitive to pressure, then a feedback process leading to sharp pressure spikes can cause simulation failure. While it is unknown how realistic this oscillation is, what seems clear is that until better relations and or data are available it cannot be discounted. Therefore, GAS-PASS/CO_2 will use average fluid property relations when devising control strategies until a better method or a clear reason for using inlet or outlet fluid properties is available.

4.6 Inventory Storage Using Only System Pressure

Inventory storage in the S-CO_2 recompression cycle provides a unique opportunity to store fluid at conditions very similar to the cold end of the cycle. Due to the high density of CO_2 at ambient temperatures (and cycle pressures) there is only a small increase in fluid density if CO_2 is liquefied. This presents the designer with opportunities and challenges.

This thesis will leave research of such a system to future work. Note that research on this option is ongoing at MIT and a similar method has been examined to some degree by Moisseytsev[62].

4.7 Chapter Summary

This chapter analyzed the control system used by GAS-PASS/CO_2 for the S-CO_2 recompression cycle. The reader was introduced to PID controllers and how they were used in GAS-PASS/CO_2, the basic set of controllers used for simulation of this cycle, the inherent difficulty of parallel compression, and the lack of attractive options for simplifying the cycle.

A significant part of the chapter discussed how inventory control can lead to oscillatory behavior. While the exact behavior of the turbomachines, when the main compressor inlet approaches the critical point, is quite uncertain at this point in time, there appears to be an attractive method for avoiding this region of rapid fluid property changes, namely using low temperature with inventory control to move away from the critical point thereby avoiding very rapid property changes.

The reader has hopefully gained an understanding of the key controls and control systems and unique issues that surrounding many of them in the S-CO_2 recompression cycle. In the next chapter the selected methods will be used in GAS-PASS/CO_2 to simulate and analyze of a variety of transients.

5 Simulation Results

This chapter will present the results of the major simulations of the S-CO_2 recompression cycle completed using GAS-PASS/CO_2. The reader is assumed to have read the preceding chapters for background on the cycle (Chapter 2), to understand the simulation code GAS-PASS/CO_2 (Chapter 3), and an overview of the control system (Chapter 4). Material presented in these earlier chapters will, in general, not be addressed in the present chapter.

This chapter will look at two different cases:
(1) part-load operation
(2) loss-of-load

The chapter will focus upon part-load operation since this case is intricately tied to the unique fluid property behavior in this cycle, especially in the case of inventory control. The reader will note that the simulations offered do not include transients focusing upon the reactor. Transients such as over-power must be resolved by reactor plant control and or operator action and are beyond the scope of this work (see Section 2.1.1).

5.1 Part-load Operation

Operating the S-CO_2 recompression cycle at part-load is more complex than in ideal gas plants due to non-linear changes in fluid properties at different temperatures and pressures, especially as these effects interact with parallel compression. The net result is that this plant requires careful control to prevent turbomachinery performance failure.

Four typical control methods are used to enable part-load operation:
- Inventory Control
- Temperature control
- Throttling
- Bypass

Each of these methods offers benefits and tradeoffs that will be addressed in the subsequent sections as will their control system. Note that shaft speed control is not an option during power operations since all the turbomachines are connected to the generator, which must be synchronized to the electrical grid.

5.1.1 Inventory Control & Low Temperature Control

This section will combine inventory with low temperature control* to simulate part-load operation. The simulation will occur in a manner slow enough to keep all system values near their design points and thus, while a transient simulation, will resemble quasi-static results.

5.1.1.1 Background Discussion

In general, the primary goal of part-load operation is to retain high efficiencies while keeping all the components within their operating range. Recall that the Carnot efficiency ($\eta = 1 - \frac{T_{low}}{T_{high}}$) is simply the ratio of the cycle high and low temperatures. To retain high efficiency at part-load one would like to keep the temperature bounds as wide as possible – close to the steady state limits.

To transfer less heat without changing temperature the mass flow rate of the system must decrease (i.e. in a PCHE: $Q = \dot{m}\Delta h \sim \dot{m} Cp \Delta T$). While one can use a form of bypass to reduce the temperature in certain loop locations, in general the work in the cycle will scale with mass flow rate (i.e. compressor work), thus to achieve highest efficiency one must decrease the mass flow rate. Finally, to decrease the mass flow rate ($\dot{m} = \rho A V$) one must decrease fluid density (at fixed compressor speed), which requires removing fluid ($M_{inventory} = \sum \rho_i V_i$) – this is inventory control.

Inventory control is quite attractive in an ideal gas (helium) plant because the fluid density and pressure are proportional. Thus, as fluid is removed the pressure drops and density decreases but the turbomachinery do not change volumetric flow rates† and stay at their (optimally) designed state points. This makes controlling part-load operation with inventory control in an ideal gas system relatively easy.

The S-CO_2 recompression cycle features non-linearly changing fluid properties, especially near the main compressor. As cycle pressure drops each turbomachine will change its volumetric flow rate differently because its relationship between pressure and density is different (each turbomachine operates at a different temperature and pressure). However, at all times, the cycle pressure changes among all three turbomachines must balance. Inventory control will move the system away from its natural balance points and, in general, will require control measures to sustain a new balance.

---

* Low temperature control is used to avoid a region of concern near the critical point (see Section 4.5) which normal inventory control operations will pass through. Depending upon the assumptions used, passing through this region can lead to flow stoppage in the compressors.

† Recall that the gas flow velocity triangle is a key factor in turbomachine performance as detailed in Section 3.4.4.

Note that Dostal speculated[4] that inventory control would be quite limited in the S-CO_2 recompression cycle due to turbomachinery pressure ratio mismatches. This issue has been studied and resolved during the present work.

Two sets of valves largely make inventory control possible in the S-CO_2 recompression cycle. The first set of valves controls the flow split mass fraction between the compressors. Normally, the compressors trade mass flow rate to balance their pressure rises. Unfortunately, as power decreases the compressors will move in opposite directions on their shaft speed curves. As the outlet pressure of the main compressor drops the compressors will rebalance by shifting mass flow from the main compressor to the recompression compressor. This will drive one or both of the compressors beyond available operating bounds and cause choke or stall. By restricting the flow rate going into one of the compressors one may force a mass flow rate split that does not produce equal compressor outlet pressures, but keeps both compressors within operating bounds.

A throttling valve can be used to match compressor outlet pressures. By placing a variable throttling valve after the recompression compressor one can artificially decrease the recompression compressor's pressure rise regardless of the recompression compressor's incoming mass flow rate and fluid property changes. In practice, this allows the main compressor and turbine to balance pressure changes, thus determining system mass flow rates, and the recompression compressor valve can drop that compressor's pressure rise to match the rest of the system.

Note that using a constant flow split with inventory control in this cycle will guarantee that the recompression compressor will have a higher outlet pressure than the main compressor due to dissimilar fluid property changes. The main compressor will see an increase in volumetric flow rate, which decreases pressure rise, and a decrease in possible pressure rise due to dropping fluid density near the critical point. Hence the main compressor outlet pressure will inevitably be lower than the recompression compressor outlet pressure if the flow split does not change.

5.1.1.2 Simulation Setup

The control system used for this simulation is the following:

1. A PI controller is used to control the precooler CO_2 outlet temperature. The temperature is initially held at 32°C, is gradually increased to 34°C as main compressor inlet pressure reaches the region of concern, and finally dropped to 31°C and held there past the region of concern. The rate at which these actions happen is matched to the main compressor inlet pressure, as shown in Figure 4-18. In general the PI controller controls this parameter within a small temperature range.

   During lower power operation the incoming cooling water temperature is raised to prevent an extremely low mass flow rate in a heat exchanger designed for a much larger flow rate. In practice this could be accomplished via a recirculation loop if necessary.

2. A PID controller is used to control fluid inventory to keep the turbine inlet temperature constant. This controller cannot easily control the temperature for rapid power changes, but will control slower transients. Keeping the error on this controller within, roughly, ten degrees Kelvin largely sets the speed of reactor power change. The maximum rate of inventory change was limited to 100 kg/s but, in general, the rate of inventory change was about 5 kg/s.
3. The reactor power and sodium mass flow rate are controlled via boundary conditions. Both are proportionally decreased. The rate of decrease is designed to allow the turbine inlet temperature to stay roughly constant. After the system low pressure drops below the critical pressure the rate of decrease is slowed to keep the system low pressure from dropping steeply.
4. A P controller is used on the flow split valves. If the main compressor exceeds 95% of the its volumetric flow rate range then flow is shifted to the recompression compressor.
5. The recompression compressor throttling valve pressure drop is a variable within the GAS-PASS/CO_2 non-linear system of equations. When a time step has converged its value will produce matching outlet pressure from the compressors.

5.1.1.3 Simulation Results

The effects of this transient are shown in figures Figure 5-1 through Figure 5-14. Each figure will be briefly addressed to give the reader an understanding of the major features and control actions.

Figure 5-1 shows the cycle net efficiency versus time. The efficiency ranges between over 47% to about 18% over 1.7 hours. The curve features three major regions:

- The first region features a roughly linear slope between 0 and 1750 seconds. In the region the flow split is held constant, the main compressor inlet moves through the region of concern with increasing temperature, and the reactor power decreases linearly.
- The second region features a mainly flat slope between 1750 seconds and 3500 seconds. Several actions occur in this time. The flow split is adjusted near the beginning of this step to shift flow from the main compressor to the recompression compressor, the main compressor inlet temperature is decreased to 31°C (see Figure 5-13), and the rate of decrease in reactor power slows.
- The third region features a smoothly sloping decrease in efficiency between 3500 and 6300 seconds. In this region the flow split is increased until around 5500 seconds and other values are held constant.

Figure 5-2 plots the net efficiency versus the normalized generator power. The graph, of course, shows identical features (although the X axis is reversed) but the reader now has context for the overall efficiency. For example, by 50% nominal generator power the net cycle efficiency is roughly 42%. The lower efficiencies are only seen at small fractions of generator power. The simulation ends at roughly 6% generator power.

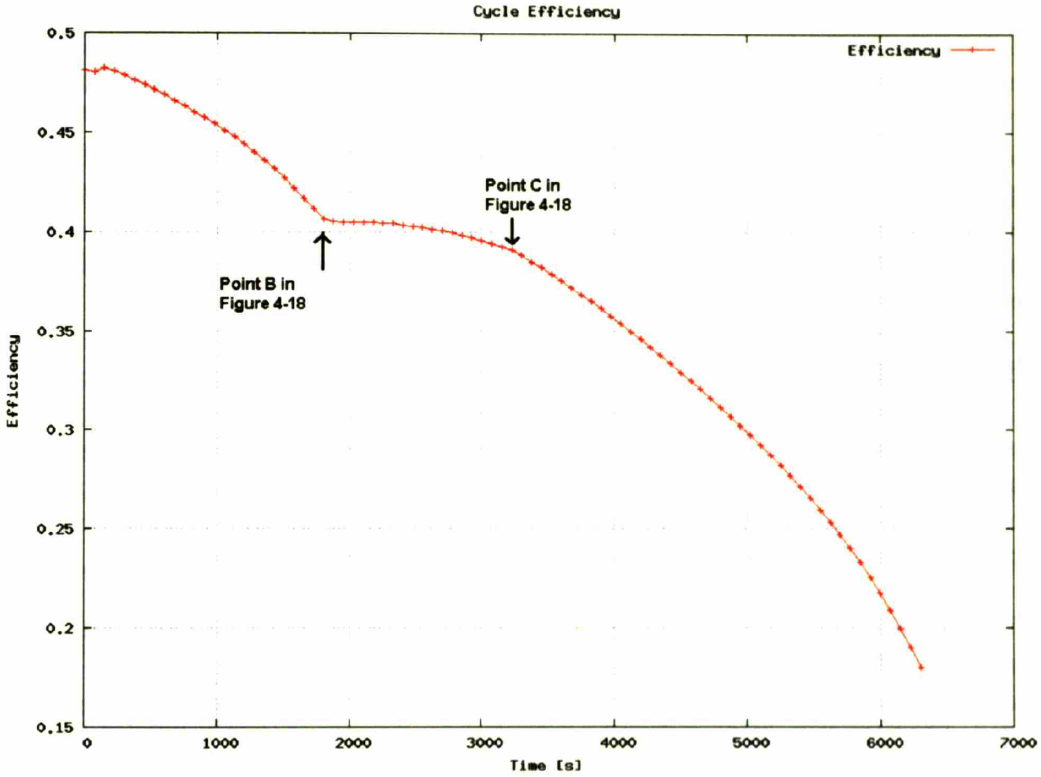

Figure 5-1: Inventory Control: Efficiency versus Time

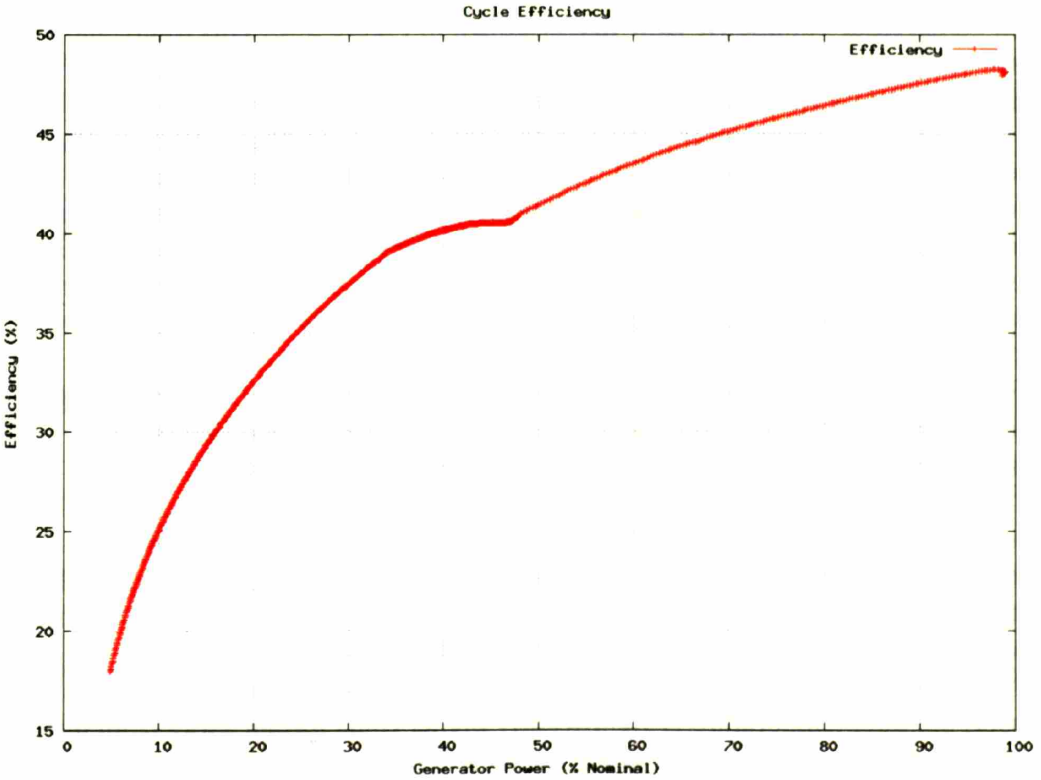

Figure 5-2: Inventory Control: Efficiency versus Generator Power

The flow split versus time is graphed in Figure 5-3. This figure shows the proportional controller actions on the compressor flow split valves to keep the volumetric flow rate of the main compressor below 95% of the total available flow rate between stall and choke.

The reader should note that the controller significantly and rapidly increases the flow split beginning at 1750 seconds (point B in Figure 4-18) when the main compressor inlet temperature has reached its maximum value. After 1750 seconds the main compressor inlet temperature falls quickly, which drops the main compressor density in a rapidly changing region as shown in Figure 4-18.

After 3500 seconds the flow split is nearly linearly increased until about 5000 seconds when it tapers off to a new value near 0.464% at 5500 seconds. At this point the main compressor inlet pressure is below the critical pressure region. During the decrease in pressure the main compressor density dropped more quickly than the mass flow rate which continuously increases the volumetric flow rate towards choke. Hence, the flow split increased to shift flow to the recompression compressor.

After 5500 seconds the main compressor enters a region where the density no longer drops faster than the mass flow rate. The mass flow rate shows a nearly constant rate of decrease and the inlet pressure is significantly below the non-linear critical property region. It is likely that the main compressor outlet pressure has dropped far enough to begin experiencing non-linear fluid property effects near the critical region.

The main compressor volumetric flow rate is shown in Figure 5-4. This figure shows the stall, choke, and operating line in terms of volumetric flow rate versus time. The operating line shows a sharp and nearly linear increase in volumetric flow rate until 1750 seconds as the main compressor inlet moves through the near critical region. Following 1750 seconds the volumetric flow rate dips as flow is shifted to the recompression compressor, and the rate mass flow rate decrease is proportionally larger than the rate of density decrease. By 1750 seconds the main compressor inlet is at its temperature and pressure apex, as shown in Figure 4-18. After this time the inlet temperature drops significantly (shown shortly) but the density decreases relatively little.

From 3500 to 5500 seconds the main compressor volumetric flow rate is kept constant by the controller on the flow split shifting the necessary flow to the recompression compressor. From 5500 to 6300 seconds the flow rate decreases slightly.

The same type of figure is shown for the recompression compressor in Figure 5-5. This figure shows the recompression compressor never operates near its choke point. This compressor shows an almost linear decrease in volumetric flow rate except when the flow split changes at 1750 seconds, and between 3500 and 5500 seconds. While the recompression compressor operates with nearly the same inlet pressure as the main compressor, the inlet temperature is significantly higher (thus further away from the critical point) and the outlet pressure is higher, as will be shown shortly.

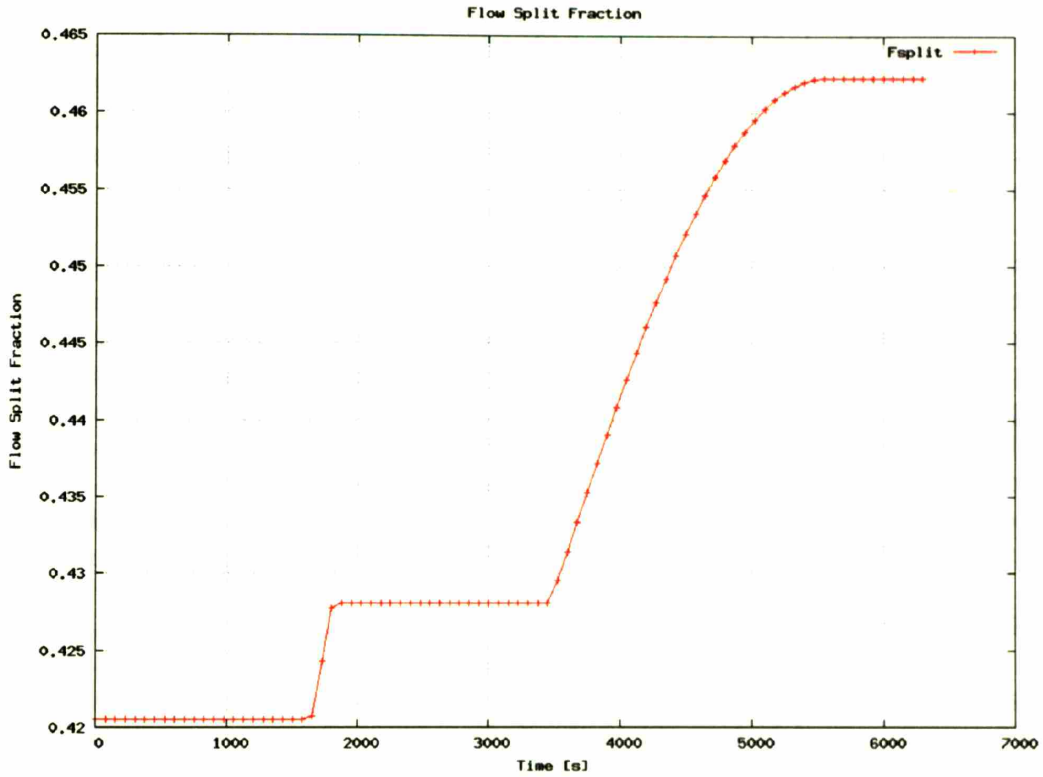

Figure 5-3: Inventory Control: Flow Split versus Time

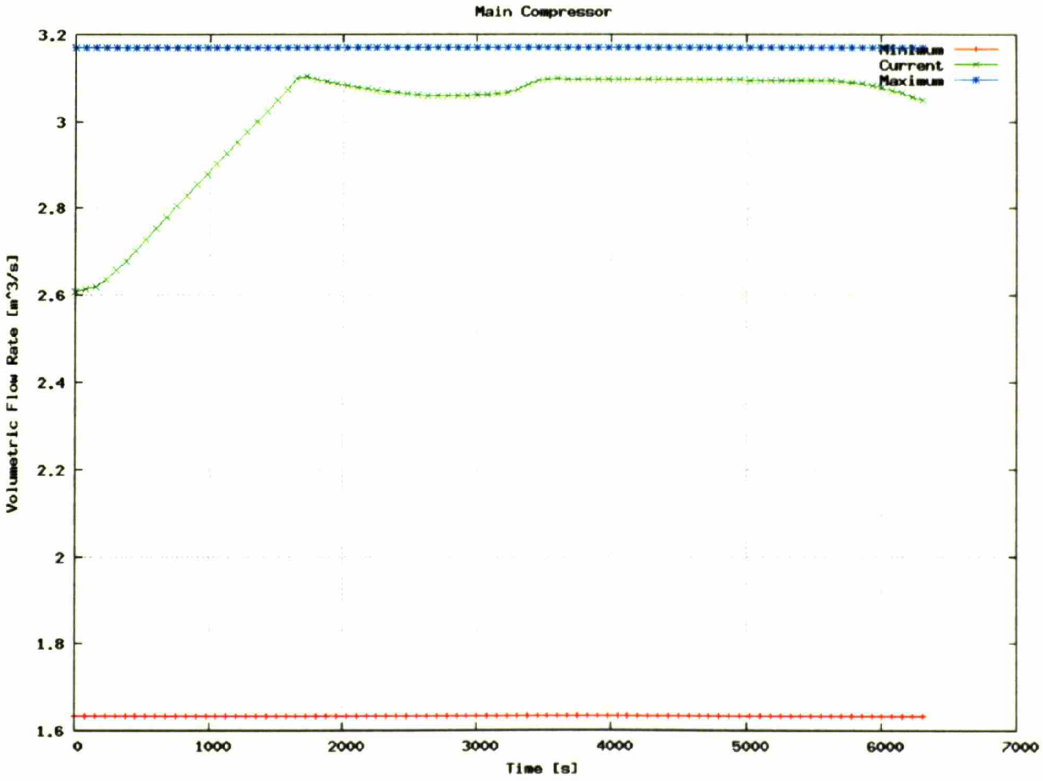

Figure 5-4: Inventory Control: Main Compressor Volumetric Flow Rate versus Time

Figure 5-6 shows the same type of figure for the turbine. The turbine volumetric flow rate shows a smoothly sloping decrease in volumetric flow rate, except at 1750 seconds. While several control actions happen at this time, it is likely that it is the slowing of the rate of decrease in heat addition that forces a leveling off between 1750 and about 2250 seconds. The turbine eventually reaches the limits of its known operation curves* near 6300 seconds, which ended the simulation.

The cycle fluid inventory is shown in Figure 5-7. The fluid inventory is controlled to keep the turbine inlet temperature constant, thus it is closely related to the ratio of reactor power to mass flow rate. The inventory show a nearly linear decrease until 1750 seconds; when the slope lessens. This stems from the slowing in the rate of decrease in reactor power at this time. The inventory ranges from over 58,000 kg at full power to about 21,000 kg at simulation failure. GAS-PASS/CO_2 predicts that about 64% of the fluid can be removed from the cycle with just inventory, low temperature, and flow split/throttling valve control. The fluid inventory versus normalized (to the steady state) generator power shown in Figure 5-8. It is included solely for reader convenience.

Figure 5-9 shows the component temperatures. This figure shows that the turbine inlet temperature is held roughly constant by the PID inventory controller, the main compressor inlet and outlet temperature are held roughly constant by the cooling water PI controller, and the rest of the loop temperatures rise.

The temperatures surrounding the low temperature recuperator, spread out from their steady state values, and will be discussed separately in Section 5.1.1.4. Note that while the reactor outlet temperature increases, it could be kept constant by changing the liquid sodium loop mass flow rate.

The component pressures are shown in Figure 5-10. This figure shows three sets of pressures: the high pressure side of the cycle, the lower pressure side of the cycle, and the very low pressure external heat addition and removal fluids. The high pressure values shows a nearly linear decrease, except where the slope moderates at 1750 seconds when the rate reactor power decrease slows until the main compressor outlet pressure reaches about 8 MPa. However, the recompression compressor shows different behavior.

The recompression compressor outlet pressure is independent of the main compressor outlet pressure due to the downstream variable throttling valve. As the main compressor experiences near critical fluid property effects, and the flow split is held constant by the upstream compressor valves, the recompression compressor outlet pressure rises above the main compressor outlet pressure. The recompression compressor outlet pressure always decreases during inventory control but it is, in general, about 2 MPa higher than the main compressor outlet pressure depending upon the flow split changes.

* While a turbine can have gas flow separation at low mass flow rates like a compressor, it will not stall, where the mass flow rate rapidly drops to zero, as occurs in a compressor.

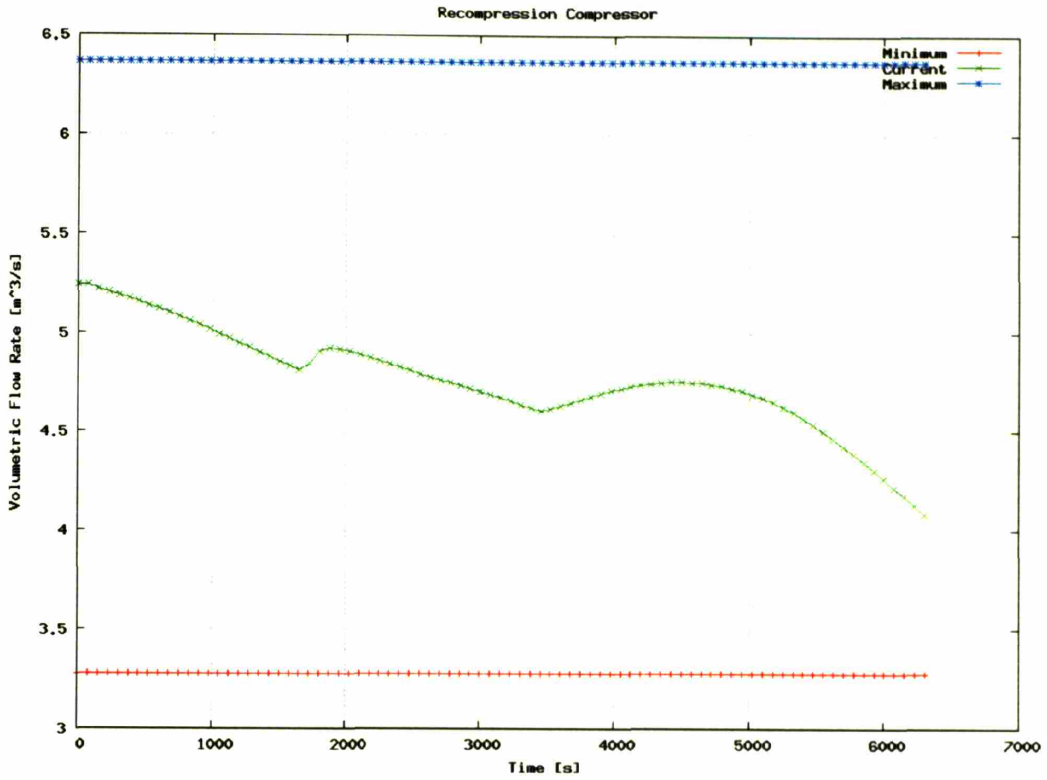

Figure 5-5: Inventory Control: Recompression Compressor Volumetric Flow Rate versus Time

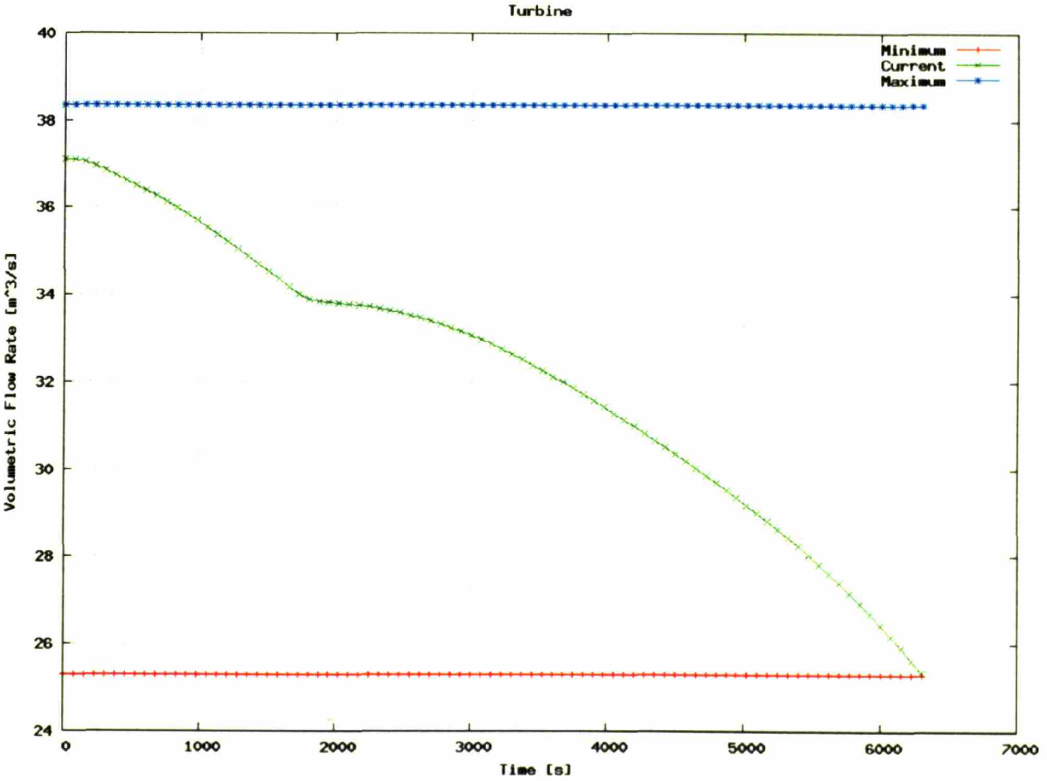

Figure 5-6: Inventory Control: Turbine Volumetric Flow Rate versus Time

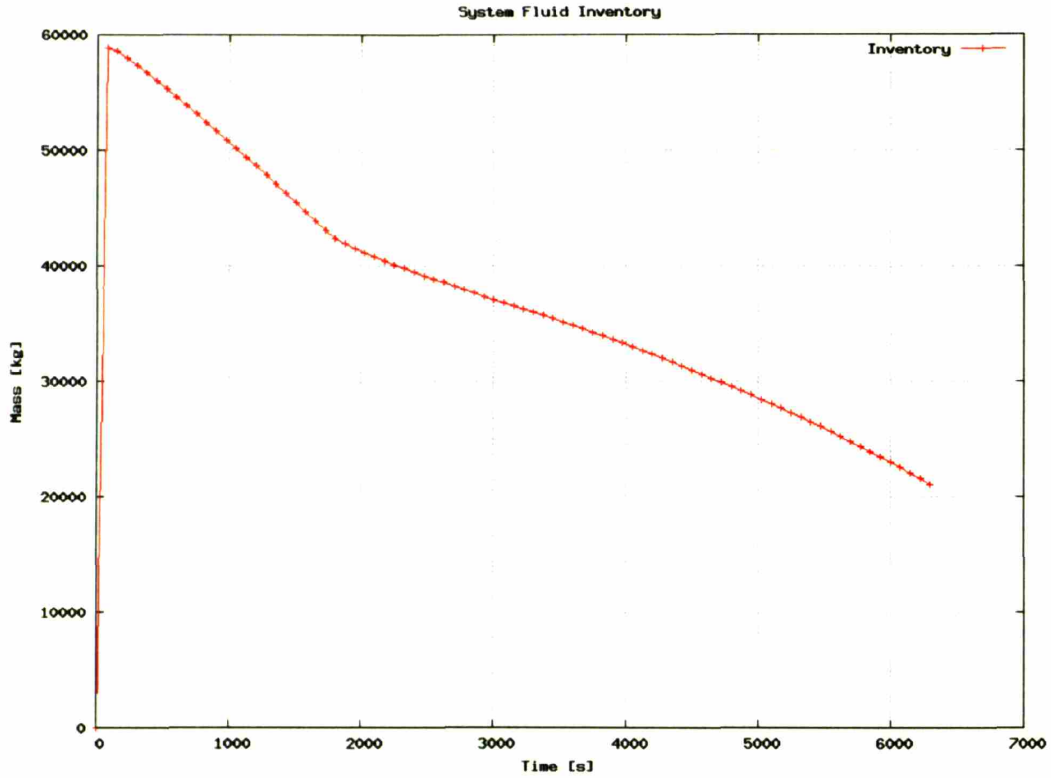

Figure 5-7: Inventory Control: Inventory versus Time

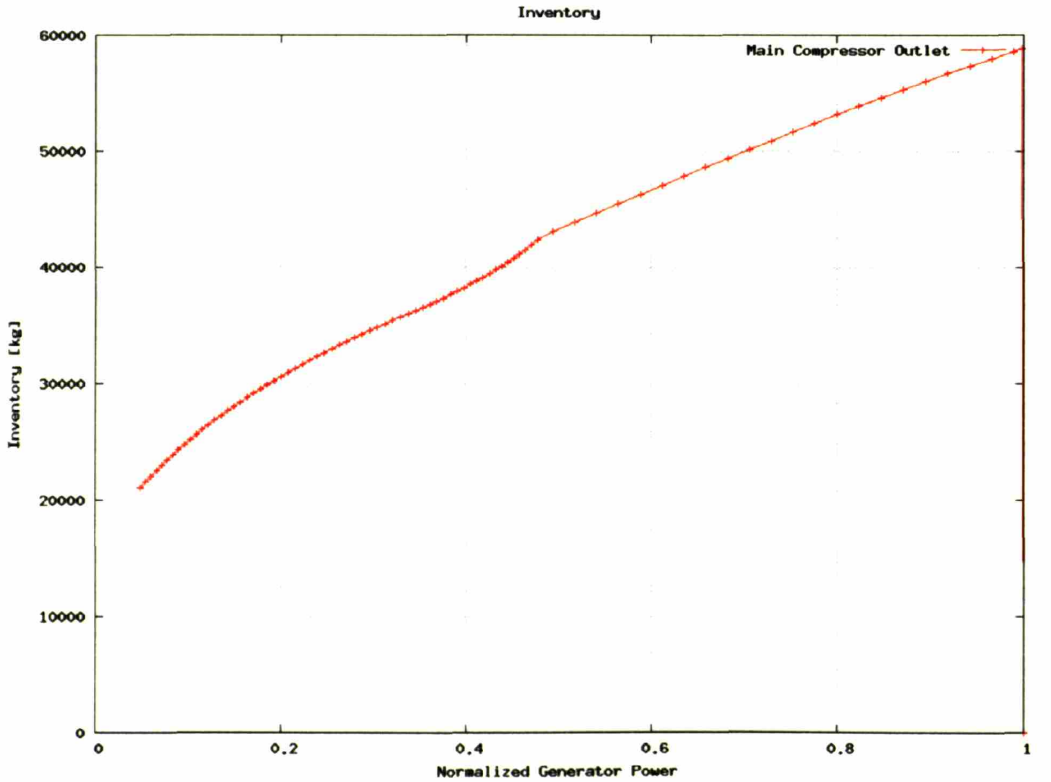

Figure 5-8: Inventory Control: Inventory versus Normalized Generator Power

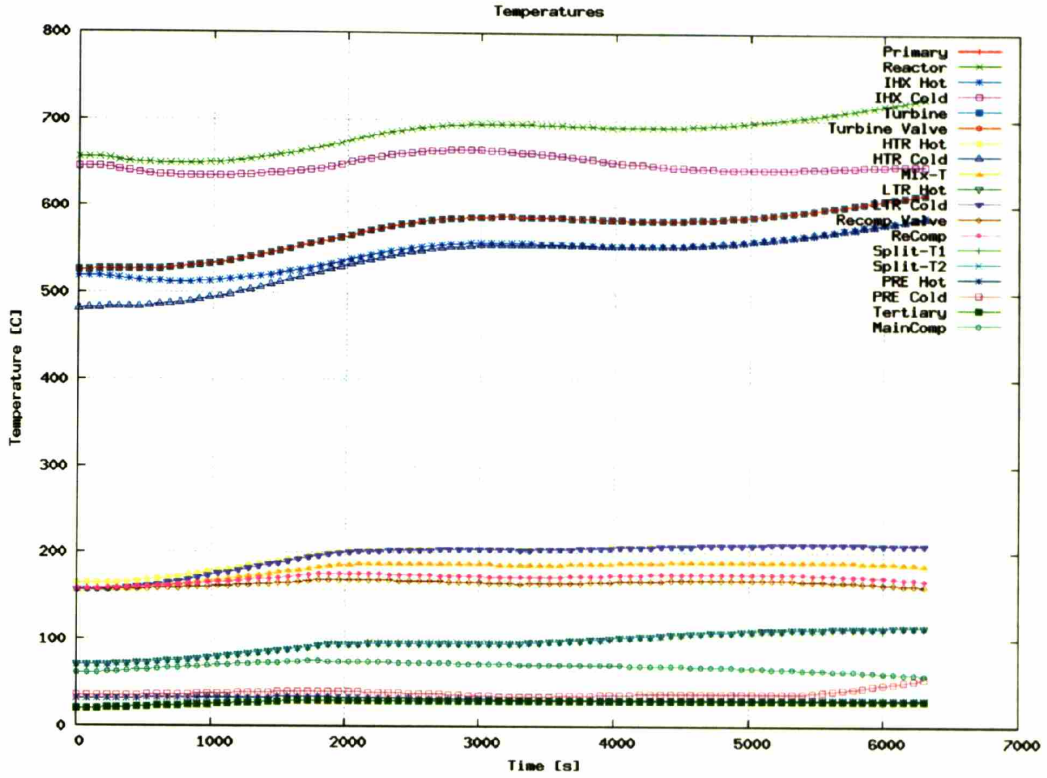

Figure 5-9: Inventory Control: Temperatures versus Time

The low pressure side of the power cycle gradually and non-linearly decreases to about 5.6 MPa. The low pressures are nearly constant until about 1750 seconds, when the main compressor inlet temperature is allowed to drop.

The heat transfer in the cycle is shown in Figure 5-11. The figure shows the reactor and IHX heat addition*, the low and high temperature recuperators, and the precooler heat removal versus time. The lines show roughly linear behavior with a decrease in slope around 1750 seconds when the rate of decrease in reactor addition slows.

The reactor heat addition line begins adding less heat than the low temperature recuperator around 3500 seconds and eventually approaches, but never reaches, the precooler heat transfer near the end of the simulation.

The low temperature recuperator and precooler heat transfer lines show a nearly constant difference in heat transfer with time. The high temperature recuperator heat transfer line decreases its heat transfer from over 1200 to less than 500 MW by the simulation conclusion.

Mass flow rates are shown in Figure 5-12. The carbon dioxide and liquid sodium mass flow rates show a nearly linear decrease in mass flow rate except for the now familiar

* Due to the modeling of the primary system these are identical. See Section 3.6.2 for more information.

change in slope at 1750 seconds. The water mass flow rate shows unique behavior and a considerable peak near 3250 seconds.

This behavior stems from the difficulty in matching the precooler water mass flow rate to the changing main compressor inlet temperature. The numerical solver used in GAS-PASS/CO_2 had trouble converging the system when the water mass flow rates dropped too far. The designer must simultaneously balance the main compressor CO_2 mass flow rate and inlet temperature to the precooler water mass flow rate and cooling water inlet temperature. This is non-trivial and the reason for the complicated behavior*. The large peak shown at 3250 seconds stems from a slight mismatch in the incoming cooling water temperature and the decrease in the main compressor inlet temperature, which reaches its minimum temperature of 31° at 3250 seconds.

Figure 5-13 shows the main compressor inlet temperature with time. This temperature is controlled by the water mass flow rate PI controller. The inlet temperature begins at 32°C a linear rise in temperature at 100 seconds and peaks at 34°C at 1750 seconds. Between 1750 and 3250 seconds the temperature linearly drops to 31°C and is held there for the rest of the simulation.

Figure 5-14 shows the precooler inlet and outlet CO_2 pressures. These lines nearly overlap (there is little pressure drop in the precooler) and show a gradual rise in pressure starting at 100 seconds and peaking around 7.8 MPa at 1750 seconds. From this point the pressure linearly decreases until 3250 seconds and then gradually slopes downwards to nearly 5.6 MPa.

* Note that there is uncertainty over how the water heat transfer coefficient changes during the transition from turbulent to laminar which occurs on this graph and may be responsible for some of the unique water mass flow rate behavior. The reader can consult, "Appendix B.1 Water Heat Transfer Correlation Uncertainty" for more information.

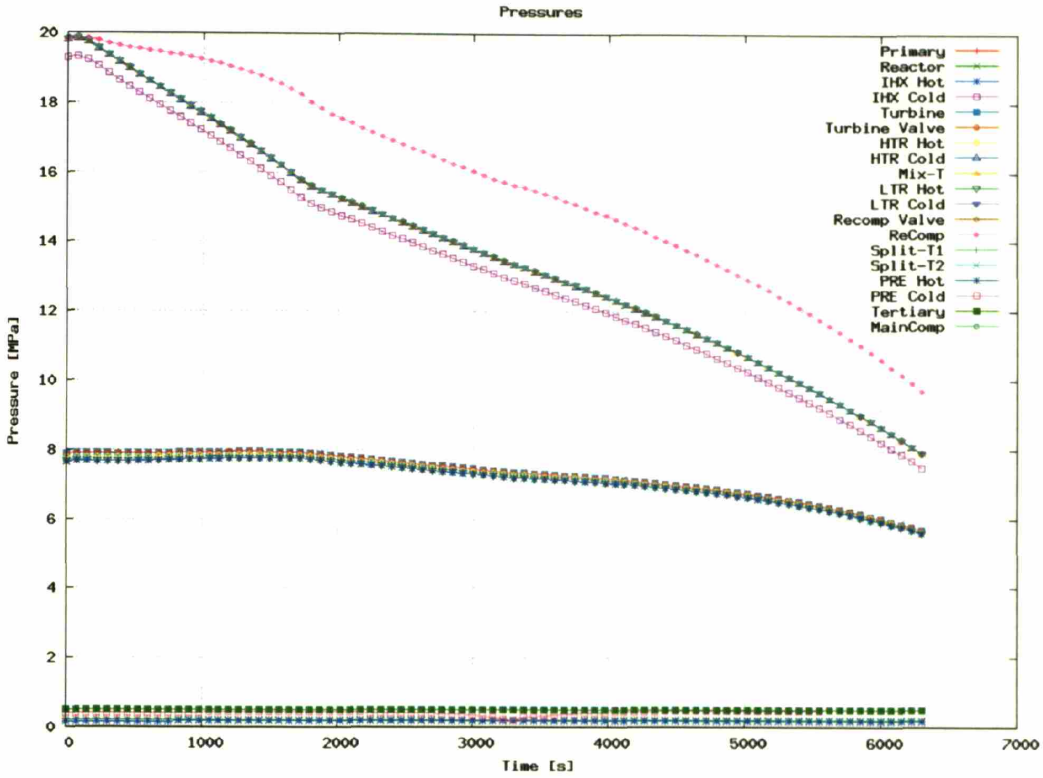

Figure 5-10: Inventory Control: Pressures versus Time

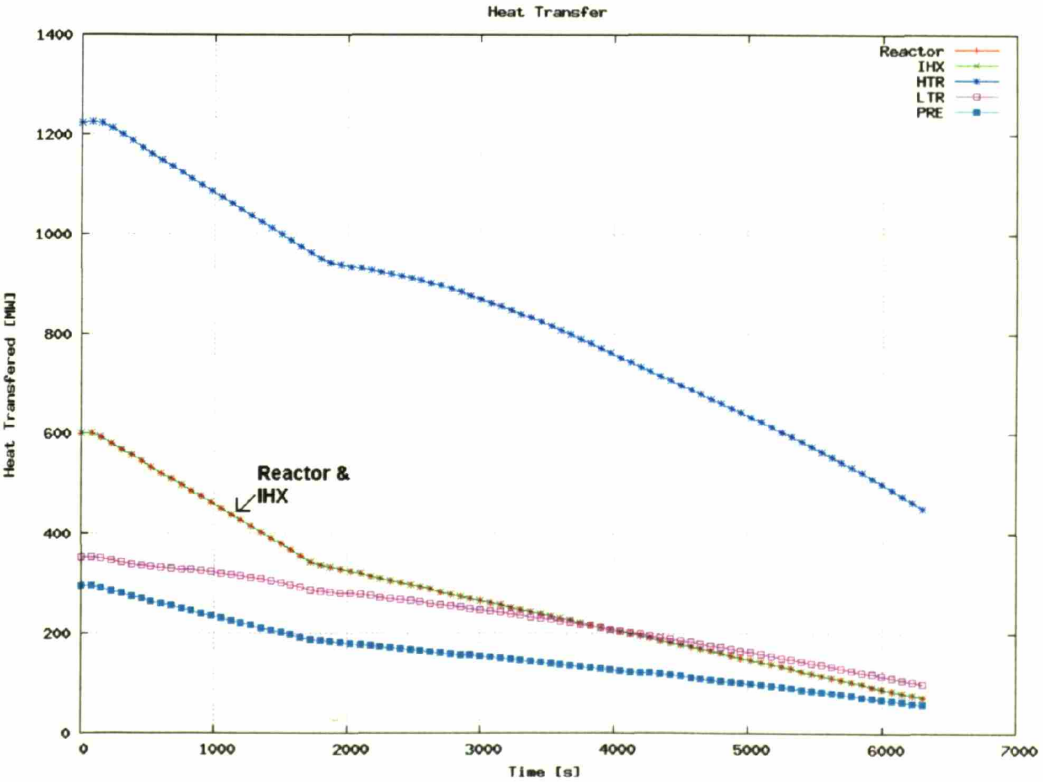

Figure 5-11: Inventory Control: Heat Transfer versus Time

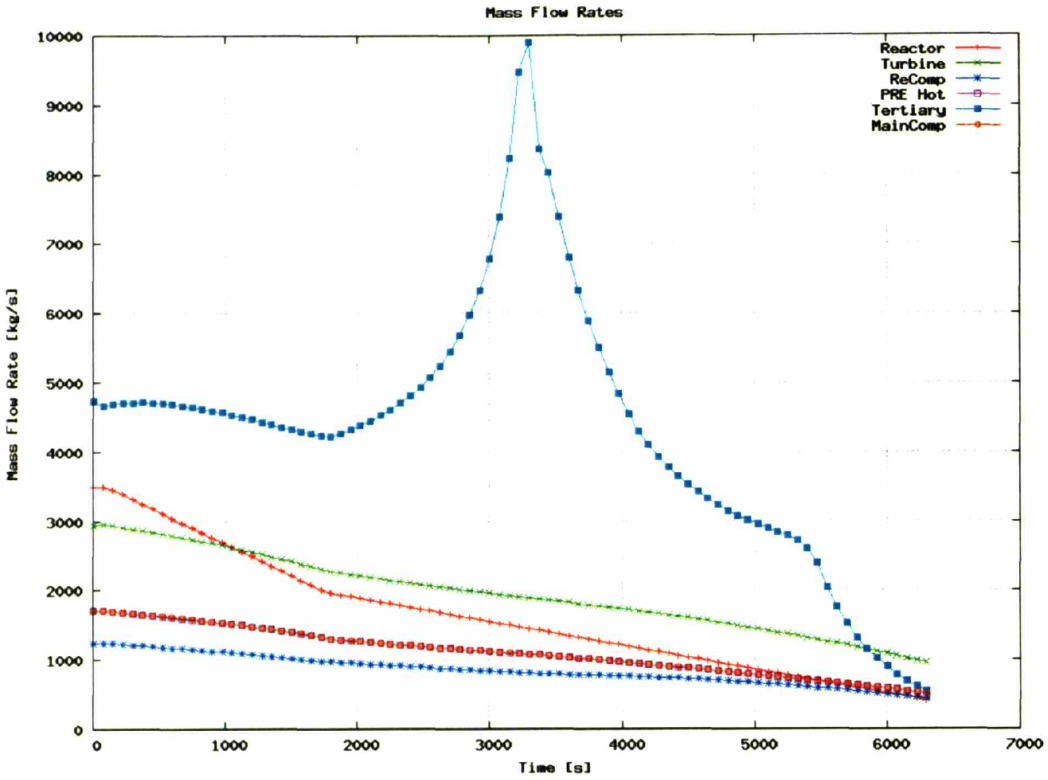

Figure 5-12: Inventory Control: Mass Flow Rates versus Time

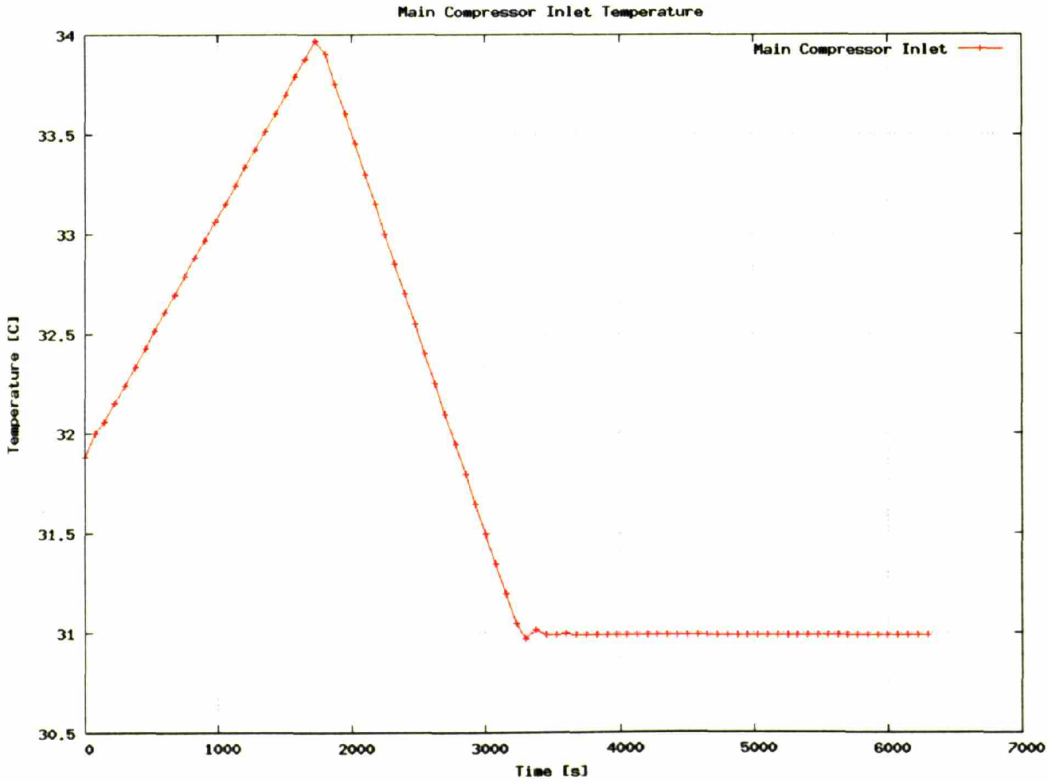

Figure 5-13: Inventory Control: Main Compressor Inlet Temperature versus Time

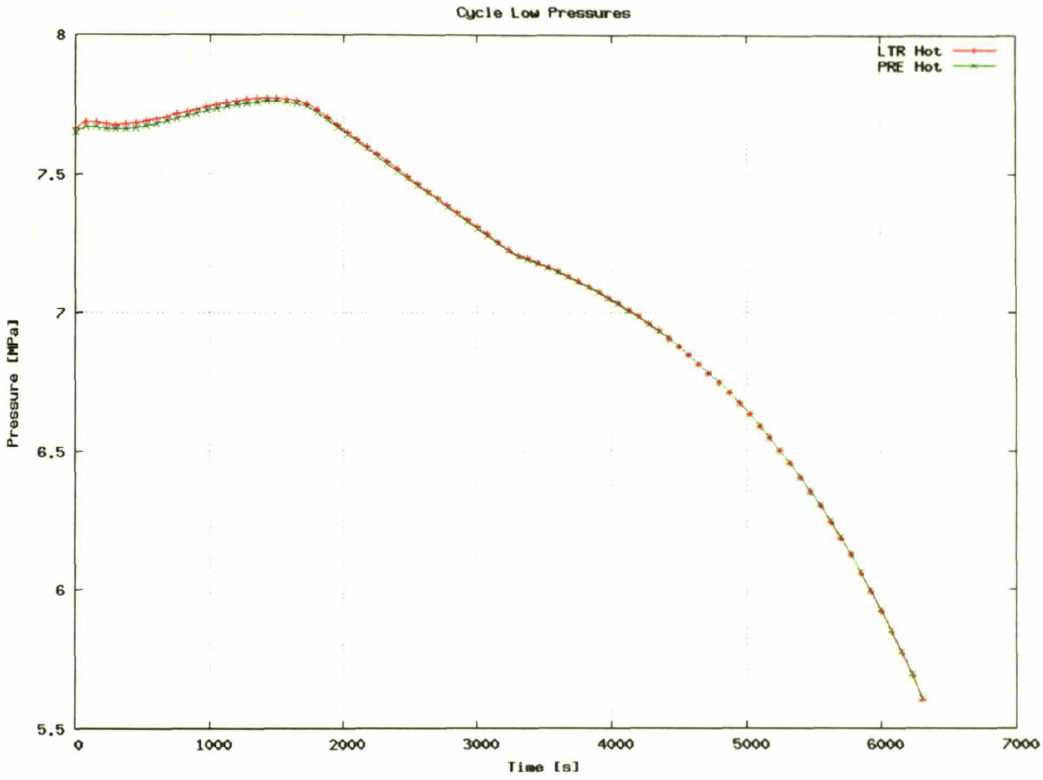

Figure 5-14: Inventory Control: Main Compressor Inlet Pressure versus Time

The three different regions in Figure 5-14 stem from control actions. The first region occurs during the rising main compressor inlet temperature when the main compressor inlet density is dropping rapidly and thus increasing the compressor's volumetric flow rate. This shifts a significant amount of dense fluid out of the main compressor and its following piping, and temporarily creates a low pressure increase. The second region coincides with falling inlet temperature, which allows pressure to drop rapidly with density change (recall Figure 4-18). The final region occurs with a constant main compressor inlet temperature. With the main compressor inlet now below the critical pressure the low pressure is allowed to naturally decrease solely due to changes in fluid inventory.

The reason for the control actions shown in Figure 5-13 and Figure 5-14 is to avoid the inventory control region of concern, as discussed in Section 4.5.

5.1.1.4 Inventory Control Heat Transfer Effects

A somewhat unexpected effect of inventory control is to proportionally increase the heat transfer and temperatures in the low temperature recuperator. This is clearly seen from the heat transfers shown among the various PCHEs in Figure 5-11. While four of the lines (including the overlapping IHX and reactor lines) move roughly in parallel, the LTR heat transfer line does not drop as quickly as expected.

Recall that the purpose of having an LTR is to prevent a pinch point arising in a single recuperating PCHE (because the isobaric specific heat of the fluids change differently due to CO_2 non-linear fluid properties). As fluid is removed from the system with inventory control the pressures decrease and the design points, where the isobaric specific heat changes were appropriately balanced, shift.

Figure 5-15 shows how isobaric specific heat varies on the cold side of the LTR during inventory control. When the high pressure is near 20 MPa the relatively sharp isobaric specific heat peak occurs near 60°C. By the time the pressure drops to 14 MPa the peak is smaller, wider, and closer to 80°C. Thus the cold side isobaric specific heat decreases with time during inventory control.

In this simulation only the hot (turbine inlet) and cold (precooler outlet) are held in place by PID controllers –the rest of the cycle temperatures are free to move at will. Thus any change in the proportional amounts of heat addition and removal will change the internal cycle temperatures. While it is complicated to account for the many fluid property effects and control actions occurring, one obvious effect is for the compressors to begin adding more heat, per unit mass, to the carbon dioxide as they work on less dense fluid. This will raise the temperatures of the middle of the system, as seen in Figure 5-9.

As middle temperatures rise, the precooler outlet temperature is held roughly constant, which feeds the main compressor and then the LTR cold inlet. Thus the LTR cold inlet only experiences the effects of additional specific main compressor work and is isolated from other cycle temperatures. The net effect is shown in Figure 5-16 where the cold inlet temperature gradually rises (note Figure 5-13 to observe how the main compressor inlet temperature is changing), then drops but stays relatively close to its steady state value. This contrasts with the other middle temperatures, which continue to rise.

Overall, the LTR experiences an ever greater temperature rise on the cold side because the incoming cold temperature is fixed by the precooler -- in effect the LTR mops up the non-proportional cycle changes at part-load. The temperature difference must rise significantly because of the already noted decrease in isobaric specific heat and the already noted relative increase in heat transfer.

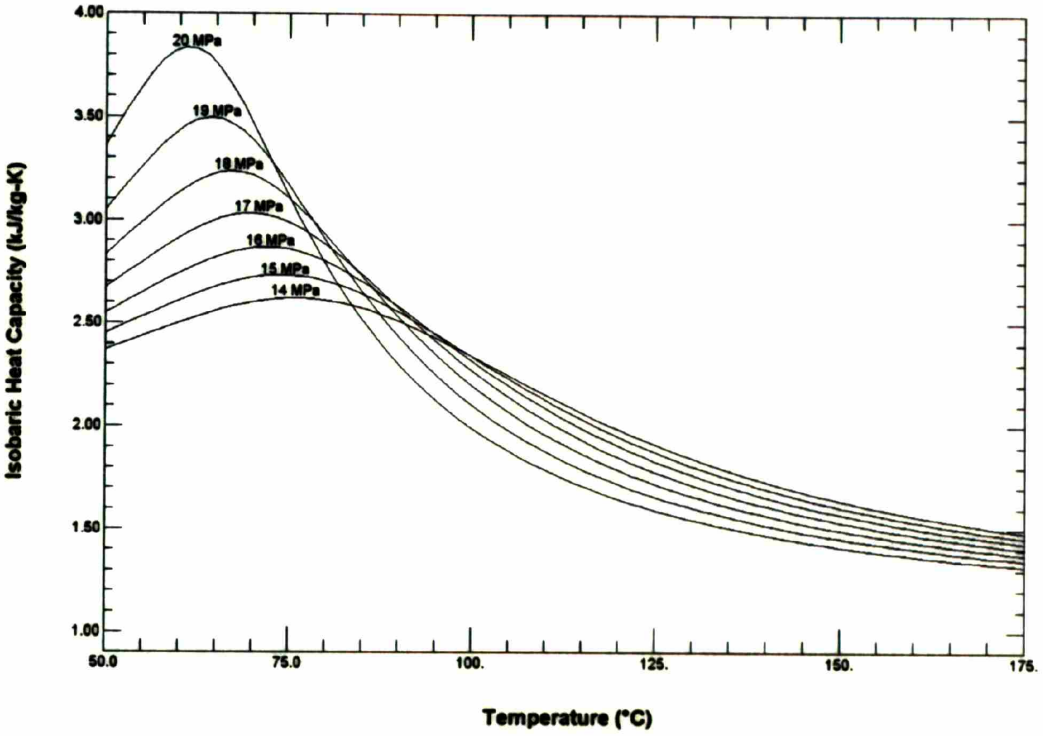

Figure 5-15: LTR Cold Side Isobaric Specific Heat during Inventory Control

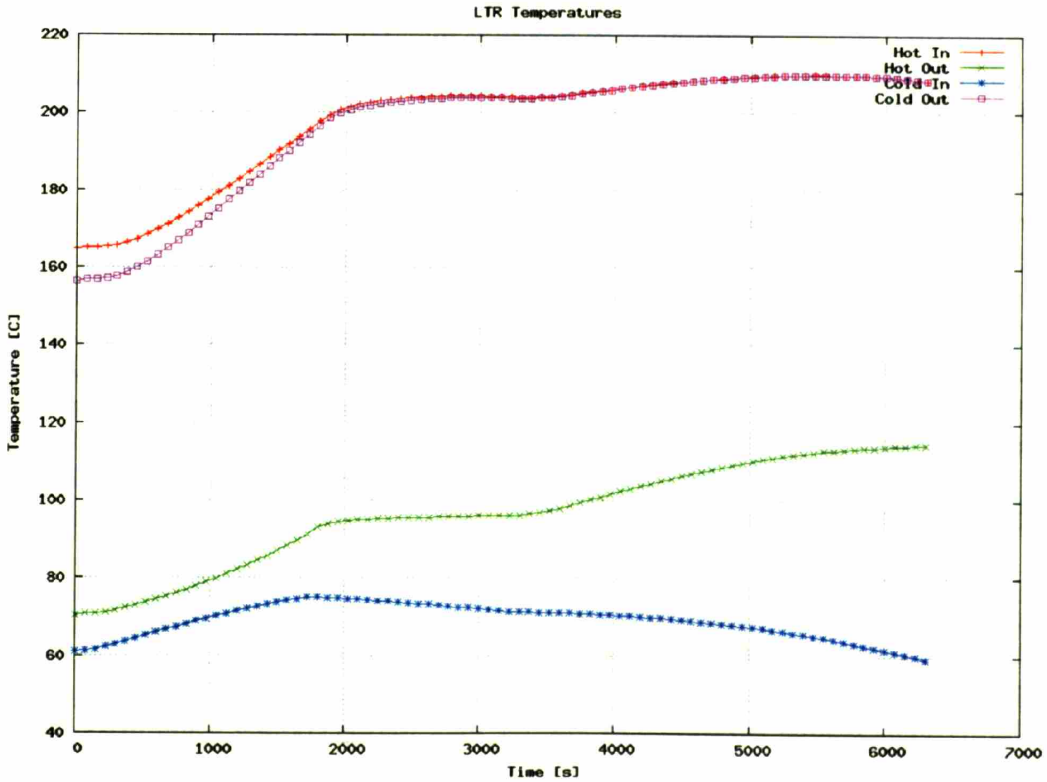

Figure 5-16: Inventory Control: LTR Temperatures

5.1.1.5 Inventory & Low Temperature Control Conclusion

GAS-PASS/CO_2 predicts that combined inventory and low temperature control for the S-CO_2 recompression cycle can work efficiently and appropriately. By carefully controlling the cycle low temperature during inventory control, rapid property changes and potential problems near the critical point can be alleviated. If inventory control is performed slowly, so that the turbine inlet temperature is approximately constant, then the part-load efficiency can be kept relatively high.

The ultimate limit of inventory control deserves more investigation, using more certain turbomachinery performance maps, but the turbine moves below known mass flow rates on the performance maps (see Section 3.4.2) used in GAS-PASS/CO_2 simulations. Using the current performance maps GAS-PASS/CO_2 predicts that the S-CO_2 recompression cycle can be operated down to about 6% generator power. This provides a relatively efficient means to move close to startup and shutdown operation before other control methods such as bypass are required.

One of the primary obstacles to reaching low power is controlling the flow split between the parallel compressors. Near full power the flow split can be matched solely by compressor outlet pressures (e.g. passive operation) but during inventory control flow must be shifted from the main to the recompression compressor to avoid choke (e.g. active control). This can be readily accomplished with variable valves upstream of the compressors and throttle valves after the compressors. For the default flow split chosen in this work the recompression compressor is always at a higher outlet pressure than the main compressor. Future researchers may optimize this flow split, but initial simulations suggest that part-load operation is more efficient when as much flow as possible is kept in the main compressor line.

Overall, combined inventory and low temperature control offer an attractive and promising method for part-load operation with the S-CO_2 recompression cycle. For example, cycle net efficiency of 39% can be maintained at 50% generator power – down only moderately from the 47% full power value. Note that the efficiency of combined inventory and low temperature control decreases significantly at low generator powers due to lower turbomachinery efficiencies (especially as the turbine approaches gas-flow separation), compression of an ever thinner fluid as system pressures drop, and parasitic cycle losses that become relatively larger.

5.1.2 Low Temperature Control

The large fluid property variations near the main compressor inlet allow significant control based on either pressure or temperature. While inventory control provides the ability to change fluid pressure, the main compressor inlet temperature (the cycle low temperature) can be readily controlled by varying the external cooling water mass flow rate in the precooler. Low temperature control effects are largely isolated to the main compressor, unlike pressure changes which affect the whole cycle.

This section will analyze the use of cycle low temperature control without inventory control. Note that one would, in many ways, prefer to decrease fluid temperature but that is not a feasible option when the low temperature is already so close, 1°C above, to the critical temperature*. If future cycle designs have a steady state operation temperature with a larger margin to the critical temperature then decreasing the cycle low temperature may become attractive.

By increasing the cycle low temperature, the incoming fluid density will drop significantly, as shown in Figure 4-18, at the same system pressure. A lower fluid density will decrease the main compressor's pressure ratio and thus decrease the system high pressure (for the same low pressure). A lower pressure ratio will allow lower power operation for the same turbine inlet temperature and thus is a part-load operation method of control.

5.1.2.1 Simulation Setup

The control system used for this simulation is the following:

1. A PI controller is used to control the precooler CO_2 outlet temperature. The temperature is initially held at 32°C until 100 seconds, then is linearly increased to 38°C by 1000 seconds and held there.
2. The reactor power is controlled via a P controller to keep the turbine inlet temperature constant. If the turbine inlet temperature falls, more heat will be added and vice versa.
3. A P controller is used on the flow split valves. If the main compressor exceeds 95% of the its volumetric flow rate range then flow is shifted to the recompression compressor.
4. The recompression compressor throttling valve is adjusted to produce matching outlet pressure from the compressors.

Note that fluid inventory is constant during this simulation.

5.1.2.2 Simulation Results

The highlights of this simulation are shown in Figure 5-17 through Figure 5-22 and will be described briefly. The main compressor inlet temperature is shown in Figure 5-17. This figure shows that the water PI controller performs quite well. The inlet temperature is held at 32°C until 100 seconds, when it is linearly increased to 38°C and held there thereafter.

The effects of the changing low temperature are shown in Figure 5-18 which graphs turbomachinery pressure ratios versus time. The main compressor pressure ratio decreases from about 2.6 to about 2.5 by 1000 seconds, then increases slightly. The turbine pressure ratio follows the same trends as the main compressor, which sets the system pressures. The recompression compressor pressure ratio increases from 2.58 to

* Dropping below risks the introduction of liquid into the loop.

nearly 2.7 by 1000 seconds, then decreases slightly. The recompression compressor does not experience the low temperature fluid property effects and actually receives an increasing fluid density, which increases its pressure ratio.

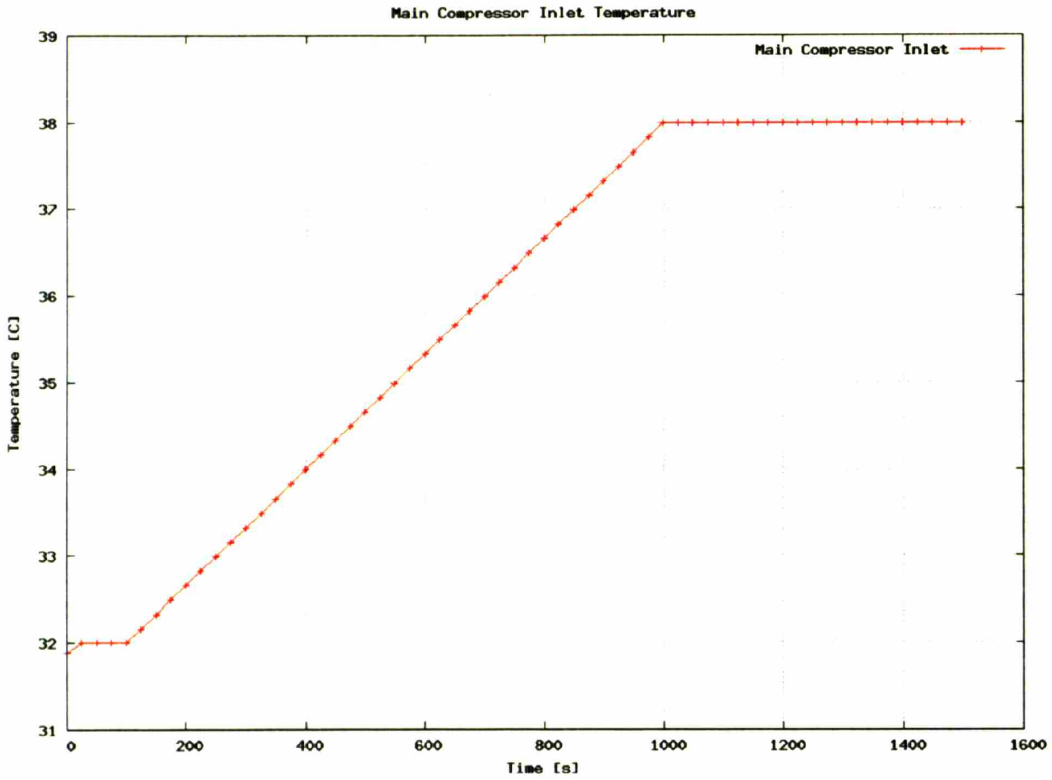

Figure 5-17: Low Temperature Control: Main Compressor Inlet Temperature versus Time

Figure 5-19 shows the cycle pressures versus time. In general, cycle pressures rise significantly. The main compressor outlet pressure rises from slightly below 20 MPa to 22.5 MPa, the main compressor inlet pressure rises from 7.69 MPa to 8.9 MPa, and the recompression compressor outlet pressure, which is throttled to match the main compressor outlet pressure, rises from less than 20 to nearly 24 MPa.

The increase in system pressures stems from decreasing fluid density in the precooler and main compressor. As the fluid temperature rises the density drops. As the dense fluid thins the excess fluid is shifted into the following components. Without inventory control the displaced fluid must distribute around the cycle, which increases pressure.

The increase in cycle pressures has an effect on cycle mass flow rates, which are shown in Figure 5-20 versus time. This figure shows that the carbon dioxide mass flow rates increase significantly. The cycle mass flow rates rise because the fluid density rises. The increase in fluid pressure increases fluid density, which will increase mass flow rates for the same fluid velocity; $\dot{m} = \rho A V$. The liquid sodium mass flow rate is constant, and the cooling water mass flow rate decreases significantly, causing the cycle low temperature to rise.

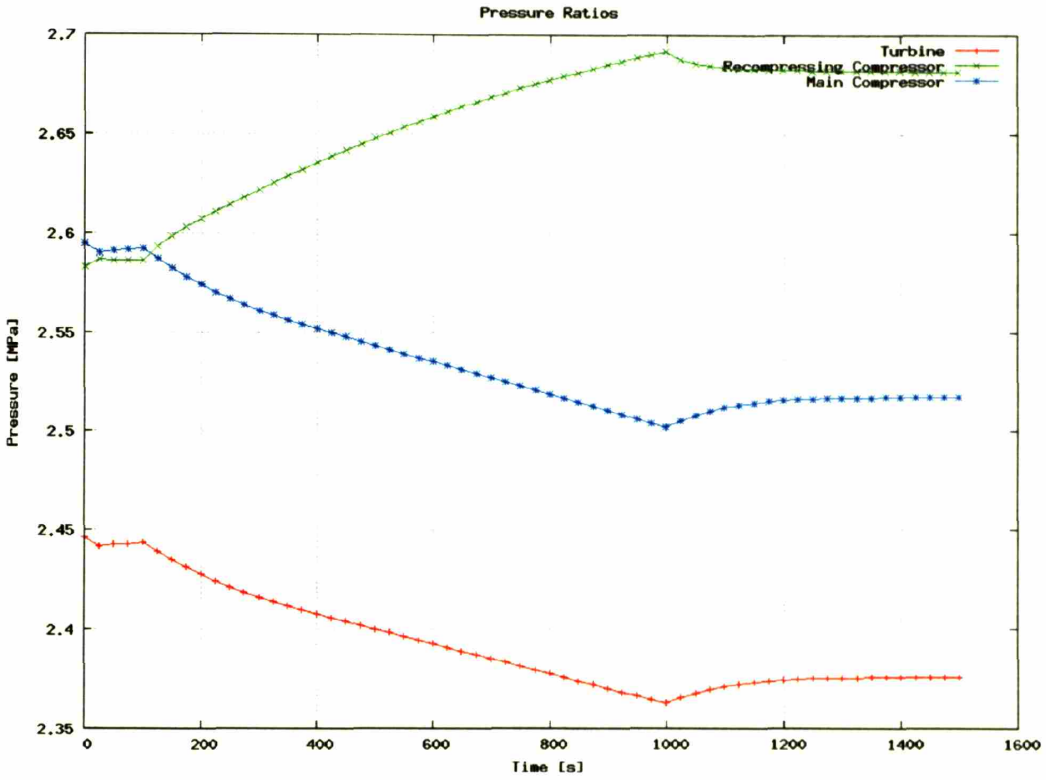

Figure 5-18: Low Temperature Control: Pressure Ratios versus Time

Recall from the discussion on the effect of inventory control (Section 5.1.1.1) that increasing mass flow rates are the opposite of that which is desired for efficient part-load operation. If reactor power were unchanged than the turbine inlet temperature would decrease (i.e. in a PCHE: $Q = m\Delta h \sim mCp\Delta T$) as mass flow rates increase. In this simulation the reactor power was allowed to change to keep the turbine inlet temperature (cycle high temperature) constant. Thus the reactor power must increase as shown in Figure 5-21*. This figure shows that reactor power increases from 600 to about 652 MW, a 8.67% increase in reactor power, by 1100 seconds.

Furthermore, due to the lower main compressor density and higher cycle densities, this method of operation is inefficient, as shown in Figure 5-22. This figure shows that cycle net efficiency drops from over 48% to about 45.25% by the end of the simulation.

5.1.2.3 Low Temperature Control Conclusion

Low temperature control in the S-CO_2 recompression cycle is not desirable without concurrent inventory control. The cycle low temperature is restrained from dropping due

* The wobble in this figure between 75 and 250 seconds stems from a poorly tuned and rarely used proportional controller changing reactor power by measuring turbine inlet temperature against reference. The controller begins operation at 75 seconds when the turbine inlet temperature is not at reference and the controller initially overcompensates due to the time lag due to thermal inertia.

to its proximity to the critical point. It produces higher reactor powers, higher system pressures, and less efficient operation when it is raised. Therefore this control method will not be used in GAS-PASS/CO_2 except in combination with inventory control.

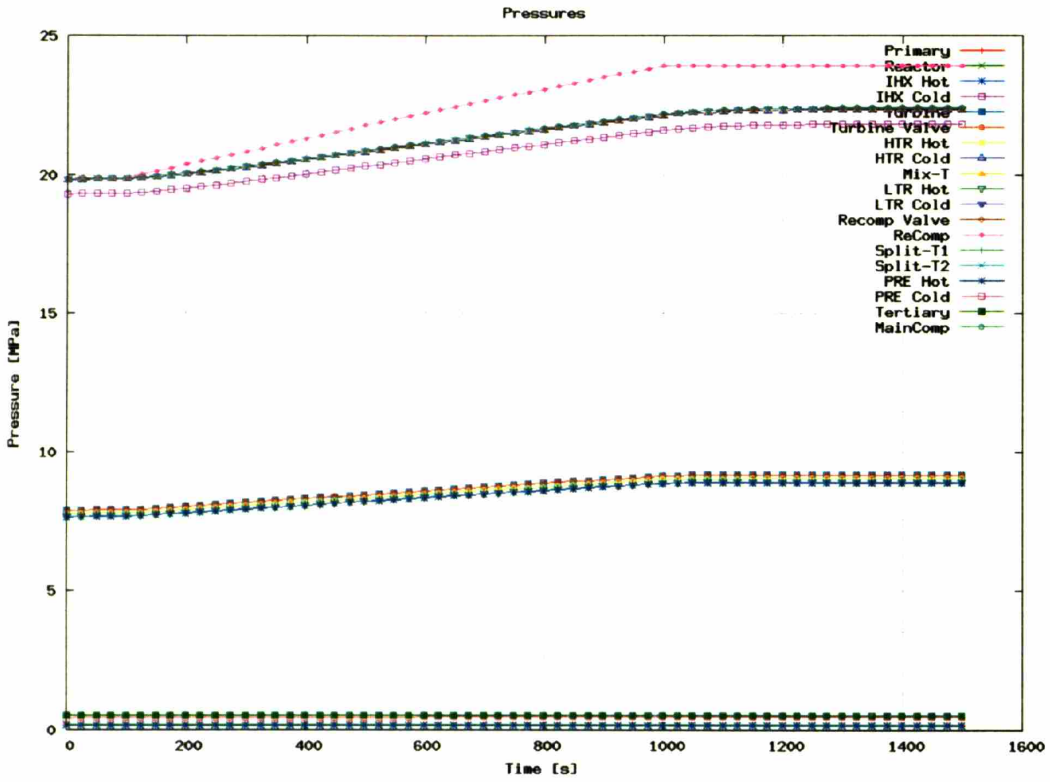

Figure 5-19: Low Temperature Control: Pressures versus Time

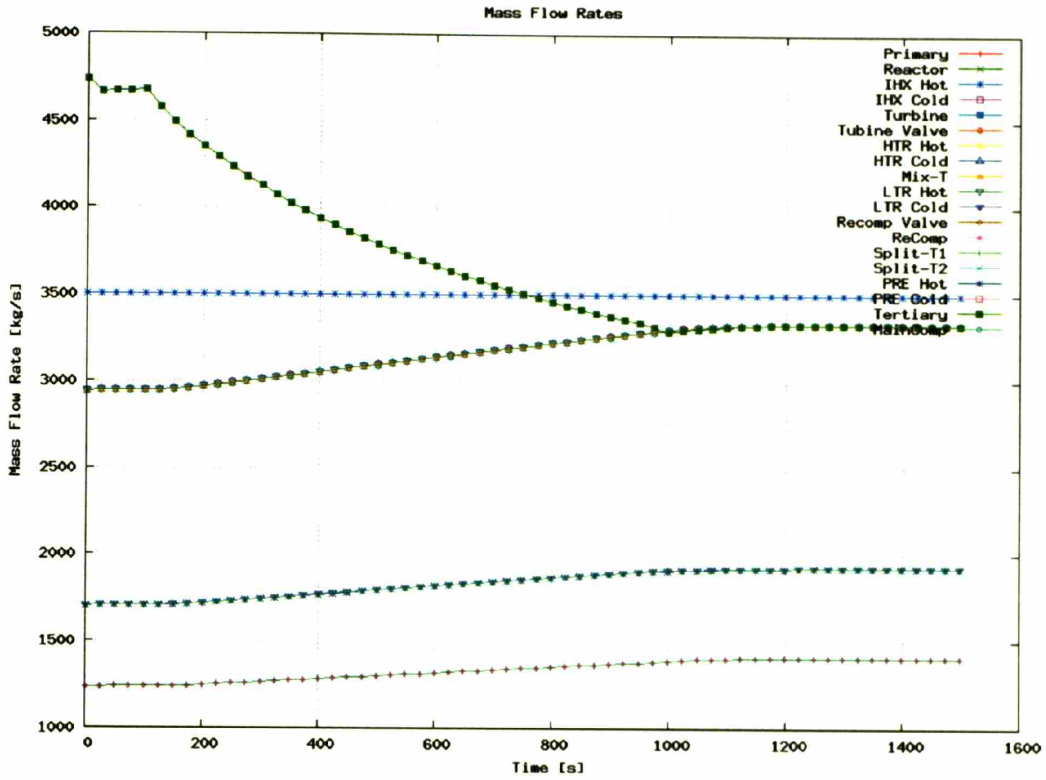

Figure 5-20: Low Temperature Control: Mass Flow Rates versus Time

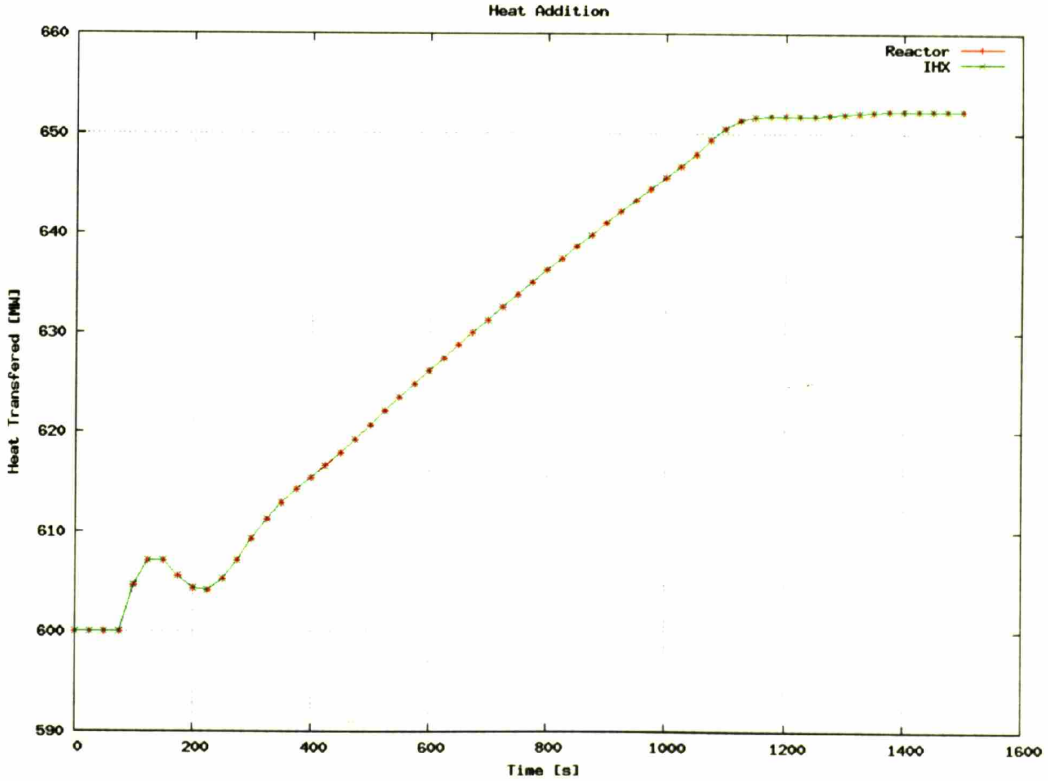

Figure 5-21: Low Temperature Control: Reactor Power versus Time

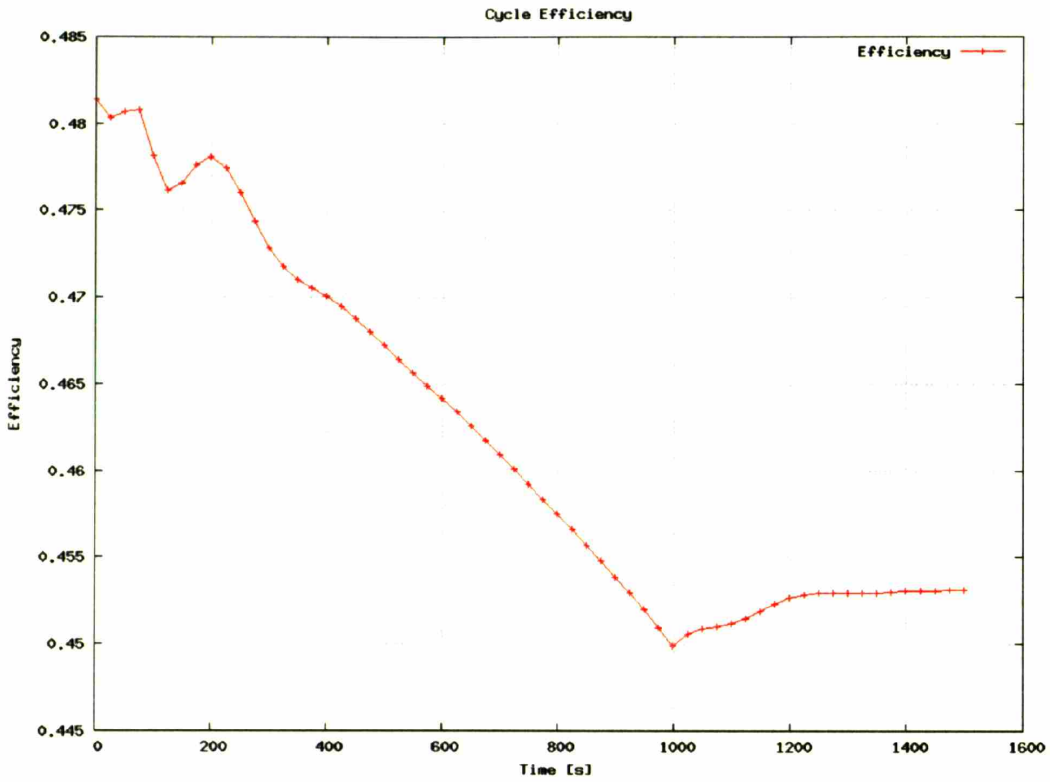

Figure 5-22: Low Temperature Control: Efficiency versus Time

5.1.3 High Temperature Control

Part-load cycle operation can be achieved by decreasing the highest cycle temperature, the turbine inlet temperature. This, inevitably, decreases the attainable cycle efficiency, but is relatively simple to implement.

This section will analyze part-load operation achieved by decreasing the turbine inlet temperature. In general, all other controlled plant components will be held to their steady state values.

5.1.3.1 Simulation Setup

The control system used for this simulation is the following:

1. A PI controller is used to control the precooler CO_2 outlet temperature and hold it at 32°C.
2. The reactor power is controlled via a P controller by measuring the turbine inlet temperature against reference. The reference value is held at 650°C until 100 seconds when it is linearly decreased until simulation failure.
3. A P controller is used on the flow split valves. If the main compressor exceeds 95% of the its volumetric flow rate range then flow is shifted to the recompression compressor.
4. The recompression compressor throttling valve is adjusted to produce matching outlet pressure from the compressors.

5.1.3.2 Simulation Results

The turbine inlet temperature linearly decreased during this simulation from the design value of 650°C to nearly 400°C by the end of the simulation near 2200 seconds. This is shown in Figure 5-23 which plots the turbine inlet and outlet temperature versus time. Note that at 20 MPa carbon dioxide's density changes from 110 kg/m^3 to 156 kg/m^3 at these temperatures and that the temperature difference across the turbine is nearly constant.

The lower turbine inlet temperature allowed part-load operation to about 52% generator power, as shown in Figure 5-24. This figure shows a nearly linear drop in efficiency from approximately 47% to 31%. The initial curl in the curve stems from stored energy in this relatively fast simulation as shown in Figure 5-25, which pictures efficiency versus time. This figure shows an initial spike in efficiency and is thereafter linear.

The simulation failed when the recompression compressor choked from too much flow, as shown in Figure 5-26. This figure shows a linear rise in volumetric flow rate until the slope increases near 1750 seconds, and the compressor reaches compressor choke around 2200 seconds. The general increase in slope will be addressed shortly but the increase in slope near 1750 seconds stems from a change in the flow split.

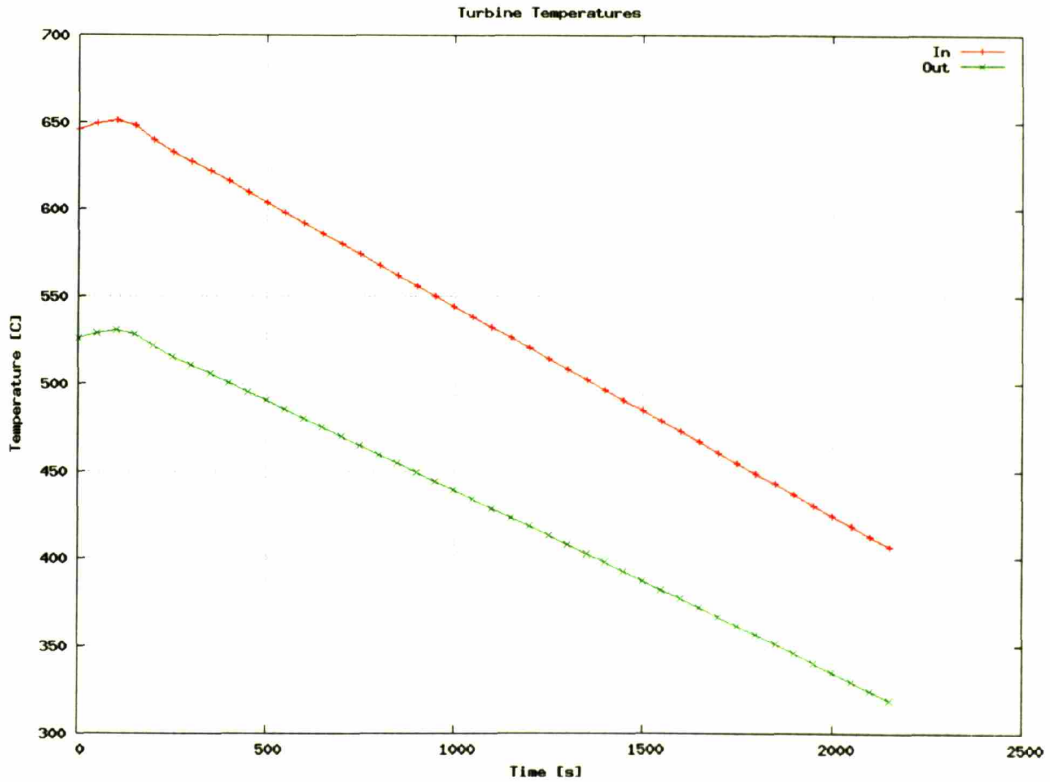

Figure 5-23: High Temperature Control: Turbine Inlet Temperature versus Time

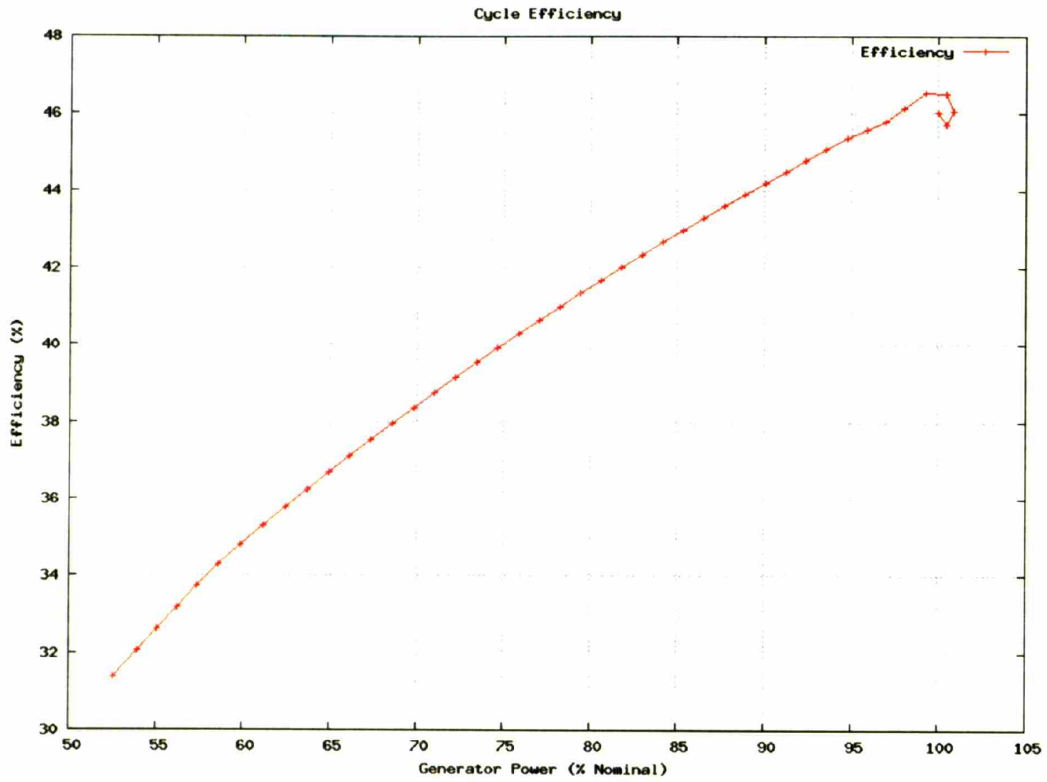

Figure 5-24: High Temperature Control: Cycle Net Efficiency versus Normalized Generator Power

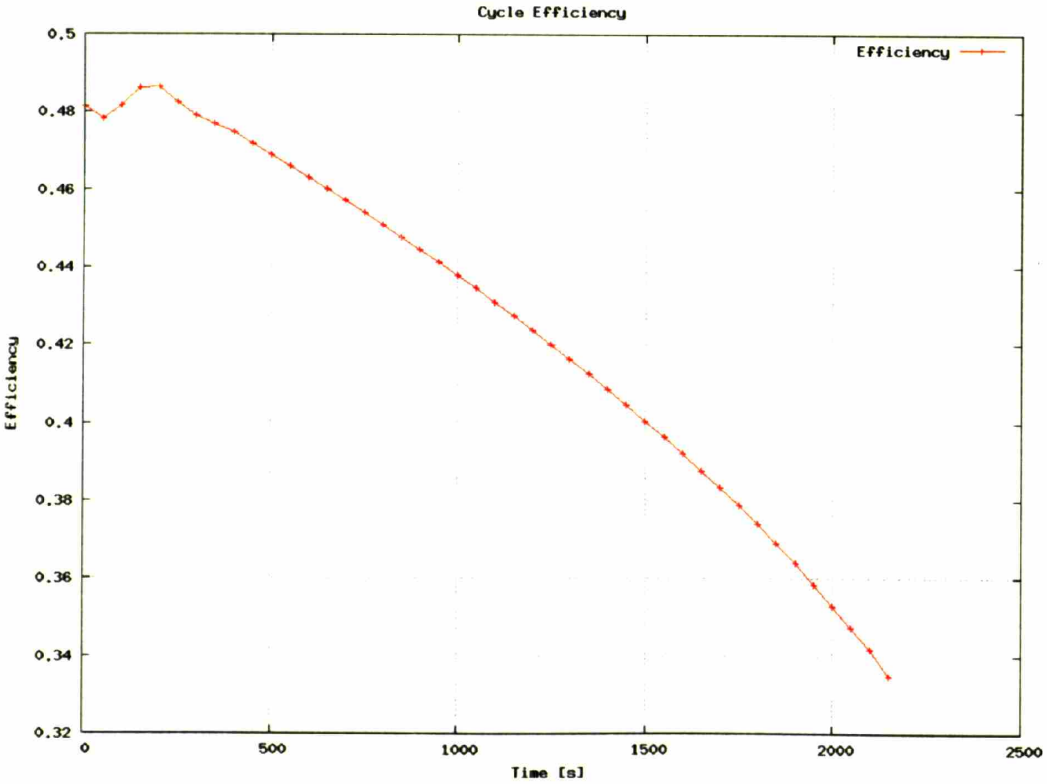

Figure 5-25: High Temperature Control: Cycle Net Efficiency versus Time

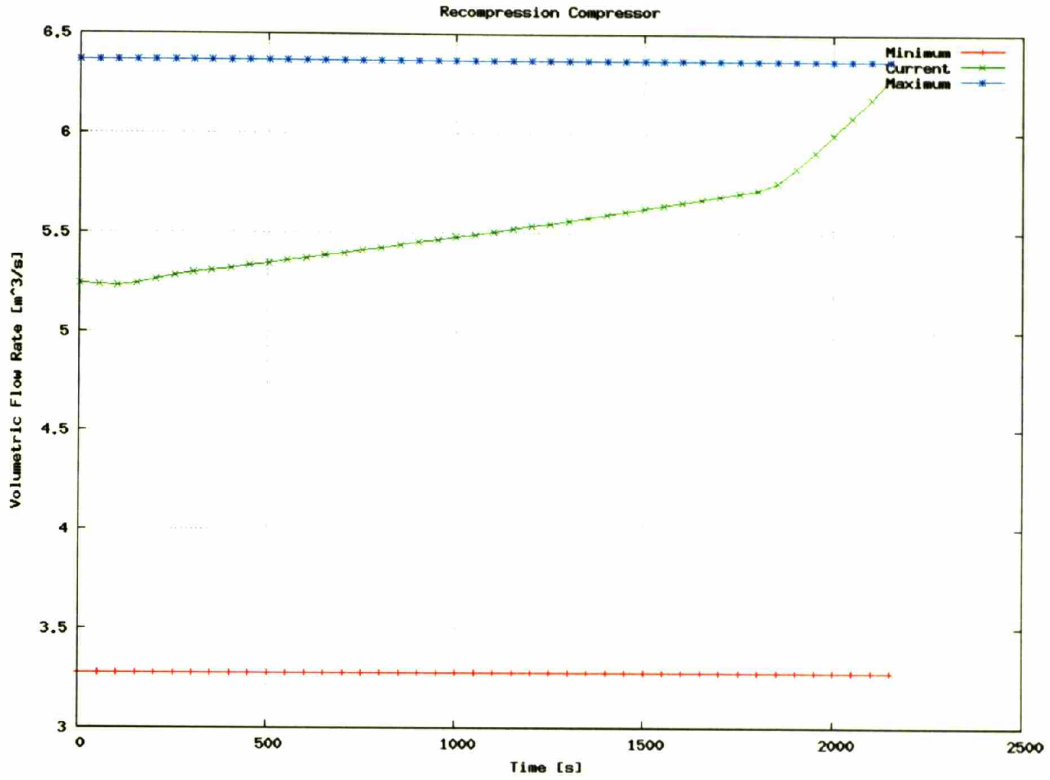

Figure 5-26: High Temperature Control: Recompression Compressor Volumetric Flow Rate versus Time

Near 1750 seconds the main compressor reaches 95% of its maximum volumetric flow rate as shown in Figure 5-27. This figure shows a nearly linear increase in volumetric flow rate until 1750 seconds, when the volumetric flow rate stops increasing. While the main compressor would increase in volumetric flow rate, the extra flow rate is shifted to the recompression compressor instead.

The increase in volumetric flow rate in the compressors stems mainly from an increase in mass flow rate as shown in Figure 5-28. Figure 5-28 shows the major system mass flow rates versus time. The carbon dioxide mass flow rates increase from about 2930 kg/s to about 3175 kg/s. The CO_2 mass flow rate also increases proportionally in the compressor loops until the flow split is changed near 1750 seconds. Note that the sodium mass flow rate is constant, but the water mass flow rate decreases to keep the cycle low temperature constant.

The mass flow rates in any cycle are a combination of the compressors' ability to raise pressure versus the turbine's ability to use that pressure by expanding dense fluid (and parasitic pressure losses). Thus the shape of the compressor and turbine pressure ratio curves largely determine loop mass flow rates.

During high temperature control the turbine inlet temperature drops significantly, as shown in Figure 5-23, which increases the density of the fluid entering the turbine and

thus decreases its volumetric flow rate (for the same mass flow rate). This decreases the turbine's pressure ratio and creates a momentary imbalance between compressor and turbine pressure rise. This is alleviated by increasing the loop mass flow rate, which decreases the compressors pressure ratios and increases the turbine's, thus establishing a new equilibrium*.

The volumetric flow rate in the turbine decreases, with increasing mass flow rates, due to its large drop in temperature, thus density, shown in Figure 5-29. This figure shows that cycle low and middle temperature change little, while cycle high temperatures drop linearly. Due to relative lack of either pressure (not shown) or temperature change in the compressors the fluid density does not change, thus increasing mass flow rates lead to increasing volumetric flow rates and, eventually, choke.

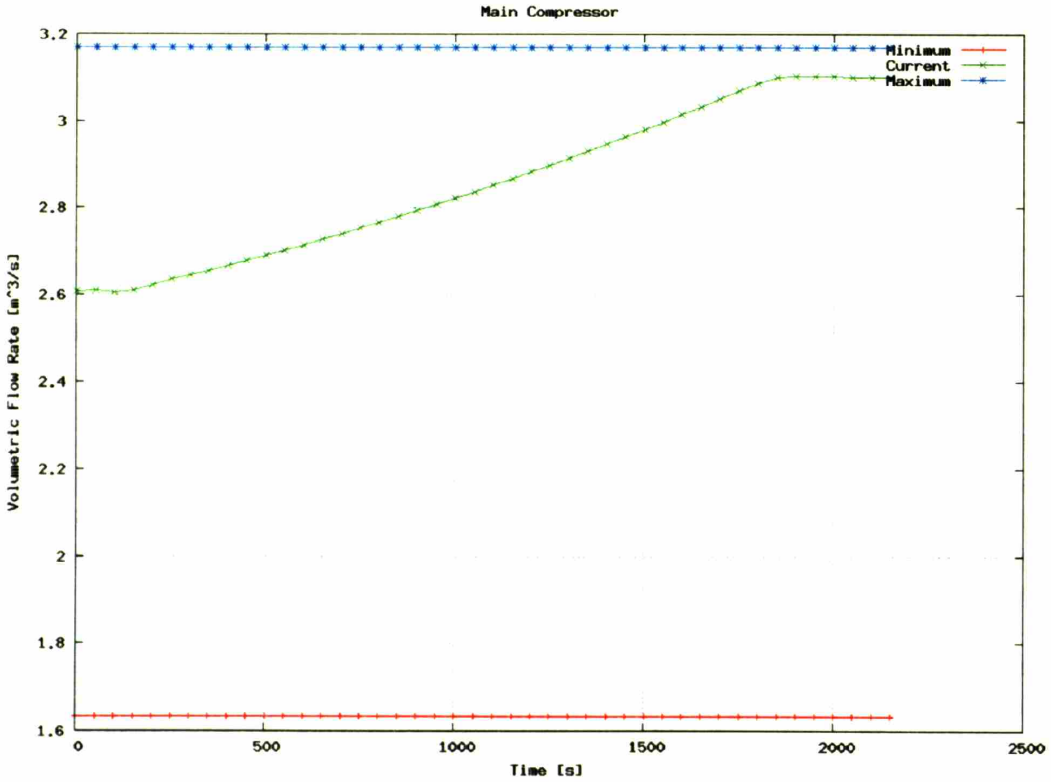

Figure 5-27: High Temperature Control: Main Compressor Volumetric Flow Rate versus Time

* The reader may consult Figure 4-13 to see the 100% shaft speed volumetric flow rates of all the turbomachines versus pressure rise.

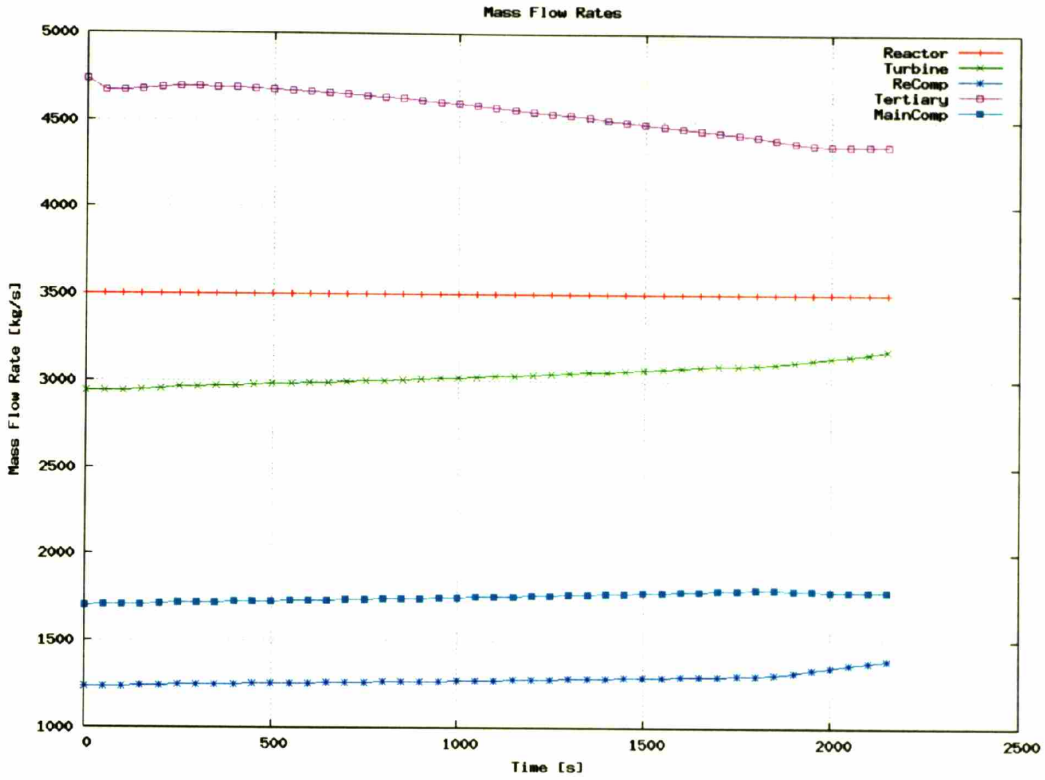

Figure 5-28: High Temperature Control: Mass Flow Rates versus Time

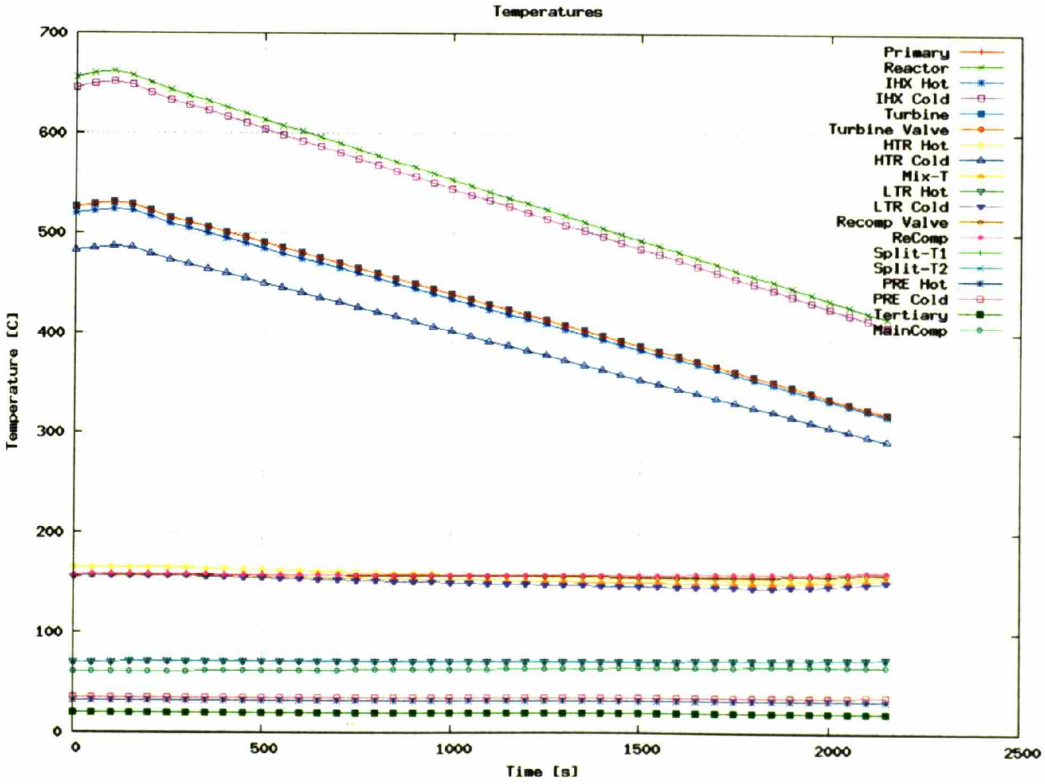

Figure 5-29: High Temperature Control: Temperatures versus Time

5.1.3.3 High Temperature Control Conclusion

High temperature control can be used to effect part-load operation between roughly 52% and 100% generator power*. Due to dissimilar property changes between the compressors and turbine, increasing loop mass flow rates will eventually produce choke in a compressor.

While effective, high temperature control is probably an undesirable method of part-load operation. Decreasing the system temperatures will probably require a slow rate of change to avoid thermal shock, and is less efficient than inventory and low temperature control. Furthermore, it will become necessary to decrease the liquid sodium temperature, which will affect reactor operation, to avoid a 250°C temperature difference in the intermediate heat exchanger.

5.1.4 Turbine Throttling

Turbine inlet throttling isenthalpically expands the fluid entering the turbine. The expansion cools the incoming flow and lowers its pressure. The turbine responds to the lower pressure ratio by decreasing the output work and mass flow rate. The feedback of the changing mass flow rate on the compressors will be addressed below.

5.1.4.1 Simulation Setup

The control system used for this simulation is the following:

1. The turbine inlet throttle is gradually constricted until simulation failure.
2. A PI controller is used to control the precooler CO_2 outlet temperature and hold it at 32°C.
3. The reactor power is controlled via a P controller to keep the turbine inlet temperature at 650°C.
4. A P controller is used on the flow split valves. If the main compressor exceeds 95% of the its volumetric flow rate range then flow is shifted to the recompression compressor.
5. The recompression compressor throttling valve is adjusted to produce matching outlet pressure from the two radial compressors.

5.1.4.2 Simulation Results

Turbine inlet throttling decreases the turbine's pressure ratio compared to the compressors as shown in Figure 5-30. This figure shows the pressure ratios of each turbomachine versus time. The recompression and the main compressor show a modest increase in pressure ratio (due to the decreasing mass flow rates shown in Figure 5-31) but stay near the design point of 2.6†. The turbine shows a, roughly, linear decrease in pressure ratio from about 2.45 to 1.65 by simulation failure around 4250 seconds.

---

* Note this is a wholly different simulation than a loss of primary heat addition (e.g. a reactor SCRAM). Besides the very different timescales, the loss of primary heating will force the disconnection of the PCS from the grid and the transient then becomes a LOL transient which will be analyzed shortly.

† Axial compressors will perform quite differently than radial compressors at low mass flow rate. An axial compressor increases its pressure rise significantly at lower mass flow rates, while a radial compressor

Due to the significant decrease in pressure ratio available to the turbine system, mass flow rates decrease. Figure 5-31 shows mass flow rates versus time. The carbon dioxide mass flow rates decrease significantly from about 2930 kg/s at time 0 to less than 1900 kg/s at simulation failure. The main compressor and recompression compressor mass flow rates decrease proportionally, since the flow split is constant for this simulation. The liquid sodium mass flow rate is constant and the precooler water mass flow rate decreases to keep the main compressor inlet temperature constant at lower powers.

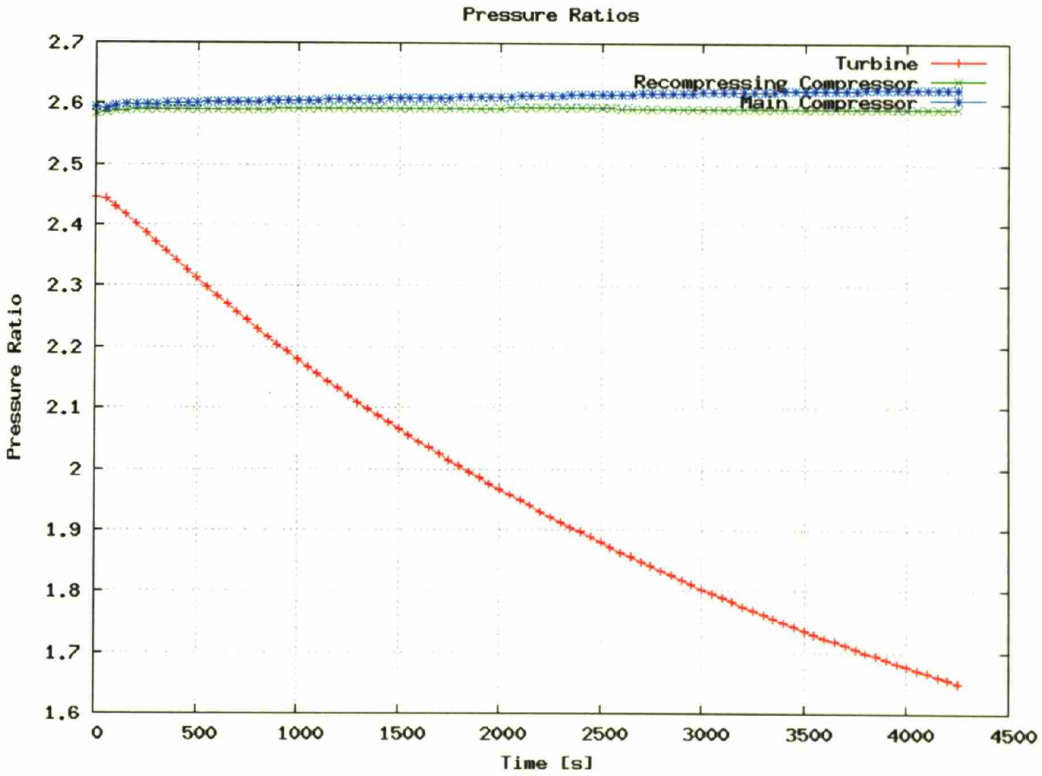

Figure 5-30: Turbine Throttling: Turbomachinery Pressure Ratios versus Time

operates close to its maximum pressure ratio at steady state. The reader may consult the compressor performance maps in Section 3.4.2 for example maps. This control method would produce different results if axial compressors were used[62].

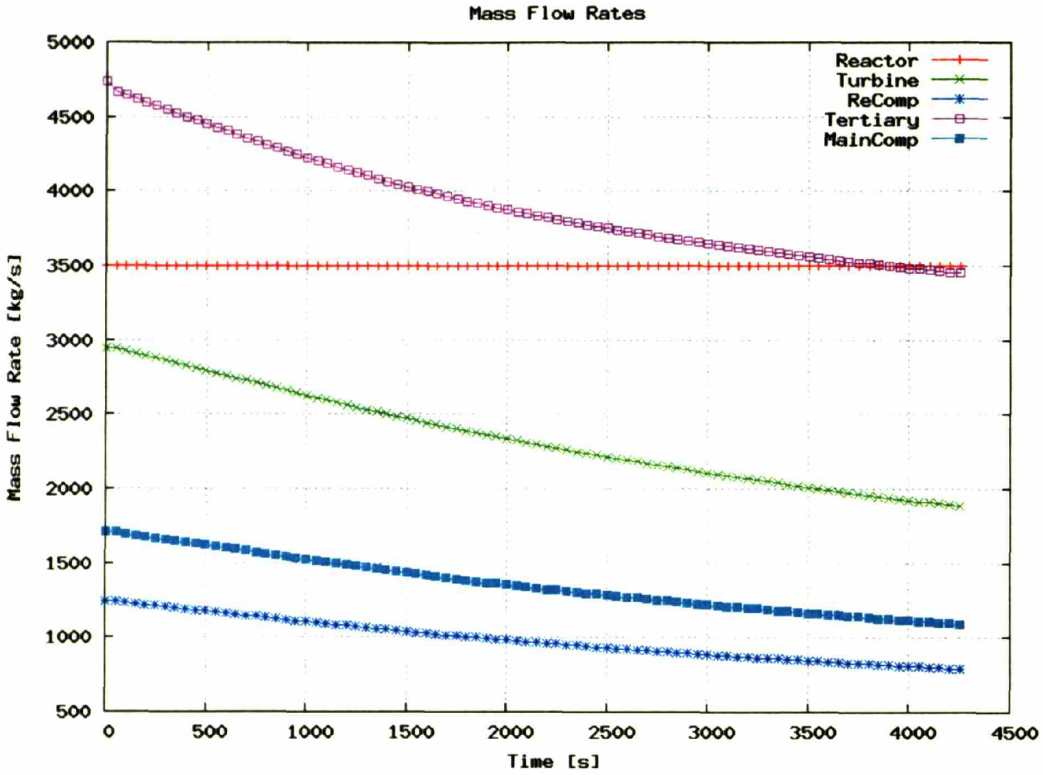

Figure 5-31: Turbine Throttling: Mass Flow Rates versus Time

The cycle temperatures are shown versus time in Figure 5-32. This figure shows that the turbine inlet temperature and cycle mid and low temperatures are nearly constant. However, the turbine outlet temperature, and its associated values in the high temperature recuperator, increase significantly due to smaller temperature differences across the turbine at lower pressure ratios.

The simulations fail due to stall in the main compressor as shown in Figure 5-33. This figure shows the main compressor's volumetric flow rate versus time and the stall and choke limits are shown as the upper and lower lines labeled minimum and maximum respectively. The main compressor's volumetric flow rate decreases nearly linearly until stall due to decreasing mass flow rates.

The recompression compressor volumetric flow rate shows similar behavior, as seen in Figure 5-34. This figure shows this compressor's volumetric flow rate linearly decreasing and ending very close to stall. If the main compressor had not stalled first the recompression compressor would have stalled shortly after.

The cycle net efficiency versus normalized generator power is shown in Figure 5-35. This figure shows that the efficiency gradually falls from the steady state value of around 47% to about 24% near 26% generator power. There is a curl in the efficiency near 100% generator power due to stored heat and controller actions at the start of this simulation.

5.1.4.3 Turbine Throttling Conclusion

Turbine inlet throttling can readily and rapidly provide part-load operation for the S-CO_2 recompression cycle between 26% and 100% generator load. By increasing turbine throttling, the turbine work and loop mass flow rates can be decreased significantly allowing part-load operation. Decreasing loop mass flow rates lead to only modest pressure rise with radial compressors but will eventually produce choke.

The reader should note that this control method could be extended to lower generator powers by avoiding compressor stall. This can be readily accomplished in two ways:

- Use inventory control to decrease fluid density, especially in the main compressor, which will increase compressor volumetric flow rates. By shifting flow between the compressors it is likely that this method of control could be extended to much lower powers.
- Recirculation lines around the compressors* would allow a fraction of the fluid flow to be reintroduced. This merits research, but in theory it could allow compressors to operate with low mass flow rates without choke. However, this method is inherently inefficient as it creates extra compressor work which is not productively used.

By using one or both of these methods it is likely that turbine throttling could be extended until the turbine reaches its performance map's minimum mass flow rate. Using the inventory and low temperature control simulation as a guideline, this will be near 6% nominal generator power.

* Note that compressor recirculation lines will very likely be necessary as a safety measure to avoid compressor stall and surge. They were not modeled in this work due to time constraints.

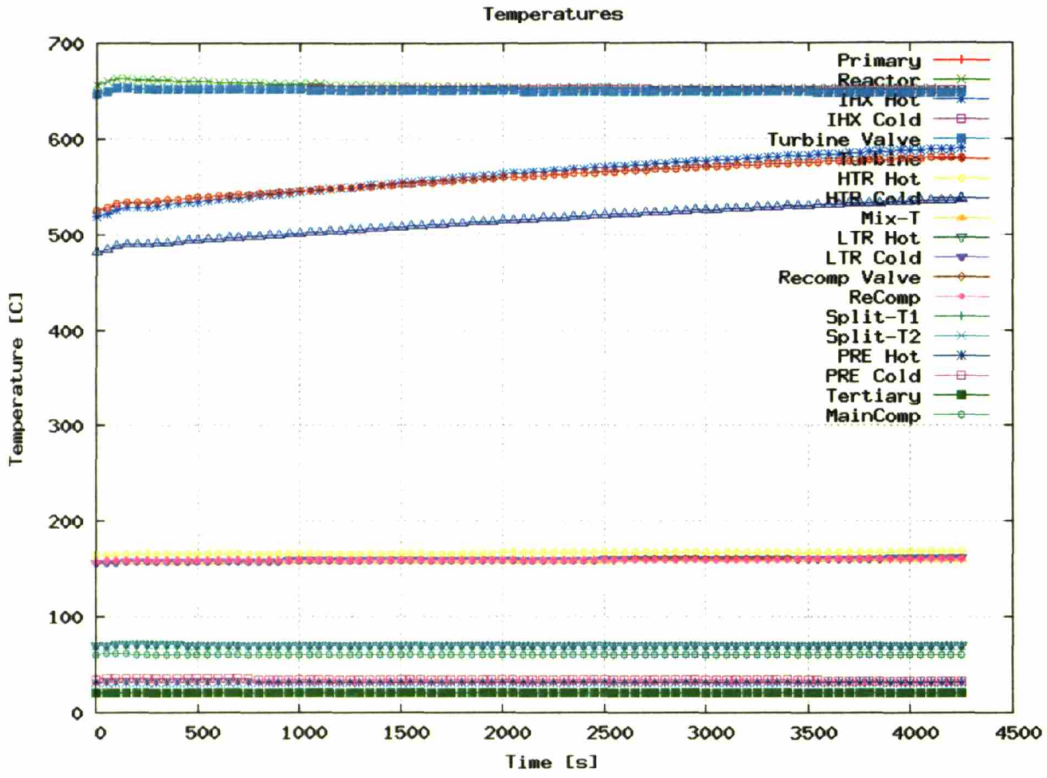

Figure 5-32: Turbine Throttling: Temperatures versus Time

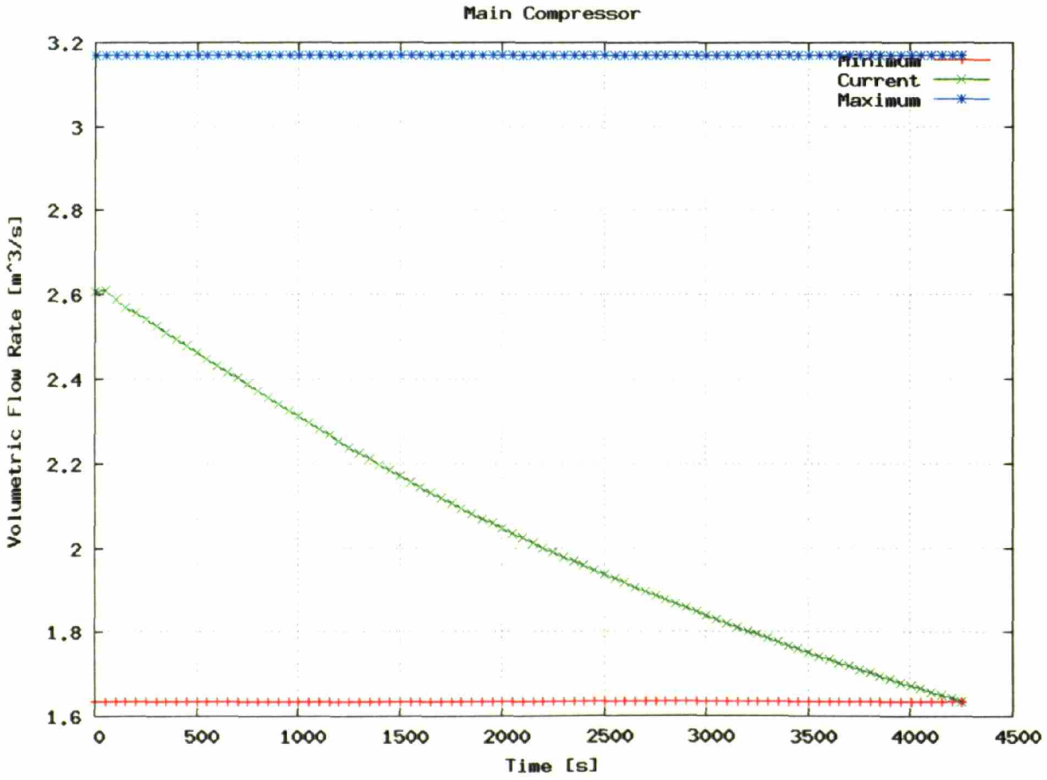

Figure 5-33: Turbine Throttling: Main Compressor Volumetric Flow Rate versus Time

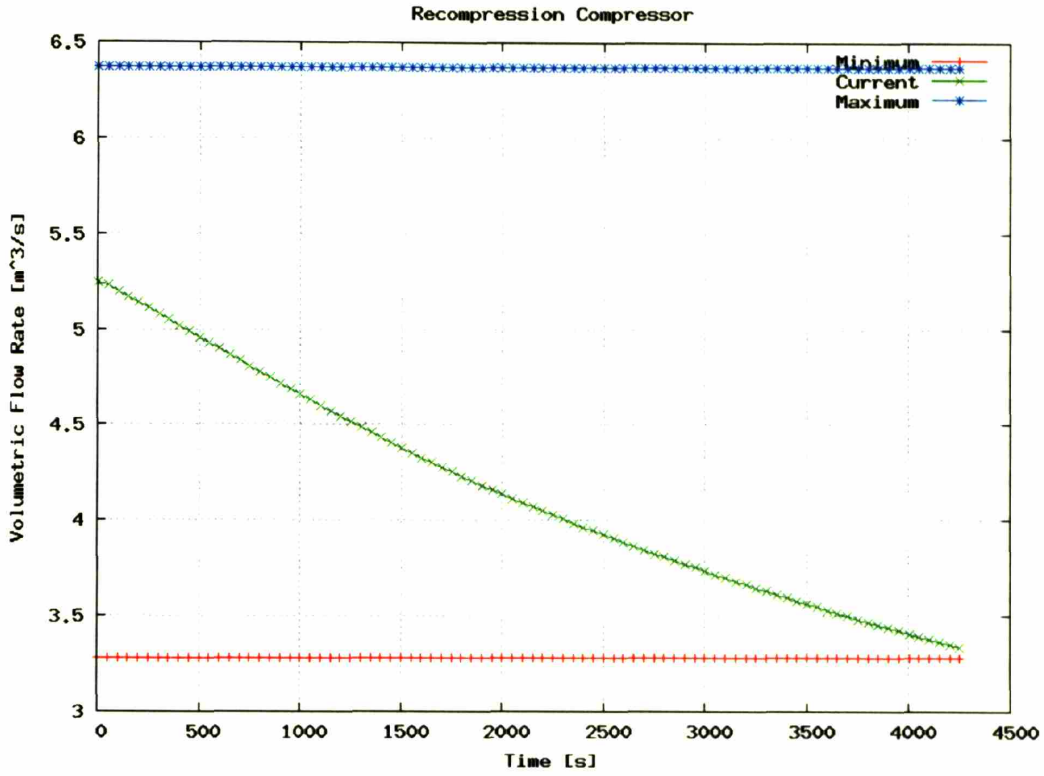

Figure 5-34: Turbine Throttling: Recompression Compressor Volumetric Flow Rate versus Time

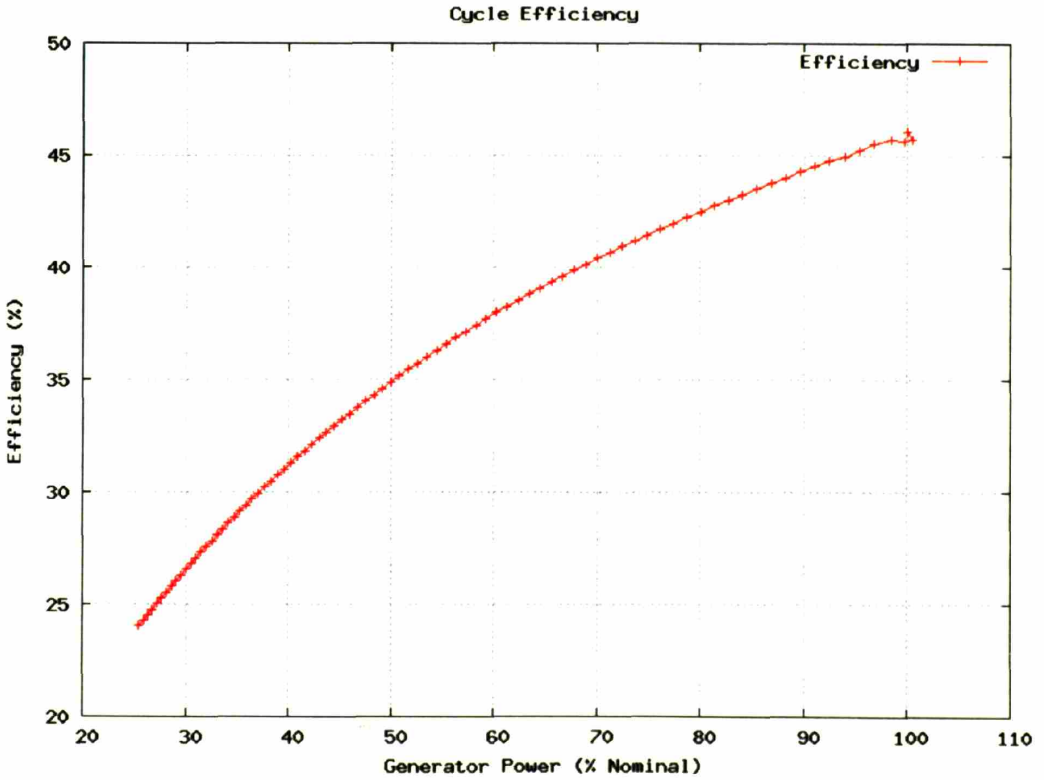

Figure 5-35: Turbine Throttling: Cycle Net Efficiency versus Normalized Generator Power

5.1.5 Turbine Bypass

Bypassing flow around the turbine allows rapid but relatively inefficient system control. This section will demonstrate the simulation results of using turbine bypass* in the S-CO_2 recompression cycle.

5.1.5.1 Simulation Setup

The control system used for this simulation is the following:

1. The turbine bypass line is gradually opened to linearly increase the proportion of bypass flow.
2. The turbine bypass throttle is used to isenthalpically expand the bypassed flow from high to low pressure.
3. A PI controller is used to control the precooler CO_2 outlet temperature and hold it at 32°C.
4. The reactor power is controlled via a P controller to keep the turbine inlet temperature at 650°C.
5. The compressors are allowed to adjust the mass flow split to match their outlet pressures.

5.1.5.2 Simulation Results

Turbine bypass can readily be used for part-load operation between zero and full generator power as seen in Figure 5-36. This figure shows the energy used in each turbomachine and the generator. The compressor works gradually decrease, but the turbine and generator works decrease significantly until the generator work approaches zero and cycle stops producing surplus work.

Decreasing the generator work to zero requires bypassing the majority of the mass flow rate around the turbine, as shown in Figure 5-37. This figure shows a linear increase in bypassed mass flow rate, ending with nearly 65% of the flow bypassed.

Bypassing the turbine increases the system mass flow rates, as shown in Figure 5-38. This figure shows key mass flow rates of interest. The reader should note several features of the system mass flow rates:

- The precooler mass flow rate initially increases (to cool the greater precooler CO2 mass flow rate to the same temperature) and later decreases, since significantly less heat is added to the cycle from the reactor.
- The "hot" side of the PCHEs experience a linear increase in mass flow rate from about 3000 kg/s to almost 4500 kg/s (at simulation failure).
- The turbine experiences a significant decrease in mass flow rate which, with the bypass mass flow rate, combine to form the PCHE hot side mass flow rate.
- Finally, both compressors experience large increases in mass flow rate.

* The location for implementing turbine bypass in the S-CO_2 recompression cycle is discussed in Section 4.2.1.

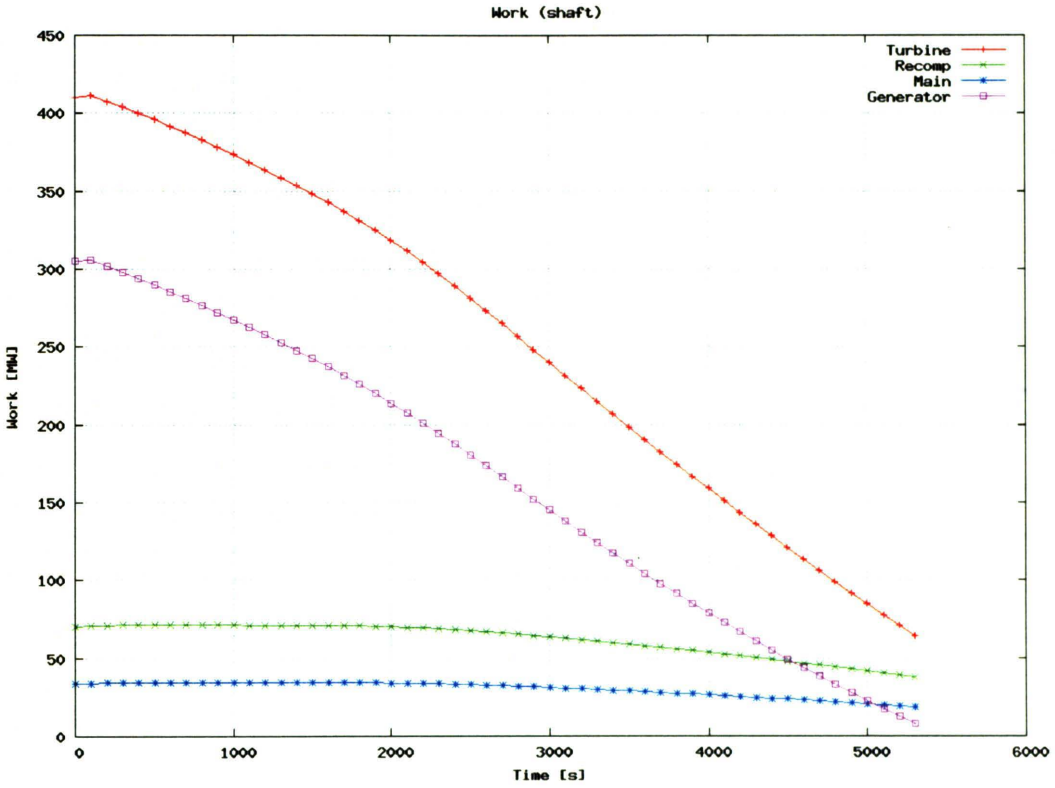

Figure 5-36: Turbine Bypass: System Work versus Time

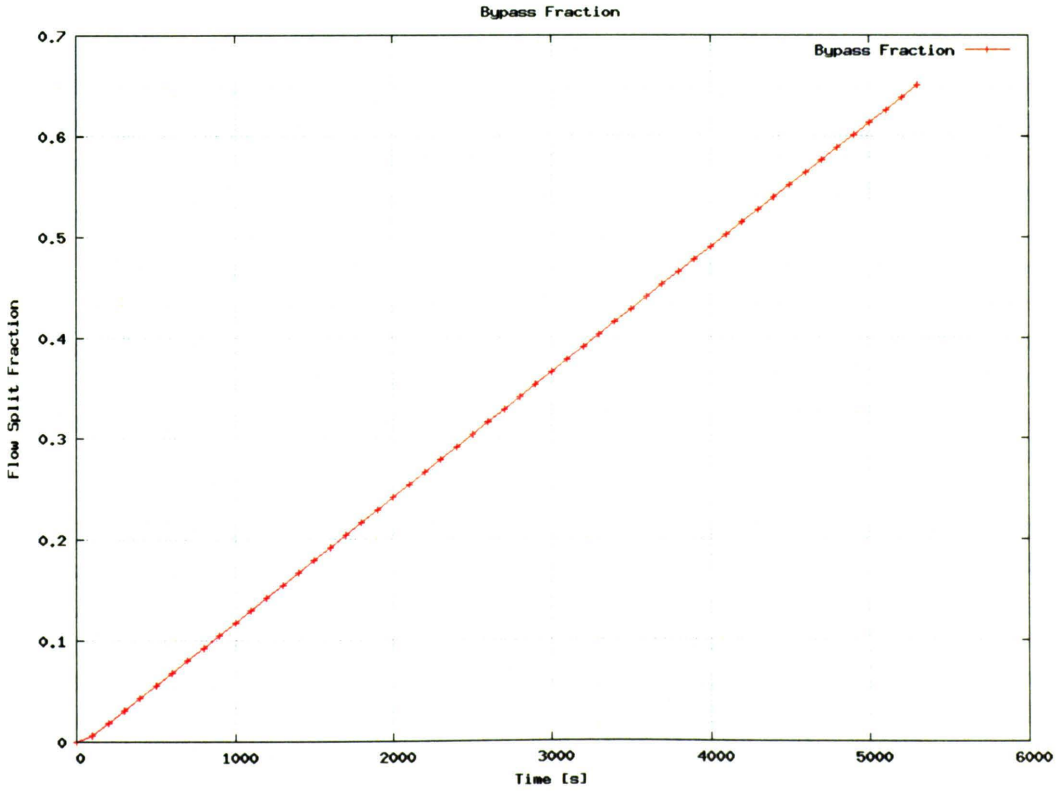

Figure 5-37: Turbine Bypass: Bypass Flow Fraction versus Time

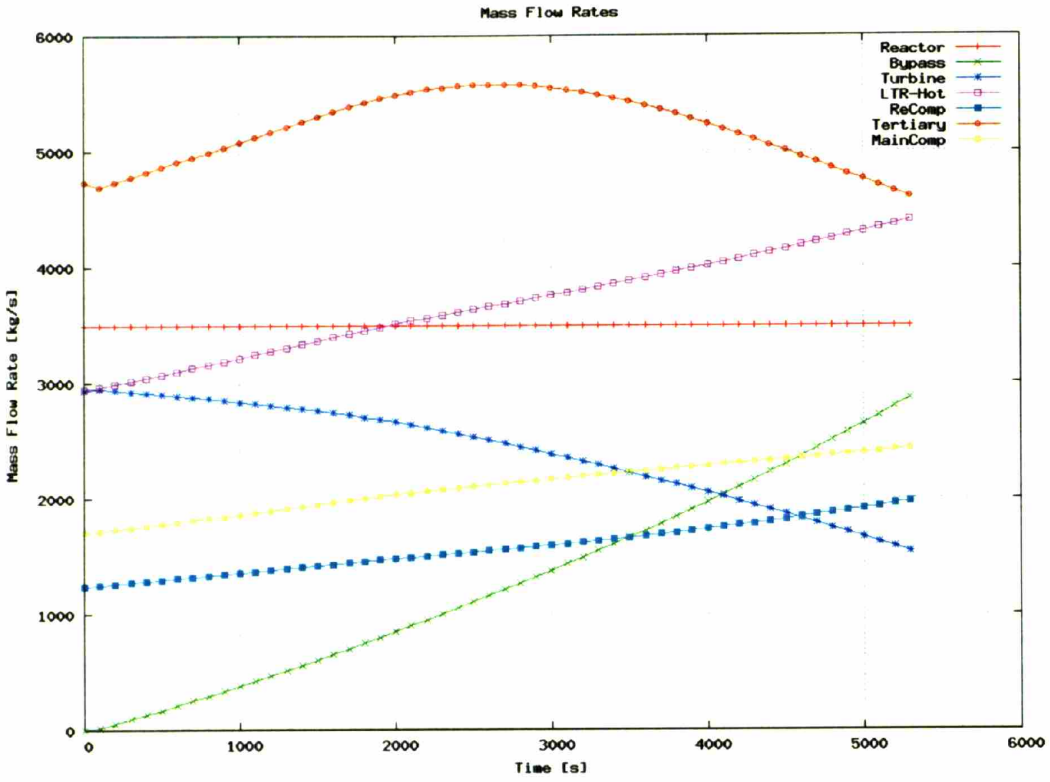

Figure 5-38: Turbine Bypass: Mass Flow Rates versus Time

For any type of bypass, that diverts flow around the turbine, the large increase in compressor mass flow rates combines with the decrease in turbine mass flow rate to decrease the system pressure ratio. However, the manner in which the pressure ratio is decreased (e.g. if the low pressure rises while the high pressure falls) varies depending upon the cycle layout and the type of bypass used.

For turbine bypass in the S-CO_2 recompression cycle, the low pressure rises while the high pressure falls as shown in Figure 5-39. This figure shows that the precooler outlet/main compressor inlet pressure rises from about 7.69 MPa to nearly 9 MPa at simulation failure. The increase in system low pressure stems from the manner in which fluid inventory is redistributed, which depends greatly upon how fluid temperatures change in components.

During turbine bypass the hot fluid exiting the IHX is diverted from the turbine inlet to the HTR. This gradually raises the HTR temperatures as ever more fluid is bypassed, until the turbine inlet temperature approaches the cycle high temperature (at the steady state there is a 120.1°C temperature difference between the IHX outlet and HTR inlet) as shown in Figure 5-40. The higher fluid temperatures in the relatively large volumes in the HTR and its associated plena and piping create a thinner fluid that pushes fluid into the colder side of the cycle (which includes the main compressor inlet).

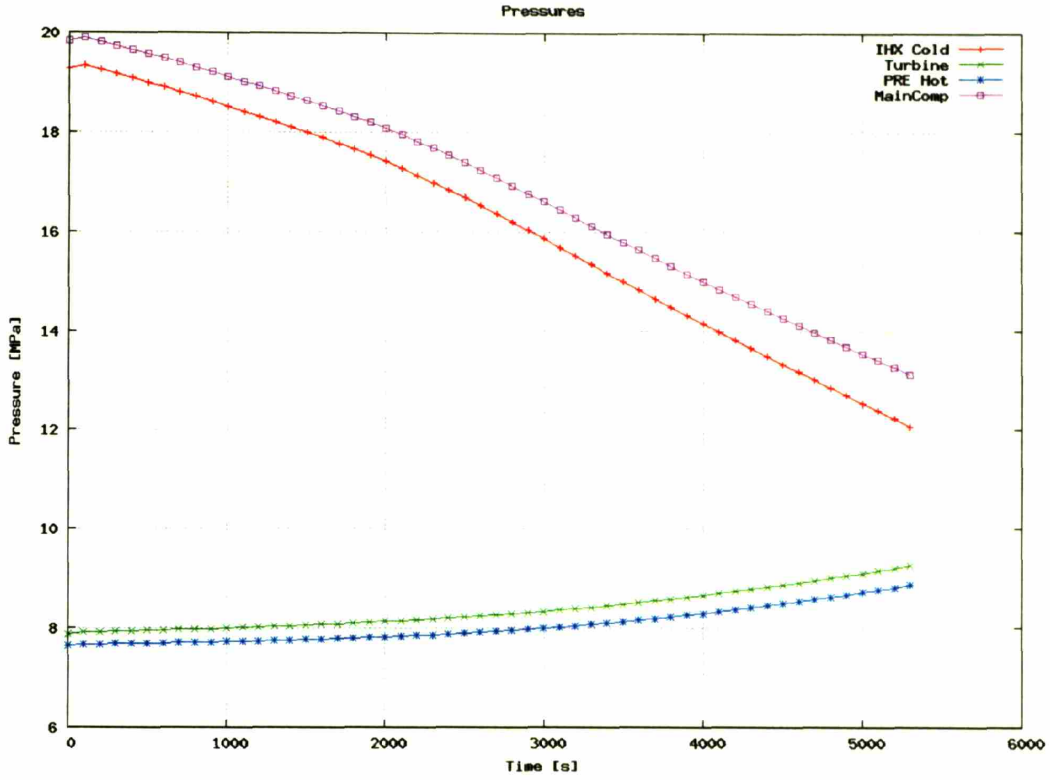

Figure 5-39: Turbine Bypass: Pressures versus Time

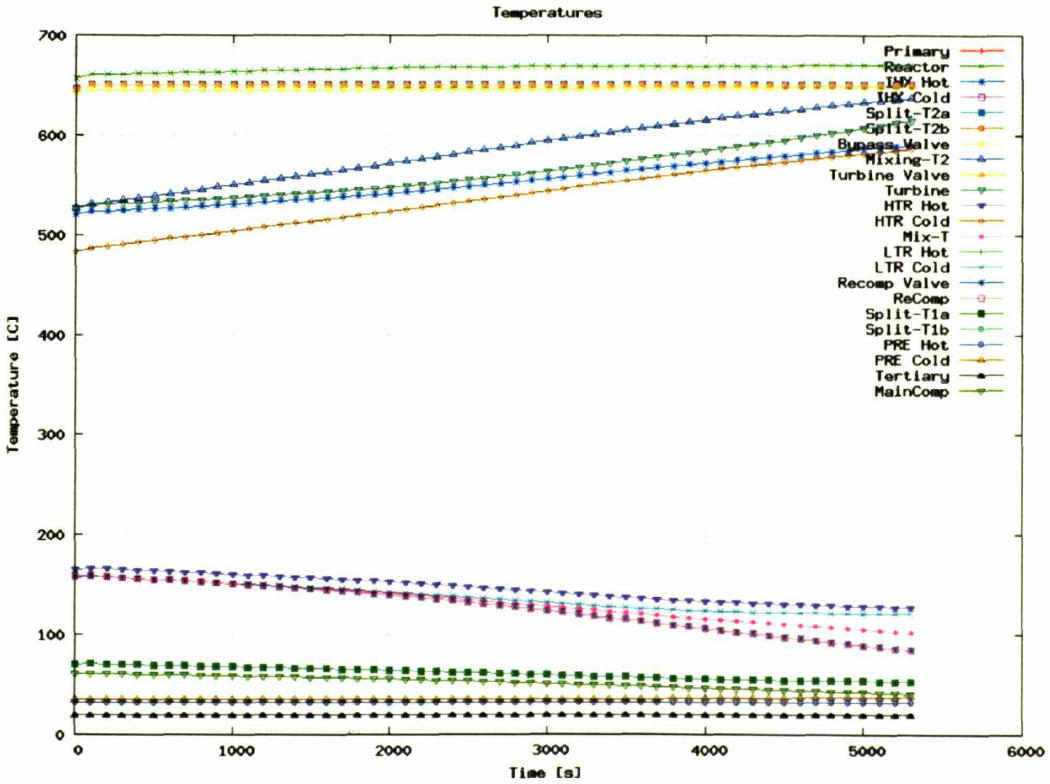

Figure 5-40: Turbine Bypass: Temperatures versus Time

Note that the middle cycle temperatures (between the LTR and HTR) drop significantly. This stems from the precooler cooling a larger mass flow rate to the (constant) main compressor inlet temperature. As the system pressure ratio drops, the main compressor performs less specific work upon this fluid and the LTR cold inlet fluid temperature gradually drops. Simultaneously, a similar process is happening in the recompression compressor which brings down the HTR outlet temperature and thus the LTR hot inlet temperature. The combined effects of these converging temperature bounds drops the outlet temperatures significantly.

The net effect of the changing mass flow rates and temperatures is to significantly increase cycle recuperation, especially in the HTR, as shown in Figure 5-41. This figure shows that while the reactor power drops to 58% nominal, the HTR recuperates over 115% more heat as the hot IHX fluid increasingly moves directly into this component. The LTR increases its heat transfer significantly. The precooler heat transfer stays roughly constant until it equals reactor power and the generator can no longer provide work.

The cycle's efficiency is relatively poor, as shown in Figure 5-42. This figure shows the net efficiency versus the nominal generator power. The turbine bypass efficiency is roughly linear until about 25% generator power, when it begins to drop off more steeply*.

5.1.5.3 Turbine Bypass Conclusion

Turbine bypass is an effective means of part-load control from zero to full power in this cycle. The method's simplicity, controlling only one valve, provides the designer and operator with an attractive method to change generator power. However, the method suffers from the drawbacks of bringing the HTR close to the maximum cycle temperature, and relatively low efficiency.

* Note that this figure shows a small range of negative generator powers. This is simply a numerical artifact since GAS-PASS/CO_2 does not force, by default, the generator to only remove power from the cycle. This simulation failed when the turbine choked, not when the net work reached zero.

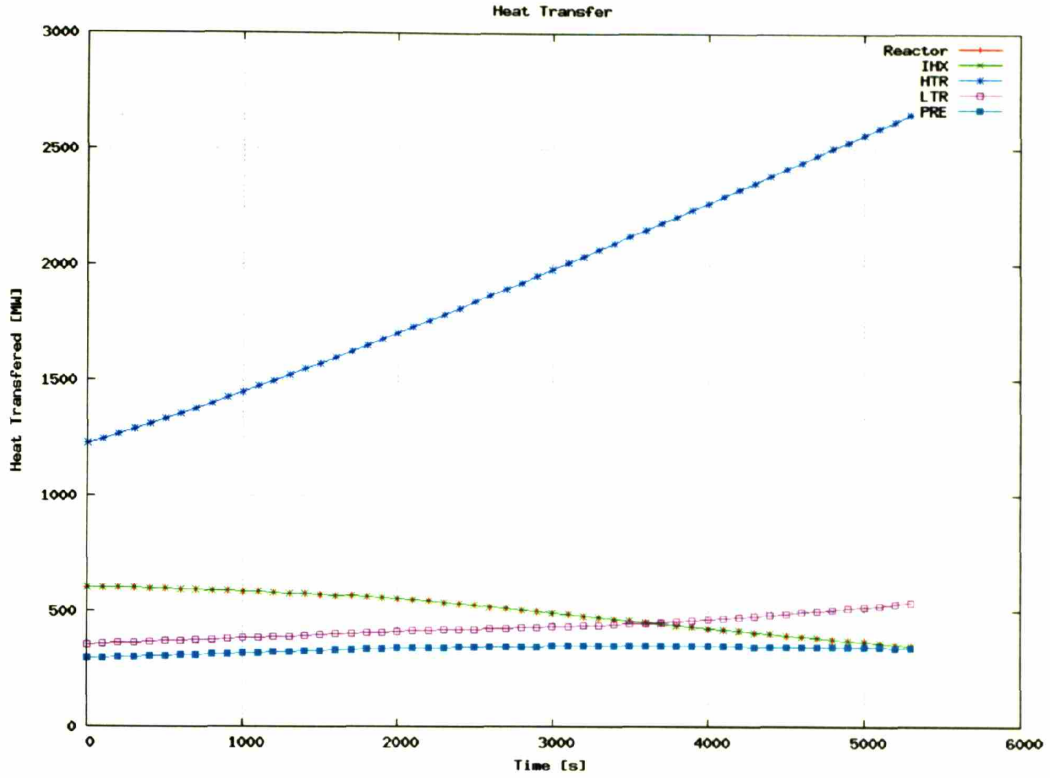

Figure 5-41: Turbine Bypass: Heat Transfer versus Time

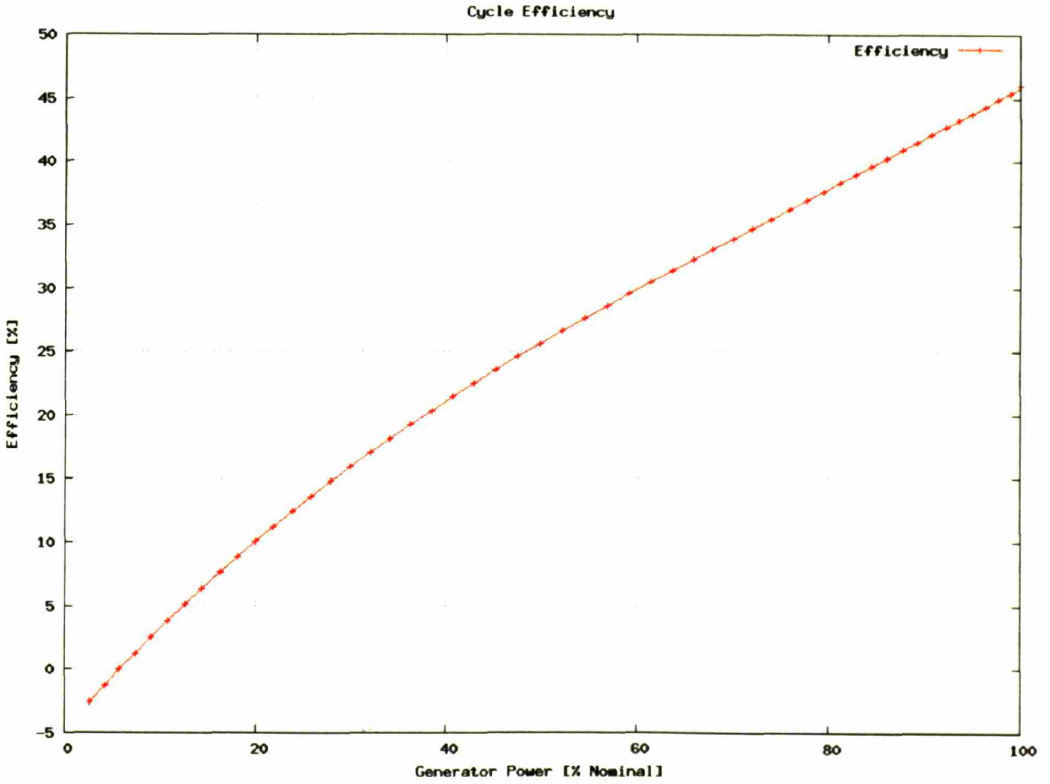

Figure 5-42: Turbine Bypass: Cycle Efficiency versus Normalized Generator Power

5.1.6 Turbine & IHX Bypass

Bypassing both the turbine and the IHX provides the advantage, over pure turbine bypass, of avoiding introducing very hot temperature fluid into the HTR. Aside from avoiding thermally stressing the PCHE, lower temperatures in the HTR will alleviate fluid displacement to the cold end of the cycle, thus leaving the lower cycle pressure closer to its design value, which should increase cycle efficiency.

5.1.6.1 Simulation Setup

The control system used for this simulation is the following:

1. The turbine and IHX bypass line is gradually opened to linearly increase the proportion of bypass flow.
2. The turbine and IHX bypass throttle is used to isenthalpically expand the bypassed flow from high to low pressure.
3. A PI controller is used to control the precooler CO_2 outlet temperature and hold it at 32°C.
4. The reactor power is controlled via a P controller to keep the turbine inlet temperature at 650°C.
5. The compressors are allowed to adjust the mass flow split to match their outlet pressures.

5.1.6.2 Simulation Results

The system works: mass flow rates, and bypass fraction all look quite similar to the previously detailed turbine bypass case, thus this section will first illustrate system pressures, as shown in Figure 5-43. This figure shows that the main compressor inlet pressure rises from 7.69 to slightly above 8 MPa. Compared to the turbine bypass case this indicates that less fluid is displaced to the cold side of the cycle; thus the system high temperatures do no rise as far.

The cycle temperatures versus time are shown in Figure 5-44. This figure shows that while the turbine outlet temperature increases, as the turbine pressure ratio decreases, the HTR inlet temperatures are roughly constant with time. Once again, the middle cycle temperatures drop as the precooler removes relatively more heat, and the compressors add less specific work.

Heat transfer during IHX and turbine bypass is similar to turbine bypass but less extreme, as shown in Figure 5-45. This figure shows a roughly 70% rise in HTR heat transfer while the reactor drops to about 52% of its nominal power. This increase comes from both the cooling of the HTR outlet temperatures and the increase in turbine outlet temperature. The LTR and precooler heat transfer are roughly constant.

Finally, the cycle net efficiency versus normalized generator power is shown in Figure 5-46. The trend of the curve is nearly identical to that of the turbine bypass case, but the efficiency is slightly higher, as will be shown in Section 5.1.8.

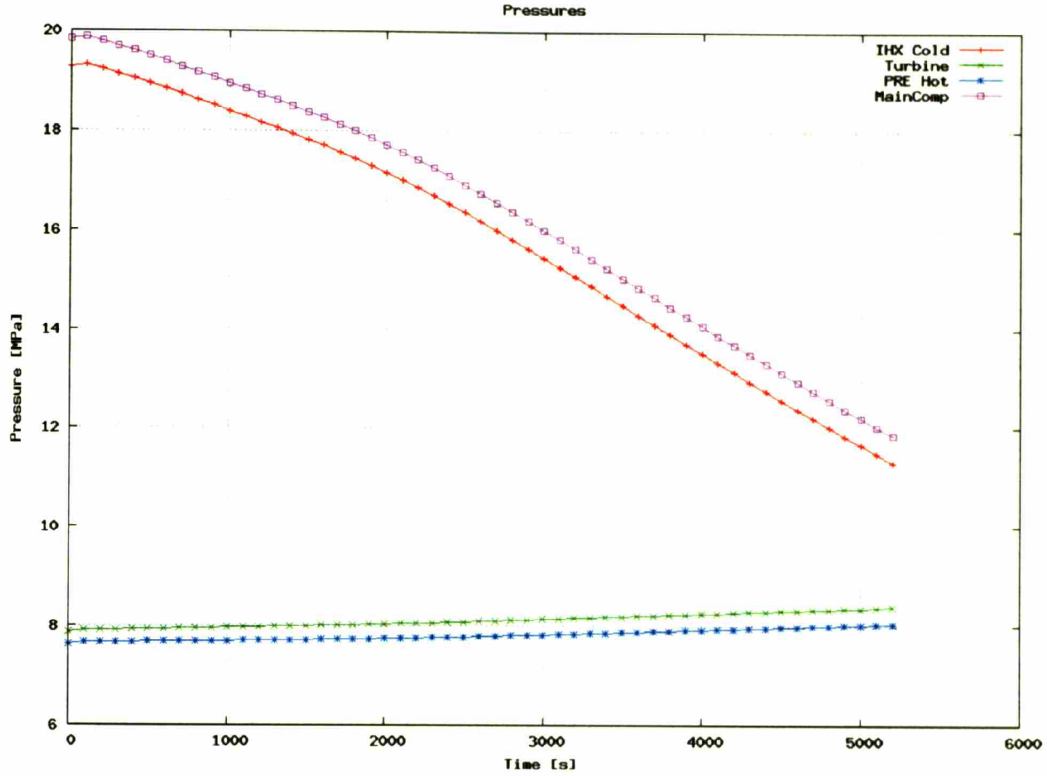

Figure 5-43: IHX Bypass: Pressures versus Time

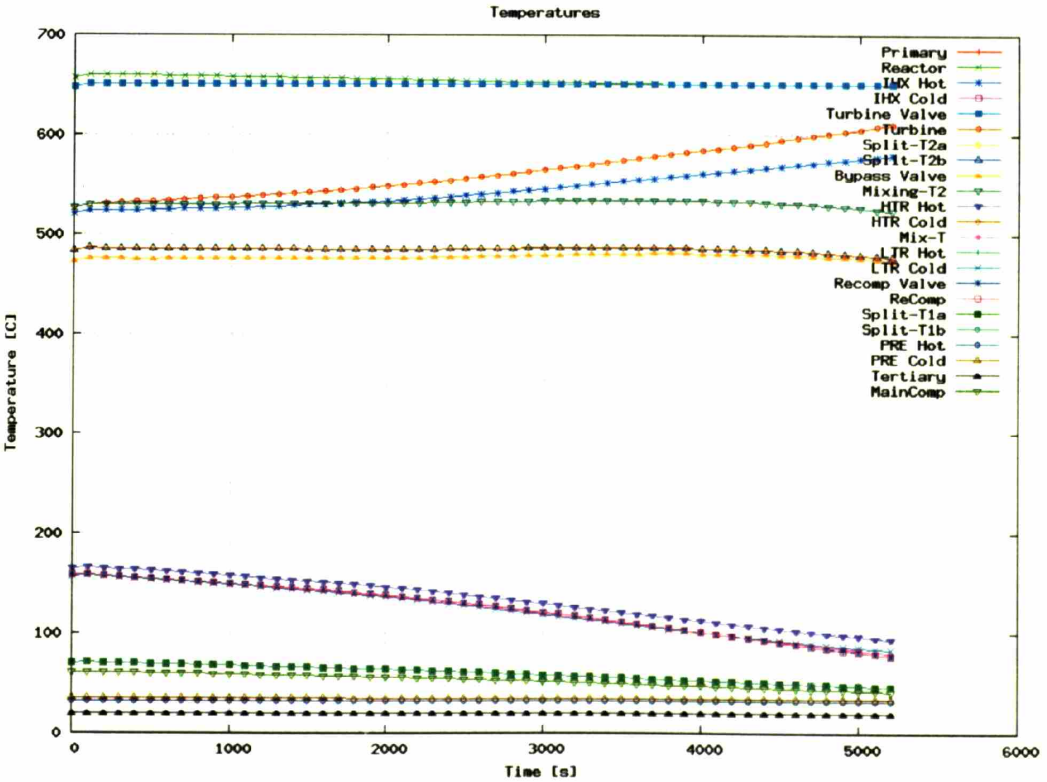

Figure 5-44: IHX Bypass: Temperatures versus Time

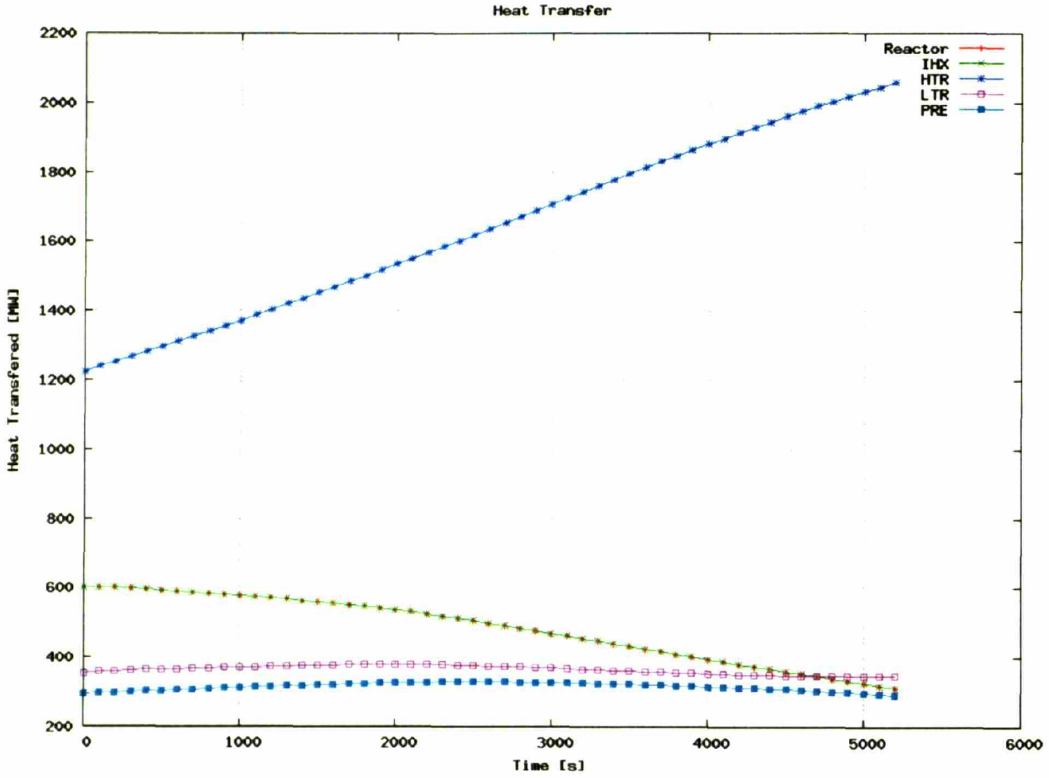

Figure 5-45: IHX Bypass: Heat Transfer versus Time

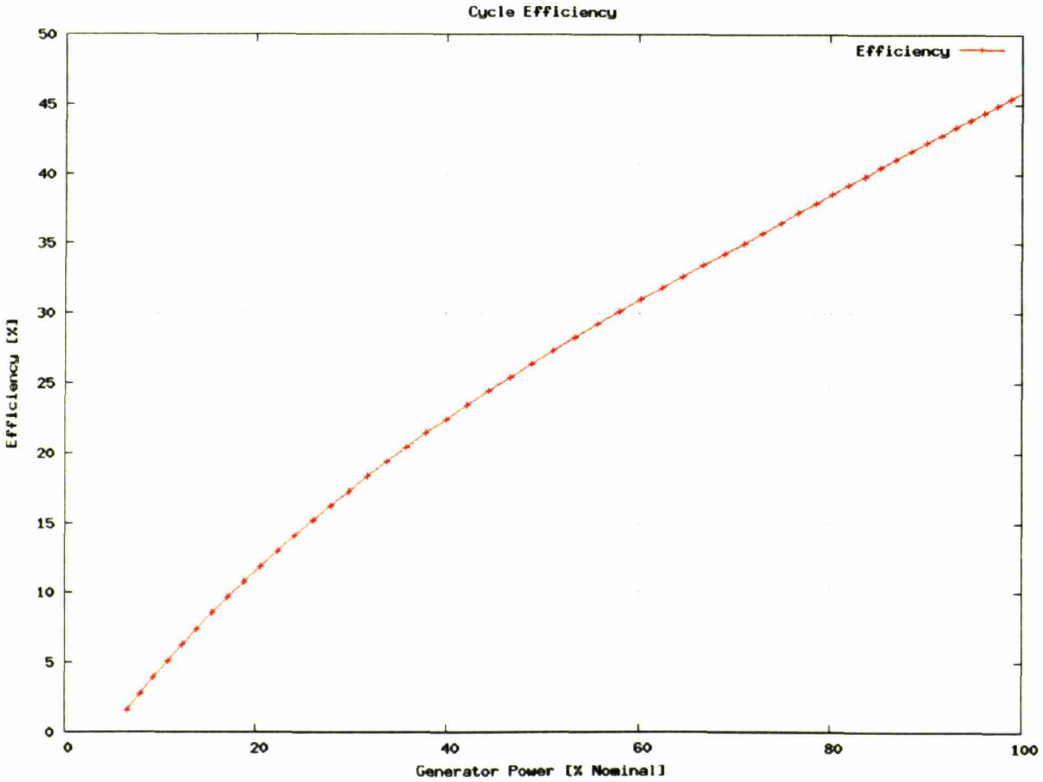

Figure 5-46: IHX Bypass: Cycle Net Efficiency versus Normalized Generator Power

5.1.6.3 Turbine & IHX Bypass Conclusion

Turbine and IHX bypass provide part-load operation over the full power range of the S-CO_2 recompression cycle. Compared to turbine bypass, this method is slightly more efficient and does not raise the HTR temperatures so close to the cycle maximum.

A possible drawback to turbine and IHX bypass was noted by Pope[9] who found that in a direct S-CO_2 recompression cycle the core fuel temperatures become unacceptably high with this method of bypass during a loss-of-load transient. His solution employed a combination of turbine and turbine & IHX bypass to assure sufficient flow in the core to keep fuel temperatures within design limits.

5.1.7 Upper Cycle Bypass

Bypassing flow between the LTR and HTR, called upper cycle bypass in this work, provides several advantages over the other bypass cases posited. The bypass occurs at significantly lower temperatures than in the other cases, the mass flow rates do not increase as much as in other bypass cases, and this method is more efficient than the others. The reasons for these differences will be explored below.

5.1.7.1 Simulation Setup

The control system used for this simulation is the following:

1. The upper cycle bypass line is gradually opened to increase the proportion of flow bypassed.
2. The upper cycle bypass throttle is used to isenthalpically expand the bypassed flow from high to low pressure.
3. A PI controller is used to control the precooler CO_2 outlet temperature and hold it at 32°C.
4. The reactor power is controlled via a P controller to keep the turbine inlet temperature at 650°C.
5. A P controller is used to keep the compressor mass flow split constant.
6. The recompression compressor throttling valve is adjusted to produce matching outlet pressure from the two radial compressors.

5.1.7.2 Simulation Results

Note, a priori, that all of these simulation results extend to only 35% generator power for reasons to be explained shortly. The difference between upper cycle bypass and other bypass methods first appears in the system mass flow rates shown in Figure 5-47. This figure shows that all the mass flow rates are smaller than in the other bypass cases.

The system mass flow rates are a combination of effects involving the compressors and turbine. As mass flow rates increase in the compressor, the pressure ratio gradually drops, and vice versa in the turbine. At a given bypass fraction, the point at which the pressure changes balance determines the loop mass flow rates.

In the upper cycle bypass case, loop mass flow rates are relatively low because the main compressors are aided, rather than hindered, by fluid density changes. In upper cycle bypass the main compressor inlet pressure drops, thus decreasing fluid density and increasing the volumetric flow rate. Since the compressors scale by volumetric flow rate (see Section 3.4.4.2) this has the effect of allowing a lower pressure ratio for a given mass flow rate. Note that this could lead to compressor stall, but this problem can be alleviated through methods already noted, such as recirculation lines.

The system pressures in this simulation are shown in Figure 5-48. This figure shows that the cycle high pressures drop, while the cycle low pressures slightly decrease. The precooler inlet and outlet pressure can be more clearly see in Figure 5-49. This figure shows that the precooler outlet pressure/main compressor inlet pressure decreases from roughly 7.69 to 7.58 MPa. Due to the non-linear nature of carbon dioxide property changes in this region the effects on fluid properties are non-trivial.

Figure 5-50 shows the isobaric specific heat peak for the beginning and ending main compressor inlet pressures. The figure shows that dropping only 0.11 MPa nearly doubles the isobaric specific heat peak and moves much of the peak below 32°C. Since the precooler outlet temperature is held very close to this value, this suggests that the peak moves at least partly out of the precooler. This has at least two important effects:

1. The precooler heat transfer coefficient drops as the large increase in isobaric specific heat is lost to this component. This will force a, potentially rapid, increase in water mass flow rate to keep the same heat transfer.
2. The main compressor receives fluid in the middle of this very rapid fluid property change. While even a small rise in pressure or temperature will move the fluid beyond this peak, it is highly uncertain how the compressor will respond to a fluid experiencing these changes.

GAS-PASS/CO_2 failed (stopped converging) in this simulation when this much larger, narrower peak began to enter the main compressor. The reason for this failure is likely numerical in nature, but future experimental testing should investigate how the compressor will physically respond to this phenomenon.

The upper cycle bypass creates a decrease in system low pressure because fluid is moved to other components as temperatures fall. Figure 5-51shows the temperatures of the cycle versus time. The figure shows that the cycle middle temperatures drop quickly towards cycle low temperatures. The LTR temperature profile makes this clear, as shown in Figure 5-52. The LTR temperature begins the simulation with a maximum temperature difference of over 110°C and ends the simulation with a maximum temperature difference of only 12°C.

The reason for the narrowing of the temperature difference in the LTR is not immediately obvious, but several factors are important:

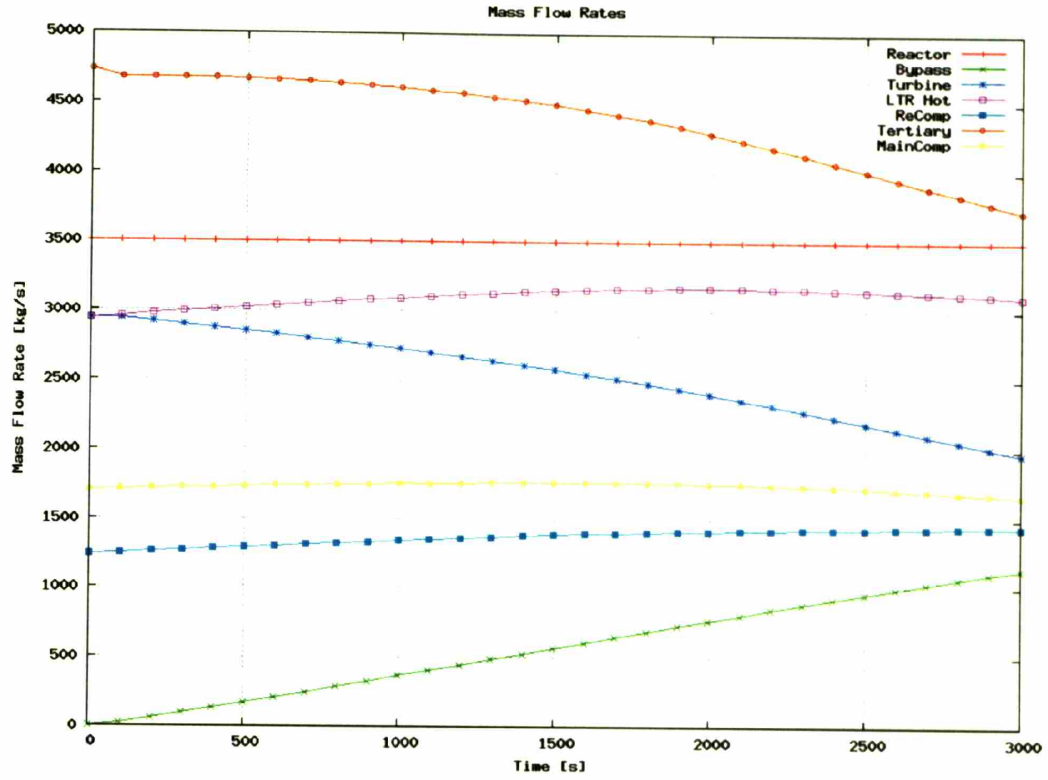

Figure 5-47: Upper Cycle Bypass: Mass Flow Rates versus Time

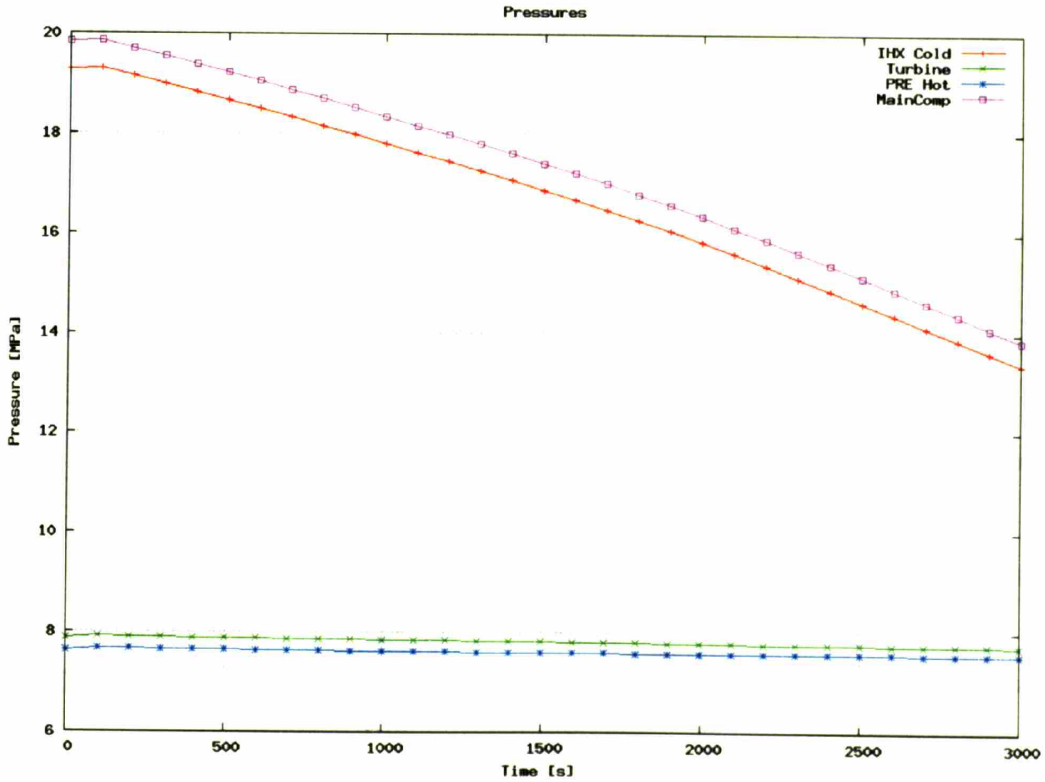

Figure 5-48: Upper Cycle Bypass: Pressures versus Time

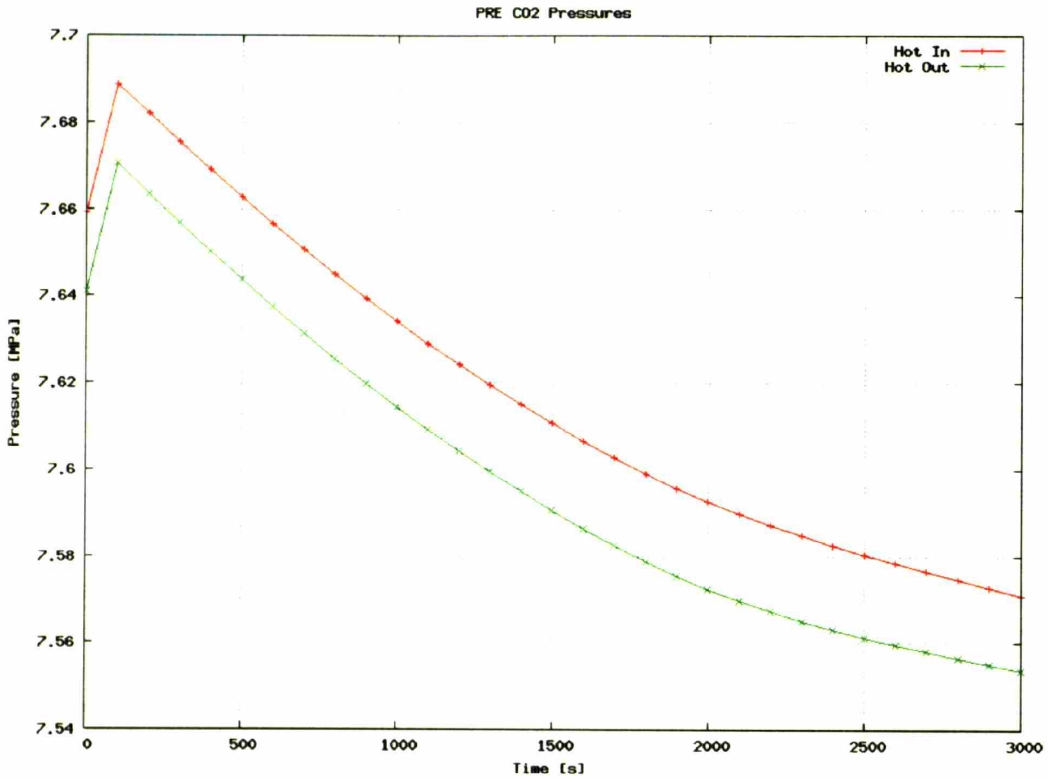

Figure 5-49: Upper Cycle Bypass: Precooler Pressures versus Time

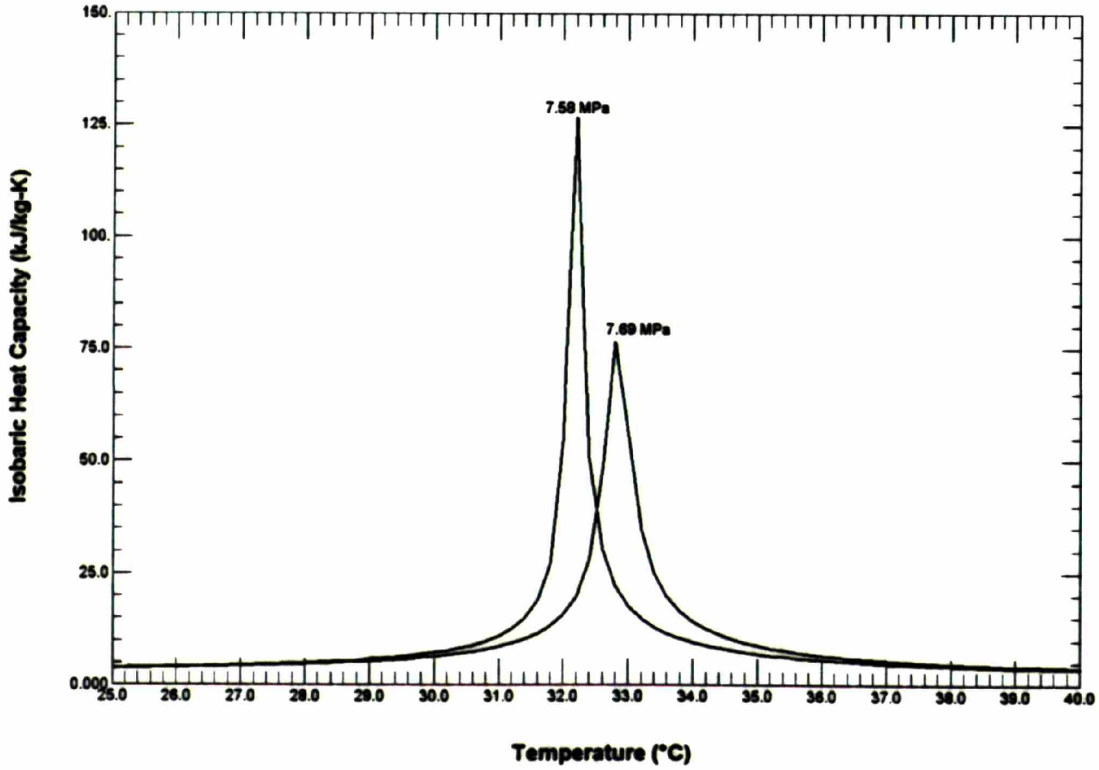

Figure 5-50: Upper Cycle Bypass: Isobaric Specific Heat at Main Compressor Inlet Pressures

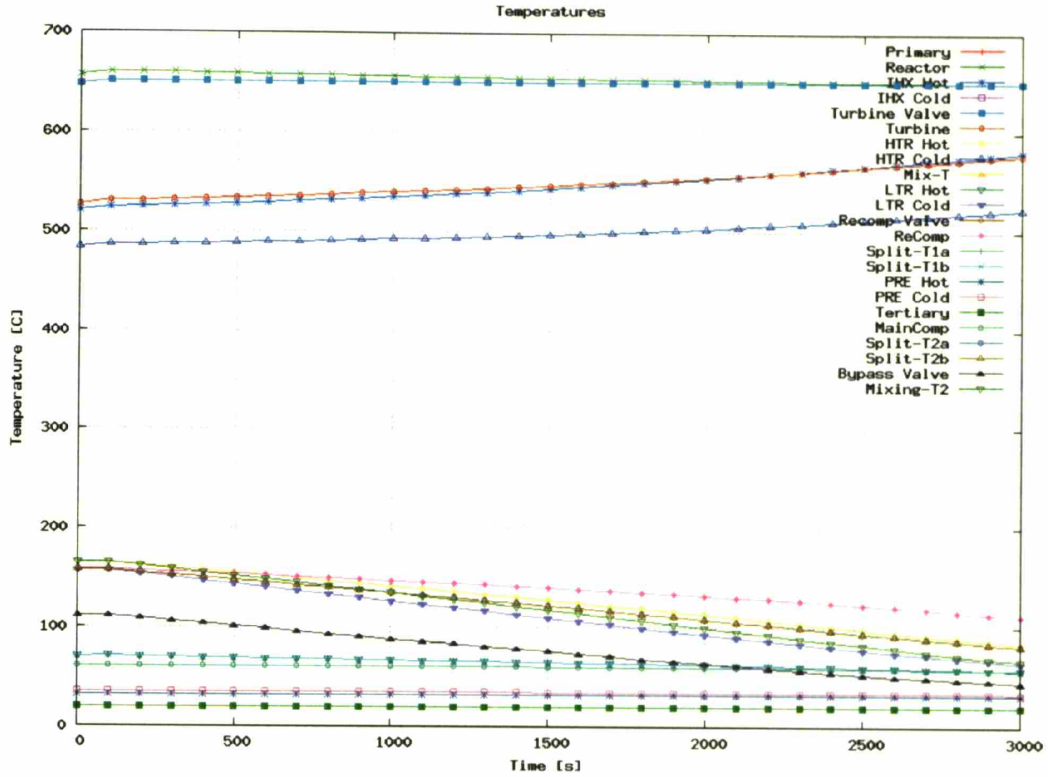

Figure 5-51: Upper Cycle Bypass: Temperatures versus Time

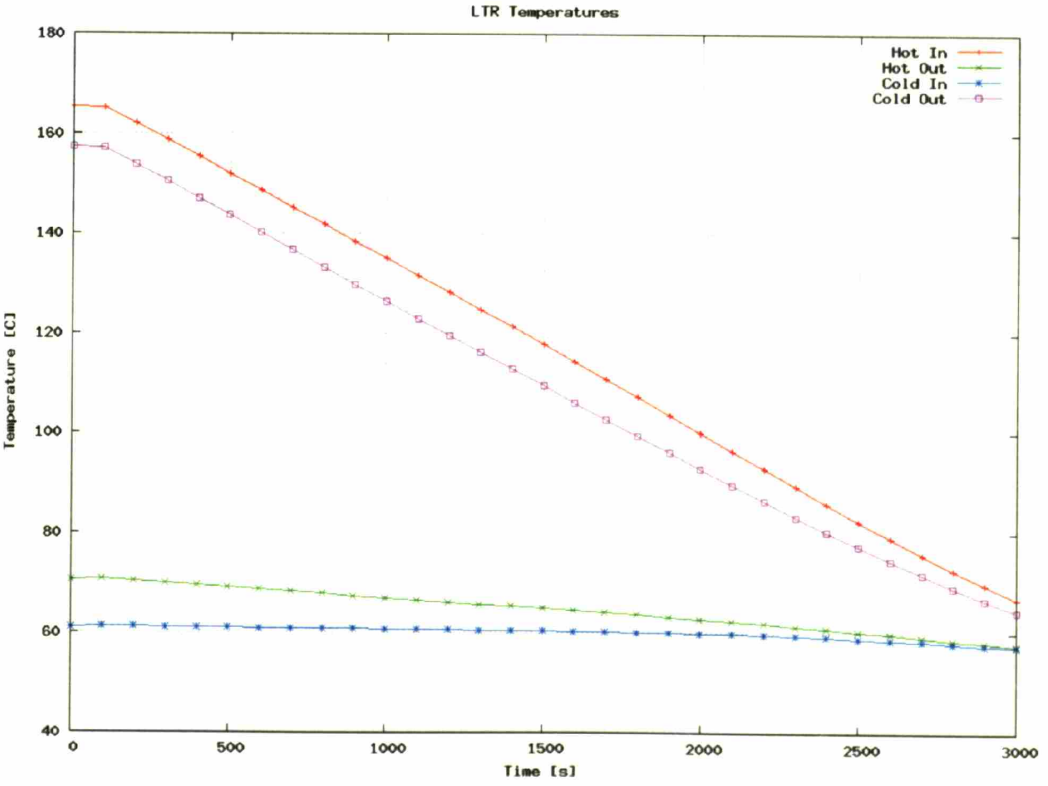

Figure 5-52: Upper Cycle Bypass: LTR Temperatures versus Time

- By holding the precooler outlet temperature to 32°C, the main compressor supplies cold fluid to the LTR at an almost constant temperature. While the HTR dropped its low temperature during turbine and turbine and IHX bypass, the LTR cannot lower its low temperature.
- The LTR cold fluid moves away from its isobaric specific heat peak as the cycle high pressure drops (see Figure 5-15), thus changing the effectiveness of the relative mass flow rates.
- As ever more fluid is bypassed, the LTR begins acting like a single recuperator and thus is prone to encounter a pinch point[3].

The effect of the difference in bypass methods becomes clear when one examines the heat transfer during upper cycle bypass as shown in Figure 5-53. This figure shows that the HTR experiences a small increase in heat transfer before decreasing, in contrast to the large increases previously seen. Furthermore, the LTR heat transfer linearly decreases to nearly zero, reflecting the small temperature difference already shown.

The cycle net efficiency versus generator power is shown in Figure 5-54. Due to the lower cycle mass flow rates, and not wasting high temperature energy, upper cycle bypass is considerably more efficient than other bypass methods.

5.1.7.3 Upper Cycle Bypass Conclusion

Upper cycle bypass presents an attractive but uncertain option to future researchers. Due to the non-linear fluid property changes in the compressors, the loop mass flow rates are relatively low and due to the bypass valve location high temperature fluid energy is not wasted thus the proposed method relatively efficient.

However, there are considerable uncertainties over the range of this method. In particular, if the pressure drops far enough to push the pseudo-critical peak into the main compressor, then it is possible that undesirable behavior will result. Future experiments (see Section 6.4.3) should examine this effect.

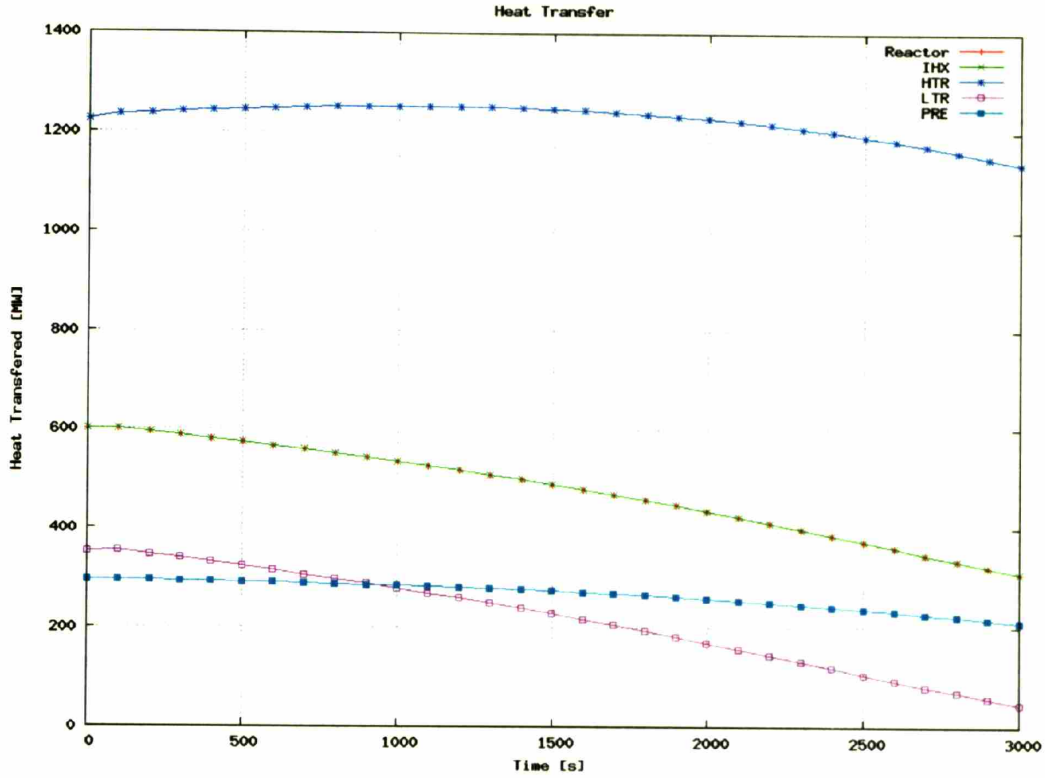

Figure 5-53: Upper Cycle Bypass: Heat Transfer versus Time

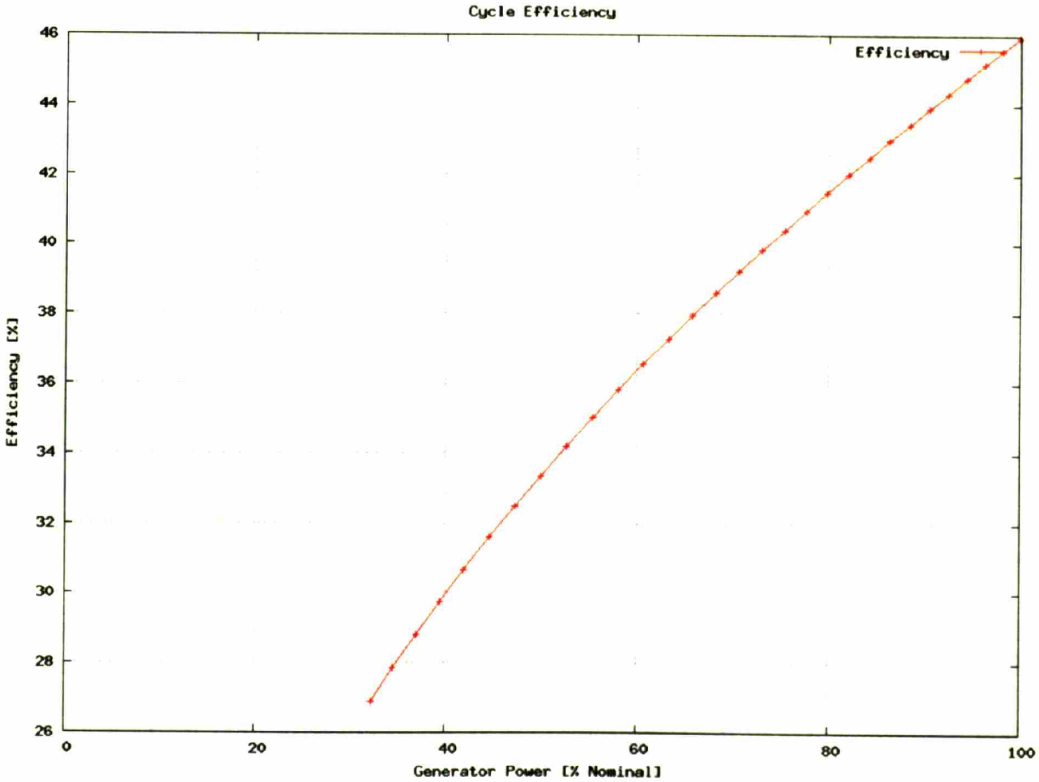

Figure 5-54: Upper Cycle Bypass: Cycle Net Efficiency versus Normalized Generator Power

5.1.8 Part-load Operation Summary

This section has reviewed a variety of part-load operation control methods for the S-CO_2 recompression cycle. Each method has advantages and disadvantages, except for pure low temperature control, which is unsuited for part-load operation and will not be addressed further, but several general features should be compared.

The net cycle efficiency of each method is shown versus nominal generator power in Figure 5-55. This figure shows that combined inventory and low temperature control is the most efficient operation method and is available over almost the full operation range of the cycle. The efficiency of this method changes significantly when the flow split changes and the cycle low pressure begins to drop quickly (see Figure 4-18), near 50% generator power, and drops rapidly near the minimum mass flow rate on the turbine performance map. This promising method suffers from several concerns:

- The fluid property effects in the near critical region on the main compressor are uncertain. If handled incorrectly these uncertain effects may cause pressure oscillations, leading to serious cycle problems. This may require relatively complicated adjustments of the main compressor inlet temperature to avoid rapid fluid property changes.
- Inventory control is a slow acting control method, and thus is unsuitable for rapid power changes.
- Inventory control requires potentially large control tanks and may require an additional compressor to move fluid rapidly. These concerns were not addressed in this work.

Turbine inlet throttling is the second most efficient control method, and operates between, roughly, 27% and 100% generator power. It features a smoothly sloping efficiency curve over its range and should be relatively easy to implement, since it requires only a single throttling valve. However, this valve may be expensive due to the size of the pipes used in this near ideal gas region, and the valve needs to accommodate throttling fluid at the cycle's high temperature.

Upper cycle bypass provides operation from at least 33% to 100% generator power and it is possible that it may extend to 0% power. Due to the relatively low temperatures and high densities seen at this bypass location, it is the preferred bypass method. However, the method presents a significant concern since, near 33% generator power in a quasi-static transient, a large and sharp pseudo-critical fluid property peak will enter the main compressor.

High temperature control is the fourth most efficient operation method, and provides control from full to slightly above 50% generator power. It shows a smoothly sloping efficiency curve over its operation range. This method of control is unlikely to be used in actual plant operations due to the large temperature changes required in the high temperature part of the cycle, including the reactor.

The turbine and IHX and turbine bypass methods are the least efficient methods, but readily extend from 0 to 100% power. The turbine and IHX bypass method prevents the HTR inlet from approaching very close to the cycle high temperature, but deprives the IHX (and reactor) of cooling fluid.

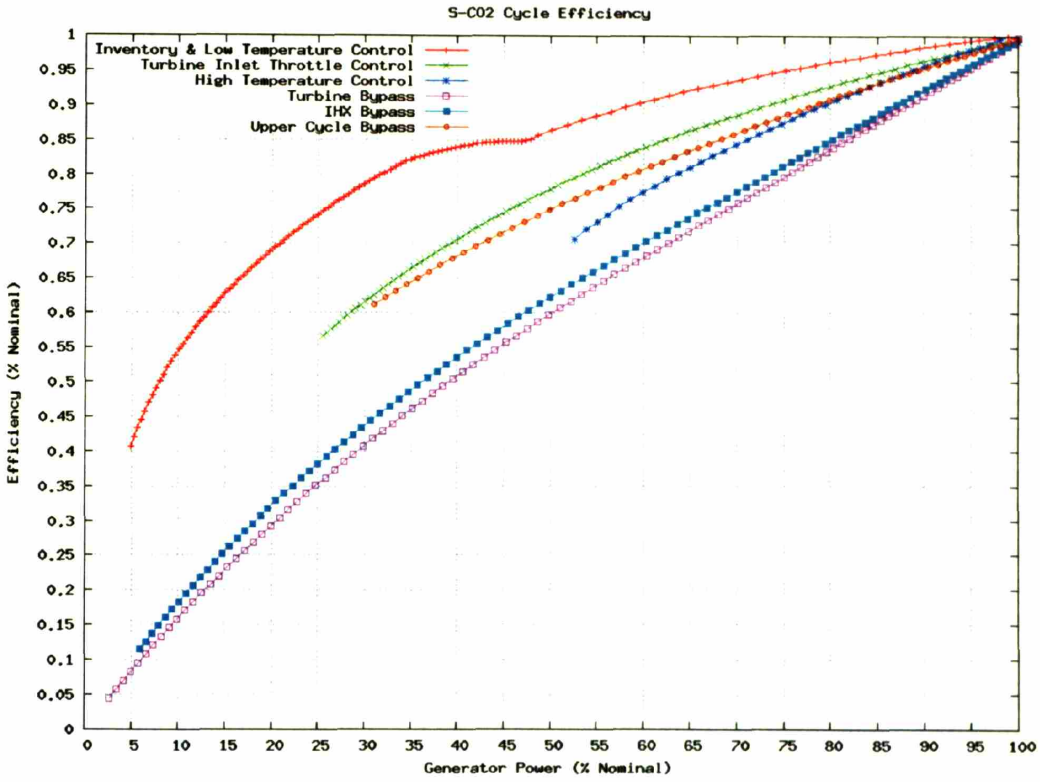

Figure 5-55: Net Cycle Efficiency versus Nominal Generator Power for Part-load Operation

5.2 Loss-of-load

The loss-of-load (LOL) transient occurs when the generator (abruptly) disconnects from the electrical grid, thus it no longer removes energy from the shaft. The very rapid decrease in generator load creates a large and positive work imbalance on the shaft which uses this energy to accelerate rapidly. Due to the S-CO_2 recompression cycle shaft's relatively low inertia*, the acceleration will rapidly lead to turbomachinery blade failure if it is not controlled†, due to an excessively high rotational speed. To control this

* This work uses the shaft inertia calculated by Pope[9] for the S-CO_2 recompression cycle of 2454.7 kg-m^2.

† Calculations indicate that S-CO_2 recompression cycle turbomachinery are limited by blade bending stress, instead of the more common tip speed stress. This suggests that the turbomachinery may be considerably more resistant to shaft overspeed (or that their construction materials may be cheaper) than is typical in a Rankine cycle. Due to the current lack of detailed blade stress calculations this work will adopt a 30% overspeed limit, which matches Pope[9] work, with the acknowledgement that this limit needs to be quantified.

transient a (turbine) bypass valve is rapidly opened to decrease the turbine work and increase compressor work to try to slow the accelerating shaft.

This simulation will use the turbine and IHX bypass valve (see Figure 4-12, Bypass valve 2) to alleviate overspeed during LOL. This valve is placed close to the turbine, yet it avoids the introduction of the cycle's hottest fluid into the HTR (and the valve). The reader should note that this valve's placement may lead to a rapid decrease in mass flow rate in the turbine and IHX. In a direct cycle this phenomena may lead to an unreasonably high fuel temperature[9] but this concern will not be addressed in this work, which focuses upon the power cycle in an indirect cycle configuration.

5.2.1 Simulation Setup

This simulation proceeded as follows:

1. The generator power used linearly decreased from full to zero power in 0.0001 seconds, within one time step, as a boundary condition.
2. The reactor is instantly scrammed upon detection of generator separation. The reactor power then follows a standard decay curve taken from Pope's LOL transient[9].
3. A PI controller is used to control the precooler CO_2 outlet temperature and hold it at 32°C. The controller varies the external cooling water mass flow rate. After the LOL is detected, the PI controller switches off and the external cooling water mass flow rate is held constant.
4. The compressor flow split is allowed to vary solely due to compressor pressure changes. Thus, changes in the precooler outlet temperature significantly affect the compressor flow split.
5. A PID controller was added to the primary loop sodium pump to keep the reactor outlet temperature constant during the first few seconds after LOL. Primarily due to the rapid reactor power decrease, the sodium temperatures entering the IHX can easily drop below the carbon dioxide outlet temperatures for short periods of time. This can produce a large spike in stored mass flow rate, which caused simulation failure in GAS-PASS/CO_2, and thus will be avoided by placing a rapid controller on the sodium pump.

   After the shaft speed has been stabilized, the sodium temperature is allowed to linearly decrease roughly in parallel with the carbon dioxide outlet temperature.
6. A PID controller is placed on the bypass valve to keep the shaft speed at reference until the LOL event is detected. The valve begins steady state with only $5*10^{-2}$% of the flow moving through it*.

   Note that the PID controller on this bypass valve required a very large derivative term to appropriately control shaft speed. The S-CO_2 recompression cycle's shaft

* The bypass valve PID controller used here required minimum and maximum bounds to prevent the controller from attempting to create flow reversal or from diverting so much flow that the turbine moved below known mass flow rates.

speed changes easily, especially when decreasing in speed, and appears to exhibit an almost exponential acceleration. If it is not carefully controlled, by anticipating its direction of travel with the derivative term, the shaft will rapidly run past realistic operating bounds before a PI controller can catch it.

7. Once the LOL event is detected, the turbine and IHX bypass valve is rapidly opened to the point where 66% of the total flow is bypassed, and held fully open until the conclusion of the simulation.

The reader should note that approximate generator and turbine shaft speed loss terms, such as windage, were added to the S-CO_2 recompression cycle model to account for changes in drag as the shaft accelerates. The coefficients used in this model were based upon Hejzlar[81].

5.2.2 Simulation Results

The shaft speed during several LOL transients is shown in Figure 5-56. This figure shows the increase in shaft speed starting at the time of LOL, at time 0, for several bypass cases. The first case, "no bypass," does not open the bypass valve during the transient and thus presents the plants uncontrolled response to this transient. This line shows a rapid and linear increase in shaft speed which ends near 140% of the nominal shaft speed, the upper limit of the turbomachinery performance curves.

The second line shows how the shaft speed increases when the bypass valve fully opens within 0.4 seconds. This line shows behavior similar to the "no bypass" case for the first half a second and then gradually peaks and decreases until the simulation ends near 7.5 seconds. The maximum shaft speed is just below 30% increase on the nominal value and the simulation ends at the minimum turbine mass flow rate on the performance curves*.

The third line shows the normalized shaft speed for a bypass valve which fully opens by 0.5 seconds. This line shows very similar behavior to the 0.4 second bypass valve case except for a slight increase in shaft speed to just above 130% shaft speed.

The final line shows normalized shaft speed for a bypass valve which fully opens by 0.6 seconds. This line is very similar to the other bypass valve cases but peaks near 132% of nominal shaft speed.

Note that the next section will present results from the 0.4 second bypass valve case to assure that the shaft speed never exceeds 130% of the nominal value.

Figure 5-58 shows the turbine and IHX fraction of bypassed flow versus time. Starting at time 0.1 the fraction of bypassed flow rises steeply until it reaches 66% of the flow at 0.4 seconds. The 66% flow fraction is held until the simulation ends.

* While a turbine can have gas flow separation at low mass flow rates like a compressor, it will not stall, where the mass flow rate rapidly drops to zero, as occurs in a compressor.

The work within the cycle versus time is shown in Figure 5-58. This figure shows the rapid decrease in generator power from full power to zero power at time zero. The turbine shows a relatively rapid but smooth decrease in work, as a significant portion of the mass flow rate is bypassed, until about 3 seconds, when it gradually decreases until simulation failure. The compressors show an initial peak in work (the compressors experience a significant peak in mass flow rate) and then gradually decrease in consumed work over time.

Figure 5-59 shows the total amount of work added and the total amount removed from the shaft versus time. Before the LOL event the works are equal, thus the shaft speed is constant. At time 0 the LOL event occurs and the amount of work removed from the shaft drops precipitously until a small peak is reached (near 0.5 seconds) and the amount of work removed slowly decreases versus time. The amount of work added to the shaft drops smoothly from about 0.1 seconds following the LOL event, until it matches and then drops below amount of work removed slightly after 3 seconds. The amount of work added then stays below the amount removed until the end of the simulation.

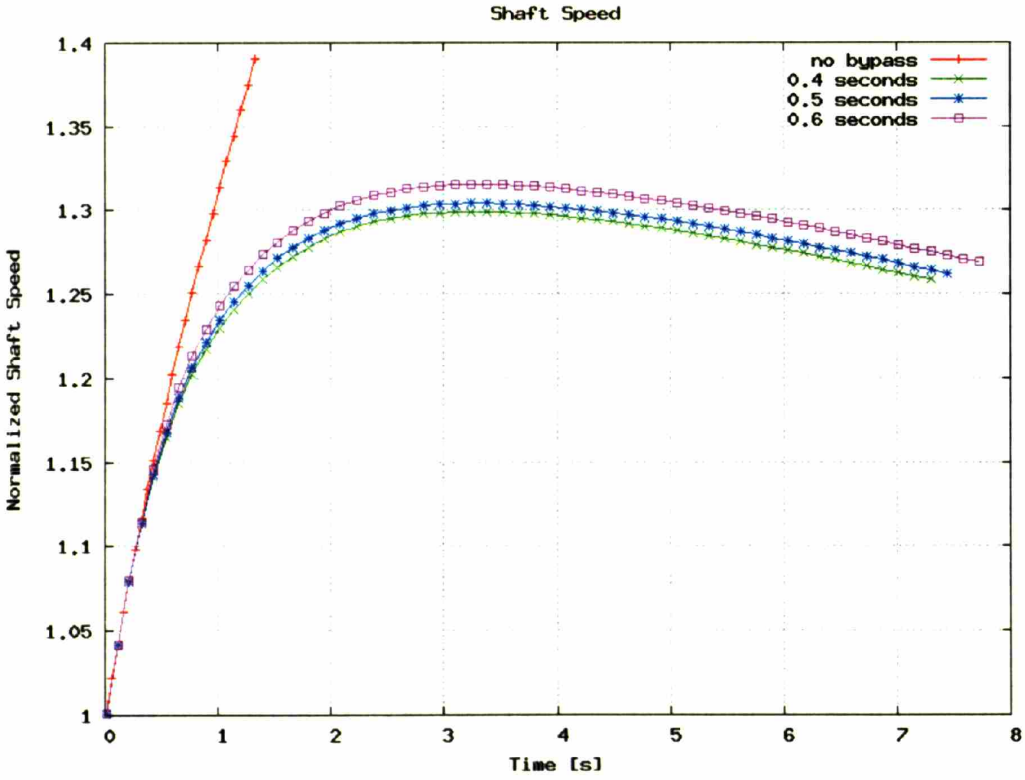

Figure 5-56: LOL Transient: Normalized Shaft Speed vs. Time

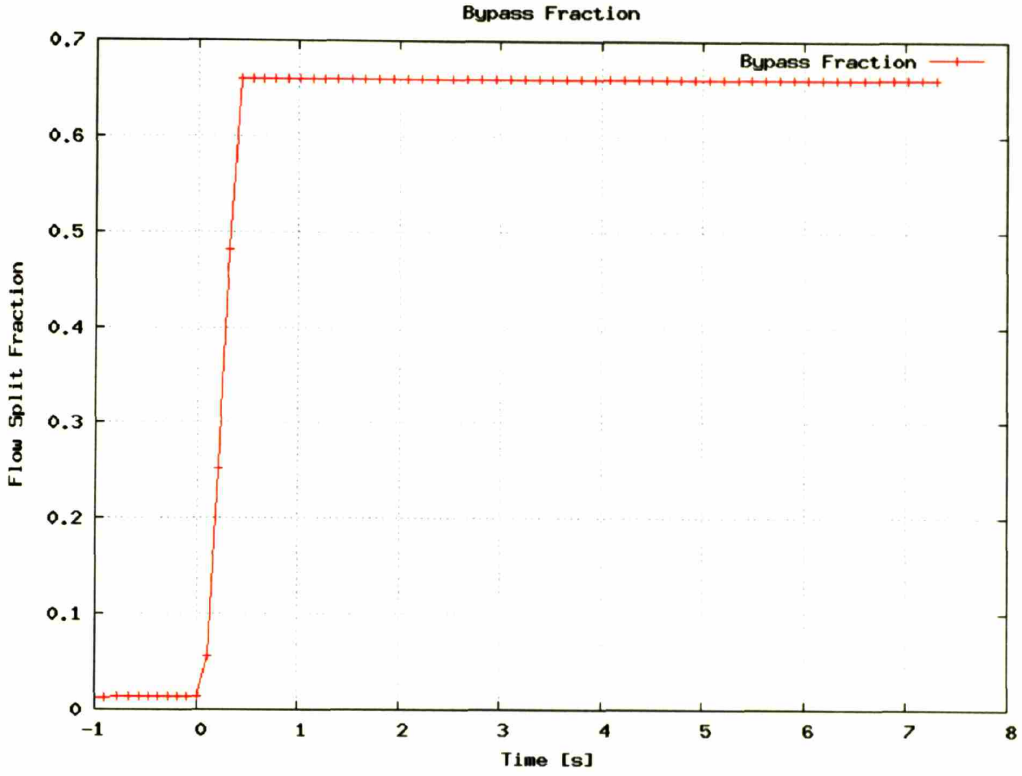

Figure 5-57: LOL Transient: Bypassed Flow Fraction vs. Time

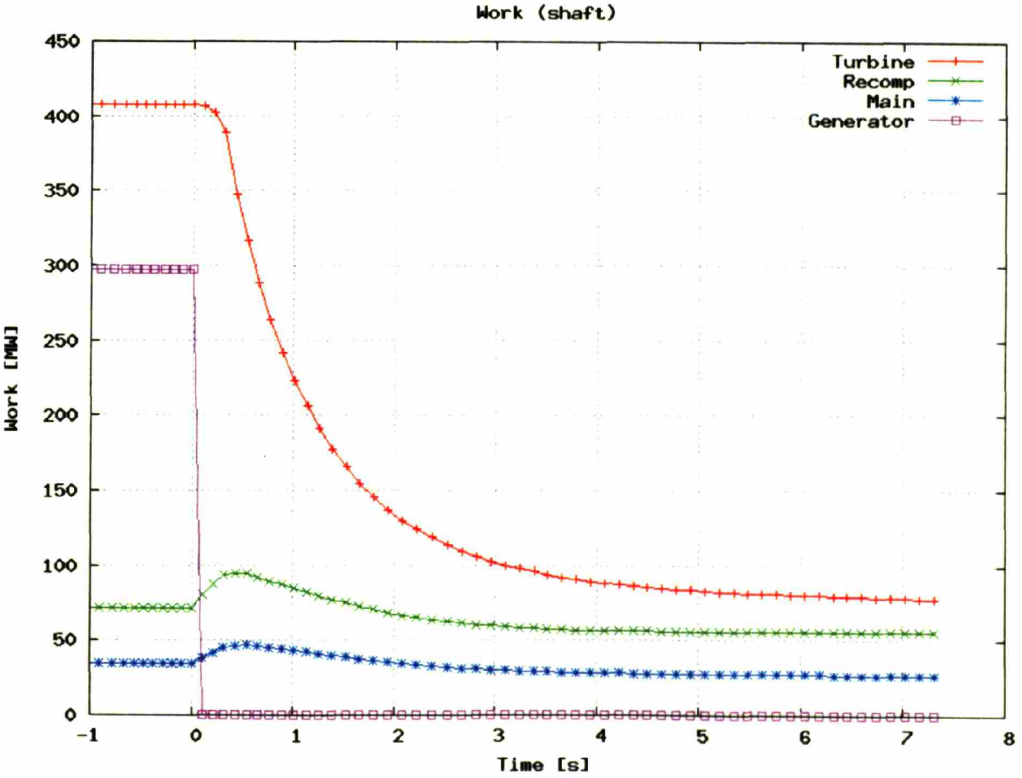

Figure 5-58: LOL Transient: Work vs. Time

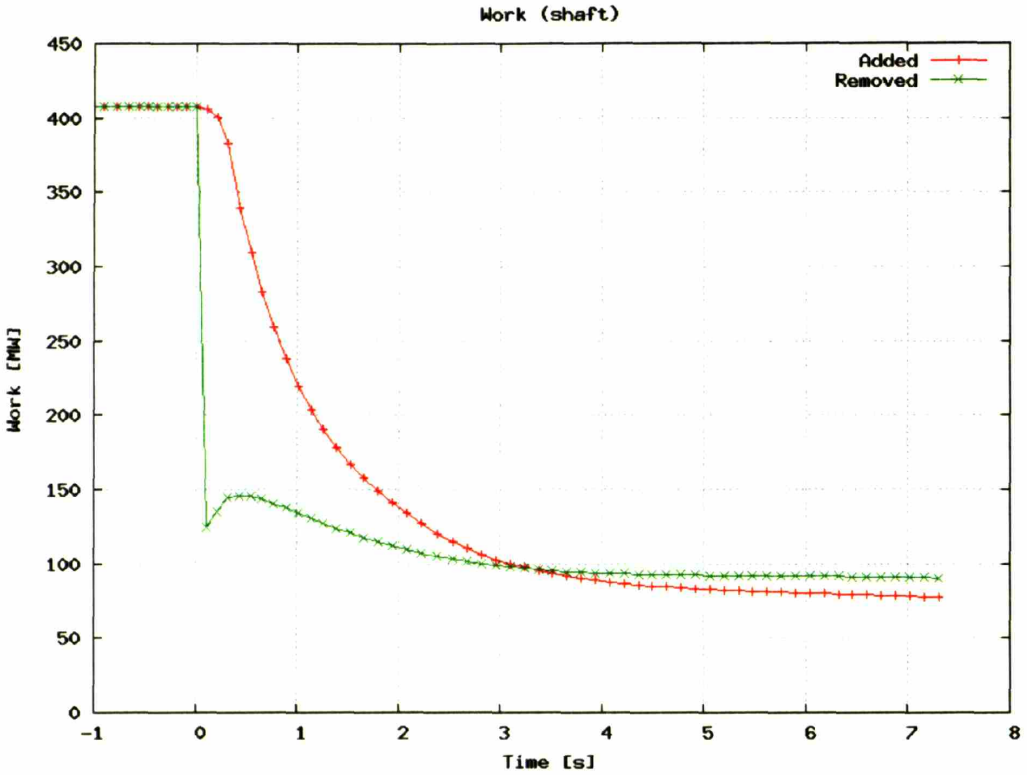

Figure 5-59: LOL Transient: Work Added & Removed vs. Time

Figure 5-60 shows heat transfer versus time. This figure shows that the reactor power exponentially and rapidly decreases from the time of LOL, time 0, until near 4 seconds, when it approaches roughly 10% power and gradually decays. The reactor power behavior is determined solely by radioactive decay constants. The high temperature recuperator shows a large increase in heat transfer with unique peaks and behavior. Much of the unique behavior stems from transient mass storage effects, especially the sharp peak near 0.5 seconds. HTR heat transfer peaks near two seconds but stays at a high value until the conclusion of the simulation. The low temperature recuperator and precooler show a rapid increase in heat transfer near 0.5 seconds, which lasts until about 2 seconds. Past two seconds these components show nearly constant heat transfer. The reader should note that the HTR is the only heat exchanger in this system to receive the full carbon dioxide mass flow rate (the LTR receives the full flow rate on only one side of the PCHE).

Several system pressures versus time are shown in Figure 5-61. This figure shows that system high and low pressure rapidly converge following the LOL transient. The main compressor outlet pressure drops from near 20 MPa around 0.5 seconds, and smoothly decreases to about 15 MPa near the end of the simulation. The precooler hot outlet pressure increases from about 7.69 MPa to over 10 MPa by 2.5 seconds and then stays at a high pressure through the simulation.

The reader should note that these large pressure changes can produce significant changes in density, especially in the non-linear region near the critical point. The large density changes create large changes in the amount of fluid stored in a component as shown in Figure 5-62. This figure shows the amount of fluid stored in each component versus time. The results show that high pressure components lose a significant amount of inventory as their pressure decreases, while low pressure components gain a significant amount as their pressure increases. Note that non-linear property effects can be seen in components like the hot/low pressure side of the LTR, which increases inventory by over 60%.

Figure 5-63 shows mass flow rates versus time. The figure shows that there is a significant spike, more than doubling, in overall mass flow rate as the bypass mass flow rate increases significantly. This spike drops quickly towards a steady state value, near four seconds, as transient mass storage effects die out. The mass storage effects are clearly seen in the outlet of the "turbine" control volume* line. The turbine control volume mass flow rate drops from nearly 3,000 kg/s per seconds to a slightly negative mass flow rate (flow reversal) near 0.5 seconds, and stabilizes near 2,000 kg/s near 4 seconds.

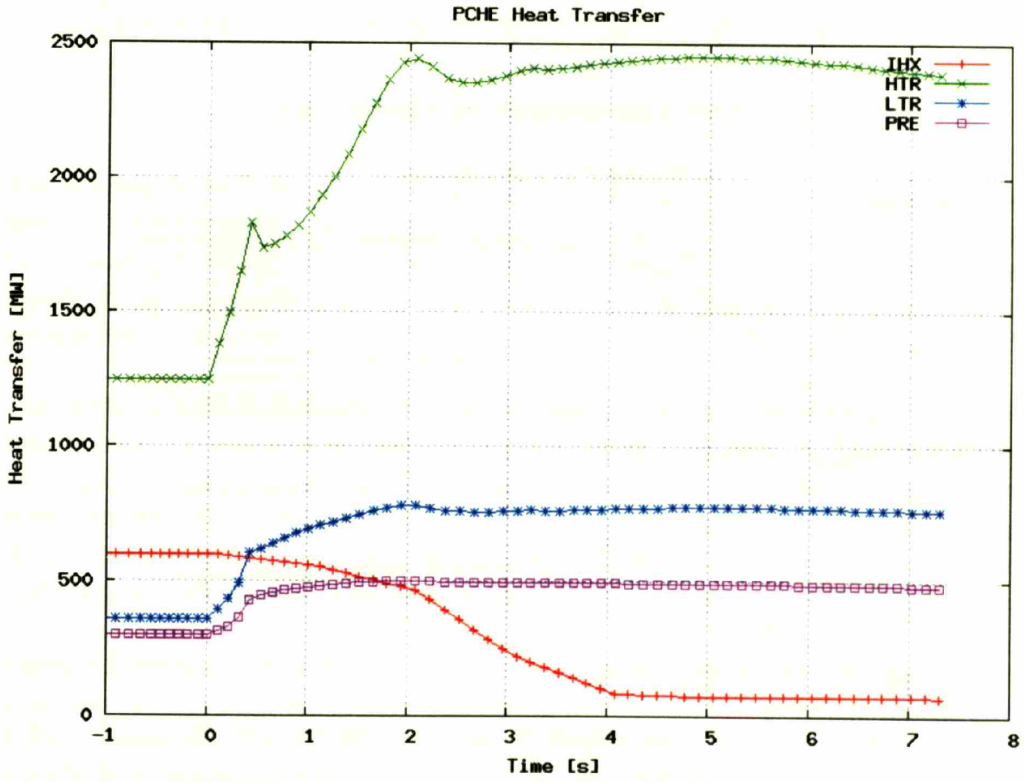

Figure 5-60: LOL Transient: Heat Transfer vs. Time

* The turbine control volume includes the passive piping following the turbine and the HTR low pressure plena. See, "Appendix B.4 Separating vs. Lumping Piping Volumes in the S-CO_2 Recompression Cycle" for more information.

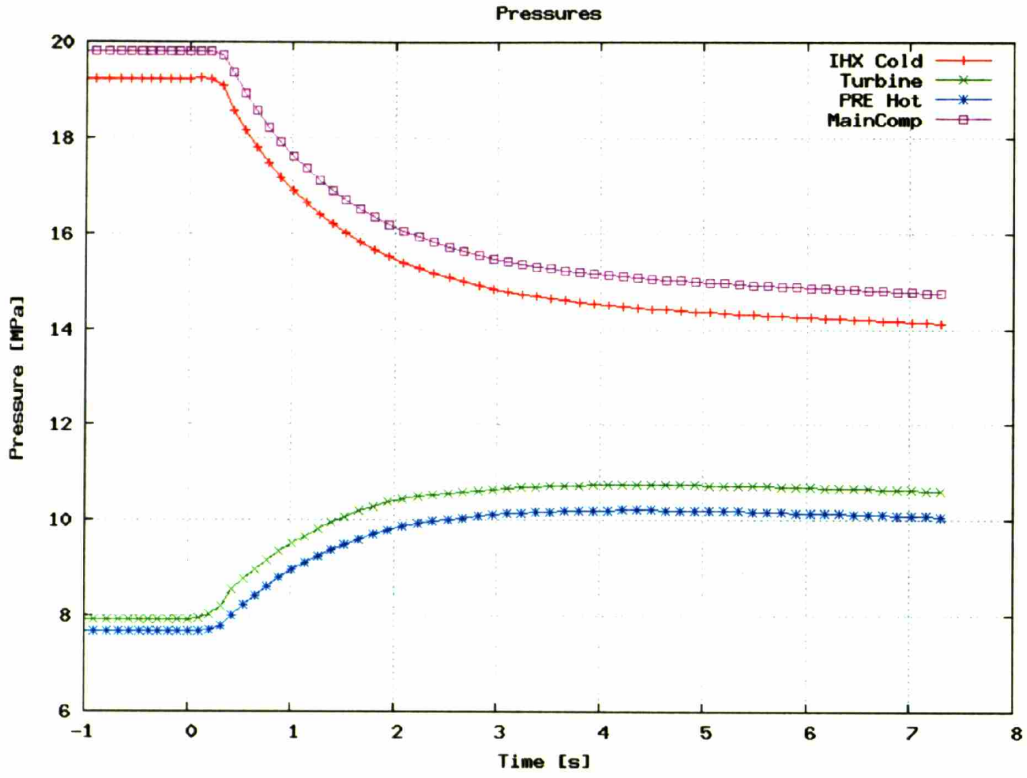

Figure 5-61: LOL Transient: Pressure vs. Time

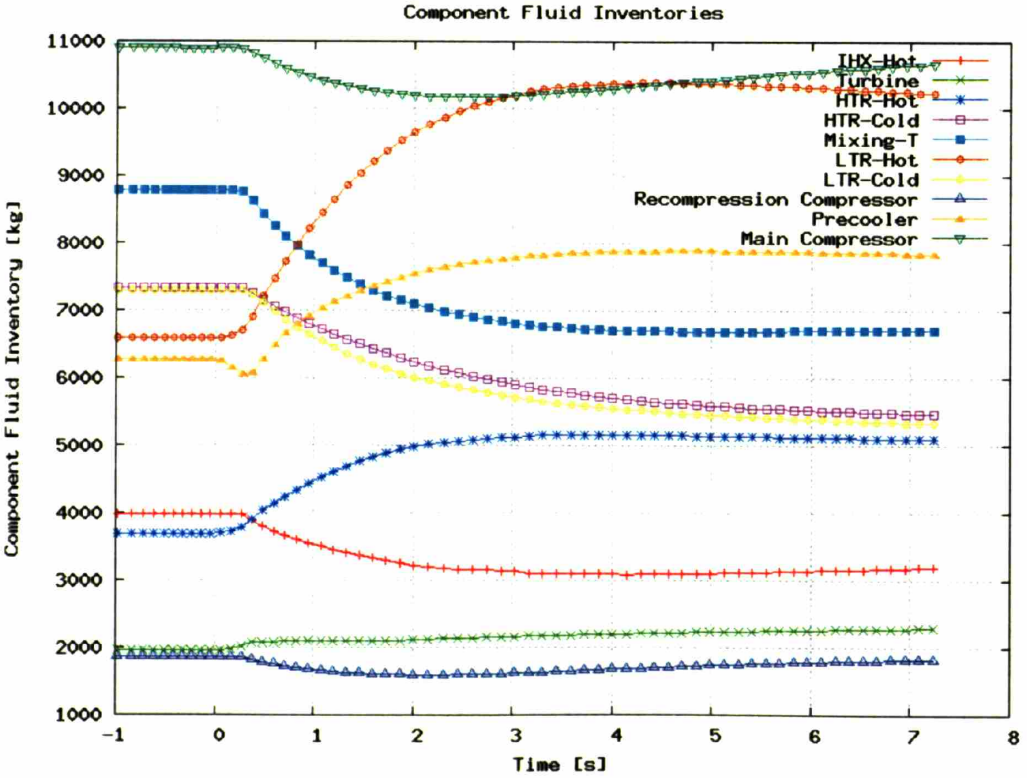

Figure 5-62: LOL Transient: Component Fluid Inventory vs. Time

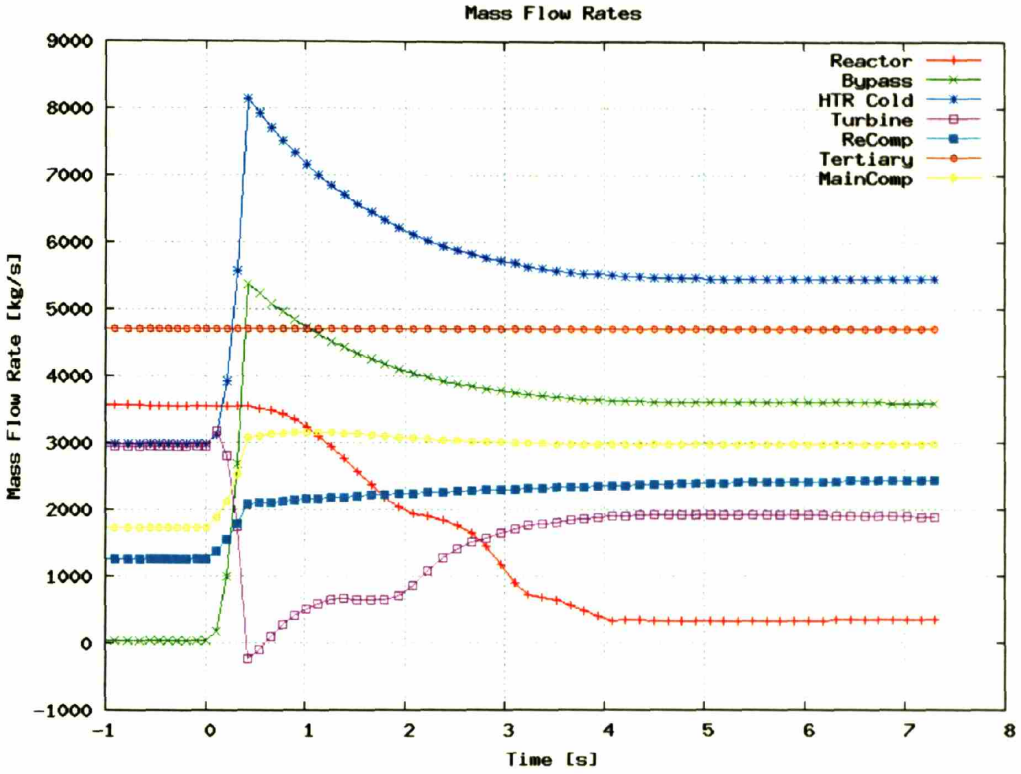

Figure 5-63: LOL Transient: Mass Flow Rates vs. Time

The sodium mass flow rate is controlled by the sodium loop PID controller to keep the reactor outlet temperature constant. The sodium mass flow rate drops significantly and non-linearly to account for the large changes in the carbon dioxide mass flow rate and the rapidly decaying reactor power. The water mass flow rate is held constant throughout the simulation.

The reader should also note that the main compressor inlet temperature will increase significantly (in terms of property changes near the critical point) due to the greatly increased carbon dioxide mass flow rate and constant water flow rate (see Figure 5-63). However, also note that the pressure at the main compressor inlet is increasing rapidly as well. Thus, an increase in main compressor inlet temperature will keep the main compressor inlet density closer to constant than an isothermal case would.

Table 5-1 shows carbon dioxide density at the main compressor inlet during the steady state and several LOL scenarios. Assuming the system low pressure increased to 10 MPa, keeping the main compressor inlet temperature constant at 32°C would significantly increase fluid density (by 25%) thus increasing main compressor pressure rise (see Section 3.4.4.2). To keep the main compressor inlet density constant would require a temperature increase to over 41°C, assuming that the low pressure once again

reached 10 MPa. The current simulation with a temperature of 34.75°C presents an intermediate, but still large, density increase*.

Table 5-1: Main Compressor Inlet Carbon Dioxide Density during Various LOL Scenarios

Temperature [°C]	Pressure [MPa]	Density [kg/m^3]	Scenario
32.000	7.6900	598.81	Steady State
32.000	10.000	749.98	Isothermal LOL
34.750	10.000	716.19	Current LOL Simulation
41.329	10.000	598.80	Constant Density LOL Simulation

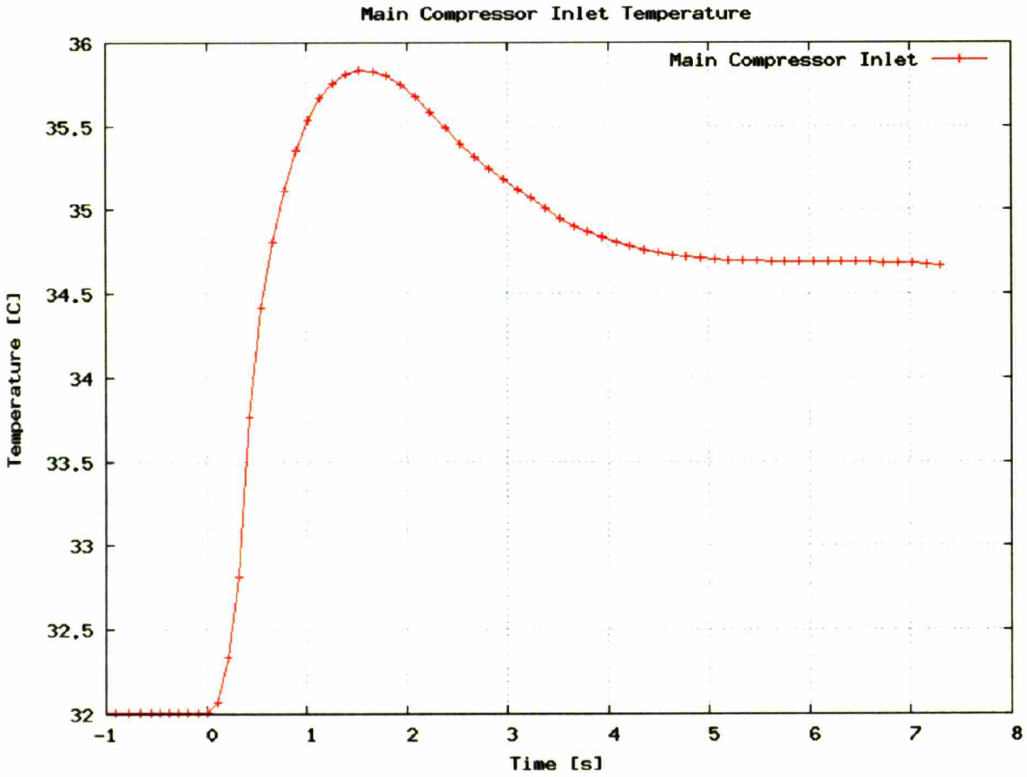

Figure 5-64: LOL Transient: Main Compressor Inlet Temperature vs. Time

* Note that initial simulations attempted to precisely control the precooler CO_2 outlet temperature by varying the external cooling water mass flow rate. Due to the rapid (bypass) changes occurring at LOL, precisely controlling the precooler CO_2 outlet temperature required very rapid and very large changes in water mass flow rates. The net result did not provide a significant improvement over constant water mass flow rates results, yet this method of control would have made significant demands on the water pump, therefore this method of control was avoided.

5.2.3 LOL Transient Conclusion

The loss-of-load event in the S-CO_2 recompression cycle can be safely controlled but it will require rapid bypass valve response due to this cycle's high turbine work to shaft inertia ratio. Current simulations show that the LOL event will require valve action on the order of 0.4 seconds for complete opening and that shaft speed will peak near 3 seconds after the LOL event. This transient also suggests that the turbine control volume can experience flow reversal for a very short time, and a relatively low exiting mass flow rate for several seconds.

Compared to similar RELAP5 LOL simulations completed by Pope, GAS-PASS/CO_2 predicts a slower shaft speed-up and slower peaking. There are numerous possibilities for these differences, but it is likely that the difference primarily stems from lumping the structure stored energy with the fluid stored energy – clearly a poor assumption on this time scale. Also note that GAS-PASS/CO_2 uses radial compressor performance curves with incompressible fluid relations, while Pope used homologous pump models. How quickly the compressor models predict an increase in work will significantly affect the rate at which the shaft speed increases and the peak shaft speed is reached.

In both RELAP5 and GAS-PASS/CO_2, maximum valve opening speed was predicted to be 0.4 seconds to keep the shaft speed less than 130% overspeed. Finally, note that using RELAP5 Pope also predicted flow reversal in the hot end of the cycle during LOL using this bypass location. Although the particulars of the flow reversal differ, the differences probably stem from Pope's use of a direct cycle and relatively finely nodalized mass storage volumes.

If future stress analysis shows that the S-CO_2 recompression cycle turbomachinery can safely handle higher than 30% increase in shaft speed, then the bypass valve requirements (and other controller requirements) may be significantly relaxed. The speed at which this transient occurs requires rapid controller actions which would be considerably relaxed if the shaft could accelerate for even half a second longer.

5.3 Chapter Summary

The S-CO_2 recompression cycle appears controllable for both part-load operation and the loss-of-load transient. This cycle has a wide variety of possible control methods for part-load operation, including low temperature and inventory control, high temperature control, turbine throttling, and at least three types of bypass control. These part-load operation methods enable efficient part-load operation, rapid load change operation, and operation between full and zero generator power. While the S-CO_2 recompression cycle shows unique behavior, one may summarize much of this behavior by stating that the proximity to the critical point should be carefully controlled, especially as this proximity applies to the main compressor inlet.

GAS-PASS/CO_2 predicts that the LOL transient can be readily controlled to keep the shaft speed within a 30% increase over the nominal shaft speed. While several details differ, previous work by Pope with RELAP5 shows similar LOL behavior with this cycle, including the possibility of flow reversal in the hot region of the cycle with rapid bypass valve opening.

6 Summary, Conclusions, & Future Work

This chapter will provide a general overview of this work. The chapter is sub-divided into five sections: summary, conclusions, safety implications, part-load cycle comparison, and recommended future work:

1. The first section provides a standalone summary of this work. Key issues regarding the simulation codes, modeling methods, and results will be briefly reviewed. The section provides no new information, but simply collates key areas of interest into one short summary.
2. Conclusions make up the second section. This brief section will highlight bottom-line findings of this work.
3. The third section is a brief review of the safety implications relevant to this indirect power conversion system. It is intended as an initial starting point for future researchers.
4. A comparison of part-load operation results between GAS-PASS/CO_2, Moisseytsev[17], and a helium cycle[19] is provided in section 4. This analysis will focus upon part-load efficiency of the different control methods and provide a brief comparison of the differences between helium and S-CO_2 storage and their possible consequences.
5. The final section provides recommendations for future work.

6.1 Summary

Increasing the temperature range a cycle operates over is a key factor affecting plant efficiency and ultimately the cost of electricity. In an ideal power cycle, a Carnot Cycle, the cycle efficiency depends only upon the ratio of the low to high temperature. To increase efficiency one must decrease the low temperature, at which heat is rejected, and/or increase the high temperature, at which heat is added. Since the cycle low temperature is typically constrained by local ambient water/air conditions, the designer must increase the high temperature to improve the cycle efficiency.

How the nuclear reactor accommodates these higher temperatures is a key design element, but the higher reactor temperatures are of little value if they cannot be efficiently converted into electricity. The power conversion system (PCS) used almost universally for today's reactors, the Rankine Cycle, cannot be easily adapted to exploit these higher temperatures, which imply very high pressures – now approaching 30 MPa. Therefore, a key consideration of the Generation IV effort is the creation of a power cycle which works efficiently at the higher temperatures envisioned. Closed Brayton Cycles are prominent candidates for this service.

One such, the supercritical carbon dioxide (S-CO_2) recompression system, couples well to advanced nuclear reactor designs. The cycle features relatively high efficiency at temperatures significantly lower (for the same efficiency) than those found in helium gas

cycles. Furthermore, this cycle is relatively compact for a given power rating, which provides significant advantages in component costs and applications where space is at a premium.

6.1.1 Indirect S-CO_2 Recompression Power Cycle

The steady state design of the S-CO_2 recompression cycle has been explored in detail elsewhere[3], but the key features of this cycle merit review. These features not only drive transient performance but they are frequently quite different than those found in other power cycles and therefore deserve examination before transient cycle aspects are introduced.

This cycle uses supercritical carbon dioxide to convert heat to electricity in a closed Brayton cycle. The cycle operates very close (in both temperature and pressure) to carbon dioxide's critical point at the cycle bottom temperature, 32°C, primarily to increase the fluid's density, thereby enabling efficient compression, but never enters the two-phase region. While a CO_2 condensing cycle (e.g. Rankine) offers many attractive options it requires cooling water too cold to be geographically available throughout the world, thus in the present work the critical point will be approached but not crossed to allow widespread deployment.

The cycle maximum temperature, the turbine inlet temperature, is 650°C in the reference design, making this cycle widely applicable to next generation reactors. The pressures within the cycle operate between 7.69 MPa to 20 MPa, making this a relatively high pressure cycle, but by no means the highest pressure cycle being designed for advanced nuclear applications. For example, the supercritical water GEN-IV concept operates at 25 MPa (water's supercritical pressure is 22.1 MPa)[82]. The cycle mass flow rates are also relatively high, approaching 3,000 kg/s. The efficiency of this power cycle is quite attractive at, roughly, 47%.

Dostal compared[3] the efficiency of several advanced nuclear power cycles as a function of turbine inlet temperature as shown in Figure 6-1. The reader should note that at 650°C the S-CO_2 recompression cycle offers higher efficiencies than those available to the water cycles and is about 200°C cooler than a helium cycle with the same efficiency. The ability to achieve this high efficiency without dealing with the materials issues present at substantially higher temperatures is a key reason for interest in this cycle.

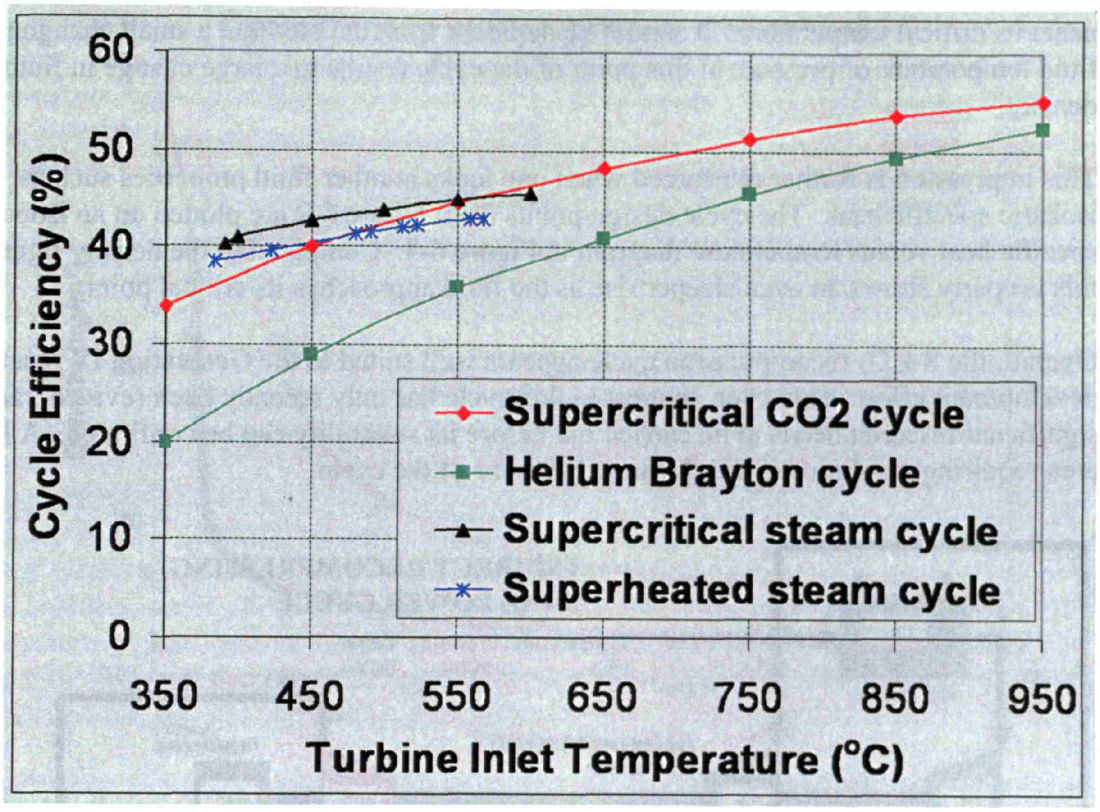

Figure 6-1: Advanced Nuclear Power Cycle Efficiency Comparison[3]

The cycle layout is shown Figure 6-2. The reader should note several features:

- all the turbomachines operate on a single shaft
- there are two compressors – the main compressor receives externally cooled fluid
- a flow split sends 42% of the flow to the recompression compressor
- there are two recuperators and the low temperature recuperator only receives the main compressor fluid on the cold side to avoid a pinch point
- the power cycle is indirect
- fluid properties vary greatly within the single phase cycle
- there are three turbomachines: an axial turbine and two radial compressors
- heat exchange occurs inside four printed circuit heat exchangers

6.1.1.1 Fluid Property Variation

Carbon dioxide shows rapidly varying property behavior near its critical point (30.978°C, 7.3773 MPa). This is one of the key enabling features for the S-CO_2 recompression cycle, but it presents challenges for modeling, and exhibits unique behavior during transients.

The cycle design points (component outlet states numbered 1 through 8 in Figure 6-2) are plotted on a density versus temperature diagram in Figure 6-3. The reader should note both the wide variation in densities within the cycle (for a single phase fluid) and especially note the very steep increase in fluid density at lower pressures as the fluid

nears its critical temperature. It should be apparent from the plot that a small change in fluid temperature or pressure at this point of the cycle results in a large change in fluid density.

This impression is further reinforced when one looks at other fluid properties such as isobaric specific heat. The cycle design points from Figure 6-2 are plotted on an isobaric specific heat versus temperature diagram in Figure 6-4. Compared to the density figure this property shows an even steeper rise as the fluid approaches its critical point.

Overall, the S-CO_2 recompression cycle appears well suited to the Generation IV reactor development effort. However, interest in this cycle has only recently been revived[3], and significant research needs to be carried out before its suitability can be confirmed. A key area requiring resolution is the dynamic behavior of the cycle.

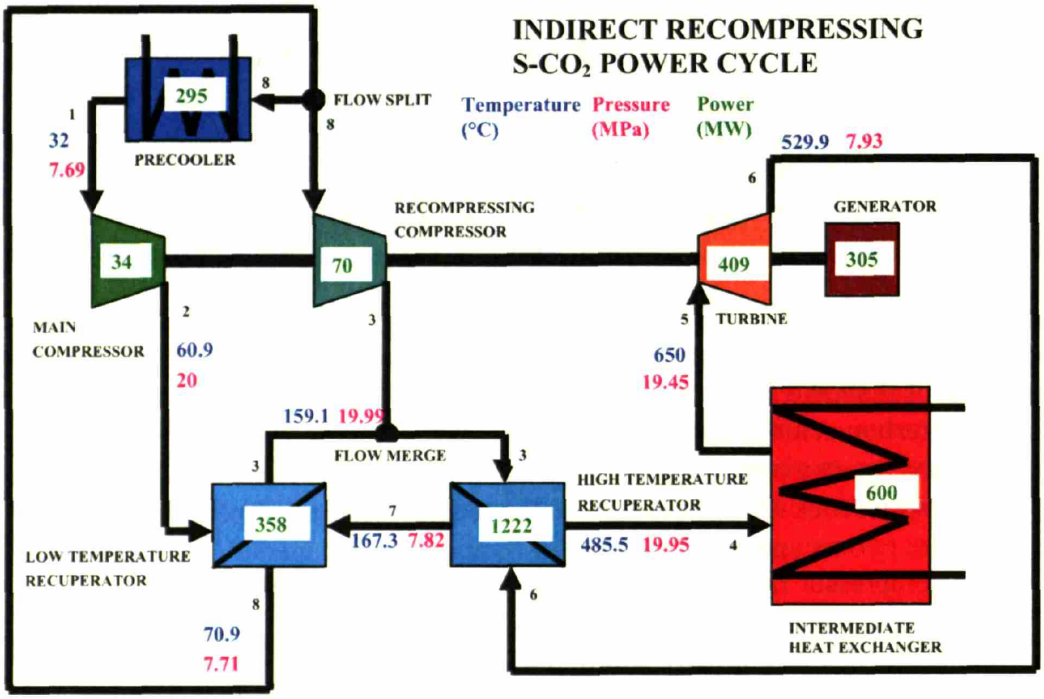

Figure 6-2: Indirect S-CO_2 Recompression Power Cycle

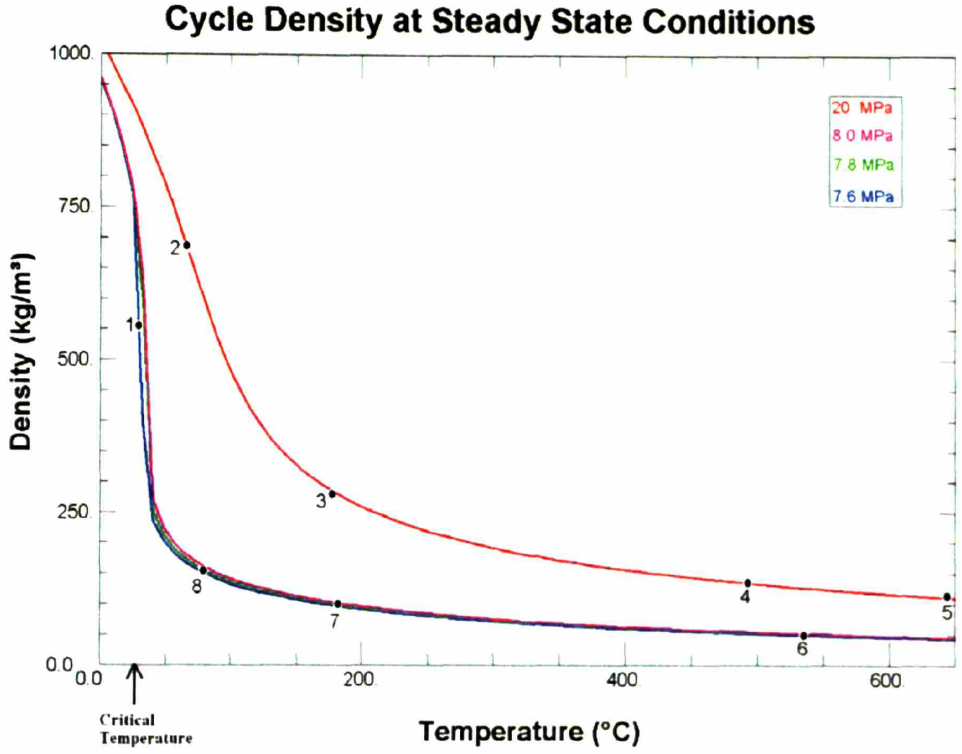

Figure 6-3: S-CO_2 Recompression Power Cycle Density vs. Temperature Diagram

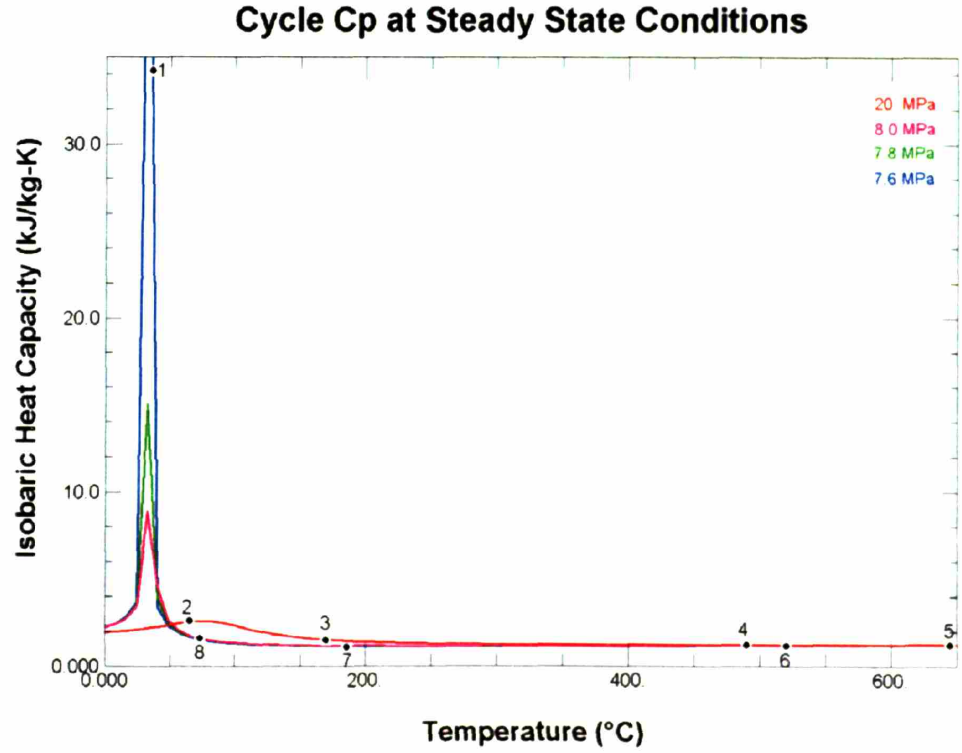

Figure 6-4: S-CO_2 Recompression Power Cycle Isobaric Specific Heat vs. Temperature Diagram

6.1.2 Dynamic Simulation of the Indirect S-CO_2 Recompression Power Cycle

Dynamic simulation of this cycle is complicated by its key features: single shaft constant speed turbomachinery, main and recompression compressor in parallel, operation of the main compressor inlet very close to the critical point, and, especially, the rapid fluid property changes surrounding the critical point. The significant property changes near the critical point are the primary reason that this cycle is more efficient than a helium power cycle at the same temperatures (and thus attractive) but they are also inherently complicating.

Many analyses have been carried out for Ideal Gas power cycles, especially helium, which share numerous characteristics – fluid properties change smoothly with pressure and temperature. Near carbon dioxide's critical point fluid properties respond in a highly non-linear manner that greatly complicate the behavior and modeling of most of the components in this cycle. These complications make many of the methods used to model the Ideal Gas cycle difficult, and frequently impossible, to use. The dynamic modeling of this new, non-linear cycle requires careful and significant development of methods to handle these issues.

Once this cycle can be realistically simulated, the questions of how it will respond to the many transients encountered in a real power plant arise. These questions will require designing and simulating a control system that allows safe and efficient operation of this unique cycle. Note that achieving high efficiency during part-load operation is a key control system consideration. This thesis is dedicated to the development of the necessary modeling methods to answering these questions as to its controllability.

6.1.3 Original Ideal Gas Simulation Code

The S-CO_2 recompression cycle has now been simulated with a greatly expanded and revised code, GAS-PASS/CO_2.* It is based upon Dr. Richard Vilim's (Argonne National Laboratory) ideal gas simulation code, GAS-PASS/H[4] (called GAS-PASS/He, for clarity, here) which will be briefly examined, since both codes share a common solution method.

GAS-PASS/He is intended for rapid assessment and appropriate placement of major system components based upon their dynamic response in a direct cycle helium nuclear power plant. To accomplish this mission GAS-PASS/He was constructed in a rapidly executable, modular, and flexible manner.

GAS-PASS/He is modular and flexible, allowing any number or order of (predefined) system components, because a defined component can be generally introduced throughout the plant. The set of defined components form a system of non-linear

* Gas Plant Analyzer and System Simulator (GAS-PASS).

equations which, along with the appropriate boundary conditions, is fed to a non-linear system of equations numerical solver. The solver uses a general Newtonian root solving technique that allows the user to change the order, number, and content of the conservation equations and variables at will.

A second part of GAS-PASS/He flexibility is the ability to interchange boundary conditions and variables. While the number of equations must match the number of unknowns, the user can readily exchange most variables for most boundary conditions. For example, if the external cooling loop is set up to provide a constant heat transfer, one can solve the system by fixing either the cooling loop mass flow rate or the cooling fluid incoming temperature; then the numerical solver determines the variable's value. Later the user can switch fixed heat rate and temperature. This allows the GAS-PASS/He user to rapidly solve the system for almost any behavior desired, which proves quite valuable for scoping calculations.

GAS-PASS/He uses a general Newtonian root-finding algorithm (a modified Powell-Hybrid method[49]), designed for non-linear systems of equations, to compute all variable values implicitly. The user specifies which inputs are variables, boundary conditions, and constants within the input deck. Once basic checks are performed, the solution process begins with a call to the numerical solver.

The numerical solver then calls a custom made function, *Fcn(x)*, which contains all of the equations necessary to solve the system at a time step. *Fcn* is organized by code modules which correspond to components within the system. Each component will contain one or more equations in the form:

$F(i) = Fcn_i(x)$

This must equal 0 to satisfy the system. Typically these equations are conservation laws or the output variables of other subprograms which apply conservation laws. In any case, these equations take the variable, x, inputs supplied by the numerical solver, and evaluate the given equation. The solver then compares the error of the solution to the change in the x inputs and modifies the variables accordingly, until tolerance is reached.

The numerical solution process is fully implicit, with iterative refinement of the user-specified variables at each time step until the system of equations is within tolerance of the system root, as outlined below:

1. At time $t_i > t_{i-1}$
2. Take X_i inputs from X_{i-1} (temperature, work ...), an initial guess
3. Calculate Jacobian (see Figure 3-1)
4. Use Jacobian to guess new X_i
5. Evaluate $F(X_i)$
6. Repeat (3), (4), and (5) as necessary to find system solution

$$J = \begin{bmatrix} \frac{\partial F_1}{\partial x_1} & \frac{\partial F_1}{\partial x_2} & \cdots & \frac{\partial F_1}{\partial x_n} \\ \frac{\partial F_2}{\partial x_1} & \frac{\partial F_2}{\partial x_2} & \cdots & \frac{\partial F_2}{\partial x_n} \\ \vdots & \vdots & \vdots & \vdots \\ \frac{\partial F_m}{\partial x_1} & \frac{\partial F_m}{\partial x_2} & \cdots & \frac{\partial F_m}{\partial x_n} \end{bmatrix}$$

Figure 6-5: Jacobian

The fundamental conservation equations are quite simple, as shown in Equation 6-1 through Equation 6-3. Note that Equation 6-3 is included solely to indicate that the momentum equation contains a significant assumption.

The momentum equation is reduced to quasi-steady state pressure drop calculations. This allows a significant simplification of the solution with a relatively small loss of accuracy in flow dynamics. Note that this dictates that GAS-PASS/He cannot be used to accurately analyze rapid (roughly less than a second) fluid inertia effects.

Equation 6-1: Mass Conservation Equation **(6-1)**

$$\frac{\partial M}{\partial t} = \dot{m}_{in} - \dot{m}_{out}$$

Equation 6-2: Energy Conservation **(6-2)**

$$\frac{dE}{dT} = \dot{E}_{in} - \dot{E}_{out}$$

Equation 6-3: Simplified Momentum Equation -- Pressure Drop **(6-3)**

$$dP^{time} = \Delta P^{time}_{calculated}$$

GAS-PASS/He required significant updating before it could be applied to the S-CO_2 recompression cycle. To simulate this cycle GAS-PASS/He required:

1. The ability to very accurately and very rapidly simulate a wide variety of real fluid properties. GAS-PASS/He used a very simple equation of state, which is not possible for carbon dioxide in this application.
2. The ability to accurately model complex turbomachinery performance. Ideal gas turbomachinery perform in a relatively simple and smooth manner that may allow a single simple polynomial to describe their behavior. This was the approach taken by GAS-PASS/He, but the behavior of S-CO_2 recompression cycle turbomachinery, while still uncertain in many respects, is significantly more complex.
3. The ability to accurately and rapidly model printed circuit heat exchangers was lacking. Due to the rapidly varying fluid properties encountered with S-CO_2, traditional simplifications such as log-mean temperature, the approach used in

GAS-PASS/He, are not appropriate. Therefore the developer must nodalize and iteratively solve this component, which rapidly becomes computationally prohibitive.

4. Numerous modifications to allow the solution process to converge the numerical system. Due to the inherently more non-linear nature of the S-CO_2 recompression cycle, using a Newtonian numerical solver presents numerous problems not seen in ideal gas applications. GAS-PASS/He required several basic modifications to make this cycle more readily solvable, and numerous computational methods to make the solution process more robust before the S-CO_2 recompression cycle could be simulated.

Overall, GAS-PASS/He performed its function well and contains several features that made its adoption for the S-CO_2 recompression cycle attractive. The process of updating and expanding the code was non-trivial and a major focus of the present work.

6.1.4 Modeling Real Fluid Properties

The ultimate source of real fluid properties for GAS-PASS/CO_2 is the NIST RefProp code[25]. The NIST RefProp code combines experimental data about a fluid into an equation of state which can be used to accurately calculate a variety of fluid properties – the current code version offers over 50 different fluids and many of their mixtures. Note that RefProp required an update (as part of this work) to its root solving techniques to achieve convergence in the highly non-linear region near carbon dioxide's critical point.

The benefits of the NIST RefProp code come at the cost of considerable complexity and therefore slow runtime. When GAS-PASS/He was originally updated to allow real fluid properties it used RefProp directly. Unfortunately, this slowed code runtime by quite a few orders of magnitude. While runtime isn't a primary concern, GAS-PASS is designed as a rapid scoping tool and this large an increase in runtime would negate much of its rationale.

The solution adopted for GAS-PASS/CO_2 is to pre-compute fluid property data and store it in tabular form. The user can still have the flexibility to create tabular data for any fluid or fluid mixture and can create tables with any input or output properties. Tables also offer the advantage of easily combining disparate property sources, such as simple liquid sodium polynomials, with the very complex RefProp carbon dioxide Helmholtz equation of state. Finally, tables offer the advantage of unrestricted distribution, whereas NIST RefProp is a commercial code. Eventual use for real time calculations as part of an automated control system also argues strongly for speed-up.

While linearly indexed tables work well with water and liquid sodium, unsurprisingly, the highly non-linear behavior of S-CO_2 properties leads to difficulty when used with linearly indexed tables. The first CO_2 tables were linearly indexed, and numerical problems were encountered during simulation that prevented solver convergence. Upon investigation it was discovered that during the calculation of the main compressor outlet pressure the

property tables were creating significant errors -- over 1 MPa in pressure at the outlet of the main compressor.

The reason for this error can be visually seen in Figure 6-6. Despite using millions of data points in the property table, the non-linear behavior of the fluid properties in the main compressor required a much tighter table spacing to avoid large property conversion errors when converting from values of enthalpy and entropy to pressure. Unfortunately, tables with this tight of a grid spacing would be far too large to be practical.

Using a variable mesh could effectively solve this problem at the cost of requiring a searching routine to find the appropriate position in the table. The large increase in computation time (compared to indexed tables) would remove much of the advantage of using tabular data in the first place. Log-indexed property tables offer many of the benefits of both methods, with few drawbacks.

If one were to plot the desired number of data points versus property value it would create a function that, beginning at the critical point, bends sharply upward, then tapers off towards a limit. The most common simple function that resembles this shape is a natural log.

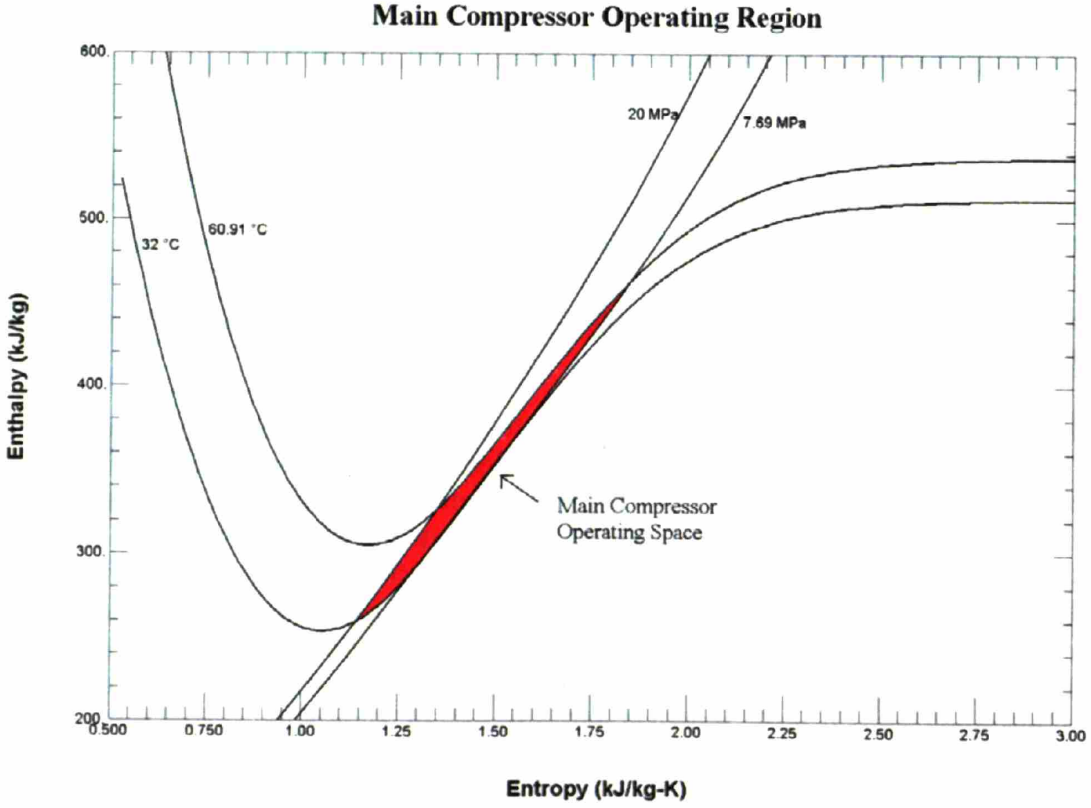

Figure 6-6: Main Compressor Enthalpy vs. Entropy Operating Region

By tailoring three coefficients, α, β, γ, to each type of fluid property table, super and sub-critical carbon dioxide property tables were created. An example of the equation used to create a supercritical property table is shown in Equation 6-4, and a plot of how this equation was applied to supercritical carbon dioxide pressures is shown in Figure 6-7. Thus, carbon dioxide tables appropriate to the S-CO_2 recompression cycle were created, which put the vast majority of the tabular data near the critical point and are computationally efficient.

Equation 6-4: Number of Data Points as a Function of Supercritical Property Value **(6-4)**

$$N_p = \alpha * \ln(P^*) + \beta$$

$$P^* = P - \gamma$$

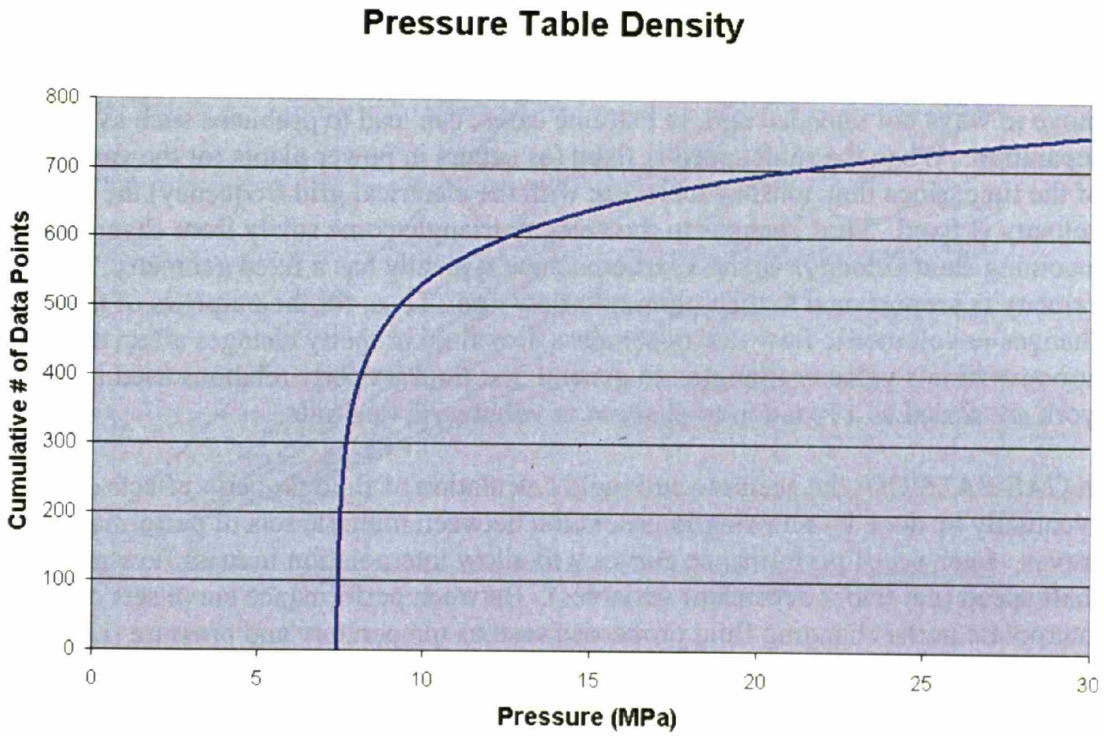

Figure 6-7: Supercritical Pressure Table Data Density

6.1.5 Modeling Turbomachinery Performance

The turbomachinery in this power conversion cycle is quite different from that encountered in typical Brayton Cycles. Compared to Ideal Gas Brayton Cycles these turbomachines have a large mass flow rate, a significant bending stress, a small Mach number, and are very compact[13]. Due to the higher "*density of CO_2, the specific enthalpy*

change is much smaller, given a pressure ratio. That translates into reduced compression work and the potential for higher efficiency."[13]

Due to the complexity of modeling turbomachinery, GAS-PASS/CO_2 uses pre-computed performance curves to estimate turbomachinery performance. This has the advantage of removing a significant computational burden from the transient code, as well as allowing rapid changes to turbomachinery, such as switching from radial to axial turbomachines, by simply switching input files. Furthermore, it allows more realistic experimental data to be easily introduced into simulations as this data becomes available.

Handling fluid property effects in turbomachinery for the S-CO_2 recompression cycle is non-trivial, and a key source of uncertainty in this work. Typical turbomachinery fluid property theory may not be applicable, as the density and other properties of S-CO_2 change significantly within the cycle.

Note that the gas flow velocity triangle between the blade and fluid vector is a critical factor in turbomachinery performance. Changes in these vectors force the gas flow to move in ways not intended and, in extreme cases, can lead to problems such as gas flow separation. When the shaft speed is fixed (as occurs in power plants for the vast majority of the time, since they must synchronize with the electrical grid frequency) the tangential velocity is fixed. Thus changes to the velocity triangle come solely from changes to the incoming fluid velocity. Since a turbomachine typically has a fixed geometry, the fluid velocity is proportional to the volumetric flow rate. Thus, for the purposes of this work, changes in volumetric flow rate encompass how fluid property changes affect a turbomachine's velocity triangle. In general, the fluid property relations used in this work are scaled as a function of changes in volumetric flow rate.

In GAS-PASS/CO_2 the accurate and rapid calculation of fluid property effects could eventually be done by allowing interpolation between multiple sets of performance curves. Each set of performance curves will allow interpolation in mass flow rate and shaft speed (i.e. two independent variables). Between performance curve sets one could interpolate in the changing fluid properties such as temperature and pressure (i.e. an additional two independent variables).

Unfortunately, these sets of performance curves are not currently available. As turbomachinery modeling codes evolve to incorporate S-CO_2, and as experimental data are generated, these performance curve sets can be incorporated into GAS-PASS/CO_2. Until then, fluid property effects will be approximated using two basic relations, which approximate the fluid property effects in the compressors and turbine.

Near the main compressor the fluid is quite dense (roughly 720 kg/m^3 at the outlet), but the fluid can still be quite sensitive to pressure changes due to its proximity to the critical point (at the compressor inlet), as shown in Figure 6-8. This figure shows the main compressor operating range, with constant density lines on a pressure versus temperature diagram. At the main compressor's outlet the constant density lines have a relatively

large spacing compared to the inlet, where the lines converge at the two-phase dome (note that two-phase values are not shown).

Compared to the main compressor, the recompression compressor operates at significantly lower densities and farther from the converging constant density lines near the critical point. The turbine operates well above the critical point in a quasi-ideal region (at steady state the turbine fluid's isobaric specific heat changes by less than 5% and γ, the ratio of specific heats, varies by less than 1%). Thus the turbine will be approximated employing ideal gas relations, while the compressors will be approximated using incompressible fluid relations. These approximations, especially in the main compressor, should be removed as experimental data become available.

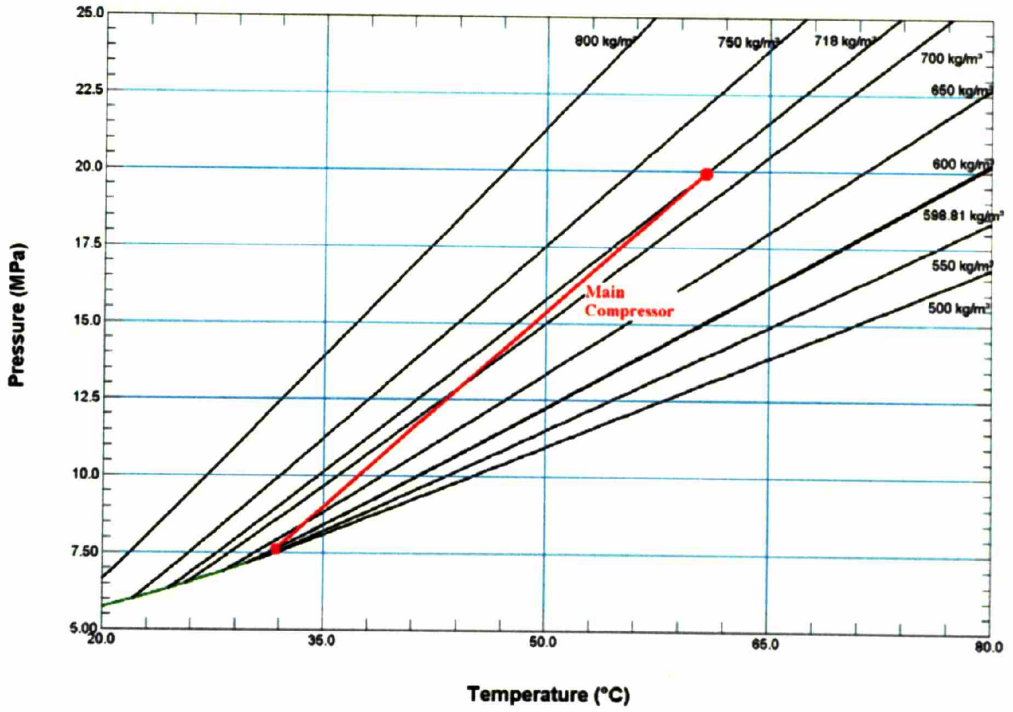

Figure 6-8: Main Compressor Operating Path Showing Pressure vs. Temperature and Iso-Density Lines

6.1.6 Modeling Printed Circuit Heat Exchangers

The S-CO_2 recompression cycle's advantageous performance is greatly enhanced by using high efficiency, yet compact, heat exchangers to significantly recuperate the cycle. This cycle's design[3] takes advantage of new heat exchanger technology in the form of printed circuit heat exchangers (PCHEs) developed by Heatric™.

Unfortunately, while the large CO_2 property variations in this cycle allow high efficiency, they also complicate standard analysis assumptions. This is especially true in the heat

exchangers, where standard procedures like log-mean temperature heat transfer are not valid due to non-linear variations in fluid properties. An example of this property-nonlinearity is shown in Figure 6-23, which shows the steady state isobaric specific heat profile in the precooler. While the water isobaric specific heat profile is constant, the carbon dioxide profile shows a large peak, which must be accurately modeled to simulate a PCHE.

If one assumes that a PCHE is adiabatic and receives perfectly mixed fluid from the plena, then one may model the heat exchanger using just one hot and one cold channel. Dostal[3] further showed that one may accurately model these single channels with one-dimensional flow with little loss of accuracy. From this point one may model the whole PCHE by axially nodalizing the heat exchanger and iteratively solving for the counter-flowing fluid's temperature, pressure, and mass flow rate based upon an initial guess at one side of the heat exchanger. Unfortunately, even this simplified solution method was far too computationally expensive for use in GAS-PASS/CO_2. The incorporation of this PCHE solution method slowed the solution process by orders of magnitude.

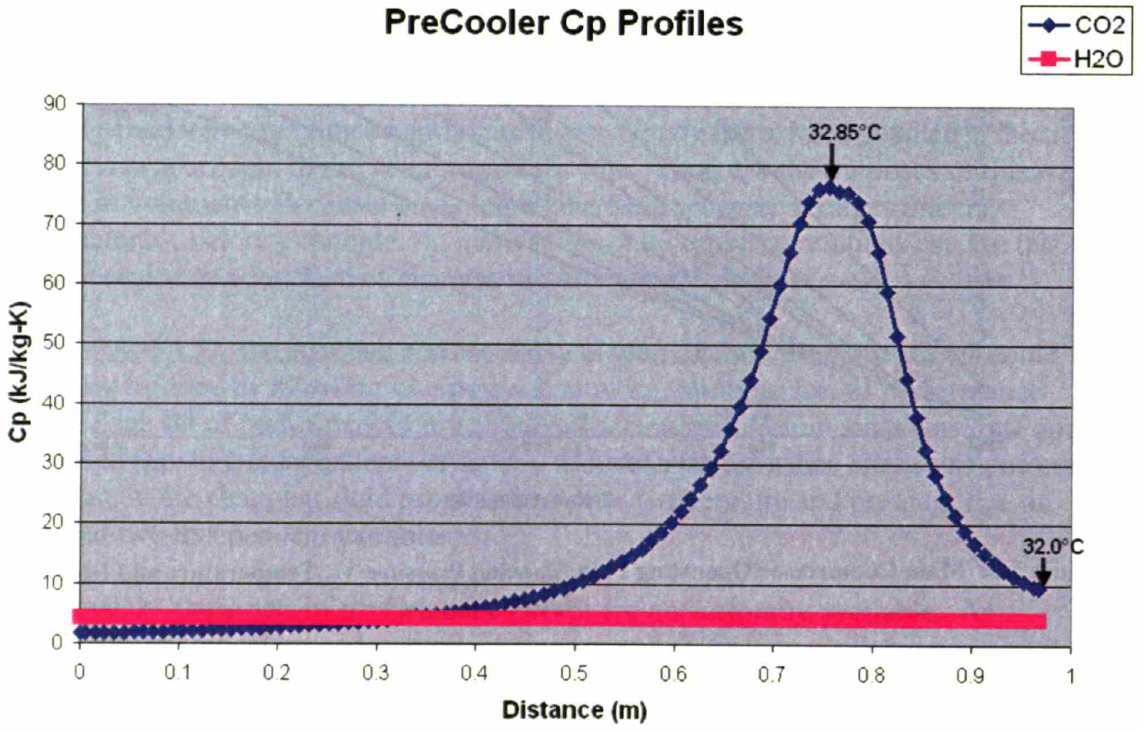

Figure 6-9: Precooler Isobaric Specific Heat Profiles

One may exploit a careful understanding of the problem to greatly speed the calculation of PCHE performance. Examples of the estimated speed-ups due to the various factors are as follows.

Starting with the axial 1D nodalized code:

- Using enthalpy instead of temperature and calculating at the node midpoint instead of at the beginning of the node allows one to reduce the number of computational nodes from approximately 40 to approximately 2 for the same accuracy, therefore a 20 fold speed-up. While temperature can be highly non-linear within a PCHE, enthalpy and pressure are both almost linear, even in the precooler, thus using the midpoint values for these variables provides an accurate node-average value even when few nodes are used.
- Using node memory to speed-up PCHE calculations decreases runtime about 10x. The convergence process from initial guesses to accurate pressure drops, heat transfers, and mass storage effects is computationally demanding. Using the previous solution as an initial guess removes much of the initial convergence work.
- Avoiding the outer three iteration loops speeds up the PCHE calculation by about 50x. A standalone counter-flow heat exchanger calculation requires an iteration to solve the PCHE, an iteration loop to correct for counter-flowing fluid's mass storage, an iteration loop to correct for counter-flowing fluid's temperature change, and an iteration to correct for the counter-flowing fluid's pressure drop. Since this solution process is already inside a general numerical solver, the three outer iteration loops can be neglected by solving from only one side of the PCHE.
- Avoiding unnecessary PCHE solutions, especially during Jacobian calculation, speeds the solution process by about another order of magnitude. Most solution variables do not directly affect other component's equations (e.g. the Jacobian is sparse) thus one can simply avoid reevaluating a component if the inputs do not change.

Thus the PCHE calculation process has been sped up by roughly a factor of 10^5 without any loss in accuracy. Since the PCHE is, by far, the most computationally demanding component in GAS-PASS/CO_2, the overall code runtime is proportional to the PCHE sub-module runtime.

6.1.7 Improved Real Gas Simulation Code

GAS-PASS/CO_2 represents a comprehensive update to GAS-PASS/He. It retains the original code structure and solution process but has been rewritten on a line by line basis where original code was retained, and the majority of the current code was written from scratch. The current code is about 24,000 lines of Fortran 90 in 27 source files.

GAS-PASS/CO_2 now includes all real fluid properties, detailed turbomachinery performance, interpolation with correction for fluid property effects, and detailed PCHE heat transfer and pressure drop calculations.

While tailored to the S-CO_2 cycle, the code is modular and general, allowing the end user to change almost any part of the plant simply by modifying simple text input files. New capabilities will, of course, require modifying the source code, but the end user could easily change the current code to something quite different without coding. For example,

the current model could be converted to a helium plant, heated by lead bismuth, with a radial turbine, and axial-radial hybrid compressors without editing the source. The major task to creating new plant designs is creating and combining new component input files.

Due to the general nature of the fluid properties code, any fluid that can be pre-computed and put in tabular format can be used. Due to the general nature of the turbomachinery methods, any design that offers sets of shaft speed curves can be modeled. Due to the general nature of the heat transfer code any type of straight-channel PCHE can be modeled for any set of fluids (assuming the current heat transfer and pressure drop correlations may be used). These capabilities should place GAS-PASS/CO_2 in an excellent position for future use.

However, converging the S-CO_2 recompression cycle in GAS-PASS/CO_2 initially proved quite difficult. This was expected given the strong non-linearity in the S-CO_2 properties near the critical point, where parts of the cycle operate. The process of overcoming the convergence problems have made GAS-PASS/CO_2 quite robust compared to past versions of GAS-PASS/He. Previously, the failure of almost any process during simulation would lead to simulation failure. Numerous modifications have been made to allow GAS-PASS/CO_2 to continue with a simulation, for as long as is reasonable, even if computation becomes difficult.

GAS-PASS/CO_2 now uses several major techniques to improve convergence including:

- Jacobian scaling. In a non-linear system the proportional region surrounding the root can be quite small. Thus, a Jacobian may greatly overestimate the distance to the root if it is taken outside of the proportional region – a two dimensional example of this is shown in Figure 6-12. GAS-PASS/CO_2 minimizes this problem by automatically scaling the (whole) Jacobian by an increasing factor if out-of-bounds flags are detected.
- Variable solution tolerance. If the user-specified default tolerance is not met and no extrapolation errors have been detected, then GAS-PASS/CO_2 will inform the user it is having trouble and attempt to converge with a looser tolerance. This process is repeated until the solution converges, or until a very large tolerance is not met and the calculation fails.
- Non-physical numerical extrapolation. During the solution process tight performance bounds, such as known turbomachinery mass flow rates, may be exceeded during the search for the system root. To avoid solution failure, dummy values (which show poor performance) are provided to inform the solver that the root is not in this region. This method is only used during the root seeking process, and is not used in a final solution.

A key part of the convergence process has been modeling components in a manner that promotes a linear solution process. Techniques such as avoiding dissimilar fluid volumes, expressing turbomachinery maps in variables directly related to the carbon dioxide equation of state, and, especially, solving in enthalpy instead of temperature have lead to the expression of the S-CO_2 recompression cycle in a more linear fashion -- this is clearly shown in the systems' Jacobian. Figure 6-10 shows the Jacobian of the S-CO_2

recompression cycle when it was first modeled. Large peaks suggest that small changes in the solution variables produce large changes in the solution equations. Figure 6-11 shows a GAS-PASS/CO_2 Jacobian where the final-version model has been designed to promote system linearity. The reader will note that there are many fewer peaks, that are much smaller in magnitude. Promoting system linearity at the model level is one of the features that enables GAS-PASS/CO_2 to solve this cycle.

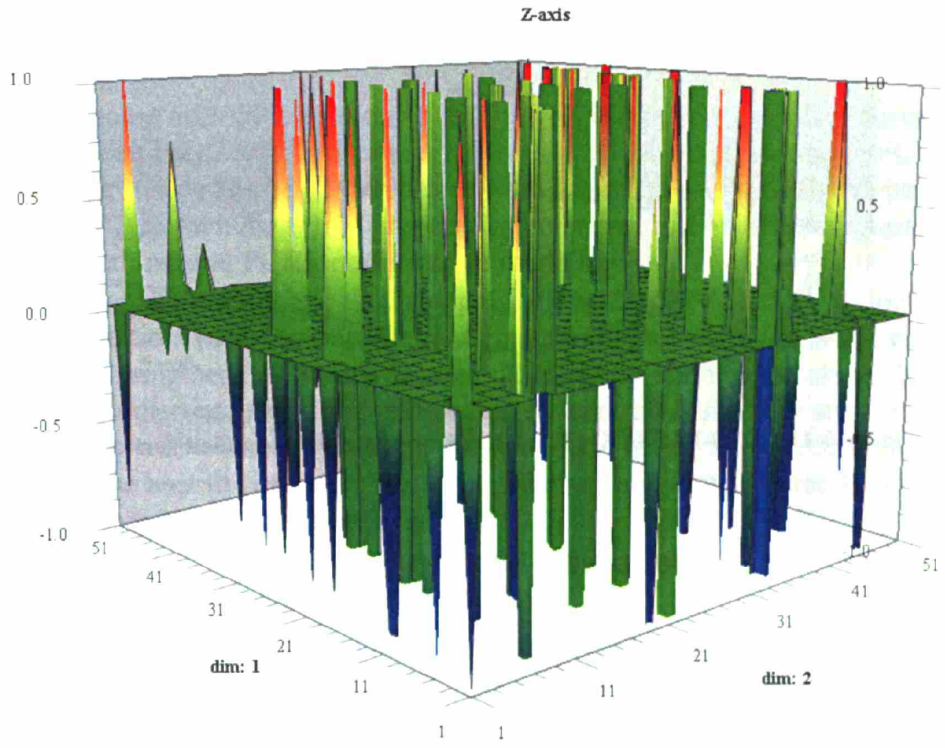

Figure 6-10: GAS-PASS/CO_2 Original Jacobian

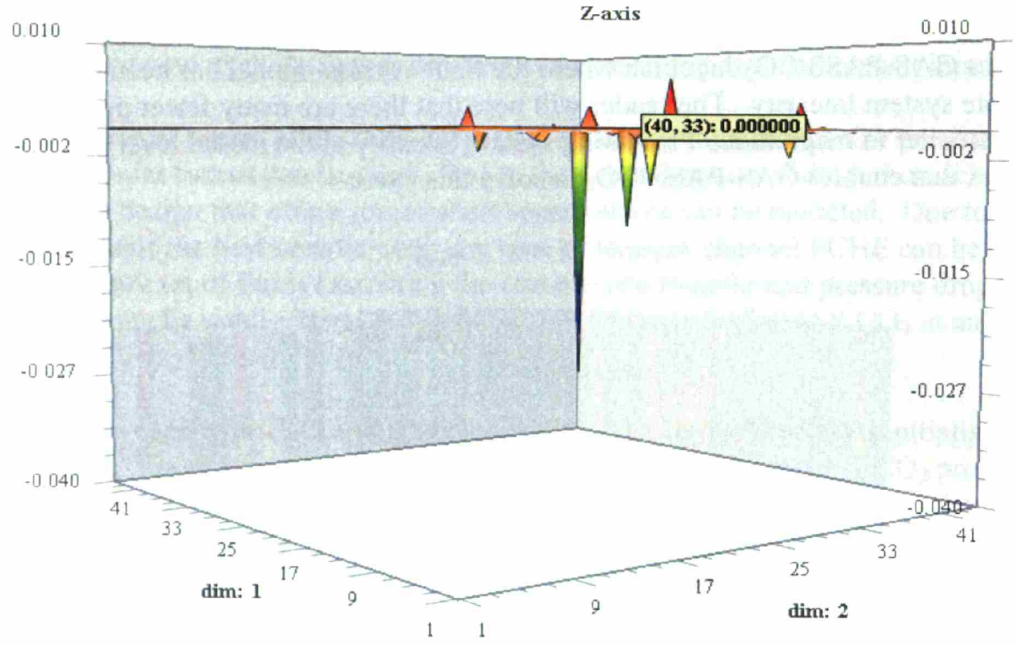

Figure 6-11: GAS-PASS/CO_2 Final Jacobian (note the expanded vertical scale)

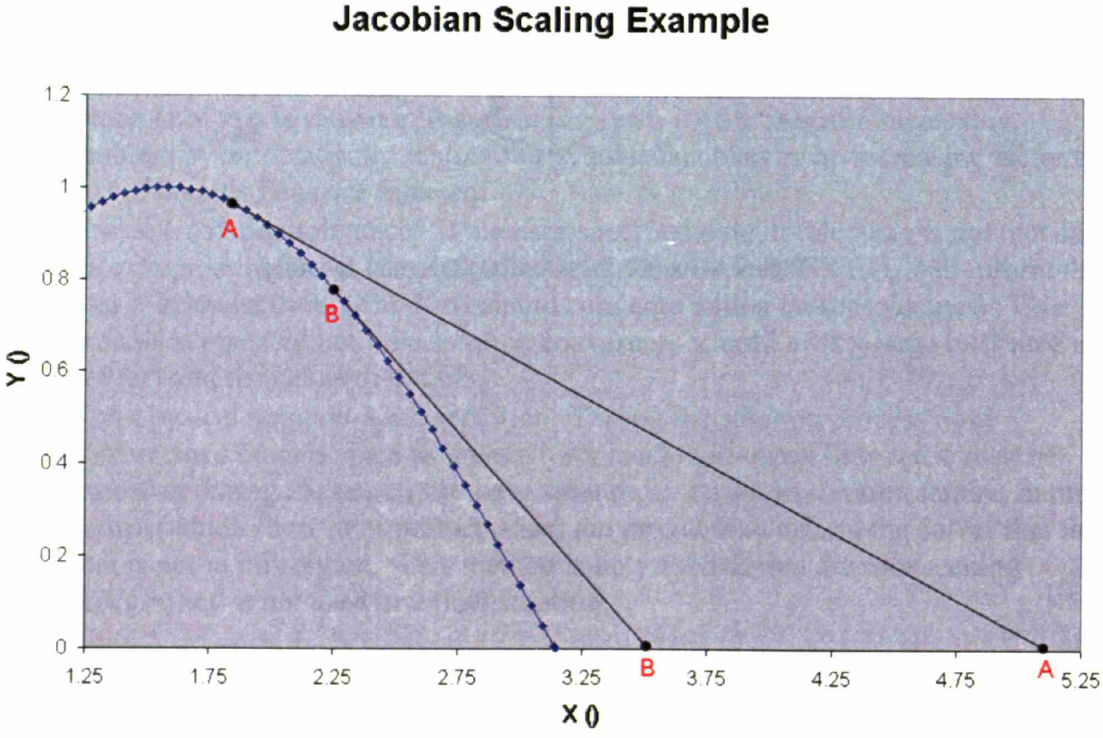

Figure 6-12: Jacobian Scaling Example

The final modifications to GAS-PASS/CO_2 generally focus upon methods to improve runtime. While the vast majority of code optimization occurred at the module level, several techniques were generally applied at the overall code level:

- Avoiding repeated evaluation of unchanging Jacobian elements. When a Jacobian is evaluated, every unknown variable is perturbed one at a time and the impact of each perturbation on every conservation equation within the system is calculated. The majority of the equations are not directly affected by perturbations in a variable, thus creating a sparse Jacobian. A typical GAS-PASS/CO_2 Jacobian is approximately 93% sparse.

  By placing a simple check on unchanging inputs to sub-modules (during a time step), one may confidently avoid useless reevaluation of sub-modules. This wrapper check has been placed on all the computationally intensive parts of GAS-PASS/CO_2, including fluid property calculations, turbomachinery performance calculations, and PCHE performance modeling.
- User controlled dynamic time stepping allows GAS-PASS/CO_2 to focus computational steps on rapidly changing parts of a simulation while minimizing effort during periods of little change. Depending on the simulation, this can lead to the numerous small time steps being concentrated in a very small time frame, and only a few time steps over a long period of time. This method can easily allow the user to simulate a transient orders of magnitude faster than would be possible with constant time steps.

6.1.8 Simulation Code Conclusion

GAS-PASS/CO_2 represents a comprehensive improvement to the GAS-PASS/He code. While designed for use with the S-CO_2 recompression cycle, it is widely applicable to generic indirect gas cycles. The flexibility and accuracy of the fluid property, turbomachinery, and heat exchanger models allow rapid yet accurate assessment of a wide variety of cycle designs.

GAS-PASS/CO_2 has also been significantly improved for the user. The code as been updated to modern coding standards and almost all the model features have been moved to simple text input files. The input format is general, thus allowing the user to specify the number of components and their location on the fly without editing the Fortran source code. When combined with the original flexibility of the GAS-PASS/He design this allows the user to rapidly alter component designs, layouts, and even fluid choices.

During the process of applying a Newtonian solver to the S-CO_2 recompression cycle, GAS-PASS/CO_2 was made significantly more robust. Various techniques such as Jacobian scaling, numerical extrapolation, and variable solution tolerance provide the ability to overcome many of the difficulties found when applying a first derivative solver to a highly non-linear system.

Significant effort has also been applied to promote computational efficiency. GAS-PASS/CO_2 uses numerous techniques to promote speed-up, ranging from a non-linearly

indexed fluid property table format to avoiding repetitive calculations in a sparse Jacobian. The overall result of these efforts is that GAS-PASS/CO_2 can simulate the S-CO_2 recompression cycle faster than real time (even without dynamic time steps) on a modern computer.

Overall, GAS-PASS/CO_2 meets its design goal of rapid cycle scoping and control system design for a wide variety of future gas cycles, including the S-CO_2 recompression cycle.

6.1.9 S-CO_2 Recompression Cycle Basic Control System

The S-CO_2 recompression cycle was successfully simulated for a variety of transients using GAS-PASS/CO_2 by employing a basic set of controls. These controls provide appropriate plant response during part-load operation, and loss-of-load events in particular. The basic controls used are shown in Figure 6-13.

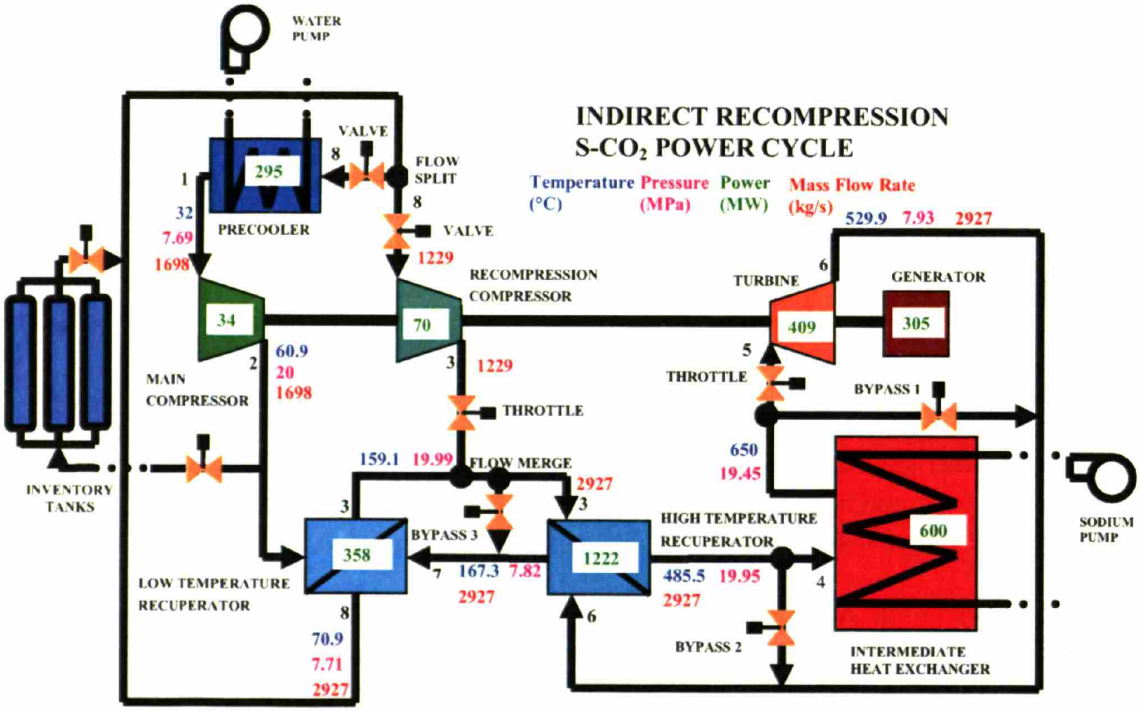

Figure 6-13: Indirect S-CO_2 Recompression Power Cycle with a Basic Control System

The controls shown in Figure 6-13 are:

- The flow split valves before the compressors. These variable valves are used to introduce a slight pressure drop to control the mass flow split going to the compressors. They can be operated in a completely open position, allowing each of the compressors to balance mass flow rates by matching outlet pressure, or one valve can be used to introduce a pressure drop until the desired mass flow rate split is achieved. Since the operator may need to introduce a pressure drop for

either compressor, depending upon desired operational parameters, one valve on each line is needed even though only one operates at any given time.

- A variable throttle is needed after the recompression compressor. If a flow split is maintained across the compressors, which does not match outlet pressures, then a throttle is needed to drop the higher outlet pressure to match the lower outlet tee pressure to prevent flow stoppage in the lower pressure line. In all observed cases the recompression compressor has achieved higher pressure than the main compressor, thus the throttle is needed only downstream of the recompression compressor. If unforeseen needs arise, then a throttle may be required after the main compressor as well.
- Valves are needed at the inlet and outlet of the inventory control tanks. The optimization of inventory control with this cycle is an area of active research[62] but in the current version of GAS-PASS/CO_2 the ability to add and remove up to 100 kg/s during part-load operation was assumed (typical removal rates are less than 10 kg/s during inventory control). The valve locations are also an area of research, but the outlet of the main compressor is a high pressure and low temperature location within the cycle, thus suggesting its use for an inventory control vessel inlet. The precooler inlet is suggested for the inventory control vessel outlet, since the precooler inlet is nearly the lowest cycle pressure, and the precooler will act as an attemperator for the main compressor, whose performance is quite sensitive to temperature.
- The bypass valves are used for rapid power changes, such as loss-of-load. Each of the three bypass valves (labeled 1-3) offer different advantages and drawbacks. Future research should establish optimal usage methods for one or more of these valves. However, each bypass valve works similarly, by bypassing part of the flow around the turbine, thus reducing the amount of work added to the shaft, and increasing the flow to the compressors, thus removing more work from the shaft.
- The turbine inlet throttle can be used to decrease the pressure ratio available to the turbine to perform work. This is another means to allow part-load operation.
- The water pump is used to control the amount of energy removed from the cycle in the precooler. The pump is used to vary the water mass flow rate, primarily to control the CO_2 outlet temperature. Note that the water temperature may need to increase during low power operation, which can be accomplished by a recirculation loop on the water side.
- The sodium pump is used to control the temperatures of the liquid sodium in the IHX. Typically, it is used to proportionally match sodium mass flow rate to reactor power. By keeping these values proportional, the sodium inlet and outlet temperatures are held close to the steady state value.

Note that this list does not include several other possible control systems or the detailed control systems required within components. For example, an S-CO_2 compressor may need a complex control system including temperature control and recirculation loops within the compressor[38,40] to provide stable operation. In the present work note that recirculation loops have not been provided for the compressors. This common control technique (employed to help prevent surge) was not needed for the transients analyzed in this work. They would likely prove useful during LOL transients when the shaft rapidly

gains excess work. Recirculating compressor flow would create additional shaft work. Recirculation loops should be added to the system model to prevent compressor surge in any case.

6.1.10 Simulation Results

Part-load operation and the loss-of-load transient have been analyzed for the S-CO_2 recompression cycle. The focus of these simulations was investigating the ability to control these operations and transients.

6.1.10.1 Part-load Operation

Operating the S-CO_2 recompression cycle at part-load is more complex than in ideal gas plants due to non-linear changes in fluid properties at off-normal temperatures and pressures, especially as these effects interact with parallel compression. The net result is that this plant requires careful control to prevent turbomachinery performance failure.

Four typical control methods* are used to enable part-load operation:

- Inventory Control
- Temperature control
- Throttling
- Bypass

Each method has advantages and disadvantages, but several general features should be compared.

The net cycle efficiency of each method is shown versus nominal generator power in Figure 6-14, as calculated using GAS-PASS/CO_2. This figure shows that combined inventory and low temperature control is the most efficient operation method, and is available over almost the full operation range of the cycle. The efficiency of this method changes significantly when the flow split changes, and the cycle low pressure begins to drop quickly near 50% generator power, and drops rapidly near the minimum mass flow rate on the turbine performance map. This promising method suffers from several concerns:

- The fluid property effects on the main compressor in the near critical region are uncertain. If handled incorrectly these effects may cause pressure oscillations, leading to serious cycle problems. This may require relatively complicated adjustments of the main compressor inlet temperature to avoid rapid fluid property changes.
- Inventory control is a slow acting control method, and thus is unsuitable for rapid power changes.

* Note that shaft speed control is not an option during power operations, since all the turbomachines are connected to the generator, which must be synchronized to the electrical grid.

- Inventory control requires potentially large control tanks and may require an additional compressor to move fluid rapidly. These concerns were not addressed in this work.

Turbine inlet throttling is the second most efficient control method, and operates between, roughly, 100% and 27% generator power before the turbine moves below known mass flow rate bounds on the turbine performance map. It features a smoothly sloping efficiency curve over its range and should be relatively easy to implement, since it requires only a single throttling valve. However, this valve may be expensive due to the size of the pipes used in this near-ideal-gas region, and the valve needs to accommodate throttling fluid at the cycle's high temperature.

Upper cycle bypass provides operation from at least 33% to 100% generator power and it is possible that it may extend to 0% power. Due to the relatively low temperatures and high densities seen at this bypass location, it is the preferred bypass method. However, the method presents a significant concern since, near 33% generator power in a quasi-static transient, a large and sharp pseudo-critical fluid property peak will enter the main compressor.

High temperature control is the fourth most efficient operation method, and provides control from full to slightly above 50% generator power. It shows a smoothly sloping efficiency curve over its operation range. This method of control is unlikely to be used in actual plant operations due to the large temperature changes required in the high temperature part of the cycle, including the reactor.

The turbine and IHX and turbine bypass methods are the least efficient methods, but readily extend from 0 to 100% power. The turbine and IHX bypass method prevents the HTR inlet from approaching very close to the cycle high temperature, but deprives the IHX (and reactor) of cooling fluid.

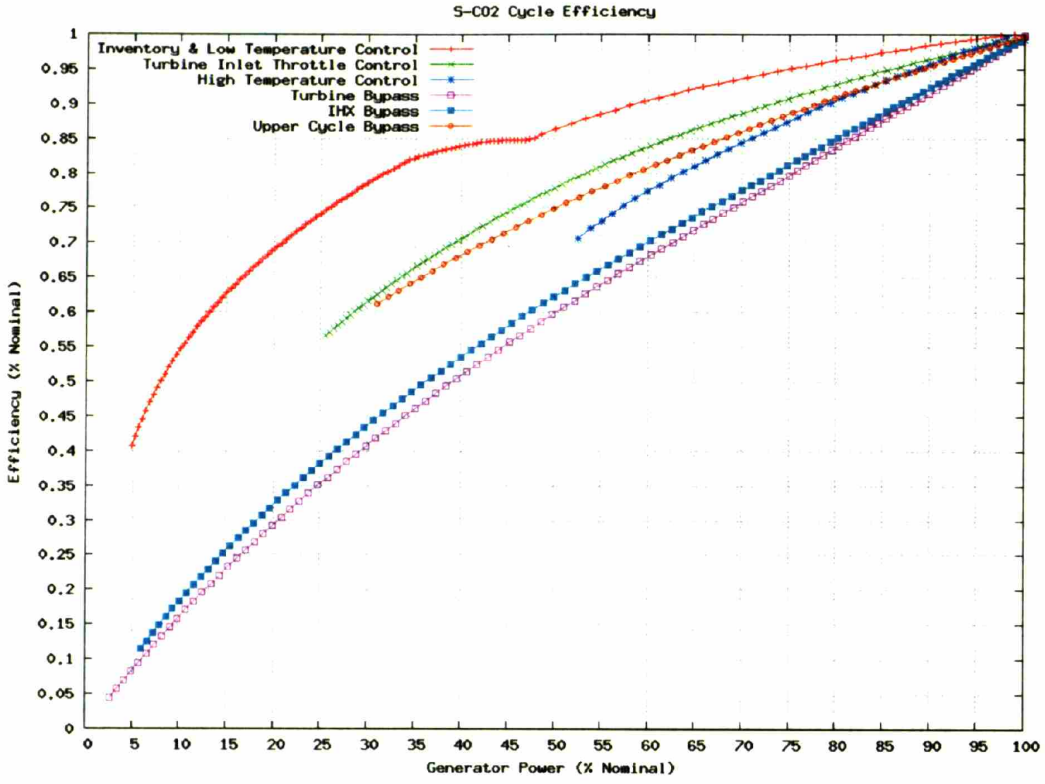

Figure 6-14: Net Cycle Efficiency versus Nominal Generator Power for Part-load Operation

6.1.10.2 Inventory Control Issues

Controlling the S-CO_2 recompression cycle presents unique problems and opportunities not seen in ideal gas cycles. In particular, part-load operation using inventory control may create undesirable turbomachinery behavior, which can be alleviated if cycle low temperature control is used as well. A set of procedures are proposed for part-load operation with inventory control for this cycle.

Inventory control removes fluid from the cycle to keep high efficiency during part-load operation. As fluid is removed, system pressure drops, which leads to lower fluid density and smaller mass flow rates. The smaller mass flow rates allow the same temperature difference (Carnot efficiency) at lower powers. In this cycle, non-linear fluid property effects dictate that, as system pressure drops, each turbomachine responds differently.

6.1.10.2.1 Non-Linear Density Change at Main Compressor Inlet

Main compressor performance is especially sensitive to pressure decrease due to its proximity to the critical point. The critical point of CO_2 is 30.978°C and 7.3773 MPa*, while the steady state main compressor inlet conditions are at 32°C and 7.69 MPa. As pressure drops, the inlet to this compressor moves through its pseudo-critical point and the incoming fluid density changes rapidly and significantly. Proximity to the critical temperature determines the magnitude of this change, as shown in Figure 6-15.

* According to NIST RefProp 7.0.

This figure shows several temperatures of interest and the liquid-vapor dome. The reader should note three key features in this graph:

- There are large density changes for relatively small pressure changes at the main compressor inlet. Starting at the design conditions the main compressor inlet density is 599 kg/m^3. If the fluid pressure drops to 7.3 MPa, then the inlet density drops by over a factor of two, to 288 kg/m^3. Note that a large density change will occur regardless of the temperature: on the right side of the dome fluid density is high while on the lower pressure left side of the dome the pressures are low.
- The isothermal lines on either side of the dome are nearly vertical. A perfectly vertical line would mean the fluid is incompressible during a pressure change. However, when lines cross over the dome they become more horizontal, especially as temperatures approach the critical temperature. This means the fluid is becoming more compressible with pressure changes. Therefore, there is a large and fundamental change in how the fluid behaves as it crosses over the dome, especially as the temperature approaches the critical temperature.
- The rate of density change versus pressure change becomes quite rapid when CO_2 approaches its critical temperature. The rate of (isothermal) density change per unit pressure is clearly shown in Figure 6-16.

Figure 6-16 shows a very large rate of density change versus pressure change close to the critical temperature. The magnitude of the peak decreases rapidly and the width of the peak spreads with increasing temperature. For example, at 31°C the main compressor inlet density would drop from 551.37 to 375.61 kg/m^3 (31.8% density change) between 7.39 and 7.37 MPa (0.2% pressure drop).

Large density changes will significantly affect main compressor performance -- especially pressure rise. The exact effects of these large non-linear density changes near the CO_2 critical point on a compressor are complex and uncertain at this time, since the performance maps are currently based on analytical models and numerical simulation and not yet supported by experimental data on actual compressors in the near critical region*.

However, it is certain that a large drop in the density of the fluid entering the main compressor will create a large drop in this machine's pressure rise†, especially near the critical temperature. The size and speed of the drop in pressure rise presents at least one significant concern: the change in pressure may produce pressure spikes in the system.

---

* Note that S-CO_2 compressors have been successfully operated and controlled while passing from subcritical to supercritical conditions.[38,39] However, in all known cases the critical point was avoided by a significant margin.

† As this density decrease happens to the main compressor, the cycle will respond with changing flow rates and, perhaps, a flow split change. It is not trivial to estimate the exact effect of fluid property changes on the main compressor due to this cycle feedback.

If the pressure rise drops quickly, then shock may be introduced to the system when an almost prompt drop in fluid density and pressure change move through the cycle. The compressor outlet pressures will not balance, and mass flow will significantly decrease in the main compressor as the flow through the recompression compressor rises to try to balance pressure*. Nearly simultaneously, the turbine will see a reduced pressure ratio and thus decrease its outgoing mass flow rate.

The combination of the main compressor, recompression compressor, and turbine nearly simultaneously making prompt changes in pressure ratio and mass flow rate may not be desirable. Furthermore, these effects may produce feedback which could make the system unstable.

GAS-PASS/CO_2 simulations using simple compressor off-density property relations show that the large and fast density changes experienced on the 32°C isotherm near the pseudo-critical point that result during inventory control can produce significant oscillation. At this time there is considerable uncertainty over the behavior in this region.

The concerns seen at 31°C are significantly alleviated when operating at 32°C. A similar change in density requires a change from roughly 7.6 to 7.5 MPa. Thus, a 1°C rise in compressor inlet temperature provides a density (and pressure drop) that is 500% less sensitive to pressure drop. For 33°C a similar density change requires a pressure change about 0.3 MPa and is about 300% less sensitive than the 32°C case.

The limiting temperature for which the main compressor can pass through its pseudo-critical peak will require detailed analysis of the effects of rapid density changes in this cycle, but it is clear that the designer can greatly alleviate the rate of change via small temperature increases. A preferred approach to isothermal operation is to use inventory control in combination with temperature control at the low-temperature end of the cycle.

6.1.10.2.2 Combined Inventory & Low Temperature Control

Due to the strong non-linear fluid property effects near the main compressor inlet, shown in Figure 6-15 and Figure 6-16, the designer has a significant and unique method of control available. Changing the cycle lower temperature (the main compressor inlet temperature) a few degrees has little direct affect on the cycle efficiency but a significant affect on the main compressor performance.

As the main compressor inlet pressure drops during inventory control, it experiences large changes in fluid properties, which decreases compressor pressure rise. If the designer keeps the main compressor inlet at a constant temperature during this process then the large fluid property changes are solely dependent upon the pressure.

---

* Note that if the system is operated with valves to control the flow split and a throttle to match the compressor pressure rise, then the change in conditions in the main compressor may not change the flow split depending upon how the control system on these valves is implemented.

If the pressure rise drops quickly, then shock may be introduced to the system when an almost prompt drop in fluid density and pressure change move through the cycle. The compressor outlet pressures will not balance, and mass flow will significantly decrease in the main compressor as the flow through the recompression compressor rises to try to balance pressure*. Nearly simultaneously, the turbine will see a reduced pressure ratio and thus decrease its outgoing mass flow rate.

The combination of the main compressor, recompression compressor, and turbine nearly simultaneously making prompt changes in pressure ratio and mass flow rate may not be desirable. Furthermore, these effects may produce feedback which could make the system unstable.

GAS-PASS/CO_2 simulations using simple compressor off-density property relations show that the large and fast density changes experienced on the 32°C isotherm near the pseudo-critical point that result during inventory control can produce significant oscillation. At this time there is considerable uncertainty over the behavior in this region.

The concerns seen at 31°C are significantly alleviated when operating at 32°C. A similar change in density requires a change from roughly 7.6 to 7.5 MPa. Thus, a 1°C rise in compressor inlet temperature provides a density (and pressure drop) that is 500% less sensitive to pressure drop. For 33°C a similar density change requires a pressure change about 0.3 MPa and is about 300% less sensitive than the 32°C case.

The limiting temperature for which the main compressor can pass through its pseudo-critical peak will require detailed analysis of the effects of rapid density changes in this cycle, but it is clear that the designer can greatly alleviate the rate of change via small temperature increases. A preferred approach to isothermal operation is to use inventory control in combination with temperature control at the low-temperature end of the cycle.

6.1.10.2.2 Combined Inventory & Low Temperature Control

Due to the strong non-linear fluid property effects near the main compressor inlet, shown in Figure 6-15 and Figure 6-16, the designer has a significant and unique method of control available. Changing the cycle lower temperature (the main compressor inlet temperature) a few degrees has little direct affect on the cycle efficiency but a significant affect on the main compressor performance.

As the main compressor inlet pressure drops during inventory control, it experiences large changes in fluid properties, which decreases compressor pressure rise. If the designer keeps the main compressor inlet at a constant temperature during this process then the large fluid property changes are solely dependent upon the pressure.

---

* Note that if the system is operated with valves to control the flow split and a throttle to match the compressor pressure rise, then the change in conditions in the main compressor may not change the flow split depending upon how the control system on these valves is implemented.

Controlling the cycle low temperature has three major advantages over pure inventory control:

1. By increasing the fluid temperature a few degrees, the rate of fluid property changes may be greatly reduced (see Figure 6-16).
2. The vast majority of the large main compressor fluid density changes (at part-load operation) can be affected through temperature control without decreasing pressure (i.e. moving isobarically between points A and B in Figure 6-17).
3. The desired main compressor inlet temperature control can be achieved by varying the external cooling water mass flow rate in the precooler immediately preceding the main compressor.

Numerical simulations using temperature control to gradually warm the main compressor inlet temperature were completed for a variety of scenarios.

- Isobarically increasing the cycle low temperature from 32°C to 38°C allows the reactor power to drop over 5% (while keeping the same turbine inlet temperature). However, due to increased cycle pressures from the displaced main compressor fluid* the cycle mass flow rates actually increase, making this method inefficient.
- The other simulations can be distilled down to the recommended method of operation analyzed in the next section.

6.1.10.2.3 Recommended Inventory & Low Temperature Control Method

A more conservative part-load control method was found by combining inventory and low temperature control. Following various numerical simulations, a recommended operational path has been developed, shown as the dotted line in Figure 6-17.

If the main compressor inlet pressure is allowed to gradually peak (the dotted line between point A and B in Figure 6-17) while the fluid temperature is increased, then the large fluid density change occurs significantly further from the critical point than in either the isothermal or isobaric case (for the same starting temperature and pressures). This significantly alleviates the rate of fluid property changes and the associated concerns.

Numerical simulations have shown that if inventory control is used to keep the turbine inlet temperature constant, then the pressure peak shown between A and B is approximately correct. Furthermore, these simulations show that point B is an appropriate temperature, 34°C, for the highest main compressor inlet temperature. Above this temperature the density is unnecessarily decreased and below this temperature there are still large density changes when decreasing fluid pressure.

From point B one could move towards point C without a significant reduction in density (which is no longer needed to decrease pressure) by removing more fluid and cooling the fluid back towards the critical temperature. This movement is clearly shown on the part-load efficiency graph, Figure 6-14, where the slope changes shape near 47% nominal

*There is a relatively large inventory of fluid (in the piping) downstream of the main compressor due to the fluid's high density as shown in, "Appendix B.4 Separating vs. Lumping Piping Volumes in the S-CO_2 Recompression Cycle."

generator power. Below point C in pressure the temperature should be kept at 31°C: the temperature with the largest fluid density that does not enter the two phase region.

Note that at some point in this path it is highly likely that flow will need to be shifted from the main to the recompression compressor to prevent the main compressor from choking. Due to the large decrease in fluid density, without a proportional decrease in loop mass flow rate, the main compressor receives ever larger volumetric flow rates during the shown operation path.

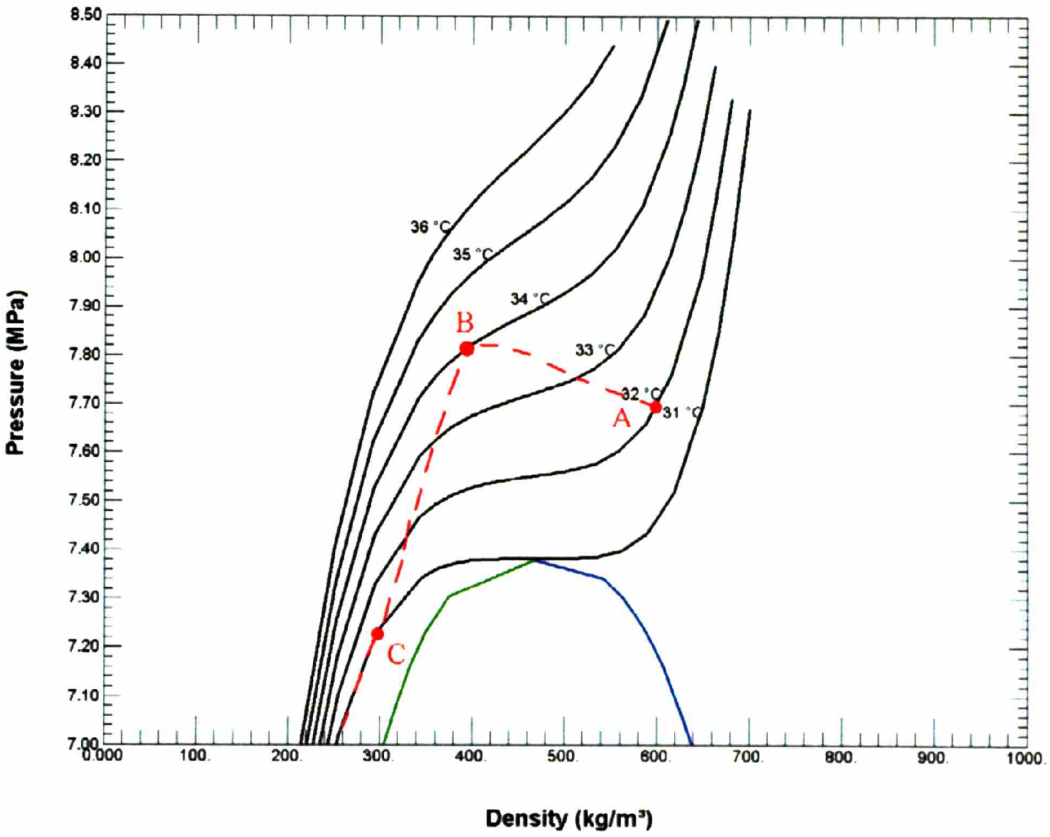

Figure 6-17: Pressure vs. Density Control Path on Main Compressor Inlet Isotherms

6.1.10.3 Loss-of-load

The loss-of-load (LOL) transient occurs when the generator (abruptly) disconnects from the electrical grid, thus it no longer removes energy from the shaft. The very rapid decrease in generator load creates a large and positive work imbalance on the shaft, which uses this energy to accelerate rapidly. Due to the S-CO_2 recompression cycle shaft's relatively low inertia*, the acceleration will rapidly lead to turbomachinery blade failure if it is not controlled†, due to an excessively high rotational speed. To control this

* This work uses the shaft inertia calculated by Pope[9] for the S-CO_2 recompression cycle of 2454.7 kg-m^2.

† Calculations indicate that S-CO_2 recompression cycle turbomachinery are limited by blade bending stress, instead of the more common tip speed stress. This suggests that the turbomachinery may be considerably more resistant to shaft overspeed (or that their construction materials may be cheaper) than is typical in a

transient a (turbine) bypass valve is rapidly opened to decrease the turbine work and increase compressor work to try to slow the accelerating shaft.

In this simulation the turbine and IHX bypass valve (see Figure 4-12) is used to alleviate overspeed during LOL. This valve is placed close to the turbine, yet it avoids the introduction of the cycle's hottest fluid into the HTR (and the valve). The reader should note that this valve's placement may lead to a rapid decrease in mass flow rate in the turbine and IHX. In a direct cycle this phenomena may lead to an unreasonably high fuel temperature[9] but this concern will not be addressed in this work, which focuses upon the power cycle in an indirect cycle configuration.

The shaft speed during several LOL transients is shown in Figure 6-18. This figure shows the increase in shaft speed starting at the time of LOL, at time 0, for several bypass cases. The first case, "no bypass," does not open the bypass valve during the transient and thus presents the plants uncontrolled response to this transient. This line shows a rapid and linear increase in shaft speed which ends near 140% of the nominal shaft speed, the upper limit of the turbomachinery performance curves.

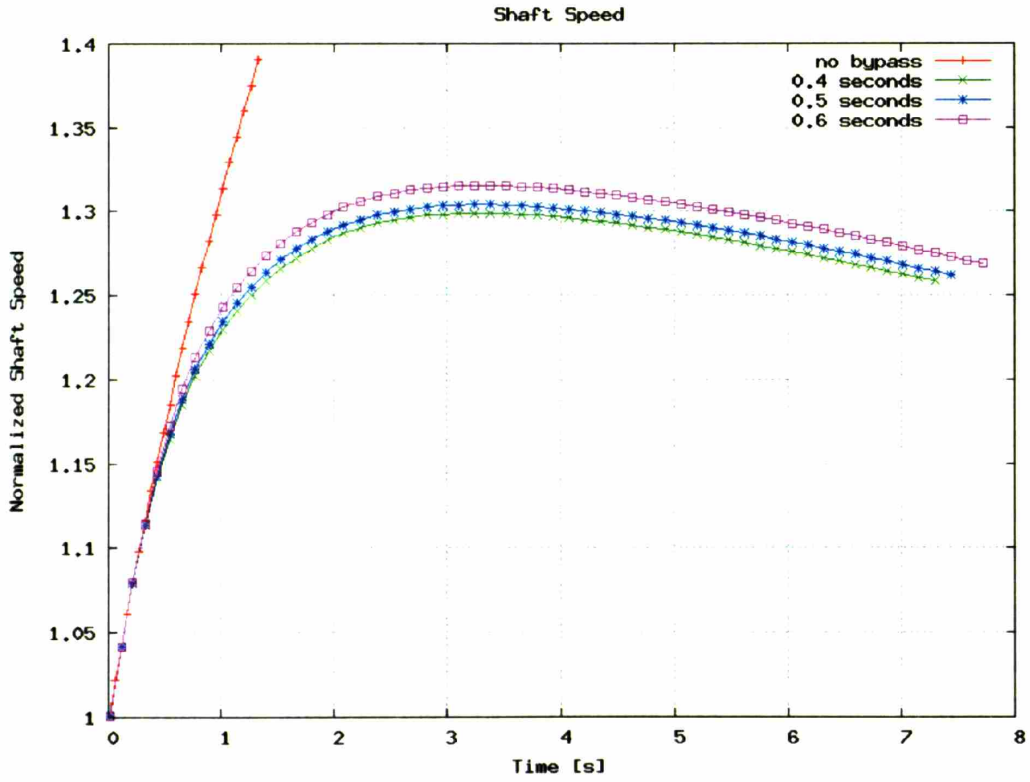

Figure 6-18: LOL Transient: Normalized Shaft Speed vs. Time

Rankine cycle. Due to the current lack of detailed blade stress calculations this work will adopt a 30% overspeed limit, which matches Pope[9] work, with the acknowledgement that this limit needs to be quantified.

The second line shows how the shaft speed increases when the bypass valve fully opens within 0.4 seconds. This line shows behavior similar to the "no bypass" case for the first half a second and then gradually peaks and decreases until the simulation ends near 7.5 seconds. The maximum shaft speed is just below a 30% increase on the nominal value, and the simulation ends at the minimum turbine mass flow rate on the performance curves*.

The third line shows the normalized shaft speed for a bypass valve which fully opens by 0.5 seconds. This line shows very similar behavior to the 0.4 second bypass valve case, except for a slight increase in shaft speed to just above 130% shaft speed.

The final line shows normalized shaft speed for a bypass valve which fully opens by 0.6 seconds. This line is very similar to the other bypass valve cases, but peaks near 132% of nominal shaft speed.

The loss-of-load event in the S-CO_2 recompression cycle can be safely controlled, but it will require rapid bypass valve response due to this cycle's high turbine work to shaft inertia ratio. Current simulations show that the LOL event will require valve action on the order of 0.4 seconds for complete opening and that shaft speed will peak near 3 seconds after the LOL event. This transient also suggests that the turbine control volume can experience flow reversal for a very short time, and a relatively low exiting mass flow rate for several seconds.

Compared to similar RELAP5 LOL simulations completed by Pope, GAS-PASS/CO_2 predicts a slower shaft speed-up and slower peaking. This is very likely due to the lumping of structure and fluid stored energy, which is a poor assumption for simulation on such a relatively short timeframe.

In both RELAP5 and GAS-PASS/CO_2, tolerable valve opening speed was found to be 0.4 seconds to keep the shaft speed less than 130% overspeed. Finally, note that using RELAP5, Pope also predicted flow reversal in the hot end of the cycle during LOL using this bypass location. Although the particulars of the flow reversal differ, the differences probably stem from Pope's use of a direct cycle and relatively finely nodalized mass storage volumes.

If future stress analysis shows that the S-CO_2 recompression cycle turbomachinery can safely handle higher than a 30% increase in shaft speed, then the bypass valve requirements (and other controller requirements) may be significantly relaxed. The speed at which this transient occurs requires rapid controller actions which would be considerably relaxed if the shaft could accelerate for even half a second longer.

* While a turbine can have gas flow separation at low mass flow rates like a compressor, it will not stall, where the mass flow rate rapidly drops to zero, as occurs in a compressor.

6.1.11 Conclusions Regarding Controllability

The S-CO_2 recompression cycle appears controllable, although it behaves differently than other power conversion cycles. The cycle is characterized by large supercritical carbon dioxide fluid property variations without a phase change. While a condensing S-CO_2 cycle presents promise, the ability to cool CO_2 below its supercritical temperature, 30.978°C, is geographically limited, therefore the present work focused solely upon operation in the supercritical region.

Within the supercritical region significant property variations can be experienced when approaching the critical point. Carbon dioxide behaves like an ideal gas at high temperatures and pressures, but shows rapid, real fluid property variations in the critical region. These property variations allow the cycle to operate at relatively high efficiencies at relatively low temperature compared to an ideal gas cycle. However, the property variations also present significant challenges not seen in an ideal gas cycle.

These challenges are varied, but generally stem from the rapidity of fluid property changes near the critical point. The S-CO_2 recompression cycle approaches closest to the critical point at the inlet to the main compressor. This enables efficient compression because of the high density fluid near the critical point, but may create problems if conditions move from their steady state design points during operation. Relatively small changes in temperature and pressure at the main compressor inlet will significantly affect the main compressor outlet pressure, which significantly affects the rest of the cycle. This can lead to complex behavior during part-load and transient operation.

The dynamic behavior of the S-CO_2 recompression cycle is an area of active research but current simulations have shown that the cycle can be controlled with a variety of part-load strategies (three different turbine bypass locations, high temperature control, turbine inlet throttling, and combined inventory and low temperature control) between zero and full power. Furthermore, a loss-of-load event can be controlled with rapid turbine bypass valve action to keep the shaft speed below 130% of its nominal value.

A key uncertainty in this work is how the main compressor changes its behavior due to changes in S-CO_2 fluid properties. During inventory control these changes can be especially rapid and large. An operation method which combines low temperature control with inventory control has been proposed and successfully simulated.

6.1.12 General Conclusions

The S-CO_2 recompression cycle appears controllable during steady state operation, a variety of part-load operations, and during the loss-of-load transient. Significant research remains before key uncertainties can be removed, but current simulations show no major obstacles to either routine operation or severe transient response.

A basic cycle control system has been advanced during this work. The control system allows efficient part-load operation via a combination of inventory and low temperature control, or by rapid load changes via flow bypass. During the extremely rapid loss-of-load transient turbine and IHX bypass has been shown to be sufficient to prevent the shaft speed from exceeding 130% of its nominal value.

Future research should characterize the performance of the main compressor, especially in regards to changing fluid properties near carbon dioxide's critical point. Depending upon the results found during these experiments, the simulations completed during this work may need to be updated. However, using the simulation code created during this work, the addition of experimental data, in the form of performance maps, can be easily accomplished.

The process of creating a simulation code which can model the S-CO_2 recompression cycle was lengthy. Numerous issues were encountered that do not feature prominently in ideal gas power cycles. In particular, accurately and rapidly simulating the widely varying carbon dioxide fluid properties, predicting turbomachinery performance, especially as fluid properties vary, and accurately and rapidly simulating printed circuit heat exchangers have proved challenging. Even with a fully functioning set of sub-modules the process of converging the S-CO_2 recompression cycle has required a variety of techniques which increase the robustness and speed of the code.

GAS-PASS/CO_2 now simulates the S-CO_2 recompression cycle for a variety of transients faster than real time on a modern computer. While the user must be careful in problem definition and error diagnosis, when properly used this tool provides capabilities not found in any other simulation code.

6.2 Safety Implications

There are several ways in which the characteristics of the supercritical CO_2 PCS can affect plant safety, broadly considered. Most are not directly linked to the principal subject of this report, system dynamics and control. However, all aspects are worthy of discussion, if only to help establish the agenda for PCS qualification in the GEN-IV context.

Since the focus of the present work has been on an indirect cycle PCS, safety issues associated with severe transients which cause, or are caused by, mechanical failure of turbomachines are not given the prominence they would merit in direct cycle applications. Thus the normal precautions observed in dealing with high energy density turbomachinery should suffice: for example, blast shields to protect personal and/or safety-related plant features in the event of blade shedding.

6.2.1.1 Physical Concerns

The S-CO_2 PCS has safety concerns associated with most other high pressure systems, for example, rapid catastrophic pipe rupture, and hot high-pressure gas jets. These appear

to be comparable to similar scenarios for steam Rankine cycle PCS. Steam cycles are currently being designed for pressures up to 28.5 MPa[83], whereas most S-CO_2 cycle designs stop at about 20 MPa, hence these aspects are not unique.

Like steam, CO_2 is not a fire hazard. However, it can be an asphyxiation hazard in the event of leakage into a confined space. Since it is not detectable by human senses, warning monitors will be required.

Unique to CO_2, leakage at the precooler outlet/main compressor inlet can produce cold liquid CO_2 and vapor, which pose a severe frostbite hazard. Likewise, rupture of a cryogenic CO_2 storage tank in the makeup tank farm must be protected against.

6.2.1.2 Chemical Compatibility

Our concern here has been with indirect cycles. Thus the consequences of intermediate heat exchanger leakage must be considered. In general, CO_2 pressure will be higher than primary coolant pressure, often much more, so that CO_2 leakage into the primary system is the principal issue. Table 6-1 summarizes the situation on a coolant-by-coolant basis. In view of the fairly recent prioritization of sodium coolant by the GNEP program[7], this item is the only one deserving of additional discussion.

While the water and CO_2 reactions with sodium are comparably exothermic, the latter is kinetically slower and does not liberate flammable hydrogen. Thus much less dramatic consequences can be anticipated. Nevertheless, avoidance and/or mitigation must be a priority, especially since elimination of the intermediate coolant loop common to past liquid metal fast breeder reactor (LMFBR) designs must be an important goal if plant capital costs are to be significantly reduced, and the attendant efficiency penalty of intermediate loop temperature drops avoided.

On the positive side of the ledger, CO_2 can be used to fight conventional fires.

Concepts have been advanced in the past to eliminate the intermediate loop even for sodium/water interfacing: for example, duplex tube heat exchangers[84], parallel tubes coupled by thermally conducting media[85], or heat pipes[86]. To this we can now add PCHE, configurations of which exist which have no possibility of plenum-to-plenum leakage. This limits leakage to that between small (a few mm) diameter channels, which can also be separated by a layer of tell-tale leak indicating channels. Thus it is highly probable that high leak rates can be avoided. Nevertheless, much more analysis and experimental verification is in order, and underway in several laboratories worldwide. Not previously suggested or evaluated is the addition of a small amount of helium to the PCS CO_2 to facilitate small leak detection by analyzing reactor core tank sodium cover gas, typically argon.

Table 6-1: Compatibility Issues for CO_2 and Primary Coolants

Primary Coolant	Comments
Helium	▪ No CO_2 chemical reaction with coolant ▪ CO_2 can attack graphite in a thermal reactor, especially when radiolysis is involved
Water (liquid or steam)	▪ No CO_2 chemical reaction with coolant ▪ $CO_2 + H_2O$ is more corrosive than either constituent alone
Lead	▪ No CO_2 chemical reaction with coolant ▪ Large gas bubbles add positive reactivity in a fast reactor core
Liquid Salts	▪ No CO_2 chemical reactions with coolant (in general) ▪ CO_2 can react with graphite in a thermal VHTR ▪ Gas bubbles have + Δk in a fast reactor core
Sodium	▪ Exothermic reaction with CO_2 ▪ Gas bubbles have + Δk in a fast reactor core ▪ Sodium oxide and carbonate can foul heat exchange surfaces and plug small channels

6.2.1.3 System Dynamics Concerns

The SCO_2 PCS has a lower thermal inertia than a Rankine cycle, particularly in view of the large thermal ballast present in the form of the liquid water inventory available in steam generators. The smaller CO_2 PCS component sizes, hence metal mass, also contribute significantly to this effect. Thus one can expect thermal transients (e.g. following loss-of-load) to proceed more rapidly. This will translate into the need for more rapid countervailing reactor control action when inherent feedback effects are not sufficient in and of themselves.

The small rotational inertia of the compact S-CO_2 turbomachinery also leads to a more nimble response to perturbations.

Although no insurmountable consequences are anticipated, it is clearly a high priority follow-on recommendation to build an SFR/ABR primary system control module and couple it to the current GAS-PASS/CO_2 PCS code (or another equivalent model), to study reactor response to coupled transients in which both those propagated back through the PCS and forward from the reactor (e.g. scram) are simulated.

6.2.1.4 Safety Concerns Summary

Finally, three of the four authors of reference[87] – a review of light water reactor safety features – were canvassed as part of the current assessment. No important issues beyond those raised in this section were identified.

6.3 Part-load Cycle Comparisons

This section will compare part-load operation efficiency results from GAS-PASS/CO_2 to independently derived results for a very similar cycle from Anton Moisseytsev[17] and helium cycle results from Xinglong Yan[19]. In all cases the comparisons will be made on a normalized (to the steady state) basis.

Part-load efficiency of the helium cycle, using several different control methods, is shown in Figure 6-19. This figure shows that, in a helium cycle, inventory control is quite efficient. Using inventory control the plant retains over 90% of its steady state efficiency until about 25% generator power. Inventory control efficiency begins to drop rapidly near 20% generator power, until near 5% power operation ends. High temperature control is the second most efficient option in a helium cycle, and ranges from full to zero power. Finally, turbine bypass shows a linear decrease in efficiency from full to zero power.

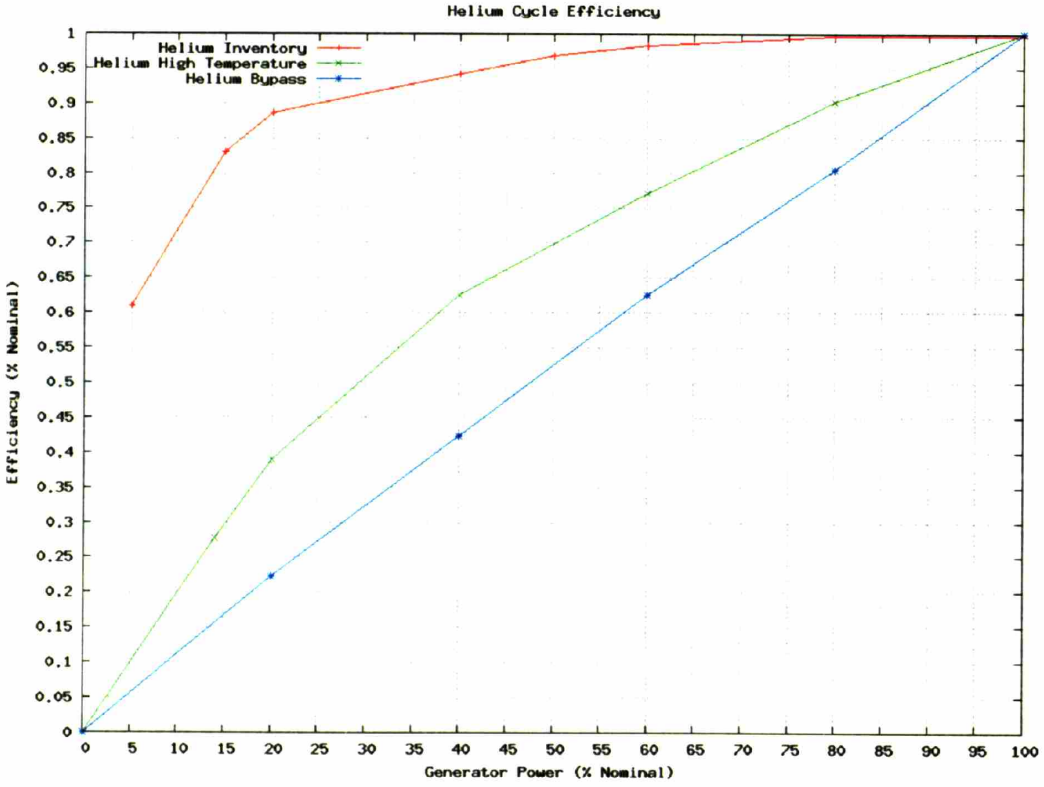

Figure 6-19: Helium Cycle: Normalized Efficiency vs. Normalized Generator Power[19]

The part-load efficiency of a S-CO_2 recompression cycle, very similar to the one examined in the present work, is shown in Figure 6-20. This figure shows the relative efficiency of inventory control, turbine inlet throttling, turbine bypass, and reactor heat exchanger bypass (this method does not apply to our indirect cycle model). The results are quite similar to the (applicable) results from GAS-PASS/CO_2 (see Figure 5-55), as will be shown in detail shortly. The reader should note that a primary difference between the Moisseytsev and GAS-PASS/CO_2 results is Moisseytsev's use of axial compressors. This type of compressor has a more restricted operation range and features a significantly

increasing pressure ratio at reduced mass flow rates (compare the relatively flat main compressor radial curves in Figure 3-16 to the axial curves in Figure 3-22) . The consequence of this difference will appear in several part-load operation results.

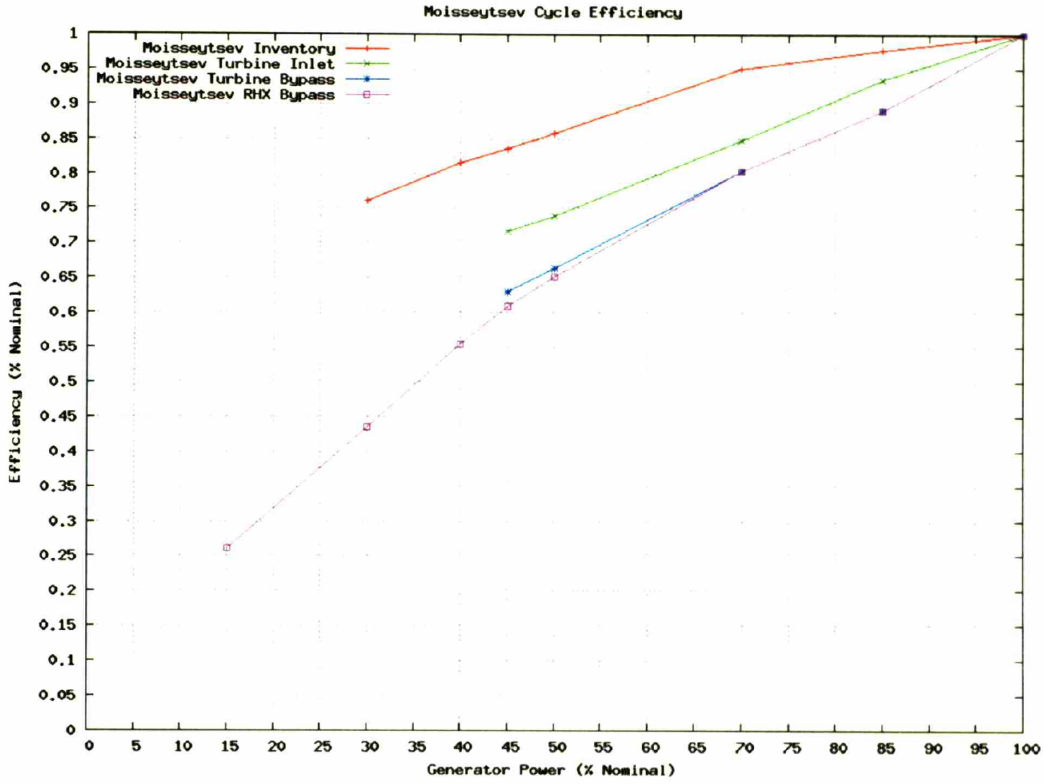

Figure 6-20: Moisseytsev Results: Normalized Part-load Efficiency vs. Normalized Generator Power[17]

High temperature control efficiencies for the helium and S-CO_2 recompression cycle* are shown in Figure 6-21. These results show close agreement between helium and S-CO_2 over the available range. The S-CO_2 recompression cycle is limited in this control method's range due to compressor choke stemming from carbon dioxide's non-linear relationship between pressure and density in the compressors, which is not experienced in the helium cycle. One possible reason for the close agreement in the results is that the decrease in cycle high temperature occurs in the part of the cycle where S-CO_2 behaves like an ideal gas (see Section 3.4.4).

* Results labeled only "S-CO2" refer to GAS-PASS/CO_2. Results for Moisseytsev are labeled "Moisseytsev S-CO2."

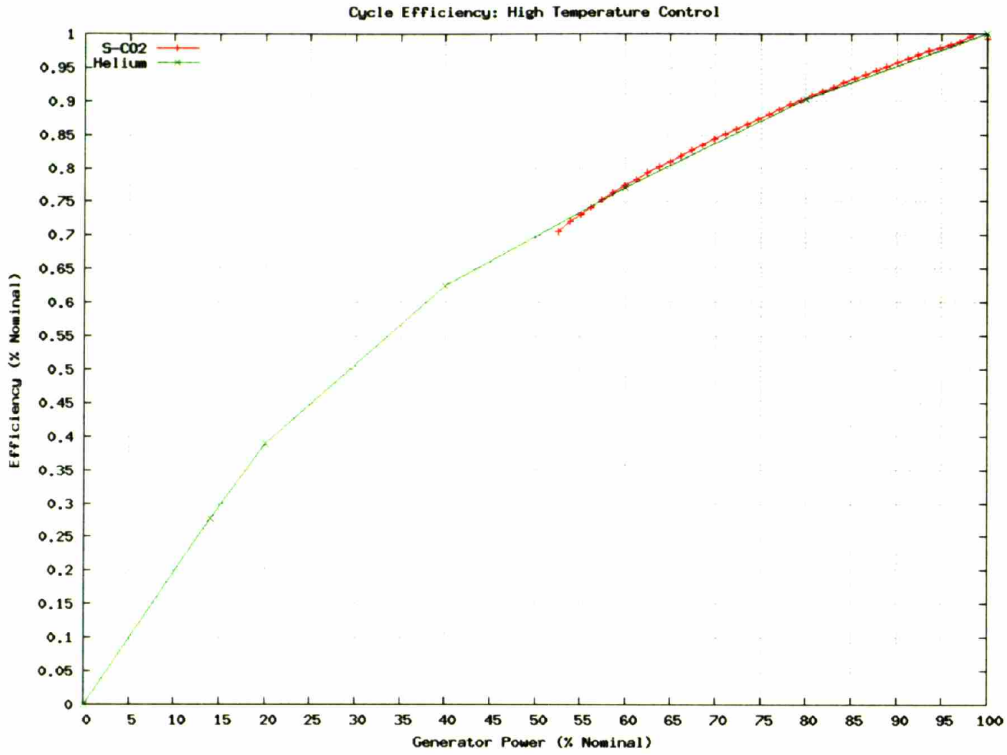

Figure 6-21: Helium vs. S-CO_2 High Temperature Control: Normalized Efficiencies vs. Normalized Generator Power

Turbine bypass control efficiency for the helium and both S-CO_2 recompression cycle simulations is shown in Figure 6-22. This figure shows that S-CO_2 is slightly more efficient under bypass control than a helium cycle, which shows a linear decrease in efficiency, but in all cases the efficiency lines show a similar trend. Moisseytsev's results show a significantly higher efficiency than those predicted by GAS-PASS/CO_2, which may stem from the differing shapes of the compressor pressure ratio curves (the compressors receive a significant increase in volumetric flow rate with this control method).

Turbine inlet throttling for both S-CO_2 simulations is shown in Figure 6-23. This figure shows that both Moisseytsev and GAS-PASS/CO_2 predict similar trends, except that GAS-PASS/CO_2 predicts significantly higher efficiencies. Once again, the difference in efficiency very likely stems from the difference in the shape of the compressor pressure ratio curves. Using axial compressors, as mass flow rates decrease the turbine receives a larger pressure ratio from compressors than it would in the case of radial compressors. Thus more pressure must be throttled with axial compressors, making the cycle less efficient. This operation method was limited by the minimum mass flow rate on the specified turbine performance map.

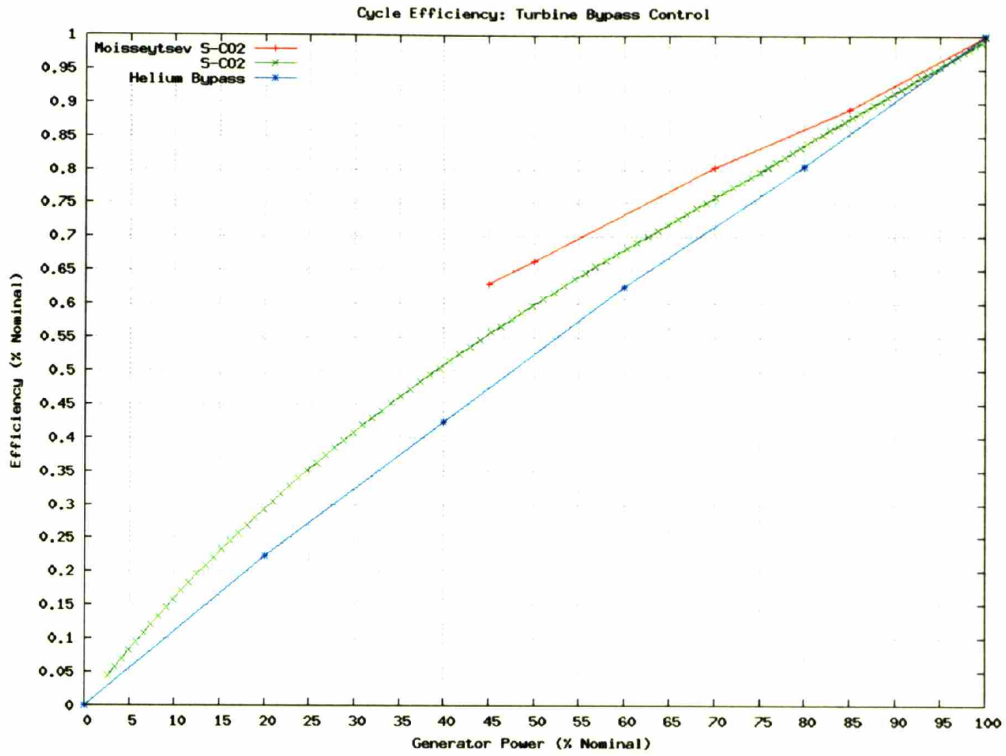

Figure 6-22: Helium vs. S-CO_2 Turbine Bypass: Normalized Efficiencies vs. Normalized Generator Power

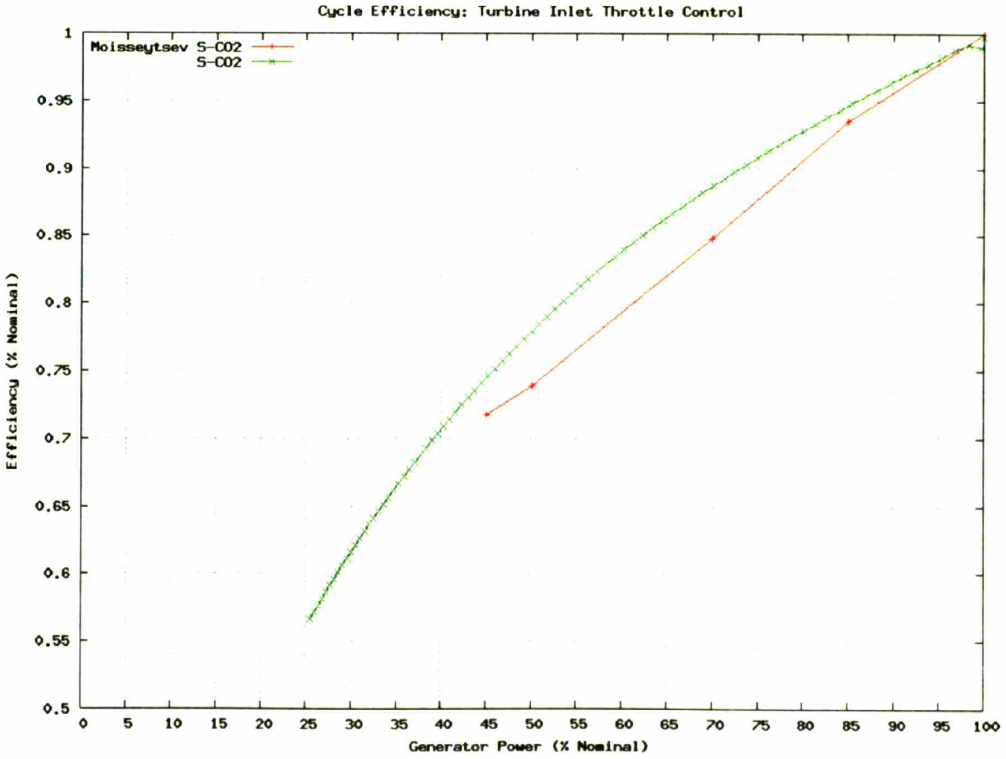

Figure 6-23: S-CO_2 Turbine Inlet Throttling: Normalized Efficiencies vs. Normalized Generator Power

The relative efficiency of inventory control for the helium and both S-CO_2 simulations is shown in Figure 6-24. This figure shows that inventory control in a helium cycle is much more efficient than in a S-CO_2 recompression cycle. The two S-CO_2 simulations show close agreement until 47% generator power, where GAS-PASS/CO_2 rapidly drops the cycle low pressure (see Figure 4-18). Once again, this operation method was limited by the minimum mass flow rate on the specified turbine performance map.

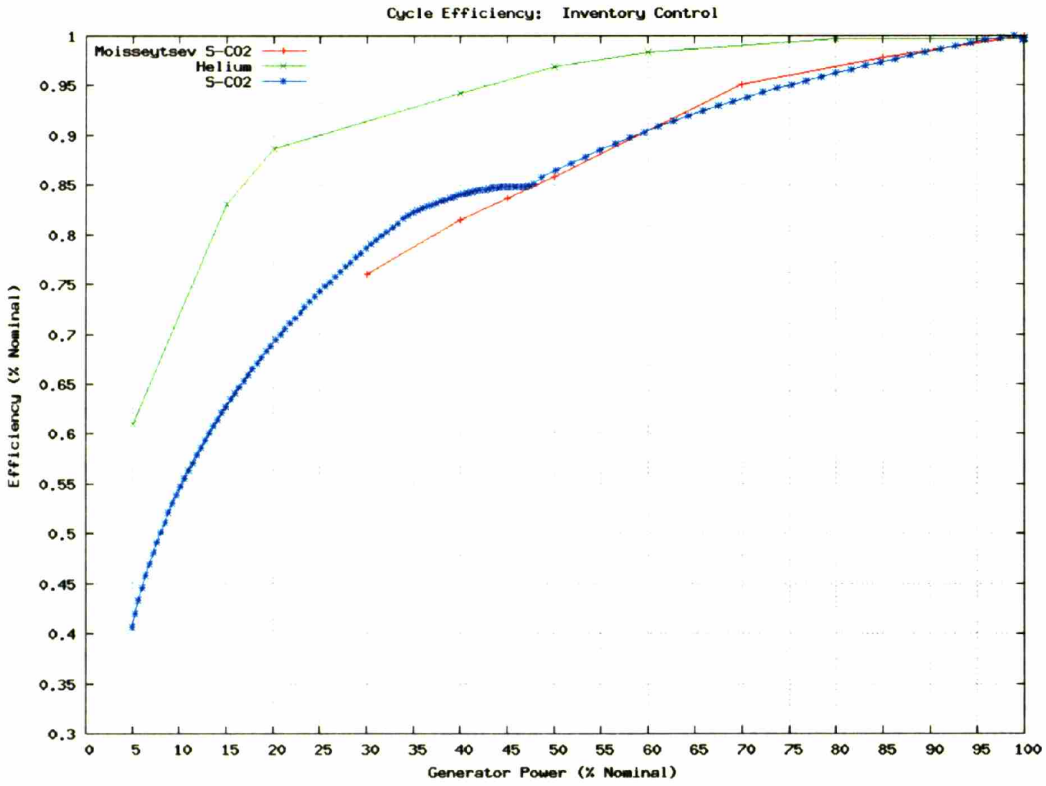

Figure 6-24: Helium vs. S-CO_2 Inventory Control: Normalized Efficiencies vs. Normalized Generator Power

One key benefit of the S-CO_2 recompression cycle is the compactness of fluid storage when using inventory control. Helium fluid density ranges from about 5-12 kg/m^3 within the cycle and the stored fluid will probably be close to the cycle's low density range (due to the loss of pressure which occurs during the filling of inventory storage tanks). This contrasts sharply with S-CO_2 fluid, which ranges from 50-720 kg/m^3 in the cycle, and the stored fluid will probably approach the upper density value. The high density of S-CO_2 (and the ability to readily change that density) allows much smaller inventory storage tanks*. Initial calculations suggest that, for the same generator power, the S-CO_2 recompression cycle only requires about 1/5 of the tank volume of a helium cycle.

* This analysis assumes that no external compressors are used to load or unload the inventory control tanks.

In practice this is likely to mean that the S-CO_2 recompression cycle can use inventory control at low generator powers, where a helium cycle will be limited using this control method to higher generator powers. If one assumes that the helium cycle cannot conveniently operate below 75% power with inventory control, then the optimal part-load efficiency of both cycles changes significantly, as shown in Figure 6-25.

Figure 6-25 shows that while helium is significantly more efficient than the S-CO_2 recompression cycle when using inventory control, it is significantly less efficient once bypass is used. Thus, it is likely that the S-CO_2 recompression cycle will be more efficient than an ideal gas cycle at low powers in an operating plant. One should also note that in a multi-loop PCS reactor plant it is possible to run one (or more) loops on idle and keep the other(s) at high powers.

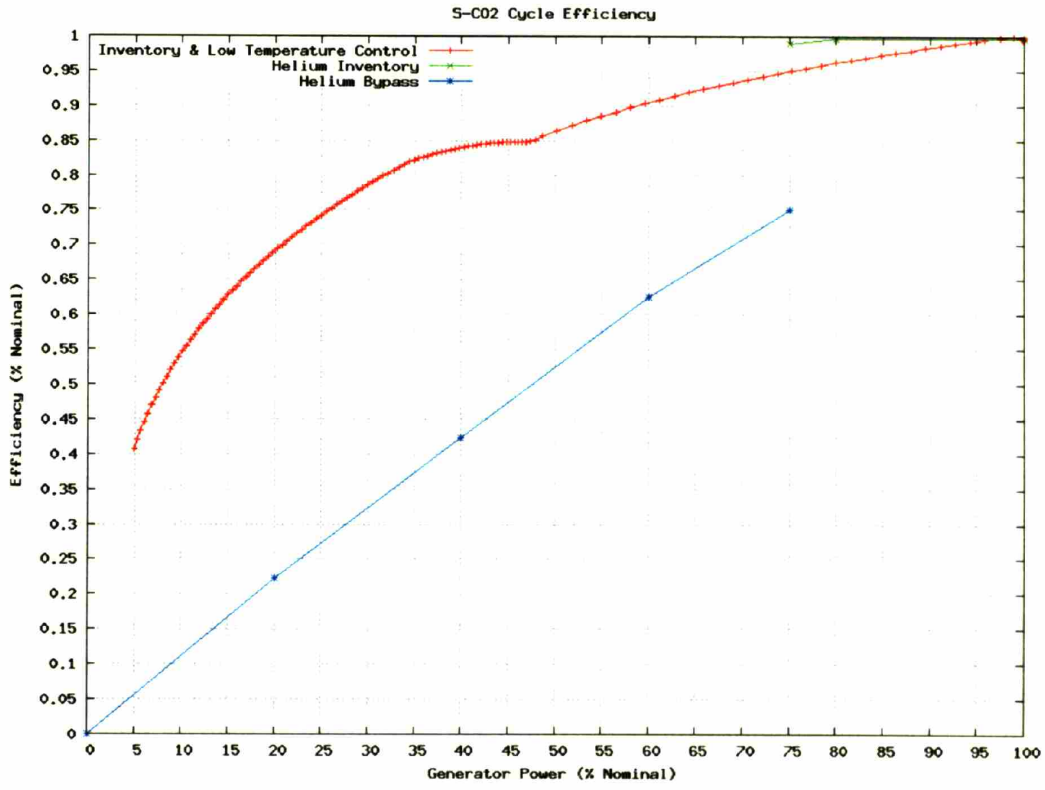

Figure 6-25: Helium vs. S-CO_2 Cycle: Optimal Part-load Efficiency Scenarios

6.4 Future Work

The discussion of future work is separated into three major sections: code improvements, model improvements, and desired testing. In general, the suggestions listed stem from a combination of the lessons learned and the key uncertainties discovered. The GAS-PASS/CO_2 improvements have been analyzed and implementation methods are offered in

Appendix B: Suggested Future Improvements. They are not included in the main text as they are lengthy and primarily of interest to future developers.

6.4.1 GAS-PASS Improvements

There are numerous improvements that could be made to GAS-PASS:

1. Replace the IMSL solvers with an open source numerical solver such as MINPACK*. This will allow two big improvements:

    a. The code would become fully reentrant and could be easily applied to multi-threaded processors (parallel computation probably isn't warranted). Multi-threading GAS-PASS is explored in, "Appendix B.2 Multi-Threading". Using today's 4 core processors it is entirely feasible to speed-up GAS-PASS runtime by more than 300%.

    b. Avoiding unnecessary Jacobian evaluation. The Jacobian is only useful to determine the slope to system root. It is very likely that this slope will change relatively little between consecutive time steps, yet it is evaluated at each time step in the current code.

    One could modify the transient solution process to only evaluate the Jacobian when the solution algorithm is not making progress. Since about 99% of the computation time is spent in the transient and over 90% of this time is spent in the Jacobian it is entirely possible that avoiding unnecessary Jacobian evaluation could speed-up the code by almost an order of magnitude. This method is not elaborated upon in the appendix because it is relatively straightforward and its implementation will depend upon the numerical solver adopted.

    Replacing the IMSL solvers would allow GAS-PASS/CO_2 to speed-up by something like 25-fold on a new computer. It would also have the added benefit of allowing future developers to avoid buying the expensive IMSL package.

2. Approximating structure conduction. Currently GAS-PASS/CO_2 treats the structure as isothermal with the fluid. While this assumption is close to true in the very thin walls inside the PCHEs, it is not true in the thick pressure boundary piping, thus GAS-PASS/CO_2 does not have the right time constants for precise simulation (the thermal inertia is stronger and acts faster than it should be).

    For first order analysis this is not critical, but before GAS-PASS/CO_2 can be benchmarked against a real plant this improvement will be required. A procedure for implementing this improvement is outlined in, "Appendix B.3 Approximating Structure Conduction". Note that some hot leg piping may be internally insulated.

* http://www.netlib.org/minpack/

3. Improving the user interface. Creating a complete cycle model input deck presents a steep learning curve, which requires considerable labor even for an experienced user. It would be relatively simple to create a graphical user interface (GUI) front end in a convenient language (e.g. Microsoft Visual Basic) which allows the user to visually construct a plant model using a library of known components. Once the plant model was designed, the GUI front end could create the GAS-PASS/CO_2 input deck and execute the computationally efficient Fortran code.

4. A more robust initial convergence mechanism would provide a significant advantage. Currently, a knowledgeable user must build up a model one component at a time until the whole system converges. This can be difficult due to the small proportional region surrounding a non-linear system of equations root. An automated process for initial converging a plant would be welcome.

6.4.2 S-CO_2 Recompression Cycle Model Improvements

The current cycle model has several areas that invite improvements:

1. Improving the turbomachinery performance maps. Once more accurate (experimental) data become available, the current maps can be replaced. Once sets of maps are available for varying fluid properties, then the basic fluid property effect relations can be removed to allow interpolation between known data.

   This may significantly change the dynamic response of this cycle. The next subsection presents an initial set of useful tests for the most uncertain turbomachine, the main compressor, to aid in the generation of these maps.

2. Heat transfer correlations and pressure drop correlations should be improved. When GAS-PASS/CO_2 was originally coded there was considerable uncertainty regarding the appropriate heat transfer correlation, especially for zig-zag PCHE flow channels (which were not used). Since that time several papers have come out which eliminate some of the uncertainty and offer more accurate correlations than the currently-used modified Gnielinski correlation, that would allow the use of different channel geometries.

   Secondly, the correlations need to be applied on a fluid-by-fluid basis. Currently, the modified Gnielinski correlation is applied to carbon dioxide, water, and liquid sodium. While accurate for the first two fluids, this correlation is not suited for liquid sodium and should be replaced. GAS-PASS/CO_2 now has the ability to easily determine which fluid is being used, and thus to apply an appropriate correlation.

   An appropriate correlation will improve the accuracy of GAS-PASS/CO_2, but not significantly. The modified Gnielinski correlation is conservative, thus it

overestimates the required heat exchanger length, and hence its pressure drop. As more accurate correlations are applied this conservatism will be removed, which will increase plant efficiency slightly.

Note that an appendix contains a brief overview, see "Appendix B: Suggested Future Improvements", of the significant uncertainty encountered in applying water heat transfer correlations in the transition region with GAS-PASS/CO_2, especially as compared to RELAP5.

3. Model the fluid in the splitting-T. Currently, GAS-PASS/CO_2 neglects this volume since its addition significantly decreases the model's condition number. One may be able to add this volume, without a significant penalty to the system's condition number, by separating the modeling of the splitting-T volume from the action of splitting the fluid flow. The splitting-T volume could simply be treated as a pipe, and a second component could actively split the flow, thus separating flow split effects from transient fluid storage (mass and energy) effects.

4. Modeling fluid piping separate from components, which would allow the addition of modeling piping pressure drops. This change should be handled with care, since it will create significant differences in volumes between the modeled components, which also contain significant differences in fluid density. This may create a stiff solution matrix, which is analyzed in greater detail in, "Appendix B.4 Separating vs. Lumping Piping Volumes in the S-CO_2 Recompression Cycle."

5. Modeling inventory control more precisely. GAS-PASS/CO_2 currently affects inventory control by changing the total amount of fluid in the system – not by removing fluid from a particular location to change the total. A complete inventory control system treatment would provide more accurate modeling of the effects of adding and removing fluid (especially on the main compressor) and would allow an integrated simulation of the inventory control tank.

6. Adding a reactor model to the primary system as an appropriate reactor design becomes available. This will allow accurate modeling of the feedback between the reactor and the power conversion cycle.

6.4.3 Suggestions for a Stand-Alone Main Compressor Test Program

Testing a S-CO_2 compressor near the critical point would remove many uncertainties from the control system design process. The following needs were identified during the course of GAS-PASS code development and initial transient simulations.

1) The shape and operating range (performance map) of the compressor at design inlet conditions for different shaft speeds. These maps will look something like Figure 6-26 and Figure 6-27. These maps should satisfy the following requirements:

a. The maps should be detailed enough to allow accurate cubic spline interpolation between data points.

b. The point of stall and choke should be clearly shown on each curve.

c. Jitter should be minimized. Sharp changes due to experimental error will affect numerical calculations.

2) A set of curves or, preferably if possible, equations to predict off-design main compressor performance (i.e. when inlet temperature/pressures change). If more curves are developed they be will similar to Figure 6-26 and Figure 6-27 but for different inlet conditions. It is likely that many sets of curves will be required.

During off-design calculations the dynamics code will interpolate for turbomachinery performance on each set of performance curves closest to the predicted inlet conditions. Then the output of these interpolations will be interpolated for the exact inlet conditions. Therefore, these surrounding sets of curves must be dense enough to permit meaningful interpolation between them. If the shapes and bounds of the curves change quickly with changing properties (i.e. near the critical point) then many sets of curves will be required.

Alternatively, if accurate equations can be developed, then they may resemble (but are likely to be more complex than) the currently used relations. Currently off-design turbomachinery performance in an Ideal Gas is estimated by applying Equation 6-5 and Equation 6-6 before interpolation on the design point shaft speed curves. Note that in all cases the reference value is the steady state value.

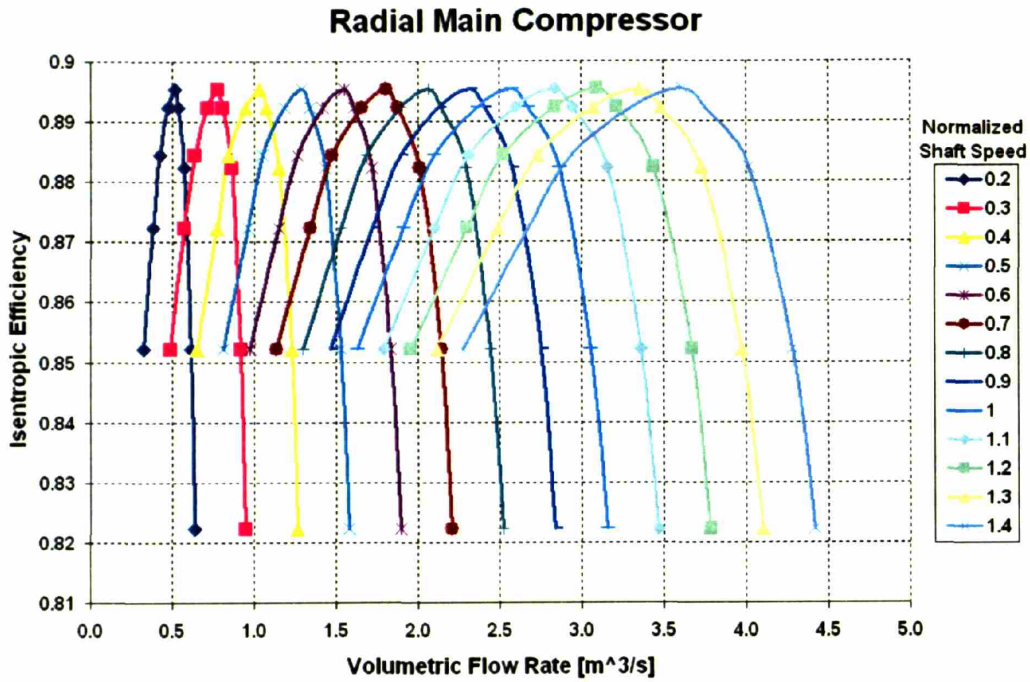

Figure 6-26: Representative Radial Main Compressor Efficiency Map - Design Conditions

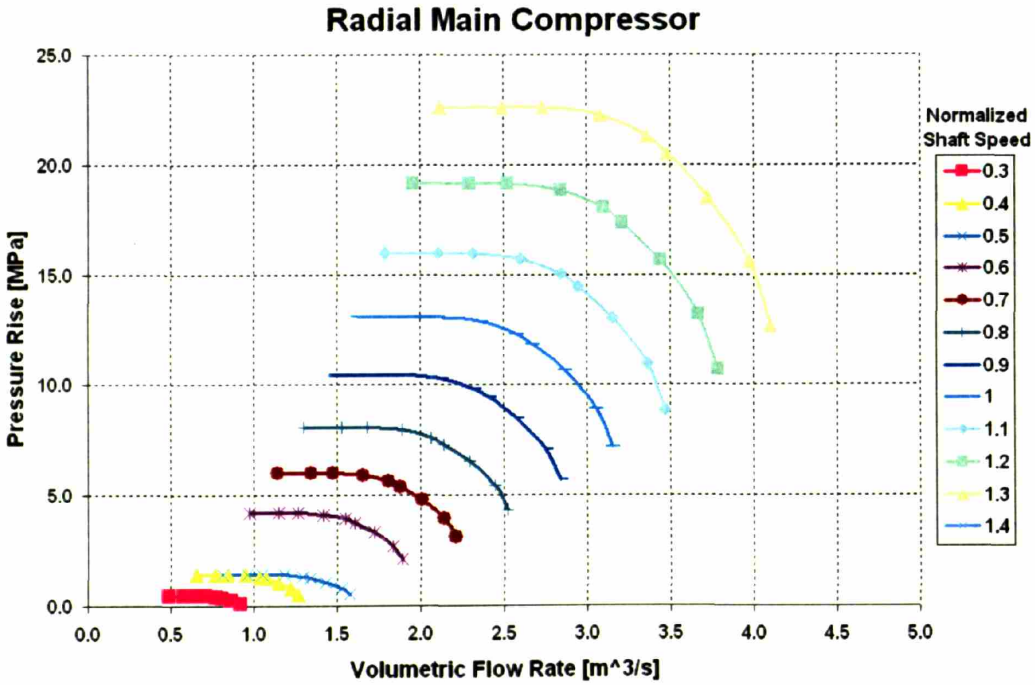

Figure 6-27: Representative Radial Main Compressor Pressure Rise Map -- Design Conditions

Equation 6-5: Ideal Gas Mass Flow Rate Property Scaling **(6-1)**

$$\dot{m}_{scaled} = \dot{m}\frac{\sqrt{T}}{\sqrt{T_{ref}}}\frac{P_{ref}}{P}$$

Equation 6-6: Ideal Gas Shaft Speed Property Scaling **(6-2)**

$$\omega_{scaled} = \omega\frac{\sqrt{T}}{\sqrt{T_{ref}}}$$

For an incompressible fluid, off-design performance is estimated by applying Equation 6-7 before interpolation to the standard curves, and Equation 6-8 to the result of that interpolation.

Equation 6-7: Mass Flow Rate Correction for Compressors **(6-3)**

$$\dot{m}_{scaled} = \dot{m}\frac{\rho_{ref}}{\rho}$$

Equation 6-8: Compressor Pressure Rise Correction **(6-4)**

$$\Delta P_{scaled} = \Delta P\frac{\rho}{\rho_{ref}}$$

Initial testing should indicate if changes in fluid density can accurately predict off-design performance (as in the incompressible relations) or if temperature and pressure change must be known (i.e. density changes don't capture all property effects in the quasi-incompressible fluid in the main compressor).

3) Due to the main compressor's proximity to the critical point, tests should go well below the critical pressure (roughly 7 MPa) and investigate inlet densities less than half the design point inlet density.

Note that an important question in these tests is how much inlet density vs. outlet density changes affect the main compressor. During inventory control the main compressor inlet may drop to ~7 MPa, and the high pressure outlet side will probably drop from 20 MPa to below 14 MPa. The main compressor will dictate the system high pressure (since it will drop faster than the recompression compressor outlet) during inventory control operation, due to the large change in inlet density.

Also note that due to the main compressor's large drop in inlet density during inventory control there will be a large increase in inlet volumetric flow rate which, in the real plant, would probably have to be partially shifted to the recompression compressor at some point. In a single compressor test loop the mass flow rate may have to decrease to avoid choke.

4) Very careful testing is needed of the main compressor's response to passing through its pseudo-critical pressure at several isotherms. The rate of density change, on an isotherm, per unit pressure can be very large near the critical point as shown in Figure 6-28. What happens to the main compressor when it goes through these large peaks is very uncertain at this point, but of great importance.

It will be critical to have very accurate temperature readings during this test. Depending upon the sensitivity of thermocouples* available it may not be feasible to measure the temperature of the CO_2 at the main compressor inlet to the required precision. Due to the large isobaric specific heat peak near the inlet of the main compressor, shown in Figure 6-29, the fluid requires large amounts of heat addition for a small temperature change. Therefore, despite the fact that most main compressor inlet properties vary rapidly, the temperature of the fluid will be almost constant. Put another way, small variations in main compressor inlet temperature will introduce large property (including density) changes, which will significantly affect turbomachine performance.

One could avoid this problem if the experiment were conducted while boundary conditions are held constant. Figure 6-30 shows a possible temperature testing layout, where warm CO_2 is cooled by external cooling water to the desired temperature before the main compressor inlet. The advantage of this, admittedly more complex, temperature sensing layout is that the CO_2 temperature is measured far from the critical point (where carbon dioxide's temperatures change significantly for a given heat transfer).

This difference between measuring carbon dioxide temperature at the precooler inlet versus the outlet is clearly shown in Figure 6-31. This figure shows† a range of precooler CO_2 inlet versus outlet temperatures with all the other boundary conditions held constant. The figure clearly shows that a relatively large change in inlet temperature produces a relatively small change in outlet temperature. If one takes a first derivative, $\frac{dT_{out}}{dT_{in}}$, of the temperatures shown, then the outlet temperature is 44 times more responsive than the inlet temperature. Measuring the temperature at the precooler CO_2 inlet is much more accurate than at the outlet regardless of the temperature measuring device.

By carrying out a heat balance‡ on the easily measured water side, adding this energy to the known incoming CO_2 fluid properties, and measuring the pressure at the outlet of the heat exchanger one may accurately calculate the CO_2 fluid temperature at the main compressor inlet without the need for extremely sensitive thermocouples. The equations for this method are shown in Equation 6-9.

---

* Note the actual measurement device may be a thermocouple, resistance temperature detector (RTD), or a thermistor. Each of these instruments will involve different accuracies, time constants, and costs, which this work will not analyze in greater detail.

† The figure is the result of simulations conducted with the standalone version of the steady state PCHE solver used in GAS-PASS/CO_2.

‡ The precooler will (inevitably) lose heat to the environment. Insulation and experimental testing should be able to eliminate much of this error.

Equation 6-9: Main Compressor Inlet Temperature Measurement Equations **(6-5)**

$$h_1 = f_{CO_2}(T_1, P_1)$$

$$Q = \dot{m}_2 \, Cp_{H_2O}(T_2 - T_3)$$

$$h_4 = h_1 + Q / \dot{m}_1$$

$$T_4 = f_{CO_2}(h_4, P_4)$$

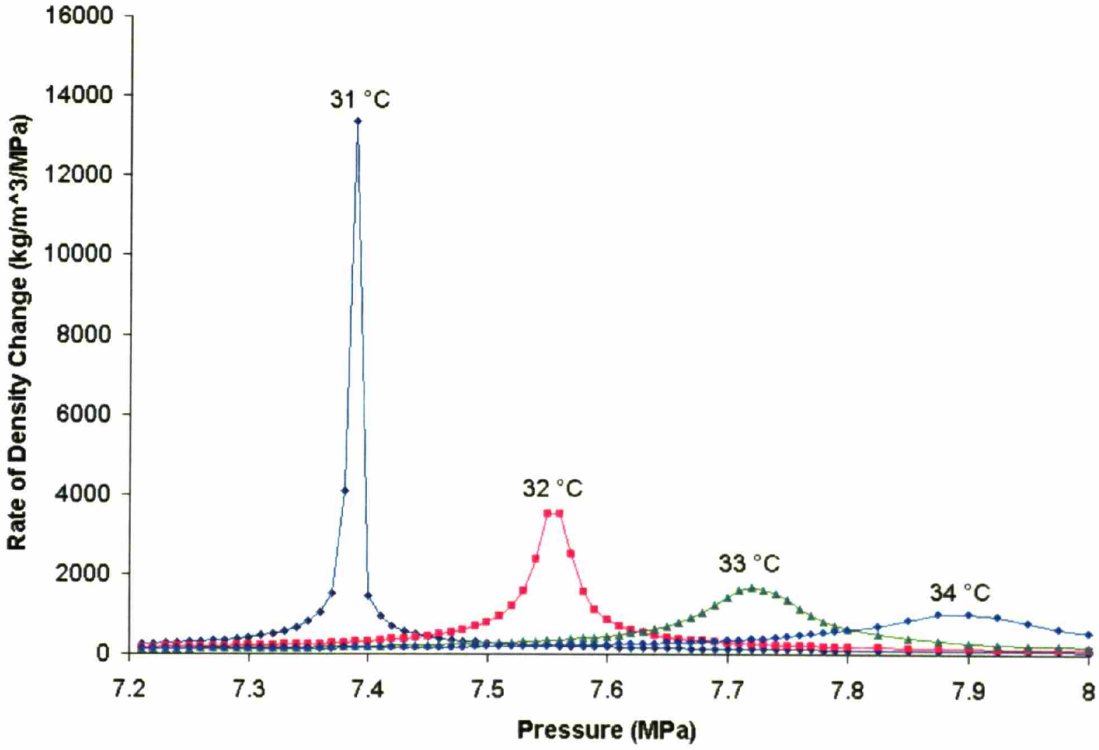

Figure 6-28: Rate of Density Change per Unit Pressure on Main Compressor Inlet Isotherms

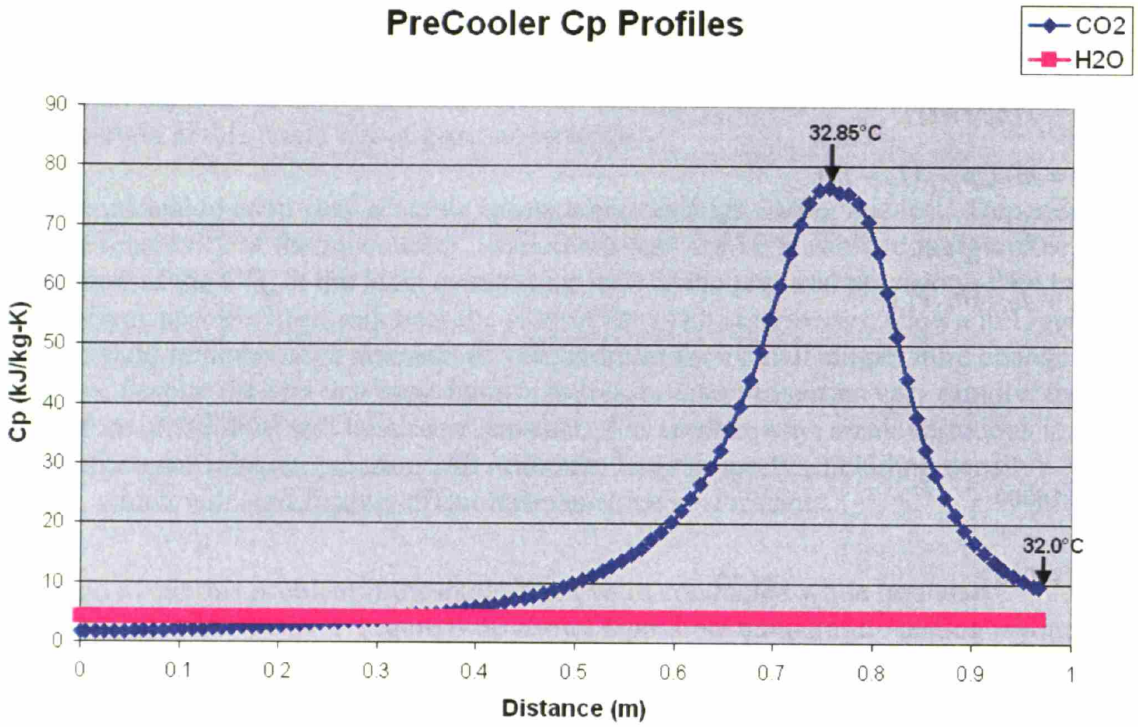

Figure 6-29: Precooler Isobaric Specific Heat Profiles

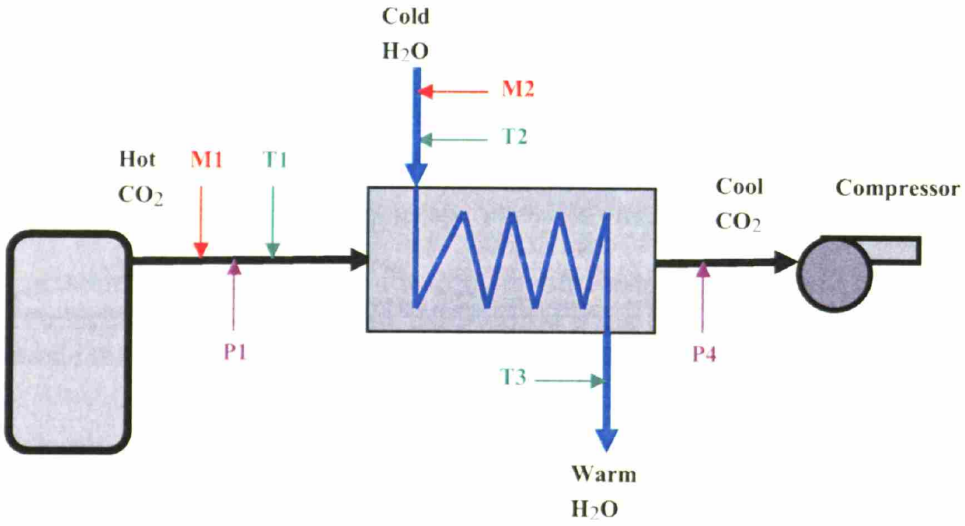

Figure 6-30: Main Compressor Accurate Temperature Testing Rig

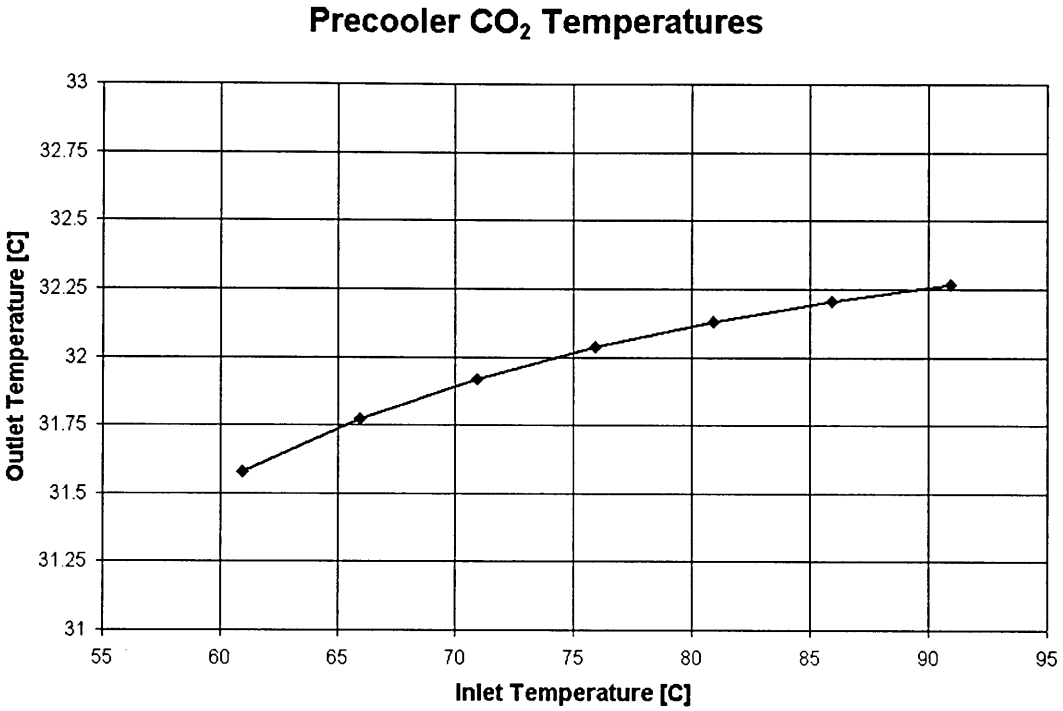

Figure 6-31: Precooler CO_2 Temperature Variation at the Outlet versus the Inlet

Of course, another potential drawback to this testing system is that the structure in the heat exchanger can absorb and release heat for a short amount of time (numerical simulations show that the internal structure in this heat exchanger approaches equilibrium within two seconds), but this concern can be easily removed if the incoming CO_2 and water properties are held constant. The success of this approach also obviously depends on accurately measuring water temperature change and flow rate. Use of a positive displacement metering pump should be considered.

In summary, the recommended method of testing avoids one very difficult temperature measurement, the precooler CO_2 outlet temperature, at the additional cost of measuring the temperature at three other (relatively easy to measure) points: the water inlet temperature, the water outlet temperature, and the CO_2 inlet temperature, and assuring the component is insulated properly to avoid environmental heat losses. Experimental testing should quickly establish the relative accuracy of these methods.

5) If possible, measuring the effect of inlet guide vanes on the main compressor would be very useful. Some literature suggests that inlet guide vanes may help correct volumetric flow rate mismatches[41], which are a key concern in the main compressor, especially during inventory control.

Inlet guide vanes are commonly used to correct mismatches in volumetric flow rates between compressor stages. For example, at lower shaft speeds (in a multiple stage high pressure ratio axial machine) the lower pressure rise in the low pressure stages leads to a thinner fluid and higher volumetric flow rate in the high pressure stages. In extreme cases this can cause the high pressure stages to choke, thus stalling the low pressure stages. The same type of problem is encountered as the CO_2 inlet density drops.

When the main compressor moves through its pseudo-critical pressure the inlet density drops significantly. Figure 6-32 shows approximate operating lines for the main compressor before inventory control begins, line 1 and (after significant fluid is removed) after the compressor inlet drops below the critical pressure, line 2. The much thinner inlet fluid will be more difficult to compress.

Besides the large drop in inlet density it is important to realize that the ratio of inlet to outlet densities in the main compressor also increases significantly – there is a large change in slope between lines 1 and 2. Therefore, there is a density/volumetric flow rate mismatch between the inlet and outlet of the compressor after dropping below the critical pressure, regardless of the effectiveness of the initial compression.

Inlet guide vanes may alleviate these (potential) problems by reducing the velocity triangle mismatch encountered at the beginning of the machine. By turning the stator guide vanes (to increase swirl) the initial compressor rotor blades can be made to work closer to their steady state design point and the mismatch between the beginning and end of the compressor can be reduced.

Note that even if the main compressor has only one (radial) stage the above analysis applies, but will simply occur within a single blade instead of over multiple stages.

6) Testing the main compressor performance when both temperature and pressure become subcritical. During rare transients it is possible that the main compressor inlet could enter the two-phase region and a two phase vapor-liquid mixture could transit the main compressor. The effects of this process are uncertain for two reasons:

- CO_2 has shown the ability to remain quite sub-cooled before droplet formation*.
- The density difference between liquid and S-CO_2 fluid near the operating point is small. A difference of 2-3 times may not readily compromise performance or damage a compressor for small liquid droplet concentrations.

7) Measurements of vibration of the compressor shaft. Mitsubishi, who developed a large S-CO_2 centrifugal compressor, warned that under the high density conditions encountered with S-CO_2, specific gravity effects become significant and the compressor

* The velocity of the fluid may be important in this calculation as well. Typically, fluid properties are evaluated at static rather than dynamic conditions. In the main compressor, near the critical point, the Mach number may approach one, thus velocity effects may be important.

rotor may vibrate unstably[40]. Therefore, vibration sensors should be installed to monitor rotor behavior under various regimes.

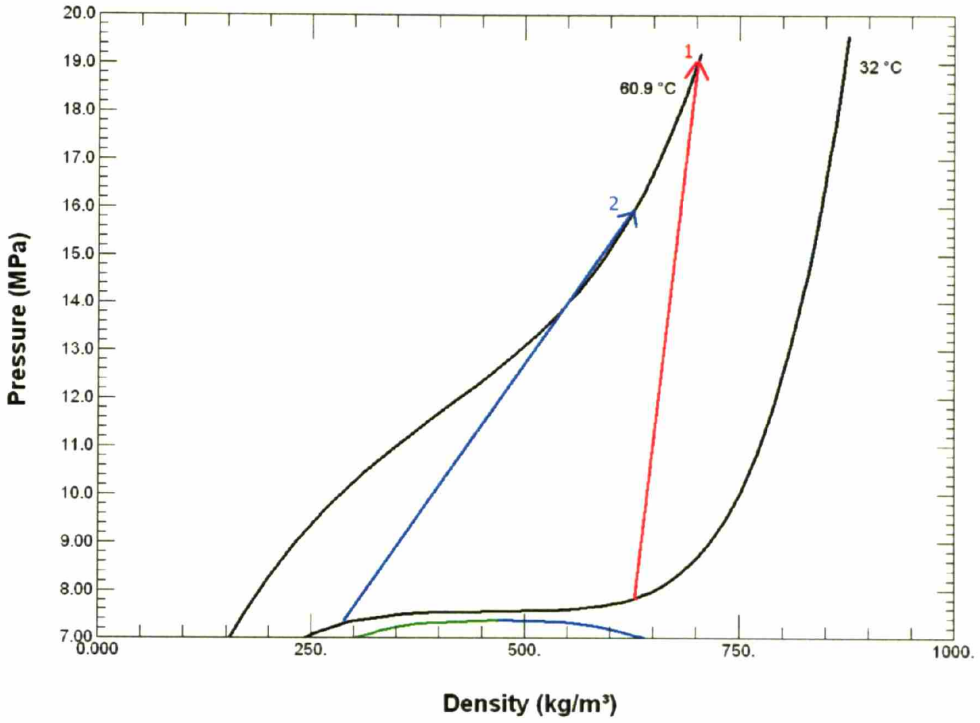

Figure 6-32: Main Compressor Operating Path Before and After Pc

Appendix A: GAS-PASS/CO_2 Equations

This appendix documents the conservation equations which are the basis for GAS-PASS/CO_2. The sections which follow describe in some detail the roster of differential equations, and their difference representations, which go to make up the program version as presently (March 2007) constituted.

This level of detail is of interest mainly to those who may become involved in validating, rewriting or extending code capabilities. Accordingly it has been relegated to an appendix, and only higher level functional descriptions presented in the main text of this report.

This appendix is broken up into three sections: an example derivation for the turbine, the steady state equations, and the transient equations. The first section illustrates the rationales for deriving the shown equations, and may prove useful for creating models of future components.

A.1 Steady State Equations

In this section we give the set of steady state equations solved when component modules are assembled to represent the plant system shown in Figure 2-2. Each of the components in this figure is represented by a module that contains the component equations as shown below. The steady state equations simulate the system with all time-changing elements removed.

All of the equations are ultimately derived from simple conservation laws, however they are expressed in two fashions. About half of the equations are in the standard conservation format which the reader will expect. The other half of the equations ask GAS-PASS/CO_2 to match a variable to a calculated value. This calculated value will be based upon a more detailed (external) calculation which GAS-PASS takes as truth, assuming that it satisfies the conservation laws.

The reader will note that several equations are trivial (i.e. $P_{in}=P_{out}$) and thus it might be possible to specify these directly in the code. This temptation (which would speed the calculation) should be avoided to assure numerical consistency. If variables are modified during a calculation then it is vital that other components have not used these variables already. With the general and somewhat complicated nature of the GAS-PASS input deck there is no easy way to assure that this is true, therefore a general rule was made:

> *variables which are used in other components can only be modified by the numerical solver.*

All of the equations are expressed as they are numerically solved, with the right hand side expected to equal 0 and all values are normalized (typically the only term in the denominator) to keep them on the same scale. It is worth noting that equation normalization is a standard practice in the numerical simulation community[88] and is required to successfully simulate this cycle with this solution method. While separate normalization of each equation will change the variables' slopes towards the root, it will not change the slopes' direction of travel (just the rate). Furthermore, as long as a root is found (all conservation equations are simultaneously satisfied), then the simulation process to arrive at the root is largely irrelevant. When one tries to converge GAS-PASS without equation normalization, the Jacobian condition number (a measure of how easy a problem is to solve digitally) becomes much smaller than machine precision, 10^{-19}, for the S-CO_2 recompression cycle, therefore the simulation fails. The current transient Jacobian condition number, including normalization, is 10^{-11}.

Note that inlet values are symbolized by a_i on the right hand side and outlet values are symbolized by a_o on the right hand side. The first time a type of equation is shown it will include a brief derivation. Future equations of the same type assume a similar derivation.

There are three fluids in the indirect cycle: the hot fluid symbolized by ^{hot} on the right-hand side, which is the sole source of heat addition, the working fluid symbolized by ^{fluid} on the right-hand side, which moves inside the cycle and performs all the work within the system, and the cold fluid symbolized by ^{cold} on the right-hand side, which removes all energy from the cycle.

Finally, note that the control volumes used in the components contain both the active component (e.g. the turbine) and all the piping following that component until the next active component begins. The volumes for the various components and piping and several reasons for lumping them are discussed in "Appendix B.4 Separating vs. Lumping Piping Volumes in the S-CO_2 Recompression Cycle."

6.4.3.1 A.1.1 Printed Circuit Heat Exchanger

The heat exchangers used in the S-CO_2 recompression cycle are all Heatric™ printed circuit heat exchangers (PCHE), and they are solved in an identical manner: via the detailed 1D modeling code which GAS-PASS/CO_2 treats as a black box producing correctly calculated values.

The calculated values take advantage of the general nature of the GAS-PASS/CO_2 numerical solver by solving for the hot fluid outlet and cold fluid ***inlet*** of this counter-flow heat exchanger. If the code were to solve for both fluid outlets it would increase, by at least an order of magnitude, the necessary run time, due to the nature of the calculation.

To solve a counter-flow heat exchanger numerically one must guess at the outlet values of one stream (say the cold fluid) then progressively march through the heat exchanger using the true hot fluid conditions and guessed cold fluid conditions. Once the other side of the PHCE is reached the calculated cold fluid enthalpy and pressure (from the guess) will not match the true incoming conditions. Thus a loop must be added to correct the fluid pressure guess, and a second loop to correct the fluid enthalpy guess. Therefore, there are two outer loops to calculate a counter-flow heat exchanger's fluid outlets in the steady state calculation (in the transient there is an additional loop to correct for mass storage).

GAS-PASS/CO_2 avoids this problem by solving from one side of the PCHE (the hot fluid inlet and cold fluid outlet) only. The numerical solver will then take care of matching the fluid inlet and outlet values of the various components in the plant. In general this will mean that GAS-PASS/CO_2 will solve for the PCHE cold fluid inlet conditions twice (also from the previous component) and the cold fluid outlet conditions not at all. However, to match the cold fluid inlet values will require varying the cold fluid outlet until the system becomes consistent. All of the subsequent PCHEs are solved in a similar manner. More detail regarding the PCHE solver code may be found in Section 3.6.2.1.

$$h_o^{hot-fluid} = h_{o-calc}^{hot-fluid} \qquad \textbf{(A-1)}$$

$$0 = h_o^{hot-fluid} - h_{o-calc}^{hot-fluid}$$

$$F(1) = \frac{h_o^{hot-fluid} - h_{o-calc}^{hot-fluid}}{h_o^{hot-fluid}}$$

Note that the F vector represents the error in each conservation equation. When $F(i)=0$ then the conservation equation is solved exactly. When all of the F vectors are simultaneously zero (to user specified tolerance) then the system is at the root – everything is conserved and the solution is achieved.

Also note that in the PCHE equations (Equation A-1 through Equation A-6) the term "calc" refers to the output of the detailed, independent PCHE computational model described in Section 3.6.2.1. At each time step, GAS-PASS/CO_2 supplies the PCHE computational model with boundary conditions to a heat exchanger which then computes the heat exchanger's performance. These calculated results are then reported back to GAS-PASS/CO_2 in the form of variables called "calc."

$$F(2) = \frac{P_o^{hot-fluid} - (P_{o-calc}^{hot-fluid} - P_{fix}^{hot-fluid})}{P_o^{hot-fluid}} \qquad \textbf{(A-2)}$$

The calculated hot outlet pressure has an addition term, $P_{fix}^{hot-fluid}$, which is specified in the input file for the IHX. This constant, non-modeled, pressure drop allows the designer to match variations in PCHE designs, such as straight versus zig-zag channels, without significantly modifying the solution process. It should be set to 0 unless the designer has a need to match non-modeled pressure drops.

$$F(3) = \frac{\dot{m}_o^{hot-fluid} - \dot{m}_{o-calc}^{hot-fluid}}{\dot{m}_o^{hot-fluid}} \tag{A-3}$$

$$F(4) = \frac{h_i^{cold-fluid} - h_{i-calc}^{cold-fluid}}{h_i^{cold-fluid}} \tag{A-4}$$

$$F(5) = \frac{P_i^{cold-fluid} - (P_{i-calc}^{cold-fluid} + P_{fix}^{cold-fluid})}{P_i^{cold-fluid}} \tag{A-5}$$

The additional term, $P_{fix}^{cold-fluid}$, serves the same purpose as the additional hot stream term for the carbon dioxide side of the PCHE.

$$F(6) = \frac{\dot{m}_i^{cold-fluid} - \dot{m}_{i-calc}^{cold-fluid}}{\dot{m}_i^{cold-fluid}} \tag{A-6}$$

6.4.3.2 A.1.2 Turbine

The turbine is the sole source of work in this cycle. The reader should note that all the turbomachines are on the same shaft, thus turbomachine work is transferred directly. These initial equations will include a brief derivation for the reader's benefit.

The turbine mass conservation equation is not used, to prevent the creation of a singular solution matrix with redundant mass variables (see Section 3.6.2.2). To avoid this problem but still allow the system to be solved, an inventory control equation will be added at the end of this section.

The energy conservation equation is:

$$\dot{E}_{in} = \dot{E}_{out} \tag{A-7}$$

$$\dot{m}_i^{fluid} * h_i^{fluid} = \dot{W} + \dot{m}_o^{fluid} * h_o^{fluid}$$

$$0 = \dot{m}_i^{fluid} * h_i^{fluid} - \dot{m}_o^{fluid} * h_o^{fluid} - \dot{W}$$

$$F(7) = \frac{\dot{m}_i^{fluid} * h_i^{fluid} - \dot{m}_o^{fluid} * h_o^{fluid} - \dot{W}}{\dot{m}_i^{fluid} * h_i^{fluid}}$$

The pressure drop equation is:

$$P_{in} - P_{out} = \Delta P \tag{A-8}$$

$$P_i^{fluid} - P_{o-Calc}^{fluid} = P_i^{fluid} - P_o^{fluid}$$

$$0 = P_o^{fluid} - P_{o-Calc}^{fluid}$$

$$F(8) = \frac{P_o^{fluid} - P_{o-Calc}^{fluid}}{P_o^{fluid}}$$

$P_{o-Calc}^{fluid} = \frac{P_{in}^{fluid}}{P_R}$, and pressure ratio, $P_R\left(\dot{m}_{in}, \omega\right)$, is interpolated with mass flow rate and shaft speed from the turbine's performance curves.

Similarly, the outlet enthalpy equation is:

$$h_{in} - h_{out} = \Delta h \tag{A-9}$$

$$h_i^{fluid} - h_{o-Calc}^{fluid} = h_i^{fluid} - h_o^{fluid}$$

$$0 = h_o^{fluid} - h_{o-Calc}^{fluid}$$

$$F(9) = \frac{h_o^{fluid} - h_{o-Calc}^{fluid}}{h_o^{fluid}}$$

$h_{o-Calc}^{fluid} = h_i^{fluid} - \eta * \left(h_i^{fluid} - h_{o-Ideal}^{fluid}\right)$, with efficiency, $\eta\left(\dot{m}_{in}, \omega\right)$, interpolated with mass flow rate and shaft speed from the turbine's performance curves, and $h_{o-Ideal}^{fluid}$ is the enthalpy change for isentropic expansion to P_o^{fluid}.

6.4.3.3 A.1.3 Compressors

The mass conservation equation is:

$$F(10) = \frac{\dot{m}_i^{fluid} - \dot{m}_o^{fluid}}{\dot{m}_i^{fluid}} \tag{A-10}$$

The energy conservation equation is:

$$F(11) = \frac{\dot{W} + \dot{m}_i^{fluid} * h_i^{fluid} - \dot{m}_o^{fluid} * h_o^{fluid}}{\dot{W} + \dot{m}_i^{fluid} * h_i^{fluid}} \tag{A-11}$$

The pressure rise equation is:

$$F(12) = \frac{P_o^{fluid} - P_{o-Calc}^{fluid}}{P_o^{fluid}} \tag{A-12}$$

Where $P_{o-Calc}^{fluid} = P_i^{fluid} * P_R$, and $P_R\left(\dot{m}, \omega\right)$ is interpolated with mass flow rate and shaft speed from the recompression compressor's performance curves.

The outlet enthalpy equation is:

$$F(13) = \frac{H_o^{fluid} - H_{o-Calc}^{fluid}}{H_o^{fluid}} \quad \textbf{(A-13)}$$

$H_{o-Calc}^{fluid} = H_i^{fluid} + \frac{\left(H_{o-Ideal}^{fluid} - H_i^{fluid}\right)}{\eta}$, with $\eta\left(\dot{m}, \omega\right)$ interpolated with mass flow rate and shaft speed from the compressor's performance curves, and $H_{o-Ideal}^{fluid}$ is the enthalpy change in isentropic compression to P_o^{fluid}.

6.4.3.4 A.1.4 Mixing Junction

The mass flow rates at a mixing-T junction, assuming incompressible flow, are related by

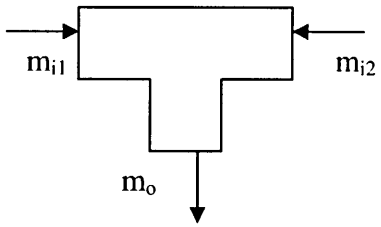

Mixing-T Junction Diagram

When applied to the steady state case one has:

$$F(14) = \frac{\dot{m}_{i1}^{fluid} + \dot{m}_{i2}^{fluid} - \dot{m}_o^{fluid}}{\dot{m}_{i1}^{fluid} + \dot{m}_{i2}^{fluid}} \quad \textbf{(A-14)}$$

The energy conservation equation is:

$$F(15) = \frac{\dot{m}_{i1}^{fluid} * h_{i1}^{fluid} + \dot{m}_{i2}^{fluid} * h_{i2}^{fluid} - \dot{m}_o^{fluid} * h_o^{fluid}}{\dot{m}_{i1}^{fluid} * h_{i1}^{fluid} + \dot{m}_{i2}^{fluid} * h_{i2}^{fluid}} \quad \textbf{(A-15)}$$

The mixing-T incoming stream1 fluid pressure assumes no pressure drop thus:

$$F(16) = \frac{P_{i1}^{fluid} - P_o^{fluid}}{P_{i1}^{fluid}} \quad \textbf{(A-16)}$$

The mixing-T incoming stream2 fluid pressure assumes no pressure drop thus:

$$F(17) = \frac{P_{i2}^{fluid} - P_o^{fluid}}{P_{i2}^{fluid}} \quad \textbf{(A-17)}$$

Note that this provides one more equation than our general derivation warrants, due to the second pressure equation. This formulation is used because it is the best alternative available, considering that:

- One could combine both pressure equations into one, but it is undesirable to use a numerical solver to solve for two pressures simultaneously. Furthermore, one would need to prevent the pressure differences between the streams from self canceling, thus some type of sign correction is necessary, which will confuse any solver.
- A second option would match both incoming fluid streams and then put that result directly into the outgoing pressure memory. Unfortunately, this may cause problems because the numerical solver is determining the outgoing pressure, thus it may try to change it before or after the memory substitution. It is somewhat dangerous to directly change the variables the solver is solving for.

This extra pressure equation is easily handled by introducing a valve before one of the mixing-T incoming streams (e.g. at the splitting-T). This valve will be used to match the desired mixing-T incoming stream pressure with that at the outlet of the previous component (in our case the recompression compressor) by changing the pressure drop coefficient, K_{valve}. Therefore, the outgoing fluid pressure of the valve is never solved for (K_{valve} is solved in its place) and we are keeping a rigorous treatment of our solution variables.

6.4.3.5 A.1.5 Valve

A valve serves solely to drop a stream's pressure to match other system pressures.

The mass conservation equation is:

$$F(18) = \frac{\dot{m}_i^{fluid} - \dot{m}_o^{fluid}}{\dot{m}_i^{fluid}} \qquad \textbf{(A-18)}$$

The energy conservation equation is:

$$F(19) = \frac{h_i^{fluid} - h_o^{fluid}}{h_i^{fluid}} \qquad \textbf{(A-19)}$$

The pressure rise equation is:

$$K_{calc} = \frac{\left(P_{in}^{fluid} - P_{o}^{fluid}\right) * 2 * \rho_{o}^{fluid} * A_{valve}^{2}}{\left(\dot{m}_{o}^{fluid}\right)^{2}} \quad \text{(A-20)}$$

$$F(20) = \frac{K_{calc} - K_{valve}}{\frac{P_{o}^{fluid} * 2 * \rho_{o}^{fluid} * A_{valve}^{2}}{\left(\dot{m}_{o}^{fluid}\right)^{2}}}$$

K is the valve pressure drop coefficient. The normalization factor, the denominator, is large to provide a reasonable condition number when this equation is used with the S-CO_2 recompression cycle.

6.4.3.6 A.1.6 Splitting Junction

A splitting-T junction presents a special case since it has two fluids exiting the component from a single input. This will be handled by treating it as two separate components in practice, with the same fluid input. The combined equations are shown below.

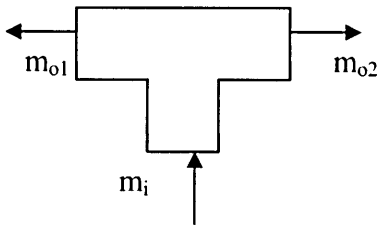

Splitting Junction Diagram

The mass conservation for the first outgoing fluid stream is:

$$F(21) = \frac{x * \dot{m}_{i}^{fluid} - \dot{m}_{o1}^{fluid}}{x * \dot{m}_{i}^{fluid}} \quad \text{(A-21)}$$

where x is the fluid fraction (a boundary condition) which goes to the first junction and is put in the input file for user convenience.

The energy conservation equation for the first stream is:

$$F(22) = \frac{h_{i}^{fluid} - h_{o1}^{fluid}}{h_{i}^{fluid}} \quad \text{(A-22)}$$

The first stream assumes no pressure drop thus:

$$F(23) = \frac{P_{i}^{fluid} - P_{o1}^{fluid}}{P_{i}^{fluid}} \quad \text{(A-23)}$$

The mass conservation for the second outgoing fluid stream is:

$$F(24) = \frac{\dot{m}_i^{fluid} - \dot{m}_{o1}^{fluid} - \dot{m}_{o2}^{fluid}}{\dot{m}_i^{fluid}} \quad \textbf{(A-24)}$$

The energy conservation equation for the second stream is:

$$F(25) = \frac{h_i^{fluid} - h_{o2}^{fluid}}{h_i^{fluid}} \quad \textbf{(A-25)}$$

The second stream assumes no pressure drop thus:

$$F(26) = \frac{P_i^{fluid} - P_{o2}^{fluid}}{P_i^{fluid}} \quad \textbf{(A-26)}$$

This formulation allows the calculation of the six outgoing fluid stream properties (two mass flow rates, two enthalpies, and two pressures) with six equations, while simultaneously forcing the matching of outgoing pressures and enthalpies which would physically happen at a splitting-T, and is therefore physically and numerically consistent. Furthermore, by using a flow split fraction the user can control the outgoing fluid mass flow rates at will.

Note that, in general, a splitting-T requires a valve and a mixing-T. If one adds all of these components together then there is one more boundary condition than the number of equations. Thus, the designer can control a splitting-T, valve, and mixing-T by either the flow split, or the valve fraction.

6.4.3.7 A.1.7 Primary

A primary component simulates a basic primary loop excluding the IHX and reactor. It does not have a mass conservation equation, to prevent linear dependence in the reactor loop. Recall that the present simulation is focused upon the power cycle.

The specific enthalpy equation is:

$$F(27) = \frac{h_i^{fluid} - h_o^{fluid}}{h_i^{fluid}} \quad \textbf{(A-27)}$$

The mass flow rate is specified by a pump work factor, which allows the designer to control the reactor loop mass flow rate via boundary conditions:

$$F(28) = \frac{f_{pump} - \dot{m}_o^{fluid}}{f_{pump}} \quad \textbf{(A-28)}$$

K is the valve pressure drop coefficient. The normalization factor is large to provide a reasonable condition number when this equation is used with the S-CO_2 recompression cycle.

6.4.3.8 A.1.8 Reactor

The reactor component provides heat addition for the system. It does not have a pressure drop equation thus the user sets the outlet pressure directly as a boundary condition.

The energy conservation equation is:

$$F(29) = \frac{h_i^{fluid} + \frac{\dot{Q}_{reactor}}{\dot{m}_{fluid}} - h_o^{fluid}}{h_i^{fluid} + \frac{\dot{Q}_{reactor}}{\dot{m}_o}} \quad \textbf{(A-29)}$$

The mass conservation equation is:

$$F(30) = \frac{\dot{m}_i^{fluid} - \dot{m}_o^{fluid}}{\dot{m}_i^{fluid}} \quad \textbf{(A-30)}$$

6.4.3.9 A.1.9 Inventory

The mass of CO_2 is computed within each component in the cycle and summed to give a total fluid inventory. The fluid density is calculated at the outlet enthalpy, and pressure and the volumes are inputs.

$$F(31) = \frac{TotMass - \sum_k Vol^k * \rho^k_{o(h,P)}}{TotMass} \quad \textbf{(A-31)}$$

6.4.3.10 A.1.10 Shaft

Conservation of mechanical energy for the turbomachinery shaft gives

$$F(32) = \frac{\sum_k \dot{W}^k_{Gen} - \sum_k \dot{W}^k_{Rem}}{\sum_k \dot{W}^k_{Gen}} \quad \textbf{(A-32)}$$

Note that the removal term includes $W_{drag} = K_{drag}\omega^2$, where ω is the rotational speed of the common shaft, and W_{gen}. In effect, this equation allows the calculation of the energy supplied (or demanded) by the generator.

A.2 Time-Difference Equations

The time-difference equations are identical to the steady state equations, with the addition of mass and energy storage terms. Only equations with the additional terms will be shown below, otherwise they are the same as in the steady state. The left hand superscript ^{n} refers to the current time step while $^{n-1}$ is from the previous time step. The first time an equation is shown a brief derivation will be shown. Future equations of the same type assume a similar derivation.

6.4.3.11 A.2.1 PCHE

The transient PCHEs are solved in a similar manner (e.g. have the same solution equations but a different, internal, calculation process) to the steady state with the addition of mass storage and energy storage terms. More detail regarding the transient PCHE solver code may be found in Section 3.5.5.

6.4.3.12 A.2.2 Turbine

The turbine is the sole source of work in this cycle. The reader should note that all the turbomachines are on the same shaft; thus turbomachine work is transferred directly. These first equations will show a brief derivation for the reader's benefit.
Recall from Section 3.2.2.2.3 that energy conservation for one dimensional flow in a stationary control volume (Equation 4-39 in Todreas and Kazimi[51]) is:

$$\dot{E}_{cv} = \sum_{i=1}^{I} \dot{m}_i \left(h_i^{\circ} + g z_i \right) + \dot{Q} + \dot{Q}_{gen} - \dot{W}_{shaft} - \dot{W}_{normal} - \dot{W}_{shear}$$

Neglecting shear work and the differences between kinetic and potential energy and conflating $\dot{Q}_{gen}$ with $\dot{E}$, the previous equation becomes (Equation 6-2 in Todreas and Kazimi[51]):

$$\dot{E}_{cv} = \sum_{i=1}^{I} \dot{m}_i h_i + \dot{Q} - \dot{W}_{shaft} - \dot{W}_{normal}$$

For a turbine the control volume is assumed to be adiabatic and kinetic energy effects are neglected, thus:

$$\frac{dE_{cv}}{dt} = -\dot{W} + \dot{m}_{in} h_{in} - \dot{m}_{out} h_{out}$$

The energy conservation equation then becomes:

$$\frac{dE_{cv}}{dt} = -\dot{W} + \dot{m}_{in} h_{in} - \dot{m}_{out} h_{out} \qquad \textbf{(A-33)}$$

$$\frac{{}^{n}E - {}^{n-1}E}{\Delta t} = {}^{n}\dot{m}_i^{fluid} * {}^{n}h_i^{fluid} - {}^{n}\dot{m}_o^{fluid} * {}^{n}h_o^{fluid} - {}^{n}\dot{W}$$

$$0 = {}^{n}\dot{m}_i^{fluid} * {}^{n}h_i^{fluid} - {}^{n}\dot{m}_o^{fluid} * {}^{n}h_o^{fluid} - {}^{n}\dot{W} - \frac{{}^{n}E - {}^{n-1}E}{\Delta t}$$

$$F(33) = \frac{{}^{n}\dot{m}_i^{fluid} * {}^{n}h_i^{fluid} - {}^{n}\dot{m}_o^{fluid} * {}^{n}h_o^{fluid} - {}^{n}\dot{W} - \frac{{}^{n}E - {}^{n-1}E}{\Delta t}}{{}^{n}\dot{m}_i^{fluid} * {}^{n}h_i^{fluid}}$$

Note that the energy stored in a component is the sum of the internal energy of the fluid and the internal energy of the structure. At any time step:

$${}^{n}E = {}^{n}E^{fluid} + {}^{n}E^{struct}$$

$${}^{n}E^{fluid} = {}^{n}M^{fluid} * {}^{n}U^{fluid}$$

$${}^{n}E^{struct} = {}^{n}M^{struct} * {}^{n}C^{struct} * {}^{n}T^{struct}$$

The pressure drop equation does not change.

The outlet enthalpy equation is replaced with a work equation. This allows the separation of turbine work effects (in the vary small volume within the turbine blades) from energy storage effects (in the large diffuser and piping volume).

$${}^{n}\dot{W}_{calc} = {}^{n}\eta * {}^{n}\dot{m}_i^{fluid} * \left({}^{n}h_i^{fluid} - h_{o-Ideal}^{fluid} \right) \qquad \textbf{(A-34)}$$

$$F(34) = \frac{{}^{n}\dot{W} - {}^{n}\dot{W}_{calc}}{{}^{n}\dot{W}}$$

The isentropic efficiency, $\eta\left(\dot{m}_{in}, \omega \right)$, is interpolated with mass flow rate and shaft speed from the turbine's performance curves, and $h_{o-Ideal}^{fluid}$ is the enthalpy change for isentropic expansion to P_o^{fluid}.

Once again there is no mass conservation equation, to prevent a singular matrix. Instead inventory control is used.

6.4.3.13 A.2.3 Compressor

The compressor mass conservation equation is:

$$F(35) = \frac{{}^{n}\dot{m}_i^{fluid} - {}^{n}\dot{m}_o^{fluid} - \frac{{}^{n}M^{fluid} - {}^{n-1}M^{fluid}}{\Delta t}}{{}^{n}\dot{m}_i^{fluid}} \qquad \textbf{(A-35)}$$

The compressor pressure equation does not change.

The energy conservation equation is:

$$F(36) = \frac{{}^{n}W + {}^{n}\dot{m}_i^{fluid} * {}^{n}h_i^{fluid} - {}^{n}\dot{m}_o^{fluid} * {}^{n}h_o^{fluid} - \frac{{}^{n}E - {}^{n-1}E}{\Delta t}}{{}^{n}W + {}^{n}\dot{m}_i^{fluid} * {}^{n}h_i^{fluid}} \quad \textbf{(A-36)}$$

The outlet enthalpy equation is replaced with a work equation. This allows the separation of compressor work effects (in the vary small volume within the compressor blades) from energy storage effects (in the large diffuser and piping volume).

$${}^{n}\dot{W}_{calc} = \frac{{}^{n}\dot{m}_i^{fluid} * \left({}^{n}h_i^{fluid} - h_{o-Ideal}^{fluid} \right)}{{}^{n}\eta} \quad \textbf{(A-37)}$$

$$F(37) = \frac{{}^{n}\dot{W} - {}^{n}\dot{W}_{calc}}{{}^{n}\dot{W}}$$

The isentropic efficiency, $\eta\left(\dot{m}_{in}, \omega \right)$, is interpolated with mass flow rate and shaft speed from the compressor's performance curves, and $h_{o-Ideal}^{fluid}$ is the enthalpy change for isentropic compression to P_o^{fluid}.

6.4.3.14 A.2.4 Mixing Junction

The mixing-T mass conservation equation is:

$$F(38) = \frac{{}^{n}\dot{m}_{i1}^{fluid} + {}^{n}\dot{m}_{i2}^{fluid} - {}^{n}\dot{m}_o^{fluid} - \frac{{}^{n}M^{fluid} - {}^{n-1}M^{fluid}}{\Delta t}}{{}^{n}\dot{m}_o^{fluid}} \quad \textbf{(A-38)}$$

The energy conservation equation is:

$$F(39) = \frac{{}^{n}\dot{m}_{i1}^{fluid} * {}^{n}h_{i1}^{fluid} + {}^{n}\dot{m}_{i2}^{fluid} * {}^{n}h_{i2}^{fluid} - {}^{n}\dot{m}_o^{fluid} * {}^{n}h_o^{fluid} - \frac{{}^{n}E - {}^{n-1}E}{\Delta t}}{{}^{n}\dot{m}_o^{fluid} * {}^{n}h_o^{fluid}} \quad \textbf{(A-39)}$$

The mixing-T pressure equations do not change.

6.4.3.15 A.2.5 Splitting Junction

The splitting -T stream 1 mass conservation equation is:

$$F(40) = \frac{{}^{n}x * {}^{n}\dot{m}_i^{fluid} - {}^{n}\dot{m}_{o1}^{fluid} - \frac{{}^{n}M_1^{fluid} - {}^{n-1}M_1^{fluid}}{\Delta t}}{x * {}^{n}\dot{m}_i^{fluid}} \quad \text{(A-40)}$$

The splitting -T stream 1 energy conservation equation is:

$$F(41) = \frac{{}^{n}x * {}^{n}\dot{m}_i^{fluid} * {}^{n}h_i^{fluid} - {}^{n}\dot{m}_{o1}^{fluid} * {}^{n}h_{o1}^{fluid} - \frac{{}^{n}E_1 - {}^{n-1}E_1}{\Delta t}}{{}^{n}x * {}^{n}\dot{m}_i^{fluid} * {}^{n}h_i^{fluid}} \quad \text{(A-41)}$$

The splitting-T pressure equations do not change.

The splitting-T stream 2 mass conservation equation is:

$$F(42) = \frac{(1 - {}^{n}x) * {}^{n}\dot{m}_i^{fluid} - {}^{n}\dot{m}_{o2}^{fluid} - \frac{{}^{n}M_2^{fluid} - {}^{n-1}M_2^{fluid}}{\Delta t}}{(1 - {}^{n}x) * {}^{n}\dot{m}_i^{fluid}} \quad \text{(A-42)}$$

The splitting -T stream 2 energy conservation equation is:

$$F(43) = \frac{(1 - {}^{n}x) * {}^{n}\dot{m}_i^{fluid} * {}^{n}h_i^{fluid} - {}^{n}\dot{m}_{o2}^{fluid} * {}^{n}h_{o2}^{fluid} - \frac{{}^{n}E_1 - {}^{n-1}E_1}{\Delta t}}{(1 - {}^{n}x) * {}^{n}\dot{m}_i^{fluid} * {}^{n}h_i^{fluid}} \quad \text{(A-43)}$$

6.4.3.16 A.2.6 Valve

The valve equations do not change since the valve has a very small volume.

6.4.3.17 A.2.7 Primary

The primary component equations do not change.

6.4.3.18 A.2.8 Reactor

The reactor equations do not change.

6.4.3.19 A.2.9 Inventory

The mass inventory equation does not change.

6.4.3.20 A.2.10 Shaft

The transient shaft equation includes shaft inertia:

$$0 = {}^{n}\omega - {}^{n-1}\omega - \frac{\sum_{k} {}^{n}\dot{W}_{Gen}^{k} - \sum_{k} {}^{n}\dot{W}_{Rem}^{k}}{{}^{n}\omega I}\Delta t \qquad \textbf{(A-44)}$$

$$F(44) = \frac{{}^{n}\omega - {}^{n-1}\omega - \frac{\sum_{k} {}^{n}\dot{W}_{Gen}^{k} - \sum_{k} {}^{n}\dot{W}_{Rem}^{k}}{{}^{n}\omega I}\Delta t}{{}^{n}\omega}$$

Appendix B: Suggested Future Improvements

This section will provide an in depth look at four possible future improvements. The first section analyses the uncertainty in the water heat transfer correlation in the transition region. The second section analyses the benefits and methods for multi-threading GAS-PASS/CO_2. The third section provides a method to more accurately model structure conduction without significant computational burden.. The final section looks at the consequences of separating volumes from components for this cycle. A general overview of recommended future improvements was offered in Section 6.4 of Chapter 6.

B.1 Water Heat Transfer Correlation Uncertainty

RELAP5 computed significantly higher precooler heat transfer than GAS-PASS/CO_2 originally did using Dostal's[3] correlations. For the tested design RELAP5 predicted 421 MW of heat transfer while the original correlations predicted only 311 MW. Upon investigation it was surprising to find that it was primarily the water heat transfer coefficients that differ between RELAP and GAS-PASS/CO_2 .

Pope[9] consulted RELAP's developer, Dr. Cliff Davis, who provided a rough understanding of RELAP's correlations, but suffice it to say that RELAP probably handles water correctly. It is the water laminar and transition regions where the correlations differ the most. If GAS-PASS/CO_2 correlations are moved to solely turbulent flow then the computed heat transferred matches within 0.5%.

After some investigation GAS-PASS/CO_2 correlations were updated by:

- Adding a laminar fluid thermodynamic entrance effect.
- Adding a turbulent fluid thermodynamic entrance effect.
- Changing the correlation transition region.

The correlation is still Gnielinski based as shown in Equation B-1.

Equation B-1: Basic Gnielinski Correlation **(B-1)**

$$Nu = \frac{f/2\,(\mathrm{Re}-1000)\mathrm{Pr}}{1+12.7\sqrt{f/2}\left(\mathrm{Pr}^{2/3}-1\right)}$$

The entrance region and effects increase the heat transfer by roughly a few percent, but the selection of the transition region is important. The previous transition region stretched from $2300 < \mathrm{Re} < 5000$, with the turbulent correlation stated to be valid from $\mathrm{Re} > 2300$. If the transition was instead shifted to a smaller band around the correlation's

starting point, i.e. 1800 < Re < 2800, the amount of heat transferred increases by a further 19% (note that the CO_2 is well within the turbulent region in the precooler).

The reason for this increase is clear from viewing the water side heat transfer coefficients without a transition region as shown in Figure B-1. The left side of the figure shows the turbulent HTC and the right side of the figure shows the laminar HTC. Clearly, a transition region that moves more of the turbulent factor to the laminar side will increase the overall heat transfer.

More importantly, there is no obvious reason to transition between the correlations between 2300 < Re < 5000, when both the correlations are stated to be valid until about Re=2300. The "transition" region is bridging two correlations, not trying to apply a separate mixed flow regime correlation, thus typical Reynolds transition numbers are required.

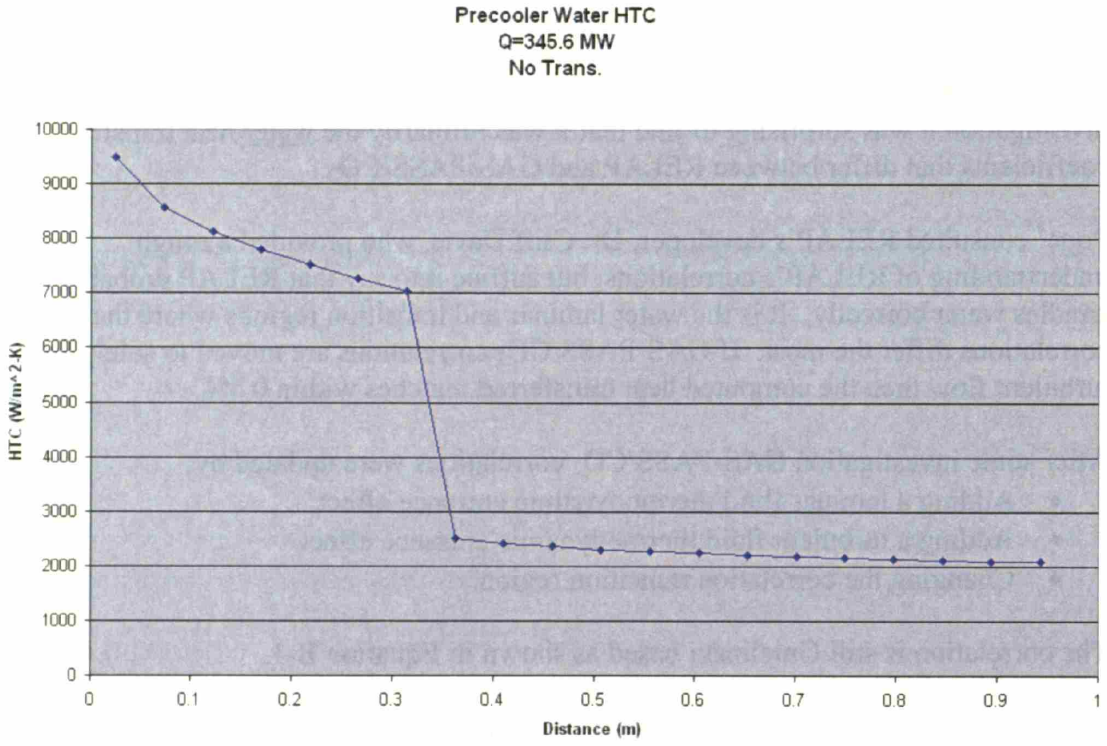

Figure B-1: Water HTC No Transition Region

It may be worth investigating why the laminar heat transfer coefficients are so much lower in GAS-PASS/CO_2 than those in RELAP. GAS-PASS/CO_2's laminar coefficient comes from Hesselgreaves[71] (2001) and is for semi-circular channels. It may also be worth noting that Wang and Hihara[66] (2002) published a detailed computational, steady state, S-CO_2-to-water heat transfer benchmark using numerous correlations but assumed fully turbulent flow in all cases. Finally, Oslen[69] (2000) performed experiments with S-CO_2 and water under somewhat different conditions than those found in a PCHE, and

found that none of the tested correlations performed well in all circumstances. The basic Gnielinski[68] (1976) correlation was found to under-predict in all cases

Using the entrance length effects and adjusted transition region, GAS-PASS/CO_2 predicts 391 MW of heat transferred in a comparison precooler compared to RELAP's 421 MW, thus showing a 7% discrepancy. Until further data become available this is assumed to be an acceptable deviation.

B.2 Multi-Threading

Moore's law has allowed many scientific advances due to the rapidly increasing computational power available to researchers. While the law is still being met, recent trends point toward significant changes that will affect scientific computation.

For several years processor clock speeds have increased relatively little, as shown in Figure B-2[89]. This decrease in clock speed improvements appears to be coming from fundamental physical limits such as current dissipation and heat generation. While it is too early to tell how close clock speeds are to this limit, there is every indication that software will have to adapt to a very different computing environment in the future.

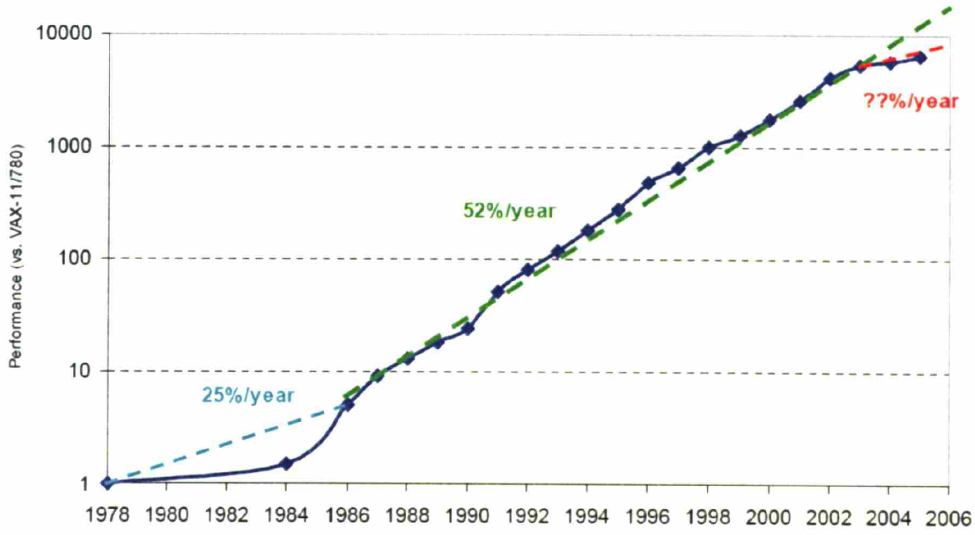

Figure 2. Processor performance improvement between 1978 and 2006 using integer SPEC [SPEC 2006] programs. RISCs helped inspire performance to improve by 52% per year between 1986 and 2002, which was much faster than the VAX minicomputer improved between 1978 and 1986. Since 2002, performance has improved less than 20% per year. By 2006, processors will be a factor of three slower than if progress had continued at 52% per year. This figure is Figure 1.1 in [Hennessy and Patterson 2007].

Figure B-2: Processor Speed Increase over Time[89]

Recall that Moore's Law originally addressed transistor density, which has proved accurate. Recent processor advances have largely come in the form of parallelism rather than clock speed. By the end of 2006, dual core chips had become standard and quad-core chips were widely available. At present it appears that most of the future

improvements in computational power will take place by means of multi-core chips rather than due to clock speed.

To take advantage of this new direction, GAS-PASS can be rewritten to allow multi-threading. Multi-threading is a subset of parallelism, where multiple jobs run on the same computer (i.e. have shared memory) which probably uses multiple processors. Where distributed parallel computation faces a major communication bottleneck, multi-threading computation starts with all threads sharing the same data and allows very rapid communication between threads. Compared to parallel computation among computers, multi-threading is a low cost, fast process.

Since each thread begins life with access to the system memory (although each thread does create its own stack) there are few startup costs and few reasons that this process cannot be expanded to a large number of processors for a large speed-up. Unfortunately, multi-threaded programming is more complex than serial programming and in many cases serial calculations are required. If a code is non-reentrant (i.e. uses global variables as GAS-PASS is forced to do when using the IMSL solvers) then numerous potential problems arise as different processes attempt to read and write from the same memory simultaneously. However, this can be alleviated by restricting the multi-threading capability to a small part of the code in GAS-PASS.

Jacobian Threading

GAS-PASS spends the majority of its time computing Jacobians to find the root of a non-linear system of equations. Computing a Jacobian requires evaluating all n equations $n+1$ times. Finding the actual root, once the Jacobian is calculated, typically requires only a few iterations (2-10) which evaluate all n equations. The S-CO_2 recompression cycle can be modeled with 57 equations, thus it is entirely possible that GAS-PASS spends 90% of its time (startup time is negligible for common transients) computing Jacobians.

$$J = \begin{bmatrix} \frac{\partial F_1}{\partial x_1} & \frac{\partial F_1}{\partial x_2} & \cdots & \frac{\partial F_1}{\partial x_n} \\ \frac{\partial F_2}{\partial x_1} & \frac{\partial F_2}{\partial x_2} & \cdots & \frac{\partial F_2}{\partial x_n} \\ \vdots & \vdots & \vdots & \vdots \\ \frac{\partial F_m}{\partial x_1} & \frac{\partial F_m}{\partial x_2} & \cdots & \frac{\partial F_m}{\partial x_n} \end{bmatrix}$$

Figure B-3: Jacobian

This presents an obvious opportunity for multi-threading. Computing a Jacobian is almost an embarrassingly parallel process, where there is no communication required to calculate rows of the Jacobian. The exception to this rule is the computation of the solution to PCHE zones. During the transient, each PCHE zone is calculated by solving a

7 equation non-linear system of equations using an IMSL solver. To make the code reentrant this global memory solver should be replaced with reentrant code. Once this has been accomplished, calculating a Jacobian can be subdivided up into n embarrassingly parallel sub-tasks.

The computation time for a job using N processors may be estimated from Equation B-2 where T_1 is the time necessary for one processor to run a simulation, η_1 is the fraction of the one-processor simulation time spent calculating Jacobians, and η_2 is the overhead required to create and merge threads. Setting the derivative of Equation B-2 equal to zero leads to an optimal number of threads, which depends solely upon the multi-threading overhead factor as shown in Equation B-3 – more processors decrease the calculation time until overhead becomes prohibitive.

Equation B-2: Multithread Performance Scaling **(B-2)**

$$T_n = (1-\eta_1)T_1 + \frac{(\eta_1 T_1)}{N} + (\eta_1 T_1)\eta_2 N$$

Equation B-3: Optimal Number of Threads **(B-3)**

$$N = \sqrt{\frac{1}{\eta_2}}$$

Figure B-4 shows the results of using Equation B-2 with some rough guesses of the applicable factors, and Table B-1 lists the optimal number of threads for several overhead factors. This figure shows that low overhead leads to large numbers of optimal processors to minimize simulation time by splitting up the Jacobian calculation.

Table B-1: Optimal Threads by Overhead

Overhead Factor	Optimal Threads
0.0001	100
0.001	32
0.01	10
0.1	3

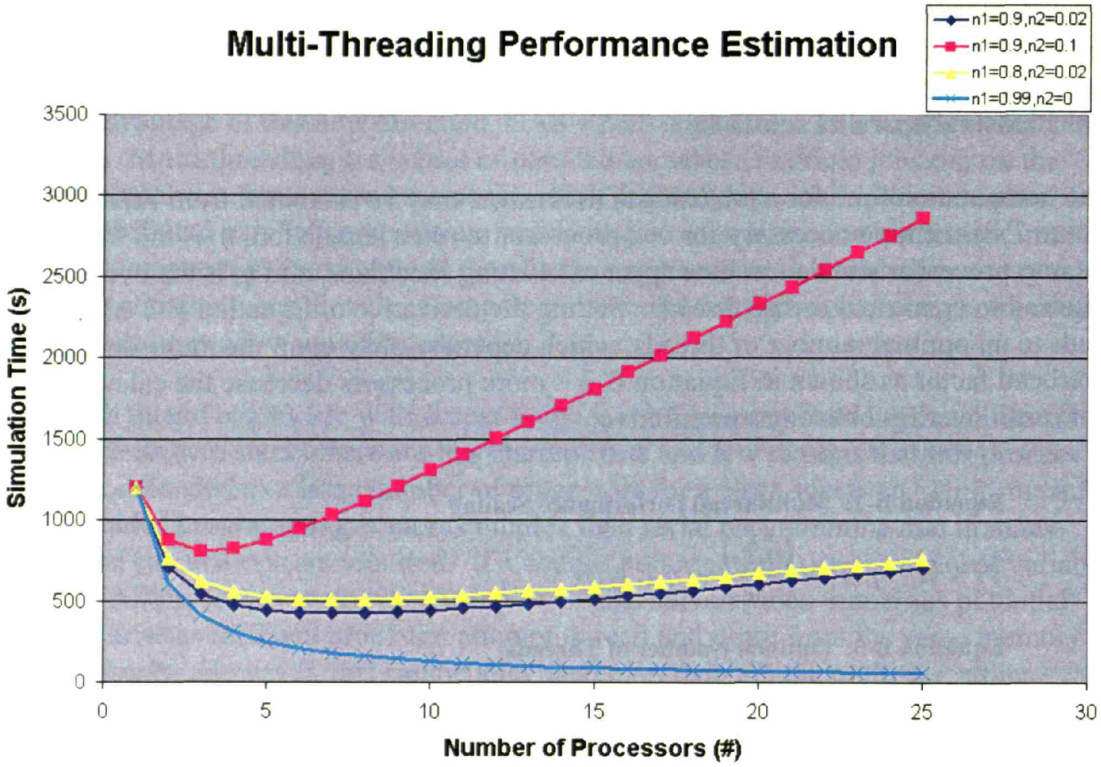

Figure B-4: Multi-Threaded Performance Estimation

Pseudo-Code

The new Jacobian algorithm could be implemented as shown in the following pseudo-code:

```
Fnorm = F(X,Variables)        !steady state values

Thread:  DO i=1,Nthreads
         DO j= Nequations/Nthreads*(i-1),Nequations/Nthreads*i
                Xmod_i = X                                  !initialize
                Xchange_i = DABS(X (j)) * change            !change to X(j)
                Xmod_i (j) = X(j) + Xchange_i               !new x
                Fnew_i = F(Xmod_i,Variables)                !new row of Fs
                Diff_i = (Fnew_i-Fnorm)                     !diff between Fs
                Jac(:,j) = Diff_i/Xchange_i                 !updated Jacobian
         ENDDO
ENDDO Thread
```

It should be apparent from this code that the Jacobian array is the only shared variable that each thread writes to, but each thread writes to a different part of this array. Therefore, there are no memory conflicts at top level coding. Significant effort has gone into making lower level coding reentrant to avoid memory conflicts.

IMSL Wrapper

The complication stems from allowing the IMSL solver to use its hard-coded function call formats. The IMSL solvers expect a format which does not allow other variables to be passed to the function, therefore global variables must be used in the function evaluation. While the Jacobian calculation could proceed on an identical but separate function not containing global variables, it is undesirable to start creating multiple copies of the same code, especially since the optimal number of copies is unknown and can be large.

The solution adopted is to create an IMSL function wrapper which provides the correct interface for IMSL solvers but makes detailed function calls to the actual solution routine. This is made clear with the pseudo code below:

```
FUNCTION IMSL(X)
        USE MGLOBAL                !global variables
        CALL FCN(X,Variables)
ENDFUNCTION IMSL
```

This code shows that there are two methods to execute *FCN*: one which accepts only one command line argument, *IMSL*, but uses global variables to supply needed data, and one which takes all the required data, *FCN*, from the command line. Although both functions perform the same calculation, only one can be used with IMSL and only one can be used with multi-threading. Using this type of interface allows only one set of code to be used for both reentrant and non-reentrant code.

Conclusion

GAS-PASS could take advantage of multithreading for its most computationally demanding operation simply by replacing the PCHE zone numerical solver. This would allow GAS-PASS to benefit from future computational improvements and largely keep pace with Moore's Law.

B.3 Approximating Structure Conduction

Estimating the thermal inertia of the metal structure in the S-CO_2 recompression cycle will be a key area of modeling for long-term transients. The difficulty of accurately estimating the temperature of the wall stems from avoiding unnecessary complexity that will significantly slow the computation while simultaneously capturing thick wall conduction effects.

GAS-PASS is a scoping and design tool that does not attempt to fully characterize a system but runs very quickly, generating approximate solutions. One of the assumptions that enables this performance is that the metal structure is assumed to be isothermal with the fluid. This assumption avoids nodalizing the structure, solving for the wall

temperature simultaneously with the fluid temperature, and calculating the relatively slowly changing wall temperatures along with the quickly changing fluid properties.

Problem

Unfortunately, this assumption is inherently limiting during time dependent simulations. While a small section of the wall will be approximately isothermal with the fluid, the thickness of this isothermal section will vary with time. One could choose the thickness of the wall to match the simulation runtime, but even within a simulation what is an accurate assumption for the end of the simulation will be inaccurate at the beginning, and vice versa. Therefore, any method that does not vary the wall temperature with time and structure thickness will be a significant approximation.

Proposal

One method to avoid this problem without significant computational burden would be to nodalize and calculate the structure wall temperature, but to do this on a different timescale than the fluid dynamic calculations. This is the method proposed here for future implementation.

The calculation process would be as follows:

a) The fluid dynamics are simulated with wall temperatures held constant. However, the wall temperature can be different than the fluid temperature.
b) When a user specified time step has passed, the structure wall temperatures would be recalculated based upon the previous wall temperatures and the current fluid temperature.

Therefore, there would be an inner and an outer calculation loop for phenomena that occur on different timescales – many simulation codes use a similar method. One of the advantages of this method would be that the GAS-PASS/CO_2 fluid dynamic solution process does not need to be changed. The GAS-PASS/CO_2 transient energy conservation equation is:

Equation B-4: Transient Energy Conservation Equation **(B-4)**

$$\frac{dE}{dt} = {}^{n}\dot{E}_{in} - {}^{n}\dot{E}_{out}$$

$$\frac{{}^{n}E - {}^{n-1}E}{\Delta t} = {}^{n}\dot{m}_{i}^{fluid} * {}^{n}h_{i}^{fluid} - {}^{n}\dot{m}_{o}^{fluid} * {}^{n}h_{o}^{fluid}$$

$$0 = {}^{n}\dot{m}_{i}^{fluid} * {}^{n}h_{i}^{fluid} - {}^{n}\dot{m}_{o}^{fluid} * {}^{n}h_{o}^{fluid} - \frac{{}^{n}E - {}^{n-1}E}{\Delta t}$$

The energy stored in the fluid and structure is calculated as follows:

Equation B-5: Transient Energy Conservation Equation **(B-5)**

$$^{n}E = {}^{n}E^{fluid} + {}^{n}E^{struct}$$

$$^{n}E^{fluid} = {}^{n}M^{fluid} * {}^{n}U^{fluid}$$

$$^{n}E^{struct} = \sum_{i}^{I} M_i^{struct} * C^{struct} * {}^{n}T_i^{struct}$$

Therefore, one need only hold the structure temperatures, $^{n}T_{i=1..I}^{struct}$, constant between structure conduction calculations, instead of setting the whole structure temperature equal to $^{n}T^{fluid}$, as is currently done. Note that the inner structure temperature, $^{n}T_{0}^{struct}$, which is in contact with the fluid, will be used in the heat transfer calculation:

$$^{n}\dot{Q} = {}^{n}HTC * A * \left({}^{n}T^{fluid} - {}^{n}T_{0}^{struct}\right).$$

The implementation of this method would be straightforward. The user would set up a structure conduction calculation with instructions similar to those used for GAS-PASS itself. For example, the conduction timing command could be:

0.01 *:default conduction time step size[s]*
5 *:# of time step instructions*
0.0 3.0 0.1 1.0 3.0 3.0 10.0 3.0 1000.0 100.0

These instructions would update the wall temperature with a default time step size of 0.01 seconds – about an order of magnitude larger than a typical fluid dynamic time step size. The instructions would also allow the user to vary the conduction time step during the simulation to account for fast and slow periods of change.

While calculating the wall structure temperatures roughly every 10^{th} time step is a significant savings, the biggest improvement is in avoiding directly coupling the solution of the fluid temperature to the wall temperature, which would greatly increase the difficulty of the solution and therefore significantly slow the calculation.

In practice one need only make the wall temperature steps small enough that the solution stops changing significantly. While each simulation may require a slightly different optimal solution, there is likely to be a good enough set of values that are widely applicable and need only be determined once.

Conclusion

One method to avoid significant computational burden but better approximate thick structure wall conduction would be to decouple the fluid dynamic calculations from conduction calculations into an inner and outer loop solution. The fast fluid dynamic calculations would occur at every time step while the slower conduction calculations would only occur as required. With proper tuning this method should be more accurate, than the currently method, and add little computational burden.

B.4 Separating vs. Lumping Piping Volumes in the S-CO_2 Recompression Cycle

This section will analyze the benefits and drawbacks of separating versus lumping piping with component volumes for the S-CO_2 cycle in GAS-PASS/CO_2. Separating components would allow active component actions, such as turbine work, to occur separately from transient mass and energy storage, which become important in the much larger, but completely passive, piping volumes. This section will refer to volumes based upon Gibbs[6] which lumped in a way appropriate for use in the GAS-PASS/CO_2 S-CO_2 recompression cycle model. The volumes are detailed in Table B-1.

Table B-1: S-CO_2 recompression Cycle Component Volumes*

Component Name	Volume [m^3]	Description of Volume
IHX - Cold	5.56	Core
IHX - Cold - After	34.22	IHX to Turbine + LP Plenum
Turbine	4.95	Turbomachine
Turbine - After	32.79	Diffuser + pipes to HTR + HTR LP inlet stuff
HTR - Hot	9.48	Core
HTR - Hot - After	24.54	Pipe + HTR plena + LTR plena
HTR - Cold	9.48	Core
HTR - Cold - After	30.82	Pipe + HTR plena + IHX plena
Mixing-T	15.76	Just T
Mixing-T - After	12.58	Piping
LTR - Hot	7.02	Core
LTR - Hot - After	10.35	LTR Plena + pipes to manifold
LTR - Cold	7.02	Core
LTR - Cold - After	8.56	Plena + Pipes to manifold
Valve	0.00	Too small to model
Valve - After	0.77	1/2 of pipe between RC and mixing-T
RC	4.45	Turbomachine
RC - After	0.77	1/2 of pipe between RC and mixing-T
Splitting-T	15.76	Just T
Splitting-T - After1	6.06	Pipe + PRE plena
Splitting-T - After2	0.69	Connected to RC?
PRE - Hot	1.98	Core
PRE - Hot - After	9.40	Pre Plena + piping + manifold
MC	0.72	Turbomachine
MC - After	14.55	Piping + Manifold + Piping + LTR Plena
Total	**268.26**	

* These volumes are based upon Gibbs[6].

Separated Component Volumes

Figure B-5 shows the volumes of the components in the S-CO_2 recompression cycle. The volumes range from ~34 m^3 to about 0.6 m^3 (note that valves are assigned a volume of 0, as they are too small to bother modeling relative to the rest of the system). There are four components which have a small volume:

- after the recompression compressor
- after the valve
- after the recompression compressor side of the splitting-T
- the main compressor itself

From a dynamic modeling perspective it is just as important to know which components behave as if they were dealing with an ideal gas, and which behave closer to an incompressible fluid. The normalized (to the largest value) volume and normalized fluid density are shown in Figure B-6. This shows that most of the high volume components are at the low density side of the system, and vice versa. This figure suggests that the low density side of the system will act like a spring (with high volumes and easy compressibility) compared to the small and dense side of the system.

Figure B-7 shows normalized volume versus normalized fluid inventory (the fluid inventory is simply a multiple if the un-normalized values in Figure B-6). This figure shows that much of the system mass is found in the dense side of the system. Furthermore, one should recall that the dense side of the system is where the fluid approaches the critical point, and thus fluid density can change rapidly.

From these figures one might speculate that:

1. The cycle would be easier to model if all of the volumes were within the same order of magnitude. Having significantly larger and smaller volumes will create phenomena on different timescales.
2. The dense side of the cycle might be difficult to model, since small volumes and high densities can create very fast phenomena. The fluid is nearly incompressible here so any fluid moving through these components will move very rapidly.
3. One may not be able to neglect the dense side of the cycle in terms of mass storage effects, since that is where most of the fluid is stored, and because this is where fluid density can change easily.

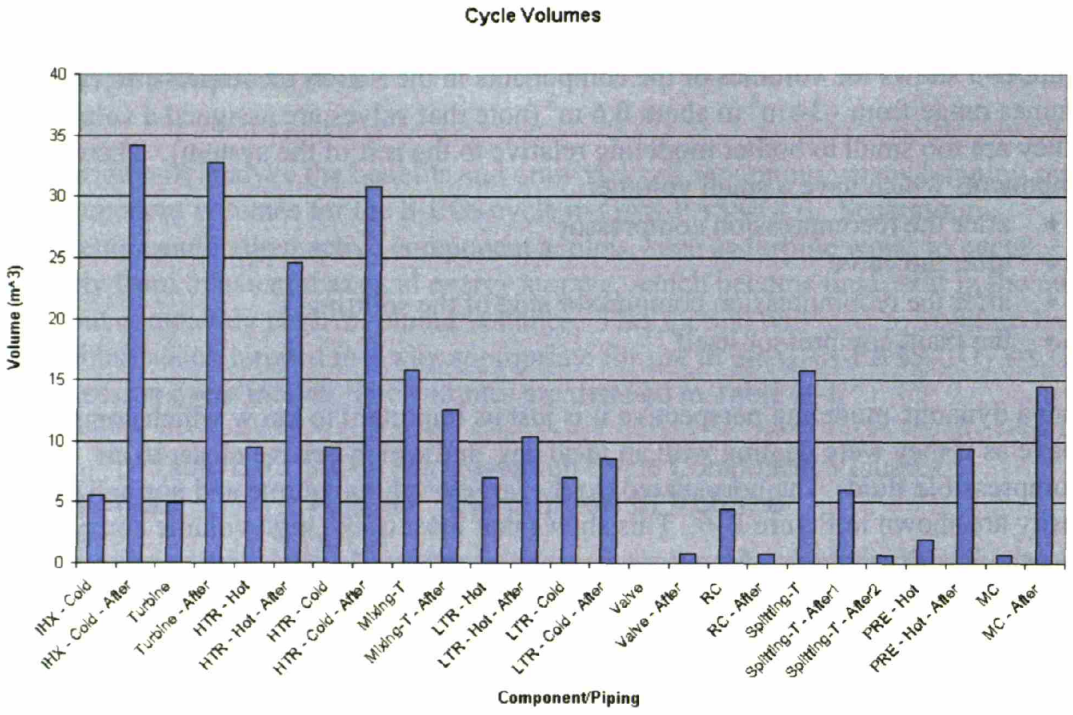

Figure B-5: Cycle Volumes for the S-CO_2 Recompression Cycle

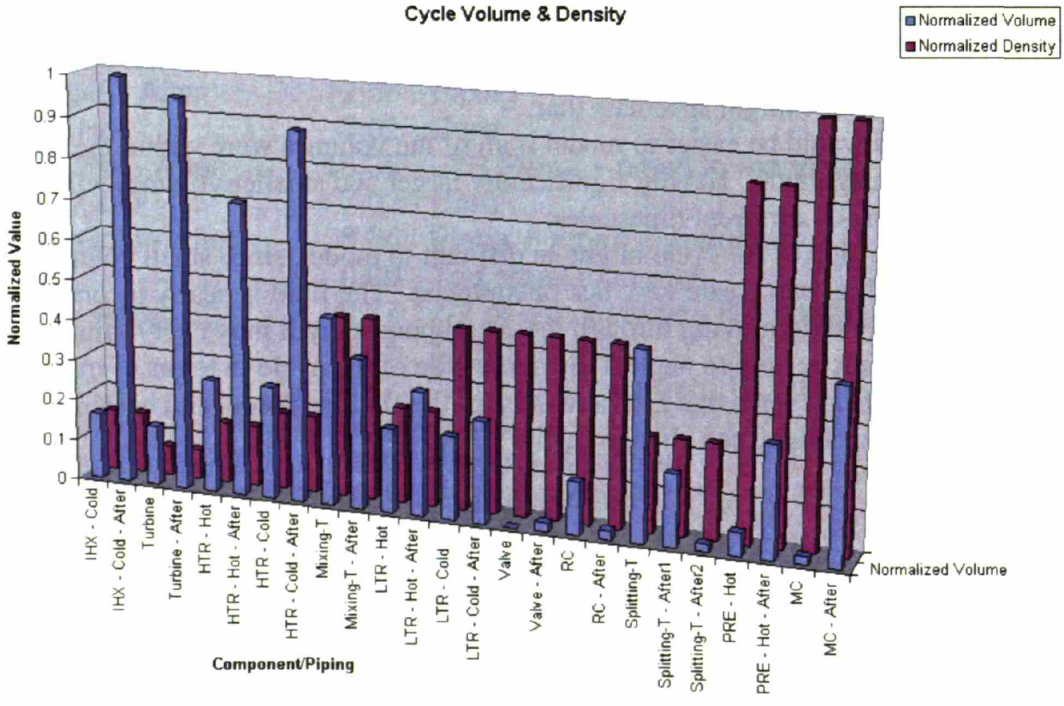

Figure B-6: Normalized Cycle Volumes & Fluid Density for a S-CO_2 Recompression Cycle

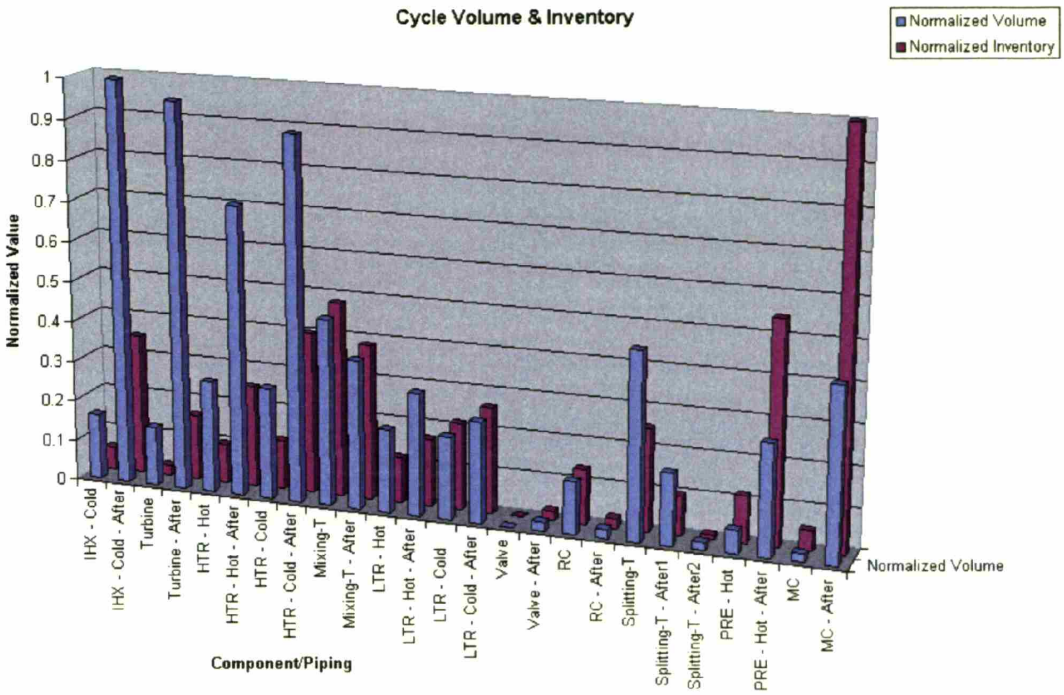

Figure B-7: Normalized Cycle Volumes & Fluid Inventory for a S-CO_2 Recompression Cycle

Lumped Volumes

Lumping components produces a very different system. While this combines transient mass and energy storage phenomena with active component actions (e.g. a turbomachine), it at least doubles the code speed and makes system volumes easier to deal with. The reason for lumped volume analyses becomes clear when the various volumes for the S-CO_2 recompression cycle are shown graphically.

Figure B-8 shows the cycle volumes lumped by component and the following (i.e. downstream) piping. Except for the representative valve, most of the component volumes are similar (within an order of magnitude).

Figure B-9 shows the same volume and density graph, but now for the lumped case. Once again, we see that the low density side of the system contains most of the volume.

Figure B-10 shows the same volume and inventory graph, here for the lumped case. Once again, we see that the high density side of the cycle contains much if not most of the cycle mass.

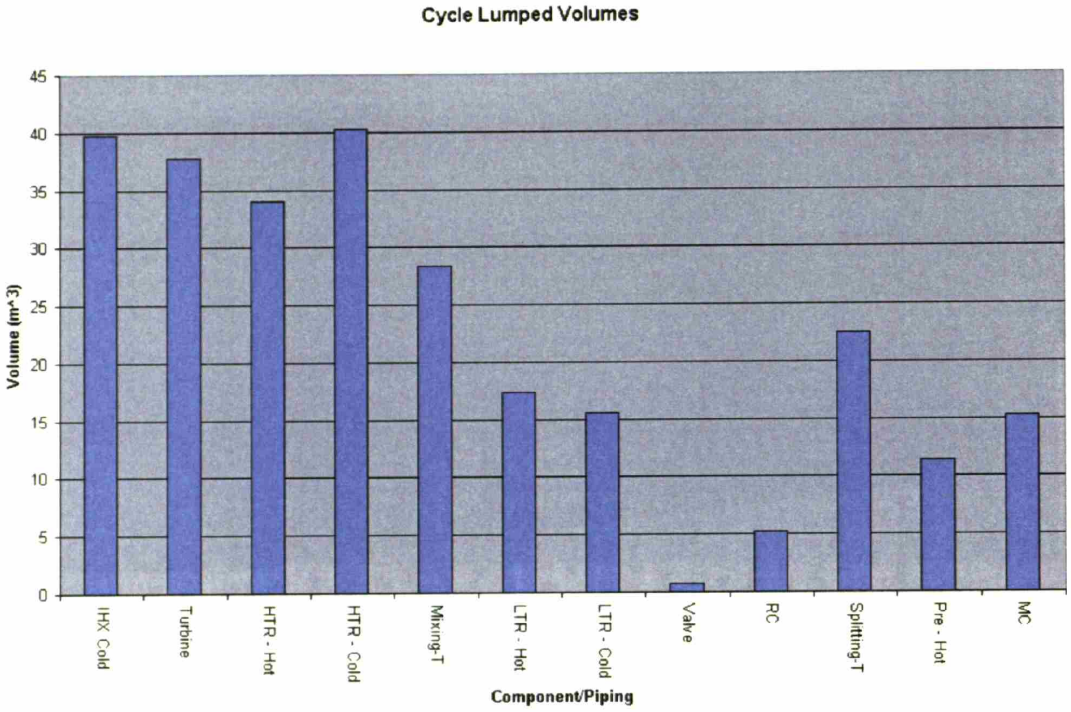

Figure B-8: Cycle Lumped Volumes for the S-CO_2 Recompression Cycle

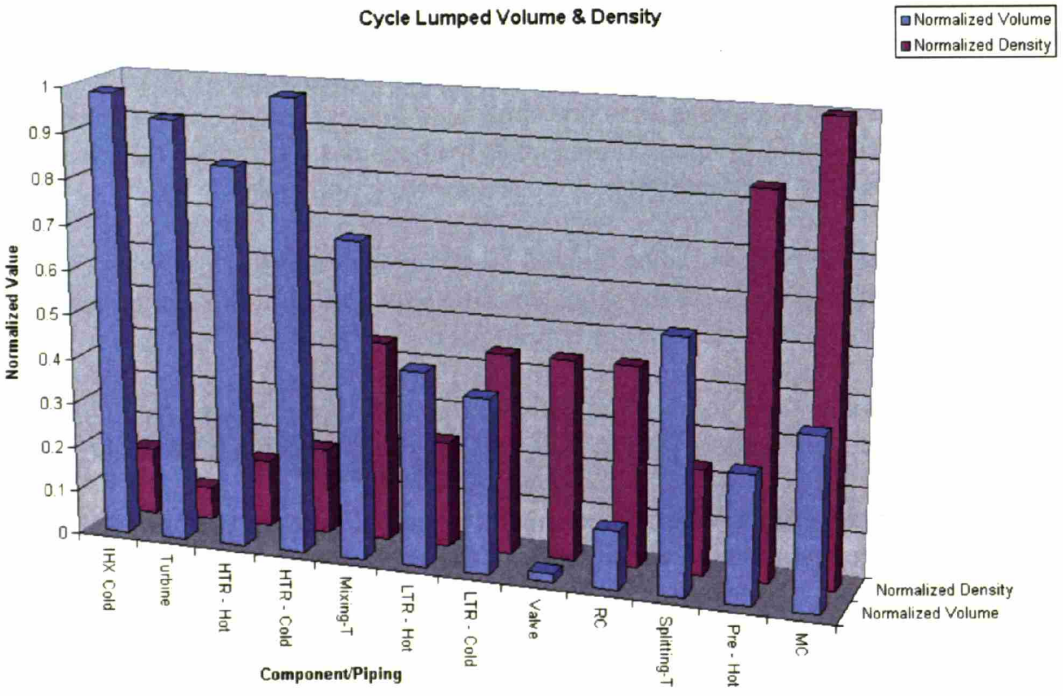

Figure B-9: Normalized Cycle Lumped and Normalized Volume & Density

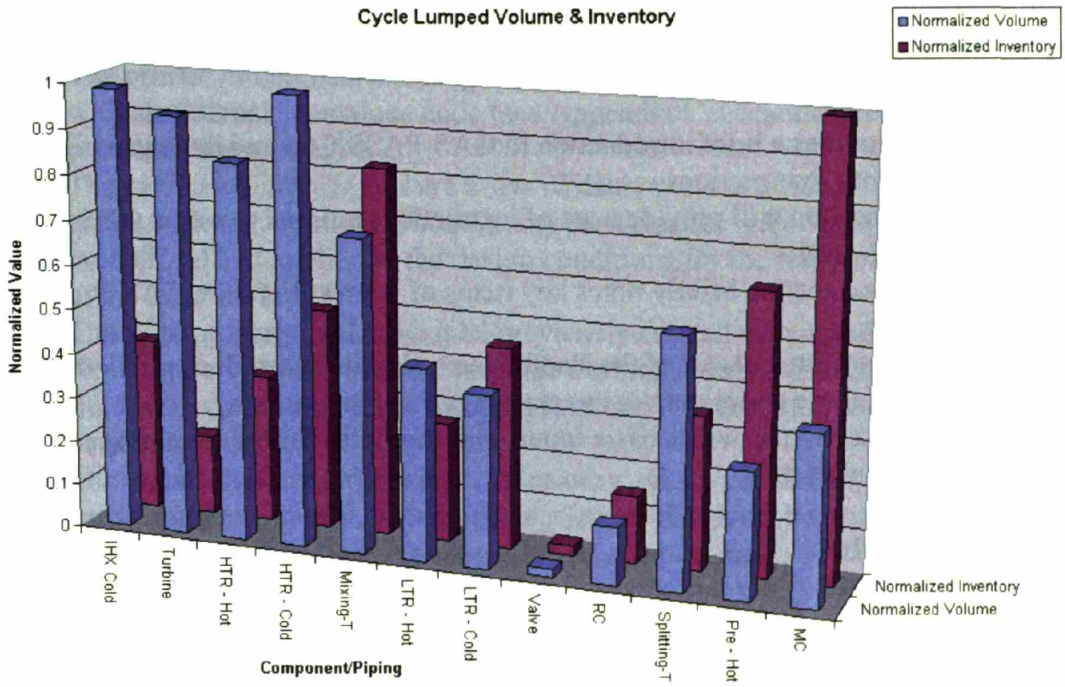

Figure B-10: Normalized Cycle Lumped and Normalized Volume & Inventory

From these figures one might speculate that:

1. The valve should be neglected in a lumped analysis.
2. The dense side of the cycle will still probably be difficult to handle, but it now has significantly larger average volumes. Furthermore, the smallest component is now the recompression compressor, with a volume of ~5 m^3 and density of ~320 kg/m^3, which should be much easier to model than the previous smallest value of the main compressor, with a volume of ~0.7 m^3 and a density of ~715 m^3.
3. Once again, one may not be able to neglect the dense side of the cycle, since that is where most of the fluid is stored, because this is where fluid may be stored or rejected most easily, and even though the fluid is cold it probably contains significant thermal inertia.

Recommendations

After looking at the pro/con of lumping and separating component volumes the author recommends using a lumped volume approach for the S-CO_2 recompression cycle. Separating components from piping in this cycle can lead to very small but dense components being modeled along with large but thin-fluid components, which may create a stiff solution matrix. GAS-PASS/CO_2 was never designed to model extremely rapid fluid density change phenomena, and thus separating component and piping volume may be unnecessarily detailed compared to other assumptions.

Appendix C: GAS-PASS/CO_2 User Manual

This appendix provides a brief introduction to GAS-PASS/CO_2 and its associated codes. It is subdivided into four sections:

1. The first section will provide a set of instructions tailored to a new GAS-PASS/CO_2 user.
2. The second section briefly notes key items of interest to future GAS-PASS/CO_2 developers.
3. The third section lists all of the standalone codes produced during this work. Several of these codes are vital to creating new plant models.
4. The final section provides basic inputs and examples for the fluid property table creation code.

C.1 User Notes

The new user of GAS-PASS/CO_2 has a non-trivial learning curve before proficiency in simulation can be obtained. While significant effort has gone into making the code easy to use, simulation results were the priority of this work, and much remains to be done to make the inherently complicated process of cycle simulation simpler. This section will attempt to provide the new user with the basic ideas and concepts necessary to successfully simulate with GAS-PASS/CO_2.

Input Files

Section 3.6.1.1 briefly discussed the various input files. In general, these files are all free format with input depending upon key words and locations. The input routines are generally intelligent and should produce error messages* pinpointing and describing obvious mistakes. The key input file, and GAS-PASS/CO_2's only command line argument, is the list of files, called *files.i* in this work. This file contains the paths to all of the other GAS-PASS/CO_2 input and output files.

The number of input files is too large to conveniently describe in detail, but several features are worth noting.

1. The main input file will be described in the next section.
2. The cond_num.i file contains a set of normalization factors to use in the transient calculation to help assure numerical stability. In general, it is not necessary to provide these values but if this file exists then they will be used. The user is cautioned to never use a normalization file if the system design has changed in any way. If a set of normalization factors worked well for a plant design and a boundary condition is then switched for a variable, it is likely that the use of the previous normalization factors will create a singular system.

* Error messages typically contain a list of the calling routine, a unique error # (to the final routine), and a brief error message describing the problem.

3. The control inputs file is currently hard coded. Users changing the control system will have to modify this file and the source code to go with it.
4. The printed circuit heat exchanger's inputs (geometry) must be previously created with an external standalone code (see Appendix C.3 Standalone Codes) for the plant conditions desired.
5. The turbomachinery inputs are a sets of data points at different shaft speeds which create a (design point fluid conditions) performance map. They will be normalized and applied to the design conditions for the turbomachinery specified in the main input file.
6. The fluid property tables must be previously created (see Appendix C.4 Creating Fluid Property Tables) for the heating, working, cooling fluids. The working fluid has two extra tables to meet the needs of the turbomachinery conservation equations.
7. The output files are largely self explanatory. GAS-PASS/CO_2 does not provide a native graphing ability, but extensive plotting files have been created for GnuPlot and will be included with the source code compact disk.

Main Input File

The main input file contains the complete system layout, variables and boundary condition specification, and initial root guesses. It will be the most commonly used and changed input file.

The input file is broken up into several sections designated by a keyword (shown in caps) starting a new line: POWER*, TEMPERATURE, PRESSURE, MASS flow rates†, COMPONENT_VOLUME, PIPING_VOLUME, COMPONENT_STRUCTURE properties, PIPING_STRUCTURE properties, and a FLUID section. Each of these sections will specify one aspect of a component and the component must be in the same order in each of these sections. Note that there are other special input sections separate from these general components. The final section of the input file, key word *DIAGRAM*, maps component fluid inputs and outputs and heat transfers.

GAS-PASS/CO_2 repeatedly uses a format which deserves mention and will become clear with an example. The following three lines are from the GAS-PASS/CO_2 temperature section:

```
20.0      1     2     :Tertiary     18     38
100 1     500 1.5
61        0     0     :MainComp     19     39
```

* Note that there is one extra power input which is always the last power input. This value corresponds to generator power. The generator does not have fluid so it is not included in the other inputs sections such as temperature and pressure.

† Note that there are several small specialized sections before the volume sections begin. They do not have fluid flow (i.e. one does not need to specify a temperature, pressure, ...) thus they are not addressed further.

The first line specifies that the first component (commented Tertiary) has an outlet temperature of 20°C and is a boundary condition which varies during the transient. The two numbers following an input value, such as a temperature, specify what type of variable this is. There are six possible choices:

```
0  0    !the input is a variable in the steady state and the transient
0  1    !the input is a variable in the steady state and a constant boundary
        !condition in the transient
0  2    ! the input is a variable in the steady state and a changing boundary
        !condition in the transient
1  0    !the input is a constant boundary condition in the steady state and a
        !variable in the transient
1  1    !the input is a constant boundary condition in the steady state and
        !the transient
1  2    !the input is a boundary condition in the steady state and a
        !changing boundary condition in the transient
```

If an input has a changing boundary condition then the next line of the input file will specify how it changes. That line provides a variable number of sets of time and fractional value inputs and linear interpolation is used in between the sets. From the temperature example (second line), the "Tertiary" temperature is specified to be constant, at 100% of its value, until 100 seconds. At 100 seconds it begins to linearly increase until, at 500 seconds, the temperature has increased by 50% to 30°C.

Note that GAS-PASS/CO_2 actually adds two data sets, which bracket the user's sets, to any time changing boundary condition. The first input specifies that all time inputs begin with a 100% value at time 0 and the last input specifies that the user's last input value will be held for the rest of the simulation. Thus in the temperature example the "Tertiary" temperature is at 100% of its steady state value from 0 to 100 seconds, linearly increases to 150% by 500 seconds, and then stays at 150% of its nominal value until the end of the simulation.

The final line of the example temperature input states that the main compressor outlet temperature is expected to start at 61°C but will be solved for in both the steady state and the transient calculations.

The rest of the input sections are largely self explanatory except:

- Every turbomachine is currently expected to reside on the same shaft with the generator. The source code will have to be edited to relax this constraint.
- The COMPUTATION section provides good general inputs and should not be adjusted without reason.
- To enable/disable energy and mass storage in the transient calculations the user must edit each PCHE file in addition to the inputs in the TRANSIENT section.

Finally, the DIAGRAM section deserves explanation. Part of the S-CO_2 recompression cycle diagram is included below as an example:

#	*Name*	*Inp1*	*Inp2*	*HX*
5	*VALVE*	*4*	*0*	*0*
6	*TURBINE*	*5*	*0*	*0*
7	*HTR*	*6*	*0*	*8*
8	*htr-cold*	*21*	*0*	*7*
9	*MIXING-T*	*11*	*12*	*0*

The first number on each line specifies the component number – they must be in numerical order (beginning with 1) and be in the same order that their inputs were listed in the earlier sections "TEMPERATURE", "PRESSURE", etc.

The name input is largely self explanatory except that these names are used as flags. For example, the word *VALVE* tells GAS-PASS/CO_2 to treat this component as a valve in the computation process.

The three numbers following the name specify component relations. Input 1 lists the incoming fluid stream. Thus, from the example, the *HTR* receives fluid (mass flow rate, enthalpy, and pressure) from the outlet of the turbine. Input 2 is only used for the mixing-T which has two incoming fluid streams. Finally, the third column, HX, specifies that this component is a heat exchanger and lists the number of the component which the energy is transferred to/from. For example, component number 7, the *HTR*, transfers heat to component number 8, the *htr-cold*, which receives heat from component 7.

Creating a New System Design

Setting up GAS-PASS/CO_2 is a five step process:

1. Obtain a steady state design for a plant from another source (e.g. the MIT CYCLES II code[55]).
2. Appropriate input files must be generated which match the steady state design. If these inputs files are not correct, GAS-PASS/CO_2 will not run for long, if at all. These files include:
    a. Hot, working, and cold fluid property tables.
    b. Turbomachinery performance curves.
    c. PCHE geometry appropriate for the system.
3. The main GAS-PASS input file must be created and converged. This will require a good knowledge of what the system looks like at the steady state (temps/pressures/heats/mass flow rates) and may be quite difficult at first. Building up the system one component at a time is the most robust and perhaps the fastest strategy in the long run.
4. Transient runs can now begin. These transients should be realistic for the plant being used (this will require some operator knowledge) or the GAS-PASS/CO_2 errors may be mistaken for a programming mistake.
5. If PIDs are used they must be devised, tuned, and coded. This requires the developer to edit the source code, have an idea of what should control what, and be able to tune a PID.

C.2 Developer Notes

These notes were put together in a somewhat random order for future developers. They present key code and simulation features in one concise list.

CODE STRUCTURE:

- IO is a significant portion of the source code. Reading in and error checking 33 free format files and outputting 11 carefully formatted output files takes a lot of coding.
- All source code is contained within modules which must be "used" except the IMSL solver routines which must be globally known. This allows clean relationships between subroutines and robust compiler checking.
- Virtually all the code is reentrant except the IMSL solver routines (used in SS, TR, and PCHE_TR). This should allow GAS-PASS/CO_2 to be multi-threaded in the future (simply replace the IMSL solvers and their calling code). Note that there are also a couple of printing flags which are not reentrant, but these need not be reentrant even in multithreaded code.
- Most GAS-PASS/CO_2 data is stored in custom data structures. This allows easy manipulation of dozens (or thousands) of data pieces and makes smart memory management feasible. The component data are incrementally built from small data structures (i.e. turbine pressure ratios) until, at the top level, all the component data is stored within a single structure called COMPONENTS.
- Effort has been made to code repeated actions only once. Thus there are layers of routines used for things like reading in a file.
- Arrays are almost always declared in an ALLOCATABLE fashion to allow general use. The developer changing GAS-PASS/CO_2 must be careful to know the state of his arrays and to DEALLOCATE them before exiting routines. If arrays are not deallocated, strange and difficult to trace memory errors can occur when using layered data structures.
- Components (except for a few exceptions like the shaft) are coded in a general fashion. Thus the main compressor would be "compressor(2)" in the S-CO_2 recompression cycle. Component are "mapped" to each other by various integer "mapping" arrays. This mapping process occurs in the INPUT routine.

ERROR HANDLING:

- Virtually all error data is sent to the routine PRINTER. This routine outputs the error message to screen and the log file, and, if instructed, exits the program.
- Virtually all errors contain a stack and a unique ID. The stack contains the pertinent history of the routine (i.e. the error was in the props routine called by the PCHE routine for the precooler called by the Jacobian routine called by transient routine). The unique ID is a number which is unique only within a subroutine. By noting the final name and number the user should be able to immediately go to

the line of code where the error occurred. By knowing the calling history one can recreate the run and watch an error occur.

- In general, GAS-PASS/CO_2 exits on read in, data processing, and readout errors. It attempts to recover from numerical convergence difficulties but logs the errors. In cases where the code is encountering a region of difficulty many errors (thousands) can be generated before the code dies or the problem passes.
- The user CANNOT know if a simulation was realistic without checking the data plots and outputs logs. GAS-PASS may run through a region of difficulty where a real plant can not. This will probably be obvious by:
    a) The plots will contain a sharp jump that is not caused by boundary conditions or PIDs (i.e. you didn't tell GP to do anything at this time).
    b) The log file will contain numerous errors at the jump time which resulted in very loose tolerances before the system began converging tightly again.
    c) The simulation continues after the problem but NO variables change. This occurs when GAS-PASS/CO_2 cannot reconverge.

  If these issues are not looked for you may be making claims which GAS-PASS/CO_2 tried to tell you wasn't realistic.
- If a time step cannot be converged its Jacobian will be output to fort.201 (and the next step to fort.202 and so on up to fort.225).
- If a property table problem is found (i.e. -1 input for a data point) then a warning message is written to fort.111. This is just to let the developer know that a bad region in a table has been reached.
- Note that if the # of fixed boundary conditions is too high then GAS-PASS/CO_2 will die with a memory error during the first steady state conservation equation evaluation. This is not a GAS-PASS/CO_2 generated (traceable) error because it is not obvious how to get an easy error message without adding a considerable amount of slow code (although in the steady state calculation this is not terribly important, but it is in the transient). However, if the number of BC's is too low then GAS-PASS/CO_2 will provide an appropriate error message. In any case you cannot solve the steady state without the number of variables equaling the number of unknowns.

RUN TIME:

- The CO_2 property tables take several seconds to read in – this only happens once.
- 99% of the solution run-time occurs in the transient, 99% of this occurs in the numerical solver and, and over 90% of this occurs when calculating the Jacobian. Within the solver the vast majority of this time is spent in the PCHE routines and much of this time is spent on fluid properties.
- The number of PCHE nodes, the time step size, and dynamic time stepping will dictate code run time.

SOLUTION PROCESS:

- The components are calculated fully implicitly by the solver.
- The boundary conditions are adjusted (if instructed) before each time step.
- The PIDs adjust boundary conditions after each time step.

C.3 Standalone Codes

This section lists the various standalone (separate from GAS-PASS/CO_2) codes produced in the present work. Some of the codes are production level (note the status) and some are not, but they are listed here for possible future use. They are listed in Table C-1.

Table C-1: External Code Modules

Name	Language	Status	Purpose
Dictionary.pl	Perl	Stable	Document code modules automatically.
pcheSS	Fortran 90	Stable	Compute a PCHE in steady state for either heat transfer or length. This has been incorporated, in an abbreviated form, into GAS-PASS/CO_2.
pcheTR	Fortran 90	Early	Dynamically simulate a PCHE while specifying the incoming fluid properties as boundary conditions changing with time. This has been incorporated, in an abbreviated form, into GAS-PASS/CO_2.
TurboSmooth	Fortran 90	Early	Smooth a turbomachinery shaft speed curve (showing jitter) for interpolation.
TurboMap	Fortran 90	Stable	To interpolate on and between a turbomachine's shaft speed curves. This has been incorporated, in an abbreviated form, into GAS-PASS/CO_2.
PropsGen	Fortran 90/77	Production	To calculate property (tables) using NIST RefProp 7.1 (beta/modified) and liquid sodium simple polynomials.
TableTester	Fortran 90	Early	To systematically compare tabular values against NIST RefProp 7.1.
Props	Fortran 90	Production	To handle and interpolate from previously made property tables. This has been incorporated, in an abbreviated form, into GAS-PASS/CO_2.
Gp.gnu	Gnuplot	Stable	Plot GAS-PASS/CO_2 output files. Note this file needs modification if the plant model changes.
Pche.pl	Perl	Early	Plot PCHE performance during GAS-PASS/CO_2 runs – creates a GIF movie.

C.4 Creating Fluid Property Tables

The Props program is run from the command line with the input and output file names as arguments. A typical command line would be:

props.exe 1.inp 1.out

Input

The input file contains a single line specifying the complete fluid property table. The format is free form but the order of values must be correct. The log and linear inputs are quite similar but both will be listed completely. For a log table there are inputs. The reader is encouraged to consult Chapter 3.3.2 if questions about tabular files arise. The log file inputs are:

1. If the 1st property is log or linearly indexed with the LOG or LIN flags respectively.
2. If the 1st property increases or decreases from its start point. Uses POS flag for increasing or NEG flag for decreasing.
3. The 1st property symbol e.g. h for enthalpy (see symbols in Table C-2).
4. The 1st property initial value e.g. 275000.
5. The 1st property alpha coefficient e.g. 100.
6. The 1st property beta coefficient e.g. -889.555.
7. The 1st property gamma coefficient e.g. 267627.
8. The 1st property number of data points e.g. 500.
9. The 1st property units e.g. J/kg.
10. If the 2nd property is log or linearly indexed with the LOG or LIN flags respectively.
11. If the 2nd property increases or decreases from its start point. Uses POS flag for increasing or NEG flag for decreasing.
12. The 2nd property symbol e.g. P for pressure (see symbols in Table C-2).
13. The 2nd property initial value e.g. 7450000..
14. The 2nd property alpha coefficient e.g. 100.
15. The 2nd property beta coefficient e.g. -1194.1.
16. The 2nd property gamma coefficient e.g. 7230035.
17. The 2nd property number of data points e.g. 500.
18. The 2nd property units e.g. Pa.
19. The fluid property state: 0 for unknown, 1 for single phase or supercritical, 2 for 2 phase. The single phase routines are relatively fast but will fail with an two phase input.
20. The fluid property phase: 0 for unknown, 1 for a liquid, or 2 for a gas or supercritical fluid. The known phase routines are faster but will fail with an incorrect input.
21. The minimum fluid density which is used for root bounding. Can be set to -1 to avoid guessing.
22. The maximum fluid density which is used for root bounding. Can be set to -1 to avoid guessing.
23. The fluid density units e.g. kg/m^3.
24. The desired fluid property symbol e.g. Cp for isobaric specific heat (see symbols in Table C-2).
25. The desired fluid property units e.g. J/kg-K.

26. The desired fluid property source. Should be NIST for using the NIST RefProp code or SODIUM for using the sodium equation of state polynomials.
27. The desired fluid to use e.g. CO2.
28. The desired fluid molar fraction e.g. 1.0

Inputs 27 and 28 may be repeated up to a mixture containing 20 fluids. These mixtures will only execute if the NIST code has predefined models for mixing these fluids but many fluid mixtures are available. An example using three fluids each taking 1/3 of the number of moles would be: *co2 0.3333 nitrogen 0.3333 helium 0.333.*

The complete log table line for the would be:

LOG POS H 275000 100.0 -889.555 267627.0 500 J/kg LOG POS P 7450000 100.0 -1194.1 7230035.0 500 PA 0 0 -1.0 -1.0 KG/M^3 Cp J/kg-K NIST CO2 1.0

A second example using a pressure which moves below the critical point is shown as well.

LOG POS H 302210 100.0 -887.1129357 295015.407 500 J/kg LOG NEG P 7500000 100.0 -1075.386425 -7547281.01 500 PA 0 0 -1.0 -1.0 KG/M^3 Cp J/kg-K NIST CO2 1.0

Once these two tables are created they can be combined into a single file for GAS-PASS/CO_2 to use. Thus GAS-PASS/CO_2 uses the above critical table by default to interpolate for Cp, but if the pressure drops below the critical value then it will automatically switch to the lower table to get Cp values.

On a *nix system the command to combine the two tables would be:
cat table1 table2 > table

The linear property table input format is highly similar except that it does not contain the log coefficients. Thus the inputs are:

1. If the 1st property is log or linearly indexed with the LOG or LIN flags respectively.
2. If the 1st property increases or decreases from its start point. Uses POS flag for increasing or NEG flag for decreasing.
3. The 1st property symbol e.g. h for enthalpy (see symbols in Table C-2).
4. The 1st property initial value e.g.8492.
5. The 1st property final value e.g. 408720.
6. The 1st property step size e.g. 408720.
7. The 1st property units e.g. J/kg.
8. If the 2nd property is log or linearly indexed with the LOG or LIN flags respectively.
9. If the 2nd property increases or decreases from its start point. Uses POS flag for increasing or NEG flag for decreasing.

10. The 2nd property symbol e.g. P for pressure (see symbols in Table C-2).
11. The 2nd property initial value e.g. 1000000..
12. The 2nd property final value e.g. 3000000.
13. The 2nd property step size e.g. 25000.
14. The 2nd property units e.g. Pa.
15. The fluid property state: 0 for unknown, 1 for single phase or supercritical, 2 for 2 phase. The single phase routines are relatively fast but will fail with an two phase input.
16. The fluid property phase: 0 for unknown, 1 for a liquid, or 2 for a gas or supercritical fluid. The known phase routines are faster but will fail with an incorrect input.
17. The minimum fluid density which is used for root bounding. Can be set to -1 to avoid guessing.
18. The maximum fluid density which is used for root bounding. Can be set to -1 to avoid guessing.
19. The fluid density units e.g. kg/m^3.
20. The desired fluid property symbol e.g. E for internal energy(see symbols in Table C-2).
21. The desired fluid property units e.g. J/kg.
22. The desired fluid property source. Should be NIST for using the NIST RefProp code or SODIUM for using the sodium equation of state polynomials.
23. The desired fluid to use e.g. WATER.
24. The desired fluid molar fraction e.g. 1.0

The complete linear table line would be:

LIN POS H 8492 408720 4000 J/KG LIN POS P 100000 3000000 25000 PA 0 0 -1.0 -1.0 KG/M^3 E J/KG NIST WATER 1.0

Note that GAS-PASS/CO_2 does not provide the ability of using combining positive and negative linear fluid property tables.

Table C-2: Tables Property Files

Description	Flag
Temperature	t
Pressure	p
Density	d
Thermal Conductivity	k
Isobaric Specific Heat	Cp
Isochoric Specific Heat	Cv
Dynamic Viscosity	v
Enthalpy	h
Entropy	s
Speed of Sound	n
Internal Energy	u

Available NIST Property Inputs

The property table creation code allows two different sets of NIST routines to be called depending on the phase of the fluid; the single phase (phase=1) and the flash routines (phase=0,2). There are 15 different property input combinations that may be used with the flash routines. If the phase is unknown then the flash routines may be used at the cost of significantly slower run time. The single phase routines are faster but may fail with an incorrect phase or return an incorrect value.

The user may also input the reverse order of the property routines i.e. pressure and temperature. They will be switched internally and returned in the order the user specified. Table C-3 lists the unknown phase routines. The flash routines require identical property inputs (using any two thermodynamic property inputs) and will ignore extra values used in other areas like state, and minimum and maximum density.

The two phase routines are exclusively called from the flash routines and require no special input cases (they are actually provided by the flash routines). The state and density limits will be ignored in these cases. The user should be aware that the isobaric specific heat and the speed of sound are not defined for two phase fluids and will return with the value -9.99998d6.

Table C-3: Unknown Phase NIST RefProp Routines

Property Input 1	Property Input 2	Symbols	Routine Name	Phase
Temperature	Pressure	T,P	TPFLSH	0/2
Temperature	Density	T,D	TDFLSH	0/2
Temperature	Internal Energy	T,E	TEFLSH	0/2
Temperature	Enthalpy	T,H	THFLSH	0/2
Temperature	Entropy	T,S	TSFLSH	0/2
Pressure	Density	P,D	PDFLSH	0/2
Pressure	Internal Energy	P,E	PEFLSH	0/2
Pressure	Enthalpy	P,H	PHFLSH	0/2
Pressure	Entropy	P,S	PSFLSH	0/2
Density	Internal Energy	D,E	DEFLSH	0/2
Density	Enthalpy	D,H	DHFLSH	0/2
Density	Entropy	D,S	DSFLSH	0/2
Enthalpy	Entropy	H,S	HSFLSH	0/2
Temperature	Quality	T,Q	TQFLSH	0/2
Pressure	Quality	P,Q	PQFLSH	0/2

The single phase subroutines offer 12 possible thermodynamic set inputs (and their reverse order) and several routines require a minimum and maximum density as inputs. The user must determine realistic limits and input these where necessary. In all other cases the density limits will not be used and any real value is acceptable but a -1.0 is recommended for clarity.

Several single phase routines require that the user specify the fluid state (liquid/gas) somewhat confusingly called the phase flag, *kph*. This input will only be used in the required cases, so any integer is acceptable, but it is recommended that the user set this input to -1 for clarity. In cases where the state is required, it should be set to 1 for liquids or 2 for vapors. The available single phase routines are shown in Table C-4.

Table C-4: Single Phase NIST RefProp Routines

Property Input 1	Property Input 2	Symbols	Routine Name	Phase	Density Limits	State
Temperature	Pressure	T,P	TPRHO	1		X
Temperature	Internal Energy	T,E	TEFL1	1	X	
Temperature	Enthalpy	T,H	THFL1	1	X	
Temperature	Entropy	T,S	TSFL1	1	X	
Pressure	Density	P,D	PDFL1	1		
Pressure	Internal Energy	P,E	PEFL1	1		X
Pressure	Enthalpy	P,H	PHFL1	1		X
Pressure	Entropy	P,S	PSFL1	1		X
Density	Internal Energy	D,E	DEFL1	1		
Density	Enthalpy	D,H	DHFL1	1		
Density	Entropy	D,S	DSFL1	1		
Enthalpy	Entropy	H,S	HSFL1	1	X	

6.4.3.21 Fluid Mixtures

The NIST code allows fluid mixtures to be used instead of pure fluids. The properties code supports mixing up to 20 fluids and includes a mixtures file, *Hmx.bnc*, which provides the mixture rules. Not all fluid mixtures are allowed[25].

Appendix D: Simple Turbomachinery Performance Equations

This appendix will offer four simple equations which capture much of the behavior of the radial compressors and axial turbine used in the S-CO_2 recompression cycle. These equations may prove useful for back of the envelope calculations or initial testing in other dynamic modeling codes.

Radial Compressors

The radial compressor pressure rise scales* as shown in Equation D-1, and the mass flow rate as shown in Equation D-2.

Equation D-1: Compressor Pressure Rise as a Function of Density and Shaft Speed **(D-1)**

$$\Delta P_2 = \Delta P \frac{\rho_{exit\_2}}{\rho_{exit\_ref}} \frac{U_2^2}{U_{ref}^2}$$

Equation D-2: Compressor Scaled Mass Flow Rate as a Function of Density and Shaft Speed **(D-2)**

$$\dot{m}_{scaled} = \dot{m} \frac{\rho_{exit\_ref}}{\rho_{exit\_2}} \frac{U_{ref}}{U_2}$$

If a trend line is fit to the original data plot (normalized pressure ratio versus normalized mass flow rate) one obtains Figure D-1. Combing the trend line in Figure D-1 with Equation D-1 and Equation D-2 creates Equation D-3†.

Equation D-3: Radial Compressor Pressure Ratio as a Function of Mass Flow Rate, Exit Density, and Shaft Speed **(D-3)**

$$\Delta P_2 = \Delta P_{ref} \left(\begin{array}{l} -4.5942 \left(\dfrac{\dot{m}_2 \dfrac{\rho_{ref}}{\rho_2} \dfrac{U_{ref}}{U_2}}{\dot{m}_{ref}} \right)^3 + 10.487 \left(\dfrac{\dot{m}_2 \dfrac{\rho_{ref}}{\rho_2} \dfrac{U_{ref}}{U_2}}{\dot{m}_{ref}} \right)^2 \\ -7.9392 \left(\dfrac{\dot{m}_2 \dfrac{\rho_{ref}}{\rho_2} \dfrac{U_{ref}}{U_2}}{\dot{m}_{ref}} \right) + 3.0484 \end{array} \right) \frac{\rho_2}{\rho_{ref}} \frac{U_2^2}{U_{ref}^2}$$

---

* Per the expert opinion of Dr. Yifang Gong from the MIT Aero/Astro Laboratory.

† Note, the user may decide what density to use (inlet/average/outlet) -- GAS-PASS/CO_2 uses average density.

The efficiency of the radial compressor is not expected to vary with density or shaft speed (e.g. no Equation D-1 for efficiency) thus its equation is solely based upon mass flow rate. The compressor normalized efficiency versus normalized mass flow rate is shown in Figure D-2 with a cubic trend-line fit. Using Figure D-2 and Equation D-2 one can create Equation D-4.

Equation D-4: Radial Compressor Efficiency as a Function of Mass Flow Rate **(D-4)**

$$\eta_2 = \eta_{ref}\left(\begin{array}{l} -1.4386\left(\dfrac{\dot{m}_2\dfrac{\rho_{ref}}{\rho_2}\dfrac{U_{ref}}{U_2}}{\dot{m}_{ref}}\right)^3 + 3.2804\left(\dfrac{\dot{m}_2\dfrac{\rho_{ref}}{\rho_2}\dfrac{U_{ref}}{U_2}}{\dot{m}_{ref}}\right)^2 \\ -2.2997\left(\dfrac{\dot{m}_2\dfrac{\rho_{ref}}{\rho_2}\dfrac{U_{ref}}{U_2}}{\dot{m}_{ref}}\right) + 1.4599 \end{array}\right)$$

These two equations encompass all the data used for radial compressor performance in the S-CO_2 recompression cycle.

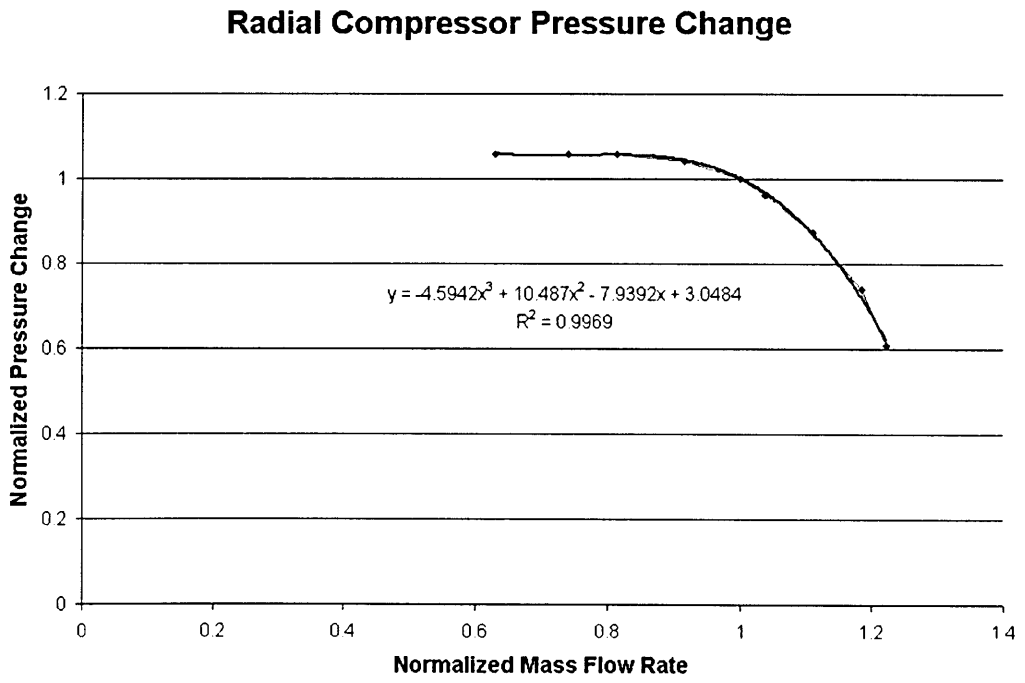

Figure D-1: Radial Compressor Pressure Ratio Curve with Trend-line

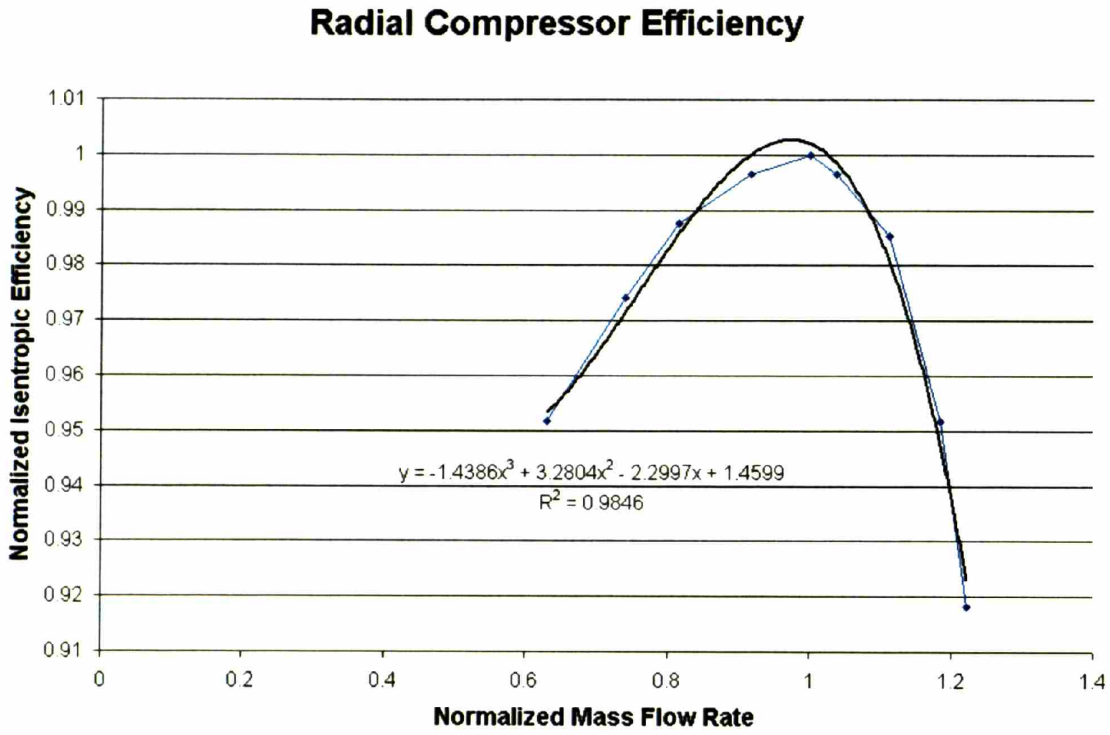

Figure D-2: Radial Compressor Efficiency Curve with Trend-line

Axial Turbine

Fitting an axial turbine is much more difficult than fitting a radial compressor. The problem stems from overlapping and conflicting pressure ratios, and is clearly illustrated by Figure D-3. This figure shows that at high shaft speeds the curves overlap in no easily recognizable pattern. It is likely that the uncertainty in creating this data is larger than the very small fractional pressure difference at these shaft speeds.

The small differences between high shaft speeds are clearly shown in Figure D-4. To a first order analysis, the 70% through 120% shaft speed curves are identical. To make the process of modeling the turbine with basic relations feasible, all but the 100% shaft speed curve will be discarded and the equations derived will be restricted to between 70% and 120% of the nominal shaft speed.

Even working with only a single axial turbine curve is more complex, because the higher mass flow rate region close to choke is so steep that polynomials will not work well. Figure D-4 shows the axial turbine with a 3^{rd} order fit and Figure D-6 shows the axial turbine with a 6^{th} order fit. No other simple function matches the shape of this curve, thus the curve must be modified before fitting.

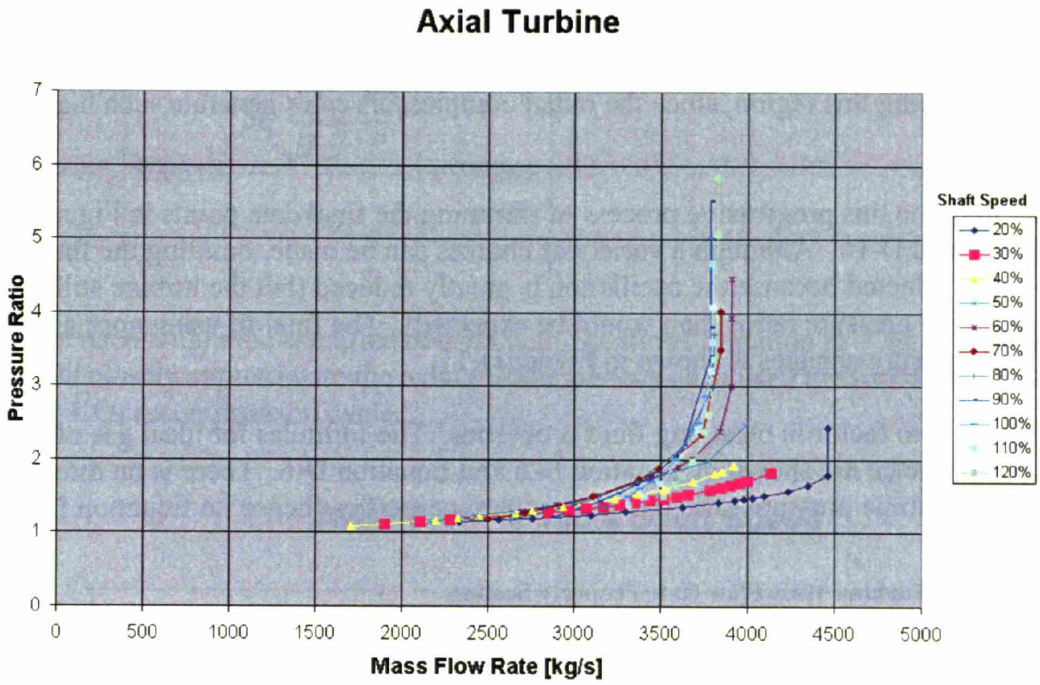

Figure D-3: Axial Turbine Pressure Ratios Curves

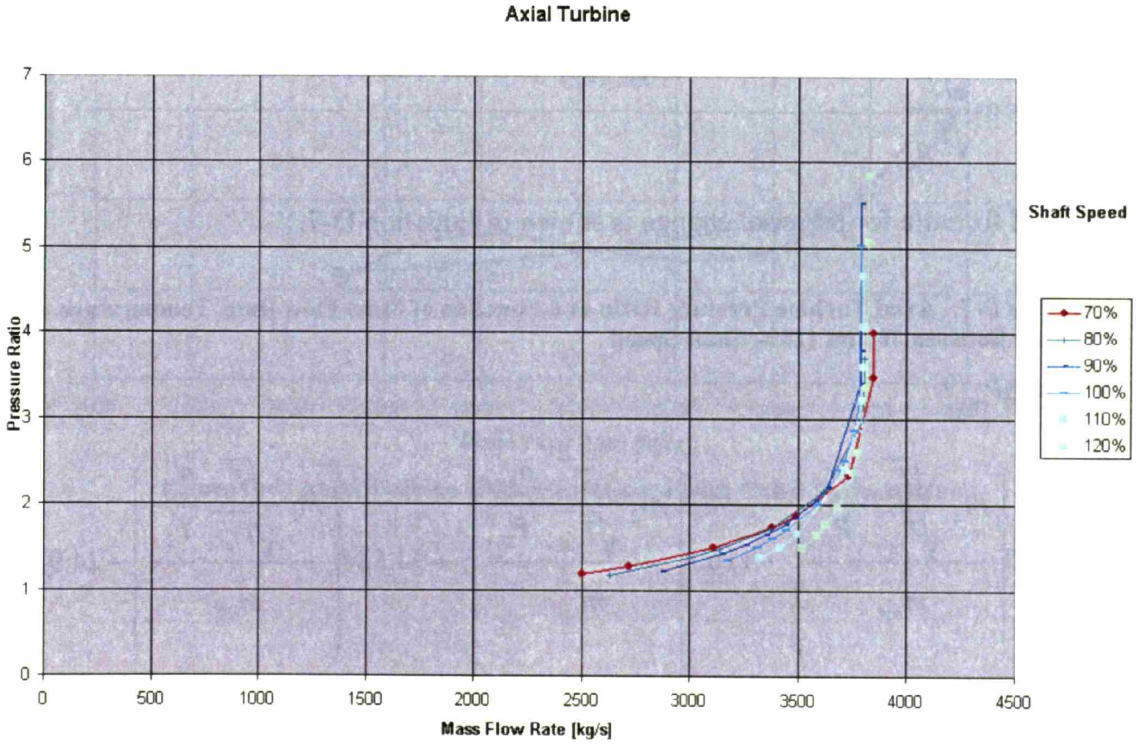

Figure D-4: Axial Turbine Pressure Ratio Curves at High Shaft Speeds

One easy solution is to remove the last data points from the curve. In this very high slope region the turbine is near choke anyway (little further information is available), the simulation code is likely to fail before reaching such a steep slope, and there is little chance of reaching this region, since the radial compressors can't generate such high pressure ratios.

The user may see this progressive process of trimming the final data points in Figure D-7 through Figured D-10. Although a variety of choices can be made, omitting the final two end points is selected because the oscillation is greatly reduced (but the turbine still achieves higher pressure ratios than would be expected). The final fit using normalized values and pressure changes is shown in Figure D-11.

The last step is to factor in changing fluid properties. The formulas for ideal gas off-design performance are shown in Equation D-5 and Equation D-6. There is no direct effect on the turbine pressure ratio due to changing properties (hence no Equation D-1).

Equation D-5: Turbine Mass Flow Rate Property Scaling **(D-5)**

$$m_{scaled} = m\frac{\sqrt{T}}{\sqrt{T_{ref}}}\frac{P_{ref}}{P}$$

Equation D-6: Turbine Shaft Speed Property Scaling **(D-6)**

$$\omega_{scaled} = \omega\frac{\sqrt{T}}{\sqrt{T_{ref}}}$$

The final formula for pressure change is shown in Equation D-7.

Equation D-7: Axial Turbine Pressure Ratio as a Function of Mass Flow Rate, Temperature, and Pressure Between 70 and 120% Shaft Speed **(D-7)**

$$\Delta P_2 = \Delta P_{ref} * \left(48.245\left(\frac{m_2 \frac{\sqrt{T_2}}{\sqrt{T_{ref}}}\frac{P_{ref}}{P_2}}{m_{ref}} \right)^3 - 116.8\left(\frac{m_2 \frac{\sqrt{T_2}}{\sqrt{T_{ref}}}\frac{P_{ref}}{P_2}}{m_{ref}} \right)^2 + 94.524\left(\frac{m_2 \frac{\sqrt{T_2}}{\sqrt{T_{ref}}}\frac{P_{ref}}{P_2}}{m_{ref}} \right) - 24.935 \right)$$

The efficiency of the axial turbine varies over a very small range, is similarly complicated, and is a second order effect during transient simulation. The single best fit line shown in Figure D-12 was adopted. Consequently the final formula for efficiency is contained in Equation D-8.

Equation D-8: Axial Turbine Efficiency as a Function of Mass Flow Rate, Temperature, and Pressure Between 70 and 120% Shaft Speed **(D-8)**

$$\eta_2 = \eta_{ref}\left(0.0518\left(\frac{\dot{m}_2\frac{\sqrt{T_2}}{\sqrt{T_{ref}}}\frac{P_{ref}}{P_2}}{\dot{m}_{ref}}\right)+0.9367\right)$$

When used within the specified bounds both equations Equation D-7 and Equation D-8 should closely approximate the axial turbine performance used in GAS-PASS/CO_2 for the S-CO_2 recompression cycle.

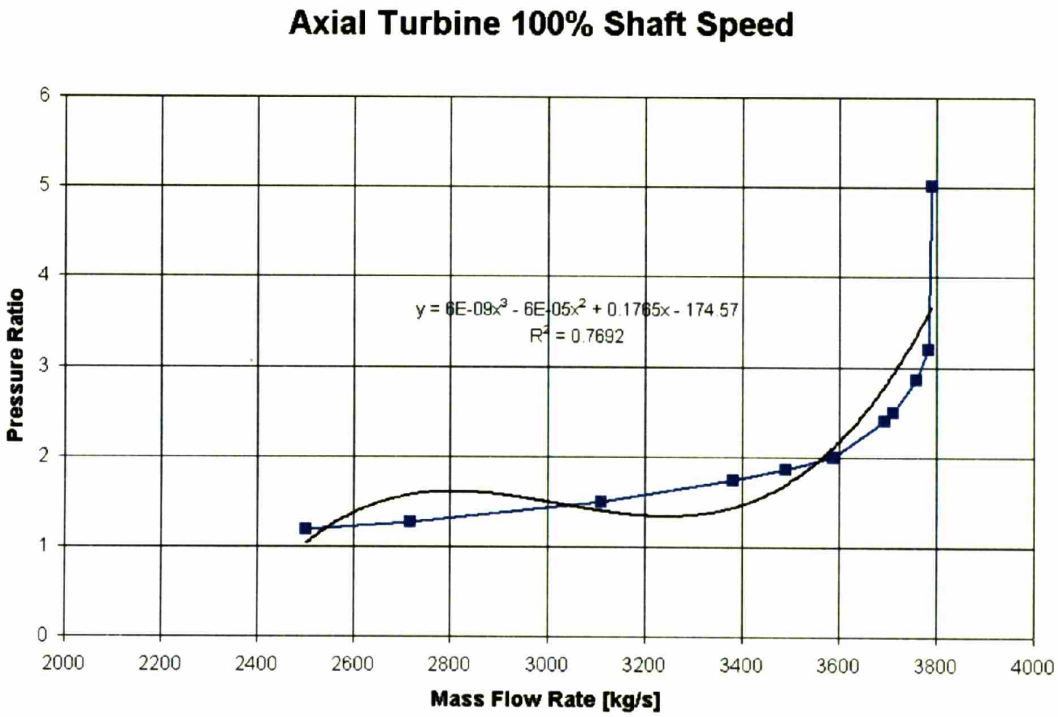

Figure D-5: Axial Turbine 100% Shaft Speed with Cubic Polynomial Fit

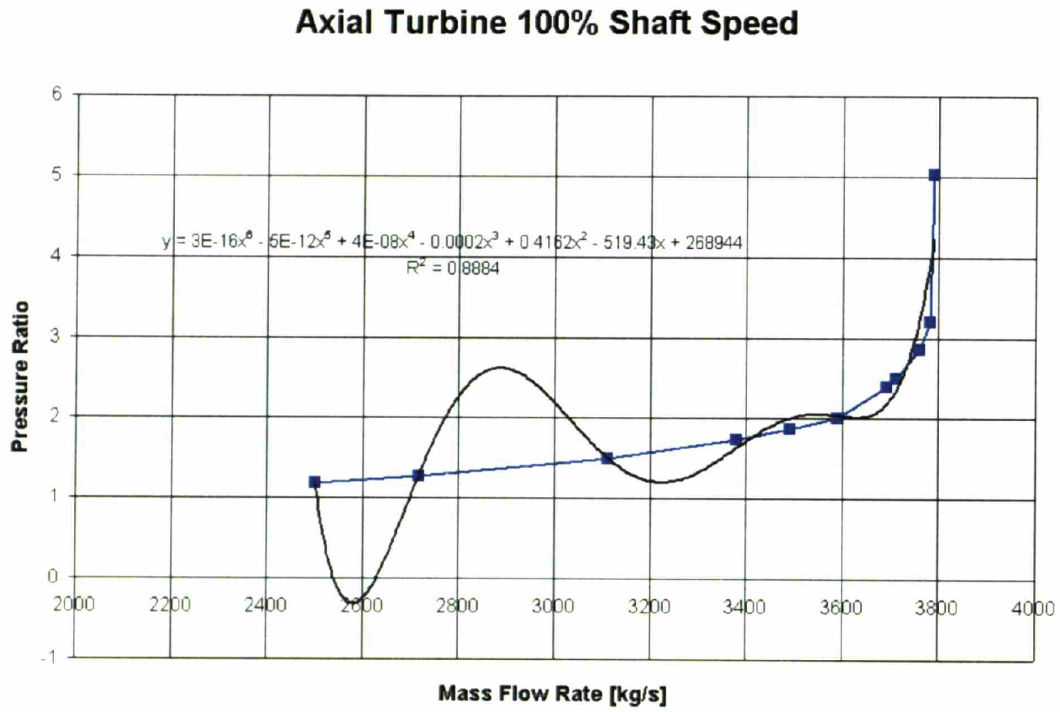

Figure D-6: Axial Turbine 100% Shaft Speed with 6th Order Polynomial Fit

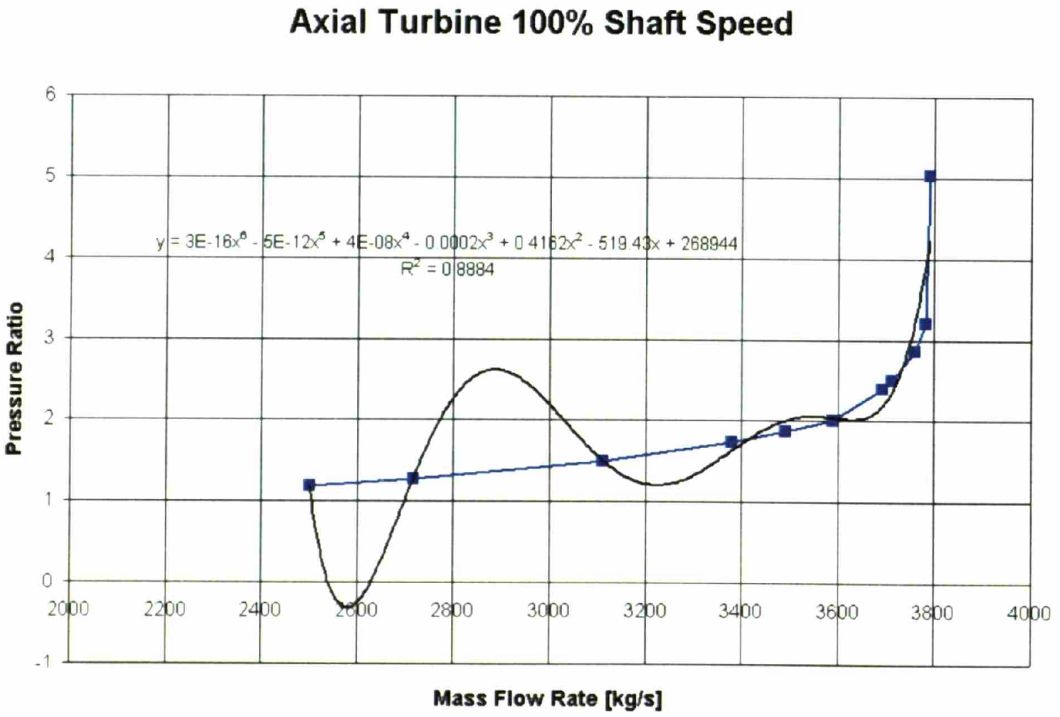

Figure D-7: Axial Turbine 100% Shaft Speed with Cubic Polynomial Fit Omitting 1 End Point

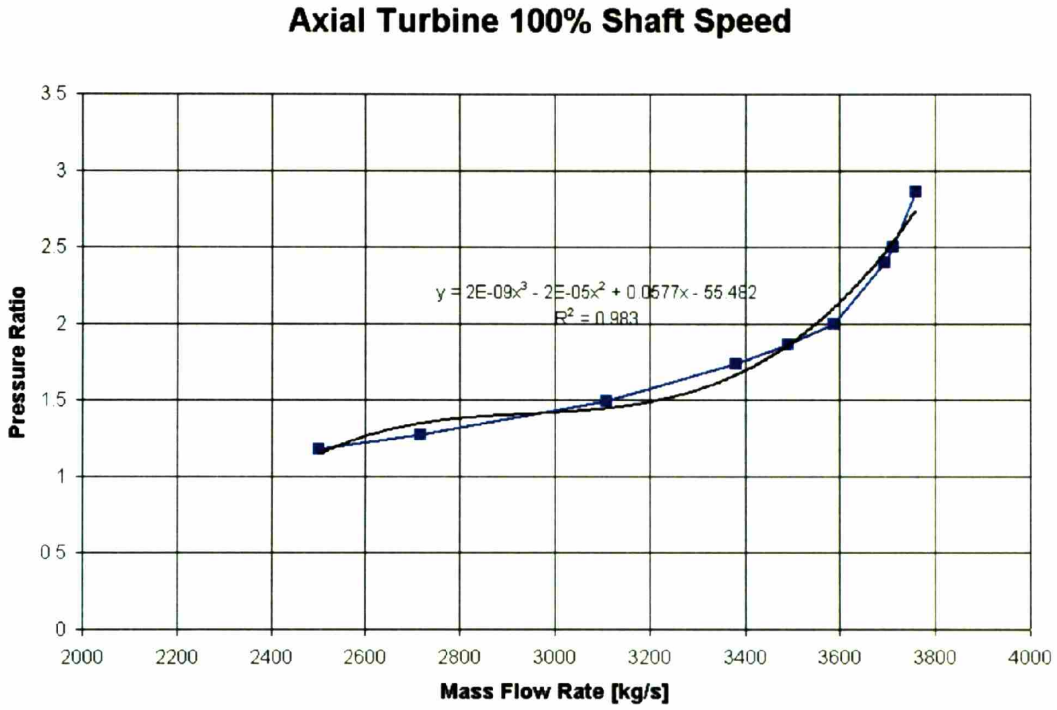

Figure D-8: Axial Turbine 100% Shaft Speed with Cubic Polynomial Fit Omitting 2 End Points

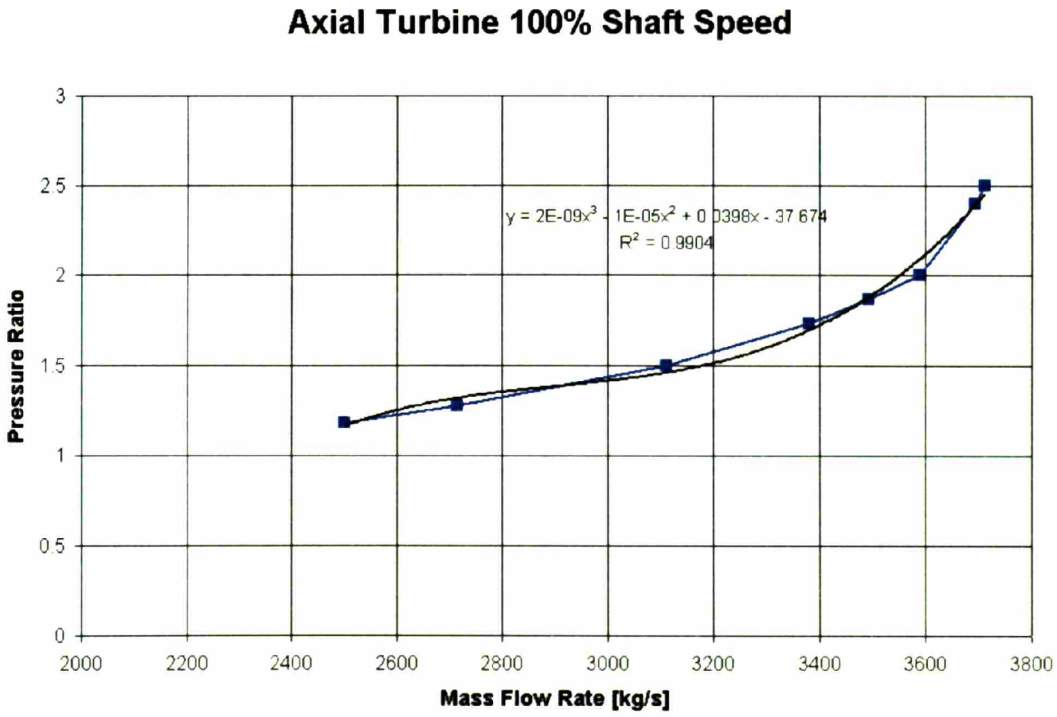

Figure D-9: Axial Turbine 100% Shaft Speed with Cubic Polynomial Fit Omitting 3 End Points

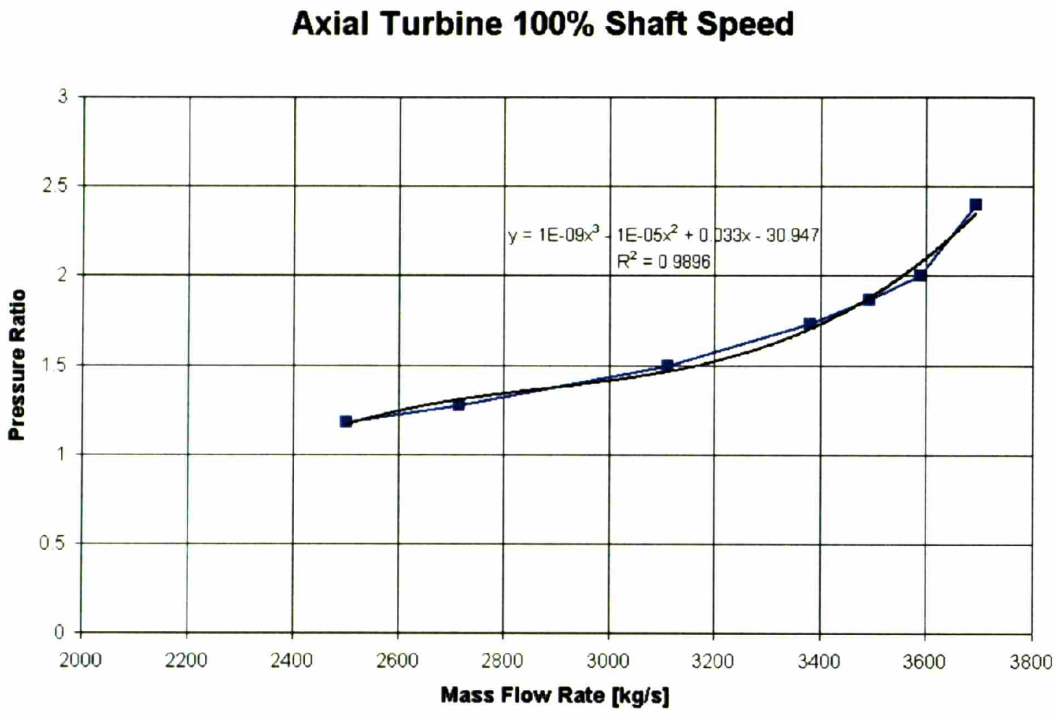

Figure D-10: Axial Turbine 100% Shaft Speed with Cubic Polynomial Fit Omitting 4 End Points

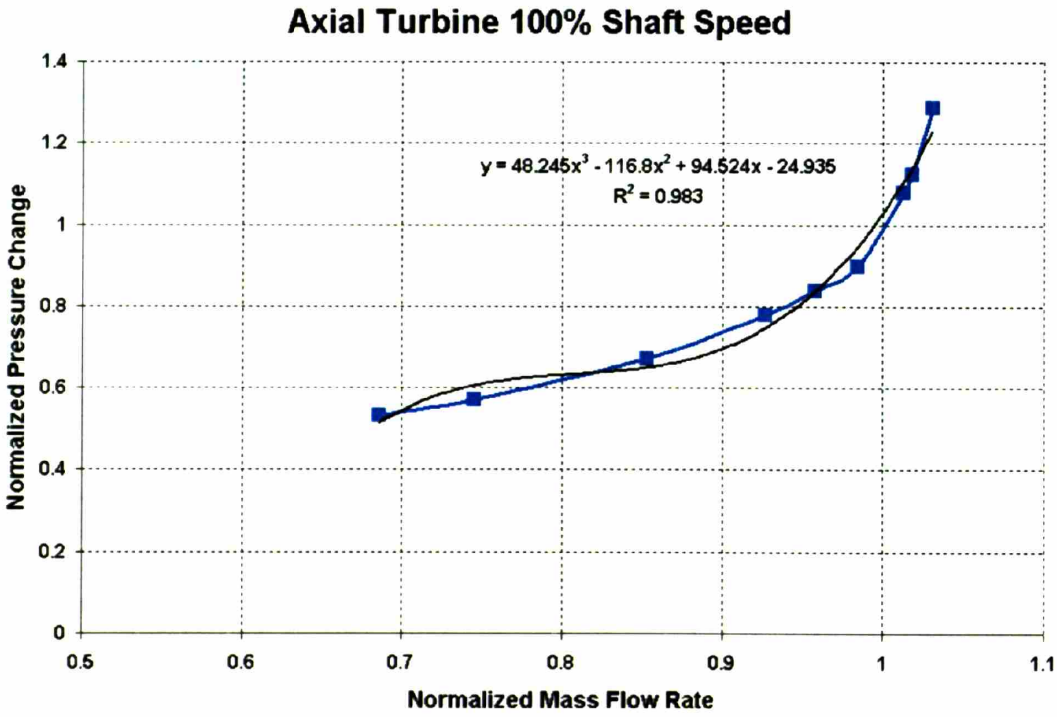

Figure D-11: Axial Turbine 100% Shaft Speed with Final Polynomial Fitted Pressure Ratio Curve

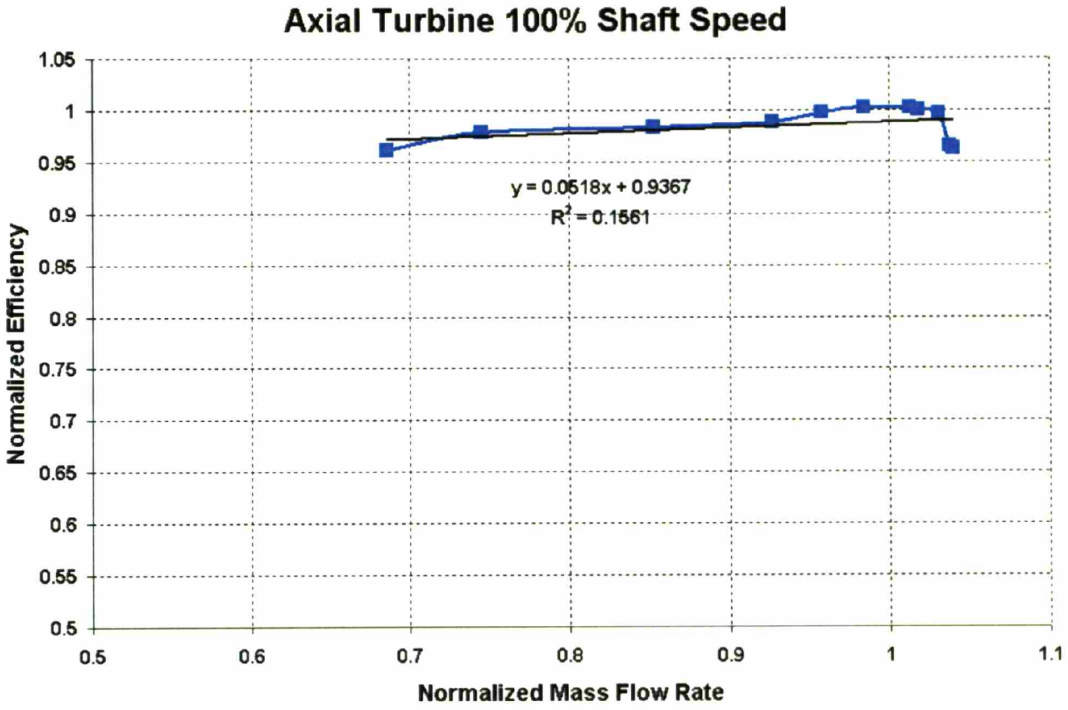

Figure D-12: Axial Turbine 100% Shaft Speed with Final Polynomial Fitted Efficiency Curve

Appendix E: References

[1] Energy Information Administration, "International Energy Outlook 2006; Highlights," June 2006, http://www.eia.doe.gov/oiaf/ieo/highlights.html

[2] Wikipedia, "Generation IV Reactor," January 2007, http://en.wikipedia.org/wiki/Generation_IV_reactor

[3] V. Dostal, M. Driscoll, P. Hejzlar, "A Supercritical Carbon Dioxide Cycle for Next Generation Reactors," MIT-ANP-TR-100, March 2004.

[4] R. Vilim, U. Mertyurek, J. Cahalan, "GAS-PASS/H: A Simulation Code for Gas Reactor Plant Systems," Argonne National Laboratory, September 2003.

[5] J. Buongiorno, "The Supercritical Water Cooled Reactor (SCWR)," Idaho National Engineering and Environmental Laboratory, PowerPoint presentation at ANS 2002 Winter Meeting, November 18, 2002.

[6] J. Gibbs, "Applicability of Supercritical CO_2 Power Conversion Systems to GEN IV Reactors," MIT-GFR-037, September 2006.

[7] DOE Office of Nuclear Energy, "The U.S. Generation IV Fast Reactor Strategy," DOE/NE-0130, December 2006.

[8] DOE, "DOE – Global Nuclear Energy Partnership," February 2007, http://www.gnep.energy.gov/

[9] M. Pope, "Thermal Hydraulic Design of a 2400 MWth Direct Supercritical CO_2-Direct Cycle GFR," MIT-ANP-TR-112, August 2006.

[10] A. Moisseytsev, J. Sienicki, "Transient Accident Analysis of a Supercritical Carbon Dioxide Brayton Cycle Energy Converter Coupled to an Autonomous Lead-Cooled Fast Reactor," ICONE 14-89544, July 2006.

[11] EPRI, "Ultra-high Temperature Coal Plants are More Efficient, Emit Much Less CO2," January 2007, http://www.epri.com/corporate/discover_epri/news/2004/052504_coalplant.html

[12] A. Hajj-Ahmad, "Use of Supercritical CO_2 Power Conversion System with Fusion Reactors," MIT-GFR-039, August 2006.

[13] Y. Wang, et. al, "Aerodynamic Design of Turbomachinery for 300 MWe Supercritical Carbon Dioxide Brayton Power Conversion System," MIT-GFR-022, March 2005.

[14] V. Dostal, "A Supercritical Carbon Dioxide Cycle for Next Generation Reactors," MIT Department of Nuclear Science and Engineering PhD Thesis, January 2004.

[15] V. Dostal, P. Hejzlar, M. Driscoll, "The Supercritical Carbon Dioxide Power Cycle: Comparison to Other Advanced Power Cycles," Nuclear Technology, Vol. 154, June 2006.

[16] P. Hejzlar, et. al., "Assessment of Gas Cooled Fast Reactor with Indirect Supercritical CO_2 Cycle," Nuclear Engineering and Technology, Vol. 38 No. 2, January 2006.

[17] A. Moisseytsev, J. Sienicki, "Control of Supercritical CO_2 Brayton Cycle for LFR Autonomous Load Following," Transactions of the American Nuclear Society, Volume 93.

[18] H. Frutschi, Closed-Cycle Gas Turbines; Operating Experience and Future Potential, ASME Press, 2005.

[19] X. Yan, "Dynamic Analysis and Control System Design for an Advanced Nuclear Gas Turbine Power Plant," MIT Department of Nuclear Science and Engineering PhD Thesis, June 1990.
[20] C. Wang, "Design, Analysis and Optimization of the Power Conversion System for the Modular Pebble Bed Reactor System," MIT Department of Nuclear Science and Engineering PhD Thesis, August 2003.
[21] J. Zhao, "Stability Analyses of Supercritical Water Cooled Reactors," MIT Department of Nuclear Science and Engineering PhD Thesis, July 2005.
[22] Burns & Roe Enterprises Inc, "Supercritical Water Reactor (SCWR), Study of Power Conversion Cycle, Reactor Control Strategy and Start-up Procedures," prepared for Idaho National Engineering Laboratory, September 2003.
[23] R. Aungier, "A Fast, Accurate Real Gas Equation of State for Fluid Dynamic Analysis Applications," Journal of Fluids Engineering, Vol. 117, June 1995.
[24] R. Aungier, Axial-Flow Compressors; A Strategy for Aerodynamic Deign and Analysis, ASME Press, 2003, pages 32-37.
[25] E. Lemmon, "REFPROP Computer Code, NIST Standard Database 23 Version 7.0," 2002, http://www.nist.gov/srd/nist23.htm
[26] R. Span, W. Wagner, "A New Equation of State for Carbon Dioxide Covering the Fluid Region from the Triple-Point Temperature to 1100 K at Pressures up to 800 MPa," Journal of Physical Chemistry Reference Data, Vol. 26, No. 6, 1996.
[27] C. Oh et. al, "Evaluation of Working Fluids in an Indirect Combined Cycle in a Very High Temperature Gas-Cooled Reactor," Nuclear Technology, Vol. 156, October 2006.
[28] C. Oh et. al., "Brayton Cycle for High-Temperature Gas-Cooled Reactors," Nuclear Technology, Vol. 149, March 2005.
[29] M. El-Genk, J. Tournier, "Noble Gases Binary Mixtures for Brayton Commercial Nuclear Power Plants," Transactions American Nuclear Society, Volume 95, November 2006.
[30] N. Tauveron, M. Saez, "Axial Turbomachine Modeling with a Quasi 2D Approach. Application to Gas Cooled Nuclear Reactor," NURETH-11, October 2005.
[31] C. Wang, "Design, Analysis and Optimization of the Power Conversion System for the Modular Pebble Bed Reactor System," MIT Department of Nuclear Science and Engineering PhD Thesis, August 2003.
[32] P. Kemp, C. Nieuwoudt, "Operation and Control of the PBMR Demonstration Power Plant," ICONE14-89359, July 2006.
[33] Y. Gong, N. Carstens, M. Driscoll, "Supercritical CO_2 Cycle Main Compressor Design and Analysis Studies," MIT-GFR-28, September 2005.
[34] Y. Gong, et. al., "Analysis of Radial Compressor Options for Supercritical CO_2 Power Conversion Cycles," MIT-GFR-034, June 2006.
[35] K. Nichols, R. Fuller, "Turbomachinery Review of MIT Supercritical CO_2 Power Cycle," Barber-Nichols Inc., August 31, 2005.
[36] J. Kurzke, C. Riegler, "A New Compressor Map Scaling Procedure for Preliminary Conceptual Design of Gas Turbines," ASME IGTI Turbo Expo, 2000.
[37] Y. Muto, Y. Kato, "Design of Turbomachinery for the Supercritical CO_2 Gas Turbine Fast Reactor," ICAPP '06, June 2006.

[38] B. Olson, H. Hage, D. Ammerman, "CO_2 Compression Using an Eight Stage, Integrally Geared, Centrifugal Compressor." International Pipeline Conference, October 2004.
[39] N. Wada et. al., "High Performance, High Reliability Re-injection Compressors for Green House Gas (CO_2)," Mitsubishi Heavy Industries, Ltd., Technical Review Vol. 41 No. 1, February 2004.
[40] T. Sato, A. Tasaki, J. Masutani, "Re-injection Compressors for Greenhouse Gas (CO_2)," Mitsubishi Heavy Industries, Ltd., Technical Review Vol. 41 No. 3, June 2004.
[41] H. Uchida, A. Kashimoto, Y. Iwakiri, "Development of Wide Flow Range Compressor with Variable Inlet Guide Vane." R&D Review of Toyota CRDL, Vol. 41 No. 3, http://www.tytlabs.co.jp/english/review/rev413epdf/e413_009uchida.pdf
[42] N. Staroselsky, L. Ladin, "More Effective Control for Centrifugal Gas Compressors Operating in Parallel," International Gas Turbine Conference and Exhibit, June 1986.
[43] K. Gezelius, M. Driscoll, P. Hejzlar, "Design of Compact Intermediate Heat Exchangers for Gas Cooled Fast Reactors," MIT-ANP-TR-103, May 2004.
[44] T. Ishizuka et. al, "Thermal-Hydraulic Characteristics of a Printed Circuit Heat Exchanger In a Supercritical CO_2 Loop," NURETH-11, October 2005.
[45] Y. Muto, M. Utamura, Y. Kato, "Present Activity of Tokyo Institute of Technology in Supercritical CO_2 Research and Future Collaboration with MIT," MIT & TIT Conference Presentation, March 2005.
[46] U. Mertyurek, R. Vilim, J. Cahalan, "GAS-PASS/H: A Simulation Code for Gas Reactor Plant Systems," ICAPP 2004, paper 4335, June 2004.
[47] R. Vilim, "ATWS Events and Control System Design for the Gas Fast Reactor," ICAPP 2005, paper 5227, May 2005.
[48] R. Vilim, "ATWS Events and Control System Design for the Gas Fast Reactor," Transactions of the American Nuclear Society, Volume 91, November 2004.
[49] Visual Numerics. IMSL Math/Library, Volume 1 848-865.
[50] Personal communication with Dr. Vilim, Argonne National Laboratory, ~June 2006.
[51] N. Todreas, M. Kazimi, Nuclear Systems I; Thermal Hydraulic Fundamentals, Taylor & Francis, 2nd printing, 1993.
[52] E. Lemmon, "REFPROP computer code help," NIST Standard Database 23 Version 7.0, 2002.
[53] Wikipedia, "Brent's Method," 2006, http://en.wikipedia.org/wiki/Brent's_method.
[54] N. Carstens, "Props 1.5: A Command Line Fluid Properties Code," MIT-GFR-030, August, 2005.
[55] D. Legault, P. Hejzlar, "CYCLES II: A Steady State Code for Supercritical CO_2 Power Conversion System Calculations," MIT-GFR-036, June 2006.
[56] R. Vilim, "International Nuclear Energy Research Initiative #2001-002-F; Development of Gen IV Advanced Gas-Cooled Reactor with Hardened/Fast Neutron Spectrum; Passive Full Power Safety," Argonne National Laboratory, January 2004, Doc. GFR-016.
[57] I. Matthews, "Characterization of Radial Compressors for Supercrtical CO_2 Power Conversion Systems," MIT-GFR-041, September 2006.
[58] D. Japikse, "Centrifugal Compressor Design and Performance," Concepts ETI, Inc., 1996.

[59] Y. Gong et. al, "Analysis of Radial Compressor Options for Supercritical CO_2 Power Conversion Cycles," MIT-GFR-034, June 2006.
[60] N. Carstens et. al., "Turbomap 1.2: A Command Line Turbomachinery Map Code," MIT-GFR-022, September, 2005.
[61] Personal communication with Dr. Yifang Gong, MIT Gas Turbine Laboratory, February 2005.
[62] J. Sienicki et. al., "Status Report on the Small Secure Transportable Autonomous Reactor (SSTAR)/Lead-Cooled Fast Reactor (LFR) and Supporting Research and Development," ANL-GenIV-089, September 2006.
[63] Press, Teukolsky et. al, Numerical Recipes in Fortran 77; The Art of Scientific Computing Volume 1, University of Cambridge, 2nd Edition, 2001.
[64] Wikipedia, "Bernoulli's principle," September 2006, http://en.wikipedia.org/wiki/Bernoulli%27s_equation
[65] Ishizuka et. al., "Thermal Hydraulic Characteristics of a Printed Circuit Heat Exchanger in a Supercritical CO_2 Loop." NURETH-11, 2005.
[66] J. Wang, and E. Hihara, "Study on carbon dioxide gas cooler heat transfer process under supercritical pressures," International Journal of Energy Research, Vol. 26, 2002.
[67] B. Petukhov, Heat Exchangers – Design and Theory Sourcebook. "Chapter 11 Turbulent heat transfer in tubes with variable fluid properties." McGraw-Hill Book Company, Afan NH, Schlunder EU (eds), 240-251, 1974.
[68] V. Gnielinski, "New Equations for heat and mass transfer in turbulent pipe and channel flow," International Chemical Engineering, Vol. 16, April 1976.
[69] D. Olsen. "Heat Transfer of Supercritical Carbon Dioxide Flowing in a Cooled Horizontal Tube." NISTIR 6496, May 2000.
[70] S. Pitla, E. Groll, S. Ramadhyani. "New Correlation to predict the heat transfer coefficient during in-tube cooling of turbulent supercritical CO_2," International Journal of Refrigeration 25, (2002), pages 887-895.
[71] J. Hesselgreaves. Compact Heat Exchangers, Selection, Design, and Operation. Pergamon 1st Edition 2001.
[72] R. Shah, M. Bhatti, Handbook of Single-Phase Convective Heat Transfer, Willy, New York, 1987.
[73] I Idelchik, Handbook of Hydraulic Resistance, Begell House Publishers, 3rd Edition, June 2001.
[74] P. Hejzlar, "Printed Circuit Heat Exchangers with Zigzag Channel," internal MIT paper, January, 2006.
[75] D. Langewisch., S. Kao, M. Driscoll, "HXMOD – A Heat Exchanger Module for Power Cycle Dynamics Modeling," MIT-GFR-040, September 2006.
[76] Wikipedia, "Biot Number," 2006, http://en.wikipedia.org/wiki/Biot_number.
[77] F. Incropera & D. Dewitt, Fundamentals of Heat and Mass Transfer, Jon Wiley & Sons, 4th Edition, 1996, page 256.
[78] Personal communication with Mike Pope, MIT, July 2006.
[79] Wikipedia, "PID Controller," November 2006, http://en.wikipedia.org/wiki/PID_controller
[80] Personal communication with Dr. Richard Vilim, Argonne National Laboratory, October 2006.

[81] P. Hejzlar, O. Ubra, J. Ambroz, "A Computer Program for Transient Analysis of Steam Turbine Generator Overspeed," Nuclear Engineering and Design, Volume 144, 1993.
[82] J. Buongiorno, "The Supercritical Water Cooled Reactor (SCWR)," Idaho National Engineering and Environmental Laboratory, PowerPoint presentation at ANS 2002 Winter Meeting, November 18, 2002.
[83] R. Duffey, S. Kuran, and I. Pioro, "Designing High Efficiency Reactors Using Existing Ultra-Supercritical Technology," 3rd International Symposium on SCWR Design and Technology, March 2007, Shanghai.
[84] A. Kubo et al., "Feasibility Study on the Reliable Steam Generator with Helically Coiled Double Wall Tubes on FBR," Proc. of ICONE-5, May 1997.
[85] C. Adkins, M. Gross, W. Harris, W. Vatter, "A Solid-Conductor Primary Steam Generator for LMFBR Plants," American Nuclear Society Transactions, Vol. 23, June 1976.
[86] C. Kirk, P. Fulford, "A Concept of Steam Generation with Heat Pipes for LMFBR Applications," American Nuclear Society Transactions, Vol. 23, June 1976.
[87] M. Gavrilas, P. Hejzlar, N. Todreas, Y. Shatilla, Safety Features of Operating Light Water Reactors of Western Design, Center for Advanced Nuclear Energy Systems, 2000.
[88] Personal communication with Dr. Richard Vilim, Argonne National Laboratory, August 2006.
[89] K. Asanovic et. al., "The Landscape of Parallel Computing Research: A View from Berkeley," Technical Report No. UCB/EECS-2006-183, http://www.eecs.berkeley.edu/Pubs/TechRpts/2006/EECS-2006-183.pdf

7237-16